TRANSCEPTORES EM BLOCO COM REDUNDÂNCIA REDUZIDA

Wallace Alves Martins

Tese de Doutorado apresentada ao Programa de Pós-graduação em Engenharia Elétrica, COPPE, da Universidade Federal do Rio de Janeiro, como parte dos requisitos necessários à obtenção do título de Doutor em Engenharia Elétrica.

Orientador: Paulo Sergio Ramirez Diniz

Rio de Janeiro
Dezembro de 2011

TRANSCEPTORES EM BLOCO COM REDUNDÂNCIA REDUZIDA

Wallace Alves Martins

TESE SUBMETIDA AO CORPO DOCENTE DO INSTITUTO ALBERTO LUIZ COIMBRA DE PÓS-GRADUAÇÃO E PESQUISA DE ENGENHARIA (COPPE) DA UNIVERSIDADE FEDERAL DO RIO DE JANEIRO COMO PARTE DOS REQUISITOS NECESSÁRIOS PARA A OBTENÇÃO DO GRAU DE DOUTOR EM CIÊNCIAS EM ENGENHARIA ELÉTRICA.

Examinada por:

Prof. Paulo Sergio Ramirez Diniz, Ph.D.

Prof. Eduardo Antônio Barros da Silva, Ph.D.

Prof. Marcello Luiz Rodrigues de Campos, Ph.D.

Prof. Raimundo Sampaio Neto, Ph.D.

Prof. Vitor Heloiz Nascimento, Ph.D.

RIO DE JANEIRO, RJ – BRASIL
DEZEMBRO DE 2011

Martins, Wallace Alves

Transceptores em Bloco com Redundância Reduzida/Wallace Alves Martins. – Rio de Janeiro: UFRJ/COPPE, 2011.

XXIII, 282 p.: il.; 29, 7cm.

Orientador: Paulo Sergio Ramirez Diniz

Tese (doutorado) – UFRJ/COPPE/Programa de Engenharia Elétrica, 2011.

Referências Bibliográficas: p. 276 – 282.

1. Processamento de sinais. 2. Comunicações. 3. Redundância reduzida. 4. Matrizes estruturadas. 5. Algoritmos rápidos. I. Diniz, Paulo Sergio Ramirez. II. Universidade Federal do Rio de Janeiro, COPPE, Programa de Engenharia Elétrica. III. Título.

A Deus,
por nos amar apesar de nós.

Agradecimentos

"God loved the people of this world so much that he gave his only Son,
so that everyone who has faith in him will have eternal life and never really die.
God did not send his Son into the world to condemn its people.
He sent him to save them!"
John 3.16-17 (Holy Bible – Contemporary English Version)

Há dois anos e nove meses aceitei o desafio de fazer o doutorado. Naquela ocasião, não esperava que me tornasse professor do CEFET/RJ (agosto/2010) e tivesse de conciliar o desafio de fazer pesquisa e ministrar aulas (doze horas semanais em sala de aula, além de outras atividades como projetos de pesquisa, não são fáceis). Agradeço a Deus por me ajudar a "concluir" etapa tão importante em minha vida.

Agradeço aos meus pais, Renê e Perpétua Martins, por me incentivarem a buscar os meus sonhos sem impor limites sobre o que eu poderia sonhar.

Agradeço à minha noiva, Claudia Lacerda, pela paciência e apoio em todos os momentos da "caminhada". Sem o seu amor seria difícil chegar até aqui.

Agradeço ao meu orientador, Prof. Paulo S. R. Diniz, pela confiança depositada em meu trabalho e pelo exemplo de profissional agregador, competente e que realmente faz a diferença na vida das pessoas. Espero que esta tese seja apenas o início de uma parceria duradoura.

Agradeço aos professores Eduardo A. B. da Silva, Marcello L. R. de Campos, Raimundo S. Neto e Vitor H. Nascimento por participarem da minha banca.

Agradeço também aos amigos do LPS pelos ensinamentos e parcerias. Correndo o risco de ser injusto, gostaria de destacar os seguintes nomes: Adriana Schulz, Alan Tygel, Alessandro Dutra, Alexandre Leizor, Prof. Amaro Lima, Ana Fernanda, André Targino, Andreas Ellmauthaler, Bernardo da Costa, Camila Gussen, Carlos Júnior, Fabiano Castoldi, Fábio Freeland, Filipe Diniz, Flávio Ávila, Prof. Gabriel Matos, Guilherme Pinto, Prof. João Terêncio, Leonardo Baltar, Leonardo Nunes, Prof. Luiz Wagner, Marcos Magalhães, Markus Lima, Prof. Michel Tcheou, Rafael de Jesus, Rafael Amado, Rodrigo Peres, Rodrigo Torres, Prof. Tadeu Ferreira (eterno orientador), Thiago Prego. Aprendi muito com vocês.

Agradeço ao Conselho Nacional de Desenvolvimento Científico e Tecnológico (CNPq) pelo suporte financeiro. Estendo estes agradecimentos ao povo brasileiro.

Resumo da Tese apresentada à COPPE/UFRJ como parte dos requisitos necessários para a obtenção do grau de Doutor em Ciências (D.Sc.)

TRANSCEPTORES EM BLOCO COM REDUNDÂNCIA REDUZIDA

Wallace Alves Martins

Dezembro/2011

Orientador: Paulo Sergio Ramirez Diniz

Programa: Engenharia Elétrica

A presente tese contém propostas de transceptores lineares e invariantes no tempo que empregam uma quantidade reduzida de redundância para eliminar a interferência entre blocos. Tais propostas englobam sistemas multiportadoras e monoportadora com equalizadores do tipo *zero-forcing* (ZF) ou de mínimo erro quadrático médio (MSE). A primeira contribuição deste trabalho é uma análise matemática que indica que a redução na quantidade relativa de redundância através do aumento do tamanho do bloco de dados, M, leva a uma perda de desempenho.

Propomos também novos transceptores que transmitem com uma quantidade menor de elementos redundantes em cada bloco, no lugar de aumentar o tamanho do bloco, M. É proposta uma modificação dos já conhecidos sistemas com redundância mínima. Além disso, propomos soluções MMSE subótimas que requerem a mesma quantidade de operações de uma solução ZF. Transceptores práticos baseados em transformadas discretas de Hartley (DHTs), matrizes diagonais e antidiagonais também são propostos.

Além de sistemas com redundância mínima, a tese apresenta propostas cuja quantidade de redundância pode variar desde a mínima, $\lceil L/2 \rceil$, até a mais comumente utilizada, L, assumindo uma resposta ao impulso do canal com ordem L. Os transceptores resultantes permitem a equalização eficiente dos blocos de dados recebidos, uma vez que eles utilizam apenas transformadas discretas de Fourier (DFTs) e equalizadores com um único coeficiente, ou DHTs e equalizadores com até dois coeficientes. Além disso, provamos matematicamente que quanto maior for a quantidade de elementos redundantes transmitidos, menor será o MSE de símbolos no receptor. As simulações indicam que nossas propostas podem alcançar taxas de transmissão maiores do que sistemas multiportadoras e monoportada tradicionais, mantendo a mesma complexidade assintótica para o processo de equalização, $\mathcal{O}(M \log_2 M)$.

Abstract of Thesis presented to COPPE/UFRJ as a partial fulfillment of the requirements for the degree of Doctor of Science (D.Sc.)

BLOCK-BASED TRANSCEIVERS WITH REDUCED REDUNDANCY

Wallace Alves Martins

December/2011

Advisor: Paulo Sergio Ramirez Diniz

Department: Electrical Engineering

This work proposes novel linear time-invariant block transceivers which employ a reduced amount of redundancy to eliminate interblock interference. The proposals encompass both multicarrier and single-carrier systems with either zero-forcing (ZF) or minimum mean-square error (MSE) equalizers. The first contribution is a mathematical analysis which indicates that the reduction in the relative amount of redundancy by increasing the block size, M, leads to loss in performance in terms of MSE and mutual information.

The work also proposes transceivers which enable transmission of a smaller amount of redundant elements in each block, instead of increasing M. It is proposed a simplification to the already known optimal MMSE-based minimum-redundancy systems. Furthermore, the work proposes suboptimal MMSE solutions requiring the same amount of computations of ZF-based ones. Practical transceivers using discrete Hartley transform (DHT), diagonal, and antidiagonal matrices are also proposed.

In addition to minimum-redundancy systems, the thesis presents practical proposals whose amount of redundancy ranges from the minimum, $\lceil L/2 \rceil$, to the most commonly used value L, assuming a channel-impulse response of order L. The resulting transceivers allow for superfast equalization of the received data blocks, since they only use discrete Fourier transform (DFT) and single-tap equalizers, or DHTs and two-tap equalizers in their structures. Moreover, it is proved mathematically that larger amounts of transmitted redundant elements lead to lower MSE of symbols at the receiver end. Computer simulations indicate that our proposals can achieve higher throughputs than the standard superfast multicarrier and single-carrier systems, while keeping the same asymptotic computational complexity for the equalization process, viz. $\mathcal{O}(M \log_2 M)$.

Sumário

Lista de Figuras

Lista de Tabelas

Lista de Abreviaturas

AMSE	Average MSE, p. 186
BER	Bit-Error Rate, p. 86
BLER	BLock-Error Rate, p. 156
CDF	Cumulative Distribution Function, p. 261
CFO	Carrier-Frequency Offset, p. 74
CP	Cyclic Prefix, p. 74
CSI	Channel-State Information, p. 78
DCT	Discrete Cosine Transform, p. 168
DFE	Decision-Feedback Equalizer, p. 77
DFT	Discrete Fourier Transform, p. 139
DHT	Discrete Hartley Transform, p. 77, 139
DSP	Digital Signal Processing, p. 81
DST	Discrete Sine Transform, p. 168
ETU	Extended Typical Urban, p. 261
FFT	Fast Fourier Transform, p. 75
FIR	Finite Impulse Response, p. 81
I/Q	Inphase/Quadrature, p. 168
IBI	InterBlock Interference, p. 74
ICI	InterCarrier Interference, p. 168
IDFT	Inverse Discrete Fourier Transform, p. 139

IIR	Infinite Impulse Response, p. 81
ISI	InterSymbol Interference, p. 74
LS	Least Square, p. 252
LTI	Linear Time-Invariant, p. 74
MC-MRBT	MultiCarrier Minimum-Redundancy Block Transceiver, p. 157
MC-RRBT	MultiCarrier Reduced-Redundancy Block Transceiver, p. 204
MIMO	Multiple-Input Multiple-Output, p. 85
MMSE	Minimum Mean-Square Error, p. 77
MSE	Mean-Square Error, p. 74
MUI	Multi-User Interference, p. 86
OFDM	Orthogonal Frequency-Division Multiplexing, p. 74
PAPR	Peak-to-Average Power Ratio, p. 74
PCG	Preconditioned Conjugate Gradient, p. 79
PDCA	Pan's Divide-and-Conquer Algorithm, p. 258
SC-FD	Single-Carrier with Frequency-Domain equalization, p. 74
SC-MRBT	Single-Carrier Minimum-Redundancy Block Transceiver, p. 157
SC-RRBT	Single-Carrier Reduced-Redundancy Block Transceiver, p. 204
SNR	Signal-to-Noise Ratio, p. 156
SVD	Singular-Value Decomposition, p. 75
TMUX	Transmultiplexer, p. 76
WSS	Wide-Sense Stationary, p. 142
ZF	Zero-Forcing, p. 77
ZJ	Zero Jamming, p. 75
ZP-OFDM	Zero-Padding OFDM, p. 93
ZP-SC-FD	Zero-Padding SC-FD, p. 95

ZP-ZJ Zero-Padding Zero-Jamming, p. 95

ZP Zero Padding, p. 74

Capítulo 1

Introdução

Uma parte significativa das pesquisas relacionadas às camadas física e de enlace de sistemas de comunicação concentra-se em desenvolver novos métodos para aumentar as taxas de transmissão de dados [1–4]. Do ponto de vista prático, tais pesquisas levam em consideração compromissos entre melhorias de desempenho e custo das soluções. A complexidade computacional está entre os fatores que determinam diretamente o custo de novos avanços na área de comunicação. Tal fato é evidenciado na escolha de transceptores lineares em várias aplicações práticas [5, 6].

Atualmente, a maior parte das especificações técnicas em comunicações recomenda a segmentação dos dados em blocos antes de começar a transmissão propriamente dita. Os blocos de dados resultantes são transmitidos separadamente naquilo que é denominado transmissão em blocos (ou por blocos). Devido à característica de seletividade em frequência própria de sistemas de comunicação em banda larga, há sempre a superposição de versões atenuadas dos sinais transmitidos. Tal superposição, também conhecida como interferência entre símbolos (ISI, da sigla em inglês, *intersymbol interference*) é induzida entre os símbolos que compõem um determinado bloco de dados. Esta superposição indesejada de sinais também gera o efeito de interferência entre blocos (IBI, da sigla em inglês, *interblock interference*).

O OFDM (do inglês, *orthogonal frequency-division multiplexing*) é o transceptor LTI (do inglês, *linear time-invariant*) sem memória e em blocos mais popular atualmente. Ele consegue eliminar o problema da IBI introduzindo redundância na transmissão. Além disso, tal redundância também age de forma a facilitar o projeto do equalizador com o intuito de eliminar ou reduzir a ISI no receptor [7–13]. A redundância pode ser inserida de várias formas, como por exemplo através de prefixo cíclico (CP, da sigla em inglês, *cyclic prefix*) ou simplesmente, pela inserção de zeros (ZP, da sigla em inglês, *zero padding*). Porém, o OFDM possui algumas desvantagens, como alto PAPR (do inglês, *peak-to-average power ratio*), alta sensibilidade ao CFO (do inglês, *carrier-frequency offset*) e, possivelmente, alta perda da eficiência espectral em razão da inserção de redundância. O SC-FD (do inglês, *single-carrier*

with frequency-domain equalization) é uma forma eficiente de reduzir ambos o PAPR e o CFO, quando comparado ao OFDM. Tais reduções são atingidas sem modificar drasticamente a complexidade computacional do transceptor [14, 15].

Quanto ao uso dos recursos espectrais, a quantidade de redundância empregada nos sistemas OFDM e SC-FD são as mesmas, dependendo apenas do espalhamento do canal (do termo em inglês, *delay spread of the channel*), o que implica que ambos transceptores gastam a mesma quantidade de banda para transmissão de dados redundantes. Entretanto, há várias formas de aumentar a eficiência espectral de sistemas de comunicação, tais como diminuindo a probabilidade de erro de símbolos na camada física de tal forma que se faça menos necessária a proteção implementada por codificadores de canais em camadas superiores. Em geral, tal abordagem aumenta os custos associados à camada física, uma vez que para alcançar tal redução na probabilidade de erro de símbolos é necessária a utilização de transceptores mais complexos, o que pode acabar por inviabilizar suas utilizações em sistemas práticos atuais.

Outros meios para aumentar a eficiência espectral são, portanto, altamente desejáveis. Reduzir a quantidade de redundância transmitida é uma solução possível. De fato, apenas poucos trabalhos propuseram a diminuição da redundância mantendo o custo computacional em níveis comparáveis aos sistemas práticos atuais (OFDM e SC-FD), através do emprego de algoritmos rápidos [16, 17]. Uma das propostas mais promissoras até então está presente no artigo pioneiro de Chung e Phoong [16]. A abordagem adotada em [16] lida com técnicas do tipo ZP-ZJ (do inglês, *zero-padding, zero-jamming*) para eliminar a IBI empregando uma quantidade reduzida de redundância associadas ao emprego de algoritmos do tipo FFT (do inglês, *fast Fourier transform*). Entretanto, o projeto resultante não possui uma estrutura bem definida e a sua complexidade computacional possui uma dependência quadrática sobre a ordem do modelo de canal. Para canais longos, o transceptor em [16] pode requerer muito mais cálculos do que aqueles propostos nesta tese. Além disso, as propostas em [16] são originalmente multiportadoras apenas. Por outro lado, a estratégia adotada em [17] é transmitir informação redundante em subportadoras não utilizadas, isto é, subportadoras que deverão ser descartadas no caso de *channel loading*. Através da exploração de tais subportadoras, é possível alcançar equalização do tipo *zero-forcing* sem enviar dados redundantes em subportadoras úteis. Usualmente, o número de subportadoras não utilizadas deve ser ao menos do tamanho da ordem do canal, restringindo a aplicação de tal técnica.

Há ainda outros trabalhos que propuseram a transmissão de dados com redundância reduzida, mas sem focar na simplicidade computacional de suas propostas. Por exemplo, o transceptor proposto em [18] requer um alto custo computacional para a equalização e para o projeto do transceptor devido à utilização de algoritmos

do tipo SVD (do inglês, *singular-value decomposition*).

Além disso, alguns trabalhos aplicaram a teoria de *displacement rank* com sucesso no contexto de processamento digital de sinais [19]. Em sistemas de comunicações, algoritmos rápidos foram aplicados em esquemas de estimação de canal empregando L (ordem do canal) elementos redundantes [20]. Os algoritmos resultantes são adequados para a deteção e a estimação dos elementos não-nulos de uma determinada resposta ao impulso de um canal de comunicação [20, 21]. Vale a pena ressaltar que, apesar da decomposição da inversa de uma matriz de Toeplitz, hermitiana [22] utilizada em [20] ser equivalente à decomposição descrita no Teorema 1 de [23], para o caso particular de uma matriz de Toeplitz hermitiana, tais decomposições não podem ser aplicadas aos receptores do tipo MMSE (do inglês, *minimum mean-squared error*) com redundância mínima. A razão é porque os transceptores propostos com redundância mínima não induzem uma estrutura de Toeplitz na matriz de correlação do canal, conforme ocorre em [20]. Tal fato, levou-nos a propor novas decomposições de bezoutianos generalizados no Teorema 2 de [23]. Conforme mencionado em [23], essas novas decomposições são fruto de adaptações realizadas em resultados descritos em [24].

1.1 Propósito deste Trabalho

O objetivo deste trabalho é propor novas estruturas para transceptores em bloco com redundância reduzida. Essas novas estruturas devem permitir a equalização dos dados recebidos de forma eficiente. Em outras palavras, tais estruturas devem empregar algoritmos rápidos [25]. De fato, nós empregamos apenas algoritmos rápidos para a implementação das transformadas discretas (de Fourier e de Hartley), juntamente com a utilização de equalizadores com no máximo dois coeficientes com o intuito de satisfazer às restrições de baixa complexidade computacional.

Vale ressaltar também que há ainda muito trabalho a ser continuado, tendo em vista que uma quantidade significativa de questões relevantes relacionadas às estruturas propostas não foram amplamente estudadas. Na verdade, nós focamos no processo de equalização ao invés de outros aspectos igualmente importantes, tais como estimação de canal, projeto do equalizador, desbalanceamento I/Q, estimação de CFO, apenas para mencionar alguns dos principais itens.

1.2 Organização

A presente tese está dividida em três partes principais: Parte I (que inclui os Capítulos 3, 4 e 5) descreve as novas contribuições feitas aos transceptores com redundância mínima; Parte II (que inclui os Capítulos 6 e 7) descreve algumas contribuições aos

sistemas com redundância reduzida; e Parte III (que inclui os Capítulos 8, 9 e 10) lida com algumas contribuições adicionais que, embora tenham suas relevâncias práticas, não fazem parte do foco principal desta tese.

No Capítulo 2, os principais conceitos relacionados à modelagem de transceptores através de banco de filtros são revisados antes de começarmos a descrever as novas contribuições desta tese (Partes I, II e III).

No Capítulo 3, analisamos o desempenho de transceptores ZP com redundância completa em termos de MSE e informação mútua. Nós demonstramos que o MSE/informação mútua relacionados a tais transceptores são: (i) funções monótonas crescentes/decrescentes do número de símbolos transmitidos por bloco; (ii) funções monótonas decrescentes/crescentes do número de símbolos redundantes utilizados na equalização de um dado bloco; (iii) acrescidos/decrescidos sempre que canais de fase não-mínima são utilizados, no lugar dos correspondentes canais de fase mínima, assumindo que apenas uma parte do bloco recebido é utilizado na equalização.

O Capítulo 4 contém novas estruturas para soluções MMSE de transceptores com redundância mínima baseados em DFT (do inglês, *discrete Fourier transform*). Tais estruturas são mais simples do que as propostas em [23] dado que elas precisam de apenas quatro ramos paralelos no equalizador, no lugar dos cinco ramos utilizados em [23]. O capítulo também descreve soluções MMSE subótimas que permitem ainda mais a redução no número de operações aritméticas utilizadas para equalizar um determinado bloco de dados.

A extensão dos resultados baseados em DFT para soluções que utilizem transformadas reais, tais como a DHT (do inglês, *discrete Hartley transform*), é descrita no Capítulo 5.

O Capítulo 6 apresenta novos transceptores LTI que empregam uma quantidade reduzida de redundância para eliminar a IBI. As propostas podem ser multiportadoras ou monoportadora, com solução ZF ou MMSE. A quantidade de redundância pode variar desde a quantidade mínima, $\lceil L/2 \rceil$, até a mais utilizada na prática, L, assumindo um canal com resposta ao impulso de ordem L.

No Capítulo 7, nós deduzimos novos transceptores LTI com redundância reduzida que empregam a DHT e equalizadores com dois coeficientes em suas estruturas. Os resultados deste capítulo são extensões naturais dos resultados propostos nos Capítulos 5 e 6.

O Capítulo 8 propõe um método ótimo para alocação de potência que minimiza os ganhos de ruído quando há acesso a informações sobre o estado do canal (CSI, do inglês, *channel-state information*) no transmissor.

O Capítulo 9 mostra como reduzir a quantidade de redundância em transceptores não-lineares do tipo DFE (do inglês, *decision-feedback equalizer*). O capítulo também

inclui resultados que permitem quantificar o desempenho de tais transceptores.

No Capítulo 10, nos concentramos no projeto dos equalizadores relacionados aos sistemas com redundância mínima, sem assumir o conhecimento prévio do canal.

As conclusões da tese estão presente no Capítulo 11.

Vale ressaltar porque escolhemos esta ordenação de capítulos para a tese. Na verdade, poderíamos começar tratando com transceptores com redundância reduzida e, a partir de tais resultados, concluir sobre os transceptores com redundância mínima. Isso faria com que o texto da tese fosse um pouco mais conciso, mas simultaneamente esconderia o trajeto que percorremos ao longo de nossa pesquisa. De fato, começamos atacando os transceptores com redundância mínima, buscando resolver pendências bem como melhorar os resultados descritos na dissertação de mestrado [23]. Após esta fase ser concluída, nos concentramos nos transceptores com redundância reduzida. Portanto, optamos por esta ordenação de capítulos para deixar claro este trajeto de pesquisa.

Encorajamos o leitor desta tese a ler os Apêndices A a L diretamente, pois eles contêm o texto na íntegra e em detalhes de toda a tese, enquanto os Capítulos 1 a 11 possuem apenas um resumo de tais apêndices.[1]

[1]Na verdade, os Capítulos 1 e 2 estão reproduzidos praticamente na íntegra.

Capítulo 2

Transceptores Multicanais

Juntamente com as técnicas modernas de codificações de fonte e de canal, além dos avanços na área de projeto de circuitos integrados, o processamento digital de sinais aplicado às telecomunicações tem viabilizado o desenvolvimento de novos sistemas que atendam às crescentes demandas por taxas de transmissão cada vez maiores. Nesse contexto, operações típicas de filtragem digital possuem um papel fundamental para processar os sinais de um ou vários usuários para que compartilhem o meio físico em questão e sejam recuperados de forma confiável no receptor.

Os filtros digitais que compõem os sistemas de comunicações podem ser fixos ou adaptativos, lineares ou não[1], com resposta ao impulso de duração finita (FIR, do inglês *Finite Impulse Response*) ou infinita (IIR, do inglês *Infinite Impulse Response*), etc [26]. Dentre essas categorias, os filtros fixos, lineares, FIR são os que possuem o maior apelo prático por admitirem uma implementação simples, sempre estável, e com um baixo custo computacional para a filtragem quando comparados às demais opções.

Porém, em várias ocasiões, os sistemas modernos de processamento de sinais exigem mais do que tais filtros (fixos, lineares, FIR) podem oferecer. Uma forma de disponibilizar mais graus de liberdade para o projetista de processamento de sinais é utilizar sistemas que trabalhem em múltiplas taxas, pois, internamente, tais sistemas comportam-se como sistemas periodicamente variantes no tempo devido à presença da operação de diminuição da taxa de amostragem.

Por isso, os sistemas que utilizam bancos de filtros têm se alastrado em várias áreas do conhecimento, especialmente em sistemas de codificação de fonte [27], [26]. Em comunicações, utilizam-se sistemas que podem ser vistos como duais dos bancos de filtros: os transceptores multicanais ou TMUXs [28], [29], [11], [30], [31]. Vários sistemas práticos podem ser modelados através da utilização de TMUXs.

Na prática, os transceptores multicanais mais comuns são os que empregam

[1]Estritamente falando, todo filtro adaptativo é não-linear [26].

filtros de comprimentos curtos quando comparados aos fatores empregados nas mudanças de taxa de amostragem. Tais transceptores são genericamente chamados de transceptores em bloco ou sem memória [32]. Os sistemas modernos mais comuns que podem ser modelados por transceptores em bloco são os sistemas OFDM e SC-FD [30], [31], [11], [33].

A principal vantagem do sistema OFDM reside em sua capacidade de eliminar a interferência entre símbolos (ISI, do inglês *InterSymbol Interference*) mantendo uma complexidade computacional relativamente baixa. Recentemente, o sistema SC-FD tem emergido como uma solução alternativa ao OFDM que é capaz de diminuir algumas de suas desvantagens, tais como altos picos de potência (PAPR, do inglês *Peak-to-Average Power Ratio*) e alta sensibilidade a deslocamentos de frequência das portadoras (CFO, do inglês *Carrier-Frequency Offset*) [14], [15]. Além disso, para alguns tipos de canais seletivos em frequência, a BER de um sistema SC-FD pode ser menor do que a BER de um sistema OFDM, especialmente se alguns subcanais possuírem alta atenuação [15]. A BER maior do OFDM se origina do fato de que a informação que é transmitida por um dado subcanal está espalhada no domínio do tempo, mas concentrada no domínio da frequência. Se a qualidade do canal for pobre naquela faixa de frequência em particular, então a informação será perdida.

No presente capítulo, são revistos brevemente os principais resultados da literatura a respeito de processamento em múltiplas taxas que possuem aplicação neste trabalho (Seção 2.1). Os transceptores multicanais são brevemente estudados na Seção 2.2. O caso particular de transceptores multicanais sem memória é modelado na Seção 2.3, destacando-se os sistemas OFDM e SC-FD, além da exposição de alguns resultados conhecidos sobre transceptores em bloco que empregam redundância reduzida.

2.1 Processamento de Sinais com Múltiplas Taxas

São várias as aplicações em processamento digital de sinais nas quais é extremamente comum coexistirem sinais e/ou filtros cujas taxas de amostragem sejam diferentes [26], [27].

Basicamente, um sistema de processamento em múltiplas taxas opera utilizando dois blocos fundamentais: o **interpolador** e o **decimador**. O processo de interpolação consiste no aumento da taxa de amostragem de um dado sinal, enquanto que o processo de decimação consiste na diminuição da taxa de amostragem. Apenas com tais definições, é possível perceber que o processo de decimação deve ser realizado com mais cuidado para que se evite perdas de informação originadas do efeito de sobreposição de espectros mais conhecido pelo termo em inglês, *aliasing* [26], [27].

A interpolação por um fator $N \in \mathbb{N}$ consiste na inserção de $N-1$ zeros entre

cada duas amostras do sinal original, gerando, assim, um novo sinal cuja taxa de amostragem é N vezes maior do que a anterior. Em termos matemáticos, dado um sinal $s(n) \in \mathbb{C}$, onde $n \in \mathbb{Z}$, então o sinal interpolado $s_{\text{int}}(k)$, com $k \in \mathbb{Z}$, é dado por $s_{\text{int}}(k) = s(n)$, sempre que $k = nN$ e $s_{\text{int}}(k) = 0$, em caso contrário.

Por outro lado, a decimação por um fator N consiste no descarte de $N - 1$ amostras a cada bloco de N amostras do sinal original, gerando, assim, um novo sinal cuja taxa de amostragem é N vezes menor do que a anterior. Matematicamente, dado $s(n)$, então o sinal decimado $s_{\text{dec}}(k)$ é definido por $s_{\text{dec}}(k) = s(n)$, sempre que $n = kN$, para todo $k \in \mathbb{Z}$.

As Figuras 2.1 e 2.2 mostram o comportamento nos domínios do tempo e da frequência de um sinal que passa por um interpolador e um decimador, respectivamente, em que $N = 2$. Os sinais dessas figuras são apenas ilustrativos de forma que não há uma correspondência válida entre os respectivos pares sinal-transformada. Através da análise de tais figuras, é possível verificar que, para que as operações

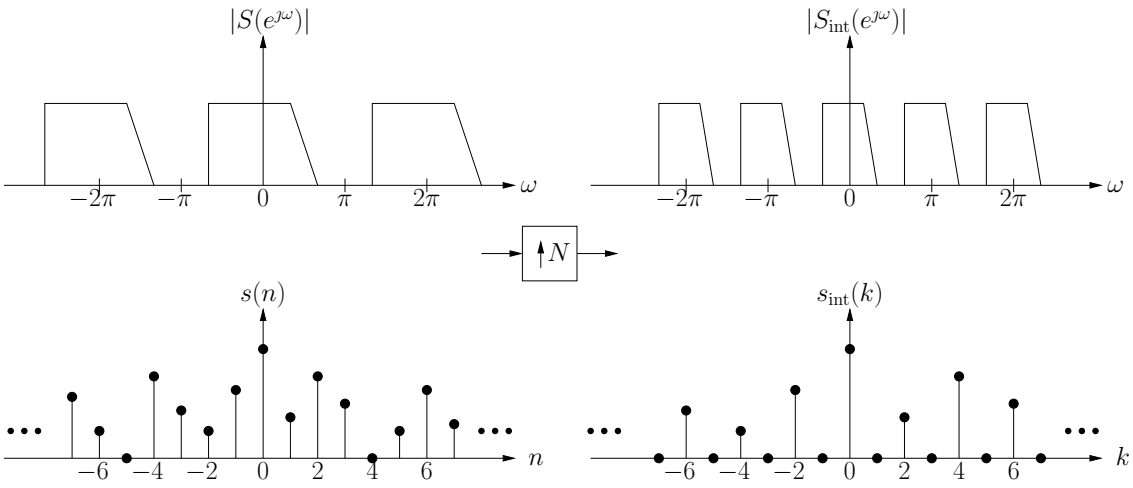

Figura 2.1: O bloco interpolador ($N = 2$).

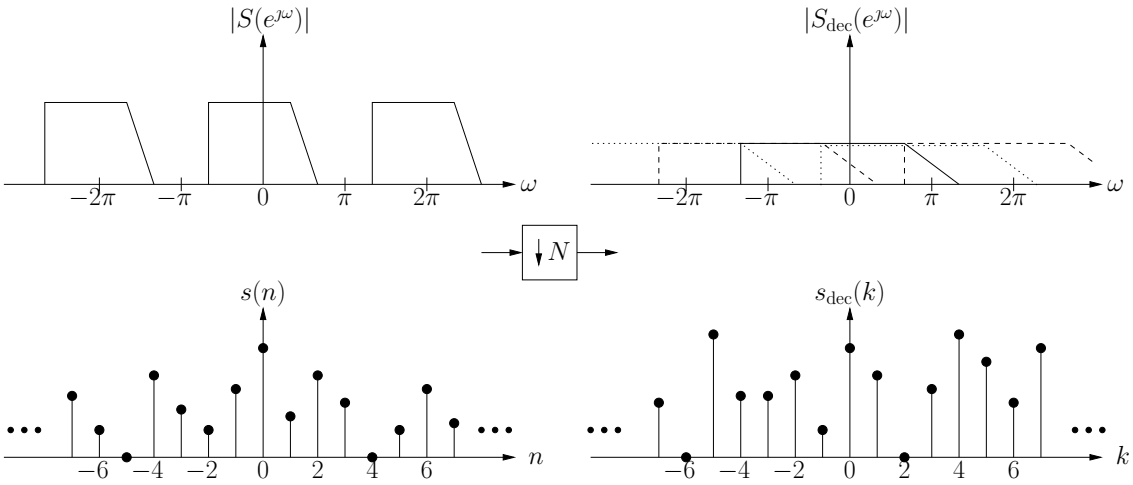

Figura 2.2: O bloco decimador ($N = 2$).

de decimação e interpolação sejam utilizadas de maneira efetiva em um sistema de processamento de sinais, é necessária a utilização de filtros digitais com o intuito de, no caso da interpolação, obter uma versão suave do sinal interpolado ou, de maneira equivalente, eliminar as imagens espectrais que surgiram **após** a inserção de zeros; e para que, no caso da decimação, não ocorra o *aliasing*, limitando-se o sinal em frequência **antes** de suas amostras serem descartadas [26], [27].

No caso da interpolação, obtém-se uma versão suave do sinal $s_{\text{int}}(k)$ processando-o com um filtro que elimine as repetições de espectro que aparecem centradas nas frequências $\pm\frac{2\pi}{N}i$, com $i \in \{\, 1, \cdots, N-1 \,\} \subset \mathbb{N}$. Semelhantemente, é necessário que se garanta que o sinal original não terá sobreposição de espectros após a sua decimação, ou seja, no caso de um sinal real passa-baixas, por exemplo, é necessário filtrar o sinal para que o mesmo fique limitado à banda $\left(-\frac{\pi}{N}, \frac{\pi}{N}\right)$. A Figura 2.3 mostra como as operações de interpolação e decimação são implementadas na prática.

Existem formas específicas para se manipular os blocos de decimação e interpolação em um sistema com múltiplas taxas. Tal manipulação pode ser particularmente interessante quando há interesse de comutar as operações de filtragem com as operações de mudança de taxa de amostragem. Essas formas específicas de manipulação baseiam-se nas chamadas **identidades nobres** [26], [27].

A Figura 2.4 contém uma descrição por diagrama de blocos dessas identidades. Em termos da interpolação, no lugar de primeiro interpolar um dado sinal para então filtrá-lo por um filtro que esteja numa taxa mais alta, é interessante primeiramente filtrar o sinal em uma taxa mais baixa para então interpolá-lo. Essa estratégia permite uma economia de operações aritméticas e de memória. Em relação à decimação, no lugar de primeiro filtrar o sinal por um filtro que esteja em uma taxa mais alta para então decimar o resultado, é possível primeiro decimar a entrada do filtro para que este trabalhe a uma taxa inferior, permitindo assim a economia de recursos computacionais.

A maior parte das aplicações de sistemas com múltiplas taxas de amostragem

Figura 2.3: Operações gerais de interpolação e decimação no domínio do tempo.

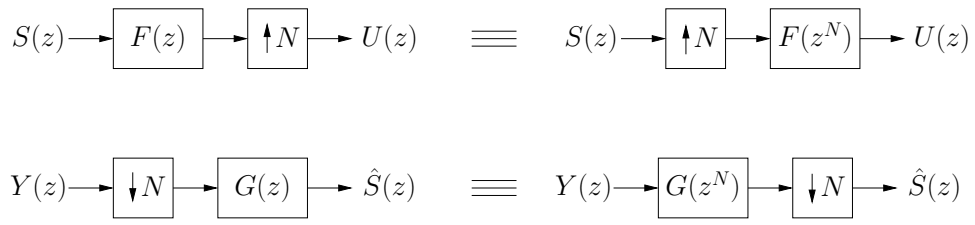

Figura 2.4: Identidades nobres no domínio $\mathcal{Z}$.

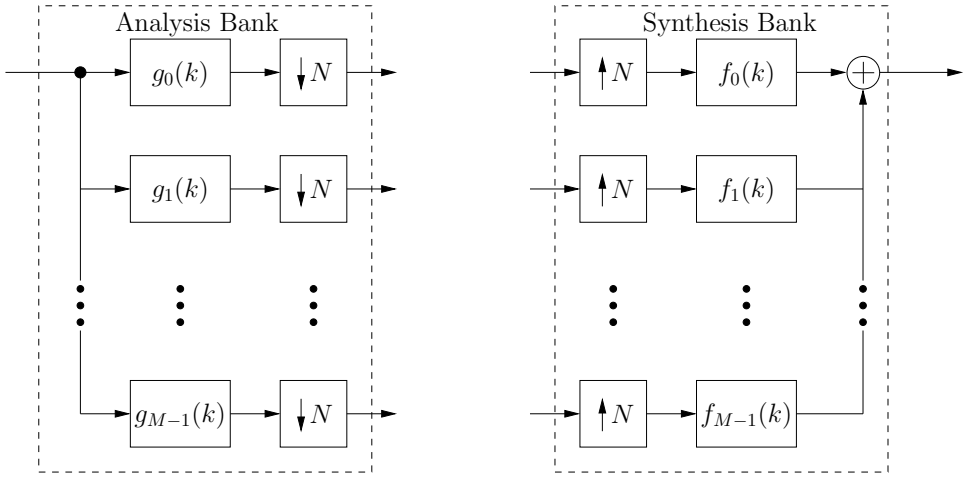

Figura 2.5: Bancos de filtros de análise e de síntese no domínio do tempo.

refere-se aos bancos de filtros [26],[27]. Um banco de filtros é um conjunto de filtros que compartilham uma entrada comum ou uma saída comum [27]. Ambos os casos são exibidos na Figura 2.5. Os filtros do conjunto $\{g_m(k)\}_{m\in\mathcal{M}}$, onde $m \in \mathcal{M} = \{0, 1, \cdots, M-1\} \subset \mathbb{N}$, compõem o chamado **banco de análise**, enquanto que os filtros do conjunto $\{f_m(k)\}_{m\in\mathcal{M}}$ compõem o chamado **banco de síntese**. Como é possível verificar, um banco de filtros aplica os blocos básicos gerais de decimação e de interpolação para dividir o sinal original em sub-bandas com o intuito de processar individualmente cada um dos subsinais resultantes na etapa de análise e, após tal processamento, recompor o sinal resultante através do banco de síntese. Mais informações a respeito de bancos de filtros e processamento em múltiplas taxas podem ser encontradas nas referências [26], [27].

2.2 Transceptores Baseados em Banco de Filtros

Considere o modelo de um transceptor multicanal [30], [27] conforme é descrito na Figura 2.6, em que um sistema de comunicação é modelado como um sistema de múltiplas entradas e múltiplas saídas (MIMO, do inglês *multiple-input multiple-output*). As amostras de cada sequência $s_m(n)$ pertencem a uma determinada constelação $\mathcal{C} \subset \mathbb{C}$ (por exemplo, PAM, QAM ou PSK [34], [35]) e representam a m-ésima entrada do transceptor, onde $m \in \mathcal{M}$ e $n \in \mathbb{Z}$. A saída correspondente do transceptor é denotada por $\hat{s}_m(n) \in \mathbb{C}$. Idealmente, $\hat{s}_m(n)$ deve ser uma estimativa confiável de $s_m(n-\delta)$, em que $\delta \in \mathbb{N}$ é o atraso introduzido pelo processo de transmissão/recepção.

Um transceptor multicanal que modela um sistema de comunicação requer um projeto apropriado para o conjunto de filtros causais de transmissão $\{f_m(k)\}_{m\in\mathcal{M}}$ e para o conjunto de filtros causais de recepção $\{g_m(k)\}_{m\in\mathcal{M}}$. Tais filtros operam com

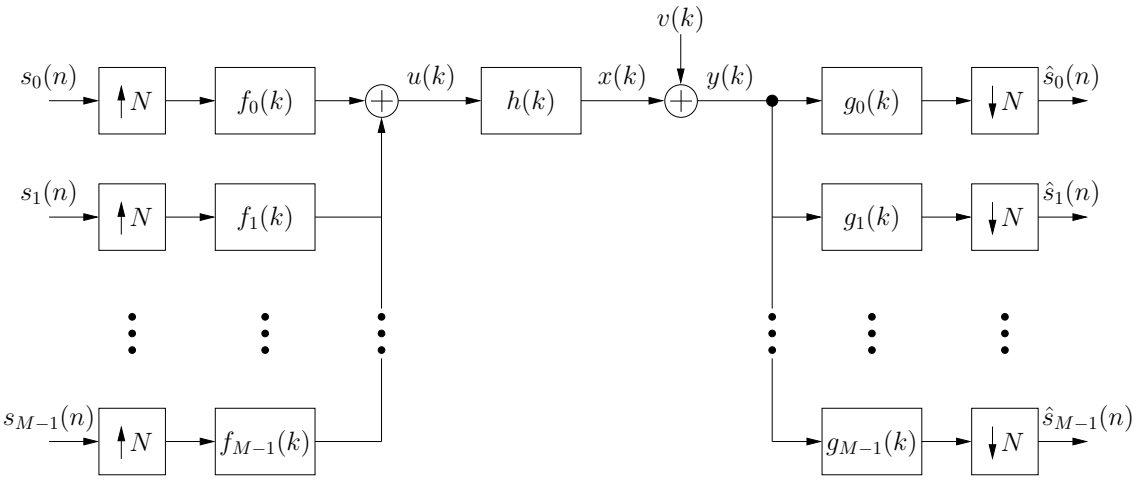

Figura 2.6: Transceptor multicanal no domínio do tempo.

uma taxa de amostragem N vezes maior do que a taxa associada a cada sequência $s_m(n)$. Note que n representa o índice de tempo para a entrada e a saída do transceptor, enquanto que um índice de tempo distinto $k \in \mathbb{Z}$ é utilizado para as respostas ao impulso dos subfiltros e para os sinais internos entre interpoladores e decimadores. Ademais, considera-se que os filtros de transmissão e recepção são fixos, isto é, não são variantes no tempo.

Os subfiltros têm como objetivo processar as sequências de entrada $s_m(n)$, para cada $m \in \mathcal{M}$, com o intuito de reduzir as distorções introduzidas pelo canal, de forma que as sequências $\hat{s}_m(n)$ são tidas como boas estimativas de $s_m(n-\delta)$ em algum sentido previamente definido. Usualmente, o objetivo final é reduzir a BER ou maximizar o *throughput*.

O modelo do canal é representado por um filtro FIR $h(k) \in \mathbb{C}$ cuja ordem é $L \in \mathbb{N}$. Esse modelo representa a propriedade de seletividade em frequência do canal. Além disso, há também um ruído aditivo $v(k) \in \mathbb{C}$, o qual modela a interferência total do ambiente, como por exemplo, a interferência multiusuário (MUI, do inglês *multi-user interference*) e o ruído térmico.

Dependendo do contexto, os sinais envolvidos no modelo serão considerados como determinísticos ou estocásticos. Entretanto, não será utilizada uma notação diferente para distingui-los, assim como é feito em vários textos técnicos [36]. Assim, apenas como um exemplo, em um contexto estocástico, poderão ser associadas a $v(k)$ ou $s_m(n)$ estatísticas de segunda ordem, tais como funções de autocorrelação $r_{vv}(l,k)$, $r_{s_m s_m}(p,n)$ ou outros tipos de estatísticas.

2.2.1 Representação no Domínio do Tempo

De acordo com a Figura 2.6 o sinal de entrada do canal $u(k)$ é dado por:

$$u(k) = \sum_{(i,m)\in\mathbb{Z}\times\mathcal{M}} s_m(i) f_m(k - iN). \tag{2.1}$$

A relação de entrada e saída do canal é representada por:

$$y(k) = \sum_{j\in\mathbb{Z}} h(j)u(k - j) + v(k). \tag{2.2}$$

No receptor, o transceptor processa o sinal $y(k)$ objetivando gerar as estimativas dos sinais transmitidos:

$$\hat{s}_m(n) = \sum_{l\in\mathbb{Z}} g_m(l)y(nN - l). \tag{2.3}$$

Assim, combinando as Eqs. (2.1), (2.2) e (2.3) é possível descrever a relação entre os sinais de entrada $s_m(n)$ e as estimativas $\hat{s}_m(n)$, conforme se segue:

$$\hat{s}_m(n) = \sum_{(i,j,l,m)\in\mathbb{Z}^3\times\mathcal{M}} g_m(l)h(j)s_m(i)f_m(nN - l - j - iN) + \sum_{l\in\mathbb{Z}} g_m(l)v(nN - l). \tag{2.4}$$

A análise das expressões anteriores pode ser um tanto difícil. Porém, há algumas ferramentas alternativas de análise, tais como expressar o sistema no domínio do tempo em forma matricial [31]. Entretanto, para os propósitos deste trabalho, é mais conveniente utilizar uma descrição no domínio da transformada $\mathcal{Z}$, através da decomposição em componentes polifásicas dos sistemas envolvidos [26], [27], [32].

2.2.2 Representação Polifásica

Uma vez que as taxas de interpolação e decimação são dadas por N, é mais apropriado representar os filtros de transmissão e de recepção utilizando suas decomposições

em componentes polifásicas de ordem N, conforme se segue [32]:

$$\begin{aligned} F_m(z) &= \sum_{k\in\mathbb{Z}} f_m(k) z^{-k} \\ &= \sum_{i\in\mathcal{N}} z^{-i} \sum_{j\in\mathbb{Z}} f_m(jN+i) z^{-jN} \\ &= \sum_{i\in\mathcal{N}} z^{-i} F_{i,m}(z^N)\,, \end{aligned} \tag{2.5}$$

$$\begin{aligned} G_m(z) &= \sum_{k\in\mathbb{Z}} g_m(k) z^{-k} \\ &= \sum_{i\in\mathcal{N}} z^{i} \sum_{j\in\mathbb{Z}} g_m(jN-i) z^{-jN} \\ &= \sum_{i\in\mathcal{N}} z^{i} G_{m,i}(z^N)\,, \end{aligned} \tag{2.6}$$

em que $m \in \mathcal{M}$, e $F_m(z)$ e $G_m(z)$ são as transformadas $\mathcal{Z}$ de $f_m(k)$ e $g_m(k)$, respectivamente. Sendo assim, pode-se reescrever os sistemas de Eqs. (2.5) e (2.6) da seguinte forma [32]:

$$\begin{aligned} \begin{bmatrix} F_0(z) & \cdots & F_{M-1}(z) \end{bmatrix} &= \underbrace{\begin{bmatrix} 1 & z^{-1} & \cdots & z^{-(M-1)} \end{bmatrix}}_{\mathbf{d}^T(z)} \underbrace{\begin{bmatrix} F_{0,0}(z^N) & \cdots & F_{0,M-1}(z^N) \\ \vdots & \ddots & \vdots \\ F_{N-1,0}(z^N) & \cdots & F_{N-1,M-1}(z^N) \end{bmatrix}}_{\mathbf{F}(z^N)}, \\ \begin{bmatrix} G_0(z) \\ \vdots \\ G_{M-1}(z) \end{bmatrix} &= \underbrace{\begin{bmatrix} G_{0,0}(z^N) & \cdots & G_{0,N-1}(z^N) \\ \vdots & \ddots & \vdots \\ G_{M-1,0}(z^N) & \cdots & G_{M-1,N-1}(z^N) \end{bmatrix}}_{\mathbf{G}(z^N)} \underbrace{\begin{bmatrix} 1 \\ \vdots \\ z^{(M-1)} \end{bmatrix}}_{\mathbf{d}(z^{-1})}, \end{aligned} \tag{2.7}$$

A Figura 2.7 mostra a representação do transceptor multicanal utilizando-se as componentes polifásicas dos filtros envolvidos. Agora, utilizando as identidades

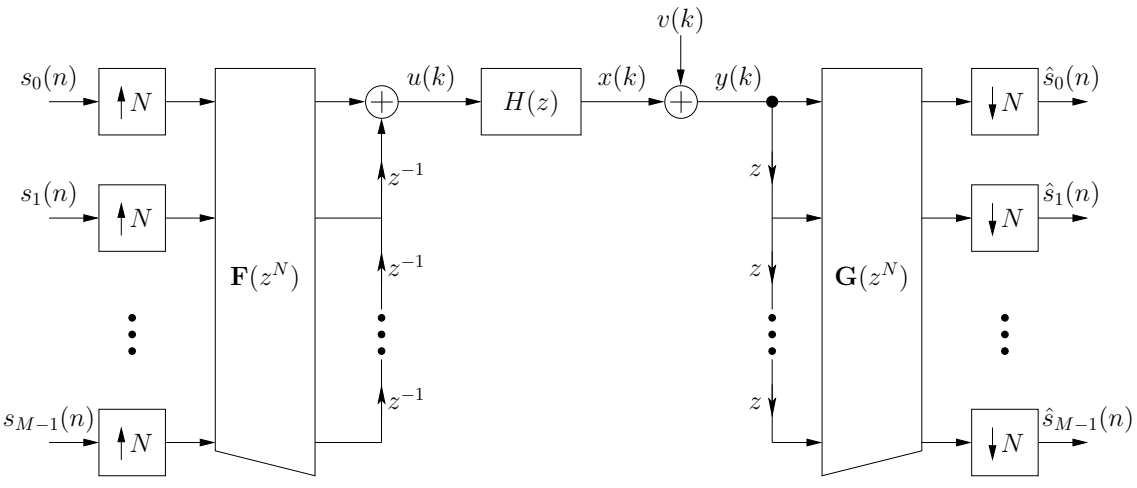

Figura 2.7: Representação polifásica do transceptor multicanal.

nobres, pode-se redesenhar o transceptor da Figura 2.7 para a forma ilustrada na Figura 2.8.

É possível mostrar que a área destacada na Figura 2.8, a qual engloba as linhas de atrasos/adiantamentos e os interpoladores/decimadores ao modelo de canal, pode ser representada por uma matriz pseudocirculante $\mathbf{H}(z)$ de dimensão $N \times N$, definida analiticamente por [11], [27], [32]:

$$\mathbf{H}(z) = \begin{bmatrix} H_0(z) & z^{-1}H_{N-1}(z) & z^{-1}H_{N-2}(z) & \cdots & z^{-1}H_1(z) \\ H_1(z) & H_0(z) & z^{-1}H_{N-1}(z) & \cdots & z^{-1}H_2(z) \\ \vdots & \vdots & \ddots & \vdots & \vdots \\ H_{N-1}(z) & H_{N-2}(z) & H_{N-3}(z) & \cdots & H_0(z) \end{bmatrix}, \tag{2.8}$$

em que [11], [27], [32]

$$H(z) = \sum_{i \in \mathcal{N}} H_i(z^N) z^{-i} \quad \text{e} \quad H_i(z) = \sum_{\substack{j \in \mathbb{Z} \\ 0 \leq jN+i \leq L}} h(jN+i) z^{-j}. \tag{2.9}$$

A Figura 2.9 descreve o sistema através das matrizes polifásicas do transceptor

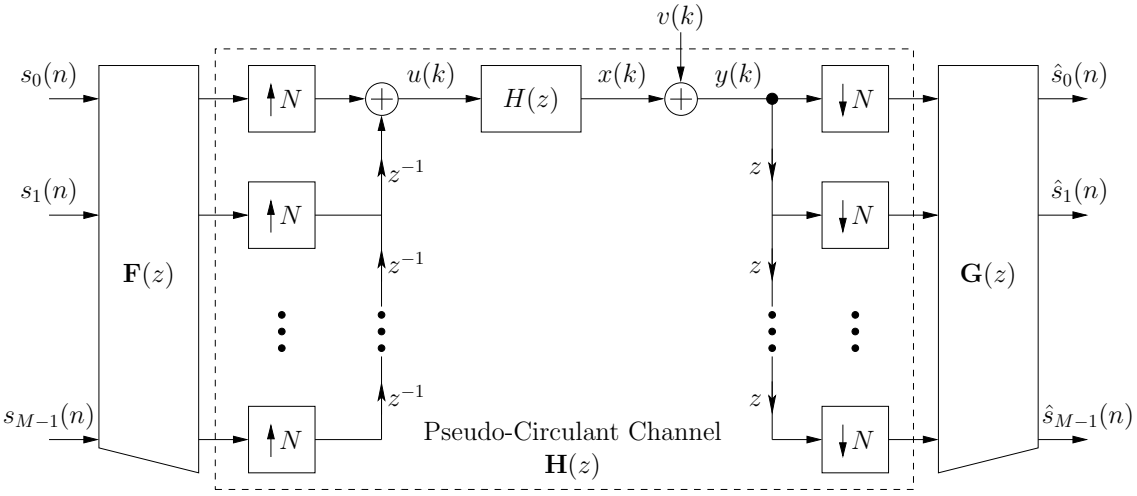

Figura 2.8: Representação polifásica modificada do transceptor multicanal.

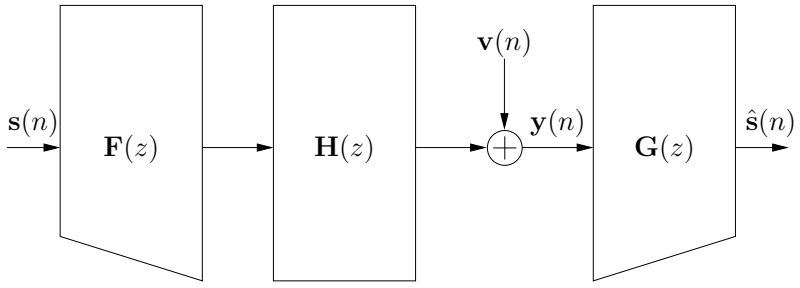

Figura 2.9: Transceptor multicanal no domínio da frequência (representação polifásica).

multicanal, incluindo a matriz pseudocirculante de canal. Essas matrizes foram definidas de forma que haja uma equivalência completa entre os sistemas modelados pelas Figuras 2.6 e 2.9.

Nesta tese, assume-se que $N \geq L$, isto é, que o fator de interpolação/decimação é maior ou igual à ordem do canal. Essa hipótese é razoável para diversas aplicações [32]. Para o caso em que $N < L$, o leitor pode verificar os resultados em [11]. Assim, quando $N \geq L$, cada um dos elementos $H_i(z)$, com $i \in \mathcal{N}$, será um filtro simples com apenas um coeficiente, ou seja, $H_i(z) = h(i)$, caso $i \leq L$, e $H_i(z) = 0$, em caso contrário. Portanto, a matriz pseudocirculante de canal pode ser representada como uma matriz FIR de primeira ordem [32]:

$$\mathbf{H}(z) = \begin{bmatrix} h(0) & 0 & 0 & \cdots & 0 \\ h(1) & h(0) & 0 & \cdots & 0 \\ \vdots & \vdots & \vdots & \vdots & \vdots \\ h(L) & h(L-1) & \ddots & \cdots & 0 \\ 0 & h(L) & \cdots & \cdots & 0 \\ \vdots & \vdots & \vdots & \vdots & \vdots \\ 0 & 0 & h(L) & \cdots & h(0) \end{bmatrix} + z^{-1} \begin{bmatrix} 0 & \cdots & 0 & h(L) & \cdots & h(1) \\ 0 & 0 & \cdots & 0 & \ddots & \vdots \\ \vdots & \vdots & \vdots & \vdots & \vdots & h(L) \\ 0 & 0 & 0 & \cdots & 0 & 0 \\ 0 & 0 & 0 & \cdots & 0 & 0 \\ \vdots & \vdots & \vdots & \vdots & \vdots & \vdots \\ 0 & 0 & 0 & 0 & \cdots & 0 \end{bmatrix}. \tag{2.10}$$

Além disso, os vetores de símbolos transmitidos e recebidos presentes na Figura 2.9 são respectivamente denotados por:

$$\mathbf{s}(n) = [\, s_0(n) \;\; s_1(n) \;\; \cdots \;\; s_{M-1}(n) \,]^T, \tag{2.11}$$

$$\hat{\mathbf{s}}(n) = [\, \hat{s}_0(n) \;\; \hat{s}_1(n) \;\; \cdots \;\; \hat{s}_{M-1}(n) \,]^T. \tag{2.12}$$

A partir da Figura 2.9 não é difícil inferir que a matriz de transferência $\mathbf{T}(z)$ do transceptor multicanal pode ser expressa como:

$$\mathbf{T}(z) = \mathbf{G}(z)\mathbf{H}(z)\mathbf{F}(z), \tag{2.13}$$

onde foi considerado o caso particular em que $v(k) \equiv 0$, motivado pelo projeto *zero-forcing* de sistemas [32]. O transceptor possui a propriedade *zero-forcing* sempre que $\mathbf{T}(z) = z^{-d}\mathbf{I}_M$, em que $d \in \mathbb{N}$.

2.3 Sistemas sem Memória Baseados em Blocos

O caso de transceptores sem memória, em que $\mathbf{F}(z) = \mathbf{F}$ e $\mathbf{G}(z) = \mathbf{G}$, é analisado nesta seção. Esse caso engloba os conhecidos transceptores em bloco [32] (em inglês, *block-based transceivers*), já que esses sistemas não utilizam informações de outros

blocos durante o processo de transmissão e recepção. Isso é possível apenas se os comprimentos dos filtros $\{f_m(k)\}_{m\in\mathcal{M}}$ e $\{g_m(k)\}_{m\in\mathcal{M}}$ são menores que ou iguais a N. Os sistemas OFDM e SC-FD tradicionais são transceptores em bloco.

2.3.1 CP-OFDM

O sistema OFDM que emprega prefixo cíclico como redundância (CP-OFDM, do inglês *Cyclic Prefix OFDM*) caracteriza-se pelas seguintes matrizes de transmissão e recepção, respectivamente [37]:

$$\mathbf{F} = \underbrace{\begin{bmatrix} \mathbf{0}_{L\times(M-L)} & \mathbf{I}_L \\ & \mathbf{I}_M \end{bmatrix}}_{\mathbf{A}_{\mathrm{CP}}\in\mathbb{C}^{N\times M}} \mathbf{W}_M^H\,, \tag{2.14}$$

$$\mathbf{G} = \mathbf{E}\mathbf{W}_M \underbrace{\begin{bmatrix}\mathbf{0}_{M\times L} & \mathbf{I}_M\end{bmatrix}}_{\mathbf{R}_{\mathrm{CP}}\in\mathbb{C}^{M\times N}}, \tag{2.15}$$

em que $\mathbf{W}_M \in \mathbb{C}^{M\times M}$ é a matriz de DFT normalizada de dimensão $M \times M$, $\mathbf{I}_M$ é a matriz identidade de dimensão $M \times M$, $\mathbf{0}_{X\times Y}$ é uma matriz de zeros de dimensão $X \times Y$ e $\mathbf{E} \in \mathbb{C}^{M\times M}$ é a matriz responsável pela equalização dos sinais após a remoção do prefixo cíclico e a aplicação da DFT. Note que o bloco de dados que se deseja transmitir possui comprimento M, mas, na verdade, transmite-se um bloco de comprimento $N = M + L$ pois os últimos L elementos do sinal resultante da aplicação da IDFT são repetidos no início do bloco, utilizando-se, assim, um prefixo cíclico como redundância.

As matrizes $\mathbf{A}_{\mathrm{CP}}$ e $\mathbf{R}_{\mathrm{CP}}$ são as matrizes responsáveis pela adição e pela remoção do prefixo cíclico, respectivamente. Note que o produto $\mathbf{R}_{\mathrm{CP}}\mathbf{H}(z)\mathbf{A}_{\mathrm{CP}} \in \mathbb{C}^{M\times M}$ é dado por:

$$\mathbf{R}_{\mathrm{CP}}\mathbf{H}(z)\mathbf{A}_{\mathrm{CP}} = \begin{bmatrix} h(0) & 0 & \cdots & 0 & h(L) & \cdots & h(1) \\ h(1) & h(0) & \cdots & 0 & 0 & \ddots & \vdots \\ \vdots & \vdots & \ddots & & & & h(L) \\ h(L) & h(L-1) & & \ddots & \ddots & & 0 \\ 0 & h(L) & & & \ddots & & \vdots \\ \vdots & \ddots & \ddots & & & \ddots & 0 \\ 0 & \cdots & 0 & h(L) & \cdots & & h(0) \end{bmatrix}, \tag{2.16}$$

ou seja, $\mathbf{R}_{\mathrm{CP}}$ remove a interferência entre os blocos, enquanto que $\mathbf{A}_{\mathrm{CP}}$ opera sobre a matriz de Toeplitz sem memória resultante $\mathbf{R}_{\mathrm{CP}}\mathbf{H}(z) \in \mathbb{C}^{M\times N}$ de forma a transformá-la em uma matriz circulante de dimensão $M \times M$.

Uma vez que a matriz de canal resultante da adição e posterior remoção do pre-

fixo cíclico é uma matriz circulante, então ela se torna diagonal após a multiplicação pelas matrizes de IDFT e de DFT no transmissor e receptor, respectivamente [22]. Assim, tem-se que o modelo equivalente de uma transmissão CP-OFDM é dado por:

$$\hat{\mathbf{s}} = \mathbf{E}\mathbf{\Lambda}\mathbf{s} + \mathbf{E}\mathbf{v}' \tag{2.17}$$

onde, por simplicidade, não foi denotada a dependência com o tempo dos sinais envolvidos e [22]

$$\mathbf{\Lambda} = \text{diag}\{\lambda_m\}_{m=0}^{M-1} = \mathbf{W}_M \mathbf{R}_{\text{CP}} \mathbf{H}(z) \mathbf{A}_{\text{CP}} \mathbf{W}_M^H \tag{2.18}$$

$$= \text{diag}\left\{ \sqrt{M} \mathbf{W}_M \begin{bmatrix} \mathbf{h} \\ \mathbf{0}_{(M-L-1)\times 1} \end{bmatrix} \right\}, \tag{2.19}$$

em que $\mathbf{h} = [\, h(0) \;\; h(1) \;\; \cdots \;\; h(L) \,]^T$ e $\mathbf{v}' = \mathbf{W}_M \mathbf{R}_{\text{CP}} \mathbf{v}$.

O equalizador $\mathbf{E}$ pode ser definido de várias formas, dentre as quais se destacam os projetos ZF e MMSE [5]. No caso do projeto ZF, assume-se que a matriz $\mathbf{\Lambda}$ é inversível, de forma que

$$\mathbf{E}_{\text{ZF}} = \mathbf{\Lambda}^{-1}. \tag{2.20}$$

No caso do projeto MMSE, não há necessidade de assumir que a matriz $\mathbf{\Lambda}$ é inversível pois a mesma não será invertida. A solução MMSE linear é dada por [38]:

$$\mathbf{E}_{\text{MMSE}} = \arg\left\{ \min_{\forall \mathbf{E} \in \mathbb{C}^{M\times M}} \mathsf{E}\left[\|\mathbf{s} - \mathbf{E}(\mathbf{\Lambda}\mathbf{s} + \mathbf{v}')\|_2^2 \right] \right\} = \mathbf{\Lambda}^H \left(\mathbf{\Lambda}\mathbf{\Lambda}^H + \frac{\sigma_v^2}{\sigma_s^2} \mathbf{I} \right)^{-1}$$

$$= \text{diag}\left\{ \frac{\lambda_m^*}{|\lambda_m|^2 + \frac{\sigma_v^2}{\sigma_s^2}} \right\}_{m=0}^{M-1}, \tag{2.21}$$

onde foi considerado que os símbolos transmitidos e o ruído na saída do canal são independentes e identicamente distribuídos (i.i.d, do inglês *independent and identically distributed*), provenientes de um processo estocástico branco com média zero e mutuamente independentes[2]. Além disso, considerou-se que $\mathsf{E}[ss^*] = \sigma_s^2$ e $\mathsf{E}[vv^*] = \sigma_v^2$.

2.3.2 ZP-OFDM

O sistema OFDM que utiliza zeros como elementos de redundância (ZP-OFDM, do inglês *Zero Padding OFDM*) caracteriza-se pelas seguintes matrizes de transmissão

[2]Note que se $\mathbf{v}$ possui tais características, então $\mathbf{v}' = \mathbf{W}_M \mathbf{R}_{\text{CP}} \mathbf{v}$ também as possui.

e recepção, respectivamente [37]:

$$\mathbf{F} = \underbrace{\begin{bmatrix} \mathbf{I}_M \\ \mathbf{0}_{L\times M} \end{bmatrix}}_{\mathbf{A}_{\mathrm{ZP}}\in\mathbb{C}^{N\times M}} \mathbf{W}_M^H\,, \tag{2.22}$$

$$\mathbf{G} = \mathbf{E}\mathbf{W}_M \underbrace{\begin{bmatrix} \mathbf{I}_M & \mathbf{I}_L \\ & \mathbf{0}_{(M-L)\times L} \end{bmatrix}}_{\mathbf{R}_{\mathrm{ZP}}\in\mathbb{C}^{M\times N}}, \tag{2.23}$$

onde, mais uma vez, são adicionados L elementos de redundância e $N = M + L$.

As matrizes $\mathbf{A}_{\mathrm{ZP}}$ e $\mathbf{R}_{\mathrm{ZP}}$ são as matrizes responsáveis pela adição e pela remoção do intervalo de guarda nulo, respectivamente. O produto $\mathbf{R}_{\mathrm{ZP}}\mathbf{H}(z)\mathbf{A}_{\mathrm{ZP}} \in \mathbb{C}^{M\times M}$ é dado por:

$$\mathbf{R}_{\mathrm{ZP}}\mathbf{H}(z)\mathbf{A}_{\mathrm{ZP}} = \begin{bmatrix} h(0) & 0 & \cdots & 0 & h(L) & \cdots & h(1) \\ h(1) & h(0) & \cdots & 0 & 0 & \ddots & \vdots \\ \vdots & \vdots & \ddots & & & & h(L) \\ h(L) & h(L-1) & & \ddots & \ddots & & 0 \\ 0 & h(L) & & & \ddots & & \vdots \\ \vdots & \ddots & \ddots & & & \ddots & 0 \\ 0 & \cdots & 0 & h(L) & \cdots & & h(0) \end{bmatrix} = \mathbf{R}_{\mathrm{CP}}\mathbf{H}(z)\mathbf{A}_{\mathrm{CP}}, \tag{2.24}$$

ou seja, $\mathbf{A}_{\mathrm{ZP}}$ remove a interferência entre os blocos, enquanto que $\mathbf{R}_{\mathrm{ZP}}$ opera sobre a matriz de Toeplitz sem memória resultante $\mathbf{H}(z)\mathbf{A}_{\mathrm{ZP}} \in \mathbb{C}^{N\times M}$ de forma a transformá-la em uma matriz circulante de dimensão $M \times M$.

Deve-se ressaltar que o ZP-OFDM considerado aqui[3] é um caso simplificado de um sistema ZP-OFDM genérico proposto em [37]. O caso mais geral de sistemas ZP-OFDM permite que se recuperem os símbolos transmitidos independentemente da localização dos zeros do modelo de canal. Porém, tal sistema é computacionalmente mais custoso do que o ZP-OFDM descrito aqui, já que a matriz equivalente de canal não é transformada em uma matriz circulante, inviabilizando sua diagonalização através de matrizes de DFT e de IDFT.

2.3.3 CP-SC-FD

O sistema SC-FD que emprega prefixo cíclico como redundância (CP-SC-FD, do inglês *Cyclic Prefix SC-FD*) é inteiramente análogo ao CP-OFDM e caracteriza-se

[3]Este sistema também é conhecido como ZP-OFDM-OLA, em que OLA provém do inglês *overlap-and-add* [37].

pelas seguintes matrizes de transmissão e recepção, respectivamente:

$$\mathbf{F} = \begin{bmatrix} \mathbf{0}_{L\times(M-L)} & \mathbf{I}_L \\ & \mathbf{I}_M \end{bmatrix}, \tag{2.25}$$

$$\mathbf{G} = \mathbf{W}_M^H \mathbf{E} \mathbf{W}_M \begin{bmatrix} \mathbf{0}_{M\times L} & \mathbf{I}_M \end{bmatrix}. \tag{2.26}$$

2.3.4 ZP-SC-FD

O sistema SC-FD que adiciona zeros como redundância (ZP-SC-FD, do inglês *Zero Padding SC-FD*) é análogo ao ZP-OFDM, sendo definido pelas seguintes matrizes de transmissão e recepção, respectivamente:

$$\mathbf{F} = \begin{bmatrix} \mathbf{I}_M \\ \mathbf{0}_{L\times M} \end{bmatrix}, \tag{2.27}$$

$$\mathbf{G} = \mathbf{W}_M^H \mathbf{E} \mathbf{W}_M \begin{bmatrix} \mathbf{I}_M & \mathbf{I}_L \\ & \mathbf{0}_{(M-L)\times L} \end{bmatrix}. \tag{2.28}$$

2.3.5 Transceptores ZP-ZJ

Lin e Phoong [2], [3], [32] mostraram que a quantidade de redundância $K \in \mathbb{N}$ de um transceptor em bloco livre de IBI deve satisfazer a desigualdade $2K \geq L$, em que $K = N - M$. Eles apresentaram uma parametrização geral de um transceptor DMT (do inglês *Discrete Multi-Tone*) sem memória, bem como um caso particular interessante que será utilizado neste trabalho. Esse caso particular é caracterizado pelas seguintes matrizes de transmissão e recepção, respectivamente [32]:

$$\mathbf{F} = \begin{bmatrix} \mathbf{F}_0 \\ \mathbf{0}_{K\times M} \end{bmatrix}_{N\times M}, \tag{2.29}$$

$$\mathbf{G} = \begin{bmatrix} \mathbf{0}_{M\times(L-K)} & \mathbf{G}_0 \end{bmatrix}_{M\times N}, \tag{2.30}$$

em que $\mathbf{F}_0 \in \mathbb{C}^{M\times M}$ e $\mathbf{G}_0 \in \mathbb{C}^{M\times(M+2K-L)}$.

Assim sendo, a matriz de transferência do transceptor multicanal é dada por:

$$\mathbf{T}(z) = \mathbf{G}\mathbf{H}(z)\mathbf{F} = \mathbf{G}_0\mathbf{H}_0\mathbf{F}_0 = \mathbf{T}, \tag{2.31}$$

onde a matriz de canal resultante após a inserção e remoção de redundância é

definida por [32]:

$$\mathbf{H}_0 = \begin{bmatrix} h(L-K) & \cdots & h(0) & 0 & 0 & \cdots & 0 \\ \vdots & \ddots & & & & & \vdots \\ h(K) & \ddots & & & & & 0 \\ \vdots & \ddots & & & \ddots & & h(0) \\ h(L) & & & & & & \vdots \\ 0 & & & & \ddots & & h(L-K) \\ \vdots & & & & & & \vdots \\ 0 & \cdots & 0 & 0 & h(L) & \cdots & h(K) \end{bmatrix} \in \mathbb{C}^{(M+2K-L)\times M}. \quad (2.32)$$

Nesse caso, considerando $v(k) = 0, \forall k \in \mathbb{Z}$, tem-se que:

$$\hat{\mathbf{s}}(n) = \mathbf{G}_0\mathbf{H}_0\mathbf{F}_0\mathbf{s}(n) = \mathbf{T}\mathbf{s}(n). \quad (2.33)$$

Há algumas restrições sobre a resposta ao impulso do canal para que exista a solução ZF. Tais restrições estão relacionadas ao conceito de zeros côngruos (em inglês, *congruous zeros*) [32], [33]. Os zeros côngruos de uma função de transferência $H(z)$ são os zeros distintos $z_0, z_1, \cdots, z_{\mu-1} \in \mathbb{C}$ dessa função que respeitam a seguinte propriedade: $z_i^N = z_j^N, \forall i, j \in \{0, 1, \cdots, \mu-1\}$. Note que μ é uma função de N. Conforme é mostrado em [32], [33], o modelo do canal deve respeitar a restrição $\mu(N) \leq K$, onde $\mu(N)$ denota a cardinalidade do maior (em termos de número de elementos) conjunto de zeros côngruos em relação a N.

Assim, é claro que se um transceptor em bloco com redundância mínima existir, ou seja, se $\mu(N) \leq L/2 = K \in \mathbb{N}$, então sua solução ZF é tal que, dado $\mathbf{H}_0 \in \mathbb{C}^{M\times M}$ e uma vez projetado/definido $\mathbf{F}_0$, deve-se ter

$$\mathbf{G}_0 = (\mathbf{H}_0\mathbf{F}_0)^{-1} = \mathbf{F}_0^{-1}\mathbf{H}_0^{-1}. \quad (2.34)$$

Obviamente, tal solução para o receptor é computacionalmente intensiva em geral por dois motivos principais:

- **O problema de projeto do receptor**: o processo de inversão de uma dada matriz $M \times M$ geralmente requer $\mathcal{O}(M^3)$ operações aritméticas. Essa complexidade é demasiadamente alta quando comparada a de sistemas práticos, tais como OFDM e SC-FD. De fato, os projetos dos equalizadores ZF e MMSE para tais sistemas possuem complexidade $\mathcal{O}(M \log M)$, uma vez que suas respectivas soluções são baseadas na aplicação da DFT sobre a resposta ao impulso do canal (vide Eqs. (2.18), (2.20) e (2.21)).
- **O problema de equalização**: em geral, o processo de multiplicar o ve-

tor recebido pela matriz receptora possui complexidade $\mathcal{O}(M^2)$. Novamente, essa complexidade é considerada muito mais alta do que $\mathcal{O}(M \log M)$, que é a complexidade de equalização nos sistemas OFDM e SC-FD tradicionais. Esse processo simples de equalização dos sistemas OFDM e SC-FD deve-se ao cálculo eficiente da DFT, bem como a multiplicações por matrizes diagonais.

2.4 Conclusões

Este capítulo tratou da modelagem de sistemas de comunicação através de transceptores multicanais ou TMUXs. Foi dada uma ênfase especial para os transceptores fixos e sem memória. Dentre esses, os transceptores que implementam os sistemas CP-OFDM, ZP-OFDM, CP-SC-FD e ZP-SC-FD foram revistos, destacando-se suas soluções ZF e MMSE. Por fim, os resultados da literatura a respeito de transceptores que empregam redundância reduzida foram descritos.

Uma questão que se levanta naturalmente a respeito das discussões deste capítulo é: por que os sistemas OFDM e SC-FD tradicionais são tão simples? A resposta encontra-se no fato de que, em ambos os casos (no problema de projeto do receptor e no problema de equalização), a matriz efetiva de canal é transformada em uma matriz circulante através do processo de inserção e remoção da redundância. Isso permite explorar a propriedade de que toda matriz circulante quadrada é diagonalizável por um par de matrizes de DFT e IDFT. Essa decomposição espectral simples é de extrema importância para implementações práticas dos sistemas OFDM e SC-FD.

Parte I

Sistemas com Redundância Mínima

Capítulo 3

Análise de Transceptores ZP com Redundância Completa

Antes de começarmos a descrever nossas propostas de transceptores com redundância mínima, primeiro iremos buscar responder o seguinte questionamento extremamente pertinente: por que pesquisar transceptores com redundância mínima/reduzida, quando já dispomos de transceptores com redundância "completa" eficientes, tais como OFDM e SC-FD? Tal questionamento é motivado pelo seguinte raciocínio: a eficiência espectral pode ser melhorada simplesmente aumentando o número de elementos não-redundantes, M, transmitidos em um bloco de dados, considerando um canal de ordem fixa L. De fato, se definirmos tal eficiência pela razão $M/(M+K)$, em que K é o número de elementos redundantes em um bloco, então $M/(M+\frac{L}{2}) = 2M/(2M+L)$, ou seja, a eficiência de um transceptor com redundância mínima seria a mesma de um transceptor com redundância completa que transmita o dobro de elementos não-redundantes em cada bloco de dados. Embora tal raciocínio seja teoricamente válido, vários sistemas práticos possuem restrições severas quanto ao valor de M, particularmente aqueles utilizados em aplicações que não podem ter um atraso relativamente grande no processamento de um bloco de dados. Entretanto, se a aplicação permitir o aumento de M, será que existe alguma desvantagem adicional em fazê-lo? A resposta é sim, conforme descrito neste capítulo.

A modelagem de sistemas de comunicações utilizando TMUXes é uma ferramenta bem conhecida, conforme descrito no capítulo anterior. Filtros FIR são mais utilizados que filtros IIR devido a dificuldades inerentes ao projeto e análise de TMUXes IIR [39]. Nesse contexto, transceptores multicanais FIR capazes de eliminar a ISI inerente às transmissões em banda-larga podem ser projetados desde que sinais redundantes sejam propriamente inseridos antes da transmissão [7, 31, 32, 40, 41]. O tipo de redundância (prefixo/sufixo cíclico, *zero-padding*, etc) colocada antes da transmissão dos sinais desempenha um papel central no processo de comunicação.

Em aplicações práticas, transceptores em bloco e sem memória são os mais utilizados. Para tais transceptores, o *zero-padding* (ZP) é uma das formas de redundância mais eficientes para eliminar a IBI. De fato, em vários cenários diferentes, sistemas do tipo ZP são tidos como soluções ótimas no sentido de MSE [40]. Tal característica de optimalidade leva a um desempenho melhor de tais transceptores ZP, quando comparados aos transceptores baseados em prefixo cíclico (CP), em várias situações [37, 42]. Além disso, sistemas baseados em ZP requerem uma potência de transmissão menor do que outros que adicionam elementos redundantes não-nulos.

Entretanto, transceptores redundantes possuem algumas desvantagens também, uma vez que a inserção de elementos redundantes (dados que não possuem informações adicionais) reduz a taxa de transmissão efetiva (*throughput*) do sistema. A redundância é empregada pelo processo de transmissão/recepção com o objetivo de suplantar as distorções introduzidas pelo canal seletivo em frequência. Como um exemplo, para um canal FIR com ordem L, um sistema ZP clássico introduz ao menos L zeros antes da transmissão. Essa característica reduz o *throughput* de tais transceptores, especialmente quando o canal é muito dispersivo.

A tendência atual de aumento da demanda por transmissões sem fio não mostra indícios de parada. A quantidade de serviços de dados *wireless* está mais do que dobrando a cada ano, fazendo com que a escassez de espectro seja um evento certo nos próximos anos. Como consequência, todos os esforços no sentido de maximizar a utilização do espectro de rádio-frequência são altamente justificáveis neste ponto. Uma alternativa para tentar superar a redução de *throughput* relacionada aos transceptores redundantes é aumentar o número de símbolos, M, transmitidos em um bloco. De fato, quando M aumenta, a razão L/M diminui, o que significa que a quantidade relativa de redundância diminui.

Entretanto, o tamanho de bloco M não pode ter qualquer valor desejado, uma vez que diversos fatores afetam a escolha de M. Um desses fatores é a restrição quanto ao atraso associado ao processamento de sinais de um dado bloco de dados. Além disso, há alguns estudos na literatura aberta indicando uma certa degradação de desempenho de transceptores *zero-padded* sempre que M aumenta [40, 42, 43].[1] Por exemplo, em [42] mostrou-se matematicamente que várias figuras de mérito que quantificam o desempenho de sistemas monoportadoras que utilizam ZP degradam com o aumento de M. Em [40], verificou-se empiricamente um comportamento semelhante para uma classe ainda maior de transceptores ZP ótimos, incluindo aqueles baseados em DFE.

Conforme os autores em [40] destacam, não há provas matemáticas de como a quantidade relativa de redundância influencia o desempenho dos transceptores

[1] Tal comportamento não se aplica a sistemas do tipo CP, conforme descrito em [42], por exemplo.

ZP ótimos, embora haja simulações indicando algumas tendências. Este capítulo fornece algumas dessas provas matemáticas não existentes na literatura. De fato, nós provamos que ambos o MSE médio de símbolos e a informação mútua entre os sinais transmitidos e estimados degradam sempre que a quantidade relativa de redundância decresce, isto é, sempre que M aumenta (para um canal de ordem fixa).

Uma outra característica interessante de transceptores ZP é o comportamento de seus desempenhos em relação à quantidade de redundância descartada no receptor. O autor em [43] mostra que os ganhos de ruído relacionados aos transceptores ZP monoportadora aumentam sempre que alguns elementos redundantes são descartados do vetor recebido com o intuito de diminuir a quantidade de operações matemáticas realizadas no processo de equalização. Este capítulo também estende o resultado de [43] para uma classe ainda maior de transceptores ZP, lineares e DFE. Mais especificamente, nós demonstramos que o MSE e a informação mútua relacionada aos transceptores ZP ótimos também são funções monótonas do número de elementos redundantes empregados na equalização.

Além disso, como uma contribuição final deste capítulo, nós mostramos que para uma classe grande de transceptores ZP lineares e DFE, o desempenho degrada sempre que um zero do canal que esteja dentro do círculo unitário é substituído por um zero fora do círculo unitário, sem que essa substituição modifique a resposta de magnitude do canal. Na verdade, tal resultado só é válido quando não utilizamos todos os elementos presentes no vetor recebido durante a equalização (ou seja, alguns elementos redundantes são descartados antes da equalização). Caso o bloco recebido seja inteiramente utilizado na equalização, então o MSE e a informação mútua relacionados a tais transceptores não serão sensíveis à localização dos zeros do canal em relação ao círculo unitário. Vale a pena destacar que tais resultados são extensões de resultados similares de [43] para uma classe grande de transceptores ZP ótimos.

3.1 Modelo e Definições de Transceptores ZP

3.1.1 Equalizadores Lineares Ótimos

Conforme indicado na Figura 3.1, foram considerados os seguintes transceptores lineares: CI-UP (ZF e Pure), UP (ZF e Pure), ZF e Pure. Neste caso, CI vem do termo em inglês *channel indepedent*, enquanto que UP vem do termo em inglês *unitary precoder*. Tais siglas indicam que tipo de restrição foi imposta para se obter a solução MMSE-ótima. Por exemplo, um transceptor linear CI-UP Pure é obtido minimizando-se o erro quadrático médio de símbolos no receptor, sujeito à restrição de que a matriz de precodificação não dependa do canal e seja, simultaneamente,

unitária. Além disso, o termo Pure indica que não foi imposta a restrição de *zero-forcing*.

Na Figura 3.1, M denota a quantidade de símbolos e L denota a quantidade de zeros inseridos. Assim, são transmitidos $N = M + L$ elementos. A definição exata das matrizes de precodificação e equalização depende do tipo de transceptor utilizado. Para mais informações, o leitor pode consultar a Subseção C.1.1.

3.1.2 Equalizadores com Realimentação de Decisão Ótimos

Conforme indicado na Figura 3.2, foram considerados os seguintes transceptores DFE: ZF e Pure. Para mais informações, o leitor pode consultar a Subseção C.1.2.

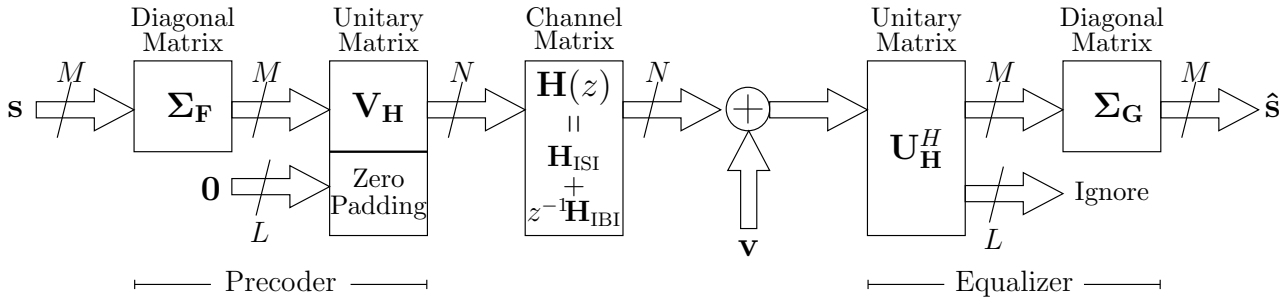

Figura 3.1: Estrutura dos transceptores lineares ZP: UP-ZF, ZF, UP-Pure e Pure.

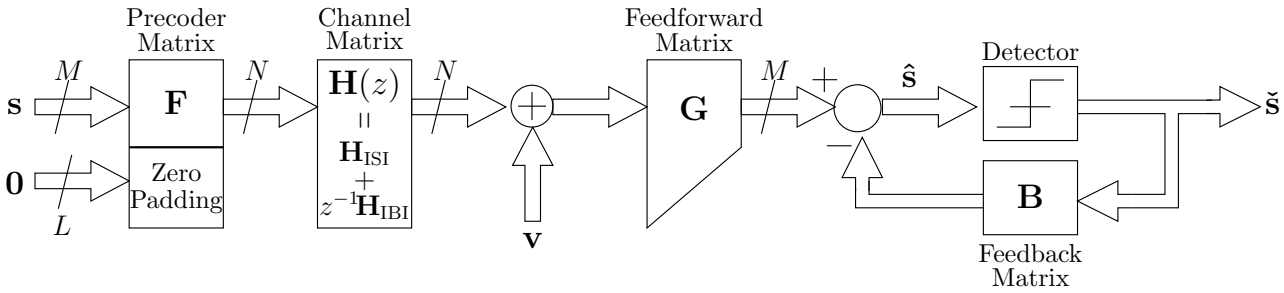

Figura 3.2: Estrutura do transceptor DFE.

3.2 Desempenho de Transceptores ZP Ótimos

Com relação ao desempenho dos transceptores ZP ótimos, é possível quantificar o MSE de símbolos da seguinte forma:

$$\mathcal{E}_{\text{ZF}}^{\text{UP}}(M) = \mathcal{E}_{\text{ZF}}^{\text{CI-UP}}(M) = \sigma_v^2 \left(\frac{1}{M} \sum_{m=0}^{M-1} \frac{1}{\sigma_m^2(M)} \right) = \sigma_v^2 \frac{\text{tr}\left\{\mathbf{S}_M\right\}}{M}, \tag{3.1}$$

$$\mathcal{E}_{\text{Pure}}^{\text{UP}}(M) = \mathcal{E}_{\text{Pure}}^{\text{CI-UP}}(M) = \sigma_v^2 \left(\frac{1}{M} \sum_{m=0}^{M-1} \frac{1}{\frac{\sigma_v^2}{\sigma_s^2} + \sigma_m^2(M)} \right) = \sigma_v^2 \frac{\text{tr}\left\{\mathbf{S}'_M\right\}}{M}, \tag{3.2}$$

$$\mathcal{E}_{\text{ZF}}(M) = \sigma_v^2 \left(\frac{1}{M} \sum_{m=0}^{M-1} \frac{1}{\sigma_m(M)} \right)^2 = \sigma_v^2 \left(\frac{\text{tr}\left\{\sqrt{\mathbf{S}_M}\right\}}{M} \right)^2, \tag{3.3}$$

$$\mathcal{E}_{\text{ZF}}^{\text{DFE}}(M) = \sigma_v^2 \left(\prod_{m=0}^{M-1} \frac{1}{\sigma_m^2(M)} \right)^{\frac{1}{M}} = \sigma_v^2 \sqrt[M]{\det\{\mathbf{S}_M\}}, \tag{3.4}$$

em que $\mathbf{S}_M = \mathbf{R}_M^{-1}$, com $\mathbf{R}_M = \mathbf{H}_M^H \mathbf{H}_M \in \mathbb{C}^{M \times M}$ e $\mathbf{H}_M$ é a matriz de convolução do canal efetiva. Analogamente, $\mathbf{S}'_M = (\mathbf{R}'_M)^{-1}$, com $\mathbf{R}'_M = \mathbf{H}_M^H \mathbf{H}_M + \frac{\sigma_v^2}{\sigma_s^2} \mathbf{I}_M \in \mathbb{C}^{M \times M}$. Por fim, $\sigma_m(M)$ é o m-ésimo valor singular de $\mathbf{H}_M$.

Já para a informação mútua entre os sinais transmitido e estimado, tem-se:

$$\begin{aligned} \mathcal{I}_{\text{ZF}}^{\text{UP}}(M) &= \mathcal{I}_{\text{Pure}}^{\text{UP}}(M) = \mathcal{I}_{\text{ZF}}^{\text{CI-UP}}(M) = \mathcal{I}_{\text{Pure}}^{\text{CI-UP}}(M) \\ &= \frac{\text{tr}\left\{\ln\left[\mathbf{I}_M + \left(\frac{\sigma_v^2}{\sigma_s^2}\mathbf{S}_M\right)^{-1}\right]\right\}}{M}, \end{aligned} \tag{3.5}$$

$$\mathcal{I}_{\text{ZF}}(M) = \frac{\text{tr}\left\{\ln\left[\mathbf{I}_M + \left(\rho_M^{\text{ZF}}\sqrt{\mathbf{S}_M}\right)^{-1}\right]\right\}}{M}, \tag{3.6}$$

$$\mathcal{I}_{\text{ZF}}^{\text{DFE}}(M) = \ln\left[1 + \frac{\sigma_s^2}{\sigma_v^2} \sqrt[M]{\det\left\{\mathbf{S}_M^{-1}\right\}}\right]. \tag{3.7}$$

Para mais informações, o leitor pode consultar a Seção C.2.

3.3 Efeito do Aumento do Tamanho do Bloco

Em termos de MSE de símbolos médio, $\mathcal{E}$, foi possível mostrar que para todo inteiro positivo M, tem-se:

$$\mathcal{E}(M) \leq \mathcal{E}(M+1), \tag{3.8}$$

conforme indicado na Figura 3.3.

Já para a informação mútua média entre símbolos transmitidos e estimados, $\mathcal{I}$,

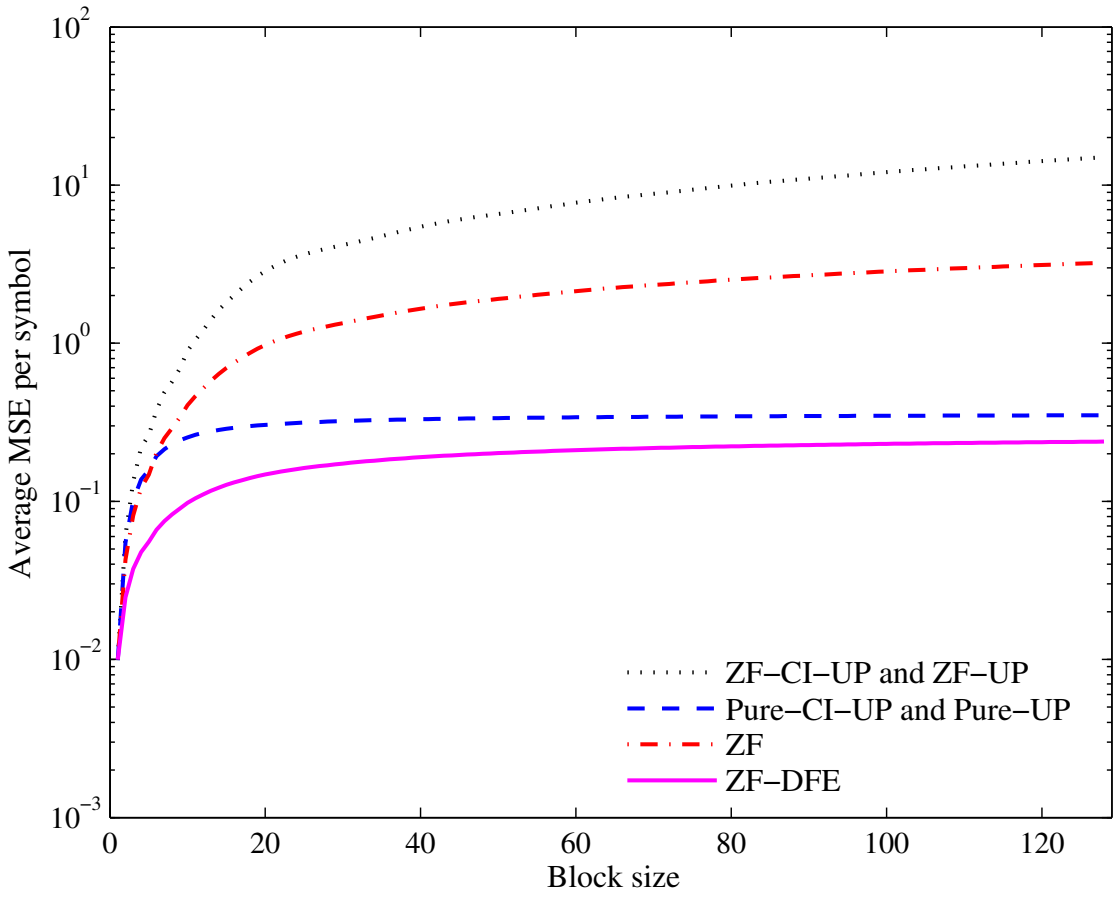

Figura 3.3: MSE de símbolos médio para os transceptores ZP ótimos em função do tamanho do bloco de dados, M.

foi possível mostrar que para todo inteiro positivo M, tem-se:

$$\mathcal{I}(M) \geq \mathcal{I}(M+1), \tag{3.9}$$

conforme indicado na Figura 3.4.

Para mais informações, o leitor pode consultar a Seção C.3.

3.4 Efeito do Descarte de Dados Redundantes

Em relação à quantidade de símbolos redundantes utilizados na equalização, K, pode-se mostrar que, para todo inteiro K entre 0 e $L-1$, tem-se:

$$\mathcal{E}(K+1) \leq \mathcal{E}(K) \quad \text{e} \quad \mathcal{I}(K+1) \geq \mathcal{I}(K), \tag{3.10}$$

conforme indicado na Tabela 3.1.

Para mais informações, o leitor pode consultar a Seção C.4.

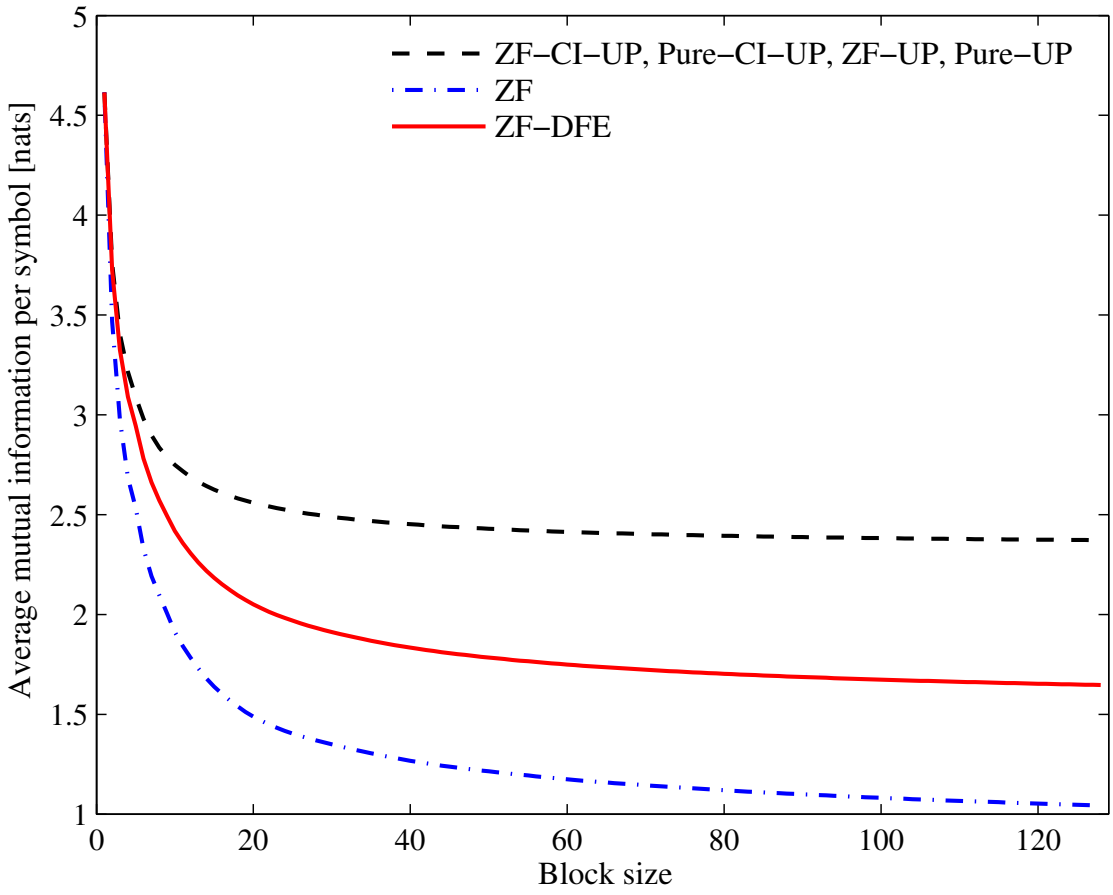

Figura 3.4: Informação mútua média entre símbolos transmitidos e estimados para os transceptores ZP ótimos em função do tamanho do bloco de dados, M.

Tabela 3.1: MSE de símbolos médio e informação mútua média para transceptores ZP em função de $K \in \mathcal{L}$.

	$K=0$	$K=1$	$K=2$	$K=3$	$K=4$	$K=5$	$K=6$	$K=7$
$\mathcal{E}_{\text{ZF}}^{\text{CI-UP}}$	3.64×10^7	2.99×10^3	1.80×10^3	14.91	11.69	8.37	7.55	6.50
$\mathcal{E}_{\text{Pure}}^{\text{CI-UP}}$	0.41	0.39	0.37	0.35	0.34	0.34	0.33	0.33
$\mathcal{E}_{\text{ZF}}$	1.16×10^6	224.64	87.90	3.87	2.99	2.26	2.07	1.85
$\mathcal{E}_{\text{ZF}}^{\text{DFE}}$	1.02	0.53	0.38	0.26	0.23	0.21	0.20	0.19

	$K=0$	$K=1$	$K=2$	$K=3$	$K=4$	$K=5$	$K=6$	$K=7$
$\mathcal{I}_{\text{ZF}}^{\text{CI-UP}}$	2.16	2.23	2.29	2.34	2.38	2.40	2.43	2.45
$\mathcal{I}_{\text{ZF}}$	0.00	0.25	0.37	0.98	1.06	1.15	1.18	1.23
$\mathcal{I}_{\text{ZF}}^{\text{DFE}}$	0.67	1.05	1.28	1.55	1.64	1.73	1.77	1.81

3.5 Efeito dos Zeros do Canal

Com relação ao efeito dos zeros do canal, nós demonstramos que o MSE de símbolos/informação mútua associado/a aos transceptores ZP ótimos diminui/aumenta sempre que ao menos um zero fora do círculo de raio unitário de um canal de fase não-mínima é substituído por um zero correspondente dentro do círculo unitário, assumindo que a equalização descarta alguns elementos redundantes para estimar o sinal transmitido.

As Tabelas 3.2 e 3.3 (vide também a Figura 3.5) ilustram este efeito dos zeros do canal.

Para mais informações, o leitor pode consultar a Seção C.5.

Tabela 3.2: Efeito dos zeros do canal: MSE de símbolos

	$K=0$	$K=1$	$K=2$	$K=3$	$K=4$	$K=5$	$K=6$	$K=7$	$K=8$	$K=9$
$\mathcal{E}_{\text{ZF}}^{\text{CI-UP}}$, $H_1(z)$	27.46	21.33	9.31	6.64	4.62	3.79	3.17	2.43	2.19	2.01
$\mathcal{E}_{\text{ZF}}^{\text{CI-UP}}$, $H_2(z)$	17.32	9.57	6.54	4.54	3.44	3.01	2.50	2.27	2.12	2.01
$\mathcal{E}_{\text{ZF}}^{\text{CI-UP}}$, $H_3(z)$	8.01	6.10	4.24	3.22	2.51	2.25	2.17	2.14	2.08	2.01
$\mathcal{E}_{\text{Pure}}^{\text{CI-UP}}$, $H_1(z)$	0.43	0.39	0.36	0.33	0.31	0.31	0.30	0.30	0.29	0.29
$\mathcal{E}_{\text{Pure}}^{\text{CI-UP}}$, $H_2(z)$	0.39	0.36	0.33	0.31	0.30	0.30	0.30	0.29	0.29	0.29
$\mathcal{E}_{\text{Pure}}^{\text{CI-UP}}$, $H_3(z)$	0.36	0.33	0.31	0.30	0.30	0.30	0.29	0.29	0.29	0.29
$\mathcal{E}_{\text{ZF}}$, $H_1(z)$	8.74	6.03	2.96	2.04	1.40	1.20	1.05	0.88	0.80	0.75
$\mathcal{E}_{\text{ZF}}$, $H_2(z)$	5.15	2.99	2.00	1.40	1.11	1.01	0.89	0.83	0.78	0.75
$\mathcal{E}_{\text{ZF}}$, $H_3(z)$	2.55	1.86	1.31	1.06	0.90	0.83	0.80	0.79	0.77	0.75
$\mathcal{E}_{\text{ZF}}^{\text{DFE}}$, $H_1(z)$	0.53	0.38	0.26	0.21	0.17	0.16	0.15	0.14	0.13	0.13
$\mathcal{E}_{\text{ZF}}^{\text{DFE}}$, $H_2(z)$	0.38	0.28	0.21	0.18	0.16	0.15	0.14	0.13	0.13	0.13
$\mathcal{E}_{\text{ZF}}^{\text{DFE}}$, $H_3(z)$	0.28	0.22	0.17	0.16	0.15	0.14	0.14	0.13	0.13	0.13

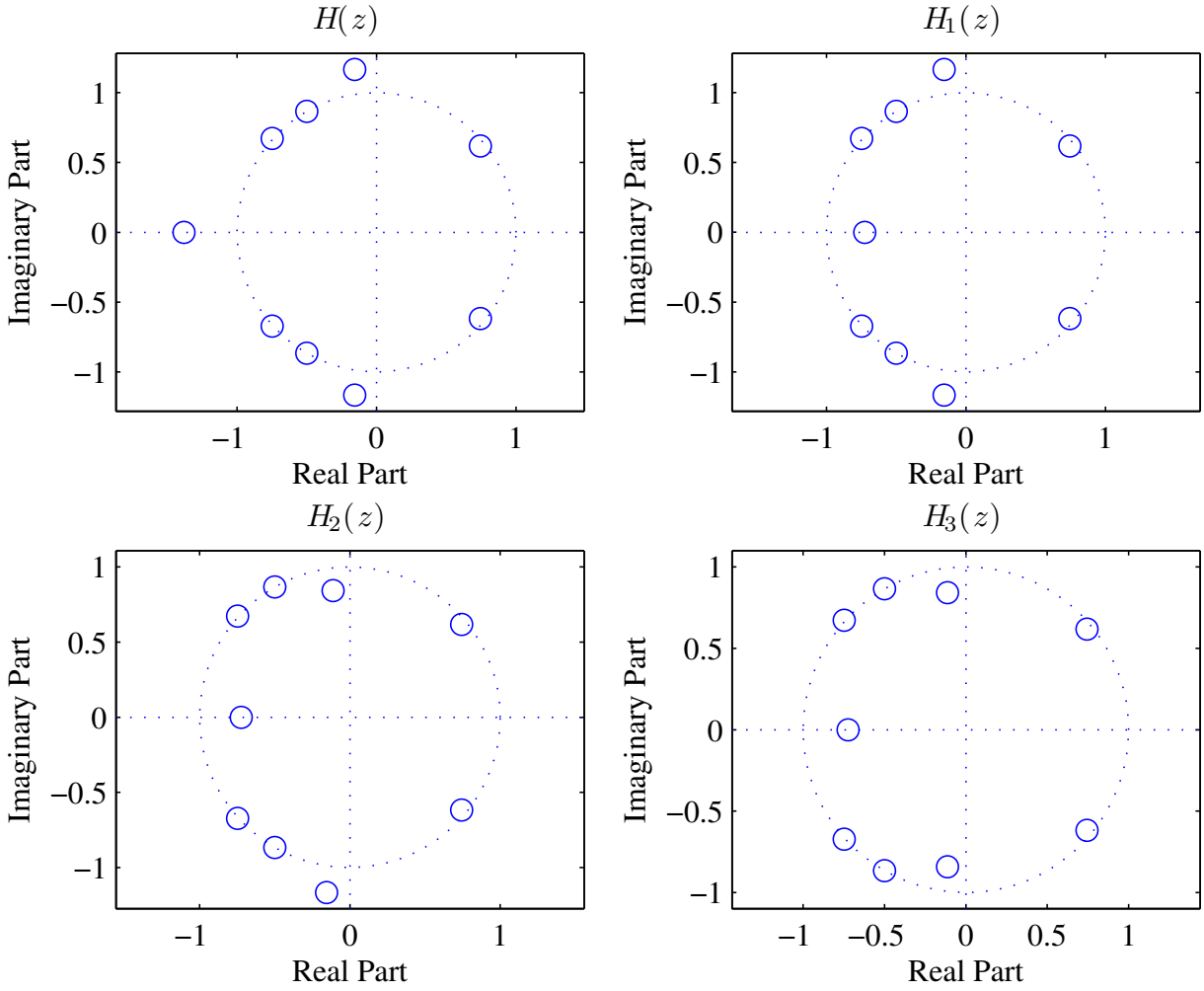

Figura 3.5: Zeros dos canais $H(z)$ e $H_i(z)$, em que $i \in \{1, 2, 3\}$, com o círculo unitário como referência. Todos os canais possuem a mesma resposta de magnitude.

Tabela 3.3: Efeito dos zeros do canal: informação mútua

	$K=0$	$K=1$	$K=2$	$K=3$	$K=4$	$K=5$	$K=6$	$K=7$	$K=8$	$K=9$
$\mathcal{I}_{\mathrm{ZF}}^{\mathrm{CI-UP}}$, $H_1(z)$	2.06	2.20	2.32	2.40	2.46	2.49	2.53	2.56	2.59	2.60
$\mathcal{I}_{\mathrm{ZF}}^{\mathrm{CI-UP}}$, $H_2(z)$	2.14	2.27	2.38	2.44	2.48	2.51	2.54	2.57	2.60	2.60
$\mathcal{I}_{\mathrm{ZF}}^{\mathrm{CI-UP}}$, $H_3(z)$	2.22	2.34	2.43	2.47	2.50	2.53	2.56	2.58	2.60	2.60
$\mathcal{I}_{\mathrm{ZF}}$, $H_1(z)$	0.69	0.81	1.03	1.17	1.32	1.39	1.45	1.52	1.57	1.60
$\mathcal{I}_{\mathrm{ZF}}$, $H_2(z)$	0.83	1.01	1.17	1.31	1.40	1.45	1.51	1.55	1.58	1.60
$\mathcal{I}_{\mathrm{ZF}}$, $H_3(z)$	1.04	1.18	1.33	1.42	1.49	1.53	1.55	1.57	1.58	1.60
$\mathcal{I}_{\mathrm{ZF}}^{\mathrm{DFE}}$, $H_1(z)$	1.04	1.27	1.55	1.73	1.89	1.95	2.01	2.07	2.12	2.15
$\mathcal{I}_{\mathrm{ZF}}^{\mathrm{DFE}}$, $H_2(z)$	1.27	1.51	1.72	1.87	1.96	2.00	2.05	2.09	2.13	2.15
$\mathcal{I}_{\mathrm{ZF}}^{\mathrm{DFE}}$, $H_3(z)$	1.51	1.70	1.88	1.96	2.02	2.06	2.09	2.11	2.13	2.15

3.6 Conclusões

Este capítulo abordou a análise de transceptores ótimos lineares e com realimentação de decisão, os quais empregam redundância completa. A classe de transceptores discutida aqui inclui sistemas ZF e MMSE, com precodificadores unitários ou não. As figuras de mérito utilizadas para aferir o desempenho de tais transceptores foram o MSE e a informação mútua entre os blocos estimado e transmitido. As análises propostas indicam que a redução na quantidade relativa de redundância em um bloco de dados leva a perdas em desempenho das referidas figuras de mérito. Mostramos também como a tentativa em diminuir o número de elementos redundantes utilizados na equalização com o intuito de reduzir a quantidade de operações matemáticas no receptor pode levar a perda de desempenho dos sistemas envolvidos. Além disso, provamos que zeros do canal fora do círculo unitário degradam o desempenho dos sistemas ZP, quando comparados a zeros relacionados dentro do círculo unitário, a menos que todo o bloco de dados recebidos seja utilizado na equalização. Os resultados das simulações corroboram com tais resultados teóricos.

Pelo o que acabamos de mostrar neste capítulo, vale a pena desenvolver transceptores que são capazes de aumentar a eficiência espectral de sistemas ZP, sem aumentar o tamanho do bloco de dados. Em outras palavras, podemos buscar transceptores em bloco práticos com redundância reduzida. Na verdade, nós descreveremos algumas propostas práticas na primeira parte desta tese e, depois disso, descreveremos o caso geral de sistemas com redundância reduzida na segunda parte da tese.

Capítulo 4

Transceptores com Redundância Mínima Baseados em DFT

Uma das principais características que ajudou na adoção ampla de sistemas baseados em OFDM e SC-FD é a inserção de redundância para a transmissão em bloco. Tal redundância elimina a IBI e permite a implementação computacionalmente eficiente de equalizadores ZF e MMSE baseados na transformada discreta de Fourier (DFT) e em matrizes diagonais [31].

Entretanto, é sabido que a redundância mínima exigida para eliminar a IBI e transceptores em bloco fixos e sem memória é apenas a metade da quantidade empregada em sistemas tradicionais baseados em OFDM [32]. O uso de redundância mínima pode levar a soluções com taxas de transmissão maiores. Entretanto, a taxa de transmissão não é a única figura de mérito que é levada em consideração, uma vez que os custos envolvidos nas soluções obtidas são também de extrema importância. De fato, transceptores práticos com redundância mínima com a restrição de serem tão simples quanto os sistemas OFDM (pelo menos do ponto de vista assintótico) já foram propostos em [23].

Em geral, os novos transceptores possuem taxas de transmissão maiores do que sistemas tradicionais baseados em OFDM e SC-FD, especialmente para canais muito dispersivos no tempo. Além disso, eles são eficientes em termos de custo computacional, uma vez que utilizam transformadas discretas rápidas e matrizes diagonais [23]. Soluções do tipo ZF e MMSE estão disponíveis e elas diferem entre si no número de ramos paralelos no receptor: dois ramos paralelos para a solução ZF e cinco ramos paralelos para a solução MMSE, conforme descrito nas Figuras 4.1, 4.2, 4.3, 4.4 e 4.5 de [23].

Embora equalizadores ZF e MMSE com redundância mínima exijam um tempo de processamento de um vetor recebido equivalente (devido ao paralelismo inerente às estruturas propostas), as soluções MMSE utilizam mais do que o dobro do número de computações relacionadas às soluções ZF. Isto é uma desvantagem óbvia do

ponto de vista computacional, o que pode dificultar o emprego de soluções MMSE com redundância mínima em alguns sistemas práticos, apesar de soluções MMSE obterem taxas maiores que as ZF em diversos ambientes, especialmente em ambientes ruidosos [23].

A desvantagem acima motivou-nos a buscar simplificar os equalizadores MMSE ótimos, reduzindo o número de ramos paralelos no receptor de cinco para quatro. Além disso, nós também investigamos soluções MMSE subótimas neste capítulo. De fato, nós propomos novos transceptores multiportadoras e monoportadora com redundância mínima que mantêm exatamente a mesma estrutura da solução ZF, enquanto se mantêm o mais próximos o possível da solução MMSE ótima. Essa proximidade é medida pela norma 2 de matrizes [44]. Como consequência, novos transceptores MMSE subótimos levam a taxas de transmissão mais altas do que as relacionadas aos sistemas ZF, com exatamente a mesma complexidade para o processo de equalização.

Para derivar os transceptores propostos, nós primeiros derivaremos novamente os transceptores MMSE ótimos com redundância mínima de uma forma ligeiramente diferente daquela descrita em [23]. Em relação às soluções subótimas, nós começamos com a solução MMSE ótima que acabamos de descrever e aplicamos a abordagem por *displacement rank* junto com decomposições SVD eficientes baseadas em fatorações de Householder e QR [44, 45]. A aplicação dessas técnicas permite o desenvolvimento de soluções MMSE subótimas que apresentam complexidade computacional comparável aos sistemas OFDM e SC-FD. Em geral, tais propostas possibilitam a transmissão através de canais bastante dispersivos com altos ganhos de *throughputs*, sendo assim uma boa solução de compromisso em termos de desempenho e custo computacional.

4.1 Transceptores ZP-ZJ Revisitados

Sabemos que os transceptores ZP-ZJ (vide Figura 4.1) são caracterizados pela seguinte relação:

$$\hat{\mathbf{s}} \triangleq \mathbf{G}\mathbf{H}(z)\mathbf{F}\mathbf{s} + \mathbf{G}\mathbf{v} = \mathbf{G}_0\mathbf{H}_0\mathbf{F}_0\mathbf{s} + \mathbf{v}_0. \tag{4.1}$$

Dada uma matriz de transmissão $\mathbf{F}_0$ e a matriz equivalente de canal $\mathbf{H}_0$, nosso objetivo será projetar a matriz de recepção $\mathbf{G}_0$. A principal ideia é utilizar o fato de a matriz de canal $\mathbf{H}_0$ ser estruturada para obtermos soluções mais simples do ponto

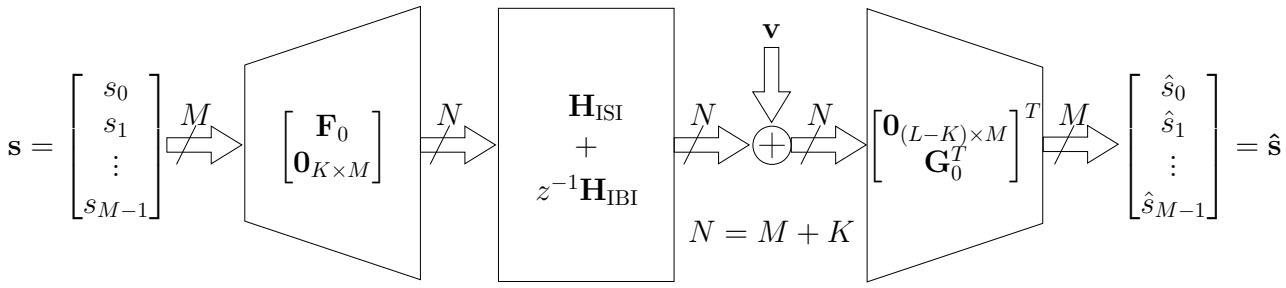

Figura 4.1: Modelo do transceptor ZP-ZJ.

de vista computacional. De fato, $\mathbf{H}_0$ é uma matriz de Toeplitz dada por

$$\mathbf{H}_0 = \begin{bmatrix} h(L-K) & \cdots & h(0) & 0 & 0 & \cdots & 0 \\ \vdots & \ddots & & & & & \vdots \\ h(K) & \ddots & & & & & 0 \\ \vdots & \ddots & & & \ddots & & h(0) \\ h(L) & & & & & & \vdots \\ 0 & & & & \ddots & & h(L-K) \\ \vdots & & & & & & \vdots \\ 0 & \cdots & 0 & 0 & h(L) & \cdots & h(K) \end{bmatrix} \in \mathbb{C}^{(M+2K-L)\times M}, \quad (4.2)$$

onde $h(0), h(1), \cdots, h(L)$ são os coeficientes do modelo FIR de canal.

Para mais informações, o leitor pode consultar a Seção D.1.

4.1.1 Sistemas com Redundância Mínima

No caso de sistemas com redundância mínima, sabemos que a matriz de recepção é dada por [23]:

$$\mathbf{G}_{0,\text{min}}^{\text{ZF}} \triangleq \mathbf{F}_0^{-1}\mathbf{H}_0^{-1}, \quad (4.3)$$

$$\mathbf{G}_{0,\text{min}}^{\text{MMSE}} \triangleq \mathbf{F}_0^{-1}\mathbf{H}_0^H \left(\mathbf{H}_0\mathbf{H}_0^H + \frac{\sigma_v^2}{\sigma_s^2}\mathbf{I}_M\right)^{-1}, \quad (4.4)$$

supondo L par, de forma que $L/2$ elementos redundantes são adicionados em cada bloco transmitido.

Tais matrizes admitem as seguintes decomposições:

$$\mathbf{G}_{0,\text{min}}^{\text{ZF}} = \frac{1}{2}\mathbf{F}_0^{-1}\mathbf{W}_M^H \left(\sum_{r=1}^{2} \mathbf{D}_{\bar{\mathbf{p}}_r}\mathbf{W}_M\mathbf{D}\mathbf{W}_M\mathbf{D}_{\bar{\mathbf{q}}_r}\right)\mathbf{W}_M^H\mathbf{D}^H, \quad (4.5)$$

$$\mathbf{G}_{0,\text{min}}^{\text{MMSE}} = \frac{1}{2}\mathbf{F}_0^{-1}\mathbf{W}_M^H \left(\sum_{r=1}^{5} \mathbf{D}_{\bar{\mathbf{p}}_r}\mathbf{W}_M\mathbf{D}\mathbf{W}_M\mathbf{D}_{\bar{\mathbf{q}}_r}\right)\mathbf{W}_M^H\mathbf{D}^H, \quad (4.6)$$

onde $\mathbf{D}_{\bar{\mathbf{p}}_r}$ e $\mathbf{D}_{\bar{\mathbf{q}}_r}$ são matrizes dependentes do modelo de canal, enquanto que $\mathbf{D}$ é uma matriz independente do modelo de canal (veja [23] para mais detalhes). Um sistema monoportadora é obtido quando $\mathbf{F}_0 \triangleq \mathbf{I}_M$, enquanto um sistemas multiportadoras é obtido quando $\mathbf{F}_0 \triangleq \mathbf{W}_M^H$.

Para mais informações, o leitor pode consultar a Subseção D.1.1.

4.1.2 Projeto de Transceptores com Redundância Mínima

A ideia do projeto de transceptores com redundância mínima é decompor de forma eficiente a matriz inversa de canal, assim como realizado nos sistemas OFDM e SC-FD. Com efeito, sistemas baseados em SC-FD, por exemplo, induzem uma matriz de canal equivalente com estrutura circulante. Como toda matriz quadrada circulante pode ser diagonalizada facilmente utilizando-se matrizes de DFT e IDFT, então a inversa de tal matriz é facilmente diagonalizada também utilizando-se matrizes de DFT e IDFT, além da inversa da matriz de autovalores original.

No caso de sistemas com redundância mínima, a matriz de canal equivalente não é circulante, mas sim de Toeplitz. Mesmo assim, ainda é possível valer-se de transformadas rápidas e matrizes diagonais para decompor (não mais diagonalizar) a inversa de tal matriz.

Para mais informações, o leitor pode consultar a Subseção D.1.2.

4.1.3 Abordagem via *Displacement Rank*

Dadas duas matrizes $\mathbf{X}, \mathbf{Y} \in \mathbb{C}^{M\times M}$, as transformações lineares [25]

$$\begin{aligned} \nabla_{\mathbf{X},\mathbf{Y}} : \mathbb{C}^{M\times M} &\to \mathbb{C}^{M\times M} \\ \mathbf{U} &\mapsto \nabla_{\mathbf{X},\mathbf{Y}}(\mathbf{U}) \triangleq \mathbf{XU} - \mathbf{UY} \end{aligned} \tag{4.7}$$

$$\begin{aligned} \Delta_{\mathbf{X},\mathbf{Y}} : \mathbb{C}^{M\times M} &\to \mathbb{C}^{M\times M} \\ \mathbf{U} &\mapsto \Delta_{\mathbf{X},\mathbf{Y}}(\mathbf{U}) \triangleq \mathbf{U} - \mathbf{XUY} \end{aligned} \tag{4.8}$$

são chamadas de *displacements* de Sylvester e de Stein, respectivamente. Quando tais transformações são devidamente aplicadas sobre matrizes estruturadas, tem-se como resultado uma matriz esparsa que depende de poucos elementos não nulos. No caso de uma matriz de Toeplitz, por exemplo, pode-se passar de uma representação com M^2 elementos não nulos para uma representação com apenas $2M$ elementos não nulos. Para mais informações, o leitor pode consultar a Subseção D.1.3.

4.2 Equalizadores MMSE Ótimos com Redundância Mínima

Aplicando-se a abordagem via *displacement rank*, é possível desenvolver decomposições eficientes para a matriz de recepção associada a sistemas com redundância mínima. Por exemplo, para um transceptor monoportadora, é possível mostrar que a solução MMSE é dada por:

$$\mathbf{F}_0 = \mathbf{I}_M, \tag{4.9}$$

$$\mathbf{G}_0 = \frac{1}{2}\mathbf{W}_M^H \left[\sum_{r=1}^{4} \mathbf{D}_{\tilde{\mathbf{p}}_r} \mathbf{W}_M \left(\text{diag}\{e^{\jmath\frac{\pi}{M}m}\}_{m=0}^{M-1}\right) \mathbf{W}_M \mathbf{D}_{\tilde{\mathbf{q}}_r}\right] \mathbf{W}_M^H \text{diag}\{e^{-\jmath\frac{\pi}{M}m}\}_{m=0}^{M-1}, \tag{4.10}$$

enquanto que um transceptor multiportadoras possui uma estrutura descrita na Figura 4.2.

Para mais informações, o leitor pode consultar a Seção D.2.

4.3 Equalizadores MMSE Subótimos com Redundância Mínima

Os equalizadores MMSE subótimos são obtidos quando ficamos com apenas dois ramos de equalização do receptor MMSE ótimos, no lugar dos quatro indicados na Figura 4.2. Na verdade, não há um simples descarte. O que se tem é uma transformação que leva a ficarmos com apenas dois ramos, mas com coeficientes de equalização diferentes dos originais. Tal transformação consiste em determinar a decomposição em valores singulares da matriz de *displacemet* associada à matriz de canal. Esta decomposição em valores singulares pode ser feita com complexidade $\mathcal{O}(M)$, uma vez que a matriz de *displacement* depende de poucos coeficientes. Depois de determinar os valores singulares, descartamos os que contribuem menos na formação da matriz (os menores valores singulares) e ficamos com apenas dois deles (num total de quatro).

Para mais informações, o leitor pode consultar a Seção D.3.

4.4 Resultados das Simulações

Equalizadores MMSE Ótimos com Redundância Mínima

Como exemplo de desempenho de nossas propostas em termos de *throughput*, considere a transmissão de 200 blocos contendo $M = 32$ símbolos BPSK por um canal

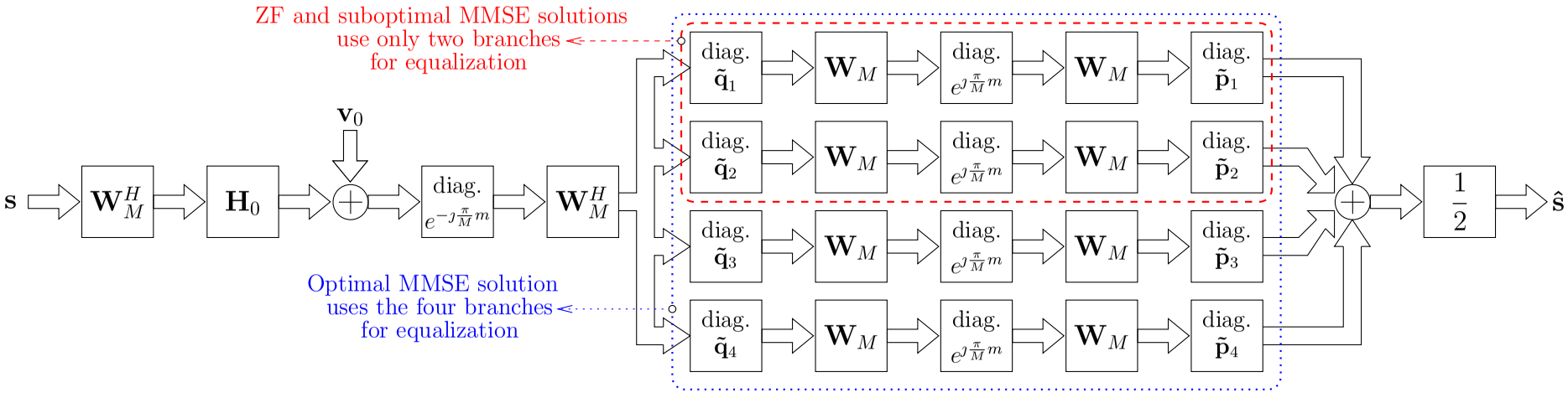

Figura 4.2: Transceptores multiportadoras em bloco com redundância mínima baseados em DFT.

Rayleigh com $L = 30$. Assuma que 10.000 simulações de Monte-Carlo foram realizadas e que a frequência de amostragem é $f_s = 1,0$ GHz. Além disso, assume-se também que o canal através do qual os sinais são transmitidos trabalha na mesma taxa de amostragem.

Neste exemplo, busca-se ilustrar uma aplicação cuja restrição em relação a atrasos seja predominante. Além disso, assume-se também que o canal modela um ambiente extremamente dispersivo. Por isso a resposta ao impulso do modelo de canal (complexo) é longa, sendo sua ordem dada por $L = 30$. Tanto a parte real como a parte imaginária são realizações de processos estocásticos gaussianos brancos, com média zero e independentes. Todos os *taps* do canal possuem a mesma potência média e o canal é sempre normalizado, ou seja, $\mathsf{E}[\|\mathbf{h}\|_2^2] = 1$. Uma nova realização do canal é gerada para cada uma das dez mil simulações. Devido à aleatoriedade na escolha dessas realizações, é muito provável que a quantidade de zeros côngruos do canal seja menor do que o comprimento da redundância, garantindo-se, assim, a existência de soluções ZF.

A definição de razão sinal-ruído (SNR, do inglês *Signal-to-Noise Ratio*) adotada nas simulações é a razão entre a potência média de um símbolo do sinal transmitido (sinal de entrada do canal) e a potência média do ruído aditivo na entrada do receptor.

A definição de *throughput* é

$$\text{Throughput} = br_c \frac{M}{M+K}(1 - \text{BLER})f_s, \tag{4.11}$$

onde $K = L/2 = 15$ e $r_c = 1/2$.

Os sistemas utilizados na transmissão são o tradicional ZP-OFDM-OLA, além dos sistemas propostos, a saber: MC-MRBT (do inglês, *multicarrier minimum-redundancy block transceiver*). Para cada um desses sistemas utilizam-se as soluções ZF e MMSE. O ZP-OFDM e ZP-SC-FD foram escolhidos porque possuem um modelo mais próximo dos sistemas propostos, já que estes utilizam a adição de zeros como redundância e também empregam transformadas rápidas.

A Figura 4.3 contém os resultados relacionados a um sistema multiportadoras. É possível verificar, neste caso em particular, que o sistema proposto MMSE-MC-MRBT possui um desempenho melhor do que a sua contraparte, MMSE-OFDM, o qual obteve exatamente o mesmo desempenho do ZF-OFDM. Já para os sistemas com redundância mínima do tipo ZF, eles são bastante vantajosos para SNRs acima de 12 dB.

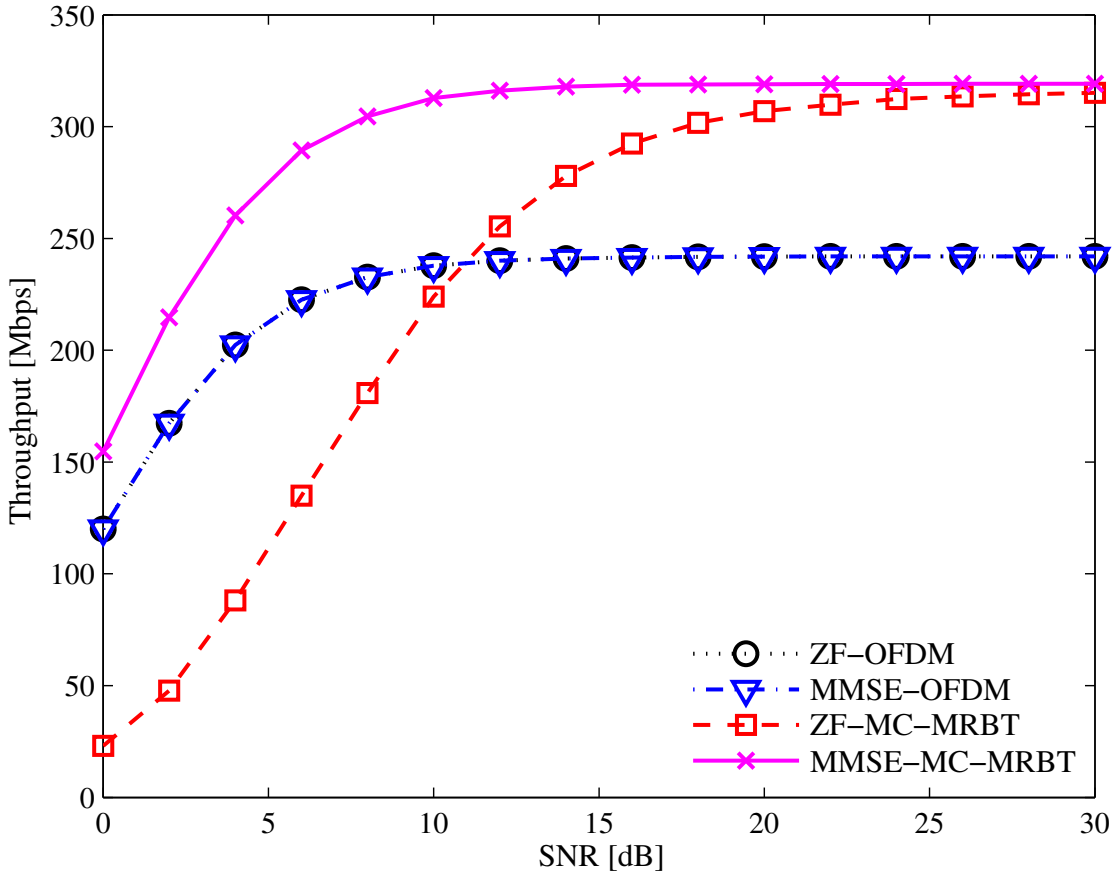

Figura 4.3: *Throughput* [Mbps] em função da SNR [dB], considerando transmissões multiportadoras (canal Rayleigh) baseadas em DFT ($M = 32$ e $L = 30$).

Equalizadores MMSE Subótimos com Redundância Mínima

Como exemplo de desempenho de nossas propostas subótimas em termos de *throughput*, considere a transmissão de 100.000 blocos contendo $M = 8$ símbolos QPSK por um canal fixo com $L = 4$. Assuma que a frequência de amostragem é $f_s = 450$ MHz.

A Figura 4.4 contém os resultados relacionados a um sistema monoportadora. É possível verificar que, com exceção do sistema ZF monoportadora com redundância mínima, os transceptores MMSE com redundância mínima obtiveram desempenho comparável ao MMSE-SC-FD ou até melhor (SNRs a partir de 25 dB). O mais importante é verificar que as soluções ótima e subótima obtiveram desempenho praticamente idêntico. O leitor deve lembrar que a solução subótima utiliza apenas dois ramos de equalizadores no receptor, no lugar dos quatro ramos utilizados pela solução MMSE ótima.

Para mais informações, o leitor pode consultar a Seção D.4.

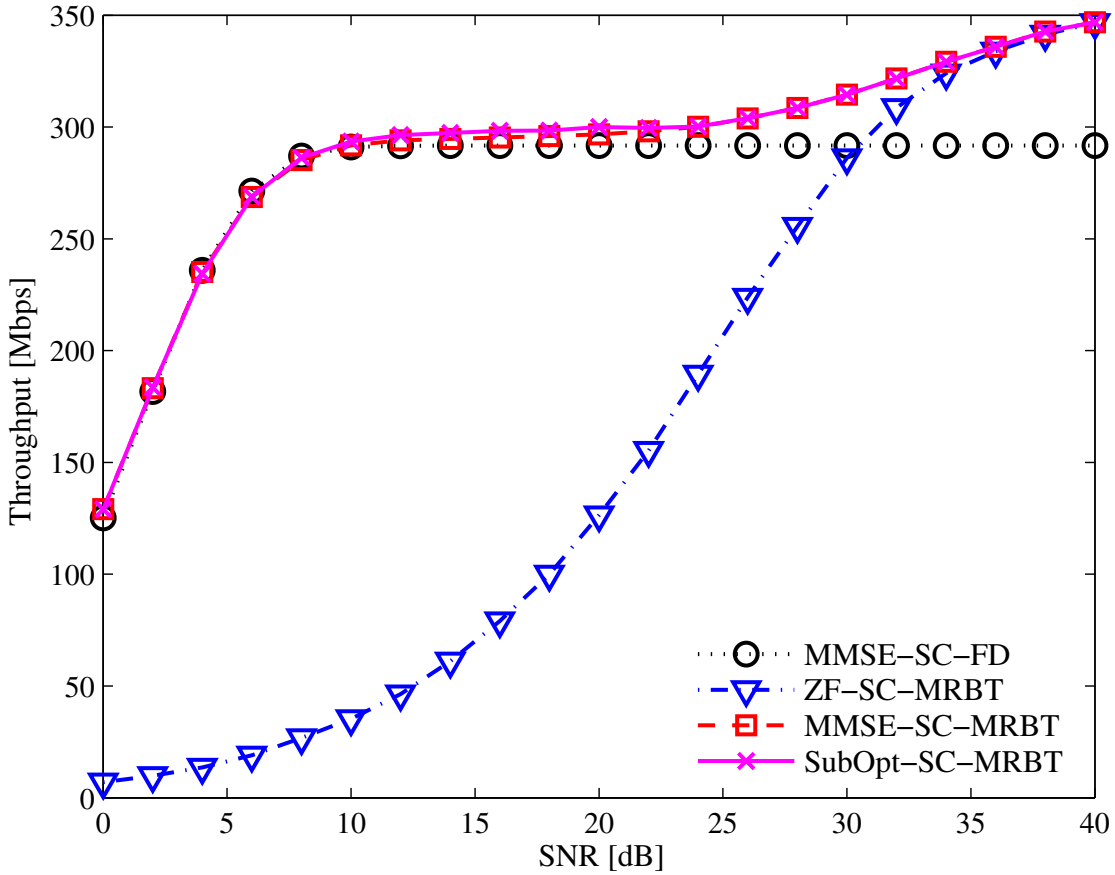

Figura 4.4: *Throughput* [Mbps] em função da SNR [dB], considerando transmissões monoportadora baseadas em DFT ($M = 8$ e $L = 4$).

4.5 Conclusões

Neste capítulo, descrevemos o modelo ZP-ZJ que é a base para os sistemas utilizados ao longo de toda o restante da tese. Através da aplicação dos conceitos de *displacement rank* nós fomos capazes de propor uma estrutura mais simples para os equalizadores MMSE ótimos baseados em DFT com redundância mínima. Além disso, novos equalizadores MMSE subótimos que requerem quase a metade do número de operações de um equalizador MMSE ótimo foram propostos. As simulações confirmam as melhorias em termos de taxa de transmissão efetiva, quando comparamos as novas propostas com sistemas OFDM e SC-FD tradicionais, especialmente quando o canal é bastante dispersivo. Uma característica chave dos sistemas propostos é a complexidade computacional assintótica para o processo de equalização, a qual é dada por $\mathcal{O}(M \log_2 M)$, a mesma complexidade de sistemas OFDM e SC-FD.

Capítulo 5

Transceptores com Redundância Mínima Baseados em DHT

O desempenho de transceptores baseados em transformadas reais que utilizam L elementos redundantes já foi estudado em diversos trabalhos, tais como [46, 47]. Algumas das vantagens em se empregar tais transceptores são provenientes dos seguintes três fatos: [46, 47]: (i) transformadas reais, tais como transformadas discretas de seno e cosseno (DST e DCT, respectivamente) possuem lóbulos laterais mais atenuados, quando comparadas à DFT. Isso implica que menos interferência entre subportadoras (ICI, do inglês *intercarrier interference*) ocorre em sistemas multiportadoras; (ii) Sistema multiportadoras podem se beneficiar com o uso de transformadas reais associado ao uso de constelações reais (PAM, por exemplo), uma vez que a transmissão de dados em fase e quadratura (I/Q) não é requerida; e (iii) DST, DCT e DHT possuem algoritmos rápidos[1], mantendo uma complexidade computacional assintótica competitiva, sendo dada por $\mathcal{O}(M \log_2 M)$, para M símbolos de dados.

Ao lidar com sistemas com redundância mínima, a primeira proposta de transceptores com transformadas reais em [23] mostrou a possibilidade de implementar sistemas de comunicação usando apenas matrizes DHT e diagonais. Entretanto, tais transceptores requeriam uma resposta ao impulso do canal simétrica. Esta condição pode ser atendida com a introdução de um pré-filtro no primeiro estágio de recepção. O pré-filtro ficaria assim responsável por fazer com que a resposta ao impulso efetiva do canal fosse simétrica. Tal abordagem foi adotada também em [46].

O objetivo deste capítulo é propor uma forma de eliminar a restrição de simetria sobre o canal mencionada acima. Para tanto, alguns novos transceptores fixos e sem memória são propostos. Tais transceptores não impõem nenhuma restrição de simetria sobre a resposta ao impulso do canal. Eles podem ser multiportadoras

[1]Isto é, transceptores que requerem $\mathcal{O}(M \log^d M)$ operações, para $d \leq 3$ [25].

ou monoportadora, com receptores ZF ou MMSE. Os transceptores usam apenas matrizes DHT, diagonais e antidiagonais em suas estruturas. Por esta razão, os sistemas propostos são computacionalmente tão simples quanto os sistemas OFDM e SC-FD, e, simultaneamente, podem ser muito mais eficientes com relação à utilização de banda disponível para transmissão.

A abordagem por *displacement rank* [25] é aplicada com o intuito de derivar os novos transceptores propostos usando novas representações de matrizes estruturadas. Tais representações novas são baseadas nas decomposições propostas em [48]. As diferenças entre este capítulo e [48] estão no fato de que a restrição de se trabalhar apenas com matrizes reais, bem como a necessidade de se estender as matrizes envolvidas com zeros não estão presentes nas deduções do presente capítulo. Tais fatores nos possibilitam trabalhar com canais complexos (canais em banda-base, por exemplo), bem como projetar sistemas multiportadoras, o que não era possível empregando diretamente as decomposições presentes em [48].

5.1 Definições das Matrizes DHTs e DFTs

Neste capítulo, consideramos as seguintes definições de matrizes DHTs e DFTs, respectivamente [48, 49]:

$$[\boldsymbol{\mathcal{H}}_X]_{ij} = \frac{\sin[\theta_X(i,j)] + \cos[\theta_X(i,j)]}{\sqrt{M}}, \tag{5.1}$$

$$[\mathbf{W}_X]_{ij} = \frac{\cos[\theta_X(i,j)] - \jmath\sin[\theta_X(i,j)]}{\sqrt{M}}, \tag{5.2}$$

em que $X \in \{\mathrm{I}, \mathrm{II}, \mathrm{III}, \mathrm{IV}\}$ e os ângulos são definidos como se segue:

$$\theta_{\mathrm{I}}(i,j) = \frac{2ij\pi}{M}, \tag{5.3}$$

$$\theta_{\mathrm{II}}(i,j) = \frac{i(2j+1)\pi}{M}, \tag{5.4}$$

$$\theta_{\mathrm{III}}(i,j) = \frac{(2i+1)j\pi}{M}, \tag{5.5}$$

$$\theta_{\mathrm{IV}}(i,j) = \frac{(2i+1)(2j+1)\pi}{2M}, \tag{5.6}$$

para todo $(i,j) \in \{\,0, 1, \cdots, M-1\,\}^2$.

Para mais informações, o leitor pode consultar a Seção E.1.

5.2 Transceptores Eficientes com Redundância Mínima Baseados em DHT

Aplicando-se a abordagem via *displacement rank*, é possível desenvolver decomposições eficientes para a matriz de recepção associada a sistemas com redundância mínima baseados em DHT. Por exemplo, para um transceptor monoportadora, é possível mostrar que a solução ZF é dada por:

$$\mathbf{F}_0 = \mathbf{I}_M \tag{5.7}$$

$$\mathbf{G}_0 = \frac{M}{2}\boldsymbol{\mathcal{H}}_{\mathrm{III}}\left(\sum_{r=1}^{2}\boldsymbol{\mathcal{X}}_{\bar{\mathbf{p}}_r}\boldsymbol{\mathcal{H}}_{\mathrm{II}}\boldsymbol{\mathcal{H}}_{\mathrm{IV}}\boldsymbol{\mathcal{X}}_{\bar{\mathbf{q}}_r}\right)\boldsymbol{\mathcal{H}}_{\mathrm{IV}}, \tag{5.8}$$

enquanto que um transceptor ZF multiportadoras possui uma estrutura descrita na Figura 5.1. Para mais informações, o leitor pode consultar a Seção E.2.

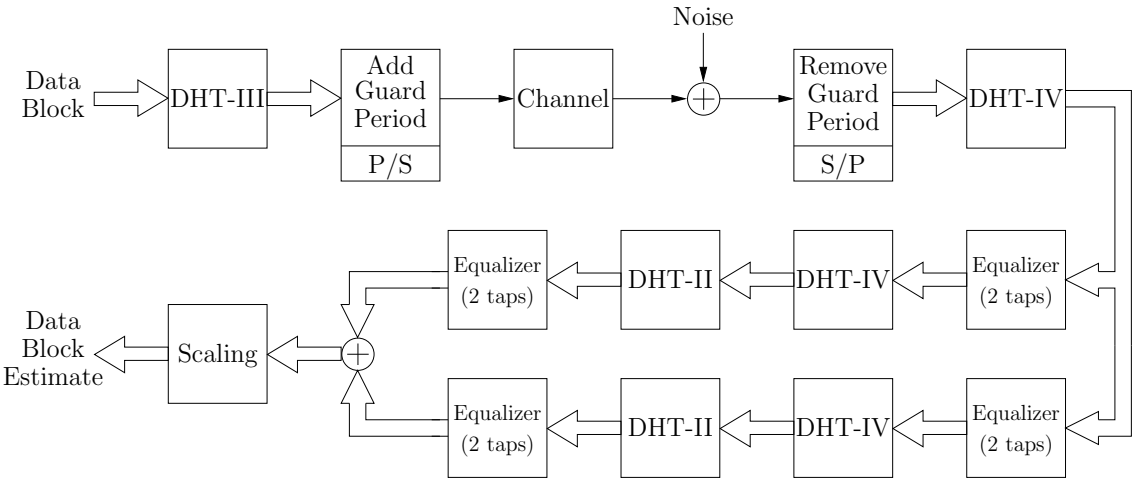

Figura 5.1: Transceptores multiportadoras em bloco com redundância mínima baseados em DHT.

5.3 Resultados das Simulações

Como exemplo de desempenho de nossas propostas em termos de *throughput*, considere a transmissão de 500 blocos contendo $M = 32$ símbolos QPSK por um canal de Rayleigh com $L = 20$. Assuma que 10.000 simulações foram realizadas e que a frequência de amostragem é $f_s = 500$ MHz. Além disso, assume-se também que o canal através do qual os sinais são transmitidos trabalha na mesma taxa de amostragem.

Tanto a parte real como a parte imaginária são realizações de processos estocásticos gaussianos brancos, com média zero e independentes. Todos os *taps* do canal possuem a mesma potência média e o canal é sempre normalizado, ou seja,

$\mathsf{E}[\|\mathbf{h}\|_2^2] = 1$. Uma nova realização do canal é gerada para cada uma das dez mil simulações. Devido à aleatoriedade na escolha dessas realizações, é muito provável que a quantidade de zeros côngruos do canal seja menor do que o comprimento da redundância, garantindo-se, assim, a existência de soluções ZF.

A definição de SNR adotada nas simulações é a razão entre a potência média de um símbolo do sinal transmitido (sinal de entrada do canal) e a potência média do ruído aditivo na entrada do receptor.

A definição de *throughput* é mesma qua já adotamos anteriormente, isto é

$$\text{Throughput} = br_c \frac{M}{M+K}(1 - \text{BLER})f_s, \tag{5.9}$$

onde $K = L/2 = 10$ (em sistemas com redundância mínima) ou $K = L = 20$ (em sistemas com redundância completa) e $r_c = 1/2$.

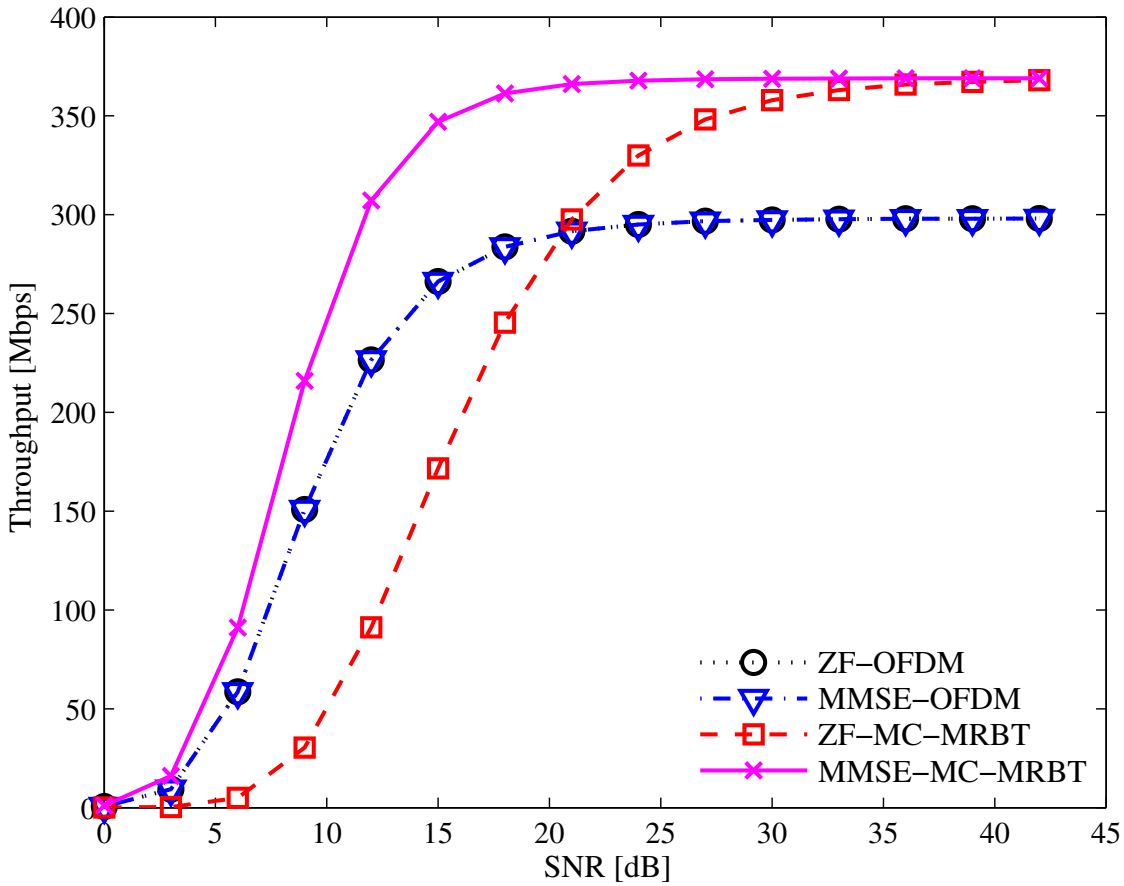

Figura 5.2: *Throughput* [Mbps] em função da SNR [dB], considerando transmissões multiportadoras (canal Rayleigh) baseadas em DHT ($M = 32$ e $L = 20$).

Os sistemas utilizados na transmissão são o tradicional ZP-OFDM-OLA, além dos sistemas propostos, a saber: MC-MRBT (do inglês, *multicarrier minimum-redundancy block transceiver*). Para cada um desses sistemas utilizam-se as soluções ZF e MMSE.

A Figura 5.2 contém os resultados relacionados a um sistema multiportadoras. É possível verificar um comportamento similar ao que foi obtido na caso de sistemas baseados em DFT. Com efeito, o sistema proposto MMSE-MC-MRBT possui um desempenho melhor do que a sua contraparte, MMSE-OFDM, o qual obteve exatamente o mesmo desempenho do ZF-OFDM. Já para os sistemas com redundância mínima do tipo ZF, eles são bastante vantajosos para SNRs acima de 20 dB.

Para mais informações, o leitor pode consultar a Seção E.3.

5.4 Conclusões

Neste capítulo nós propomos a utilização de transformadas discretas de Hartley em sistemas de transmissão em blocos com redundância mínima. As soluções ZF e MMSE empregam matrizes DHT, diagonais e antidiagonais, o que faz com que os novos transceptores sejam computacionalmente eficientes. Nossa abordagem baseia-se nas propriedades de matrizes estruturadas e utiliza os conceitos de *displacement* de Sylvester e de Stein. Foram derivadas novas representações baseadas em DHTs para inversas e pseudo-inversas de matrizes de Toeplitz. Uma característica marcante dos sistemas propostos é o fato de não haver restrições de simetria sobre a resposta ao impulso do canal, ao contrário do que ocorre em [23]. Os resultados das simulações demonstram que as soluções encontradas viabilizam a transmissão com taxas maiores.

Parte II

Sistemas com Redundância Reduzida

Capítulo 6

Transceptores com Redundância Reduzida Baseados em DFT

Este capítulo apresenta novos transceptores lineares invariantes no tempo que empregam uma quantidade reduzida de redundância para eliminar a interferência entre blocos. Tais propostas englobam sistemas multiportadoras e monoportadora com equalizadores ZF e MMSE. A quantidade de redundância varia desde a mínima, $\lceil L/2 \rceil$, até a mais comumente utilizada, L, assumindo um canal com resposta ao impulso de ordem L. Os transceptores resultantes permitem a equalização eficiente dos blocos de dados recebidos, uma vez que eles utilizam transformadas rápidas de Fourier e equalizadores com um único coeficiente em suas estruturas. O capítulo também inclui uma análise do MSE associado aos transceptores propostos com respeito à quantidade de redundância. De fato, nós demonstramos que, quanto maior for a quantidade de redundância transmitida, menor será o MSE de símbolos na recepção. Diversas simulações indicam que, se escolhermos uma quantidade adequada de redundância, então os transceptores propostos podem alcançar taxas de transmissão maiores do que os transceptores multiportadoras e monoportadora tradicionais. Tais ganhos são obtidos sem sacrificar a complexidade computacional assintótica associada ao processo de equalização.

Neste capítulo, nós consideramos o modelo ZP-ZJ [16, 41] que permite a transmissão com uma quantidade menor de redundância, mais ainda evitando a IBI. Na verdade, os transceptores ZP-ZJ com redundância mínima propostos em [23] podem ser considerados como o estado da arte neste tópico particular, o que naturalmente nos leva ao questionamento: por que investigar transceptores com redundância reduzida quando transceptores com redundância mínima já estão disponíveis? A resposta a tal questionamento bem como a estratégia para projetar esses novos transceptores são os tópicos centrais deste capítulo.

6.1 Redundância Reduzida *versus* Redundância Mínima

Considerando $M + K$ dados transmitidos com K zeros redundantes, temos os seguintes MSE de símbolos:

$$\mathrm{AMSE}^{\mathrm{MMSE}}(K, M) = \frac{\sigma_v^2}{M}\mathrm{tr}\left\{\left[\mathbf{H}_0^H(K, M)\mathbf{H}_0(K, M) + \rho\mathbf{I}_M\right]^{-1}\right\} \tag{6.1}$$

$$= \frac{\sigma_v^2}{M}\sum_{m\in\mathcal{M}}\frac{1}{\sigma_m^2(K, M) + \rho}, \tag{6.2}$$

$$\mathrm{AMSE}^{\mathrm{ZF}}(K, M) = \frac{\sigma_v^2}{M}\mathrm{tr}\left\{\left[\mathbf{H}_0^H(K, M)\mathbf{H}_0(K, M)\right]^{-1}\right\}$$

$$= \frac{\sigma_v^2}{M}\sum_{m\in\mathcal{M}}\frac{1}{\sigma_m^2(K, M)}. \tag{6.3}$$

Sendo assim, é possível mostrar que, para todo inteiro positivo K entre $L/2$ e L, tem-se:

$$\mathrm{AMSE}^{\mathrm{MMSE}}(K + 1, M) \leq \mathrm{AMSE}^{\mathrm{MMSE}}(K, M), \tag{6.4}$$

$$\mathrm{AMSE}^{\mathrm{ZF}}(K + 1, M) \leq \mathrm{AMSE}^{\mathrm{ZF}}(K, M). \tag{6.5}$$

O resultado acima mostra que o aumento de elementos redundantes transmitidos permite a redução do erro quadrático médio de tais transceptores. Para mais informações, o leitor pode consultar a Seção F.1.

6.2 Novas Decomposições de Matrizes Estruturadas Retangulares

6.2.1 Abordagem do *Displacement-Rank*

De forma similar à descrita na Subseção 4.1.3, se assumirmos que $\mathbf{X} \in \mathbb{C}^{M_1\times M_1}$ e $\mathbf{Y} \in \mathbb{C}^{M_2\times M_2}$ são duas matrizes de operação dadas, onde M_1 e M_2 são inteiros positivos, as transformações lineares [25]

$$\nabla_{\mathbf{X},\mathbf{Y}} : \mathbb{C}^{M_1\times M_2} \to \mathbb{C}^{M_1\times M_2}$$

$$\mathbf{U} \mapsto \nabla_{\mathbf{X},\mathbf{Y}}(\mathbf{U}) \triangleq \mathbf{XU} - \mathbf{UY}, \tag{6.6}$$

$$\Delta_{\mathbf{X},\mathbf{Y}} : \mathbb{C}^{M_1\times M_2} \to \mathbb{C}^{M_1\times M_2}$$

$$\mathbf{U} \mapsto \Delta_{\mathbf{X},\mathbf{Y}}(\mathbf{U}) \triangleq \mathbf{U} - \mathbf{XUY} \tag{6.7}$$

são extensões dos *displacements* de Sylvester and Stein para lidar com os casos de matrizes retangulares. Para mais informações, o leitor pode consultar a Subseção F.2.1.

6.2.2 *Displacement* das Matrizes de Receptores ZF e MMSE

Dadas as matrizes de operação $\mathbf{Z}_\xi \in \mathbb{C}^{M\times M}$ e $\mathbf{Z}_{1/\eta} \in \mathbb{C}^{(M+2K-L)\times(M+2K-L)}$, a matriz $\mathbf{K}_{\text{MMSE}} = (\mathbf{H}_0^H\mathbf{H}_0 + \rho\mathbf{I}_M)^{-1}\mathbf{H}_0^H$ possui a seguinte matriz de *displacement* $\nabla_{\mathbf{Z}_\xi,\mathbf{Z}_{1/\eta}}(\mathbf{K}_{\text{MMSE}}) = \mathbf{P}\mathbf{Q}^T$, em que

$$\mathbf{P} = \left[\rho\left(\mathbf{H}_0^H\mathbf{H}_0 + \rho\mathbf{I}_M\right)^{-1}\hat{\mathbf{P}}' \quad -\mathbf{K}_{\text{MMSE}}\hat{\mathbf{P}}\right]_{M\times 4}, \tag{6.8}$$

$$\mathbf{Q} = \left[\left(\mathbf{H}_0\mathbf{H}_0^H + \rho\mathbf{I}_{(M+2K-L)}\right)^{-T}\hat{\mathbf{Q}}' \quad \mathbf{K}_{\text{MMSE}}^T\hat{\mathbf{Q}}\right]_{(M+2K-L)\times 4}, \tag{6.9}$$

com $(\hat{\mathbf{P}},\hat{\mathbf{Q}}) \in \mathbb{C}^{(M+2K-L)\times 2}\times\mathbb{C}^{M\times 2}$ e $(\hat{\mathbf{P}}',\hat{\mathbf{Q}}') \in \mathbb{C}^{M\times 2}\times\mathbb{C}^{(M+2K-L)\times 2}$ sendo os pares geradores de *displacement* $\nabla_{\mathbf{Z}_{1/\eta},\mathbf{Z}_\xi}(\mathbf{H}_0)$ e $\nabla_{\mathbf{Z}_\xi,\mathbf{Z}_{1/\eta}}(\mathbf{H}_0^H)$, respectivamente. Para mais informações, o leitor pode consultar a Subseção F.2.2.

6.2.3 Representação de Bezoutianos Retangulares Baseada em DFT

Dados dois números complexos não-nulos η e ξ, e dados dois números naturais M_1 e M_2, assuma que $\mathbf{B}$ é uma matriz de Bézout de dimensão $M_2\times M_1$ tal que $\nabla_{\mathbf{Z}_\xi,\mathbf{Z}_{1/\eta}}(\mathbf{B}) = \mathbf{P}\mathbf{Q}^T$. O par gerador $(\mathbf{P},\mathbf{Q})$ está no conjunto $\mathbb{C}^{M_2\times R}\times\mathbb{C}^{M_1\times R}$, onde o número natural R é o posto da matriz de *displacement* de Sylvester. Assim, se $M_1 \geq M_2$, então

$$\mathbf{B} = \sqrt{M_1M_2}\mathbf{V}_{\boldsymbol{\xi}}^{-1}\left[\sum_{r=1}^{R}\text{diag}\{\bar{\mathbf{p}}_r\}\mathbf{W}_{M_2}\left[\text{diag}\{(\xi_0\eta_0)^{m_2}\}_{m_2=0}^{M_2-1} \quad \mathbf{0}_{M_2\times(M_1-M_2)}\right]\times\right.$$
$$\left.\times\,\mathbf{W}_{M_1}\text{diag}\{\bar{\mathbf{q}}_r\}\right]\mathbf{V}_{\boldsymbol{\eta}}^{-T}, \tag{6.10}$$

onde o vetor $\boldsymbol{\eta}$ de dimensão $M_1\times 1$ contém as raízes M_1-ésimas de η, i.e., para cada índice $m_1 \in \mathcal{M}_1 \triangleq \{0,1,\cdots,M_1-1\}$, tem-se $[\boldsymbol{\eta}]_{m_1} = \eta_{m_1} \triangleq \eta_0 W_{M_1}^{m_1}$, com $W_{M_1} \triangleq \text{e}^{-\jmath\frac{2\pi}{M_1}}$ e $\eta_0 \triangleq |\eta|^{1/M_1}\text{e}^{\jmath\frac{\angle\eta}{M_1}}$, enquanto que o vetor $\boldsymbol{\xi}$ de dimensão $M_2\times 1$ contém as raízes M_2-ésimas de ξ, i.e., para cada índice $m_2 \in \mathcal{M}_2 \triangleq \{0,1,\cdots,M_2-1\}$, tem-se

$[\boldsymbol{\xi}]_{m_2} = \xi_{m_2} \triangleq \xi_0 W_{M_2}^{m_2}$, com $\xi_0 \triangleq |\xi|^{1/M_2} \mathrm{e}^{\jmath \frac{\angle \xi}{M_2}}$. Além disso, temos que

$$\bar{\mathbf{P}} \triangleq [\, \bar{\mathbf{p}}_1 \ \cdots \ \bar{\mathbf{p}}_R \,] = -\mathbf{V}_{\boldsymbol{\xi}} \mathbf{P} \tag{6.11}$$

$$\bar{\mathbf{Q}} \triangleq [\, \bar{\mathbf{q}}_1 \ \cdots \ \bar{\mathbf{q}}_R \,] = \left(\mathrm{diag} \left\{ \frac{1}{1 - \xi \eta_{m_1}^{M_2}} \right\}_{m_1=0}^{M_1-1} \right) \mathbf{V}_{\boldsymbol{\eta}} \mathbf{Z}_{\eta} \mathbf{Q}, \tag{6.12}$$

onde assumimos que $\xi \eta_{m_1}^{M_2} \neq 1$, para todo $m_1 \in \mathcal{M}_1$.

Para mais informações, o leitor pode consultar a Subseção F.2.3.

6.3 Transceptores Eficientes com Redundância Reduzida Baseados em DFT

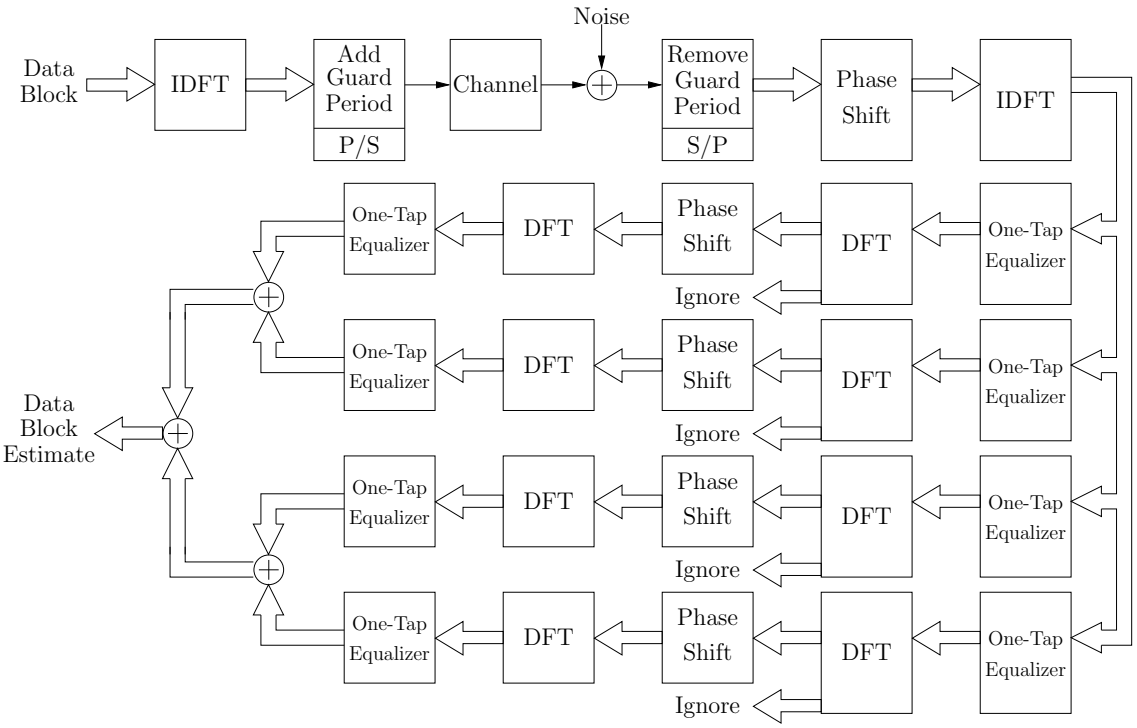

Figura 6.1: Transceptores multiportadoras em bloco com redundância reduzida baseados em DFT.

Aplicando-se a abordagem via *displacement rank*, é possível desenvolver decomposições eficientes para a matriz de recepção associada a sistemas com redundância reduzida baseados em DFT. Por exemplo, para um transceptor monoportadora, é

possível mostrar que:

$$\mathbf{F}_0 = \mathbf{I}_M \tag{6.13}$$

$$\mathbf{G}_0 = \mathbf{W}_M^H \left[\sum_{r=1}^{4} \mathbf{D}_{\bar{\mathbf{p}}_r} \mathbf{W}_M \begin{bmatrix} \mathbf{D}_M & \mathbf{0}_{M\times(2K-L)} \end{bmatrix} \mathbf{W}_{(M+2K-L)} \mathbf{D}_{\bar{\mathbf{q}}_r} \right] \mathbf{W}_{(M+2K-L)}^H \mathbf{D}_{(M+2K-L)}^H, \tag{6.14}$$

enquanto que para um transceptor multiportadoras, tem-se conforme descrito na Figura 6.1. Para mais informações, o leitor pode consultar a Seção F.3.

6.4 Resultados das Simulações

Como exemplo de desempenho de nossas propostas em termos de *throughput*, considere a transmissão de 50.000 blocos contendo $M = 16$ símbolos 64-QAM por um canal fixo com $L = 4$. Assuma que a frequência de amostragem é $f_s = 100$ MHz.

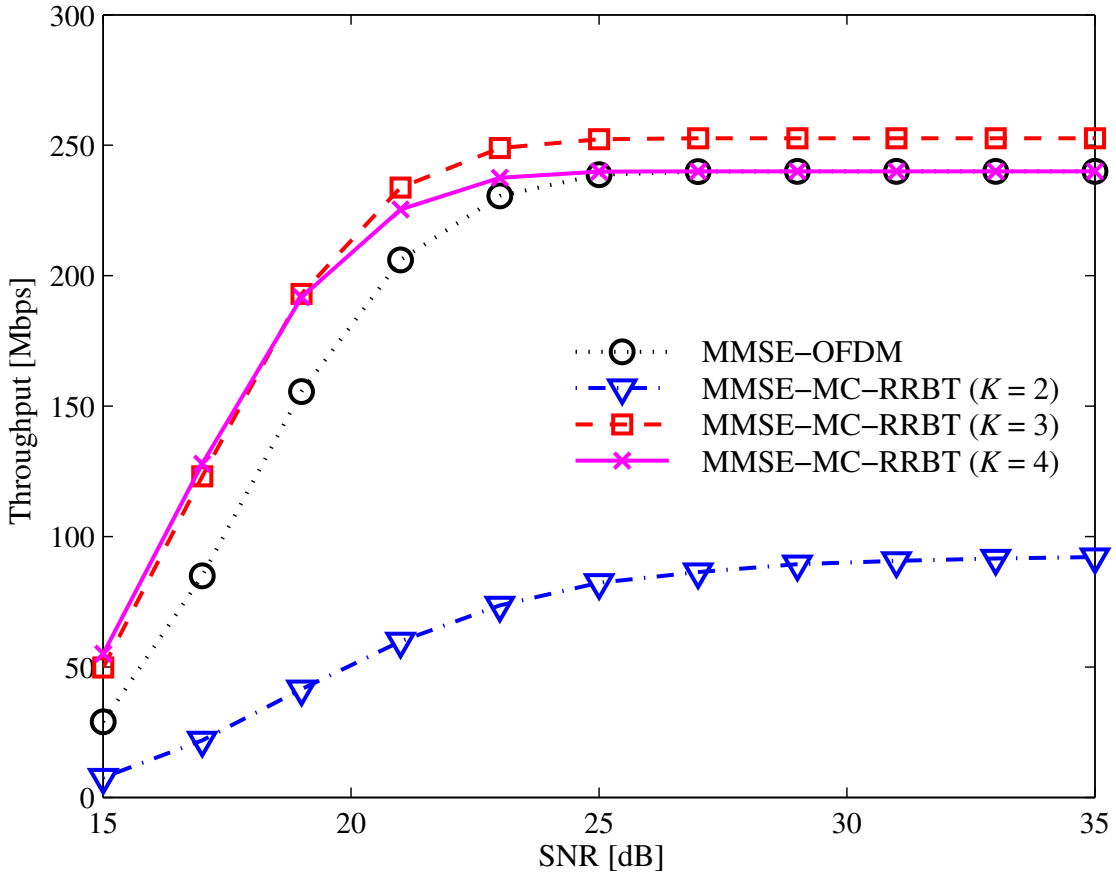

Figura 6.2: *Throughput* [Mbps] em função da SNR [dB], considerando transmissões multiportadoras com redundância reduzida baseadas em DFT ($M = 16$ e $L = 4$).

Os sistemas utilizados na transmissão são o tradicional ZP-OFDM-OLA, além dos sistemas propostos, a saber: MC-RRBT (do inglês, *multicarrier reduced-redundancy block transceiver*). Para cada um desses sistemas utiliza-se a solução

MMSE.

A Figura 6.2 contém os resultados relacionados a um sistema multiportadoras. É possível verificar que o sistema com redundância mínima ($K = 2$) não obteve um bom desempenho neste cenário de simulação. Entretanto, ao transmitirmos apenas um elemento redundante adicional, obtivemos uma melhora significativa, conforme ilustrado na figura ($K = 3$).

Para mais informações, o leitor pode consultar a Seção F.4.

6.5 Conclusões

Neste capítulo, nós propomos novos transceptores em bloco lineares e invariantes no tempo com redundâncias variando desde a mínima até a usualmente utilizada na prática, a qual coincide com o máximo *delay-spread* (em amostras) esperado para o modelo de canal. As propostas incluem soluções práticas de transceptores multiportadoras e monoportadora. As soluções ZF e MMSE requerem apenas DFTs, IDFTs e matrizes diagonais, de forma que os transceptores se tornam computacionalmente eficientes. As soluções foram obtidas novamente adequando os conceitos de *displacement* de Sylvester e Stein para lidar com matrizes estruturadas retangulares. Resultados teóricos mostraram pela primeira vez que o aumento na quantidade de redundância associada a sistemas ZP-ZJ pode trazer benefícios em termos de desempenho de MSE, mas, ao mesmo tempo, piora a eficiência espectral.

As simulações confirmam os resultados teóricos e mostram também que o desempenho relativo dos transceptores com redundância reduzida pode variar muito dependendo das características do modelo de canal. Nós acreditamos que os resultados deste capítulo respondem diversas questões em aberto relacionadas a inserção de redundância em sistemas em bloco.

Capítulo 7

Transceptores com Redundância Reduzida Baseados em DHT

Conforme mencionado no Capítulo 5, há várias vantagens em se utilizar transformadas reais em sistemas multiportadoras e monoportadora, quando comparados a sistemas que utilizam transformadas complexas. O Capítulo 6 introduziu os transceptores com redundância reduzida baseados em DFT, que é uma transformada complexa. Os resultados do Capítulo 6 podem ser utilizados juntamente com os resultados do Capítulo 5 com o intuito de derivar os transceptores com redundância reduzida baseados na transformada discreta de Hartley, que é uma transformada real.

Neste capítulo, nós propomos algumas possíveis estruturas para transceptores baseados em DHT com redundância reduzida. Começando a partir das derivações dos transceptores com redundância mínima baseados em DHT e dos transceptores com redundância reduzida baseados em DFT, nós podemos conceber as estruturas propostas para transceptores com redundância reduzida baseados em DHT através de adaptações dos resultados dos Capítulos 5 e 6.

7.1 Transceptores Eficientes com Redundância Reduzida Baseados em DHT

Mais uma vez, aplicando-se a abordagem via *displacement rank*, é possível desenvolver decomposições eficientes para a matriz de recepção associada a sistemas com redundância reduzida baseados em DHT. Por exemplo, para um transceptor mono-

portadora, é possível mostrar que

$$\mathbf{F}_0 = \mathbf{I}_M \tag{7.1}$$

$$\mathbf{G}_0 = \boldsymbol{\mathcal{H}}_{M,\mathrm{II}} \left[\sum_{r=1}^{4} \boldsymbol{\mathcal{X}}_{\bar{\mathbf{p}}_r} \boldsymbol{\mathcal{H}}_{M,\mathrm{III}} \begin{bmatrix} \mathbf{I}_M & \mathbf{0}_{M\times(2K-L)} \end{bmatrix} \boldsymbol{\mathcal{H}}_{(M+2K-L),\mathrm{I}} \boldsymbol{\mathcal{X}}_{\bar{\mathbf{q}}_r} \right] \boldsymbol{\mathcal{H}}_{(M+2K-L),\mathrm{I}}, \tag{7.2}$$

enquanto que um transceptor multiportadoras possui a estrutura descrita na Figura 7.1. Para mais informações, o leitor pode consultar a Seção G.1.

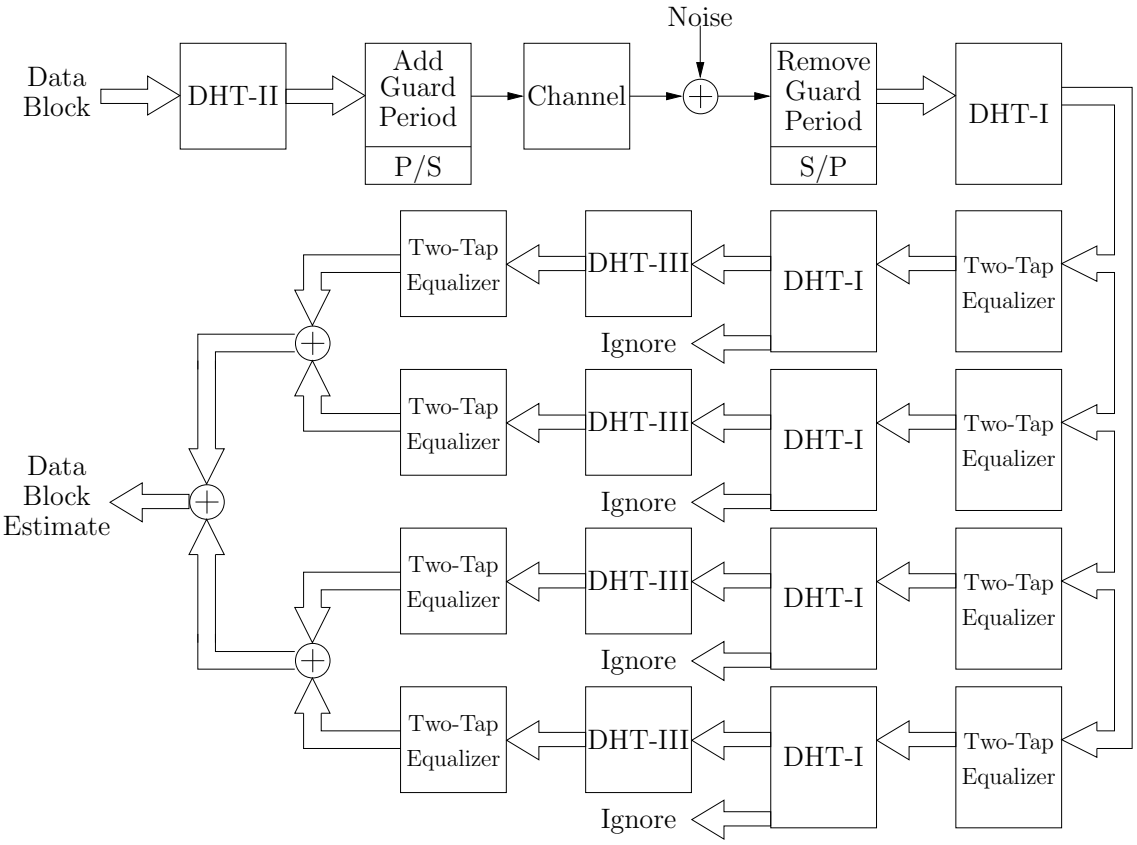

Figura 7.1: Transceptores multiportadoras em bloco com redundância reduzida baseados em DHT.

7.2 Resultados das Simulações

Como exemplo de desempenho de nossas propostas em termos de *throughput*, considere a transmissão de 50.000 blocos contendo $M = 16$ símbolos 64-QAM por um canal fixo com $L = 4$. Assuma que a frequência de amostragem é $f_s = 100$ MHz.

Os sistemas utilizados na transmissão são o tradicional ZP-OFDM-OLA, além dos sistemas propostos, a saber: MC-RRBT (do inglês, *multicarrier reduced-redundancy block transceiver*). Para cada um desses sistemas utiliza-se a solução

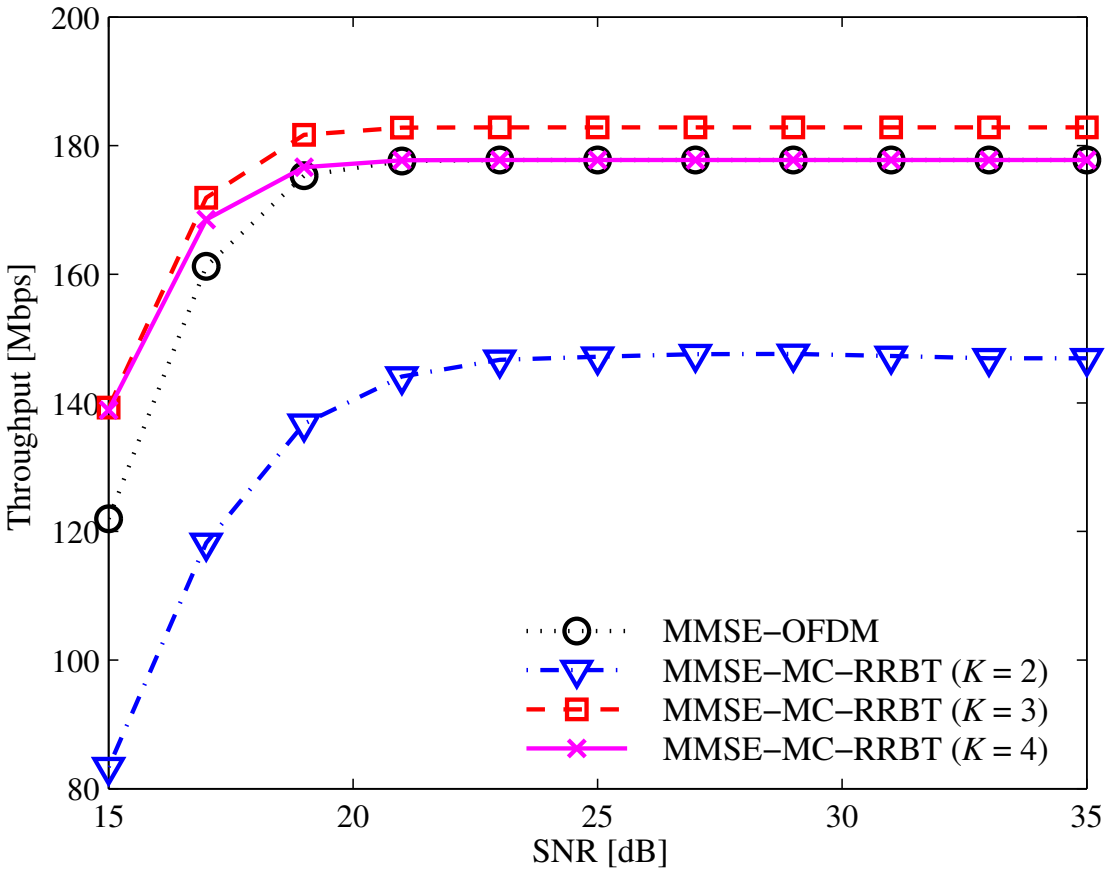

Figura 7.2: *Throughput* [Mbps] em função da SNR [dB], considerando transmissões multiportadoras com redundância reduzida baseadas em DHT ($M = 16$ e $L = 4$).

MMSE.

A Figura 7.2 contém os resultados relacionados a um sistema multiportadoras. É possível verificar que o sistema com redundância mínima ($K = 2$) não obteve um bom desempenho neste cenário de simulação. Entretanto, assim como ocorreu no caso de transceptores baseados em DFT, ao transmitirmos apenas um elemento redundante adicional, obtivemos uma melhora significativa, conforme ilustrado na figura ($K = 3$).

Para mais informações, o leitor pode consultar a Seção G.2.

7.3 Conclusões

Neste capítulo, propomos transceptores com redundância reduzida para transmissões em bloco. Mais especificamente, estendemos os resultados do Capítulo 7 utilizando agora transformadas discretas de Hartley no lugar de transformadas discretas de Fourier. As soluções ZF e MMSE empregam apenas matrizes DHTs e matrizes diagonais/antidiagonais. Tal característica faz com que os transceptores resultantes sejam computacionalmente eficientes. A abordagem adotada no capítulo passou por

adaptar os resultados relacionados a matrizes estruturadas descritos nos Capítulos 5 e 6. Os resultados das simulações reafirmam as boas propriedades em termos de taxa de transmissão dos transceptores propostos.

Parte III

Contribuições Adicionais

Capítulo 8

Alocação de Potência em Transceptores com Redundância Mínima

Observamos que, depois do processo de equalização, os transceptores com redundância reduzida poderiam eventualmente sofrer mais com ganhos de ruído do que transceptores tradicionais, tais como OFDM e SC-FD. (veja o Capítulo 4 de [23]). Isso ocorre por conta da dificuldade adicional em equalizar a matriz de Toeplitz efetiva de canal, a qual é induzida pelos transceptores com redundância mínima, quando comparada à matriz circulante associada aos sistemas OFDM e SC-FD [23]. Este fato nos motivou a realizar pesquisas neste tópico para minimizar esses ganhos de ruído.

Neste capítulo, consideramos um esquema onde transceptores em bloco com redundância mínima possuem conhecimento do canal no transmissor. Nós utilizamos tal conhecimento para distribuir a potência de transmissão disponível entre os símbolos. A alocação de potência é realizada objetivando minimizar os ganhos de ruído no receptor.

O método de alocação de potência proposto é implementado multiplicando cada símbolo a ser transmitido por um número real positivo. Tais números reais são soluções de um problema de otimização com restrições: minimizar a potência do vetor de ruído depois do processamento no receptor, sem modificar a potência média transmitida.

8.1 Alocação Ótima de Potência

Conforme já foi dito, queremos minimizar os ganhos de ruído no receptor sem aumentar de forma significativa o custo computacional na transmissão. Isso pode ser

traduzido no seguinte problema de otimização:

$$\min \sum_{m=0}^{M-1} t_m^2 \|\mathbf{g}_m\|_2^2 \,, \quad \text{sujeito a} \quad \sum_{m=0}^{M-1} t_m^{-2} = M, \tag{8.1}$$

em que $\mathbf{g}_m$ é a m-ésima linha da matriz de recepção $\mathbf{G}_0$.

O método de alocação ótima de potência que propomos é descrito na Figura 8.2, onde

$$t_m^* = \sqrt{\frac{\sum_{m'=0}^{M-1} \|\mathbf{g}_{m'}\|_2}{M\|\mathbf{g}_m\|_2}}, \quad \forall m \in \{0, 1, \cdots, M-1\}, \tag{8.2}$$

é a solução do problema de otimização descrito acima.

Para mais informações, o leitor pode consultar a Seção H.1.

8.2 Resultados das Simulações

Como exemplo de desempenho das propostas em termos de *throughput*, considere a transmissão de 100.000 blocos contendo $M = 16$ símbolos 16-QAM por um canal fixo com $L = 4$. Assuma que a frequência de amostragem é $f_s = 100$ MHz. A Figura 8.1 contém os resultados relacionados a um sistema multiportadoras. É possível verificar uma melhora significativa dos transceptores que utilizam a alocação de potência proposta (indicados pela letra "P" na legenda da figura).

Para mais informações, o leitor pode consultar a Seção H.2.

8.3 Conclusões

Neste capítulo, apresentamos um método de alocação de potência especialmente projetado para minimizar os ganhos de ruídos presentes em sistemas em bloco com redundância mínima. Os transceptores resultantes ainda requerem $\mathcal{O}(M \log_2 M)$ operações numéricas para equalizar um vetor recebido. Além disso, o desempenho em termos de taxa de transmissão apresenta melhoras, conforme indicado nos resultados das simulações.

O problema de alocar potência objetivando maximizar a capacidade do canal ainda é um problema em aberto e deve ser abordado em um trabalho futuro.

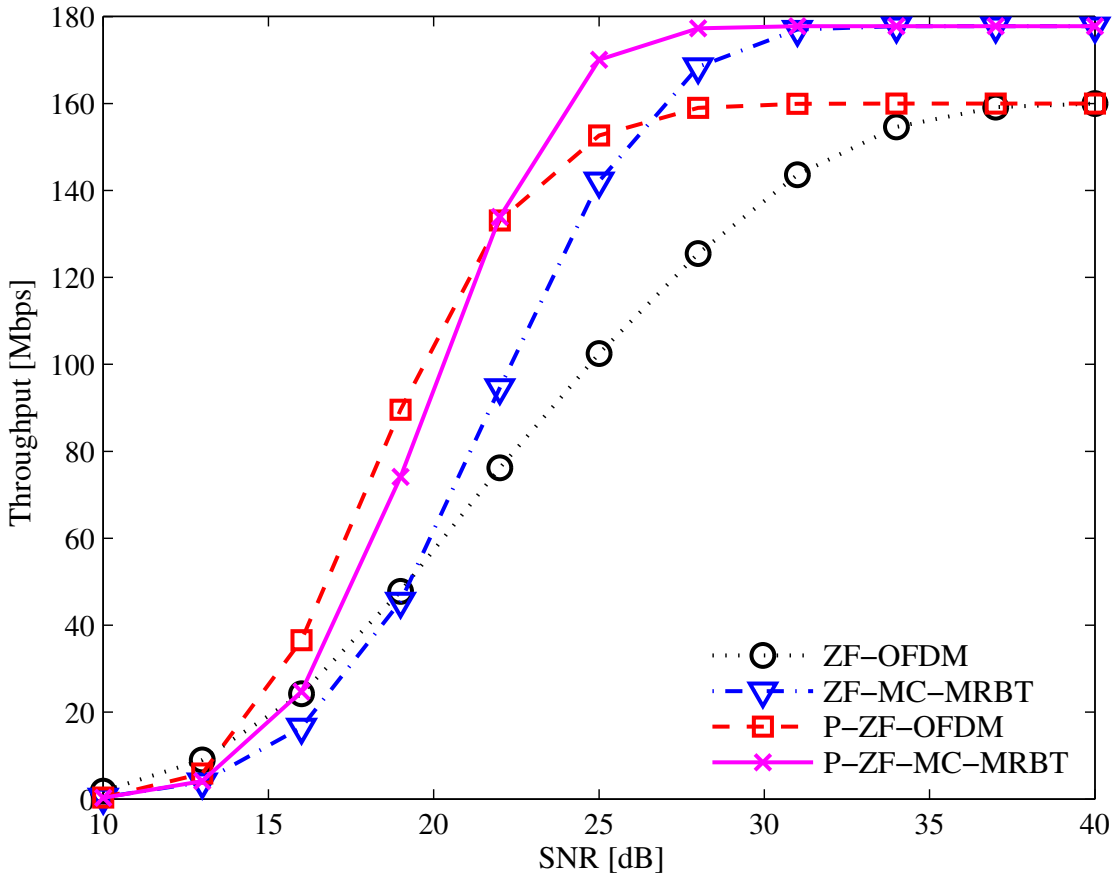

Figura 8.1: *Throughput* [Mbps] em função da SNR [dB], considerando transmissões multiportadoras com redundância mínima baseadas em DFT e com alocação de potência ($M = 16$ e $L = 4$).

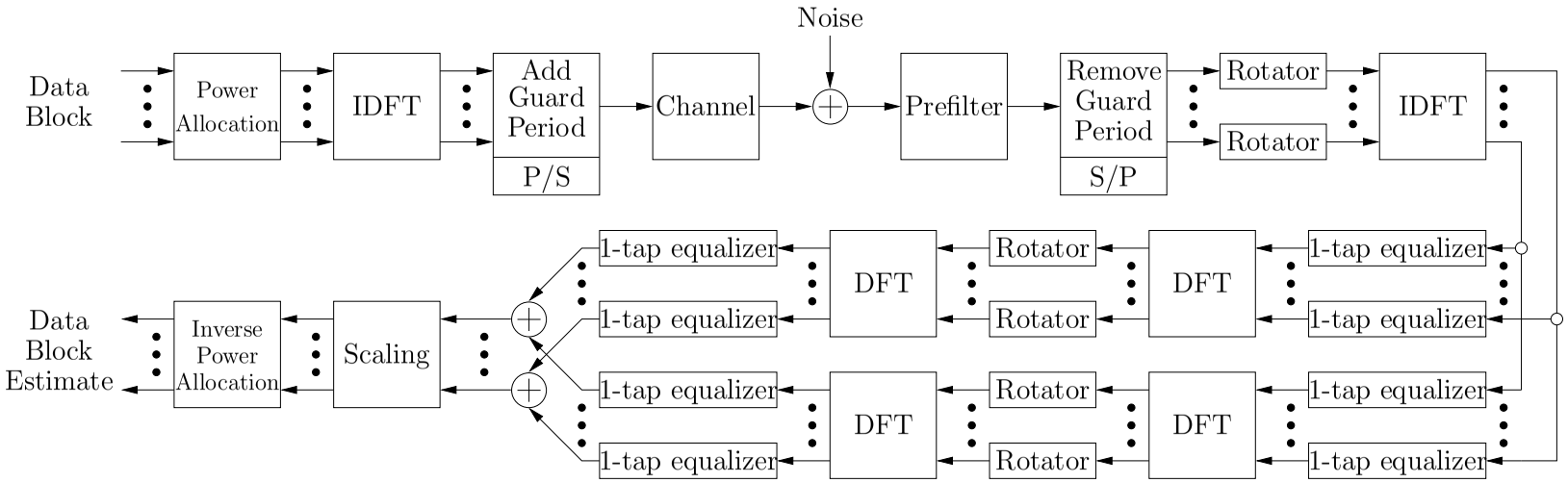

Figura 8.2: Transceptor ZF com redundância mínima e alocação de potência.

Capítulo 9

DFE em Blocos com Redundância Reduzida

A equalização desempenha um papel importante em qualquer esquema moderno de transmissão digital. Equalizadores lineares são ainda a escolha preferida em sistemas práticos devido às suas simplicidades computacionais. Entretanto, a melhora constante no desempenho de processadores digitais possibilitou o uso de equalizadores não-lineares também. As não-linearidades induzem certos graus de liberdade que não são explorados na equalização linear. Entre os receptores não-lineares, o DFE (do inglês, *decision-feedback equalizer*) [40, 50–52] está entre os mais populares devido ao bom compromisso atingido entre melhoria em desempenho e complexidade computacional.

Em comunicações modernas, é prática comum a segmentação dos dados em blocos que são transmitidos separadamente na transmissão em bloco. Tal separação em blocos é bastante útil em DFEs em blocos, uma vez que qualquer erro de deteção em um símbolo não é propagado por diferentes blocos de dados. Entretanto, a superposição indesejada de sinais inerente às comunicações em banda larga gera a IBI entre blocos adjacentes. A IBI pode ser eliminada transmitindo sinais redundantes, tais como sinais *zero-padded* ou prefixo cíclico [7, 40]. Entretanto, é necessário otimizar o uso de recursos espectrais em transmissões em banda larga. Uma possibilidade é atacar este problema reduzindo a quantidade de redundância requerida por transmissões em bloco para eliminar a IBI. Uma solução eficiente é empregar transceptores ZP-ZJ, os quais permitem a transmissão com redundância reduzida. Entretanto, apenas alguns poucos trabalhos empregam transceptores ZP-ZJ e todos consideram apenas equalizadores lineares.

Este capítulo mostra que técnicas ZP-ZJ podem ser aplicadas com sucesso no contexto de sistemas DFEs. Nós descrevemos como aplicar soluções MMSE e ZF conhecidas para sistemas DFEs em bloco dentro do contexto de redundância reduzida. O capítulo também inclui alguns resultados matemáticos que descrevem o compor-

tamento monótono de figuras de mérito relacionadas aos sistemas DFEs ZP-ZJ (tais como MSE de símbolos, informação mútua, probabilidade de erro de símbolos, etc). As análises propostas indicam que a redução na quantidade de redundância pode levar à uma degradação de desempenho de tais figuras de mérito, as quais não incluem o *throughput*. De fato, *throughput* pode aumentar ao reduzirmos a quantidade de sinais redundantes, conforme ficará claro nos resultados das simulações.

9.1 DFE com Redundância Reduzida

Nossa proposta para sistemas DFEs com redundância reduzida está ilustrada na Figura 9.1, em que

$$\mathbf{F} = \mathbf{V_H S}, \tag{9.1}$$

$$\mathbf{G} = \mathbf{R S}^H \mathbf{\Sigma}_\mathbf{H}^{-1} [\mathbf{I}_M \;\; \mathbf{0}_{M\times(2K-L)}] \mathbf{U}_\mathbf{H}^H, \tag{9.2}$$

$$\mathbf{B} = \mathbf{R} - \mathbf{I}_M, \tag{9.3}$$

onde as matrizes acima provêm de decomposições SVD da matriz de canal efetiva $\mathbf{H}$ e de decomposições QRS [40] de $\mathbf{\Sigma_H}$, como se segue:

$$\mathbf{H} = \begin{bmatrix} h(L-K) & \cdots & h(0) & 0 & 0 & \cdots & 0 \\ \vdots & \ddots & & & & & \vdots \\ h(K) & \ddots & & & & & 0 \\ \vdots & \ddots & & & \ddots & & h(0) \\ h(L) & & & & & & \vdots \\ 0 & & & & \ddots & & h(L-K) \\ \vdots & & & & & & \vdots \\ 0 & \cdots & 0 & 0 & h(L) & \cdots & h(K) \end{bmatrix} \in \mathbb{C}^{(M+2K-L)\times M}$$

$$= \underbrace{\mathbf{U_H}}_{(M+2K-L)\times(M+2K-L)} \underbrace{\begin{bmatrix} \mathbf{\Sigma_H} \\ \mathbf{0}_{(2K-L)\times M} \end{bmatrix}}_{(M+2K-L)\times M} \underbrace{\mathbf{V}_\mathbf{H}^H}_{M\times M}, \tag{9.4}$$

$$\mathbf{\Sigma_H} = \sqrt[M]{\prod_{m=0}^{M-1} \sigma_m} \mathbf{Q R S}^H. \tag{9.5}$$

Neste caso $\mathbf{\Sigma_H} = \mathbf{\Sigma}_\mathbf{H}^H > O$ é uma matriz diagonal $M \times M$ contendo os M valores singulares de $\mathbf{H}$. Além disso, $\mathbf{Q}$ e $\mathbf{S}$ são matrizes unitárias de dimensão $M \times M$, enquanto que $\mathbf{R}$ é uma matriz triangular superior $M \times M$ contendo apenas 1s em sua diagonal.

Para mais informações, o leitor pode consultar a Seção I.1.

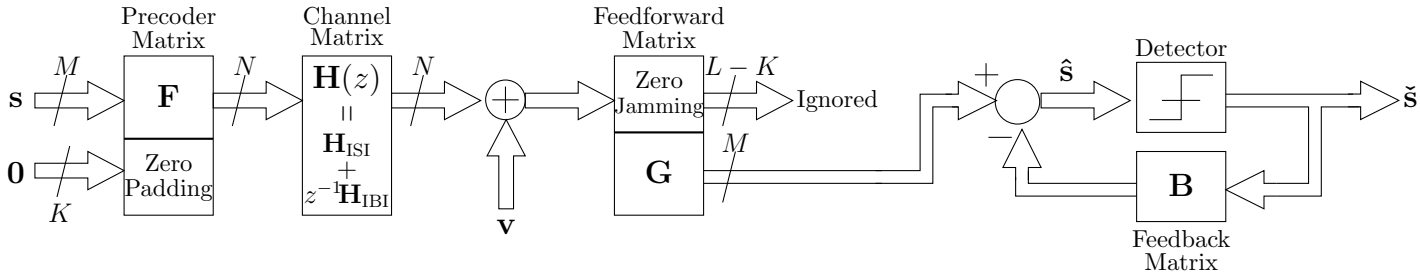

Figura 9.1: Estrutura geral dos sistemas DFE ZP-ZJ propostos.

9.2 Análise de Desempenho

Em termos de desempenho, para cada $m \in \{0, 1, \cdots, M-1\}$, assuma que exista uma função $f_m : \mathbb{R}_+ \to \mathbb{R}$ tal que o desempenho dos transceptores DFEs com redundância reduzida possa ser quantificado pela função $\mathcal{J} : \{\lceil L/2 \rceil, \lceil L/2 \rceil + 1, \cdots, L\} \to \mathbb{R}$ definida por

$$\mathcal{J}(K) \triangleq \frac{1}{M} \sum_{m=0}^{M-1} f_m(\sigma_m(K)) \;\text{ ou }\; \mathcal{J}(K) \triangleq \sqrt[M]{\prod_{m=0}^{M-1} f_m(\sigma_m(K))}. \tag{9.6}$$

Se f_m é monótona crescente para todo m, então $\mathcal{J}(K+1) \geq \mathcal{J}(K)$, para todo K. Analogamente, se f_m é monótona decrescente para todo m, então $\mathcal{J}(K+1) \leq \mathcal{J}(K)$, para todo K.

Para mais informações, o leitor pode consultar a Seção I.2.

9.3 Resultados das Simulações

Como exemplo de desempenho de nossas propostas em termos de *throughput*, considere a transmissão de 10.000 blocos contendo $M = 16$ símbolos 16-QAM por um canal fixo com $L = 5$. Assuma que a frequência de amostragem é $f_s = 400$ MHz. A Figura 9.2 contém os resultados relacionados a um sistema multiportadoras.

Para mais informações, o leitor pode consultar a Seção I.3.

9.4 Conclusões

Neste capítulo, propomos transceptores ZP-ZJ com realimentação de decisão (DFE). Tais transceptores possuem um bom compromisso entre desempenho e taxa de transmissão, viabilizando a otimização dos recursos espectrais em sistemas de banda larga. A redundância presente em tais transceptores pode variar da mínima, $L/2$, até a máxima, L. Algumas ferramentas para a análise de desempenho (em termos de MSE, informação mútua, probabilidade de erro de símbolos, etc) tais transceptores

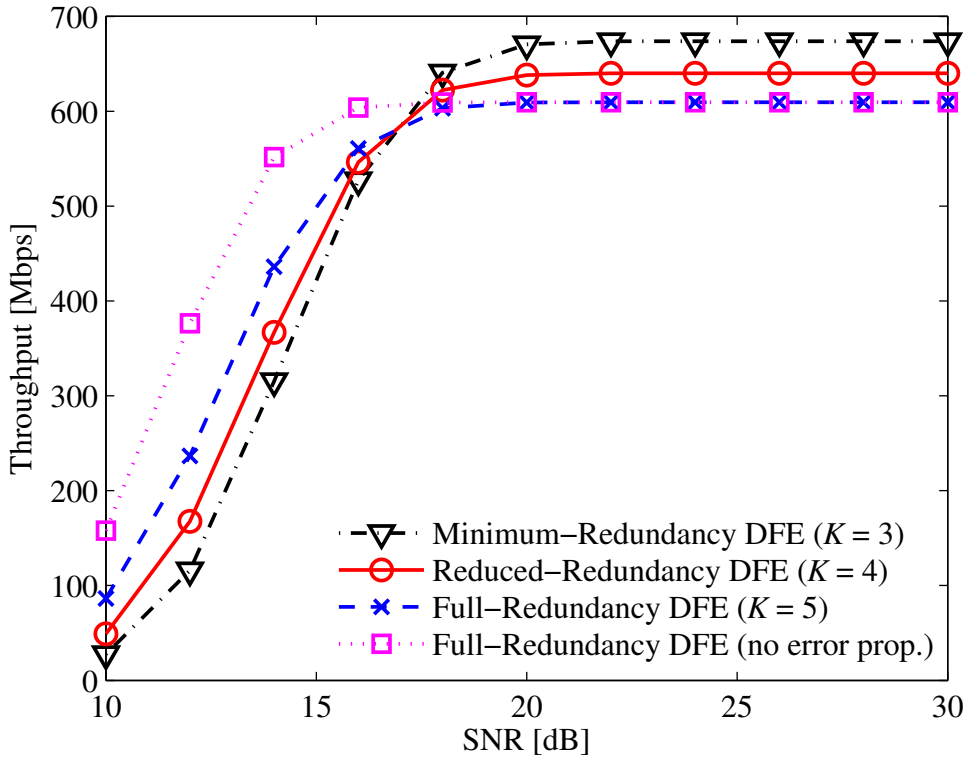

Figura 9.2: *Throughput* [Mbps] em função da SNR [dB] para sistemas DFEs.

também foram propostas.

A principal conclusão deste capítulo é que transceptores ZP-ZJ do tipo DFE permitem o aumento do *throughput*, conforme indicado nas simulações. Esta pesquisa ainda está em seu estado inicial, consistindo apenas de resultados preliminares. Uma linha interessante de pesquisa futura é o desenvolvimento de algoritmos eficientes para implementar as soluções não-lineares propostas.

Capítulo 10

Projeto de Transceptores com Redundância Mínima

Na Parte I desta tese, propomos transceptores multiportadoras e monoportadora em blocos com redundância mínima, os quais podem ser boas alternativas aos tradicionais sistemas OFDM e SC-FD. Conforme ressaltado anteriormente, tais transceptores com redundância mínima podem alcançar taxas de transmissão maiores do que sistemas OFDM e SC-FD, requerendo a mesma complexidade computacional para a equalização, $\mathcal{O}(M \log_2 M)$, para M símbolos. Entretanto, as propostas de tais transceptores se baseavam na hipótese de que o canal já era conhecido no receptor. Além disso, eles também assumiam que os equalizadores já haviam sido previamente projetados, focando no problema de equalização apenas.

O propósito deste capítulo é apresentar alguns resultados teóricos relacionados ao projeto de equalizadores com redundância mínima, sem assumir o conhecimento prévio do canal. Mais precisamente, neste capítulo mostramos como estimar o canal quando sistemas com redundância mínima são empregados e como utilizar tal estimativa para resolver os sistemas de equações lineares que definem os equalizadores. O resultado principal deste capítulo mostra que é possível projetar tais equalizadores com base em informações de piloto e usando algoritmos iterativos que requerem $\mathcal{O}(M \log_2 M)$ operações por iteração. Vale a pena ressaltar que as propostas deste capítulo são resultados preliminares de uma pesquisa que ainda está em processo, mas que não é o foco principal desta tese.

10.1 Estimação de Canal Assistida no Domínio do Tempo

No caso monoportadora, a estimação de canal no domínio do tempo pode ser feita utilizando a expressão

$$\hat{\mathbf{h}} = \left(\mathbf{R}^H\mathbf{R} + \rho\mathbf{I}_{(L+1)}\right)^{-1}\mathbf{R}^H\mathbf{y}, \tag{10.1}$$

em que $\mathbf{R} \in \mathbb{C}^{M\times(L+1)}$ é uma matriz de Toeplitz contendo os sinais piloto. A primeira linha de $\mathbf{R}$ é $[\,r(L/2) \;\; r(L/2-1) \;\; \cdots \;\; r(0) \;\; \mathbf{0}_{1\times L/2}\,]$ e a primeira coluna é $[\,r(L/2) \;\; \cdots \;\; r(M-1) \;\; \mathbf{0}_{1\times L/2}\,]^T$. Além disso, o vetor $\mathbf{h} \in \mathbb{C}^{(L+1)\times 1}$ contém os coeficientes da resposta ao impulso do canal. O vetor $\mathbf{y}$ contém os sinais recebidos no receptor.[1]

Para mais informações, o leitor pode consultar a Seção J.1.

10.2 Projeto do Equalizador Utilizando Iterações de Newton

O projeto do equalizador está intimamente ligado a inversões de matrizes, as quais podem ser implementadas utilizando iterações de Newton. De fato, defina a função

$$\begin{aligned} f_{\mathbf{X}} \,:\, \mathbb{C}^{M\times M} &\to \mathbb{C}^{M\times M} \\ \mathbf{U} &\mapsto \mathbf{U} - \mathbf{X}^{-1}, \end{aligned} \tag{10.2}$$

onde $\mathbf{X} \in \mathbb{C}^{M\times M}$ é uma matriz inversível, cuja inversa queremos determinar. É possível mostrar que as iterações de Newton melhoram uma aproximação inicial $\mathbf{U}_0 \in \mathbb{C}^{M\times M}$ para a inversa de $\mathbf{X}$ utilizando a seguinte recursão [25, 53]:

$$\mathbf{U}_{i+1} = \mathbf{U}_i(2\mathbf{I} - \mathbf{X}\mathbf{U}_i), \tag{10.3}$$

para $i \in \mathbb{N}$.

Para mais informações, o leitor pode consultar a Seção J.2.

[1] A estimação descrita nesta seção é uma alternativa à forma usual de estimação utilizando sinais piloto, no domínio da frequência, em sistemas (CP, por exemplo) que induzem uma matriz de canal circulante.

10.3 Heurísticas Alternativas para o Projeto de Equalizadores

10.3.1 Algoritmo PCG

A ideia de algoritmos PCG (do inglês, *preconditioned conjugate gradient*) é solucionar problemas da forma $\mathbf{H}_0\mathbf{p} = \hat{\mathbf{p}}$ resolvendo o problema equivalente $\boldsymbol{\mathcal{P}}^{-1}\mathbf{H}_0\mathbf{p} = \boldsymbol{\mathcal{P}}^{-1}\hat{\mathbf{p}}$, que é melhor condicionado que o problema original, usando algoritmos de gradiente conjugado [54]. A matriz $\boldsymbol{\mathcal{P}}$ é a matriz de precondicionamento e deve ser mais fácil de inverter do que a matriz $\mathbf{H}_0$ e, ao mesmo tempo, deve ser uma boa aproximação para $\mathbf{H}_0^{-1}$, isto é, $\boldsymbol{\mathcal{P}}^{-1}\mathbf{H}_0 \approx \mathbf{I}$ [54]. Como todas as matrizes envolvidas são estruturadas, tais algoritmos podem ser implementados de forma eficiente.

Para mais informações, o leitor pode consultar a Subseção J.3.1.

10.3.2 Algoritmo Dividir-e-Conquistar

A ideia de aplicar algoritmos dividir-e-conquistar no contexto de projeto dos equalizadores é simplificar a inversão de matrizes do tipo Toeplitz. De fato, dada uma matriz de Toeplitz $\mathbf{T} \in \mathbb{C}^{M\times M}$, temos [19, 25, 55]:

$$\mathbf{T} = \begin{bmatrix} \mathbf{T}_{00} & \mathbf{T}_{01} \\ \mathbf{T}_{10} & \mathbf{T}_{11} \end{bmatrix} = \begin{bmatrix} \mathbf{I} & \mathbf{0} \\ \mathbf{T}_{10}\mathbf{T}_{00}^{-1} & \mathbf{I} \end{bmatrix} \begin{bmatrix} \mathbf{T}_{00} & \mathbf{0} \\ \mathbf{0} & \mathbf{S} \end{bmatrix} \begin{bmatrix} \mathbf{I} & \mathbf{T}_{00}^{-1}\mathbf{T}_{01} \\ \mathbf{0} & \mathbf{I} \end{bmatrix}, \tag{10.4}$$

em que $\mathbf{S} = \mathbf{T}_{11} - \mathbf{T}_{10}\mathbf{T}_{00}^{-1}\mathbf{T}_{01} \in \mathbb{C}^{\frac{M}{2}\times\frac{M}{2}}$ é o complemento de Schur da matriz $\mathbf{T}_{00}$ na matriz $\mathbf{T}$ [19]. É possível verificar que [19, 25, 55]:

$$\mathbf{T}^{-1} = \begin{bmatrix} \bar{\mathbf{T}}_{00} & \bar{\mathbf{T}}_{01} \\ \bar{\mathbf{T}}_{10} & \bar{\mathbf{T}}_{11} \end{bmatrix} = \begin{bmatrix} \mathbf{I} & -\mathbf{T}_{00}^{-1}\mathbf{T}_{01} \\ \mathbf{0} & \mathbf{I} \end{bmatrix} \begin{bmatrix} \mathbf{T}_{00}^{-1} & \mathbf{0} \\ \mathbf{0} & \mathbf{S}^{-1} \end{bmatrix} \begin{bmatrix} \mathbf{I} & \mathbf{0} \\ -\mathbf{T}_{10}\mathbf{T}_{00}^{-1} & \mathbf{I} \end{bmatrix}. \tag{10.5}$$

Podemos trabalhar de forma recursiva com tais expressões para calcular a inversa de $\mathbf{T}$ de forma eficiente. Para mais informações, o leitor pode consultar a Subseção J.3.2.

10.4 Conclusões

Neste capítulo, propomos novos métodos para o projeto dos coeficientes dos equalizadores presentes em sistemas com redundância mínima. As novas propostas são baseadas em transmissão de sinais piloto e requerem apenas $\mathcal{O}(M \log_2 M)$ para estimar o modelo de canal no domínio do tempo. Além disso, as novas propostas também empregam algoritmos iterativos que requerem $\mathcal{O}(M \log_2 M)$ operações por

iteração. Estes são resultados teóricos preliminares de uma pesquisa que ainda está em progresso, mas que não é a linha central de investigação da presente tese.

Capítulo 11

Conclusão

Neste trabalho, propomos soluções práticas e efetivas para transceptores multiportadoras e monoportadora usando redundância mínima, ou mais geralmente, redundância reduzida. As respectivas soluções ZF e MMSE empregam apenas DFTs, IDFTs e matrizes diagonais, ou DHTs e matrizes diagonais e antidiagonais. Tais características fazem com que os novos transceptores sejam computacionalmente eficientes. A abordagem adotada baseia-se nas propriedades de matrizes estruturadas usando os conceitos de *displacement* de Sylvester e Stein. Tais conceitos tem como objetivo explorar as propriedades estruturais de representações típicas de matrizes de canais, tais como matrizes de Toeplitz, de Vandermonde e de Bézout. Utilizando propriedades adequadas inerentes à abordagem de *displacement rank*, fomos capazes de derivar novas decomposições de bezoutianos generalizados baseadas em DFT e DHT. Essas novas decomposições foram a chave para as propostas de transceptores multiportadoras e monoportadora em bloco que utilizam redundância mínima/reduzida.

Simulações mostraram que os transceptores propostos podem alcançar taxas de transmissão maiores do que sistemas baseados em OFDM e SC-FD, especialmente quando canais longos são utilizados. A complexidade computacional utilizada no processo de equalização permanece sendo $\mathcal{O}(M \log_2 M)$.

11.1 Contribuições

Segue-se uma lista mais específica contendo as inovações desta tese:

- Foi desenvolvida uma análise matemática completa sobre o MSE e a informação mútua presente em transceptores em bloco com redundância completa que empregam *zero-padding*;

- Foi proposta uma modificação nas soluções MMSE com redundância mínima descrita em [23]. De fato, as novas estruturas propostas são mais simples do que aquelas propostas em [23], uma vez que elas empregam apenas quatro

ramos de equalização paralelos, enquanto que as propostas de [23] utilizam cinco ramos;

- Foram propostos novos equalizadores MMSE subótimos com redundância mínima que requerem a mesma quantidade de operações de equalizadores ZF;
- Foram propostos novos transceptores com redundância mínima baseados em DHT. Tais transceptores não impõem nenhuma restrição de simetria sobre a resposta ao impulso do canal, ao contrário do que foi feito em [23];
- Foram apresentados novos transceptores com redundância reduzida baseados em DFTs;
- Foram apresentados novos transceptores com redundância reduzida baseados em DHTs;
- Foi desenvolvida uma análise do MSE relacionado aos transceptores propostos com redundância reduzida com respeito à quantidade de redundância. De fato, nós demonstramos que quantidades maiores de redundância levam a MSEs de símbolos menores;
- Foi desenvolvido um método de alocação de potência que permite minimizar os ganhos de ruído quando há conhecimento do modelo de canal no transmissor;
- Foram propostos novos sistemas DFEs em blocos com redundância reduzida;
- Foram propostos alguns métodos de projeto dos equalizadores com redundância mínima com base em pilotos e usando algoritmos iterativos eficientes [25, 53, 56] que utilizam $\mathcal{O}(M \log_2 M)$ operações por iteração. Outra abordagem proposta foi a aplicação de algoritmos do tipo dividir-e-conquistar [25, 55] para o projeto dos equalizadores.

11.2 Sugestões de Trabalhos Futuros

Segue-se uma lista de possíveis trabalhos futuros:

- Desenvolver transceptores variantes no tempo que sigam as mesmas linhas dos sistemas com redundância reduzida propostos nesta tese. Transceptores variantes no tempo permitem a transmissão com apenas um elemento redundante, independentemente da ordem do modelo de canal, conforme descrito em [57];
- Desenvolver versões MIMO de transceptores com redundância reduzida para lidar com sistemas com diversidade espaço-temporal, conformação de feixes e multiplexação espacial;

- Desenvolver esquemas de múltiplo acesso baseados nas propostas desta tese;
- Estudar problemas de desbalanceamento I/Q em transceptores com redundância reduzida;
- Estudar o efeito de CFO, bem como formas de diminuir tais efeitos em transceptores com redundância reduzida.

Apêndice A

Introduction

A significant part of physical- and link-layer research in communication systems focuses on either developing new methods or enhancing the existing ones in order to increase throughput [1–4]. From a practical point of view, these investigations should always take into account the fundamental trade-off between performance gains and cost effectiveness.[1] The computational complexity[2] is amongst the factors that directly affects the cost effectiveness of new advances in communications. This explains why linear transceivers are still preferred in several practical applications [5, 6].

Nowadays, most telecommunication specifications recommend the segmentation of data in blocks before starting the transmission. The resulting data blocks are usually transmitted separately in the so-called block-based transmission. Due to the characteristic of frequency selectivity inherent to broadband communications, there is a superposition of attenuated versions of the transmitted signal. This superposition, called intersymbol interference (ISI), is induced among the symbols that compose a given data block. The undesired superposition of signals also generates interblock interference (IBI) between adjacent transmitted data blocks.

The orthogonal frequency-division multiplexing (OFDM) is the most popular memoryless linear time-invariant (LTI) block-based transceiver that circumvents the IBI problem by inserting redundancy in the transmission. In addition, the redundancy leads to the elimination of ISI or the minimization of the mean-square error (MSE) of symbols at the receiver end [7–13]. Whether the redundancy consists of cyclic prefix (CP) or zero padding (ZP), simple equalizer structures can always be induced. However, the OFDM has some drawbacks, such as high peak-to-average power ratio (PAPR), high sensitivity to carrier-frequency offset (CFO), and (possibly) significant loss on spectral efficiency due to the redundancy inser-

[1] In this work, performance improvements mean higher throughputs, whereas low costs mean low power consumption and easy-to-implement characteristics.

[2] Total amount of complex-valued additions and multiplications.

tion. The single-carrier with frequency-domain (SC-FD) equalization technique is an efficient way to reduce both PAPR and CFO as compared to the OFDM system. These advantages are attained without changing the overall complexity of the transceiver [14, 15].

Regarding the spectral-resource usage, the amount of redundancy employed in both OFDM and SC-FD systems depends on the delay spread of the channel, implying that both transceivers waste the same bandwidth on redundant data. Nevertheless, there are many ways to increase the spectral efficiency of communication systems, such as by decreasing the overall symbol-error probability in the physical layer, so that less redundancy needs to be inserted in upper-layers by means of channel coding. In general, this approach increases the costs in the physical layer, since it leads to more computationally complex transceivers, hindering its implementation in some practical applications.

Other means to improve spectral efficiency are, therefore, highly desirable. Reducing the amount of transmitted redundancy inserted in the physical layer is a possible solution. Just few works had proposed decreasing the redundancy while constraining the transceiver to employ superfast algorithms [16, 17]. One of the most successful proposals comes from the pioneering paper [16]. The approach adopted in [16] relies on both the zero-padding (ZP) and the zero-jamming (ZJ) techniques to eliminate IBI employing a reduced amount of redundancy along with fast Fourier transform (FFT) algorithms. Nonetheless, the resulting designs do not have well-defined structures and their computational complexity associated with the equalization process depends quadratically on the channel order. For long channels, the transceivers in [16] may require much more computations than those proposed in this work, as will be clearer later on. Besides, the proposals from [16] are originally multicarrier systems only. On the other hand, the strategy in [17] is to transmit redundant information in the unused subcarriers, that is, the subcarriers that will be discarded in the case of channel loading. By exploiting these unused subcarriers it is possible to achieve zero-forcing equalization without sending redundant information in useful subcarriers. Usually, the number of unused subcarriers should be at least as large as the channel order, restricting its application.

There are other works that had also proposed to transmit data incorporating reduced redundancy, without focusing on the computational simplicity. The capacity-approaching block-based transceivers with reduced redundancy proposed in [18], for instance, entail high computational burden, since they are based on general singular-value decompositions (SVDs) of the involved matrices.

Besides, some works had applied the displacement rank theory successfully in the context of digital signal processing [19]. In communication systems, superfast algorithms were applied to pilot-based channel estimation schemes employing L

(channel order) redundant elements [20]. The resulting algorithms are suitable for detection and estimation of the nonzero taps of a given channel impulse response [20, 21]. It is worth mentioning that, even though the decomposition for the inverse of a given nonsingular Hermitian Toeplitz matrix [22] used in [20] is equivalent to the decomposition found in Theorem 1 of [23], for the particular case of Hermitian Toeplitz matrix, such decompositions cannot be applied to the minimum redundant MMSE-based receivers. The reason is that the proposed transceivers with minimum redundancy do not induce a Toeplitz structure in the channel correlation matrix, as in [20]. This property originated the proposals of new generalized-Bezoutian decompositions in Theorem 2 of [23]. As indicated in [23], these new decompositions stem from adaptations of results taken from [24].

A.1 Purpose of This Work

This work aims at proposing new structures for block-based transceivers with reduced redundancy. Such new structures must allow one to equalize the received data blocks efficiently. In other words, the structures are constrained to use only superfast algorithms [25]. Indeed, we employ only discrete Fourier transforms and discrete Hartley transforms along with one/two-tap equalizers in the transceiver structures in order to satisfy the aforementioned computational-complexity constraints.[3]

It is worth highlighting that there are plenty of work to be continued, since a number of relevant issues related to the proposed structures are not fully addressed yet. In fact, we focus on the equalization process rather than on other practical aspects, such as channel estimation, equalizer design, I/Q imbalance, CFO estimation, just to mention a few.[4]

A.2 Organization

We have divided the contributions of this thesis into three main parts: Part I (which includes Chapters C, D, and E) describes novel contributions to minimum-redundancy transceivers; Part II (which includes Chapter F and G) describes some key contributions to reduced-redundancy systems, whose amount of redundancy is greater than the minimum; and Part III (which includes Chapter H, I, and J) deals with some additional proposals which are rather important in practical systems, but that are not on the main research stream of this thesis.

[3]The only exception is the proposed DFE system with reduced redundancy, for which we have not developed superfast structures (see Chapter I).

[4]Even though such issues are not our focus, we did develop some algorithms for channel estimation and equalizer design, as one can verify in Part III.

In Chapter B, the main concepts related to the modeling of transceivers using filter banks are revised before starting with the novel contributions of this thesis (Parts I, II, and III). In order to do that, we first describe briefly both multirate and filter-bank systems. After that, the transmultiplexer (TMUX) is mathematically modeled in time-domain and through polyphase decompositions. The chapter ends with a description of memoryless TMUXes, highlighting the particular cases of OFDM and SC-FD systems, as well as the block-based transceivers with reduced redundancy.

Chapter C analyzes both the MSE and the mutual information in block-based transceivers with full-redundancy that employ zero-padding. We consider both linear transceivers and decision-feedback equalizers (DFEs) that minimize the MSE of symbols. These systems may enjoy the zero-forcing property or not, and may use unitary precoder or not. We demonstrate mathematically that the MSE/mutual information related to these transceivers are: (i) monotone increasing/decreasing functions of the number of transmitted symbols per block; (ii) monotone decreasing/increasing functions of the number of redundant data used in the equalization process of a block; and (iii) increased/decreased whenever non-minimum phase channels are utilized, instead of their minimum phase counterparts, assuming that one does not use the whole received data block to estimate the transmitted signal. As consequence of the former results, we also prove that, for both DFE and minimum error-probability systems, the average error-probability of symbols maintains the same monotonic behavior as the average MSE of symbols.

In [23], we have proposed practical zero-forcing (ZF) and linear minimum MSE (MMSE) solutions for fixed and memoryless block-based transceivers with minimum redundancy, using only half the amount of redundancy employed in standard systems. Their equalization processes require only $\mathcal{O}(M \log_2 M)$ operations. Chapter D contains a new structure for linear MMSE-based minimum-redundancy transceivers using DFTs. Such a structure is simpler than the one proposed in [23], since it employs only four parallel branches at the receiver end instead of the previous five branches. However, it may still be difficult to apply MMSE equalizers with minimum redundancy in some practical systems, given their higher number of operations. This chapter also proposes novel suboptimal MMSE equalizers with minimum redundancy that require the same amount of computations of ZF equalizers, with a mild decrease in the throughput performance when compared to the optimal MMSE solution.

The extension of the aforementioned DFT-based solutions to real transforms, such as the discrete Hartley transform (DHT), is not straightforward. The only known solution imposes a symmetry on the channel model that is unlikely to be met in practice [23]. Chapter E proposes transceivers with practical ZF and MMSE

receivers using DHT, diagonal, and antidiagonal matrices as building blocks. The resulting systems are asymptotically as simple as OFDM and SC-FD equalization transceivers. In addition, they do not enforce constraints on the channel model. Several computer simulations indicate the higher throughput of the proposed transceivers as compared to the standard solutions.

Chapter F presents new LTI block-based transceivers which employ a reduced amount of redundancy to eliminate the interblock interference. The proposals encompass both multicarrier and single-carrier systems with either ZF or MSE equalizers. The amount of redundancy ranges from the minimum, $\lceil L/2 \rceil$, to the most commonly used value, L, assuming a channel-impulse response of order L. The resulting transceivers allow for superfast equalization of the received data blocks, since they only use fast Fourier transforms and single-tap equalizers in their structures. The chapter also includes an MSE analysis of the proposed transceivers with respect to the amount of redundancy. Indeed, we demonstrate that larger amounts of transmitted redundant elements lead to lower MSE of symbols at the receiver end. Several computer simulations indicate that, by choosing an appropriate amount of redundancy, our proposals in this chapter can achieve higher throughputs than the standard superfast multicarrier and single-carrier systems, while keeping the same asymptotic computational complexity for the equalization process.

In Chapter G, we deduce new LTI reduced-redundancy transceivers which employ only discrete Hartley transforms and two-tap equalizers in their structures. The results of this chapter are natural extensions of the results proposed in Chapter E and Chapter F. The simulation results of Chapter G also indicate that the real-transform-based transceivers with reduced redundancy can outperform OFDM and SC-FD systems with respect to the throughput performance.

Block-based transceivers with minimum redundancy induce a Toeplitz effective channel matrix that may lead to higher noise gains than circulant channel matrices. This occurs due to the additional difficulty in equalizing the Toeplitz effective channel matrix induced by the minimum-redundancy transceivers, as compared to the circulant channel matrix associated with OFDM and SC-FD systems [23]. This fact motivated us to perform research on methods to minimize these noise gains. Chapter H proposes an optimal power-allocation method that minimizes the noise gains when channel-state information (CSI) is available at the transmitter end. Simulation results demonstrate that the design approaches allow higher throughputs in a number of situations, revealing the potential usefulness of the proposed solutions.

Chapter I shows how one can reduce the amount of transmitted redundancy in block nonlinear decision-feedback equalization. Some performance analyses based on the resulting mean-square error of symbols, mutual information between transmitted and estimated symbols, and average error probability of symbols are included

to assess the effects of the reduction in the amount of redundancy. Simulation results illustrate that data throughput can be increased without affecting the system performance, for a certain level of signal-to-noise ratio at the receiver.

In Chapter J, we concentrate on the equalizer-design problem related to the minimum-redundancy systems proposed in the first part of the thesis, without assuming CSI. We do so by first adapting recently proposed pilot-based channel estimation methods [20] to these minimum-redundancy transceivers. After that, we apply three iterative algorithms to invert structured matrices in order to design the equalizers, namely: Newton's iteration, homotopic Newton's iteration [25, 53], and preconditioned conjugate gradient (PCG) [54] methods. A key feature of the proposed designs is that they employ superfast algorithms that require only $\mathcal{O}(M \log_2 M)$ complex-valued operations. This is achieved by using the displacement approach [25, 58] in association with all the utilized algorithms.

The concluding remarks of this thesis as well as some suggestions for future works are in Chapter K.

Chapter L contains a complete list of publications and invited lectures related to this thesis.

It is worth mentioning at this point why we have chosen such ordering for the chapters. One could argue that, as reduced-redundancy systems include minimum-redundancy systems as special cases, why we have not described only reduced-redundancy systems and derived minimum-redundancy systems as subproducts? This would led us to a simpler and more concise text. However, this would also hide the path that we have followed throughout the entire research which we have been conducting since the master thesis [23]. We therefore have chosen this chapter ordering to keep the same historical development of this research.[5]

A.3 Notation and Terminology

Scalars are denoted by italic letters, while vectors and matrices are denoted by boldface letters (lowercase for vectors and uppercase for matrices). All vectors are column vectors. The notations $[\cdot]^T$, $[\cdot]^*$, $[\cdot]^H$, $[\cdot]^\dagger$, and $\mathsf{E}[\cdot]$ stand for transpose, conjugate, Hermitian transpose, pseudo-inverse, and expectation operations on $[\cdot]$, respectively. We shall denote the sets of natural, real, positive real, and complex numbers as $\mathbb{N}$, $\mathbb{R}$, $\mathbb{R}_+$, and $\mathbb{C}$, respectively. The set $\mathbb{C}^{M_1 \times M_2}$ denotes all $M_1 \times M_2$ matrices comprised of complex entries, whereas $\mathbb{C}^{M_1 \times M_2}[x]$ denotes all polynomials in the variable x with $M_1 \times M_2$ complex-valued matrices as coefficients. The (m_1, m_2)th element of an $M_1 \times M_2$ matrix $\mathbf{X}$ may be denoted as $[\mathbf{X}]_{m_1,m_2}$. The operator $\mathrm{diag}\{\cdot\}$

[5]The exception is Part III since Chapters H and J were developed before the chapters that form Part II.

represents a diagonal matrix whose elements are the entries of the argument vector. The operator $\mathrm{tr}\{\cdot\}$ outputs the trace of a given matrix. In addition, the operator $\mathrm{toeplitz}\{\mathbf{c}, \mathbf{r}^T\}$ denotes a Toeplitz matrix whose first column is $\mathbf{c}$ and whose first row is $\mathbf{r}^T$. The symbols $\mathbf{0}_{M_1 \times M_2}$ and $\mathbf{I}_M$ denote an $M_1 \times M_2$ matrix with zero entries and the $M \times M$ identity matrix (sometimes we may drop the index M without loss of clarity). Moreover, the following matrices will be used: $\mathbf{J} = [\, \mathbf{e}_M \;\; \mathbf{e}_{M-1} \;\; \cdots \;\; \mathbf{e}_2 \;\; \mathbf{e}_1 \,]$, $\mathbf{J}' = [\, \mathbf{e}_1 \;\; \mathbf{e}_M \;\; \cdots \;\; \mathbf{e}_3 \;\; \mathbf{e}_2 \,]$, and $\mathbf{J}'' = [\, -\mathbf{e}_1 \;\; \mathbf{e}_M \;\; \cdots \;\; \mathbf{e}_3 \;\; \mathbf{e}_2 \,]$, where the vector $\mathbf{e}_m \in \mathbb{C}^{M \times 1}$, with $m \in \{\, 1, 2, \cdots, M \,\}$, has its mth element equal to 1 and all the others equal to 0. Given a real number x, $\lceil x \rceil$ stands for the smallest integer greater than or equal to x. When we refer to computational complexity, we mean the total amount of complex operations (additions and multiplications). In this context, an algorithm is $\mathcal{O}(f(M))$ when it is possible to implement it with at most $cf(M)$ complex operations, for some positive real constant c. The differential entropy of a random vector $\boldsymbol{r}$ is denoted as $\mathcal{H}(\boldsymbol{r})$, whereas the mutual information between the random vectors $\boldsymbol{r}_1$ and $\boldsymbol{r}_2$ is denoted as $\mathcal{I}(\boldsymbol{r}_1, \boldsymbol{r}_2)$. Given two sets $\mathcal{A}$ and $\mathcal{B}$, the set $\mathcal{A} \backslash \mathcal{B}$ contains the elements of $\mathcal{A}$ that are not elements of $\mathcal{B}$ and the set $\mathcal{A} \times \mathcal{B}$ denotes the usual Cartesian product. The notation $\| \cdot \|_2$ denotes the standard norm-2 of a vector (when the argument is a matrix such a notation denotes the induced Euclidean norm of matrices), whereas $\| \cdot \|_{\mathrm{F}}$ denotes the standard Frobenius norm of a matrix. The notation $\mathbf{A} \geq \mathbf{B}$, means that $\mathbf{A} - \mathbf{B} \geq O$, i.e., $\mathbf{A} - \mathbf{B}$ is a positive semidefinite matrix. Similarly, the notation $\mathbf{A} > \mathbf{B}$, means that $\mathbf{A} - \mathbf{B} > O$, i.e., $\mathbf{A} - \mathbf{B}$ is a positive definite matrix. The set $\mathbb{H}_M(a, b)$ denotes all $M \times M$ positive semidefinite Hermitian matrices whose eigenvalues are within the open interval $(a, b) \subset \mathbb{R}$. Given a function $f : (a, b) \to \mathbb{R}$ and a matrix $\mathbf{A} \in \mathbb{H}_M(a, b)$, then one can define the mapping $f(\mathbf{A}) = \mathbf{U} f(\mathbf{\Lambda}) \mathbf{U}^H$, in which $\mathbf{A} = \mathbf{U} \mathbf{\Lambda} \mathbf{U}^H$ is the eigendecomposition of $\mathbf{A}$. In this context, a function $f : (a, b) \to \mathbb{R}$ is matrix-monotone on $\mathbb{H}_M(a, b)$ if $f(\mathbf{A}) \geq f(\mathbf{B})$, for all $\mathbf{A}, \mathbf{B} \in \mathbb{H}_M(a, b)$ such that $\mathbf{A} \geq \mathbf{B}$. Moreover, a function $f : (a, b) \to \mathbb{R}$ is matrix-concave on $\mathbb{H}_M(a, b)$ if $f(\alpha \mathbf{A} + (1 - \alpha)\mathbf{B}) \geq \alpha f(\mathbf{A}) + (1 - \alpha) f(\mathbf{B})$, for all $\mathbf{A}, \mathbf{B} \in \mathbb{H}_M(a, b)$ and for all $\alpha \in [0, 1]$.

Apêndice B

Transmultiplexers

The proposals of novel schemes for channel and source coding, allied with the development of integrated circuits and the use of digital signal processing (DSP) for communications, have allowed the deployment of several communication systems to meet the demands for increasing data-transmission rates. Indeed, common DSP tools, such as digital filtering, are crucial to retrieve at the receiver end reliable estimates of signals associated with one or several users that share the same physical channel.

There is a variety of classes of digital filters. In communication systems, for instance, they can be either fixed or adaptive, linear or nonlinear, with finite impulse response (FIR) or with infinite impulse response (IIR), etc. When compared to the other possibilities, fixed, linear, and FIR filters are the most common ones in practice, due to their simpler implementation, stability properties, and low costs.

However, modern communication systems usually require more features than fixed, linear, and FIR filters can offer. In this context, multirate signal processing adds some degrees of freedom to the standard linear time-invariant (LTI) signal processing through the inclusion of decimators and interpolators. These degrees of freedom are key to develop some important representations of communication systems based on filter banks.

Filter-bank representations are widely employed in spectral analysis and source coding [26, 27]. In communications, the transmultiplexer (TMUX) configuration can be employed to represent multicarrier or single-carrier transceivers, and can be considered a system dual to the filter-bank configuration [1, 28–31]. Indeed, several practical systems can be modeled using TMUXes.

Differently from sharp frequency-selective filter banks, practical multicarrier and single-carrier transceivers can be modeled as TMUXes which employ short length subfilters. Most of such practical cases are implemented as memoryless block-based transceivers [32]. As previously mentioned, the most commonly used block-based transceivers are OFDM and SC-FD systems [30, 31], which are memoryless LTI

systems.

The main feature related to OFDM-based transceivers is the elimination of intersymbol interference (ISI) with low computational complexity. An alternative to OFDM is the SC-FD transceiver, which presents lower peak-to-average power ratio (PAPR) and lower sensitivity to carrier-frequency offset (CFO) [14, 15]. In addition, for frequency-selective channels, the BER of SC-FD can be lower than for its OFDM counterpart, particularly for the cases in which the channel has high attenuation at some subchannel central frequencies [15].

In this introductory chapter some important multirate signal-processing tools are revised aiming at their use in the modeling of communication systems. These tools will be employed to represent OFDM and SC-FD systems, as well as to introduce some results related to block-based transceivers using reduced redundancy.

B.1 Multirate Signal Processing

It is rather common that signals with distinct sampling rates coexist in many signal-processing applications [26, 27]. In general, multirate signal-processing systems include as building blocks both the interpolator and the decimator. The interpolation consists of increasing the sampling rate of a given signal, whilst the decimation entails a sampling-rate reduction of its input signal. The loss of data inherent to decimation may generate aliasing in the decimated signal spectrum [26, 27].

The interpolation by a factor $N \in \mathbb{N}$ consists of including $N-1$ zeros between each pair of adjacent samples, creating a signal whose sampling rate is N times larger than the original signal. Indeed, given a complex-valued signal $s(n)$, where $n \in \mathbb{Z}$, the interpolated signal $s_{\text{int}}(k)$, with $k \in \mathbb{Z}$, is given by $s_{\text{int}}(k) \triangleq s(n)$, whenever $k = nN$, otherwise $s_{\text{int}}(k) \triangleq 0$. In the frequency domain, the effect of interpolation can be described as [26, 27]:

$$S_{\text{int}}(\mathrm{e}^{\mathrm{j}\omega}) = S(\mathrm{e}^{\mathrm{j}\omega N}), \tag{B.1}$$

where $X(\mathrm{e}^{\mathrm{j}\omega}) \triangleq \mathcal{F}\{x(n)\}$ is the discrete-time Fourier transform of the sequence $x(n)$.

The decimation by a factor N consists of discarding $N-1$ samples from each block of N samples of the input signal. The resulting signal has a sampling rate N times lower than the original signal. Indeed, given the signal $s(n)$, the decimated signal $s_{\text{dec}}(k)$ is defined by $s_{\text{dec}}(k) \triangleq s(n)$, whenever $n = kN$, for all $k \in \mathbb{Z}$. In the frequency domain, it is possible to show that the decimated signal is represented

by [26, 27]:

$$S_{\text{dec}}(\mathrm{e}^{\mathrm{j}\omega}) = \frac{1}{N} \sum_{n \in \mathcal{N}} S\left(\mathrm{e}^{\mathrm{j}\frac{\omega - 2\pi n}{N}}\right), \tag{B.2}$$

in which $\mathcal{N} \triangleq \{0, 1, \cdots, N-1\} \subset \mathbb{N}$. Unlike the interpolation, the decimation is a periodically time-varying operation [26, 27].

The effects of interpolation and decimation in both time and frequency domains of a signal interpolated and decimated by $N = 2$ are respectively depicted in Figures B.1 and B.2. Those signals in time and frequency domains are only for illustration purposes since they do not represent a true time-frequency pair. The careful examination of Figures B.1 and B.2 shows that a digital filtering operation is required before the decimation and after the interpolation in order to avoid aliasing due to decimation and in order to eliminate the spectrum repetition due to inter-

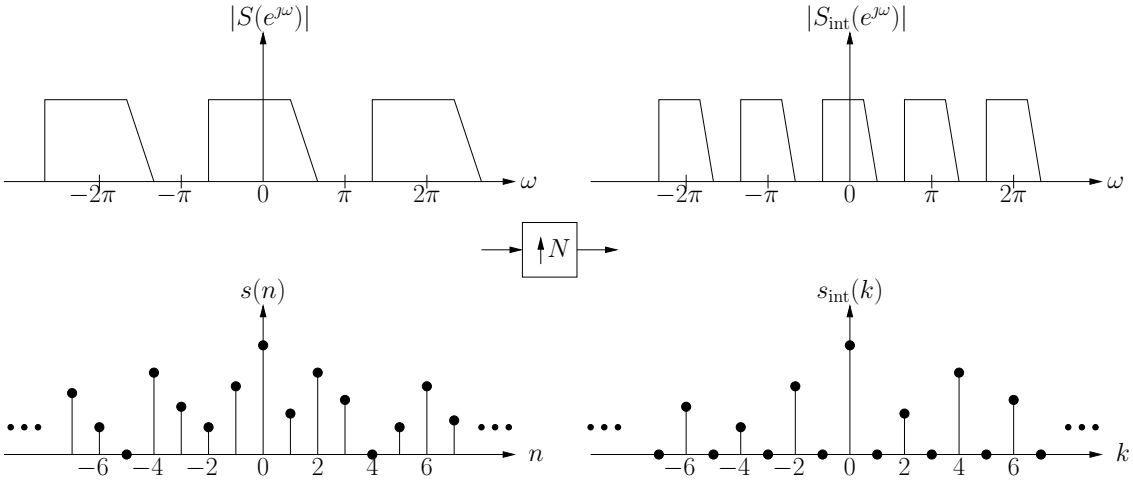

Figure B.1: Interpolation ($N = 2$).

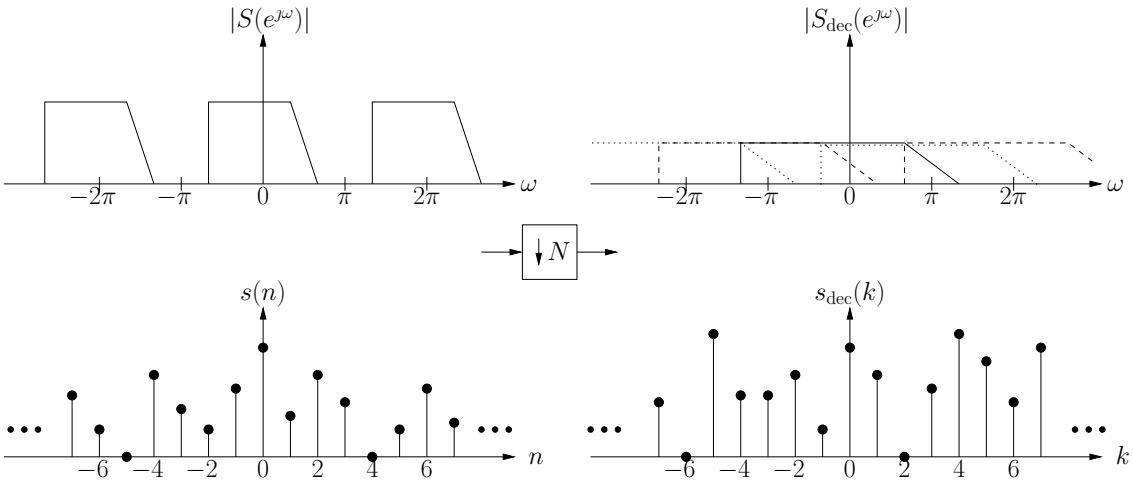

Figure B.2: Decimation ($N = 2$).

polation [26, 27]. The decimation filter narrows the spectrum of the input signal in order to avoid that aliasing corrupt the spectrum of the resulting decimated signal. For a lowpass real signal, for instance, we have to maintain the input signal information only at the lower frequencies in the range $\left(-\frac{\pi}{N}, \frac{\pi}{N}\right)$, so that the spectrum at this range is not corrupted after decimation. The interpolation filter smooths the interpolated signal $s_{\text{int}}(k)$, eliminating the abrupt transition between nonzero and zero samples, which is the source of the spectrum repetition. The central frequencies of the spectrum repetitions are located at $\pm\frac{2\pi}{N}n$, with $n \in \mathcal{N}$. Figure B.3 illustrates how the decimation and interpolation operations are implemented in practice.

There are useful ways to manipulate the interpolation and decimation blocks in multirate systems. We are particularly interested in manners to commute the decimation and interpolation operations with LTI filters. Some forms of commuting are based on the so-called noble identities [26, 27].

Figure B.4 illustrates the building-block representations of the noble identities. In the interpolation process, instead of first filtering the input signal and then upsampling it, one can first upsample the input signal and then perform a filtering operation with a filter whose impulse response is upsampled. This strategy allows one to reduce the number of operations required by the process. For decimation, the decimator followed by a filter is equivalent to filter the input signal by the interpolated filter followed by decimation. These operations can be described mathematically as [26, 27]:

$$[S(z)F(z)]_{\uparrow N} \triangleq U(z) = [S(z)]_{\uparrow N} F(z^N), \tag{B.3}$$

$$[Y(z)]_{\downarrow N} G(z) \triangleq \hat{S}(z) = \left[Y(z)G(z^N)\right]_{\downarrow N}, \tag{B.4}$$

in which $[(\cdot)]_{\uparrow N}$ and $[(\cdot)]_{\downarrow N}$ denote the interpolation and decimation by N applied to $(\cdot)$, respectively.

A widespread application of multirate systems is the filter-bank design [26, 27].

Figure B.3: Interpolation and decimation operations in time domain.

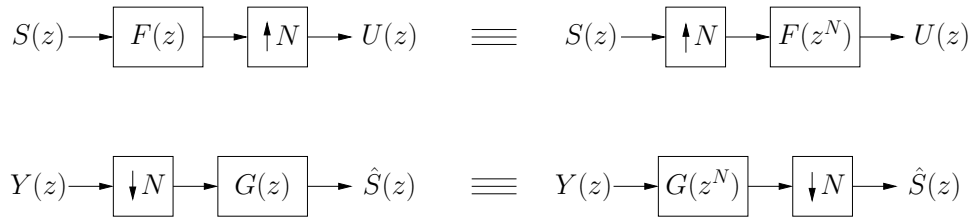

Figure B.4: Noble identities in $\mathcal{Z}$-domain.

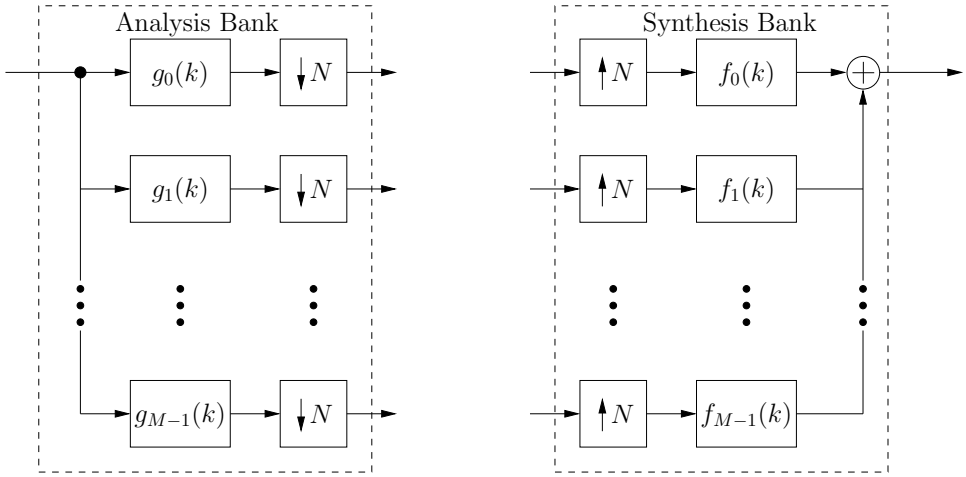

Figure B.5: Analysis and synthesis filter banks in time domain.

A filter bank consists of a set of filters with the same input signal, or a set of filters whose outputs are added to form the output signal [27], as depicted in Figure B.5. The set of filters $\{g_m(k)\}_{m\in\mathcal{M}}$, where $\mathcal{M} \triangleq \{0, 1, \cdots, M-1\} \subset \mathbb{N}$, is the so-called analysis filter bank, whereas the set of filters $\{f_m(k)\}_{m\in\mathcal{M}}$ is the synthesis filter bank. It is possible to verify that the analysis filter bank divides the input signal in subbands of narrowband frequencies, so that their outputs can be decimated. The subband signal can be employed for analysis and manipulations according to the particular application. For reconstruction, the subband signals are interpolated and combined by the synthesis filter bank [26, 27, 29].

Filter-bank transceivers, also known as transmultiplexers, are considered systems dual to the filter-bank configurations, since the roles of analysis and synthesis banks are interchanged in transmultiplexers. Indeed, the input of a transmultiplexer is first synthesized by the synthesis bank and, after some processing stages, the outputs are obtained as a result from the analysis bank.

B.2 Filter-Bank Transceivers

Further improvements in communication systems may call for sophisticated transmultiplexer designs in which the transmitted signal is filtered by a precoder with memory consisting of a multiple-input multiple output (MIMO) FIR filter. The inherent memory at the transmitter can be viewed as a kind of redundancy since a given signal block is transmitted more than once along with neighboring blocks. Sophisticated transmitters may call for more complex receivers, but they might also allow a reduction in the amount of prefix signals necessary to attain zero-forcing solution, for example.

Let us consider the model of a transceiver [27, 29, 30] as depicted in Figure B.6,

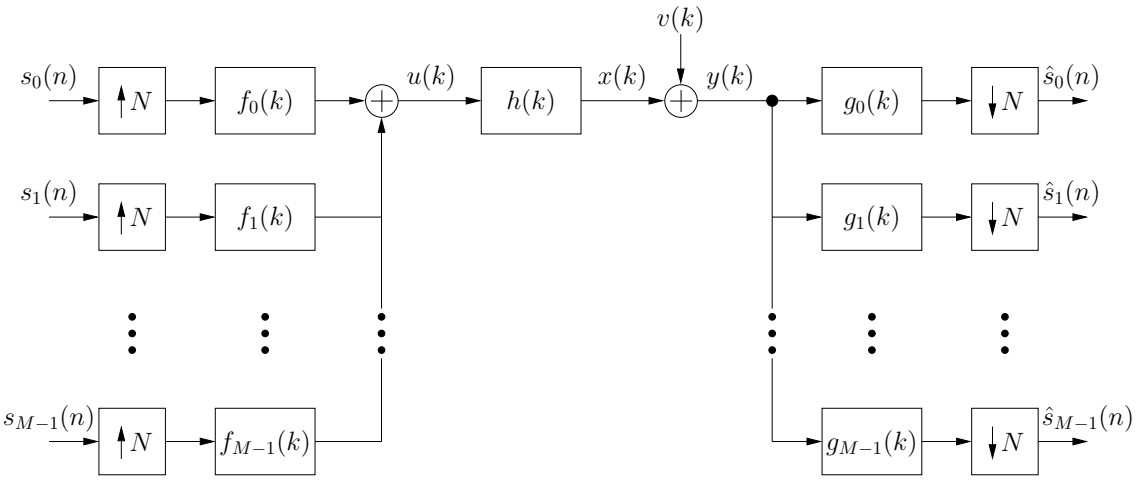

Figure B.6: TMUX system in time domain.

in which a communication system is modeled as a MIMO system. The data samples of each sequence $s_m(n)$ belong to a particular constellation $\mathcal{C} \subset \mathbb{C}$, such as PAM, QAM, or PSK[1] [34]. The sequence $s_m(n)$ represents the mth transceiver input, where $m \in \mathcal{M}$ and $n \in \mathbb{Z}$. The corresponding transceiver output is denoted as $\hat{s}_m(n) \in \mathbb{C}$, which should be a reliable estimate of $s_m(n-\delta)$, where $\delta \in \mathbb{N}$ represents the delay introduced by the overall transmission/reception process.

A communication system can be designed by choosing carefully the set of causal transmitter filters with impulse responses represented by $\{f_m(k)\}_{m\in\mathcal{M}}$, and the set of causal receiver filters represented by $\{g_m(k)\}_{m\in\mathcal{M}}$. These filters operate at a sampling rate N times larger than the sampling rate of the sequences $s_m(n)$. Note that the index n represents the sample index at the input and output of the transceiver, whereas $k \in \mathbb{Z}$ is employed to represent the sample index of the subfilters and of the internal signals between the interpolators and decimators. In our discussions, we shall consider that the transmitter and receiver subfilters are LTI.

The input signals $s_m(n)$, for each $m \in \mathcal{M}$, are processed by the subfilters aiming at reducing the channel distortion, so that the output signals $\hat{s}_m(n)$ can give rise to good estimates of the corresponding transmitted signals. The usual goal in a communication system is to produce estimates of $s_m(n-\delta)$ achieving low bit-error rate (BER) and/or maximizing the data throughput.

The channel model can be represented by an FIR filter whose impulse response is $h(k) \in \mathbb{C}$ of order $L \in \mathbb{N}$. The FIR transfer function accounts for the frequency-selective behavior of the physical channel. The additive noise $v(k) \in \mathbb{C}$ accounts for the thermal noise from the environment and for the multi-user interference (MUI).

[1]Pulse-amplitude modulation, quadrature-amplitude modulation, or phase-shift keying, respectively.

B.2.1 Time-Domain Representation

Based on Figure B.6, one can deduce that the channel input signal is given as

$$u(k) \triangleq \sum_{(i,m)\in\mathbb{Z}\times\mathcal{M}} s_m(i) f_m(k - iN). \tag{B.5}$$

The channel input to output relation is described by:

$$y(k) \triangleq \sum_{j\in\mathbb{Z}} h(j)u(k - j) + v(k). \tag{B.6}$$

The signal $y(n)$ is processed at the receiver end to generate estimates of the transmitted data according to:

$$\hat{s}_m(n) \triangleq \sum_{l\in\mathbb{Z}} g_m(l)y(nN - l). \tag{B.7}$$

By using Eqs. (B.5), (B.6), and (B.7) we can describe the relation between the input signal $s_m(n)$ and its estimate $\hat{s}_m(n)$, as follows:

$$\hat{s}_m(n) = \sum_{(i,j,l,m)\in\mathbb{Z}^3\times\mathcal{M}} g_m(l)h(j)s_m(i)f_m(nN - l - j - iN) + \sum_{l\in\mathbb{Z}} g_m(l)v(nN - l). \tag{B.8}$$

The description above is not the easiest one to analyze the system and draw conclusions. For example, a polyphase approach in the $\mathcal{Z}$-domain is much more appropriate in this context [26, 27, 32].

B.2.2 Polyphase Representation

By assuming that the interpolation and decimation factors are equal to N, it is convenient to describe the transmitter and receiver filters by their polyphase de-

compositions of order N, according to the expressions [32]:

$$\begin{aligned} F_m(z) &\triangleq \sum_{k\in\mathbb{Z}} f_m(k) z^{-k} \\ &= \sum_{i\in\mathcal{N}} z^{-i} \sum_{j\in\mathbb{Z}} f_m(jN+i) z^{-jN} \\ &= \sum_{i\in\mathcal{N}} z^{-i} F_{i,m}(z^N)\,, \end{aligned} \tag{B.9}$$

$$\begin{aligned} G_m(z) &\triangleq \sum_{k\in\mathbb{Z}} g_m(k) z^{-k} \\ &= \sum_{i\in\mathcal{N}} z^{i} \sum_{j\in\mathbb{Z}} g_m(jN-i) z^{-jN} \\ &= \sum_{i\in\mathcal{N}} z^{i} G_{m,i}(z^N)\,, \end{aligned} \tag{B.10}$$

so that $m \in \mathcal{M}$, $F_m(z) \triangleq \mathcal{Z}\{f_m(k)\}$, and $G_m(z) \triangleq \mathcal{Z}\{g_m(k)\}$ are the $\mathcal{Z}$-transforms of $f_m(k)$ and $g_m(k)$, respectively. In such a case, we can rewrite Eqs. (B.9) and (B.10) as follows [32]:

$$\begin{bmatrix} F_0(z) & \cdots F_{M-1}(z) \end{bmatrix} = \underbrace{\begin{bmatrix} 1 & z^{-1} & \cdots & z^{-(N-1)} \end{bmatrix}}_{\mathbf{d}^T(z)} \underbrace{\begin{bmatrix} F_{0,0}(z^N) & \cdots & F_{0,M-1}(z^N) \\ \vdots & \ddots & \vdots \\ F_{N-1,0}(z^N) & \cdots & F_{N-1,M-1}(z^N) \end{bmatrix}}_{\mathbf{F}(z^N)}, \tag{B.11}$$

$$\begin{bmatrix} G_0(z) \\ \vdots \\ G_{M-1}(z) \end{bmatrix} = \underbrace{\begin{bmatrix} G_{0,0}(z^N) & \cdots & G_{0,N-1}(z^N) \\ \vdots & \ddots & \vdots \\ G_{M-1,0}(z^N) & \cdots & G_{M-1,N-1}(z^N) \end{bmatrix}}_{\mathbf{G}(z^N)} \underbrace{\begin{bmatrix} 1 \\ \vdots \\ z^{(N-1)} \end{bmatrix}}_{\mathbf{d}(z^{-1})}. \tag{B.12}$$

Now, by defining $S_m(z) \triangleq \mathcal{Z}\{s_m(n)\}$, $U(z) \triangleq \mathcal{Z}\{u(k)\}$, $X(z) \triangleq \mathcal{Z}\{x(k)\}$,

$V(z) \triangleq \mathcal{Z}\{v(k)\}$, $Y(z) \triangleq \mathcal{Z}\{y(k)\}$, and $\hat{S}_m(z) \triangleq \mathcal{Z}\{\hat{s}_m(n)\}$, then one can write

$$U(z) = \mathbf{d}^T(z)\mathbf{F}(z^N) \underbrace{\begin{bmatrix} S_0(z^N) \\ \vdots \\ S_{M-1}(z^N) \end{bmatrix}}_{\mathbf{s}(z^N)}, \tag{B.13}$$

$$X(z) = H(z)U(z), \tag{B.14}$$

$$Y(z) = X(z) + V(z), \tag{B.15}$$

$$\begin{bmatrix} \hat{S}_0(z) \\ \vdots \\ \hat{S}_{M-1}(z) \end{bmatrix} = \Big[\mathbf{G}(z^N)\mathbf{d}(z^{-1})Y(z)\Big]_{\downarrow N}. \tag{B.16}$$

The transceiver model utilizing the polyphase decompositions of the transmitter and receiver subfilters is illustrated in Figure B.7. By employing the noble identities described in Section B.1, it is possible to transform the transceiver of Figure B.7 into the equivalent transceiver of Figure B.8.

The highlighted area of Figure B.8 that includes delays, forward delays, decimators, interpolators, and the SISO channel model can be represented by a pseudo-circulant matrix $\mathbf{H}(z)$ of dimension $N \times N$, given by [27, 32]:

$$\mathbf{H}(z) \triangleq \begin{bmatrix} H_0(z) & z^{-1}H_{N-1}(z) & z^{-1}H_{N-2}(z) & \cdots & z^{-1}H_1(z) \\ H_1(z) & H_0(z) & z^{-1}H_{N-1}(z) & \cdots & z^{-1}H_2(z) \\ \vdots & \vdots & \ddots & \vdots & \vdots \\ H_{N-1}(z) & H_{N-2}(z) & H_{N-3}(z) & \cdots & H_0(z) \end{bmatrix}, \tag{B.17}$$

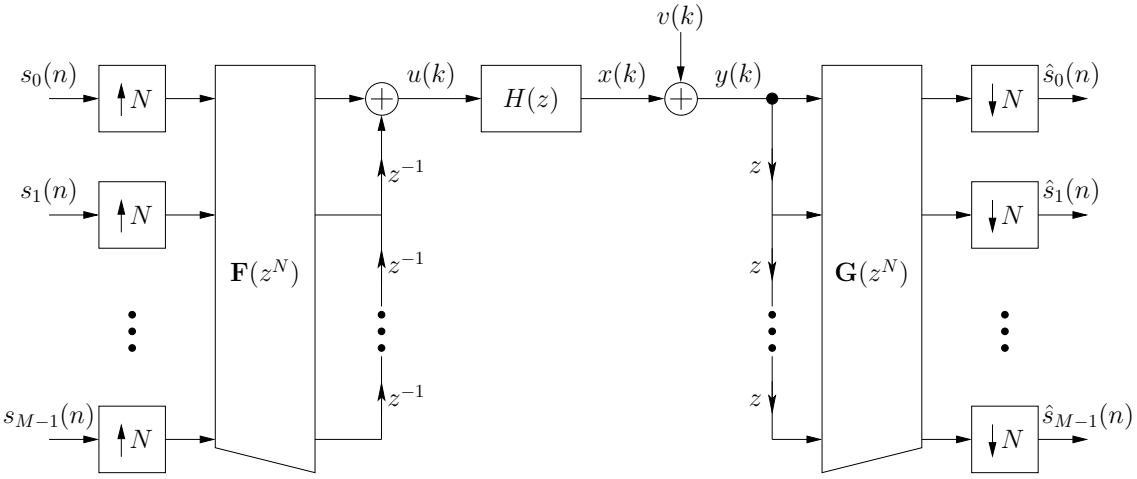

Figure B.7: Polyphase representation of TMUX systems.

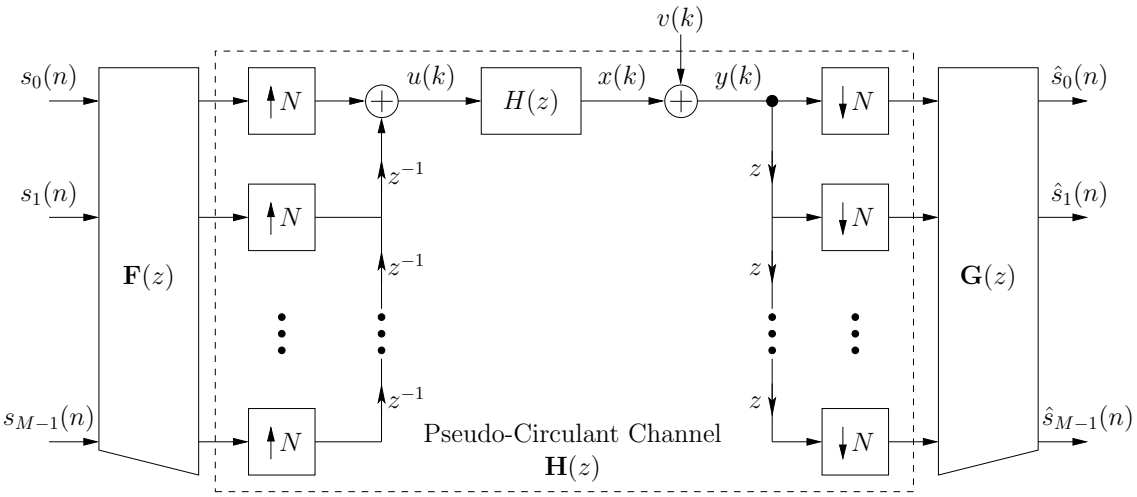

Figure B.8: Equivalent representation of TMUX systems employing polyphase decompositions.

in which [27, 32]

$$H(z) \triangleq \sum_{i \in \mathcal{N}} H_i(z^N) z^{-i} \quad \text{and} \quad H_i(z) \triangleq \sum_{\substack{j \in \mathbb{Z} \\ 0 \leq jN+i \leq L}} h(jN+i) z^{-j}. \tag{B.18}$$

Figure B.9 describes the transceiver through the polyphase decomposition of appropriate matrices, including the pseudo-circulant representation of the channel matrix. It is worth noting that the descriptions of Figures B.6 and B.9 are equivalent.

Moreover, let us consider that $N \geq L$, i.e., the interpolation/decimation factor is greater than or equal to the channel order, a common situation in practice [32]. For $N \geq L$, each element of matrix $H_i(z)$, for $i \in \mathcal{N}$, will consist of filters with a single coefficient so that $H_i(z) = h(i)$, for $i \leq L$, and $H_i(z) = 0$, for $i > L$. In this case the pseudo-circulant channel matrix is represented by a first-order FIR matrix

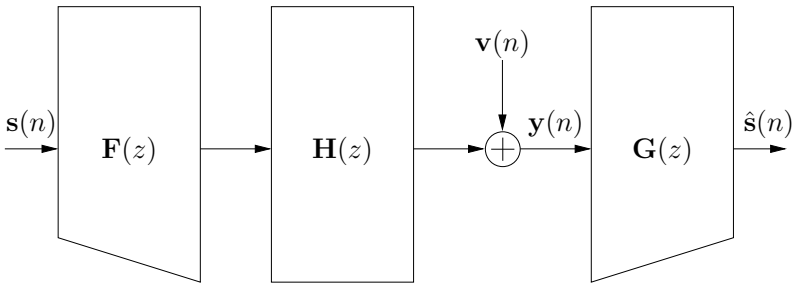

Figure B.9: Block-based transceivers in $\mathcal{Z}$-domain employing polyphase decompositions.

described by [32]:

$$\mathbf{H}(z) = \begin{bmatrix} h(0) & 0 & 0 & \cdots & 0 \\ h(1) & h(0) & 0 & \cdots & 0 \\ \vdots & \vdots & \vdots & \vdots & \vdots \\ h(L) & h(L-1) & \ddots & \cdots & 0 \\ 0 & h(L) & \cdots & \cdots & 0 \\ \vdots & \vdots & \vdots & \vdots & \vdots \\ 0 & 0 & h(L) & \cdots & h(0) \end{bmatrix} + z^{-1} \begin{bmatrix} 0 & \cdots & 0 & h(L) & \cdots & h(1) \\ 0 & 0 & \cdots & 0 & \ddots & \vdots \\ \vdots & \vdots & \vdots & \vdots & \vdots & h(L) \\ 0 & 0 & 0 & \cdots & 0 & 0 \\ 0 & 0 & 0 & \cdots & 0 & 0 \\ \vdots & \vdots & \vdots & \vdots & \vdots & \vdots \\ 0 & 0 & 0 & 0 & \cdots & 0 \end{bmatrix}. \tag{B.19}$$

As Figure B.9 illustrates, the transmitted and received vectors are denoted as:

$$\mathbf{s}(n) \triangleq [\, s_0(n) \;\; s_1(n) \;\; \cdots \;\; s_{M-1}(n) \,]^T, \tag{B.20}$$

$$\hat{\mathbf{s}}(n) \triangleq [\, \hat{s}_0(n) \;\; \hat{s}_1(n) \;\; \cdots \;\; \hat{s}_{M-1}(n) \,]^T. \tag{B.21}$$

Based on Figure B.9, we can infer that the transfer matrix $\mathbf{T}(z)$ of the transceiver can be expressed as:

$$\mathbf{T}(z) \triangleq \mathbf{G}(z)\mathbf{H}(z)\mathbf{F}(z), \tag{B.22}$$

where we considered the particular case in which $v(k) \equiv 0$, inspired by the zero-forcing (ZF) design [32]. A transceiver is zero forcing whenever $\mathbf{T}(z) = z^{-d}\mathbf{I}_M$, with $d \in \mathbb{N}$.

B.3 Memoryless Block-Based Systems

The particular and very important case where the transceivers are LTI and memoryless, that is, $\mathbf{F}(z) = \mathbf{F}$ and $\mathbf{G}(z) = \mathbf{G}$, is addressed in this section. This case encompasses the memoryless block-based transceivers [32], since these systems do not use data from previous or future blocks in the transmission and reception processing of the current data block. That is, only the current block takes part in the transceiver computations. This non-overlapping behavior is only possible if the length of the subfilters $\{f_m(k)\}_{m\in\mathcal{M}}$ and $\{g_m(k)\}_{m\in\mathcal{M}}$ are less than or equal to N. The traditional OFDM and SC-FD transceivers are examples of memoryless block-based systems.

B.3.1 CP-OFDM

The cyclic-prefix OFDM, or just CP-OFDM, is a transceiver which employs cyclic prefix as redundancy. It is described by the following transmitter and receiver matrices, respectively [37]:

$$\mathbf{F} \triangleq \underbrace{\begin{bmatrix} \mathbf{0}_{L\times(M-L)} & \mathbf{I}_L \\ & \mathbf{I}_M \end{bmatrix}}_{\mathbf{A}_{\mathrm{CP}}\in\mathbb{C}^{N\times M}} \mathbf{W}_M^H, \tag{B.23}$$

$$\mathbf{G} \triangleq \mathbf{E}\mathbf{W}_M \underbrace{\begin{bmatrix} \mathbf{0}_{M\times L} & \mathbf{I}_M \end{bmatrix}}_{\mathbf{R}_{\mathrm{CP}}\in\mathbb{C}^{M\times N}}, \tag{B.24}$$

where $\mathbf{W}_M$ is the normalized $M \times M$ DFT matrix, $\mathbf{I}_M$ is the $M \times M$ identity matrix, $\mathbf{0}_{M\times N}$ is an $M \times N$ matrix whose entries are zero, and $\mathbf{E} \in \mathbb{C}^{M\times M}$ is the equalizer matrix placed after the removal of the cyclic prefix and the application of the DFT matrix. Observe that the data block to be transmitted has length M, however, due to the prefix, the transceiver actually transmits a block of length $N = M + L$. The first L elements are repetitions of the last L elements of the IDFT output in order to implement the cyclic prefix as redundancy.

Matrices $\mathbf{A}_{\mathrm{CP}}$ and $\mathbf{R}_{\mathrm{CP}}$ include and remove the related cyclic prefix, respectively. Note that the product $\mathbf{R}_{\mathrm{CP}}\mathbf{H}(z)\mathbf{A}_{\mathrm{CP}} \in \mathbb{C}^{M\times M}$ is given by:

$$\mathbf{R}_{\mathrm{CP}}\mathbf{H}(z)\mathbf{A}_{\mathrm{CP}} = \begin{bmatrix} h(0) & 0 & \cdots & 0 & h(L) & \cdots & h(1) \\ h(1) & h(0) & \cdots & 0 & 0 & \ddots & \vdots \\ \vdots & \vdots & \ddots & & & & h(L) \\ h(L) & h(L-1) & & \ddots & \ddots & & 0 \\ 0 & h(L) & & & \ddots & & \vdots \\ \vdots & \ddots & \ddots & & & \ddots & 0 \\ 0 & \cdots & 0 & h(L) & \cdots & & h(0) \end{bmatrix}, \tag{B.25}$$

where we can observe that $\mathbf{R}_{\mathrm{CP}}$ removes the interblock interference, whereas matrix $\mathbf{A}_{\mathrm{CP}}$ pre-multiplies the resulting memoryless matrix $\mathbf{R}_{\mathrm{CP}}\mathbf{H}(z) \in \mathbb{C}^{M\times N}$ so that the overall matrix product is a circulant matrix of dimension $M \times M$. Indeed, one can observe that each row of matrix $\mathbf{R}_{\mathrm{CP}}\mathbf{H}(z)\mathbf{A}_{\mathrm{CP}}$ can be obtained by right-rotating the related previous row.

After inclusion and removal of the cyclic prefix, the resulting circulant matrix can be diagonalized by its pre-multiplication by the IDFT and post-multiplication by the DFT matrices, with these matrices placed at the transmitter and receiver,

respectively [22]. Therefore, the model of a CP-OFDM transceiver is described by:

$$\hat{\mathbf{s}} = \mathbf{E}\mathbf{\Lambda}\mathbf{s} + \mathbf{E}\mathbf{v}', \tag{B.26}$$

with $\mathbf{v}' \triangleq \mathbf{W}_M\mathbf{R}_{\text{CP}}\mathbf{v}$ and, for the sake of simplicity, the time dependency of the expressions was omitted [22]. As can be noted, the estimates of the transmitted symbols are uncoupled, that is, each symbol can be estimated independently of any other symbol within the related block, avoiding intersymbol interference.

Matrix $\mathbf{\Lambda}$ includes at its diagonal the distortion imposed by the channel on each symbol of the data block. This eigenvalue matrix can be described by [40, 41]:

$$\begin{aligned}\mathbf{\Lambda} &\triangleq \text{diag}\{\lambda_m\}_{m=0}^{M-1} \\ &= \mathbf{W}_M\mathbf{R}_{\text{CP}}\mathbf{H}(z)\mathbf{A}_{\text{CP}}\mathbf{W}_M^H \\ &= \text{diag}\left\{\sqrt{M}\mathbf{W}_M\begin{bmatrix}\mathbf{h} \\ \mathbf{0}_{(M-L-1)\times 1}\end{bmatrix}\right\},\end{aligned} \tag{B.27}$$

in which $\mathbf{h} \triangleq [\,h(0)\;\; h(1)\;\; \cdots\;\; h(L)\,]^T$.

The equalizer $\mathbf{E}$ for this transceiver can be defined in several ways, where the most popular ones are the ZF and MMSE equalizers [5]. In the ZF solution, it is assumed that matrix $\mathbf{\Lambda}$ can be inverted, such that

$$\mathbf{E}_{\text{ZF}} \triangleq \mathbf{\Lambda}^{-1}. \tag{B.28}$$

As for the MMSE solution, there is no requirement that matrix $\mathbf{\Lambda}$ be invertible since this latter operation is not needed. The linear MMSE solution is given by:

$$\begin{aligned}\mathbf{E}_{\text{MMSE}} &\triangleq \arg\left\{\min_{\forall\mathbf{E}\in\mathbb{C}^{M\times M}} \mathsf{E}\left[\|\mathbf{s} - \mathbf{E}(\mathbf{\Lambda}\mathbf{s} + \mathbf{v}')\|_2^2\right]\right\} \\ &= \mathbf{\Lambda}^H\left(\mathbf{\Lambda}\mathbf{\Lambda}^H + \frac{\sigma_v^2}{\sigma_s^2}\mathbf{I}\right)^{-1} \\ &= \text{diag}\left\{\frac{\lambda_m^*}{|\lambda_m|^2 + \frac{\sigma_v^2}{\sigma_s^2}}\right\}_{m=0}^{M-1},\end{aligned} \tag{B.29}$$

where the derivation assumes that the transmitted symbols and environment noise are independent and identically distributed (i.i.d.), originating from white stochastic processes with zero means and mutually independent. In the derivation above it was also considered that $\mathsf{E}[ss^*] = \sigma_s^2 \in \mathbb{R}_+$ and $\mathsf{E}[vv^*] = \sigma_v^2 \in \mathbb{R}_+$.

B.3.2 ZP-OFDM

An alternative OFDM system inserts zeros as redundancy and is called zero-padding OFDM (ZP-OFDM). There are many variants of ZP-OFDM. One possible choice is the ZP-OFDM-OLA (overlap-and-add) whose transmitter and receiver matrices are given as [37]:

$$\mathbf{F} \triangleq \underbrace{\begin{bmatrix} \mathbf{I}_M \\ \mathbf{0}_{L\times M} \end{bmatrix}}_{\mathbf{A}_{\mathrm{ZP}}\in\mathbb{C}^{N\times M}} \mathbf{W}_M^H, \tag{B.30}$$

$$\mathbf{G} \triangleq \mathbf{E}\mathbf{W}_M \underbrace{\begin{bmatrix} \mathbf{I}_M & \mathbf{I}_L \\ & \mathbf{0}_{(M-L)\times L} \end{bmatrix}}_{\mathbf{R}_{\mathrm{ZP}}\in\mathbb{C}^{M\times N}}, \tag{B.31}$$

where, as in the CP-OFDM case, L elements are inserted as redundancy, and $N = M + L$.

Matrices $\mathbf{A}_{\mathrm{ZP}}$ and $\mathbf{R}_{\mathrm{ZP}}$ perform the insertion and removal of the guard period of zero redundancy, respectively. The matrix product $\mathbf{R}_{\mathrm{ZP}}\mathbf{H}(z)\mathbf{A}_{\mathrm{ZP}} \in \mathbb{C}^{M\times M}$ is given by:

$$\mathbf{R}_{\mathrm{ZP}}\mathbf{H}(z)\mathbf{A}_{\mathrm{ZP}} = \begin{bmatrix} h(0) & 0 & \cdots & 0 & h(L) & \cdots & h(1) \\ h(1) & h(0) & \cdots & 0 & 0 & \ddots & \vdots \\ \vdots & \vdots & \ddots & & & & h(L) \\ h(L) & h(L-1) & & \ddots & \ddots & & 0 \\ 0 & h(L) & & & \ddots & & \vdots \\ \vdots & \ddots & \ddots & & & \ddots & 0 \\ 0 & \cdots & 0 & h(L) & \cdots & & h(0) \end{bmatrix} = \mathbf{R}_{\mathrm{CP}}\mathbf{H}(z)\mathbf{A}_{\mathrm{CP}}. \tag{B.32}$$

As can be verified, matrix $\mathbf{A}_{\mathrm{ZP}}$ removes the interblock interference, whereas matrix $\mathbf{R}_{\mathrm{ZP}}$ post-multiplies the resulting memoryless Toeplitz matrix $\mathbf{H}(z)\mathbf{A}_{\mathrm{ZP}} \in \mathbb{C}^{N\times M}$ so that the overall product becomes a circulant matrix of dimension $M \times M$. The reader should note that $\mathbf{R}_{\mathrm{ZP}}\mathbf{H}(z)\mathbf{A}_{\mathrm{ZP}} = \mathbf{R}_{\mathrm{CP}}\mathbf{H}(z)\mathbf{A}_{\mathrm{CP}}$.

The ZP-OFDM-OLA transceiver discussed here is a simplified version of a more general transceiver proposed in [37].[2] In fact, the general transceiver allows the recovery of the transmitted symbols using zero-forcing equalizers independently of the locations of the channel zeros, unlike the ZP-OFDM-OLA or CP-OFDM that might have zero eigenvalues under certain channel conditions. Unfortunately the general ZP-OFDM implementation is computationally complex since the equivalent

[2]There are other variants of ZP-OFDM, such as the ZP-OFDM-FAST [37].

channel matrix is not circulant, turning its diagonalization through fast transforms such as FFT impossible.[3]

B.3.3 CP-SC-FD

The cyclic-prefix single-carrier frequency-domain transceiver (CP-SC-FD) employs cyclic prefix as redundancy and it is closely related to the CP-OFDM transceiver. The CP-SC-FD system is described by the following transmitter and receiver matrices [37]:

$$\mathbf{F} \triangleq \begin{bmatrix} \mathbf{0}_{L\times(M-L)} & \mathbf{I}_L \\ & \mathbf{I}_M \end{bmatrix}, \tag{B.33}$$

$$\mathbf{G} \triangleq \mathbf{W}_M^H \mathbf{E} \mathbf{W}_M \begin{bmatrix} \mathbf{0}_{M\times L} & \mathbf{I}_M \end{bmatrix}, \tag{B.34}$$

respectively.

B.3.4 ZP-SC-FD

The zero-padding single-carrier frequency-domain (ZP-SC-FD) transceiver inserts zero redundancy to the transmitted block as in the ZP-OFDM transceiver. The ZP-SC-FD-OLA version may be modeled through the following transmitter and receiver matrices [37]:

$$\mathbf{F} \triangleq \begin{bmatrix} \mathbf{I}_M \\ \mathbf{0}_{L\times M} \end{bmatrix}, \tag{B.35}$$

$$\mathbf{G} \triangleq \mathbf{W}_M^H \mathbf{E} \mathbf{W}_M \begin{bmatrix} \mathbf{I}_M & \mathbf{I}_L \\ & \mathbf{0}_{(M-L)\times L} \end{bmatrix}, \tag{B.36}$$

respectively.

B.3.5 ZP-ZJ Transceivers

Lin and Phoong [2, 3, 32] had shown that the amount of redundancy $K \triangleq N - M \in \mathbb{N}$ required to eliminate IBI in memoryless block-based transceivers must satisfy the inequality $2K \geq L$. They proposed a family of memoryless discrete multitone transceivers with reduced redundancy. A particular transceiver of interest for our studies here is the zero-padding zero-jamming (ZP-ZJ) system, which is

[3] Actually, it is possible to implement ZP-OFDM systems using FFTs, but without diagonalizing the equivalent channel matrix.

characterized by the following transmitter and receiver matrices [32]:

$$\mathbf{F} \triangleq \begin{bmatrix} \mathbf{F}_0 \\ \mathbf{0}_{K\times M} \end{bmatrix}_{N\times M}, \tag{B.37}$$

$$\mathbf{G} \triangleq \begin{bmatrix} \mathbf{0}_{M\times(L-K)} & \mathbf{G}_0 \end{bmatrix}_{M\times N}, \tag{B.38}$$

where $\mathbf{F}_0 \in \mathbb{C}^{M\times M}$ and $\mathbf{G}_0 \in \mathbb{C}^{M\times(M+2K-L)}$.

The transfer matrix related to this transceiver is given by:

$$\mathbf{T}(z) = \mathbf{G}\mathbf{H}(z)\mathbf{F} = \mathbf{G}_0\mathbf{H}_0\mathbf{F}_0 = \mathbf{T}, \tag{B.39}$$

where, after removing the redundancy, the effective channel matrix is defined as [32]:

$$\mathbf{H}_0 \triangleq \begin{bmatrix} h(L-K) & \cdots & h(0) & 0 & 0 & \cdots & 0 \\ \vdots & \ddots & & & & & \vdots \\ h(K) & \ddots & & & & & 0 \\ \vdots & \ddots & & & \ddots & & h(0) \\ h(L) & & & & & & \vdots \\ 0 & & & & \ddots & & h(L-K) \\ \vdots & & & & & & \vdots \\ 0 & \cdots & 0 & 0 & h(L) & \cdots & h(K) \end{bmatrix} \in \mathbb{C}^{(M+2K-L)\times M}. \tag{B.40}$$

Considering $v(k) = 0, \forall k \in \mathbb{Z}$, we have:

$$\hat{\mathbf{s}}(n) = \mathbf{G}_0\mathbf{H}_0\mathbf{F}_0\mathbf{s}(n) = \mathbf{T}\mathbf{s}(n). \tag{B.41}$$

For this transceiver there are some constraints to be imposed upon the channel impulse response model so that a zero-forcing solution exists. These constraints are related to the concept of congruous zeros [32]. The congruous zeros of a transfer function $H(z)$ are the distinct zeros $z_0, z_1, \cdots, z_{\mu-1} \in \mathbb{C}$ which meet the following condition: $z_i^N = z_j^N, \forall i, j \in \{0, 1, \cdots, \mu-1\} \subset \mathbb{N}$. Note that μ is a function of N. As shown in [32], the channel model must satisfy the constraint $\mu(N) \leq K$, where $\mu(N)$ denotes the cardinality (number of elements) of the larger set of congruous zeros with respect to N.

Therefore, assuming the existence of minimum-redundancy solutions for a given channel, i.e., considering that $\mu(N) \leq L/2 \in \mathbb{N}$, then the ZF solution is such that its associated receiver matrix is given by:

$$\mathbf{G}_0 \triangleq (\mathbf{H}_0\mathbf{F}_0)^{-1} = \mathbf{F}_0^{-1}\mathbf{H}_0^{-1}, \tag{B.42}$$

where $\mathbf{H}_0 \in \mathbb{C}^{M\times M}$ is given and $\mathbf{F}_0$ is predefined.

This solution is computationally intensive since it requires the inversions of $M \times M$ matrices, requiring $\mathcal{O}(M^3)$ arithmetic operations. The conventional OFDM and SC-FD transceivers need $\mathcal{O}(M \log M)$ operations for the implementation of ZF and MMSE equalizers. The equalizer associated with the minimum-redundancy solution consists of multiplying the received vector by the receiver matrix entailing, $\mathcal{O}(M^2)$ operations. This complexity is high as compared to that of $\mathcal{O}(M \log M)$ required by traditional OFDM and SC-FD transceivers. This efficient equalization originates from the use of DFT matrices as well as the multiplication by memoryless diagonal matrices.

More details about ZP-ZJ transceivers will be given in Section D.1.

B.4 Concluding Remarks

This chapter has briefly reviewed the modeling of communication systems using the transmultiplexer framework. The LTI memoryless transceivers were the main focus of our presentation. Among these transceivers we particularly addressed the CP-OFDM, ZP-OFDM, CP-SC-FD, and ZP-SC-FD transceivers, highlighting their corresponding ZF and MMSE designs. Some results taken from the open literature related to transceivers with reduced redundancy were also discussed.

A lesson learned from this chapter is that the conventional OFDM and SC-FD transceivers are rather simple since the receiver and the equalizer have very simple implementations. These systems take advantage of the related circulant structure of the effective channel matrix. The circulant matrices can be diagonalized using a pair of DFT and IDFT transformations.

A further query is if it is possible to derive similar transceivers to the OFDM and SC-FD employing minimum redundancy, whose implementations rely on fast transforms as well. In fact, this is the focus of this thesis.

Part I

Minimum-Redundancy Systems

Apêndice C

Analysis of Zero-Padded Transceivers with Full-Redundancy

Before addressing the proposals of practical minimum-redundancy systems, one should first answer the relevant question: why investigating minimum/reduced-redundancy transceivers when efficient full-redundancy systems, such as OFDM and SC-FD, are already available? Such a question is related to the following reasoning: one may argue that the spectral efficiency can be enhanced by increasing the number M of transmitted data elements in a block, for a fixed channel order L. Let us define the bandwidth efficiency of a block-based transmission as $M/(M+K)$, in which K denotes the number of redundant elements in a block. Notice that $M/(M+\frac{L}{2}) = 2M/(2M+L)$, i.e., the bandwidth efficiency of a minimum-redundancy transceiver is the same of a full-redundancy system that uses twice as much the number of data symbols. Even though this approach is theoretically valid, several practical systems have strict requirements with respect to the value of M, particularly those dealing with delay-constrained applications. Nevertheless, if the particular application allows us to increase M, are there any additional drawbacks in doing so? The answer is yes, as described in this chapter.

The modeling of communication systems by using transmultiplexers is a well-known analysis tool [26–31, 40, 59]. Finite impulse-response (FIR) filters are preferred to infinite impulse-response (IIR) filters due to the difficulties inherent to both the design and analysis of IIR transmultiplexers [39]. In this context, FIR transmultiplexers capable of eliminating the intersymbol interference (ISI) intrinsic to broadband transmissions can be designed when redundant signals are properly inserted [7, 31, 32, 40, 41]. The type of redundancy (cyclic-prefix/suffix, zero-padding/jamming, etc) appended before transmitting the signals plays a central

role in the whole communication process.

In practical applications, memoryless block-based transmultiplexers are the prevalent choice. For such transceivers, zero-padding (ZP) is a quite effective way to eliminate the interblock interference (IBI) that pervades block-based transmissions. Indeed, in several different setups, ZP systems are optimal solutions in the mean-square error (MSE) sense [40]. This optimality characteristic leads to better performance of ZP-based transceivers, as compared to cyclic-prefix-based systems in a number of situations [37, 42]. Besides, ZP-based systems require lower transmission power than nonzero-padded solutions.

Nevertheless, redundant transceivers have some drawbacks, given that the insertion of redundant elements (data that, a priori, do not contain any additional information) reduces the effective data rate or throughput. The redundancy is employed by the transmission/reception processing to overcome the distortion effects introduced by frequency-selective channels. As an example, for an FIR-channel model with order L, a classical ZP-based system introduces at least L zeros before the transmission. This requirement reduces the throughput of these transceivers, especially when the channel is very dispersive.

The current trend of increasing the demand for radio transmissions shows no sign of settling. The amount of wireless data services is more than doubling each year leading to spectrum shortage as a sure event in the years to come. As a consequence, all efforts to maximize the spectrum usage are highly justifiable at this point. A possible way to cope with the throughput reduction related to redundant transceivers is to increase the number of data symbols, M, in a block. Indeed, as M increases, the ratio L/M decreases, which means that the relative amount of redundancy diminishes.

However, the block size M cannot have any desired value, since there are many factors that affect the choice of M. One of them is the delay constraint associated with the signal processing of a data block. Besides, there are some studies in the literature indicating a performance degradation of zero-padded transceivers whenever M increases [40, 42, 43].[1] The author in [42], for instance, has theoretically proved that several figures of merit that quantify the performance of ZP-based single-carrier optimal linear transceivers (either zero-forcing or minimum MSE optimal solutions) degrade as M increases. The authors in [40] have empirically verified a similar performance behavior for a wide class of zero-padded optimal transceivers, including DFE-based systems.

As the authors in [40] point out, for most of the available solutions there is no mathematical proof of how the relative amount of redundancy influences the transceiver performance, although in some cases there are simulation results that

[1] Such a behavior does not appear in CP-based transceivers, as described, for example, in [42].

indicate some trends. This chapter provides some of these missing mathematical proofs. Indeed, we prove that both the average MSE of symbols and the average mutual information between transmitted and estimated signals degrade whenever one decreases the relative amount of redundancy in the system, i.e., whenever M increases (for a fixed channel order).

Another interesting feature of the ZP-based transceivers is the performance behavior when one discards redundant data at the receiver side. The author in [43] has proved that the noise gains related to ZP-based single-carrier linear systems increase when one removes some redundant elements from the received vector in the attempt to diminish the amount of numerical operations in the equalization process. This chapter also extends the results from [43] to a wider class of ZP-based linear and DFE transceivers. More specifically, we demonstrate that the MSE and the mutual information related to ZP-based optimal transceivers are also monotone functions of the number of redundant elements employed in the equalization.

Moreover, as a final contribution, this chapter shows that, for a wide class of ZP-based linear and DFE systems, the performance degrades whenever a channel zero inside the unit circle is replaced by a related zero outside the unit circle, without changing the magnitude response of the channel. Actually, this result holds when one does not use the whole received data block in the equalization, i.e., when some redundant elements are discarded. If the whole received data block is employed, then the MSE and the mutual information related to such transceivers are not sensitive to whether the channel zeros are inside or outside the unit circle. It is worth mentioning that these results are extensions of similar results from [43] to a wider class of ZP-based optimal transceivers.

The organization of the chapter is as follows: Section C.1 gives the background of zero-padded optimal transceivers (linear and DFE). In Section C.2, some results that quantify the performance of zero-padded optimal transceivers are described. Section C.3 shows the monotonic behavior of the performance metrics described in Section C.2 when the block size varies. Section C.4 contains the results that characterize the monotonic behavior of the performance metrics described in Section C.2 when the number of redundant symbols used in the equalization process varies. The effect of the zero locations of the channel on the performance of zero-padded optimal transceivers is analyzed in Section C.5. The concluding remarks are described in Section C.6.

C.1 Model and Definitions of ZP Transceivers

Let $\mathbf{s} \in \mathcal{C}^{M\times 1} \subset \mathbb{C}^{M\times 1}$ be a vector containing $M \in \mathbb{N}$ symbols of a constellation $\mathcal{C}$. This vector is transmitted through a frequency-selective channel, whose matrix

model is

$$\mathbf{H}(z) = \mathbf{H}_{\text{ISI}} + z^{-1}\mathbf{H}_{\text{IBI}} \in \mathbb{C}^{N\times N}[z^{-1}], \tag{C.1}$$

where $M \leq N \in \mathbb{N}$ and $\mathbb{C}^{N\times N}[z^{-1}]$ denotes all polynomials in the variable z^{-1} with $N \times N$ complex-valued matrices as coefficients. The matrix $\mathbf{H}_{\text{ISI}}$ models the intersymbol-interference (ISI) characteristic of the channel, being defined as [31, 40]

$$\mathbf{H}_{\text{ISI}} = \begin{bmatrix} h(0) & 0 & 0 & \cdots & 0 \\ h(1) & h(0) & 0 & \cdots & 0 \\ \vdots & \vdots & \vdots & \vdots & \vdots \\ h(L) & h(L-1) & \ddots & \cdots & 0 \\ 0 & h(L) & \cdots & \cdots & 0 \\ \vdots & \vdots & \vdots & \vdots & \vdots \\ 0 & 0 & h(L) & \cdots & h(0) \end{bmatrix} \in \mathbb{C}^{N\times N}, \tag{C.2}$$

whereas the matrix $\mathbf{H}_{\text{IBI}}$ models the presence of interblock interference (IBI) inherent to all block-based transmissions, being defined as [31, 40]

$$\mathbf{H}_{\text{IBI}} = \begin{bmatrix} 0 & \cdots & 0 & h(L) & \cdots & h(1) \\ 0 & 0 & \cdots & 0 & \ddots & \vdots \\ \vdots & \vdots & \vdots & \vdots & \vdots & h(L) \\ 0 & 0 & 0 & \cdots & 0 & 0 \\ 0 & 0 & 0 & \cdots & 0 & 0 \\ \vdots & \vdots & \vdots & \vdots & \vdots & \vdots \\ 0 & 0 & 0 & 0 & \cdots & 0 \end{bmatrix} \in \mathbb{C}^{N\times N}. \tag{C.3}$$

The previous channel matrices have dimensions $N \times N$ since, in general, some sort of redundant signals (whose amount is $N - M$) are inserted before transmitting $\mathbf{s}$. This redundancy aims at eliminating the IBI. In this chapter, we shall consider zero-padded transceivers, i.e., the redundant signals are zeros that are inserted at the end of each data block.

Thus, by assuming an FIR-channel model $\{h(l)\}_{l\in\mathcal{L}}$ with complex-valued taps $h(l)$, for each $l \in \mathcal{L} = \{0, 1, \cdots, L\} \subset \mathbb{N}$, one can define the *effective channel matrix*

as [31, 40]

$$\mathbf{H} = \begin{bmatrix} h(0) & 0 & \cdots & 0 \\ h(1) & h(0) & \cdots & 0 \\ \vdots & \vdots & \ddots & \vdots \\ h(L) & & & \\ 0 & h(L) & & \\ \vdots & & \ddots & \vdots \\ 0 & 0 & \cdots & h(L) \end{bmatrix} \in \mathbb{C}^{(M+L)\times M}, \tag{C.4}$$

in which the IBI effect has already been eliminated by means of the insertion of L zeros in the transmitted data block. Notice that, in this case, $N = M + L$. In some situations, we shall also denote the effective-channel matrix in Eq. (C.4) as $\mathbf{H}_M$ in order to highlight that M symbols are transmitted per block.

Before starting the transmission, a pre-processing is implemented at the transmitter side through the multiplication of the vector $\mathbf{s}$ by the transmitter matrix $\mathbf{F} \in \mathbb{C}^{M\times M}$. The resulting data vector $\mathbf{x} = \mathbf{Fs}$ is the input of the effective channel. Hence, the received vector $\mathbf{y} = \mathbf{Hx} + \mathbf{v} \in \mathbb{C}^{(M+L)\times 1}$ is used to estimate the transmitted data, where $\mathbf{v}$ models the additive channel noise. The particular way the symbols are estimated at the receiver end depends on the transceiver structure. In this chapter, we shall consider only linear (see Subsection C.1.1) and DFE-based (see Subsection C.1.2) structures.

C.1.1 ZP Optimal Linear Equalizers

The symbol estimation in ZP optimal linear transceivers is implemented by means of a multiplication of the vector $\mathbf{y}$ by the receiver matrix $\mathbf{G} \in \mathbb{C}^{M\times(M+L)}$. Thus, we have the estimate $\hat{\mathbf{s}} = \mathbf{GHFs} + \mathbf{Gv}$.

There are many ways to design the transmitter and receiver matrices $\mathbf{F}$ and $\mathbf{G}$. In this chapter we shall focus mainly on minimizing the MSE of symbols, $\mathcal{E}_{\text{MSE}} \in \mathbb{R}_+$. The minimum MSE (MMSE) designs are very common in practical systems and their solutions are well-known [40]. The overall MSE of symbols is given by [40]

$$\begin{aligned} \mathcal{E}_{\text{MSE}} &= \mathsf{E}\{\|\hat{\boldsymbol{s}} - \boldsymbol{s}\|_2^2\} \\ &= \text{tr}\left\{(\mathbf{GHF} - \mathbf{I}_M)\mathbf{R}_{\boldsymbol{ss}}(\mathbf{GHF} - \mathbf{I}_M)^H\right\} + \text{tr}\left\{\mathbf{GR}_{\boldsymbol{vv}}\mathbf{G}^H\right\}, \end{aligned} \tag{C.5}$$

in which we have assumed that the transmitted vector $\mathbf{s}$ and the channel-noise vector $\mathbf{v}$ are respectively drawn from the zero-mean jointly wide-sense stationary (WSS) random processes $\boldsymbol{s}$ and $\boldsymbol{v}$.[2] In addition, we have assumed that $\boldsymbol{s}$ and $\boldsymbol{v}$ are

[2]We have omitted the time-index for the sake of simplicity.

uncorrelated, i.e. $\mathbf{R}_{\boldsymbol{sv}} = \mathsf{E}\{\boldsymbol{sv}^H\} = \mathsf{E}\{\boldsymbol{s}\}\mathsf{E}\{\boldsymbol{v}\}^H = \mathbf{0}_{M\times 1}\mathbf{0}_{1\times N} = \mathbf{0}_{M\times N}$.

Furthermore, let us assume that $\mathbf{R}_{\boldsymbol{ss}} = \mathsf{E}\{\boldsymbol{ss}^H\} = \sigma_s^2\mathbf{I}_M$ and $\mathbf{R}_{\boldsymbol{vv}} = \mathsf{E}\{\boldsymbol{vv}^H\} = \sigma_v^2\mathbf{I}_N$, with $\sigma_s^2, \sigma_v^2 \in \mathbb{R}_+$. The authors in [40] (pp. 399–400) show that the assumption $\mathbf{R}_{\boldsymbol{vv}} = \sigma_v^2\mathbf{I}_N$ is not a loss of generality. On the other hand, the assumption $\mathbf{R}_{\boldsymbol{ss}} = \sigma_s^2\mathbf{I}_M$ is adequate only in the cases of single-user systems employing neither bit nor power loading.[3] We therefore have

$$\mathcal{E}_{\mathrm{MSE}} = \sigma_s^2\|\mathbf{GHF} - \mathbf{I}_M\|_{\mathrm{F}}^2 + \sigma_v^2\|\mathbf{G}\|_{\mathrm{F}}^2. \tag{C.6}$$

Let us formulate the problem of designing the matrices $\mathbf{F}$ and $\mathbf{G}$ as an optimization problem:

$$\min_{\mathbf{F},\mathbf{G}} \left\{\sigma_s^2\|\mathbf{GHF} - \mathbf{I}_M\|_{\mathrm{F}}^2 + \sigma_v^2\|\mathbf{G}\|_{\mathrm{F}}^2\right\}, \tag{C.7}$$

subject to:

$$(\mathbf{GHF} - \mathbf{I}_M)\, i_{\mathrm{ZF}} = 0, \tag{C.8}$$

$$\left(\mathbf{FF}^H - \mathbf{I}_M\right) i_{\mathrm{UP}} = 0, \tag{C.9}$$

$$\left(\|\mathbf{F}\|_{\mathrm{F}}^2 - \frac{p_{\mathrm{T}}}{\sigma_s^2}\right)(1 - i_{\mathrm{UP}}) = 0, \tag{C.10}$$

$$\left(\mathbf{F}_0\mathbf{F}^H - \mathbf{I}_M\right) i_{\mathrm{CI-UP}} = 0, \tag{C.11}$$

where $i_{\mathrm{ZF}} \in \{0, 1\}$ is an indicator variable: the zero-forcing constraint is enforced whenever $i_{\mathrm{ZF}} = 1$. For $i_{\mathrm{ZF}} = 0$, one has a pure MMSE-based solution. Similarly, $i_{\mathrm{UP}} \in \{0, 1\}$ is also an indicator variable: a unitary-precoder (UP) system is designed whenever $i_{\mathrm{UP}} = 1$. Note that, for $i_{\mathrm{UP}} = 0$, the only restriction on the precoder matrix is to satisfy the power constraint. In this context, $p_{\mathrm{T}} \in \mathbb{R}_+$ denotes the total-power input to the channel. It is common to assume that $p_{\mathrm{T}} = p_{\mathrm{T}}(M) = M\sigma_s^2$, i.e., the average transmitted power per symbol is σ_s^2. Likewise, $i_{\mathrm{CI-UP}} \in \{0, 1\}$ is also an indicator variable: a channel-independent unitary-precoder (CI-UP) transceiver is designed whenever $i_{\mathrm{CI-UP}} = 1$. In general, the precoder matrix is a predefined unitary matrix $\mathbf{F}_0 \in \mathbb{C}^{M\times M}$. Two of the most useful examples of such a matrix are $\mathbf{F}_0 = \mathbf{I}_M$ (single-carrier transmission) and $\mathbf{F}_0 = \mathbf{W}_M^H$ (multicarrier transmission), in which $\mathbf{W}_M^H$ is the $M \times M$ normalized discrete Fourier transform (DFT) matrix [40, 41].

Note that the aforementioned optimization problem has six possible solutions. Each solution is associated with a choice of the indicator variables i_{ZF}, i_{UP}, and $i_{\mathrm{CI-UP}}$. Thus, we have the following transceiver types (see Table C.1):

1. CI-UP ZF system: an MMSE-based solution under both the zero-forcing and

[3] That is, equal-energy symbols.

channel-independent unitary-precoder constraints;

2. CI-UP Pure system: an MMSE-based solution under the channel-independent unitary-precoder constraint;

3. UP ZF system: an MMSE-based solution under both the zero-forcing and unitary-precoder constraints;

4. UP Pure system an MMSE-based solution under the unitary-precoder constraint;

5. ZF system an MMSE-based solution under both the zero-forcing and transmitter-power constraints;

6. Pure system an MMSE-based solution under the transmitter-power constraint.[4]

The solutions to the above optimization problem related to the first two transceiver types (CI-UP ZF[5] and CI-UP Pure) are given by [40] (p. 479 and p. 483):[6]

$$\mathbf{F}_{\text{ZF}}^{\text{CI-UP}} = \mathbf{F}_{\text{Pure}}^{\text{CI-UP}} = \mathbf{F}_0, \tag{C.12}$$

$$\mathbf{G}_{\text{ZF}}^{\text{CI-UP}} = \mathbf{F}_0^H \left(\mathbf{H}^H\mathbf{H}\right)^{-1} \mathbf{H}^H = \mathbf{F}_0^H \mathbf{H}^\dagger, \tag{C.13}$$

$$\mathbf{G}_{\text{Pure}}^{\text{CI-UP}} = \mathbf{F}_0^H \left(\mathbf{H}^H\mathbf{H} + \frac{\sigma_v^2}{\sigma_s^2}\mathbf{I}\right)^{-1} \mathbf{H}^H. \tag{C.14}$$

The other four linear solutions (whether UP-ZF, ZF, UP-Pure, or Pure MMSE-based solutions) to the above optimization problem share the same structure depicted in Figure C.1. The unitary matrices appearing in this figure stem from the singular-value decomposition (SVD) of the $N \times M$ effective channel matrix $\mathbf{H}$; that

[4]Note that CI-UP Pure and UP Pure transceivers do not meet the ZF constraint.

[5]Even though the CI-UP ZF transceiver does not depend upon any information about the statistics of the noise $\mathbf{v}$, it is a solution to the optimization problem defined in Eqs. (C.7)–(C.11) anyway. Thus, we shall still refer to it as a particular type of MMSE-based transceiver for the sake of conciseness.

[6]We shall assume that the matrix $\mathbf{H}$ has full column rank.

Table C.1: Six different choices of MMSE-based linear transceivers.

MMSE-based transceivers	$i_{\text{ZF}} = 1$	$i_{\text{ZF}} = 0$
$(i_{\text{UP}}, i_{\text{CI-UP}}) = (1, 1)$	CI-UP ZF	CI-UP Pure
$(i_{\text{UP}}, i_{\text{CI-UP}}) = (1, 0)$	UP ZF	UP Pure
$(i_{\text{UP}}, i_{\text{CI-UP}}) = (0, 1)$	CI-UP ZF	CI-UP Pure
$(i_{\text{UP}}, i_{\text{CI-UP}}) = (0, 0)$	ZF	Pure

is

$$\mathbf{H} = \underbrace{\mathbf{U}_{\mathbf{H}}}_{N\times N} \underbrace{\begin{bmatrix} \mathbf{\Sigma}_{\mathbf{H}} \\ \mathbf{0}_{L\times M} \end{bmatrix}}_{N\times M} \underbrace{\mathbf{V}_{\mathbf{H}}^{H}}_{M\times M}, \tag{C.15}$$

where $\mathbf{\Sigma}_{\mathbf{H}} = \mathbf{\Sigma}_{\mathbf{H}}^{H} > O$ is an $M \times M$ diagonal matrix containing the M nonzero singular values of $\mathbf{H}$. The mth diagonal element of $\mathbf{\Sigma}_{\mathbf{H}}$ is denoted as σ_m. In addition, the $M \times M$ diagonal matrices $\mathbf{\Sigma}_{\mathbf{F}}$ and $\mathbf{\Sigma}_{\mathbf{G}}$ depend on the particular design. Note that the optimal transmitter and receiver matrices are respectively given by [40] (p. 814):

$$\mathbf{F} = \mathbf{V}_{\mathbf{H}}\mathbf{\Sigma}_{\mathbf{F}}, \tag{C.16}$$

$$\mathbf{G} = \mathbf{\Sigma}_{\mathbf{G}}[\mathbf{I}_M \;\; \mathbf{0}_{M\times L}]\mathbf{U}_{\mathbf{H}}^{H}. \tag{C.17}$$

Furthermore, let us observe that if one substitutes $\mathbf{F}$ by $\mathbf{FU}$ and $\mathbf{G}$ by $\mathbf{U}^H\mathbf{G}$, where $\mathbf{U}$ is an $M\times M$ unitary matrix, the resulting MSE remains unchanged. Indeed, this occurs since

$$\begin{aligned} \mathcal{E}_{\text{MSE}} &= \sigma_s^2\|\mathbf{GHF} - \mathbf{I}_M\|_{\text{F}}^2 + \sigma_v^2\|\mathbf{G}\|_{\text{F}}^2 \\ &= \sigma_s^2\|\mathbf{U}^H(\mathbf{GHF} - \mathbf{I}_M)\mathbf{U}\|_{\text{F}}^2 + \sigma_v^2\|\mathbf{U}^H\mathbf{G}\|_{\text{F}}^2 \\ &= \sigma_s^2\|(\mathbf{U}^H\mathbf{G})\mathbf{H}(\mathbf{FU}) - \mathbf{I}_M\|_{\text{F}}^2 + \sigma_v^2\|(\mathbf{U}^H\mathbf{G})\|_{\text{F}}^2, \end{aligned} \tag{C.18}$$

for any unitary matrix $\mathbf{U}$. We therefore can insert a unitary matrix $\mathbf{U}$ at the transmitter (before the precoding process) and its inverse $\mathbf{U}^H$ at the receiver (after the equalization process) without changing the ZF-property, the transmitter power, or the MSE of symbols. Nevertheless, the additional unitary matrix $\mathbf{U}$ can be used to further minimize the average error-probability of symbols [40] (pp. 494–499).

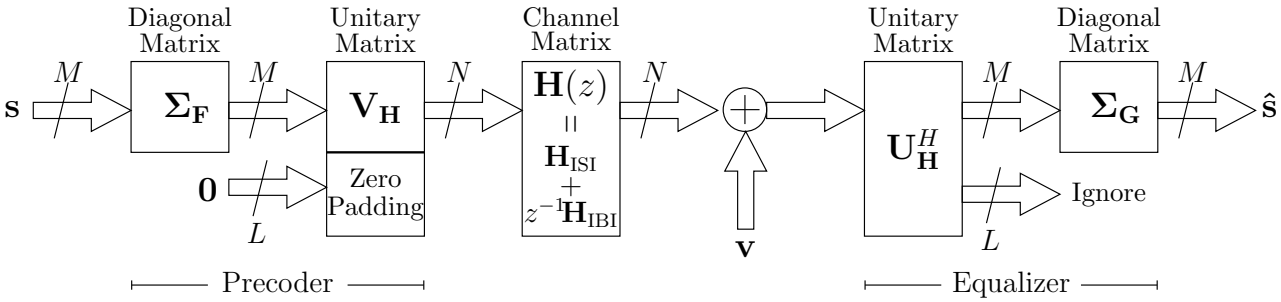

Figure C.1: Structure of the zero-padded UP-ZF, ZF, UP-Pure, and Pure MMSE-based transceivers.

C.1.2 ZP Optimal DFEs

Figure C.2 depicts the general structure of the DFE system. In this figure, $\check{\mathbf{s}} \in \mathbb{C}^{M\times 1}$ denotes the vector containing the detected symbols at the receiver end. The detected symbols are nonlinear functions of the estimated symbols. The estimation in ZP-DFE systems is implemented by means of a subtraction of the vector $\mathbf{B}\check{\mathbf{s}}$ from the vector $\mathbf{Gy}$. The $M \times (M + L)$ complex-valued matrix $\mathbf{G}$ is the so-called feedforward matrix, whereas the $M \times M$ complex-valued matrix $\mathbf{B}$ is the feedback matrix. Thus, we have the estimate $\hat{\mathbf{s}} = \mathbf{GHFs} + \mathbf{Gv} - \mathbf{B}\check{\mathbf{s}}$. Note that, since the detection is implemented based on the estimate $\hat{\mathbf{s}}$ itself, the matrix $\mathbf{B}$ is chosen to be strictly upper triangular, so that the symbol estimation within a data block is sequentially performed, guaranteeing the causality of the process [40].

The presence of a nonlinear function in the basic DFE model hinders the search for optimal solutions, even within the simple MMSE approach. A key hypothesis that helps one simplify the mathematical deduction of optimal solutions is the assumption of perfect decisions [40]. Thus, we shall assume that $\check{\mathbf{s}} = \mathbf{s}$ from now on. It is rather intuitive that this assumption is suitable only when the error-probability of symbols is small. Note that, by assuming perfect decisions, the estimate can be rewritten as $\hat{\mathbf{s}} = (\mathbf{GHF} - \mathbf{B})\mathbf{s} + \mathbf{Gv}$.

As in the linear case, there are many ways to design the transmitter, feedforward, and feedback matrices $\mathbf{F}$, $\mathbf{G}$, and $\mathbf{B}$. Once again, we will focus on minimizing the MSE of symbols, $\mathcal{E}_{\text{MSE}}^{\text{DFE}}$. Using the same hypotheses of the linear case, the overall MSE of symbols is given by [40]

$$\mathcal{E}_{\text{MSE}}^{\text{DFE}} = \sigma_s^2 \|\mathbf{GHF} - \mathbf{B} - \mathbf{I}_M\|_{\text{F}}^2 + \sigma_v^2 \|\mathbf{G}\|_{\text{F}}^2. \tag{C.19}$$

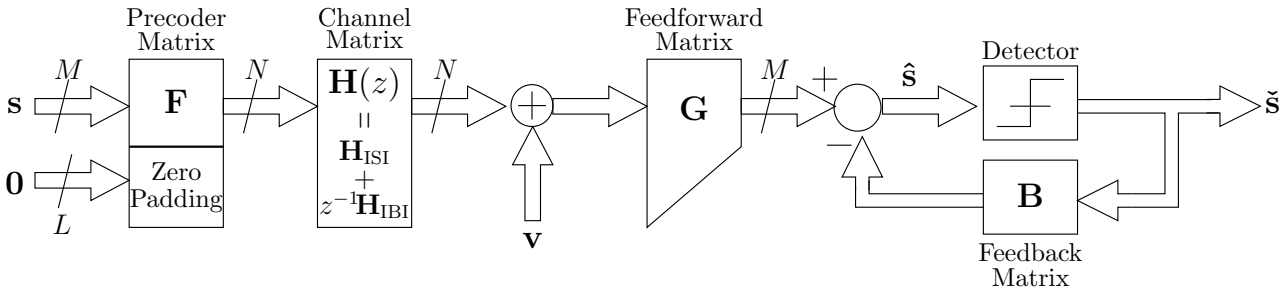

Figure C.2: General structure of an MMSE-based optimal DFE employing zero-padding.

Let us formulate the problem of designing the matrices $\mathbf{F}$, $\mathbf{G}$, and $\mathbf{B}$ as an

optimization problem:

$$\min_{\mathbf{F},\mathbf{G},\mathbf{B}} \left\{\sigma_s^2\|\mathbf{GHF}-\mathbf{B}-\mathbf{I}_M\|_{\mathrm{F}}^2+\sigma_v^2\|\mathbf{G}\|_{\mathrm{F}}^2\right\}, \tag{C.20}$$

subject to:

$$(\mathbf{GHF}-\mathbf{B}-\mathbf{I}_M)\, i_{\mathrm{ZF}}=0, \tag{C.21}$$

$$\|\mathbf{F}\|_{\mathrm{F}}^2=\frac{p_{\mathrm{T}}}{\sigma_s^2}=M, \tag{C.22}$$

$$[\mathbf{B}]_{mn}=0,\ \ \forall m\geq n, \tag{C.23}$$

where $i_{\mathrm{ZF}}\in\{0,1\}$ is an indicator variable: the zero-forcing constraint is enforced whenever $i_{\mathrm{ZF}}=1$. For $i_{\mathrm{ZF}}=0$, one has a pure MMSE-based solution. Hence, for the DFE system, we have only two distinct solutions: ZF and Pure MMSE-based solutions. We do not consider other solutions since they are all related to each other. The ZF solution, for instance, is also a unitary-precoder solution and it also minimizes the error-probability of symbols [40] (pp. 619–621).

The solutions to the above optimization problem related to the two DFE systems are given by [40] (p. 816):

$$\mathbf{F}=\mathbf{V}_{\mathbf{H}}\mathbf{\Sigma}_{\mathbf{F}}\mathbf{S}, \tag{C.24}$$

$$\mathbf{G}=(\mathbf{I}+\mathbf{B})\mathbf{S}^H\mathbf{\Lambda}[\mathbf{I}_M\ \ \mathbf{0}_{M\times L}]\mathbf{U}_{\mathbf{H}}^H, \tag{C.25}$$

$$\mathbf{B}=\mathbf{R}-\mathbf{I}, \tag{C.26}$$

in which $\mathbf{\Lambda}$ and $\mathbf{\Sigma}_{\mathbf{F}}$ are diagonal matrices, whereas $\mathbf{S}$ is an $M\times M$ unitary matrix, and $\mathbf{R}$ is an $M\times M$ upper triangular matrix containing only 1s in its main diagonal. In fact, the exact definitions of the diagonal matrices $\mathbf{\Lambda}$ and $\mathbf{\Sigma}_{\mathbf{F}}$, as well as the unitary matrices $\mathbf{S}$ and $\mathbf{R}$ depend on the particular design, whether a ZF or a Pure MMSE-based solution is chosen. However, the matrices $\mathbf{S}$ and $\mathbf{R}$ always come from QRS decompositions of diagonal matrices for both designs [40] (pp. 646–656). In the ZF case, for instance, the related QRS decomposition is $\mathbf{\Sigma}_{\mathbf{H}}=\sigma\mathbf{QRS}^H$, where $\mathbf{Q}$ and $\mathbf{S}$ are unitary matrices, whereas $\mathbf{R}$ is upper triangular with diagonal elements $[\mathbf{R}]_{mm}=1$. In addition, $\sigma\in\mathbb{R}_+$ is the geometric mean of the diagonal elements of $\mathbf{\Sigma}_{\mathbf{H}}$. See [40] and references therein for further detailed information.

C.2 Performance of Optimal ZP Transceivers

This section characterizes the performance of zero-padded optimal transceivers by using some appropriate figures of merit. We shall focus mainly on the MSE of symbols and the mutual information between transmitted and estimated signals. In addition, we shall also describe the error-probability of symbols associated with

some of these transceivers, namely: minimum error-probability and DFE MMSE-based systems.

The MSE of symbols is a widely used figure of merit since it allows one to quantify the overall amount of symbol errors throughout the estimation process. The mathematical simplicity inherent to MSE-based analyses is perhaps the main reason for their overwhelming adoption [60]. Nonetheless, the conclusions taken from an MSE analysis must be regarded with care, since the MSE does not necessarily capture all the aspects of the transceiver performance. The error-probability of symbols, for instance, may be different for systems with the same MSE of symbols.

In order to characterize the MSE performance of the ZP transceivers, let us first define $\mathbf{S}_M = \mathbf{R}_M^{-1}$, in which $\mathbf{R}_M = \mathbf{H}_M^H \mathbf{H}_M \in \mathbb{C}^{M\times M}$ is the deterministic channel-correlation matrix, considering the transmission of M data symbols. Similarly, let us assume that $\mathbf{S}'_M = (\mathbf{R}'_M)^{-1}$, where $\mathbf{R}'_M = \mathbf{H}_M^H \mathbf{H}_M + \frac{\sigma_v^2}{\sigma_s^2}\mathbf{I}_M \in \mathbb{C}^{M\times M}$ enjoys the same structure as $\mathbf{R}_M$. Moreover, we shall denote explicitly that the singular values of $\mathbf{H}_M$ depend on M. Thus, $\sigma_m(M)$ is the mth singular value of $\mathbf{H}_M$. By using these definitions, we have the following result concerning the average MSE of symbols related to each ZP optimal transceiver.

Proposition 1. *The zero-padded MMSE-based optimal transceivers have the following average MSE of symbols:*[7]

$$\mathcal{E}_{\text{ZF}}^{\text{UP}}(M) = \sigma_v^2 \left(\frac{1}{M} \sum_{m=0}^{M-1} \frac{1}{\sigma_m^2(M)} \right) = \sigma_v^2 \frac{\text{tr}\left\{\mathbf{S}_M\right\}}{M}, \tag{C.27}$$

$$\mathcal{E}_{\text{Pure}}^{\text{UP}}(M) = \sigma_v^2 \left(\frac{1}{M} \sum_{m=0}^{M-1} \frac{1}{\frac{\sigma_v^2}{\sigma_s^2} + \sigma_m^2(M)} \right) = \sigma_v^2 \frac{\text{tr}\left\{\mathbf{S}'_M\right\}}{M}, \tag{C.28}$$

$$\mathcal{E}_{\text{ZF}}^{\text{CI-UP}}(M) = \sigma_v^2 \left(\frac{1}{M} \sum_{m=0}^{M-1} \frac{1}{\sigma_m^2(M)} \right) = \sigma_v^2 \frac{\text{tr}\left\{\mathbf{S}_M\right\}}{M}, \tag{C.29}$$

$$\mathcal{E}_{\text{Pure}}^{\text{CI-UP}}(M) = \sigma_v^2 \left(\frac{1}{M} \sum_{m=0}^{M-1} \frac{1}{\frac{\sigma_v^2}{\sigma_s^2} + \sigma_m^2(M)} \right) = \sigma_v^2 \frac{\text{tr}\left\{\mathbf{S}'_M\right\}}{M}, \tag{C.30}$$

$$\mathcal{E}_{\text{ZF}}(M) = \sigma_v^2 \left(\frac{1}{M} \sum_{m=0}^{M-1} \frac{1}{\sigma_m(M)} \right)^2 = \sigma_v^2 \left(\frac{\text{tr}\left\{\sqrt{\mathbf{S}_M}\right\}}{M} \right)^2, \tag{C.31}$$

$$\mathcal{E}_{\text{ZF}}^{\text{DFE}}(M) = \sigma_v^2 \left(\prod_{m=0}^{M-1} \frac{1}{\sigma_m^2(M)} \right)^{\frac{1}{M}} = \sigma_v^2 \sqrt[M]{\det\{\mathbf{S}_M\}}. \tag{C.32}$$

Proof. We have just rewritten the results from Tables I.1, I.2, and I.3 in Appendix I of [40] (pp. 814–816).[8] □

[7] When the block size is M, we set $\mathcal{E}(M) = \frac{\mathcal{E}_{\text{MSE}}}{M}$ (see Eqs. (C.5) and (C.6)).

[8] The notation $\sqrt{\mathbf{S}}$ means $\mathbf{U}\sqrt{\mathbf{\Lambda}}\mathbf{U}^H$, considering the eigendecomposition $\mathbf{S} = \mathbf{U}\mathbf{\Lambda}\mathbf{U}^H$. The square root of a diagonal matrix $\mathbf{\Lambda} = \text{diag}\{\lambda_m\}_{m=0}^{M-1}$ is $\sqrt{\mathbf{\Lambda}} = \text{diag}\{\sqrt{\lambda_m}\}_{m=0}^{M-1}$.

The reader should notice the close relationship between the MSE of symbols and the singular values of the effective-channel matrix. Indeed, smaller singular values of the effective-channel matrix lead to larger average MSE of symbols. With respect to the average MSE of symbols related to Pure MMSE-based systems (linear and DFE), we did not include them in Proposition 1 since the exact expressions for $\mathcal{E}_{\text{Pure}}(M)$ and $\mathcal{E}_{\text{Pure}}^{\text{DFE}}(M)$, without assuming that the transmitted power is large, are too complicated to be analyzed here (see Eqs. (13.50) and (19.113) from [40]). For this reason, we shall refer to zero-padded optimal transceivers without including Pure MMSE-based systems (linear and DFE) from now on.

Another very useful figure of merit is the mutual information between the transmitted and estimated signals. Mutual information allows one to quantify the mutual statistical dependence related to these two random variables. This dependence can be thought as the statistical information that the transmitted and the estimated signals share. For example, a really poor transmission/reception process is such that the transmitted vector $\mathbf{s}$ is not strongly related to the estimate $\hat{\mathbf{s}}$. In this case, the related mutual information between $\boldsymbol{s}$ and $\hat{\boldsymbol{s}}$ is close to zero, revealing some statistical independence. On the other hand, a perfect transmission/reception process is such that $\hat{\mathbf{s}} = \mathbf{s}$. In this particular case, the mutual information between $\boldsymbol{s}$ and $\hat{\boldsymbol{s}}$ is maximum (i.e., it is equal to the entropy of $\boldsymbol{s}$).

By taking this fact into account, we have developed the following result concerning the average mutual information between the transmitted vector $\boldsymbol{s}$ and its estimate $\hat{\boldsymbol{s}}$ related to each ZP optimal transceiver.

Theorem 1. *For the zero-padded MMSE-based optimal transceivers, the average*

mutual information between the transmitted vector $\boldsymbol{s}$ and its estimate $\hat{\boldsymbol{s}}$ is given by:[9]

$$\mathcal{I}_{\mathrm{ZF}}^{\mathrm{UP}}(M) = \frac{\mathrm{tr}\left\{\ln\left[\mathbf{I}_M + \left(\frac{\sigma_v^2}{\sigma_s^2}\mathbf{S}_M\right)^{-1}\right]\right\}}{M}, \tag{C.33}$$

$$\mathcal{I}_{\mathrm{Pure}}^{\mathrm{UP}}(M) = \frac{\mathrm{tr}\left\{\ln\left[\mathbf{I}_M + \left(\frac{\sigma_v^2}{\sigma_s^2}\mathbf{S}_M\right)^{-1}\right]\right\}}{M}, \tag{C.34}$$

$$\mathcal{I}_{\mathrm{ZF}}^{\mathrm{CI-UP}}(M) = \frac{\mathrm{tr}\left\{\ln\left[\mathbf{I}_M + \left(\frac{\sigma_v^2}{\sigma_s^2}\mathbf{S}_M\right)^{-1}\right]\right\}}{M}, \tag{C.35}$$

$$\mathcal{I}_{\mathrm{Pure}}^{\mathrm{CI-UP}}(M) = \frac{\mathrm{tr}\left\{\ln\left[\mathbf{I}_M + \left(\frac{\sigma_v^2}{\sigma_s^2}\mathbf{S}_M\right)^{-1}\right]\right\}}{M}, \tag{C.36}$$

$$\mathcal{I}_{\mathrm{ZF}}(M) = \frac{\mathrm{tr}\left\{\ln\left[\mathbf{I}_M + \left(\rho_M^{\mathrm{ZF}}\sqrt{\mathbf{S}_M}\right)^{-1}\right]\right\}}{M}, \tag{C.37}$$

$$\mathcal{I}_{\mathrm{ZF}}^{\mathrm{DFE}}(M) = \ln\left[1 + \frac{\sigma_s^2}{\sigma_v^2}\sqrt[M]{\det\left\{\mathbf{S}_M^{-1}\right\}}\right], \tag{C.38}$$

where ρ_M^{ZF} is a positive number that depends on M. In addition, we have assumed that $\boldsymbol{s}$ and $\boldsymbol{v}$ are independent zero-mean circularly symmetric complex Gaussian random vectors.

Proof. Let us first consider the two channel-independent unitary-precoder linear transceivers. Recalling that the differential entropy of a random vector $\boldsymbol{r}$ is denoted as $\mathcal{H}(\boldsymbol{r})$, then from the hypotheses of Theorem 1 and by considering that $\hat{\boldsymbol{s}} = \mathbf{GHF}_0\boldsymbol{s} + \mathbf{G}\boldsymbol{v} = \mathbf{GHF}_0\boldsymbol{s} + \boldsymbol{v}'$, we can write

$$\begin{aligned}
\mathcal{I}(\boldsymbol{s};\hat{\boldsymbol{s}}) &= \mathcal{H}(\hat{\boldsymbol{s}}) - \mathcal{H}(\hat{\boldsymbol{s}}|\boldsymbol{s}) \\
&= \mathcal{H}(\hat{\boldsymbol{s}}) - \mathcal{H}(\mathbf{GHF}_0\boldsymbol{s} + \boldsymbol{v}'|\boldsymbol{s}) \\
&= \mathcal{H}(\hat{\boldsymbol{s}}) - \mathcal{H}(\boldsymbol{v}') \\
&= \ln\left[\det\left(\pi e\mathbf{C}_{\hat{\boldsymbol{s}}\hat{\boldsymbol{s}}}\right)\right] - \ln\left[\det\left(\pi e\mathbf{C}_{\boldsymbol{v}'\boldsymbol{v}'}\right)\right] \\
&= \ln\left[\frac{\det\left(\mathbf{C}_{\hat{\boldsymbol{s}}\hat{\boldsymbol{s}}}\right)}{\det\left(\mathbf{C}_{\boldsymbol{v}'\boldsymbol{v}'}\right)}\right] \\
&= \ln\left[\det\left(\mathbf{C}_{\boldsymbol{v}'\boldsymbol{v}'}^{-1}\mathbf{C}_{\hat{\boldsymbol{s}}\hat{\boldsymbol{s}}}\right)\right],
\end{aligned} \tag{C.39}$$

where $\mathbf{C}_{\hat{\boldsymbol{s}}\hat{\boldsymbol{s}}} = \sigma_s^2\mathbf{GHH}^H\mathbf{G}^H + \sigma_v^2\mathbf{GG}^H$ and $\mathbf{C}_{\boldsymbol{v}'\boldsymbol{v}'} = \sigma_v^2\mathbf{GG}^H$. One therefore has

$$\mathbf{C}_{\boldsymbol{v}'\boldsymbol{v}'}^{-1}\mathbf{C}_{\hat{\boldsymbol{s}}\hat{\boldsymbol{s}}} = \mathbf{I} + \frac{\sigma_s^2}{\sigma_v^2}(\mathbf{GG}^H)^{-1}\mathbf{GHH}^H\mathbf{G}^H. \tag{C.40}$$

[9]When the block size is M, we set $\mathcal{I}(M) = \frac{\mathcal{I}(\boldsymbol{s};\hat{\boldsymbol{s}})}{M}$, where $\mathcal{I}(\boldsymbol{s};\hat{\boldsymbol{s}})$ is the mutual information between the complex-valued vectors $\boldsymbol{s}$ and $\hat{\boldsymbol{s}}$.

Using Eqs. (C.13) and (C.14), it is possible to verify that

$$\begin{aligned}\mathbf{C}_{\boldsymbol{v}'\boldsymbol{v}'}^{-1}\mathbf{C}_{\hat{\boldsymbol{s}}\hat{\boldsymbol{s}}} &= \mathbf{I} + \frac{\sigma_s^2}{\sigma_v^2}\mathbf{F}_0^H(\mathbf{H}^H\mathbf{H})\mathbf{F}_0 \\ &= \mathbf{F}_0^H\left(\mathbf{I} + \frac{\sigma_s^2}{\sigma_v^2}\mathbf{R}_M\right)\mathbf{F}_0 \\ &= \mathbf{F}_0^H\left[\mathbf{I} + \left(\frac{\sigma_v^2}{\sigma_s^2}\mathbf{S}_M\right)^{-1}\right]\mathbf{F}_0, \end{aligned} \tag{C.41}$$

where, in the case of CI-UP-Pure transceivers, we have used the fact that

$$\mathbf{H}^H\mathbf{H}\left(\mathbf{H}^H\mathbf{H} + \frac{\sigma_v^2}{\sigma_s^2}\mathbf{I}\right)^{-1} = \left(\mathbf{H}^H\mathbf{H} + \frac{\sigma_v^2}{\sigma_s^2}\mathbf{I}\right)^{-1}\mathbf{H}^H\mathbf{H}, \tag{C.42}$$

which yields

$$\mathbf{G}\mathbf{H}\mathbf{H}^H\mathbf{G}^H = (\mathbf{G}\mathbf{G}^H)(\mathbf{F}_0^H\mathbf{H}^H\mathbf{H}\mathbf{F}_0). \tag{C.43}$$

Hence, by substituting Eq. (C.41) into Eq. (C.39), we finally arrive at

$$\begin{aligned}\mathcal{I}_{\mathrm{ZF}}^{\mathrm{CI-UP}}(M) = \mathcal{I}_{\mathrm{Pure}}^{\mathrm{CI-UP}}(M) &= \frac{1}{M}\mathcal{I}(\boldsymbol{s};\hat{\boldsymbol{s}}) \\ &= \frac{1}{M}\ln\det\left\{\mathbf{F}_0^H\left[\mathbf{I}_M + \left(\frac{\sigma_v^2}{\sigma_s^2}\mathbf{S}_M\right)^{-1}\right]\mathbf{F}_0\right\} \\ &= \frac{1}{M}\ln\det\left[\mathbf{I}_M + \left(\frac{\sigma_v^2}{\sigma_s^2}\mathbf{S}_M\right)^{-1}\right] \\ &= \frac{\mathrm{tr}\left\{\ln\left[\mathbf{I}_M + \left(\frac{\sigma_v^2}{\sigma_s^2}\mathbf{S}_M\right)^{-1}\right]\right\}}{M}. \end{aligned} \tag{C.44}$$

Considering the other three linear solutions (UP-ZF, UP-Pure, or ZF MMSE-based linear transceivers), we know from Eqs. (C.16) and (C.17) that

$$\begin{aligned}\hat{\boldsymbol{s}} &= \left([\boldsymbol{\Sigma}_{\mathbf{G}} \;\; \mathbf{0}_{M\times L}]\mathbf{U}_{\mathbf{H}}^H\right)\left(\mathbf{U}_{\mathbf{H}}\begin{bmatrix}\boldsymbol{\Sigma}_{\mathbf{H}} \\ \mathbf{0}_{L\times M}\end{bmatrix}\mathbf{V}_{\mathbf{H}}^H\right)(\mathbf{V}_{\mathbf{H}}\boldsymbol{\Sigma}_{\mathbf{F}})\,\boldsymbol{s} + \left([\boldsymbol{\Sigma}_{\mathbf{G}} \;\; \mathbf{0}_{M\times L}]\mathbf{U}_{\mathbf{H}}^H\right)\boldsymbol{v} \\ &= \boldsymbol{\Sigma}_{\mathbf{G}}\boldsymbol{\Sigma}_{\mathbf{H}}\boldsymbol{\Sigma}_{\mathbf{F}}\boldsymbol{s} + \boldsymbol{\Sigma}_{\mathbf{G}}\overline{\boldsymbol{v}}, \end{aligned} \tag{C.45}$$

where $\overline{\boldsymbol{v}} = [\mathbf{I}_M \;\; \mathbf{0}_{M\times L}]\mathbf{U}_{\mathbf{H}}^H\boldsymbol{v}$. Note that there is no interference among symbols within a block in these ZP-MMSE-based optimal transceivers. In other words, the resulting transceivers are comprised of M parallel complex Gaussian channels. The

SNR for the mth channel is given by

$$\mathrm{SNR}_m(M) = \sigma_m^2(M)\sigma_{\mathbf{F},m}^2(M)\frac{\sigma_s^2}{\sigma_v^2}, \tag{C.46}$$

in which $\sigma_{\mathbf{F},m}(M)$ is the mth diagonal element of $\mathbf{\Sigma}_{\mathbf{F}}$, assuming the transmission of M data symbols. Thus, whenever a unitary-precoder system is designed, one has $\sigma_{\mathbf{F},m}(M) = 1$ for all m [40]. In this case,

$$\mathrm{SNR}_m(M) = \frac{\sigma_s^2}{\sigma_v^2}\sigma_m^2(M). \tag{C.47}$$

If the ZF MMSE-based design is employed, then $\sigma_{\mathbf{F},m}^2(M) = \frac{\sigma_v}{\sqrt{\mathcal{E}_{\mathrm{ZF}}(M)}}\frac{1}{\sigma_m}$ [40], where $\mathcal{E}_{\mathrm{ZF}}(M)$ is defined in Eq. (C.31). Hence,

$$\mathrm{SNR}_m(M) = \frac{\sigma_s^2}{\sigma_v^2}\frac{\sigma_v}{\sqrt{\mathcal{E}_{\mathrm{ZF}}(M)}}\sigma_m. \tag{C.48}$$

All these three cases yield

$$\mathcal{I}(\boldsymbol{s};\hat{\boldsymbol{s}}) = \sum_{m=0}^{M-1}\ln\left[1+\mathrm{SNR}_m(M)\right]. \tag{C.49}$$

Thus, for unitary-precoder systems, we finally arrive at

$$\begin{aligned}\mathcal{I}_{\mathrm{ZF}}^{\mathrm{UP}}(M) = \mathcal{I}_{\mathrm{Pure}}^{\mathrm{UP}}(M) &= \frac{1}{M}\mathcal{I}(\boldsymbol{s};\hat{\boldsymbol{s}}) \\ &= \frac{1}{M}\sum_{m=0}^{M-1}\ln\left[1+\frac{\sigma_s^2}{\sigma_v^2}\sigma_m^2(M)\right] \\ &= \frac{\mathrm{tr}\left\{\ln\left[\mathbf{I}_M+\left(\frac{\sigma_v^2}{\sigma_s^2}\mathbf{S}_M\right)^{-1}\right]\right\}}{M},\end{aligned} \tag{C.50}$$

whereas for the ZF MMSE-based systems, we arrive at

$$\begin{aligned}\mathcal{I}_{\mathrm{ZF}}(M) &= \frac{1}{M}\mathcal{I}(\boldsymbol{s};\hat{\boldsymbol{s}}) \\ &= \frac{1}{M}\sum_{m=0}^{M-1}\ln\left[1+\frac{\sigma_s^2}{\sigma_v^2}\frac{\sigma_v}{\sqrt{\mathcal{E}_{\mathrm{ZF}}(M)}}\sigma_m\right] \\ &= \frac{1}{M}\sum_{m=0}^{M-1}\ln\left[1+\frac{\sigma_m}{\rho_M^{\mathrm{ZF}}}\right] \\ &= \frac{\mathrm{tr}\left\{\ln\left[\mathbf{I}_M+\left(\rho_M^{\mathrm{ZF}}\sqrt{\mathbf{S}_M}\right)^{-1}\right]\right\}}{M},\end{aligned} \tag{C.51}$$

in which

$$\rho_M^{\mathrm{ZF}} = \frac{\sigma_v^2}{\sigma_s^2}\frac{\sqrt{\mathcal{E}_{\mathrm{ZF}}(M)}}{\sigma_v}. \tag{C.52}$$

With respect to the ZF-DFE system, we know from [40] that $\mathbf{\Sigma_H} = \sigma\mathbf{QRS}^H$, where $\mathbf{Q}$ and $\mathbf{S}$ are unitary matrices. In addition, we also know from [40] that

$$\hat{\boldsymbol{s}} = \boldsymbol{s} + \mathbf{RS}^H{\mathbf{\Sigma_H}}^{-1}\overline{\boldsymbol{v}} = \boldsymbol{s} + \sigma^{-1}\mathbf{Q}^H\overline{\boldsymbol{v}}, \tag{C.53}$$

where $\overline{\boldsymbol{v}}$ is also a zero-mean circularly symmetric complex Gaussian random vector. In addition, we still have that $\boldsymbol{s}$ and $\overline{\boldsymbol{v}}$ are jointly WSS random vectors, with $\mathbf{R}_{\overline{\boldsymbol{v}}\overline{\boldsymbol{v}}} = \sigma_v^2\mathbf{I}_M$ and $\mathbf{R}_{\boldsymbol{s}\overline{\boldsymbol{v}}} = \mathbf{0}_{M\times M}$. Hence, by using the same reasoning that we have just employed to derive the results related to channel-independent unitary-precoder transceivers, one has

$$\begin{aligned}
\mathcal{I}_{\mathrm{ZF}}^{\mathrm{DFE}}(M) &= \frac{1}{M}\mathcal{I}(\boldsymbol{s};\hat{\boldsymbol{s}}) \\
&= \frac{1}{M}\ln\det\left\{\left[\sigma_v^2\sigma^{-2}\mathbf{I}_M\right]^{-1}\left[(\sigma_s^2+\sigma_v^2\sigma^{-2})\mathbf{I}_M\right]\right\} \\
&= \frac{1}{M}\ln\det\left\{\left(\frac{\sigma_s^2}{\sigma_v^2}\sigma^2+1\right)\mathbf{I}_M\right\} \\
&= \ln\left\{1+\frac{\sigma_s^2}{\sigma_v^2}\sigma^2\right\} \\
&= \ln\left[1+\frac{\sigma_s^2}{\sigma_v^2}\sqrt[M]{\det\left\{\mathbf{S}_M^{-1}\right\}}\right],
\end{aligned} \tag{C.54}$$

where we have used the fact that [40]

$$\sigma^2 = \sqrt[M]{\det\left\{\mathbf{R}_M\right\}} = \sqrt[M]{\det\left\{\mathbf{S}_M^{-1}\right\}}. \tag{C.55}$$

The authors in [40] have derived the above result in a distinct way. □

Once again, the average mutual information is a figure of merit which is strongly related to the singular values of the effective-channel matrix. Indeed, the smaller the singular values of the effective-channel matrix are, the smaller the average mutual information is.

The ultimate goal of a transmission/reception process is to allow one to transmit symbols that, ideally, could be perfectly detected at the receiver end. The error-probability of symbols is, therefore, a very appealing figure of merit to quantify the performance of communication systems. For the case of both the minimum error-probability and the DFE MMSE-based systems (see Section C.1), the resulting error-probability of symbols are directly associated with the average MSE of symbols.

Indeed, it is possible to show that, for such transceivers, the average error-probability of symbols is a monotone increasing function of the corresponding average MSE of symbols [40] (p. 579 and p. 619). This close relationship between these two important figures of merit is quite useful, since any monotonic behavior associated with the MSE of symbols is automatically transferred to the error-probability of symbols associated with both the minimum error-probability and the DFE MMSE-based systems.[10]

C.3 Effect of Increasing the Block Size

This section analyzes the behavior of both the MSE and the mutual information associated with the optimal ZP transceivers as the number of transmitted symbols, M, increases. With such an analysis we aim at evaluating the effect of increasing the bandwidth efficiency upon the performance of optimal ZP transceivers. Indeed, when we consider the transmission of signals through an Lth-order channel, the percentage of redundant signals in the whole data block always decreases when one increases the number of data symbols from M to $M+1$. On the other hand, one is not allowed to increase M substantially due to delays introduced by the signal-processing building blocks of the transceivers.

The block size M does interfere in the performance of the optimal ZP transceivers, in addition to its drawbacks in delay-constraint applications. As a matter of fact, the performance of optimal ZP transceivers tends to degrade as the block size increases. The author in [42] has proved that several figures of merit that quantify the performance of single-carrier ZP transceivers present a monotone behavior with respect to M. For example, the average MSE and the average error-probability of symbols are monotone increasing functions of M. A similar behavior has also been reported in [40] for the other optimal ZP transceivers after performing thorough simulation experiments. Nonetheless, as highlighted in [40] (p. 590), no theoretical proof of this monotonic behavior is known for the case of jointly optimized transceivers (linear or DFE), except for the single-carrier ZP transceiver [40, 42]. The following results are the first attempt to bridge this gap.

Theorem 2. *The average MSE of symbols associated with the zero-padded MMSE-based optimal transceivers is a monotone increasing function of the number of transmitted symbols per block. Mathematically, for all positive integer M, one has $\mathcal{E}(M) \leq \mathcal{E}(M+1)$.*

[10] The reader should remember from the discussions in the last paragraph of Section C.1 that minimum error-probability systems can be designed by introducing a unitary matrix $\mathbf{U}$ at the transmitter side and its inverse, $\mathbf{U}^H$, at the receiver end aiming at minimizing the overall average error-probability of symbols (see pp. 494–499 in [40]).

Proof. Before proving Theorem 2, we shall state two important auxiliary results, as follows.

Lemma 1. *Given two sets of real numbers* $\{a_0, a_1, \cdots, a_{M-1}\}$ *and* $\{b_0, b_1, \cdots, b_M\}$*, if their elements respect the following inequalities:* $b_m \geq a_m$ *and* $b_{m+1} \geq a_m$*, for all* $m \in \{0, 1, \cdots, M-1\}$*, then one always has*

$$\frac{1}{M+1}\sum_{m=0}^{M} b_m \geq \frac{1}{M}\sum_{m=0}^{M-1} a_m. \tag{C.56}$$

Proof. See [40, 42]. □

Lemma 2. *For any positive semidefinite Hermitian matrix* $\mathbf{S}$*, the function* $\sqrt{\mathbf{S}}$ *is monotone, i.e.,* $\sqrt{\mathbf{S}_a} \geq \sqrt{\mathbf{S}_b}$ *whenever* $\mathbf{S}_a \geq \mathbf{S}_b \geq O$*.*

Proof. See [61]. □

Now, we are able to demonstrate Theorem 2. First of all, note that the $(M+1)\times(M+1)$ complex-valued matrix $\mathbf{R}_{M+1} = \mathbf{H}_{M+1}^H \mathbf{H}_{M+1}$ can be partitioned as

$$\mathbf{R}_{M+1} = \begin{bmatrix} \mathbf{R}_M & \mathbf{u}_M \\ \mathbf{u}_M^H & c \end{bmatrix} = \begin{bmatrix} c & \mathbf{w}_M \\ \mathbf{w}_M^H & \mathbf{R}_M \end{bmatrix}. \tag{C.57}$$

Now, by defining both $\delta_u = \sqrt{c - \mathbf{u}_M^H \mathbf{S}_M \mathbf{u}_M}$ and $\delta_w = \sqrt{c - \mathbf{w}_M^H \mathbf{S}_M \mathbf{w}_M}$, and by using the formula for inverse of matrices in partitioned form [40], one gets

$$\begin{aligned} \mathbf{S}_{M+1} &= \underbrace{\begin{bmatrix} \mathbf{S}_M & \mathbf{0}_{M\times 1} \\ \mathbf{0}_{1\times M} & 0 \end{bmatrix}}_{\overline{\mathbf{S}}_M} + \begin{bmatrix} \frac{\mathbf{S}_M \mathbf{u}_M}{\delta_u} \\ -\frac{1}{\delta_u} \end{bmatrix} \begin{bmatrix} \frac{\mathbf{S}_M \mathbf{u}_M}{\delta_u} \\ -\frac{1}{\delta_u} \end{bmatrix}^H \\ &= \underbrace{\begin{bmatrix} 0 & \mathbf{0}_{1\times M} \\ \mathbf{0}_{M\times 1} & \mathbf{S}_M \end{bmatrix}}_{\underline{\mathbf{S}}_M} + \begin{bmatrix} -\frac{1}{\delta_w} \\ \frac{\mathbf{S}_M \mathbf{w}_M}{\delta_w} \end{bmatrix} \begin{bmatrix} -\frac{1}{\delta_w} \\ \frac{\mathbf{S}_M \mathbf{w}_M}{\delta_w} \end{bmatrix}^H. \end{aligned} \tag{C.58}$$

These identities imply that $\mathbf{S}_{M+1} \geq \overline{\mathbf{S}}_M$ and $\mathbf{S}_{M+1} \geq \underline{\mathbf{S}}_M$. In other words, we can state that the diagonal elements of $\mathbf{S}_{M+1}$ and $\mathbf{S}_M$ respect the hypotheses of Lemma 1. This, in turn, implies that the arithmetic mean of the diagonal elements of $\mathbf{S}_{M+1}$ is, at least, as large as the arithmetic mean of the diagonal elements of $\mathbf{S}_M$.

We therefore arrive at our first result:

$$\begin{aligned}\sigma_v^2\frac{\mathrm{tr}\left\{\mathbf{S}_M\right\}}{M} &= \mathcal{E}_{\mathrm{ZF}}^{\mathrm{CI-UP}}(M)\\ &= \mathcal{E}_{\mathrm{ZF}}^{\mathrm{UP}}(M)\\ &\leq \mathcal{E}_{\mathrm{ZF}}^{\mathrm{UP}}(M+1)\\ &= \mathcal{E}_{\mathrm{ZF}}^{\mathrm{CI-UP}}(M+1) = \sigma_v^2\frac{\mathrm{tr}\left\{\mathbf{S}_{M+1}\right\}}{M+1}.\end{aligned} \tag{C.59}$$

It should be mentioned that, for the CI-UP system employing the precoder $\mathbf{F}_0 = \mathbf{I}_M$, the inequality expressed in (C.59) is not a new result [40, 42]. Nevertheless, it has fundamental importance for the derivation of the subsequent novel contributions. Indeed, by using Lemma 2 along with the inequality expressed in (C.58), we get

$$\begin{bmatrix} 0 & \mathbf{0}_{1\times M} \\ \mathbf{0}_{M\times 1} & \sqrt{\mathbf{S}_M} \end{bmatrix} = \sqrt{\underline{\mathbf{S}}_M} \leq \sqrt{\mathbf{S}_{M+1}} \geq \sqrt{\overline{\mathbf{S}}_M} = \begin{bmatrix} \sqrt{\mathbf{S}_M} & \mathbf{0}_{M\times 1} \\ \mathbf{0}_{1\times M} & 0 \end{bmatrix}. \tag{C.60}$$

Thus, we can apply Lemma 1 once again, since the diagonal elements of $\sqrt{\mathbf{S}_{M+1}}$ and $\sqrt{\mathbf{S}_M}$ respect the hypotheses of the lemma. Hence, the arithmetic mean of the diagonal elements of $\sqrt{\mathbf{S}_{M+1}}$ is, at least, as large as the arithmetic mean of the diagonal elements of $\sqrt{\mathbf{S}_M}$. We therefore arrive at our second result:

$$\sigma_v^2\left(\frac{\mathrm{tr}\left\{\sqrt{\mathbf{S}_M}\right\}}{M}\right)^2 = \mathcal{E}_{\mathrm{ZF}}(M) \leq \mathcal{E}_{\mathrm{ZF}}(M+1) = \sigma_v^2\left(\frac{\mathrm{tr}\left\{\sqrt{\mathbf{S}_{M+1}}\right\}}{M+1}\right)^2. \tag{C.61}$$

Now, observe that

$$\begin{aligned}\mathbf{R}'_{M+1} = \mathbf{R}_{M+1} + \beta\mathbf{I}_{M+1} &= \begin{bmatrix} \mathbf{R}_M + \beta\mathbf{I}_M & \mathbf{u}_M \\ \mathbf{u}_M^H & c+\beta \end{bmatrix}\\ &= \begin{bmatrix} \mathbf{R}'_M & \mathbf{u}_M \\ \mathbf{u}_M^H & c' \end{bmatrix}\\ &= \begin{bmatrix} c' & \mathbf{w}_M \\ \mathbf{w}_M^H & \mathbf{R}'_M \end{bmatrix},\end{aligned} \tag{C.62}$$

where $c' = c + \beta$. Hence, our third result follows directly from the observation that this is exactly the same type of problem we have already solved to prove our first

result. It is then possible to reach our third result:

$$\begin{aligned}\sigma_v^2 \frac{\mathrm{tr}\left\{\mathbf{S}'_M\right\}}{M} &= \mathcal{E}_{\mathrm{Pure}}^{\mathrm{CI-UP}}(M) \\ &= \mathcal{E}_{\mathrm{Pure}}^{\mathrm{UP}}(M) \\ &\leq \mathcal{E}_{\mathrm{Pure}}^{\mathrm{UP}}(M+1) \\ &= \mathcal{E}_{\mathrm{Pure}}^{\mathrm{CI-UP}}(M+1) = \sigma_v^2 \frac{\mathrm{tr}\left\{\mathbf{S}'_{M+1}\right\}}{M+1}. \end{aligned} \tag{C.63}$$

Let us recall some important definitions [62]: the notation $\mathbf{A} \geq \mathbf{B}$, means that $\mathbf{A} - \mathbf{B} \geq O$, i.e., $\mathbf{A} - \mathbf{B}$ is a positive semidefinite matrix. Similarly, the notation $\mathbf{A} > \mathbf{B}$, means that $\mathbf{A} - \mathbf{B} > O$, i.e., $\mathbf{A} - \mathbf{B}$ is a positive definite matrix. The set $\mathbb{H}_M(a, b)$ denotes all $M \times M$ positive semidefinite matrices whose eigenvalues are within the open interval $(a, b) \subset \mathbb{R}$. Given a function $f : (a, b) \to \mathbb{R}$ and a matrix $\mathbf{A} \in \mathbb{H}_M(a, b)$, then one can define the mapping $f(\mathbf{A}) = \mathbf{U} f(\mathbf{\Lambda}) \mathbf{U}^H$, in which $\mathbf{A} = \mathbf{U}\mathbf{\Lambda}\mathbf{U}^H$ is the eigendecomposition of $\mathbf{A}$. In this context, a function $f : (a, b) \to \mathbb{R}$ is matrix-monotone on $\mathbb{H}_M(a, b)$ if $f(\mathbf{A}) \geq f(\mathbf{B})$, for all $\mathbf{A}, \mathbf{B} \in \mathbb{H}_M(a, b)$ such that $\mathbf{A} \geq \mathbf{B}$. Moreover, a function $f : (a, b) \to \mathbb{R}$ is matrix-concave on $\mathbb{H}_M(a, b)$ if $f(\alpha\mathbf{A} + (1 - \alpha)\mathbf{B}) \geq \alpha f(\mathbf{A}) + (1 - \alpha) f(\mathbf{B})$, for all $\mathbf{A}, \mathbf{B} \in \mathbb{H}_M(a, b)$ and for all $\alpha \in [0, 1]$.

Now, in order to prove that $\mathcal{E}_{\mathrm{ZF}}^{\mathrm{DFE}}(M) \leq \mathcal{E}_{\mathrm{ZF}}^{\mathrm{DFE}}(M+1)$, we will first state three important results:

Lemma 3. *A nonnegative continuous function on* $[0, \infty)$ *is matrix-monotone if and only if it is matrix-concave.*

Proof. See [62, 63]. □

It is worth highlighting a fact described in Corollary 3.1 from [62]:

> "Every matrix-monotone function is monotonic (increasing or decreasing) whereas not every monotonic function is matrix-monotone. Every matrix-convex function is convex whereas not every convex function is matrix-convex."

In other words, the properties of a matrix function can be transferred to the related scalar function, but not vice-versa. For example, $\mathbf{A}^{-1}$ is a strictly decreasing matrix-function, whilst $\mathbf{A}^2$ is not a matrix-monotone function on the set of positive definite matrices (see Lemma 3.1 and Remark 3.3 in [62]).

Lemma 4. *Given a twice-differentiable function* $f : \mathbb{R}_+ \to \mathbb{R}$*, let us define* $\mathbf{G}(t) = f(t\mathbf{A} + (1-t)\mathbf{B})$*, in which* $\mathbf{A}$ *and* $\mathbf{B}$ *are any positive semidefinite matrices, whereas* t *is a real number within the interval* $(0, 1)$*. Then,* f *is matrix-concave if and only*

if the matrix $\dfrac{d^2\mathbf{G}(t)}{dt^2}$ *is negative semidefinite for all positive semidefinite matrices* $\mathbf{A}$ *and* $\mathbf{B}$*, and for all* $t \in (0,1)$*.*

Proof. See [62, 64]. □

Lemma 5. *Given a constant* $k_0 \in \mathbb{R}$*, the function* $f(x) = \ln(x) + k_0$*, with* $x \in \mathbb{R}_+$*, is matrix-concave.*

Proof. For all positive semidefinite Hermitian matrices $\mathbf{X}$ and $\mathbf{Y}$ and for all $t \in (0,1)$, let us consider the following derivative [62, 65]

$$\frac{d^2}{dt^2}\left\{\ln(t(\mathbf{X}-\mathbf{Y})+\mathbf{Y})+k_0\mathbf{I}\right\} = -(\mathbf{X}-\mathbf{Y})[t(\mathbf{X}-\mathbf{Y})+\mathbf{Y}]^{-2}(\mathbf{X}-\mathbf{Y}). \quad \text{(C.64)}$$

Note that the former expression can be seen as a product, let us say $-\mathbf{Z}^H\mathbf{Z}$, in which $\mathbf{Z} = [t(\mathbf{X}-\mathbf{Y})+\mathbf{Y}]^{-1}(\mathbf{X}-\mathbf{Y})$. As a result, for $\mathbf{G}(t) = f(t\mathbf{A}+(1-t)\mathbf{B})$, one has

$$\frac{d^2\mathbf{G}(t)}{dt^2} \leq O, \quad \text{(C.65)}$$

for all positive semidefinite Hermitian matrices $\mathbf{A}$ and $\mathbf{B}$, and for all $t \in (0,1)$. From Lemma 4, we have that f is matrix-concave. □

Now we can prove that $\mathcal{E}_{\text{ZF}}^{\text{DFE}}(M) \leq \mathcal{E}_{\text{ZF}}^{\text{DFE}}(M+1)$. Indeed, for each natural number n, one can always define the function

$$\begin{aligned} f_n : \left(\frac{1}{n}, \infty\right) &\longrightarrow \mathbb{R}_+ \\ x &\longmapsto f_n(x) = f(x) + \ln(n), \end{aligned} \quad \text{(C.66)}$$

where $f(x) = \ln(x)$. Note that $f_n(x) = \ln\left(\frac{x}{1/n}\right) > 0$, since $x > 1/n$. Now, let us define the set $\mathbb{H}_M(1/n,\infty)$ of all $M \times M$ positive semidefinite Hermitian matrices whose eigenvalues are within the open interval $\left(\frac{1}{n},\infty\right)$. Thus, based on Lemma 5, it is rather straightforward to verify that f_n is a matrix-concave function on $\mathbb{H}_M(1/n,\infty)$. Hence, f_n satisfies all the hypotheses present in Lemma 3. Therefore, the function f_n is also matrix-monotone on $\mathbb{H}_M(1/n,\infty)$. This means that for all $\mathbf{A} \geq \mathbf{B} \geq O$ in $\mathbb{H}_M(1/n,\infty)$, one has

$$\begin{aligned} f_n(\mathbf{A}) = f(\mathbf{A}) + \ln(n)\,\mathbf{I}_M &\geq f(\mathbf{B}) + \ln(n)\,\mathbf{I}_M = f_n(\mathbf{B}) \\ &\Updownarrow \\ f(\mathbf{A}) &\geq f(\mathbf{B}). \end{aligned} \quad \text{(C.67)}$$

Note that, from Proposition 1, one gets

$$f\left(\mathcal{E}_{\mathrm{ZF}}^{\mathrm{DFE}}(M)\right) = \ln\left(\sigma_v^2\right) + \frac{1}{M}\sum_{m=0}^{M-1}\ln\left[\frac{1}{\sigma_m^2(M)}\right]$$
$$= \ln\left(\sigma_v^2\right) + \frac{1}{M}\mathrm{tr}\left\{f(\mathbf{S}_M)\right\}. \tag{C.68}$$

Since $\mathbf{S}_{M+1} \geq \overline{\mathbf{S}}_M$ and $\mathbf{S}_{M+1} \geq \underline{\mathbf{S}}_M$, then, from the above results, we have $f(\mathbf{S}_{M+1}) \geq f(\overline{\mathbf{S}}_M)$ and $f(\mathbf{S}_{M+1}) \geq f(\underline{\mathbf{S}}_M)$. In other words, we can state that the diagonal elements of $f(\mathbf{S}_{M+1})$ and $f(\mathbf{S}_M)$ respect the hypotheses of Lemma 1. This, in turn, implies that the arithmetic mean of the diagonal elements of $f(\mathbf{S}_{M+1})$ is, at least, as large as the arithmetic mean of the diagonal elements of $f(\mathbf{S}_M)$. This result yields $f\left(\mathcal{E}_{\mathrm{ZF}}^{\mathrm{DFE}}(M)\right) \leq f\left(\mathcal{E}_{\mathrm{ZF}}^{\mathrm{DFE}}(M+1)\right)$. As f is a strictly monotone increasing real function, we arrive at our last result:

$$\sigma_v^2\sqrt[M]{\det\{\mathbf{S}_M\}} = \mathcal{E}_{\mathrm{ZF}}^{\mathrm{DFE}}(M) \leq \mathcal{E}_{\mathrm{ZF}}^{\mathrm{DFE}}(M+1) = \sigma_v^2\sqrt[(M+1)]{\det\{\mathbf{S}_{M+1}\}}, \tag{C.69}$$

as desired. □

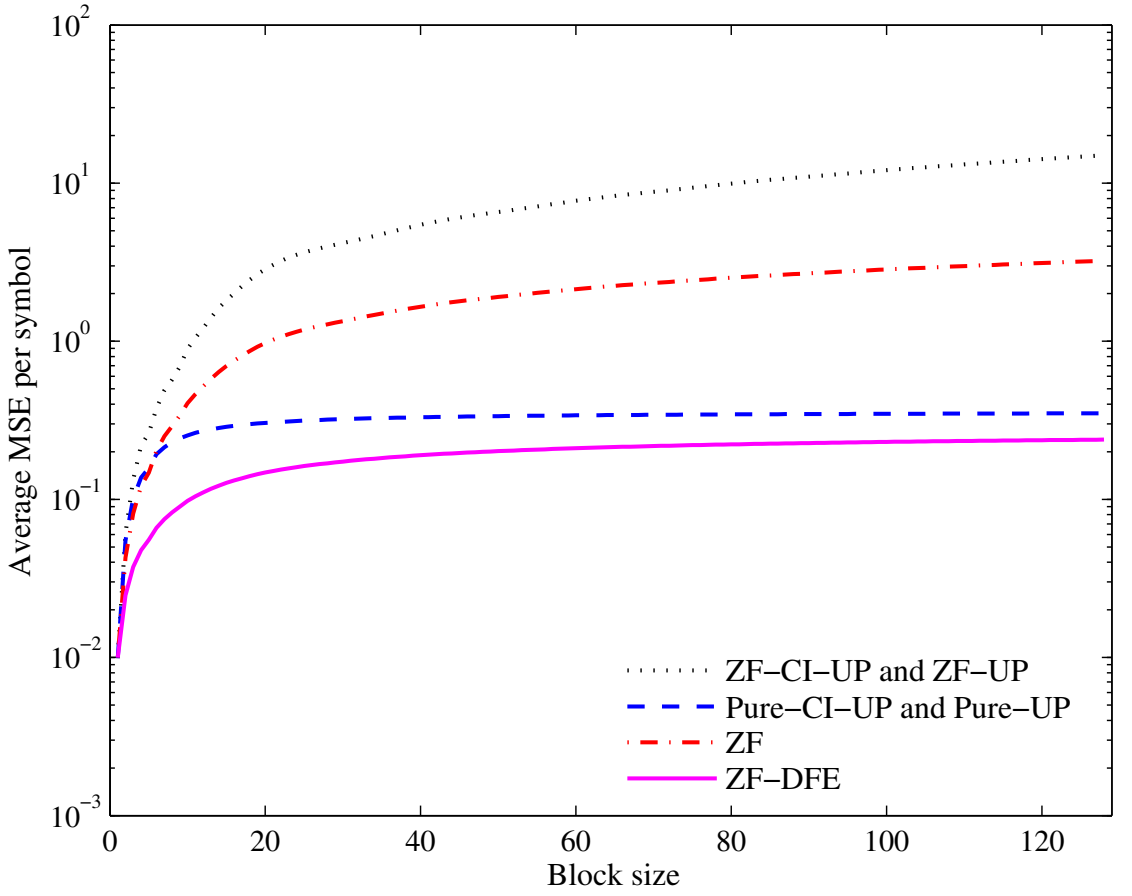

Figure C.3: Average MSE of symbols of optimal ZP transceivers as a function of block size M.

Figure C.3 illustrates the monotonic behavior of the average MSE of symbols as a function of the block size, M, for ZP-based optimal transceivers, namely: CI-UP-ZF, CI-UP-Pure, UP-ZF, UP-Pure, ZF, and ZF-DFE systems. For this experiment, we have used $\sigma_s^2 = 1$, $\sigma_v^2 = 0.01$, and the channel transfer function, $H(z)$, given by [40] (p. 580)

$$\begin{aligned} H(z) =& 0.0986 + 0.2664z^{-1} + 0.4192z^{-2} + 0.4535z^{-3} + 0.3129z^{-4} \\ &+ 0.2464z^{-5} + 0.2628z^{-6} + 0.4139z^{-7} + 0.3275z^{-8} + 0.1782z^{-9}, \end{aligned} \quad \text{(C.70)}$$

where $\|H(z)\|_2 = 1$ (i.e., the channel is normalized). Figure C.4 depicts the magnitude response of this channel. Notice that, for this case, $L = 9$, which means that 9 zeros are inserted at the end of each data block before transmitting them. Other experiments with different setups are quite well-documented in [40].

Moreover, a straightforward corollary from Theorem 2 is that the average error-probability of symbols is also a monotone increasing function of M, for the case of both the minimum error-probability and the DFE MMSE-based systems. Such a result follows from the fact that the average error-probability of symbols is a

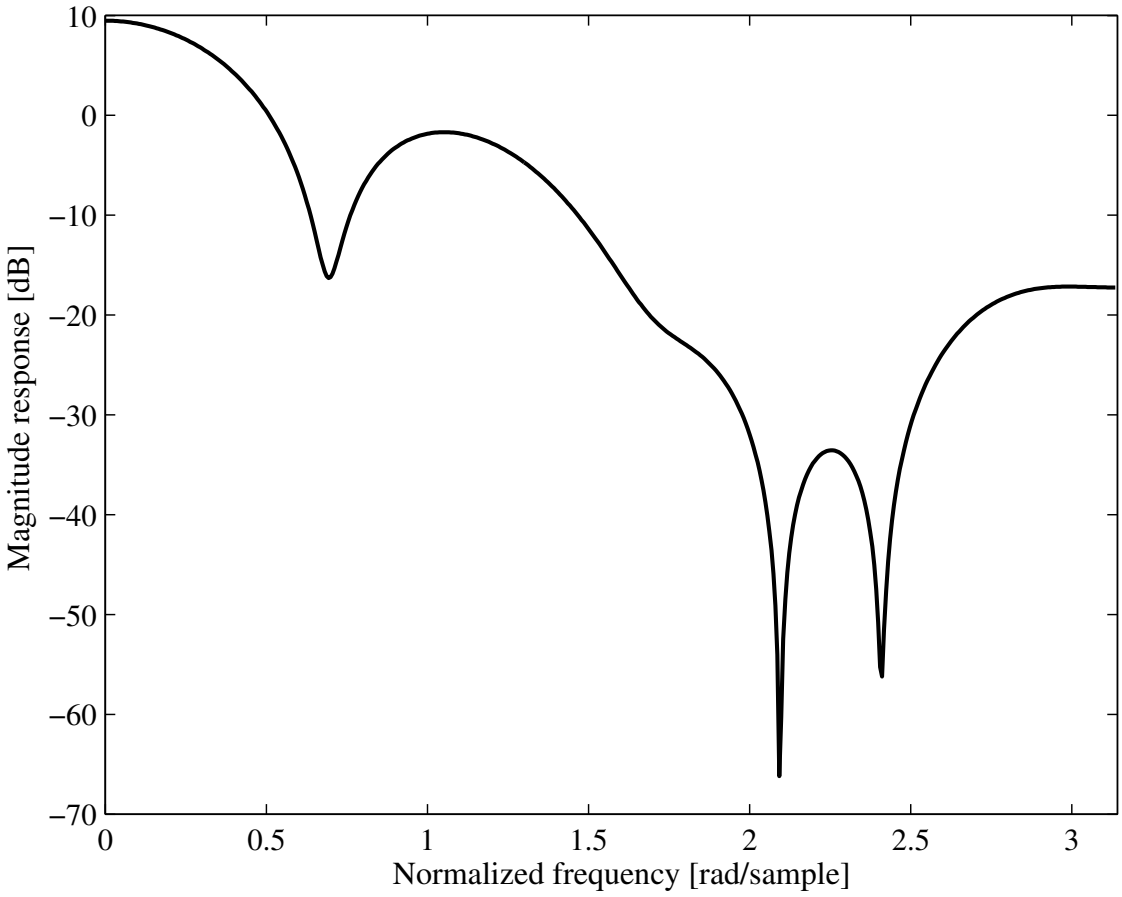

Figure C.4: Magnitude frequency response of the channel $H(z)$ defined in Eq. (C.70).

monotone increasing function of the average MSE of symbols for both the minimum error-probability and the DFE MMSE-based systems [40]. Note, however, that such analysis does not relate the performance among different systems, i.e., we are not making any comparisons between different systems. In fact, we are fixing one system and analyzing the performance behavior of this predefined system.

Theorem 3. *The average mutual information between transmitted and estimated symbols of the zero-padded MMSE-based optimal transceivers is a monotone decreasing function of the number of transmitted symbols per block. Mathematically, for all positive integer M, one has $\mathcal{I}(M) \geq \mathcal{I}(M+1)$.*

Proof. Before demonstrating Theorem 3, let us state the following auxiliary result.

Lemma 6. *Given a constant $k_0 \in \mathbb{R}$, the function $f(x) = \ln(x) - \ln(x+1) + k_0$, with $x \in \mathbb{R}_+$, is matrix-concave.*

Proof. For all distinct positive definite Hermitian matrices $\mathbf{X}$ and $\mathbf{Y}$ and for all $t \in (0,1)$, one has

$$\frac{d^2}{dt^2}\left\{\ln(t(\mathbf{X}-\mathbf{Y})+\mathbf{Y})+k_0\mathbf{I}\right\} = -(\mathbf{X}-\mathbf{Y})[t(\mathbf{X}-\mathbf{Y})+\mathbf{Y}]^{-2}(\mathbf{X}-\mathbf{Y}), \tag{C.71}$$

$$\frac{d^2}{dt^2}\left\{\ln[t(\mathbf{X}-\mathbf{Y})+\mathbf{Y}+\mathbf{I}]\right\} = -(\mathbf{X}-\mathbf{Y})[t(\mathbf{X}-\mathbf{Y})+\mathbf{Y}+\mathbf{I}]^{-2}(\mathbf{X}-\mathbf{Y}). \tag{C.72}$$

Now, observe that

$$\begin{aligned}(\mathbf{X}-\mathbf{Y})^{-1}[t(\mathbf{X}-\mathbf{Y})+\mathbf{Y}+\mathbf{I}]^2(\mathbf{X}-\mathbf{Y})^{-1} &= (\mathbf{X}-\mathbf{Y})^{-1}[t(\mathbf{X}-\mathbf{Y})+\mathbf{Y}]^2(\mathbf{X}-\mathbf{Y})^{-1} \\ &\quad + 2(\mathbf{X}-\mathbf{Y})^{-1}[t(\mathbf{X}-\mathbf{Y})+\mathbf{Y}](\mathbf{X}-\mathbf{Y})^{-1} \\ &\quad + (\mathbf{X}-\mathbf{Y})^{-2} \\ &> (\mathbf{X}-\mathbf{Y})^{-1}[t(\mathbf{X}-\mathbf{Y})+\mathbf{Y}]^2(\mathbf{X}-\mathbf{Y})^{-1},\end{aligned} \tag{C.73}$$

where the last inequality comes from the fact that $2(\mathbf{X}-\mathbf{Y})^{-1}[t(\mathbf{X}-\mathbf{Y})+\mathbf{Y}](\mathbf{X}-\mathbf{Y})^{-1}+(\mathbf{X}-\mathbf{Y})^{-2} > O$, since $[t(\mathbf{X}-\mathbf{Y})+\mathbf{Y}] > O$ (remember that $0 < t < 1$). Now, by using the fact that $\mathbf{A}^{-1} < \mathbf{B}^{-1}$ whenever $\mathbf{A} > \mathbf{B} > O$ [61], we get

$$(\mathbf{X}-\mathbf{Y})[t(\mathbf{X}-\mathbf{Y})+\mathbf{Y}+\mathbf{I}]^{-2}(\mathbf{X}-\mathbf{Y}) < (\mathbf{X}-\mathbf{Y})[t(\mathbf{X}-\mathbf{Y})+\mathbf{Y}]^{-2}(\mathbf{X}-\mathbf{Y}). \tag{C.74}$$

This implies

$$\begin{aligned}\frac{d^2}{dt^2}\left\{f[t\mathbf{X}+(1-t)\mathbf{Y}]\right\} &= (\mathbf{X}-\mathbf{Y})[t(\mathbf{X}-\mathbf{Y})+\mathbf{Y}+\mathbf{I}]^{-2}(\mathbf{X}-\mathbf{Y}) \\ &\quad - (\mathbf{X}-\mathbf{Y})[t(\mathbf{X}-\mathbf{Y})+\mathbf{Y}]^{-2}(\mathbf{X}-\mathbf{Y}) < O.\end{aligned} \tag{C.75}$$

As a result, for $\mathbf{G}(t) = f(t\mathbf{A} + (1-t)\mathbf{B})$, one has $\frac{d^2\mathbf{G}(t)}{dt^2} \leq O$, for all positive semidefinite Hermitian matrices $\mathbf{A}$ and $\mathbf{B}$, and for all $t \in (0,1)$. From Lemma 4, we have that f is matrix-concave. $\square$

Now we can prove Theorem 3. Let us first note that, from Theorem 1, the average mutual information related to the linear transceivers is nothing but the normalized trace of a matrix $\ln(\mathbf{I} + \mathbf{X}^{-1})$, where the specific matrix $\mathbf{X}$ depends on the particular type of transceiver. For instance, if the transceiver is a UP-Pure MMSE-based system, then $\mathbf{X} = \frac{\sigma_v^2}{\sigma_s^2}\mathbf{S}_M$. One therefore can write the average mutual information between the transmitted and estimated vectors as the normalized trace of the matrix $-[\ln(\mathbf{X}) - \ln(\mathbf{I} + \mathbf{X})] = -f(\mathbf{X})$, in which f is as defined in Lemma 6, with $k_0 = 0$. We already know that f is a matrix-concave function. In addition, f is also a matrix-monotone function. Indeed, for each natural number n one can always define the function

$$\begin{aligned} f_n : \left(\frac{1}{n}, n\right) &\longrightarrow \mathbb{R}_+ \\ x &\longmapsto f_n(x) = f(x) + \ln\left(n^2 + n\right). \end{aligned} \tag{C.76}$$

Note that $f_n(x) = \ln\left(\frac{x}{x+1} \times \frac{n+1}{1/n}\right) > 0$, since $n + 1 > x + 1$ and $x > 1/n$. Now, let us define the set $\mathbb{H}_M(1/n, n)$ of all $M \times M$ positive semidefinite Hermitian matrices whose eigenvalues are within the open interval $\left(\frac{1}{n}, n\right)$. Thus, based on Lemma 6, it is rather straightforward to verify that f_n is a matrix-concave function on $\mathbb{H}_M(1/n, n)$ and therefore satisfies all the hypotheses present in Lemma 3. Hence, the function f_n is also matrix-monotone on $\mathbb{H}_M(1/n, n)$. This means that for all $\mathbf{A} \geq \mathbf{B} \geq O$ in $\mathbb{H}_M(1/n, n)$, one has

$$\begin{gathered} f(\mathbf{A}) + \ln\left(n^2 + n\right)\mathbf{I}_M \geq f(\mathbf{B}) + \ln\left(n^2 + n\right)\mathbf{I}_M \\ \Updownarrow \\ f(\mathbf{A}) \geq f(\mathbf{B}). \end{gathered} \tag{C.77}$$

Now, let us remember from the proof of Theorem 2 that

$$\mathbf{S}_{M+1} \geq \overline{\mathbf{S}}_M \tag{C.78}$$

$$\mathbf{S}_{M+1} \geq \underline{\mathbf{S}}_M \tag{C.79}$$

$$\sqrt{\mathbf{S}_{M+1}} \geq \sqrt{\overline{\mathbf{S}}_M} \tag{C.80}$$

$$\sqrt{\mathbf{S}_{M+1}} \geq \sqrt{\underline{\mathbf{S}}_M}. \tag{C.81}$$

Thus, these inequalities yield

$$\frac{\sigma_v^2}{\sigma_s^2}\mathbf{S}_{M+1} \geq \frac{\sigma_v^2}{\sigma_s^2}\overline{\mathbf{S}}_M \tag{C.82}$$

$$\frac{\sigma_v^2}{\sigma_s^2}\mathbf{S}_{M+1} \geq \frac{\sigma_v^2}{\sigma_s^2}\underline{\mathbf{S}}_M \tag{C.83}$$

$$\rho_{M+1}\sqrt{\mathbf{S}_{M+1}} \geq \rho_M\sqrt{\overline{\mathbf{S}}_M} \tag{C.84}$$

$$\rho_{M+1}\sqrt{\mathbf{S}_{M+1}} \geq \rho_M\sqrt{\underline{\mathbf{S}}_M}, \tag{C.85}$$

for any increasing sequence $\{\rho_M\}_{M\in\mathbb{N}}$ of positive real numbers. Furthermore, we know that there always exists a sufficiently large natural number n_0 such that $\frac{\sigma_v^2}{\sigma_s^2}\mathbf{S}_{M+1}, \frac{\sigma_v^2}{\sigma_s^2}\overline{\mathbf{S}}_M,\ \frac{\sigma_v^2}{\sigma_s^2}\underline{\mathbf{S}}_M, \rho_{M+1}\sqrt{\mathbf{S}_{M+1}}, \rho_M\sqrt{\overline{\mathbf{S}}_M}, \rho_M\sqrt{\underline{\mathbf{S}}_M} \in \mathcal{H}_{M+1}(1/n_0, n_0)$. Hence, from what we have just proved, one has

$$f\left(\frac{\sigma_v^2}{\sigma_s^2}\mathbf{S}_{M+1}\right) \geq f\left(\frac{\sigma_v^2}{\sigma_s^2}\overline{\mathbf{S}}_M\right) \tag{C.86}$$

$$f\left(\frac{\sigma_v^2}{\sigma_s^2}\mathbf{S}_{M+1}\right) \geq f\left(\frac{\sigma_v^2}{\sigma_s^2}\underline{\mathbf{S}}_M\right) \tag{C.87}$$

$$f\left(\rho_{M+1}\sqrt{\mathbf{S}_{M+1}}\right) \geq f\left(\rho_M\sqrt{\overline{\mathbf{S}}_M}\right) \tag{C.88}$$

$$f\left(\rho_{M+1}\sqrt{\mathbf{S}_{M+1}}\right) \geq f\left(\rho_M\sqrt{\underline{\mathbf{S}}_M}\right). \tag{C.89}$$

Now, one can apply Lemma 1 once again, since the diagonal elements of $f\left(\frac{\sigma_v^2}{\sigma_s^2}\mathbf{S}_{M+1}\right)$ and $f\left(\frac{\sigma_v^2}{\sigma_s^2}\mathbf{S}_M\right)$ respect the hypotheses of such a lemma. Hence, the arithmetic mean of the diagonal elements of $f\left(\frac{\sigma_v^2}{\sigma_s^2}\mathbf{S}_{M+1}\right)$ is, at least, as large as the arithmetic mean of the diagonal elements of $f\left(\frac{\sigma_v^2}{\sigma_s^2}\mathbf{S}_M\right)$. Similarly, the arithmetic mean of the diagonal elements of $f\left(\rho_{M+1}\sqrt{\mathbf{S}_{M+1}}\right)$ is, at least, as large as the arithmetic mean of the diagonal elements of $f\left(\rho_M\sqrt{\mathbf{S}_M}\right)$. We therefore arrive at our

desired results:

$$
\begin{aligned}
-\frac{\mathrm{tr}\left\{f\left(\frac{\sigma_v^2}{\sigma_s^2}\mathbf{S}_M\right)\right\}}{M} &= \mathcal{I}_{\mathrm{ZF}}^{\mathrm{CI-UP}}(M) \\
&= \mathcal{I}_{\mathrm{Pure}}^{\mathrm{CI-UP}}(M) \\
&= \mathcal{I}_{\mathrm{ZF}}^{\mathrm{UP}}(M) \\
&= \mathcal{I}_{\mathrm{Pure}}^{\mathrm{UP}}(M) \\
&\geq \mathcal{I}_{\mathrm{Pure}}^{\mathrm{UP}}(M+1) \\
&= \mathcal{I}_{\mathrm{ZF}}^{\mathrm{UP}}(M+1) \\
&= \mathcal{I}_{\mathrm{Pure}}^{\mathrm{CI-UP}}(M+1) \\
&= \mathcal{I}_{\mathrm{ZF}}^{\mathrm{CI-UP}}(M+1) = -\frac{\mathrm{tr}\left\{f\left(\frac{\sigma_v^2}{\sigma_s^2}\mathbf{S}_{M+1}\right)\right\}}{M+1},
\end{aligned}
\tag{C.90}
$$

whereas

$$
-\frac{\mathrm{tr}\left\{f\left(\rho_M^{\mathrm{ZF}}\sqrt{\mathbf{S}_M}\right)\right\}}{M} = \mathcal{I}_{\mathrm{ZF}}(M) \geq \mathcal{I}_{\mathrm{ZF}}(M+1) = -\frac{\mathrm{tr}\left\{f\left(\rho_{M+1}^{\mathrm{ZF}}\sqrt{\mathbf{S}_{M+1}}\right)\right\}}{M+1}, \tag{C.91}
$$

in which we have used the fact that $\rho_M^{\mathrm{ZF}} = \frac{\sigma_v^2}{\sigma_s^2}\frac{\sqrt{\mathcal{E}_{\mathrm{ZF}}(M)}}{\sigma_v}$ increases as M increases (see Theorem 2).

Now, from the proof of Theorem 2, we know that $\sigma_v^2 \sqrt[M]{\det\{\mathbf{S}_M\}} \leq \sigma_v^2 \sqrt[(M+1)]{\det\{\mathbf{S}_{M+1}\}}$, which implies $1 + \frac{\sigma_s^2}{\sigma_v^2}\sqrt[M]{\det\{\mathbf{S}_M^{-1}\}} \geq 1 + \frac{\sigma_s^2}{\sigma_v^2}\sqrt[(M+1)]{\det\{\mathbf{S}_{M+1}^{-1}\}}$. Since $\ln(\cdot)$ is a strictly monotone increasing real function, one has

$$
\begin{aligned}
\ln\left[1 + \frac{\sigma_s^2}{\sigma_v^2}\sqrt[M]{\det\{\mathbf{S}_M^{-1}\}}\right] &= \mathcal{I}_{\mathrm{ZF}}^{\mathrm{DFE}}(M) \\
&\geq \mathcal{I}_{\mathrm{ZF}}^{\mathrm{DFE}}(M+1) = \ln\left[1 + \frac{\sigma_s^2}{\sigma_v^2}\sqrt[(M+1)]{\det\{\mathbf{S}_{M+1}^{-1}\}}\right],
\end{aligned}
\tag{C.92}
$$

as desired. □

Figure C.5 confirms the monotonic behavior of the average mutual information between transmitted and estimated symbols as a function of the block size, M, for ZP-based optimal transceivers. In this experiment, we have used the same scenario previously described. Once again, it is rather clear that such a figure of merit also degrades as M increases.

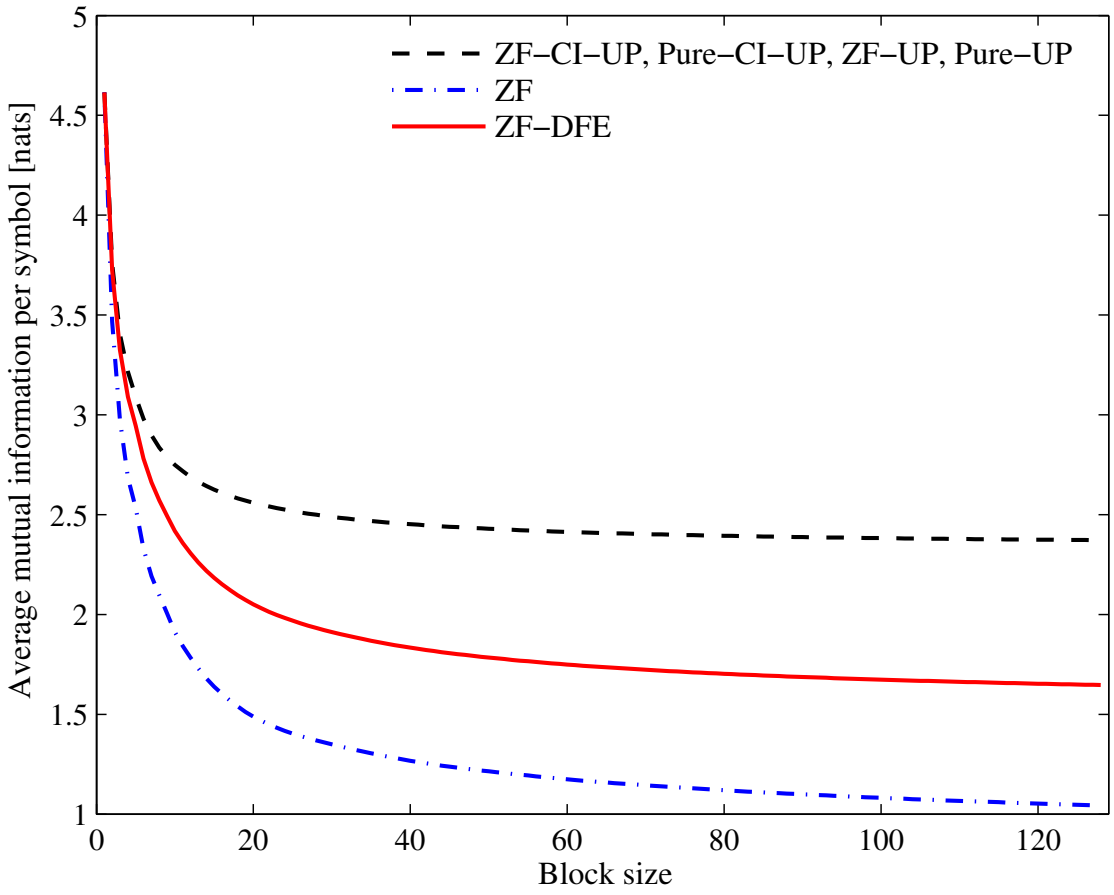

Figure C.5: Average mutual information between transmitted and estimated symbols as a function of block size M.

C.4 Effect of Discarding Redundant Data

Throughout this section, let us assume that both the order of the FIR-channel model, L, and the number of transmitted data symbols, M, are two fixed natural numbers.[11] As previously described, the task of the receiver is to generate an estimate $\hat{\mathbf{s}}$ of the transmitted vector $\mathbf{s}$ by processing the received vector $\mathbf{y} = \mathbf{H}\mathbf{x} + \mathbf{v}$, with $\mathbf{x} = \mathbf{F}\mathbf{s}$. The received vector $\mathbf{y}$ has $M + L$ elements due to the redundancy that is inserted at the transmitter side. In order to decrease the number of samples to be processed, one can discard up to L elements of the received vector $\mathbf{y}$, yielding a new vector $\mathbf{y}(K) = \mathbf{H}(K)\mathbf{x} + \mathbf{v}(K) \in \mathbb{C}^{(M+K)\times M}$, where $K \in \mathcal{L} = \{0, 1, \cdots, L\}$ denotes the amount of redundancy used in the equalization process.

As a particular example, if $K = 0$ (which means that L elements are removed before starting the equalization), one could discard, for instance, the first $L/2$ elements of $\mathbf{y}$ as well as the last $L/2$ elements of $\mathbf{y}$ to generate the new vector $\mathbf{y}(0)$. Observe that, in this case, $\mathbf{y}(0) = \mathbf{H}(0)\mathbf{x} + \mathbf{v}(0) \in \mathbb{C}^{M\times M}$. The matrix $\mathbf{H}(0)$ is generated from $\mathbf{H}$ by discarding the first $L/2$ rows of $\mathbf{H}$, as well as the last $L/2$ rows

[11] We therefore shall omit any dependence on these variables.

of $\mathbf{H}$. Alternatively, one could simply discard the last L elements of $\mathbf{y}$ in order to generate $\mathbf{y}(0)$. Note that the adopted notations for $\mathbf{y}(K)$, $\mathbf{H}(K)$, and $\mathbf{v}(K)$ do not specify which elements/rows are discarded, for the sake of notation simplicity. The choice of the rows of $\mathbf{H}$ to be discarded is such that $\mathbf{H}(K)$ can be obtained from $\mathbf{H}(K+1)$ by removing a given row of $\mathbf{H}(K+1)$, without mattering which row is discarded. In addition, the resulting matrix $\mathbf{H}(K)$ must keep the full-column-rank property. The full-column-rank property guarantees that $\mathbf{H}(K) \in \mathbb{C}^{(M+K)\times M}$ has exactly M nonzero singular values, for all $K \in \mathcal{L}$.

Thus, given both an Lth-order channel-impulse response and a fixed rule for discarding a row of $\mathbf{H}(K+1)$ to generate $\mathbf{H}(K)$ (e.g., to remove the first row of $\mathbf{H}(K+1)$ to yield $\mathbf{H}(K)$), we can generate $L+1$ distinct matrices $\mathbf{H}(K)$, for $K \in \mathcal{L}$.[12] All these matrices with reduced redundancy are constructed from their related effective-channel matrix $\mathbf{H}$ as previously described. Once again, in the case of single-carrier ZP zero-forcing linear transceiver, the authors in [40, 43] have proved theoretically that the MSE performance improves as $K \in \mathcal{L}$ increases, i.e., larger amounts of samples used in the equalization lead to better MSE performance. Nevertheless, not even similar empirical results had been reported for the other ZP transceivers yet. The following theorem is an important result towards the clarification of this point.

Theorem 4. *For each $K \in \mathcal{L}$, let $\sigma_0(K) \geq \sigma_1(K) \geq \cdots \geq \sigma_{M-1}(K) > 0$ be the M nonzero singular values of $\mathbf{H}(K)$. Thus, one always has*

$$\sigma_m(K+1) \geq \sigma_m(K),\ \forall (K,m) \in (\mathcal{L} \setminus \{L\}) \times \mathcal{M}, \tag{C.93}$$

where $\mathcal{M} = \{0, 1, \cdots, M-1\}$.

Proof. Before starting the proof of Theorem 4, we shall state a very useful supporting result.

Lemma 7. *Let $\mathbf{X} \in \mathbb{C}^{M_1\times M_2}$ be a rectangular matrix whose SVD is $\mathbf{X} = \mathbf{U}_{M_1}\mathbf{\Sigma}_{M_1\times M_2}\mathbf{V}_{M_2}^H$, where $\mathbf{U}_{M_1}$ and $\mathbf{V}_{M_2}$ are unitary matrices, and $\mathbf{\Sigma}_{M_1\times M_2} = [\mathrm{diag}\{\sigma_m\}_{m=0}^{M_2-1} \quad \mathbf{0}_{M_2\times(M_1-M_2)}]^T$, with $M_1 \geq M_2$. By assuming that $\sigma_0 \geq \sigma_1 \geq \cdots \geq \sigma_{S-1} > \sigma_S = \cdots = \sigma_{M_2-1} = 0$, and $\mathrm{rank}\{\mathbf{X}\} = S \in \mathbb{N}$, one has*

$$\min_{\substack{\mathrm{rank}\{\mathbf{Y}\}=R<S \\ \mathbf{Y}\in\mathbb{C}^{M_1\times M_2}}} \{\|\mathbf{X}-\mathbf{Y}\|_2\} = \|\mathbf{X}-\bar{\mathbf{X}}\|_2 = \sigma_R, \tag{C.94}$$

in which $\bar{\mathbf{X}} = \mathbf{U}_{M_1}\bar{\mathbf{\Sigma}}_{M_1\times M_2}\mathbf{V}_{M_2}^H$, with $\bar{\mathbf{\Sigma}}_{M_1\times M_2} = [\mathrm{diag}\{\bar{\sigma}_m\}_{m=0}^{M_2-1} \quad \mathbf{0}_{M_2\times(M_1-M_2)}]^T$. In addition, $\bar{\sigma}_m = \sigma_m$, for all $m \in \{0, 1, \cdots, R-1\}$, and $\bar{\sigma}_m = 0$ otherwise.

Proof. See [44]. □

[12] In fact, $\mathbf{H}(L) = \mathbf{H}$.

Now, note that $\sigma_0(K+1) = \|\mathbf{H}(K+1)\|_2 = \max\|\mathbf{H}(\mathrm{K}+1)\mathbf{x}\|_2$, in which $\mathbf{x} \in \mathbb{C}^{M\times 1}$ is a unit vector, i.e., $\|\mathbf{x}\|_2 = 1$. Since, for each $K \in (\mathcal{L} \setminus L)$, the matrix $\mathbf{H}(K)$ can be obtained from $\mathbf{H}(K+1)$ by discarding a predefined row of $\mathbf{H}(K+1)$, denoted as $\mathbf{h}_{\mathrm{d}}^H(K+1)$, then one has

$$\begin{aligned}
\sigma_0(K+1) &= \|\mathbf{H}(K+1)\|_2 \\
&= \max_{\|\mathbf{x}\|_2=1} \|\mathbf{H}(K+1)\mathbf{x}\|_2 \\
&= \max_{\|\mathbf{x}\|_2=1} \sqrt{\|\mathbf{H}(K)\mathbf{x}\|_2^2 + |\mathbf{h}_{\mathrm{d}}^H(K+1)\mathbf{x}|^2} \\
&\geq \max_{\|\mathbf{x}\|_2=1} \|\mathbf{H}(K)\mathbf{x}\|_2 \\
&= \|\mathbf{H}(K)\|_2 = \sigma_0(K). \qquad \text{(C.95)}
\end{aligned}$$

Now, by taking into account the SVD decomposition of the matrix $\mathbf{H}(K+1)$, one has

$$\mathbf{H}(K+1) = \sum_{m\in\mathcal{M}} \sigma_m(K+1)\mathbf{u}_m(K+1)\mathbf{v}_m^H(K+1), \qquad \text{(C.96)}$$

where $\mathcal{M} = \{0, 1, \cdots, M-1\}$.

In addition, one can also define a reduced-rank approximation for $\mathbf{H}(K+1)$ as follows:

$$\mathbf{H}_R(K+1) = \sum_{r=0}^{R} \sigma_r(K+1)\mathbf{u}_r(K+1)\mathbf{v}_r^H(K+1), \ \forall R \in \mathcal{M} \setminus \{M-1\}, \quad \text{(C.97)}$$

where $\mathbf{H}_R(K+1)$ is a rank-$(R+1)$ matrix. By using Lemma 7, we have

$$\begin{aligned}
\sigma_{(R+1)}(K+1) &= \|\mathbf{H}(K+1) - \mathbf{H}_R(K+1)\|_2 \\
&= \max_{\|\mathbf{x}\|_2=1} \left\| \left(\mathbf{H}(K+1) - \sum_{r=0}^{R} \sigma_r(K+1)\mathbf{u}_r(K+1)\mathbf{v}_r^H(K+1) \right) \mathbf{x} \right\|_2 \\
&= \max_{\|\mathbf{x}\|_2=1} \sqrt{\left\| \left(\mathbf{H}(K) - \sum_{r=0}^{R} \sigma_r(K+1)\bar{\mathbf{u}}_r(K+1)\mathbf{v}_r^H(K+1) \right) \mathbf{x} \right\|_2^2 + |\delta_{\mathbf{x}}|^2} \\
&\geq \max_{\|\mathbf{x}\|_2=1} \left\| \left(\mathbf{H}(K) - \sum_{r=0}^{R} \sigma_r(K+1)\bar{\mathbf{u}}_r(K+1)\mathbf{v}_r^H(K+1) \right) \mathbf{x} \right\|_2 \\
&= \left\| \mathbf{H}(K) - \sum_{r=0}^{R} \sigma_r(K+1)\bar{\mathbf{u}}_r(K+1)\mathbf{v}_r^H(K+1) \right\|_2 \\
&\geq \|\mathbf{H}(K) - \mathbf{H}_R(K)\|_2 = \\
&= \sigma_{(R+1)}(K), \qquad \text{(C.98)}
\end{aligned}$$

where, for each $r \in \{0, 1, \cdots, R\}$, the column vector $\bar{\mathbf{u}}_r(K+1)$ is obtained from

the column vector $\mathbf{u}_r(K+1)$ by discarding a given element. In addition, $|\delta_{\mathbf{x}}|$ is a nonnegative real number that depends on $\mathbf{x}$. As R can assume any value within the set $\mathcal{M} \setminus \{M-1\}$, we have therefore proved that $\sigma_m(K+1) \geq \sigma_m(K)$, for all $m \in \mathcal{M}$. □

All figures of merit that we presented in Section C.2 depend crucially on the singular values of the effective-channel matrix. Theorem 4 shows the monotonic increase of these singular values with respect to $K \in \mathcal{L}$. Hence, Theorem 4 sums up the monotonic behavior of any figure of merit that directly depends on the singular values of the effective-channel matrix. Such a monotonic behavior does not depend on which row of $\mathbf{H}(K+1)$ is discarded to generate $\mathbf{H}(K)$. Corollary 1 gives a more formal and complete description of the utility of Theorem 4 in the analysis of ZP-based systems.

Corollary 1. *Let us assume that, for each $m \in \mathcal{M}$, there exists a function $f_m : \mathbb{R}_+ \to \mathbb{R}$ such that a performance measure $\mathcal{J} : \mathcal{L} \to \mathbb{R}$ associated with each ZP transceiver can be defined as*

$$\mathcal{J}(K) = \frac{1}{M}\sum_{m=0}^{M-1} f_m(\sigma_m(K)) \quad \text{or} \quad \mathcal{J}(K) = \sqrt[M]{\prod_{m=0}^{M-1} f_m(\sigma_m(K))}. \tag{C.99}$$

If f_m is monotone increasing for all $m \in \mathcal{M}$, then $\mathcal{J}$ is monotone increasing on $\mathcal{L}$, i.e. $\mathcal{J}(K+1) \geq \mathcal{J}(K)$, for all $K \in \mathcal{L} \setminus \{L\}$. Likewise, if f_m is monotone decreasing for all $m \in \mathcal{M}$, then $\mathcal{J}$ is monotone decreasing on $\mathcal{L}$, i.e. $\mathcal{J}(K+1) \leq \mathcal{J}(K)$, for all $K \in \mathcal{L} \setminus \{L\}$.

Proof. This is a straightforward application of Theorem 4. □

Corollary 1 is a quite generic result that characterizes the monotonic behavior of several figures of merit associated with the performance of optimal ZP transceivers. A particular application of the former corollary is the next result.

Corollary 2. *For all $K \in \mathcal{L} \setminus \{L\}$, one has $\mathcal{E}(K+1) \leq \mathcal{E}(K)$ and $\mathcal{I}(K+1) \geq \mathcal{I}(K)$, for zero-padded MMSE-based optimal transceivers.*

Proof. This is a consequence of Theorem 4 along with both Proposition 1 and Theorem 1. □

Table C.2 exemplifies the monotonic behavior of the average MSE of symbols as a function of the number of redundant elements, K, used in the equalization. To obtain such results, we have used the same scenario previously described, except for the block size that we have fixed at $M = 32$. Once again, it is rather clear that such a figure of merit also degrades as K decreases. Note that we have omitted the

Table C.2: Average MSE of symbols of optimal ZP transceivers as a function of $K \in \mathcal{L}$ ($M = 32$ data symbols).

	$K=0$	$K=1$	$K=2$	$K=3$	$K=4$	$K=5$	$K=6$	$K=7$	$K=8$	$K=9$
$\mathcal{E}_{\mathrm{ZF}}^{\mathrm{CI-UP}}$	3.64×10^7	2.99×10^3	1.80×10^3	14.91	11.69	8.37	7.55	6.50	5.27	4.39
$\mathcal{E}_{\mathrm{Pure}}^{\mathrm{CI-UP}}$	0.41	0.39	0.37	0.35	0.34	0.34	0.33	0.33	0.32	0.32
$\mathcal{E}_{\mathrm{ZF}}$	1.16×10^6	224.64	87.90	3.87	2.99	2.26	2.07	1.85	1.61	1.40
$\mathcal{E}_{\mathrm{ZF}}^{\mathrm{DFE}}$	1.02	0.53	0.38	0.26	0.23	0.21	0.20	0.19	0.18	0.17

Table C.3: Average mutual information (in nats) between transmitted and estimated symbols of optimal ZP transceivers as a function of $K \in \mathcal{L}$ ($M = 32$ data symbols).

	$K=0$	$K=1$	$K=2$	$K=3$	$K=4$	$K=5$	$K=6$	$K=7$	$K=8$	$K=9$
$\mathcal{I}_{\mathrm{ZF}}^{\mathrm{CI-UP}}$	2.16	2.23	2.29	2.34	2.38	2.40	2.43	2.45	2.46	2.48
$\mathcal{I}_{\mathrm{ZF}}$	0.00	0.25	0.37	0.98	1.06	1.15	1.18	1.23	1.28	1.33
$\mathcal{I}_{\mathrm{ZF}}^{\mathrm{DFE}}$	0.67	1.05	1.28	1.55	1.64	1.73	1.77	1.81	1.85	1.89

results for $\mathcal{E}_{\mathrm{ZF}}^{\mathrm{UP}}$ and $\mathcal{E}_{\mathrm{Pure}}^{\mathrm{UP}}$ since they are respectively equal to $\mathcal{E}_{\mathrm{ZF}}^{\mathrm{CI-UP}}$ and $\mathcal{E}_{\mathrm{Pure}}^{\mathrm{CI-UP}}$ (see Proposition 1). Likewise, Table C.3 exemplifies the monotonic behavior of the average mutual information between the transmitted and estimated symbols as a function of the number of redundant elements used in the equalization. Note that we have omitted the results for $\mathcal{I}_{\mathrm{ZF}}^{\mathrm{UP}}$, $\mathcal{I}_{\mathrm{Pure}}^{\mathrm{UP}}$, and $\mathcal{I}_{\mathrm{Pure}}^{\mathrm{CI-UP}}$ since all of them are equal to $\mathcal{I}_{\mathrm{ZF}}^{\mathrm{CI-UP}}$ (see Theorem 1). One can observe that this figure of merit also degrades as K decreases.

It is important to note that, as a consequence of Corollary 1, the average error-probability of symbols associated with both the minimum error-probability and the DFE MMSE-based systems also increases whenever K decreases.

C.5 Effect of Zeros of the Channel

The FIR-channel model associated with some particular applications may be either a minimum or a non-minimum phase channel. For the single-carrier ZP zero-forcing linear transceiver, the authors in [40, 43] have empirically shown that the MSE performance gets worse whenever non-minimum phase channels are utilized, as compared to their minimum phase counterparts. Nonetheless, an analogous empirical result had not been reported for the other ZP transceivers yet. In this section, we shall mathematically clarify this point by proving that, for both linear and DFE optimal ZP transceivers, several figures of merit degrade in the transmissions with non-minimum phase channels, when some redundant elements are discarded. On the other hand, if the whole received data block is employed to estimate the transmitted symbols, then the figures of merit related to such transceivers are not sensitive to whether the channel zeros are inside or outside the unit circle.

Hence, we shall verify the effect of the locations of the zeros of the channel on the performance of ZP transceivers. Let us assume that the FIR channel-impulse response $\{h(l)\}_{l\in\mathcal{L}}$ is such that its associated transfer function

$$H(z) = h(0) + h(1)z^{-1} + \cdots + h(L)z^{-L} \tag{C.100}$$

has at least one zero within the unit circle. The lth zero of $H(z)$ is denoted as

$z_l \in \mathbb{C}$, where $l \in \{0, 1, \cdots, L-1\} = \mathcal{L} \setminus \{L\}$. Suppose we create a new channel

$$\begin{aligned} H_{\text{new}}(z) &= \sum_{l=0}^{L} h_{\text{new}}(l) z^{-l} \\ &= h(0) \frac{z_0^* - z^{-1}}{1 - z^{-1} z_0} \prod_{l=0}^{L-1} (1 - z^{-1} z_l) \\ &= \frac{z_0^* - z^{-1}}{1 - z^{-1} z_0} H(z). \end{aligned} \tag{C.101}$$

Thus, $H_{\text{new}}(z)$ is an FIR channel transfer function with the 0th zero, z_0, replaced by $1/z_0^*$. Note that $|H_{\text{new}}(e^{\jmath\omega})| = |H(e^{\jmath\omega})|$ for all real ω, since the factor

$$A(z) = \frac{z_0^* - z^{-1}}{1 - z^{-1} z_0} \tag{C.102}$$

is an all-pass filter, i.e., $|A(e^{\jmath\omega})| = 1$, for all real ω. In addition, let us define $\mathbf{S}_{\text{new}}(K) = \mathbf{R}_{\text{new}}^{-1}(K)$, where $\mathbf{R}_{\text{new}}(K) = \mathbf{H}_{\text{new}}^H(K)\mathbf{H}_{\text{new}}(K) \in \mathbb{C}^{M \times M}$ and $K \in \mathcal{L}$. Moreover, we will restrict ourselves to the cases in which $\mathbf{H}(K)$ is generated from $\mathbf{H}(K+1)$ by discarding the last row of the former matrix, as performed in [40, 43]. Thus, the following key result holds.

Theorem 5. *Let us assume that the 0th zero of $H(z)$, z_0, is such that $|z_0| < 1$. Thus,*

$$\mathbf{S}_{\text{new}}(K) \geq \mathbf{S}(K) > O, \ \forall K \in \mathcal{L}. \tag{C.103}$$

Proof. First of all, observe that proving that $\mathbf{S}_{\text{new}}(K) \geq \mathbf{S}(K)$ is equivalent to proving that $O < \mathbf{R}_{\text{new}}(K) \leq \mathbf{R}(K)$. The former matrix-inequality, however, is equivalent to demonstrating that

$$\|\mathbf{H}_{\text{new}}(K)\mathbf{w}\|_2 \leq \|\mathbf{H}(K)\mathbf{w}\|_2, \ \forall \mathbf{w} \in \mathbb{C}^{M \times 1}. \tag{C.104}$$

One can interpret the elements of the vector $\mathbf{H}(K)\mathbf{w}$ as the first $M+K$ samples of the signal resulting from the linear convolution $(h * w)(n)$, where $\{w(m)\}_{m \in \mathcal{M}}$ is a finite causal signal whose samples are the elements of $\mathbf{w}$ (see Eq. (C.4)). By using this interpretation, we shall adapt the ideas present in the demonstration of Lemma 4.5 from [66] in order to arrive at the desired result. Hence, from Parseval's theorem, one can rewrite inequality (C.104) as

$$\|[A(e^{\jmath\omega})H(e^{\jmath\omega})W(e^{\jmath\omega})]_{\text{f},(M+K)}\|_2 \leq \|[H(e^{\jmath\omega})W(e^{\jmath\omega})]_{\text{f},(M+K)}\|_2, \ \forall \{w(m)\}_{m \in \mathcal{M}}, \tag{C.105}$$

in which $[T(z)]_{\text{f},(M+K)}$ denotes the first $M+K$ terms of the polynomial $T(z) = t(0) +$

$t(1)z^{-1}+\cdots+t(M+L-1)z^{-(M+L-1)}$, for $K \in \mathcal{L}$.[13] In other words, $[T(z)]_{\mathrm{f},(M+K)} = t(0)+t(1)z^{-1}+\cdots+t(M+K-1)z^{-(M+K-1)}$. Note that for a given sequence $t(n)$ whose Fourier transform is $T(e^{\jmath\omega})$, the Parseval's identity holds, i.e.,

$$\|t(n)\|_2^2 = \sum_{n=-\infty}^{\infty} |t(n)|^2 = \frac{1}{2\pi}\int_{-\pi}^{\pi} |T(e^{\jmath\omega})|^2 d\omega = \|T(e^{\jmath\omega})\|_2^2. \tag{C.106}$$

Now, assuming that $[T(z)]_{\mathrm{l},(L-K)}$ denotes the last $L-K$ terms of the polynomial $T(z)$, one has

$$H(e^{\jmath\omega})W(e^{\jmath\omega}) = [H(e^{\jmath\omega})W(e^{\jmath\omega})]_{\mathrm{f},(M+K)} + [H(e^{\jmath\omega})W(e^{\jmath\omega})]_{\mathrm{l},(L-K)}, \tag{C.107}$$

yielding

$$\begin{aligned} A(e^{\jmath\omega})H(e^{\jmath\omega})W(e^{\jmath\omega}) &= A(e^{\jmath\omega})[H(e^{\jmath\omega})W(e^{\jmath\omega})]_{\mathrm{f},(M+K)} \\ &\quad + A(e^{\jmath\omega})[H(e^{\jmath\omega})W(e^{\jmath\omega})]_{\mathrm{l},(L-K)} \\ &= e^{-\jmath\omega(M+K-1)}\Big(A(e^{\jmath\omega})[H(e^{\jmath\omega})W(e^{\jmath\omega})]^{\mathrm{NC}}_{\mathrm{f},(M+K)} \\ &\quad + A(e^{\jmath\omega})[H(e^{\jmath\omega})W(e^{\jmath\omega})]^{\mathrm{SC}}_{\mathrm{l},(L-K)}\Big), \end{aligned} \tag{C.108}$$

in which we have

$$[H(e^{\jmath\omega})W(e^{\jmath\omega})]^{\mathrm{NC}}_{\mathrm{f},(M+K)} = e^{\jmath\omega(M+K-1)}[H(e^{\jmath\omega})W(e^{\jmath\omega})]_{\mathrm{f},(M+K)}, \tag{C.109}$$

$$[H(e^{\jmath\omega})W(e^{\jmath\omega})]^{\mathrm{SC}}_{\mathrm{l},(L-K)} = e^{\jmath\omega(M+K-1)}[H(e^{\jmath\omega})W(e^{\jmath\omega})]_{\mathrm{l},(L-K)}, \tag{C.110}$$

where NC stands for noncausal signal, whereas SC stands for strictly causal signal (all coefficients of the discrete-time Fourier transform multiply a power of $e^{-\jmath\omega}$).[14]

Let us observe that, since $|z_0| < 1$, then $A(e^{\jmath\omega})$ is the discrete-time Fourier transform of a causal sequence $a(n)$. This means that the product $A(e^{\jmath\omega})[H(e^{\jmath\omega})W(e^{\jmath\omega})]^{\mathrm{SC}}_{\mathrm{l},(L-K)}$ represents the discrete-time Fourier transform of a strictly causal signal. This implies that $e^{-\jmath\omega(M+K-1)}A(e^{\jmath\omega})[H(e^{\jmath\omega})W(e^{\jmath\omega})]^{\mathrm{SC}}_{\mathrm{l},(L-K)}$ only has powers of $e^{-\jmath\omega}$ higher than or equal to $M+K$. On the other hand, $A(e^{\jmath\omega})[H(e^{\jmath\omega})W(e^{\jmath\omega})]^{\mathrm{NC}}_{\mathrm{f},(M+K)}$ may have causal and noncausal parts. We therefore

[13] Remember that, since $\{w(m)\}_{m\in\mathcal{M}}$ and $\{h(l)\}_{l\in\mathcal{L}}$ are causal signals, then $H(z)W(z)$ is a polynomial in the variable z^{-1}.

[14] Indeed, due to the definition of $[H(e^{\jmath\omega})W(e^{\jmath\omega})]_{\mathrm{f},(M+K)}$, we have that $[H(e^{\jmath\omega})W(e^{\jmath\omega})]^{\mathrm{NC}}_{\mathrm{f},(M+K)}$ is a polynomial in $e^{\jmath\omega}$, which means that the associated time-domain sequence is noncausal. On the other hand, as $[T(z)]_{\mathrm{l},(L-K)}$ denotes the last $L-K$ terms of the polynomial $T(z) = t(0) + t(1)z^{-1}+\cdots+t(M+L-1)z^{-(M+L-1)}$, for $K \in \mathcal{L}$, i.e., $[T(z)]_{\mathrm{l},(L-K)} = t(M+K)z^{-(M+K)}+t(M+K+1)z^{-(M+K+1)}+\cdots+t(M+L-1)z^{-(M+L-1)}$, then $[H(e^{\jmath\omega})W(e^{\jmath\omega})]^{\mathrm{NC}}_{\mathrm{l},(L-K)}$ is a polynomial in $e^{-\jmath\omega}$ whose independent coefficient equals to zero, which means that the associated time-domain sequence is a strictly causal signal.

have

$$[A(e^{\jmath\omega})H(e^{\jmath\omega})W(e^{\jmath\omega})]_{\mathrm{f},(M+K)} = \left[e^{-\jmath\omega(M+K-1)}A(e^{\jmath\omega})[H(e^{\jmath\omega})W(e^{\jmath\omega})]^{\mathrm{NC}}_{\mathrm{f},(M+K)}\right]_{\mathrm{f},(M+K)}$$
$$= \left[A(e^{\jmath\omega})[H(e^{\jmath\omega})W(e^{\jmath\omega})]_{\mathrm{f},(M+K)}\right]_{\mathrm{f},(M+K)}. \qquad \text{(C.111)}$$

Remember that our aim is to prove inequality (C.105). From the former identity, it follows that

$$\|[A(e^{\jmath\omega})H(e^{\jmath\omega})W(e^{\jmath\omega})]_{\mathrm{f},(M+K)}\|_2 = \left\|\left[A(e^{\jmath\omega})[H(e^{\jmath\omega})W(e^{\jmath\omega})]_{\mathrm{f},(M+K)}\right]_{\mathrm{f},(M+K)}\right\|_2$$
$$\leq \left\|A(e^{\jmath\omega})[H(e^{\jmath\omega})W(e^{\jmath\omega})]_{\mathrm{f},(M+K)}\right\|_2$$
$$= \left\|[H(e^{\jmath\omega})W(e^{\jmath\omega})]_{\mathrm{f},(M+K)}\right\|_2, \ \forall\{w(m)\}_{m\in\mathcal{M}}, \qquad \text{(C.112)}$$

where the last inequality is a consequence of the fact that $A(e^{\jmath\omega})$ is a filter that does not modify the magnitude of discrete-time Fourier transform of signals (all-pass filter). □

Theorem 5 plays a central role in the characterization of the monotonic behavior associated with the MSE and mutual information in ZP-based systems. This occurs since both of these figures of merit are directly related to the matrix $\mathbf{S}(K)$ (or $\mathbf{S}'(K)$), as can be readily seen in Proposition 1 and Theorem 1. In fact, we can be more specific in this matter by stating the following corollary.

Corollary 3. *The average MSE/mutual information associated with the zero-padded MMSE-based optimal transceivers is decreased/increased whenever at least one zero outside the unit circle of a non-minimum phase channel is replaced by the related zero inside the unit circle, assuming that one does not use the whole received data block to estimate the transmitted signal.*

Proof. We know that $\mathbf{S}_{\mathrm{new}}(K) \geq \mathbf{S}(K)$ implies that the diagonal elements of $\mathbf{S}_{\mathrm{new}}(K)$ are at least as large as the diagonal elements of $\mathbf{S}(K)$. Moreover, we also know that $\mathbf{S}_{\mathrm{new}}(K) \geq \mathbf{S}(K) > O$ implies that $\mathbf{R}_{\mathrm{new}}(K) \leq \mathbf{R}(K)$. The former expression yields

$$\mathbf{R}'_{\mathrm{new}}(K) = \mathbf{R}_{\mathrm{new}}(K) + \frac{\sigma_v^2}{\sigma_s^2}\mathbf{I} \leq \mathbf{R}(K) + \frac{\sigma_v^2}{\sigma_s^2}\mathbf{I} = \mathbf{R}'(K). \qquad \text{(C.113)}$$

Thus, we also have

$$[\mathbf{R}'_{\mathrm{new}}(K)]^{-1} = \mathbf{S}'_{\mathrm{new}}(K) \geq \mathbf{S}'(K) = [\mathbf{R}'(K)]^{-1}. \qquad \text{(C.114)}$$

These facts eventually yield that the normalized trace of $\mathbf{S}_{\text{new}}(K)$ (or $\mathbf{S}'_{\text{new}}(K)$) is at least as large as the normalized trace of $\mathbf{S}(K)$ (or $\mathbf{S}'(K)$). Due to Lemma 2, it is also true that $\sqrt{\mathbf{S}_{\text{new}}(K)} \geq \sqrt{\mathbf{S}(K)}$ and $\sqrt{\mathbf{S}'_{\text{new}}(K)} \geq \sqrt{\mathbf{S}'(K)}$. From Lemma 5, we know that $\ln\{\mathbf{S}_{\text{new}}(K)\} \geq \ln\{\mathbf{S}(K)\}$. Such fact implies that the normalized trace of $\ln\{\mathbf{S}_{\text{new}}(K)\}$ is at least as large as the normalized trace of $\ln\{\mathbf{S}(K)\}$. The former sentence can be rewritten as

$$\ln\left(\sqrt[M]{\det\{\mathbf{S}_{\text{new}}(K)\}}\right) \geq \ln\left(\sqrt[M]{\det\{\mathbf{S}(K)\}}\right), \tag{C.115}$$

which yields

$$\sqrt[M]{\det\{\mathbf{S}_{\text{new}}(K)\}} \geq \sqrt[M]{\det\{\mathbf{S}(K)\}}. \tag{C.116}$$

In summary, all these facts show that the average MSE associated with the new channel, $\mathbf{H}_{\text{new}}(K)$, is larger than or equal to the average MSE associated with the original channel, $\mathbf{H}(K)$.

Regarding the average mutual information (see Theorem 1), the aforementioned arguments along with Lemmas 3 and 6 allow one to show that the average mutual information associated with the new channel, $\mathbf{H}_{\text{new}}(K)$, is smaller than or equal to the average mutual information associated with the original channel, $\mathbf{H}(K)$. □

Table C.4 exemplifies the results contained in Corollary 3 related to the average MSE of symbols. In order to obtain these data, we have used $\sigma_s^2 = 1$, $\sigma_v^2 = 0.01$, and channels $H_i(z)$, with $i \in \{1, 2, 3\}$. The previously described channel $H(z)$ (see Eq. (C.70) and Figure C.4) has three zeros outside the unit circle. Channel $H_1(z)$ is obtained from $H(z)$ by replacing one of these zeros outside the unit circle, let us say z_1, by $1/z_1^*$, in such a way that the magnitude responses of channels $H_1(z)$ and $H(z)$ are the same. Likewise, $H_2(z)$ is generated from $H_1(z)$ by substituting one zero that is outside the unit circle by a zero inside, in such a way that the magnitude responses of channels $H_2(z)$ and $H_1(z)$ are the same. The same procedure has been applied to generate the minimum phase channel $H_3(z)$ from $H_2(z)$. Thus, one should read Table C.4 in a per-column basis. As an example, for $K = 2$, the average MSE decreases whenever we substitute a zero outside the unit circle by a related zero inside the unit circle, irrespective of the transceiver type. One can also notice that the average MSE does not change whenever one uses all the redundant elements ($K = L = 9$) to estimate the symbols. This occurs since $\mathbf{R}_{\text{new}}(L) = \mathbf{R}(L)$ [43].

Table C.5 exemplifies the results contained in Corollary 3 related to the average mutual information between transmitted and estimated symbols. To obtain such results, we have used the same scenario previously described. Once again, one can verify that the mutual information increases when one substitutes a zero outside the

Table C.4: Average MSE of symbols of optimal ZP transceivers as a function of $K \in \mathcal{L}$ ($M = 16$ data symbols). The zeros of channels $H_i(z)$, with $i \in \{1, 2, 3\}$, are all depicted in Figure C.6.

	$K=0$	$K=1$	$K=2$	$K=3$	$K=4$	$K=5$	$K=6$	$K=7$	$K=8$	$K=9$
$\mathcal{E}_{\text{ZF}}^{\text{CI-UP}}$, $H_1(z)$	27.46	21.33	9.31	6.64	4.62	3.79	3.17	2.43	2.19	2.01
$\mathcal{E}_{\text{ZF}}^{\text{CI-UP}}$, $H_2(z)$	17.32	9.57	6.54	4.54	3.44	3.01	2.50	2.27	2.12	2.01
$\mathcal{E}_{\text{ZF}}^{\text{CI-UP}}$, $H_3(z)$	8.01	6.10	4.24	3.22	2.51	2.25	2.17	2.14	2.08	2.01
$\mathcal{E}_{\text{Pure}}^{\text{CI-UP}}$, $H_1(z)$	0.43	0.39	0.36	0.33	0.31	0.31	0.30	0.30	0.29	0.29
$\mathcal{E}_{\text{Pure}}^{\text{CI-UP}}$, $H_2(z)$	0.39	0.36	0.33	0.31	0.30	0.30	0.30	0.29	0.29	0.29
$\mathcal{E}_{\text{Pure}}^{\text{CI-UP}}$, $H_3(z)$	0.36	0.33	0.31	0.30	0.30	0.30	0.29	0.29	0.29	0.29
$\mathcal{E}_{\text{ZF}}$, $H_1(z)$	8.74	6.03	2.96	2.04	1.40	1.20	1.05	0.88	0.80	0.75
$\mathcal{E}_{\text{ZF}}$, $H_2(z)$	5.15	2.99	2.00	1.40	1.11	1.01	0.89	0.83	0.78	0.75
$\mathcal{E}_{\text{ZF}}$, $H_3(z)$	2.55	1.86	1.31	1.06	0.90	0.83	0.80	0.79	0.77	0.75
$\mathcal{E}_{\text{ZF}}^{\text{DFE}}$, $H_1(z)$	0.53	0.38	0.26	0.21	0.17	0.16	0.15	0.14	0.13	0.13
$\mathcal{E}_{\text{ZF}}^{\text{DFE}}$, $H_2(z)$	0.38	0.28	0.21	0.18	0.16	0.15	0.14	0.13	0.13	0.13
$\mathcal{E}_{\text{ZF}}^{\text{DFE}}$, $H_3(z)$	0.28	0.22	0.17	0.16	0.15	0.14	0.14	0.13	0.13	0.13

Table C.5: Average mutual information between transmitted and estimated symbols of optimal ZP transceivers as a function of $K \in \mathcal{L}$ ($M = 16$ data symbols). The zeros of channels $H_i(z)$, with $i \in \{1, 2, 3\}$, are all depicted in Figure C.6.

	$K=0$	$K=1$	$K=2$	$K=3$	$K=4$	$K=5$	$K=6$	$K=7$	$K=8$	$K=9$
$\mathcal{I}_{\text{ZF}}^{\text{CI-UP}}$, $H_1(z)$	2.06	2.20	2.32	2.40	2.46	2.49	2.53	2.56	2.59	2.60
$\mathcal{I}_{\text{ZF}}^{\text{CI-UP}}$, $H_2(z)$	2.14	2.27	2.38	2.44	2.48	2.51	2.54	2.57	2.60	2.60
$\mathcal{I}_{\text{ZF}}^{\text{CI-UP}}$, $H_3(z)$	2.22	2.34	2.43	2.47	2.50	2.53	2.56	2.58	2.60	2.60
$\mathcal{I}_{\text{ZF}}$, $H_1(z)$	0.69	0.81	1.03	1.17	1.32	1.39	1.45	1.52	1.57	1.60
$\mathcal{I}_{\text{ZF}}$, $H_2(z)$	0.83	1.01	1.17	1.31	1.40	1.45	1.51	1.55	1.58	1.60
$\mathcal{I}_{\text{ZF}}$, $H_3(z)$	1.04	1.18	1.33	1.42	1.49	1.53	1.55	1.57	1.58	1.60
$\mathcal{I}_{\text{ZF}}^{\text{DFE}}$, $H_1(z)$	1.04	1.27	1.55	1.73	1.89	1.95	2.01	2.07	2.12	2.15
$\mathcal{I}_{\text{ZF}}^{\text{DFE}}$, $H_2(z)$	1.27	1.51	1.72	1.87	1.96	2.00	2.05	2.09	2.13	2.15
$\mathcal{I}_{\text{ZF}}^{\text{DFE}}$, $H_3(z)$	1.51	1.70	1.88	1.96	2.02	2.06	2.09	2.11	2.13	2.15

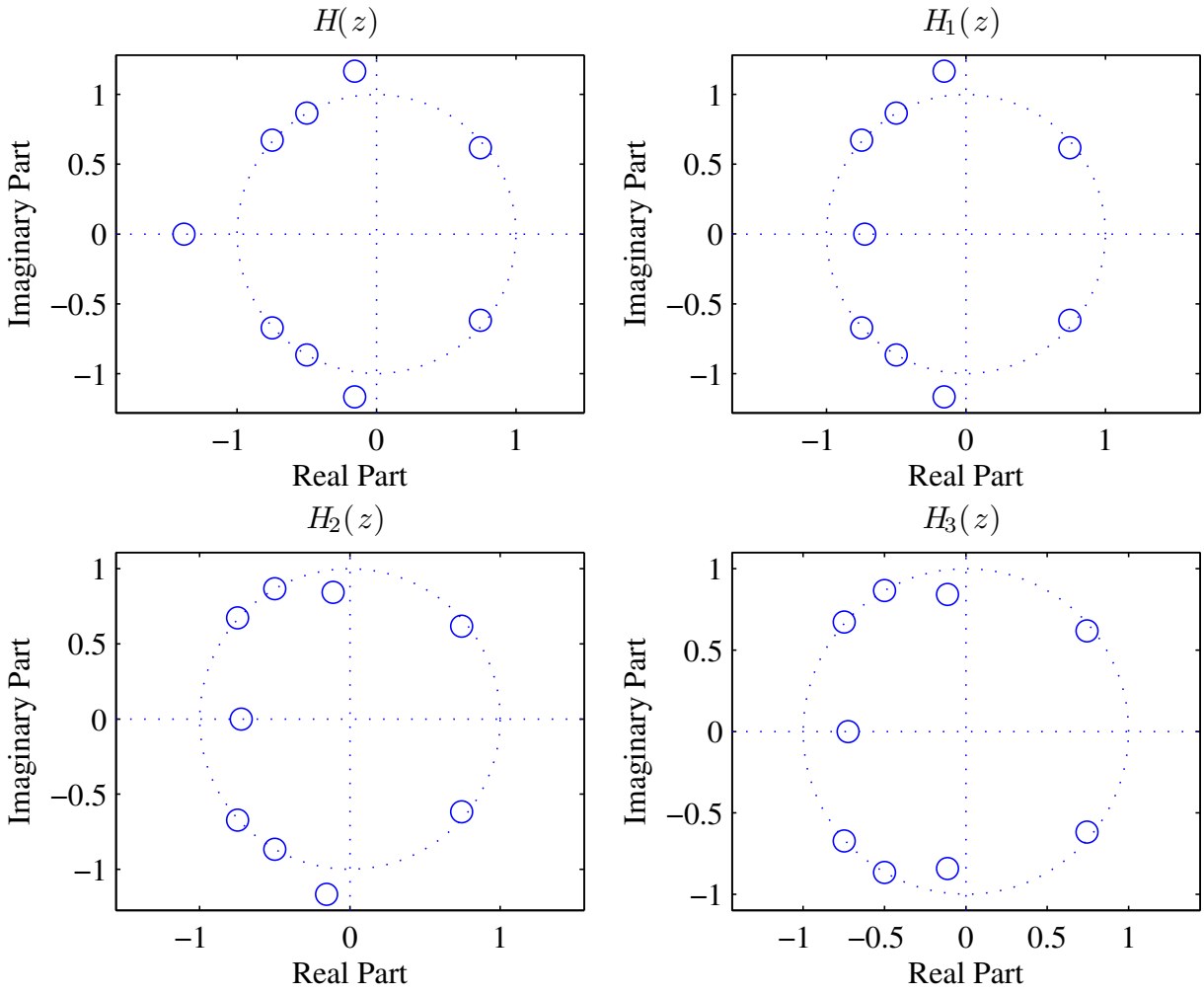

Figure C.6: Zeros of channels $H(z)$ and $H_i(z)$, where $i \in \{1, 2, 3\}$, with the unit circle for reference. All of these channels have the same magnitude response.

unit circle by a related zero inside the unit circle.

Another consequence of Corollary 3 is that the average MSE of symbols associated with the zero-padded MMSE-based optimal transceivers is increased whenever non-minimum phase channels are utilized, instead of their minimum phase counterparts. Similarly, the average mutual information between transmitted and estimated symbols of the zero-padded MMSE-based optimal transceivers is decreased whenever non-minimum phase channels are utilized, instead of their minimum phase counterparts. It is worth mentioning that such conclusions are valid assuming that some redundant elements are not used in the equalization.

Moreover, as a consequence of Corollary 3, the error-probability of symbols associated with both the minimum error-probability and the DFE MMSE-based systems also decreases whenever a zero outside the unit circle is replaced by a related zero inside the unit circle. Once again, such a monotonic behavior takes place since the

error-probability of symbols related to these particular transceivers is a monotone increasing function of the average MSE of symbols in many scenarios [40]. In fact, if the entire received data block is employed in the equalization, then the error-probability of symbols related to such transceivers is not sensitive to whether the channel zeros are inside or outside the unit circle.

C.6 Concluding Remarks

This chapter addressed the analysis of zero-padded optimal linear and DFE transceivers with full-redundancy. The class of transceivers discussed here includes zero-forcing and minimum mean-square-error systems, with unitary or non-unitary precoders. The figures of merit utilized to assess the performance of the various transceivers analyzed in this chapter were the MSE and the mutual information between the transmitted and received blocks. The proposed analyses indicated that the reduction in the relative amount of redundancy leads to loss in performance in terms of MSE and mutual information, which ultimately may lead to an increase in the bit-error rate. It is also shown how an attempt to decrease the number of redundant elements in the equalization in order to reduce the amount of computations might lead to loss in performance. Moreover, we also proved that channel zeros outside the unit circle degrade the performance as compared to related channel zeros inside the unit circle, unless the whole received data block is employed in the equalization process. Simulation results corroborate the theoretical findings.

From what we have proved in this chapter one can conclude it is worth developing transceivers which are capable of enhancing the bandwidth efficiency of ZP transceivers without increasing the data block length. In other words, it is worthwhile searching for practical block-based transceivers with reduced redundancy. In fact, we shall describe some practical minimum-redundancy proposals in the first part of this work and, after that, we will address the general reduced-redundancy systems in the second part of the work.

Apêndice D

DFT-Based Transceivers with Minimum Redundancy

One of the key features that enables the widespread adoption of both OFDM and SC-FD systems is the insertion of redundancy for the block-based transmission. This redundancy eliminates the IBI and allows computationally efficient implementations of ZF and MMSE equalizers based on discrete Fourier transform (DFT) and diagonal matrices [31].

Nonetheless, it is known that the minimum redundancy, required to eliminate IBI in fixed and memoryless block-based transceivers, is only half the amount employed in standard OFDM and SC-FD systems [32]. Minimum redundancy may lead to solutions with higher throughputs. However, throughput is not the only figure of merit to be considered, since cost effectiveness is an important issue. Indeed, practical transceivers with minimum redundancy, constrained to be asymptotically as simple as OFDM and SC-FD systems, have already been proposed [23].

In general, these new transceivers feature higher throughputs than standard OFDM and SC-FD systems, especially for channels with a large delay spread. In addition, they are cost effective, since they require either DFT, inverse DFT (IDFT), and diagonal matrices, or discrete Hartley transforms (DHT) and diagonal matrices [23]. Both ZF and MMSE solutions are available and they differ from each other in the number of parallel branches at the receiver end: two parallel branches for the ZF solutions and five parallel branches for the MMSE solutions, as depicted in Figures 4.1, 4.2, 4.3, 4.4, and 4.5 from [23].

Even though those ZF- and MMSE-based equalizers with minimum redundancy [23] may require equivalent time for processing a received vector (due to the inherent parallelism of the receiver structures), the MMSE solutions perform more than twice the number of computations related to the ZF solutions. This is an obvious drawback from a cost effectiveness (power consumption) perspective, and may hinder the use of MMSE-based equalizers with minimum redundancy in some

practical systems, despite the fact that MMSE-based solutions achieve much higher throughputs than ZF-based ones, especially for noisy environments [23].

The aforementioned drawback motivated us to further simplify the optimal MMSE-based equalizers, reducing the number of parallel branches at the receiver from five to four. In addition we also investigate suboptimal MMSE solutions in this chapter. Indeed, we propose novel multicarrier and single-carrier transceivers with minimum redundancy that keep the structure of the ZF solutions, while remaining as "close" to the optimal MMSE solution as possible. This closeness is measured by the standard 2-norm of matrices [44]. As a result, the new suboptimal MMSE transceivers lead to higher throughputs than the related ZF systems, with exactly the same complexity for the equalization process.

In order to derive the proposed transceivers, we first re-derive the optimal MMSE equalizers with minimum redundancy in a slightly different manner of that performed in [23]. As for the suboptimal solutions, we start from the brand-new optimal MMSE equalizers with minimum redundancy and apply the displacement approach [25] along with computationally simple singular-value decompositions (SVD) based on Householder-QR factorizations [44, 45]. The application of these techniques allows the development of suboptimal MMSE solutions that present comparable computational complexity to OFDM and SC-FD systems. In general, the proposals enable transmissions through long channels with higher throughputs than these traditional systems, achieving a good trade-off between performance and cost effectiveness.

This chapter is organized as follows: Section D.1 contains the mathematical description of the memoryless LTI transceiver model adopted in this work: the ZP-ZJ model. By stating some mathematical results, we also present the minimum-redundancy systems in Subsection D.1.1. This section also includes a description of the strategy to devise low complexity ZP-ZJ transceivers with minimum redundancy in Subsection D.1.2. In order to introduce the new decompositions of structured matrices, Subsection D.1.3 briefly presents the main ideas of the displacement theory. The simplification of the optimal MMSE equalizers proposed in [23] is described in Section D.2. The proposed suboptimal MMSE solutions are derived in Section D.3. Several simulation results are presented in Section D.4. The chapter includes some concluding remarks in Section D.5.

D.1 Zero-Padded Zero-Jammed Transceivers

As any other communication model, the ZP-ZJ system is comprised of five components, namely: channel, transmitter, receiver, input (or message), and output (or estimated message). As performed in Section C.1, we assume an FIR baseband-

channel model $\{h(l)\}_{l\in\mathcal{L}}$, with $h(l) \in \mathbb{C}$ for each $l \in \mathcal{L} \triangleq \{0, 1, \cdots, L\} \subset \mathbb{N}$. As long as the channel order L is not greater than the length of the transmitted message $N \in \mathbb{N}$, the ISI and IBI effects are respectively modeled by the $N \times N$ matrices $\mathbf{H}_{\text{ISI}}$ and $\mathbf{H}_{\text{IBI}}$ defined in Eqs. (C.2) and (C.3), respectively. The transmitter is responsible for linearly processing the input vector $\mathbf{s} \in \mathcal{C}^{M\times 1} \subset \mathbb{C}^{M\times 1}$, where $M \in \mathbb{N}$ is the number of symbols pertaining to a given constellation $\mathcal{C}$. Such a processing is defined by the matrix $\mathbf{F} \triangleq [\mathbf{F}_0^T \ \mathbf{0}_{M\times K}]^T$, with $\mathbf{F}_0 \in \mathbb{C}^{M\times M}$. The number of redundant elements inserted in this transmission is $K \triangleq N - M \in \mathbb{N}$. In order to generate an estimate $\hat{\mathbf{s}} \in \mathbb{C}^{M\times 1}$ of the input message, the receiver also processes the received vector through a linear transformation [67, 68] represented by the matrix $\mathbf{G} \triangleq [\mathbf{0}_{M\times(L-K)} \ \mathbf{G}_0]$, with $\mathbf{G}_0 \in \mathbb{C}^{M\times(M+2K-L)}$ [16].

Figure D.1 depicts the ZP-ZJ model, including an additive noise $\mathbf{v} \in \mathbb{C}^{N\times 1}$ at the receiver front-end. Note that this model yields the following input-output relationship:

$$\hat{\mathbf{s}} \triangleq \mathbf{G}\mathbf{H}(z)\mathbf{F}\mathbf{s} + \mathbf{G}\mathbf{v} = \mathbf{G}_0\mathbf{H}_0\mathbf{F}_0\mathbf{s} + \mathbf{v}_0\,, \tag{D.1}$$

in which $\mathbf{H}_0$ is the effective channel matrix defined as

$$\mathbf{H}_0 = \begin{bmatrix} h(L-K) & \cdots & h(0) & 0 & 0 & \cdots & 0 \\ \vdots & \ddots & & & & & \vdots \\ h(K) & \ddots & & & & & 0 \\ \vdots & \ddots & & & \ddots & & h(0) \\ h(L) & & & & & & \vdots \\ 0 & & & & \ddots & & h(L-K) \\ \vdots & & & & & & \vdots \\ 0 & \cdots & 0 & 0 & h(L) & \cdots & h(K) \end{bmatrix} \in \mathbb{C}^{(M+2K-L)\times M}. \tag{D.2}$$

Hence, the way the redundancy is padded at the transmitter and jammed at the receiver end is such that the IBI effect is completely eliminated. The amount

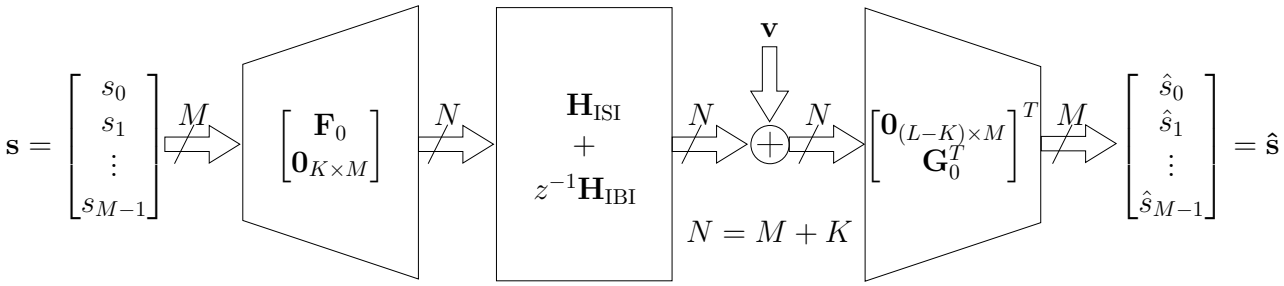

Figure D.1: ZP-ZJ transceiver model.

of redundancy, however, cannot be arbitrarily small, as discussed in the following proposition.

Proposition 2. *Assuming that the matrices* $\mathbf{F}$ *and* $\mathbf{G}$ *are full-rank, the ZP-ZJ transceiver is IBI-free, i.e.* $\mathbf{G}\mathbf{H}_{\text{IBI}}\mathbf{F} = \mathbf{0}$*, only when the number of redundant elements* K *is such that* $2K \geq L$*.*

Proof. See Lemma 5.1 in [32]. □

Let us consider that we insert at least $\lceil L/2 \rceil$ zeros before the transmission takes place. Thus, assuming both that channel-state information (CSI) is available at the receiver and that the transmitter uses a channel-independent unitary precoder $\mathbf{F}_0$, the designer task is to define the rectangular matrix $\mathbf{G}_0$. The most widely used techniques minimize either the ISI or the MSE of symbols at the receiver end. The ZF and the MMSE receivers are the respective solutions to such problems. Analytically, one has

$$\mathbf{G}_0^{\text{ZF}} \triangleq (\mathbf{H}_0\mathbf{F}_0)^{\dagger} = [(\mathbf{H}_0\mathbf{F}_0)^H(\mathbf{H}_0\mathbf{F}_0)]^{-1}(\mathbf{H}_0\mathbf{F}_0)^H = \mathbf{F}_0^{-1}(\mathbf{H}_0^H\mathbf{H}_0)^{-1}\mathbf{H}_0^H = \mathbf{F}_0^H\mathbf{H}_0^{\dagger}, \tag{D.3}$$

$$\mathbf{G}_0^{\text{MMSE}} \triangleq \left[(\mathbf{H}_0\mathbf{F}_0)^H(\mathbf{H}_0\mathbf{F}_0) + \frac{\sigma_v^2}{\sigma_s^2}\mathbf{I}_M\right]^{-1}(\mathbf{H}_0\mathbf{F}_0)^H = \mathbf{F}_0^H\left(\mathbf{H}_0^H\mathbf{H}_0 + \frac{\sigma_v^2}{\sigma_s^2}\mathbf{I}_M\right)^{-1}\mathbf{H}_0^H, \tag{D.4}$$

where, for the MMSE solution, the vectors $\mathbf{s}$ and $\mathbf{v}_0$ are drawn from zero-mean uncorrelated wide-sense stationary (WSS) random processes $\boldsymbol{s}$ and $\boldsymbol{v}_0$.[1] Note that $\mathsf{E}[\boldsymbol{s}\boldsymbol{v}_0^H] = \mathsf{E}[\boldsymbol{s}]\mathsf{E}[\boldsymbol{v}_0^H] = \mathbf{0}_{M\times M} = \mathsf{E}[\boldsymbol{v}_0]\mathsf{E}[\boldsymbol{s}^H] = \mathsf{E}[\boldsymbol{v}_0\boldsymbol{s}^H]$. We also assume that $\mathsf{E}[\boldsymbol{s}\boldsymbol{s}^H] = \sigma_s^2\mathbf{I}_M$ and $\mathsf{E}[\boldsymbol{v}_0\boldsymbol{v}_0^H] = \sigma_v^2\mathbf{I}_M$, for some $\sigma_v^2, \sigma_s^2 \in \mathbb{R}_+$. Observe that the definition of $\mathbf{G}_0^{\text{ZF}}$ only makes sense when $\mathbf{H}_0$ is full-rank. We shall consider that $\{h(l)\}_{l\in\mathcal{L}}$ induces a matrix $\mathbf{H}_0$ with rank M.

Assuming the adoption of a more traditional methodology of first estimating the channel-impulse response and then detecting the symbols, we now proceed to define two distinct problems: equalization and receiver design. The equalization problem is simply the processing of the received and jammed vector through the multiplication by $\mathbf{G}_0$. As a result, the computational complexity of the equalization is $\mathcal{O}(M^2)$ complex-valued numerical operations for general unstructured matrices. Nevertheless, the equalizer matrix depends on the knowledge of $\mathbf{H}_0$ and its (possibly regularized) pseudo-inverse. This knowledge is acquired during the receiver design. As a consequence, the computational complexity of the receiver design is $\mathcal{O}(M^3)$ complex-valued numerical operations for general unstructured matrices. It is worth

[1] The time index was omitted for the sake of conciseness.

mentioning that CP-OFDM and CP-SC-FD solve both the receiver-design and the equalization problems using only $\mathcal{O}(M \log_2 M)$ complex-valued operations [41].

With respect to the ZP-ZJ transceivers, the minimum-redundancy systems [23] are the state of the art. They only use $L/2$ redundant elements, considering an even-order FIR channel model. Besides their high throughput gains in delay constrained applications in very dispersive environments ($L/M \approx 1$), the minimum-redundancy transceivers are also computationally efficient, since they require only $\mathcal{O}(M \log_2 M)$ complex-valued operations for the equalization [23].

D.1.1 Minimum-Redundancy Systems

The ZF- and the MMSE-equalizer matrices of minimum-redundancy ZP-ZJ systems are nonsingular square matrices given by [23]

$$\mathbf{G}_{0,\min}^{\mathrm{ZF}} \triangleq \mathbf{F}_0^{-1}\mathbf{H}_0^{-1}, \tag{D.5}$$

$$\mathbf{G}_{0,\min}^{\mathrm{MMSE}} \triangleq \mathbf{F}_0^{-1}\mathbf{H}_0^{H}\left(\mathbf{H}_0\mathbf{H}_0^{H} + \frac{\sigma_v^2}{\sigma_s^2}\mathbf{I}_M\right)^{-1}, \tag{D.6}$$

in which we have considered that L is even, yielding only $L/2$ redundant elements for each data block.

These matrices admit decompositions that employ only DFT, IDFT, and diagonal matrices, as described in the following proposition.

Proposition 3. *The matrices* $\mathbf{G}_{0,\min}^{\mathrm{ZF}}$ *and* $\mathbf{G}_{0,\min}^{\mathrm{MMSE}}$ *can be expressed as*

$$\mathbf{G}_{0,\min}^{\mathrm{ZF}} = \frac{1}{2}\mathbf{F}_0^{-1}\mathbf{W}_M^{H}\left(\sum_{r=1}^{2}\mathbf{D}_{\bar{\mathbf{p}}_r}\mathbf{W}_M\mathbf{D}\mathbf{W}_M\mathbf{D}_{\bar{\mathbf{q}}_r}\right)\mathbf{W}_M^{H}\mathbf{D}^{H}, \tag{D.7}$$

$$\mathbf{G}_{0,\min}^{\mathrm{MMSE}} = \frac{1}{2}\mathbf{F}_0^{-1}\mathbf{W}_M^{H}\left(\sum_{r=1}^{5}\mathbf{D}_{\bar{\mathbf{p}}_r}\mathbf{W}_M\mathbf{D}\mathbf{W}_M\mathbf{D}_{\bar{\mathbf{q}}_r}\right)\mathbf{W}_M^{H}\mathbf{D}^{H}, \tag{D.8}$$

where $\mathbf{D}_{\bar{\mathbf{p}}_r}$ *and* $\mathbf{D}_{\bar{\mathbf{q}}_r}$ *are channel-dependent diagonal matrices, whereas* $\mathbf{D}$ *is a channel-independent diagonal matrix (see [23] for further details). A single-carrier system is obtained when* $\mathbf{F}_0 \triangleq \mathbf{I}_M$*, while a multicarrier system is obtained when* $\mathbf{F}_0 \triangleq \mathbf{W}_M^{H}$*.*

Proof. See Chapter 4 in [23]. □

This proposition indicates the low computational complexity of the minimum-redundancy transceivers. The decompositions of $\mathbf{G}_{0,\min}^{\mathrm{ZF}}$ and $\mathbf{G}_{0,\min}^{\mathrm{MMSE}}$ are not limited to DFT-based representations. Indeed, real-transform-based representations are also available [23]. Such alternative decompositions use discrete Hartley transform (DHT), which can also be implemented in a superfast way.

D.1.2 Strategy to Devise Transceivers with Minimum Redundancy

It is well-known that OFDM-based systems enjoy several good properties due to their structural simplicity. The use of DFT and IDFT in order to decouple the estimation of the symbols at the receiver end are paramount to the success of such systems. Unfortunately, we cannot decouple so easily the estimation of the symbols in a ZP-ZJ system with minimum redundancy. Indeed, such decoupling process requires the computation of singular-value decompositions (SVD), hindering its implementation in several practical problems.

Despite this potential drawback, we show that there are low complexity ZP-ZJ system with minimum redundancy. As a motivating example, let us consider how a zero forcing SC-FD system using cyclic prefix is implemented. The insertion of the cyclic prefix turns the linear convolution into a circular convolution between the transmitted data symbols and the channel impulse response. Using the vector notation for a noiseless channel, we can write $\mathbf{y} \triangleq \mathbf{C}\mathbf{s}$, where $\mathbf{C}$ is a circulant matrix that contains the channel coefficients. From linear algebra, we know that all circulant matrices may be diagonalized by using the same set of orthonormal eigenvectors. These eigenvectors are the columns of the normalized DFT matrix. In addition, the eigenvalues of circulant channel matrices are easily computed by means of the DFT of the first column of the circulant matrix. Thus, we have $\mathbf{y} = \mathbf{W}^H\mathbf{\Lambda}\mathbf{W}\mathbf{s} \Leftrightarrow \mathbf{s} = \mathbf{W}^H\mathbf{\Lambda}^{-1}\mathbf{W}\mathbf{y} = \mathbf{C}^{-1}\mathbf{y}$, considering that $\mathbf{\Lambda}^{-1}$ is computable, i.e., all eigenvalues of $\mathbf{C}$ are nonzero. Hence, the ZF-SC-FD system that employs cyclic prefix decomposes the inverse of the effective channel matrix using DFT and diagonal matrices. In fact, this decomposition is quite special since it is a diagonalization of the inverse of the effective channel matrix.

Our aim is to propose a similar approach: to look for an efficient decomposition of the "inverse" of the effective channel matrix associated with ZP-ZJ systems with minimum redundancy. In such systems, the effective channel matrix $\mathbf{H}_0$ is no longer circulant, in fact, it is an $M \times M$ Toeplitz matrix. Nevertheless, we still can take into account the Toeplitz structure in order to decompose the generalized inverse of $\mathbf{H}_0$ using only DFT and diagonal matrices. Our approach conveys the same basic ideas present in OFDM-based systems, except for two main features present only in OFDM-based systems: (i) the inverse of the effective channel matrix has exactly the same structure of the effective channel matrix (circulant structure); and (ii) the efficient decomposition of the inverse of the effective channel matrix corresponds to its diagonalization.

D.1.3 Displacement-Rank Approach

Intuitively, a matrix is said to have structure when its coefficients follow a given formation rule regarding either their relative position in the matrix or their mutual relationship. This implies that the matrix entries are defined by few parameters according to a compact formula.

A useful tool for exploiting the structure of a matrix is the displacement approach [58]. In order to introduce the main concepts of this theory, let us start with a particular example: consider a nonsingular square Toeplitz matrix $\mathbf{T} \in \mathbb{C}^{M\times M}$, whose ijth entry is defined as $[\mathbf{T}]_{ij} = t_{(i-j)}$, for all pair of integers i, j between 0 and $M-1$. Note that, when this matrix is either multiplied by a vector or inverted, all its M^2 entries are used in such operations. However, this matrix is completely defined by up to $2M-1$ elements, since the vector $[\, t_{1-M} \;\; \cdots \;\; t_0 \;\; \cdots \;\; t_{M-1} \,]$ defines the entire matrix $\mathbf{T}$. This way, it would be quite reasonable to expect that matrix operations may be performed faster by using a reduced amount of parameters. For instance, instead of using M^2 additions to add two Toeplitz matrices, the same result can be achieved by adding $2(2M-1) = 4M-2$ elements and then rearranging them accordingly.

This simple discussion motivates the definition of linear displacement operators: given two matrices $\mathbf{X}, \mathbf{Y} \in \mathbb{C}^{M\times M}$, the linear transformations [25]

$$\begin{aligned} \nabla_{\mathbf{X},\mathbf{Y}} \,:\, & \mathbb{C}^{M\times M} \to \mathbb{C}^{M\times M} \\ & \mathbf{U} \mapsto \nabla_{\mathbf{X},\mathbf{Y}}(\mathbf{U}) \triangleq \mathbf{XU} - \mathbf{UY} \end{aligned} \tag{D.9}$$

$$\begin{aligned} \Delta_{\mathbf{X},\mathbf{Y}} \,:\, & \mathbb{C}^{M\times M} \to \mathbb{C}^{M\times M} \\ & \mathbf{U} \mapsto \Delta_{\mathbf{X},\mathbf{Y}}(\mathbf{U}) \triangleq \mathbf{U} - \mathbf{XUY} \end{aligned} \tag{D.10}$$

are the so-called *Sylvester and Stein displacement operators*, respectively.

With these displacement operators, one can choose the *operator matrices* $\mathbf{X}$ and $\mathbf{Y}$ in a clever way in order to *compress* a given structured matrix $\mathbf{U}$. The resulting matrix $\nabla_{\mathbf{X},\mathbf{Y}}(\mathbf{U})$ or $\Delta_{\mathbf{X},\mathbf{Y}}(\mathbf{U})$ is the compressed form of $\mathbf{U}$ if its *displacement rank* is small, i.e., $R = \operatorname{rank}\{\nabla_{\mathbf{X},\mathbf{Y}}(\mathbf{U})\} \ll M$ or $R = \operatorname{rank}\{\Delta_{\mathbf{X},\mathbf{Y}}(\mathbf{U})\} \ll M$, where R is not a function of M. The idea behind the displacement approach is that the compressed form of a structured matrix contains all the information of the original matrix, but with a reduced amount of elements. Besides, with some rather mild constraints on $\mathbf{X}$ and $\mathbf{Y}$, it is possible to *decompress* the matrix $\nabla_{\mathbf{X},\mathbf{Y}}(\mathbf{U})$ or $\Delta_{\mathbf{X},\mathbf{Y}}(\mathbf{U})$ in order to recover the original matrix $\mathbf{U}$. Thus, *operations* with the original matrix can be directly translated into operations with its compressed forms [25].

As an example, it is easy to verify that, given the operator matrix $\mathbf{Z}_\lambda = [\, \mathbf{e}_2 \;\; \cdots \;\; \mathbf{e}_M \;\; \lambda\mathbf{e}_1 \,]$, for some $\lambda \in \mathbb{C}$, the Sylvester operator $\nabla_{\mathbf{Z}_\eta,\mathbf{Z}_\xi}$ applied to a

Toeplitz matrix $\mathbf{T}$ yields

$$
\begin{aligned}
\nabla_{\mathbf{Z}_\eta,\mathbf{Z}_\xi}(\mathbf{T}) &= \mathbf{Z}_\eta\mathbf{T} - \mathbf{T}\mathbf{Z}_\xi \\
&= \begin{bmatrix} \eta t_{M-1} & \eta t_{M-2} & \cdots & \eta t_0 \\ t_0 & t_{-1} & \cdots & t_{1-M} \\ \vdots & \vdots & \ddots & \vdots \\ t_{M-2} & t_{M-1} & \cdots & t_{-1} \end{bmatrix} - \begin{bmatrix} t_{-1} & \cdots & t_{1-M} & \xi t_0 \\ \vdots & \ddots & \vdots & \xi t_1 \\ t_{M-3} & \cdots & t_{-1} & \vdots \\ t_{M-2} & \cdots & t_0 & \xi t_{M-1} \end{bmatrix} \\
&= \begin{bmatrix} \eta t_{M-1} - t_{-1} & \cdots & \eta t_1 - t_{1-M} & \eta t_0 - \xi t_0 \\ 0 & \cdots & 0 & t_{1-M} - \xi t_1 \\ \vdots & & \vdots & \vdots \\ 0 & \cdots & 0 & t_{-1} - \xi t_{M-1} \end{bmatrix} \\
&= \underbrace{\begin{bmatrix} 1 \\ 0 \\ \vdots \\ 0 \end{bmatrix}}_{\hat{\mathbf{p}}_1} \underbrace{\begin{bmatrix} \eta t_{M-1} - t_{-1} & \cdots & \eta t_1 - t_{1-M} & \eta t_0 \end{bmatrix}}_{\hat{\mathbf{q}}_1^T} \\
&\quad + \underbrace{\begin{bmatrix} -\xi t_0 \\ t_{1-M} - \xi t_1 \\ \vdots \\ t_{-1} - \xi t_{M-1} \end{bmatrix}}_{\hat{\mathbf{p}}_2} \underbrace{\begin{bmatrix} 0 & 0 & \cdots & 1 \end{bmatrix}}_{\hat{\mathbf{q}}_2^T} \\
&= \hat{\mathbf{p}}_1\hat{\mathbf{q}}_1^T + \hat{\mathbf{p}}_2\hat{\mathbf{q}}_2^T = \begin{bmatrix} \hat{\mathbf{p}}_1 & \hat{\mathbf{p}}_2 \end{bmatrix} \begin{bmatrix} \hat{\mathbf{q}}_1^T \\ \hat{\mathbf{q}}_2^T \end{bmatrix} = \hat{\mathbf{P}}\hat{\mathbf{Q}}^T. \qquad \text{(D.11)}
\end{aligned}
$$

Hence, for $\eta = -1$ and $\xi = 1$, $\nabla_{\mathbf{Z}_{-1},\mathbf{Z}_1}(\mathbf{T}) = \hat{\mathbf{P}}\hat{\mathbf{Q}}^T = \hat{\mathbf{p}}_1\hat{\mathbf{q}}_1^T + \hat{\mathbf{p}}_2\hat{\mathbf{q}}_2^T$, with $\hat{\mathbf{p}}_1 = [\,1 \quad 0 \quad \cdots \quad 0\,]^T$, $\hat{\mathbf{q}}_1 = -[\,(t_{M-1} + t_{-1}) \quad \cdots \quad (t_1 + t_{1-M}) \quad t_0\,]^T$, $\hat{\mathbf{p}}_2 = [\,-t_0 \quad (t_{1-M} - t_1) \quad \cdots \quad (t_{-1} - t_{M-1})\,]^T$, and $\hat{\mathbf{q}}_2 = [\,0 \quad 0 \quad \cdots \quad 1\,]^T$. The pair of matrices $(\hat{\mathbf{P}}, \hat{\mathbf{Q}}) \in \mathbb{C}^{M\times 2} \times \mathbb{C}^{M\times 2}$ is the so-called *displacement-generator pair*. From this example, it is obvious that a Toeplitz matrix can be compressed, whenever $M \gg R \leq 2$.

The operations with a compressed form of a given matrix may be efficiently performed if some well-known results are applied, for instance (see Theorems 1.5.1,

1.5.3, and 1.5.4 in [25]):

$$\nabla_{\mathbf{Y},\mathbf{X}}(\mathbf{U}^{-1}) = -\mathbf{U}^{-1}\nabla_{\mathbf{X},\mathbf{Y}}(\mathbf{U})\mathbf{U}^{-1}, \tag{D.12}$$

$$\Delta_{\mathbf{X},\mathbf{Y}^{-1}}(\mathbf{U}) = -\nabla_{\mathbf{X},\mathbf{Y}}(\mathbf{U})\mathbf{Y}^{-1}, \tag{D.13}$$

$$\nabla_{\mathbf{X},\mathbf{Z}}(\mathbf{U}\mathbf{V}) = \nabla_{\mathbf{X},\mathbf{Y}}(\mathbf{U})\mathbf{V} + \mathbf{U}\nabla_{\mathbf{Y},\mathbf{Z}}(\mathbf{V}), \tag{D.14}$$

$$\nabla_{\mathbf{X},\mathbf{Y}}(\alpha\mathbf{U} + \beta\mathbf{V}) = \alpha\nabla_{\mathbf{X},\mathbf{Y}}(\mathbf{U}) + \beta\nabla_{\mathbf{X},\mathbf{Y}}(\mathbf{V}), \tag{D.15}$$

for any scalars α, β, and any 5-tuple $\{\mathbf{U}, \mathbf{V}, \mathbf{X}, \mathbf{Y}, \mathbf{Z}\}$ of complex-valued matrices with compatible dimensions and, when necessary, nonsingular.

D.2 Optimal MMSE Equalizers with Minimum Redundancy

Even though the existence of practical ZF solutions is important, most real-world systems work in environments where noise cannot be considered null. In such scenarios, the MMSE designs are more suitable. In this section we develop a novel DFT-based structure for linear MMSE block-based transceivers with minimum redundancy. Such a new result is distinct from the one described in Eq. (D.8), since it employs only four parallel branches at the equalizer, instead of five branches.

The result of this section exemplifies the operation stage associated with the displacement-rank approach. Indeed, let us define the transmitter-independent receiver matrix $\mathbf{K} \triangleq \mathbf{F}_0\mathbf{G}_{0,\min}^{\text{MMSE}} \in \mathbb{C}^{M\times M}$. From Eq. (D.6), one can easily verify that $\mathbf{K} = \mathbf{H}_0^H(\mathbf{H}_0\mathbf{H}_0^H + \rho\mathbf{I}_M)^{-1}$. Note that for the MMSE solution, the related transmitter-independent receiver matrix $\mathbf{K}$ is obtained from operations upon the effective channel matrix $\mathbf{H}_0$. One may therefore argue if there is any relationship between the displacement-generator pair of $\mathbf{K}$ and the displacement-generator pair of $\mathbf{H}_0$. Theorem 6 contains a result which shows how to operate on the displacement-generator pairs of $\mathbf{H}_0$ and $\mathbf{H}_0^H$ in order to derive the displacement-generator pair of $\mathbf{K}$.

Theorem 6. *For all $(\xi, \eta) \in \mathbb{C}^2$, with $\eta \neq 0$, one has $\nabla_{\mathbf{Z}_\xi,\mathbf{Z}_{1/\eta}}(\mathbf{K}) = \mathbf{P}\mathbf{Q}^T$, where*

$$\mathbf{P} = \left[\frac{\sigma_v^2}{\sigma_s^2}\left(\mathbf{H}_0^H\mathbf{H}_0 + \frac{\sigma_v^2}{\sigma_s^2}\mathbf{I}\right)^{-1}\hat{\mathbf{P}}' \quad -\mathbf{K}\hat{\mathbf{P}}\right]_{M\times 4}, \tag{D.16}$$

$$\mathbf{Q} = \left[\left(\mathbf{H}_0\mathbf{H}_0^H + \tfrac{\sigma_v^2}{\sigma_s^2}\mathbf{I}\right)^{-T}\hat{\mathbf{Q}}' \quad \mathbf{K}^T\hat{\mathbf{Q}}\right]_{M\times 4}, \tag{D.17}$$

with $(\hat{\mathbf{P}}, \hat{\mathbf{Q}}) \in \mathbb{C}^{M\times 2} \times \mathbb{C}^{M\times 2}$ and $(\hat{\mathbf{P}}', \hat{\mathbf{Q}}') \in \mathbb{C}^{M\times 2} \times \mathbb{C}^{M\times 2}$ being the displacement-generator pairs of $\nabla_{\mathbf{Z}_{1/\eta},\mathbf{Z}_\xi}(\mathbf{H}_0)$ and $\nabla_{\mathbf{Z}_\xi,\mathbf{Z}_{1/\eta}}(\mathbf{H}_0^H)$, respectively. These generators are easily found by using Eq. (D.11).

Proof. By using the result expressed in Eq. (D.14), we have

$$\nabla_{\mathbf{z}_{1/\eta},\mathbf{z}_{1/\eta}}(\mathbf{H}_0\mathbf{H}_0^H) = \underbrace{\begin{bmatrix}\hat{\mathbf{P}} & \mathbf{H}_0\hat{\mathbf{P}}'\end{bmatrix}}_{\bar{\mathbf{P}}} \underbrace{\begin{bmatrix}\hat{\mathbf{Q}}^T\mathbf{H}_0^H \\ \hat{\mathbf{Q}}'^T\end{bmatrix}}_{\bar{\mathbf{Q}}^T} = \bar{\mathbf{P}}\bar{\mathbf{Q}}^T. \tag{D.18}$$

Now, define $\mathbf{A} = \left(\mathbf{H}_0\mathbf{H}_0^H + \frac{\sigma_v^2}{\sigma_s^2}\mathbf{I}\right)$. Since $\nabla_{\mathbf{z}_{1/\eta},\mathbf{z}_{1/\eta}}(\mathbf{I}) = \mathbf{0}_{M\times M}$, then $\nabla_{\mathbf{z}_{1/\eta},\mathbf{z}_{1/\eta}}(\mathbf{A}) = \bar{\mathbf{P}}\bar{\mathbf{Q}}^T$. From Eq. (D.12), it follows that

$$\nabla_{\mathbf{z}_{1/\eta},\mathbf{z}_{1/\eta}}\left(\mathbf{A}^{-1}\right) = -\mathbf{A}^{-1}\nabla_{\mathbf{z}_{1/\eta},\mathbf{z}_{1/\eta}}(\mathbf{A})\,\mathbf{A}^{-1} = \underbrace{\left[-\mathbf{A}^{-1}\bar{\mathbf{P}}\right]}_{\check{\mathbf{P}}}\underbrace{\left[\mathbf{A}^{-T}\bar{\mathbf{Q}}\right]^T}_{\check{\mathbf{Q}}^T} = \check{\mathbf{P}}\check{\mathbf{Q}}^T \tag{D.19}$$

Thus, by again using Eq. (D.14), one has

$$\nabla_{\mathbf{z}_{\xi},\mathbf{z}_{1/\eta}}\left(\mathbf{H}_0^H\mathbf{A}^{-1}\right) = \underbrace{\begin{bmatrix}\hat{\mathbf{P}}' & \mathbf{H}_0^H\check{\mathbf{P}}\end{bmatrix}}_{\mathbf{P}} \underbrace{\begin{bmatrix}\hat{\mathbf{Q}}'^T\mathbf{A}^{-1} \\ \check{\mathbf{Q}}^T\end{bmatrix}}_{\mathbf{Q}^T} = \mathbf{P}\mathbf{Q}^T \tag{D.20}$$

Hence, the displacement generator of the MMSE solution is given by the pair

$$\mathbf{P} = \begin{bmatrix}\hat{\mathbf{P}}' & -\mathbf{K}\hat{\mathbf{P}} & -\mathbf{K}\mathbf{H}_0\hat{\mathbf{P}}'\end{bmatrix}_{M\times 6}, \tag{D.21}$$

$$\mathbf{Q} = \begin{bmatrix}\mathbf{A}^{-T}\hat{\mathbf{Q}}' & \mathbf{K}^T\hat{\mathbf{Q}} & \mathbf{A}^{-T}\hat{\mathbf{Q}}'\end{bmatrix}_{M\times 6}. \tag{D.22}$$

By applying the matrix inversion lemma [16], it is possible to show that

$$\mathbf{P}\mathbf{Q}^T = \frac{\sigma_v^2}{\sigma_s^2}\left(\mathbf{H}_0^H\mathbf{H}_0 + \frac{\sigma_v^2}{\sigma_s^2}\mathbf{I}\right)^{-1}\hat{\mathbf{P}}'\hat{\mathbf{Q}}'^T\mathbf{A}^{-1} - \mathbf{K}\hat{\mathbf{P}}\hat{\mathbf{Q}}^T\mathbf{K}, \tag{D.23}$$

resulting in a more compact definition for $(\mathbf{P},\mathbf{Q}) \in \mathbb{C}^{M\times 4}\times\mathbb{C}^{M\times 4}$, as in Eqs. (D.16) and (D.17). □

Hence, by using the result of Theorem 1 from [23], combined with Theorem 6 of this chapter, and considering that $(\xi,\eta) = (1,-1)$, we have

$$\mathbf{K} = \frac{1}{2}\mathbf{W}_M^H\left[\sum_{r=1}^{4}\mathbf{D}_{\tilde{\mathbf{p}}_r}\mathbf{W}_M\left(\mathrm{diag}\{e^{\jmath\frac{\pi}{M}m}\}_{m=0}^{M-1}\right)\mathbf{W}_M\mathbf{D}_{\tilde{\mathbf{q}}_r}\right]\mathbf{W}_M^H\mathrm{diag}\{e^{-\jmath\frac{\pi}{M}m}\}_{m=0}^{M-1}, \tag{D.24}$$

with $\tilde{\mathbf{P}} = [\,\tilde{\mathbf{p}}_1\ \cdots\ \tilde{\mathbf{p}}_4\,]$ and $\tilde{\mathbf{Q}} = [\,\tilde{\mathbf{q}}_1\ \cdots\ \tilde{\mathbf{q}}_4\,]$ defined as in Theorem 1 from [23]. Note that we have introduced the notation $\mathbf{D}_{\boldsymbol{\nu}} \triangleq \mathrm{diag}\{\boldsymbol{\nu}\}$, for any vector $\boldsymbol{\nu}$.

Thus, in the multicarrier transmission, we can define

$$\mathbf{F}_0 = \mathbf{W}_M^H, \tag{D.25}$$

$$\mathbf{G}_0 = \frac{1}{2}\left[\sum_{r=1}^{4} \mathbf{D}_{\tilde{\mathbf{p}}_r} \mathbf{W}_M \left(\text{diag}\{e^{\jmath\frac{\pi}{M}m}\}_{m=0}^{M-1}\right) \mathbf{W}_M \mathbf{D}_{\tilde{\mathbf{q}}_r}\right] \mathbf{W}_M^H \text{diag}\{e^{-\jmath\frac{\pi}{M}m}\}_{m=0}^{M-1}, \tag{D.26}$$

in order to achieve the linear MMSE solution. Similarly, in the single-carrier transmission, we can define

$$\mathbf{F}_0 = \mathbf{I}_M, \tag{D.27}$$

$$\mathbf{G}_0 = \frac{1}{2}\mathbf{W}_M^H \left[\sum_{r=1}^{4} \mathbf{D}_{\tilde{\mathbf{p}}_r} \mathbf{W}_M \left(\text{diag}\{e^{\jmath\frac{\pi}{M}m}\}_{m=0}^{M-1}\right) \mathbf{W}_M \mathbf{D}_{\tilde{\mathbf{q}}_r}\right] \mathbf{W}_M^H \text{diag}\{e^{-\jmath\frac{\pi}{M}m}\}_{m=0}^{M-1}, \tag{D.28}$$

in order to achieve the linear MMSE solution.

Note that the equalization process of the linear MMSE solution requires almost the same processing time of the ZF solution, since the structures of the receivers are very similar and it is also possible to take advantage of the inherent parallel structures (see Figure D.2). Nevertheless, the MMSE solution entails four parallel branches instead of only two employed in the ZF solution.

In order to illustrate the computations related to the proposed decompositions of $\mathbf{F}_0$ and $\mathbf{G}_0$, especially concerning the definitions of the one-tap equalizers, let us consider a toy example of a minimum-redundancy single-carrier transmission through an FIR baseband channel model

$$H(z) = (1-\jmath) + (2+\jmath)z^{-1} + (3-\jmath)z^{-2}. \tag{D.29}$$

In addition, assume that $M = 3$ innovative data symbols are transmitted per block. In such a case, we have $L = 2$, implying that only one redundant element is transmitted per block. Under these conditions, one can set $\mathbf{F}_0 = \mathbf{I}_3$ while $\mathbf{G}_0$ is defined as in Eq. (D.28), considering an MMSE-based equalizer, in which

$$\mathbf{W}_3 = \frac{1}{\sqrt{3}}\begin{bmatrix} 1 & 1 & 1 \\ 1 & e^{-\jmath\frac{2\pi}{3}} & e^{-\jmath\frac{4\pi}{3}} \\ 1 & e^{-\jmath\frac{4\pi}{3}} & e^{-\jmath\frac{2\pi}{3}} \end{bmatrix}, \tag{D.30}$$

$$\text{diag}\{e^{\jmath\frac{\pi}{3}m}\}_{m=0}^{2} = \begin{bmatrix} 1 & 0 & 0 \\ 0 & e^{\jmath\frac{\pi}{3}} & 0 \\ 0 & 0 & e^{\jmath\frac{2\pi}{3}} \end{bmatrix}. \tag{D.31}$$

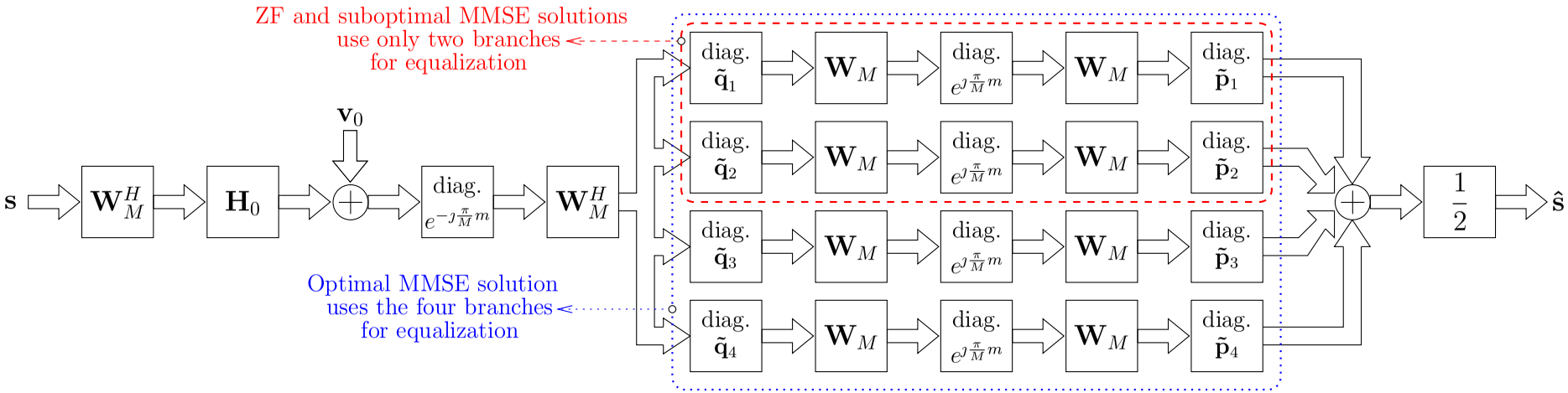

Figure D.2: DFT-based multicarrier minimum-redundancy block transceiver (MC-MRBT).

As for the diagonal matrices $\mathbf{D}_{\tilde{\mathbf{p}}_r}$ and $\mathbf{D}_{\tilde{\mathbf{q}}_r}$, they depend on the channel model. Indeed, we have the following matrices for the chosen channel model:

$$\mathbf{H}_0 = \begin{bmatrix} (2+\jmath) & (1-\jmath) & 0 \\ (3-\jmath) & (2+\jmath) & (1-\jmath) \\ 0 & (3-\jmath) & (2+\jmath) \end{bmatrix}, \tag{D.32}$$

$$\nabla_{\mathbf{Z}_{-1},\mathbf{Z}_1}(\mathbf{H}_0) = \hat{\mathbf{P}}\hat{\mathbf{Q}}^T = \begin{bmatrix} (-1+\jmath) & (-3+\jmath) & (-4-2\jmath) \\ 0 & 0 & (-3+\jmath) \\ 0 & 0 & (1-\jmath) \end{bmatrix}, \tag{D.33}$$

$$\hat{\mathbf{P}} = \begin{bmatrix} 1 & (-2-\jmath) \\ 0 & (-3+\jmath) \\ 0 & (1-\jmath) \end{bmatrix}, \tag{D.34}$$

$$\hat{\mathbf{Q}} = \begin{bmatrix} (-1+\jmath) & 0 \\ (-3+\jmath) & 0 \\ (-2-\jmath) & 1 \end{bmatrix}. \tag{D.35}$$

With the help of such matrices, one can compute the equalizer matrices $\mathbf{D}_{\tilde{\mathbf{p}}_r}$ and $\mathbf{D}_{\tilde{\mathbf{q}}_r}$, with $r \in \{1,2,3,4\}$, by first determining the matrices $\tilde{\mathbf{P}} = [\,\tilde{\mathbf{p}}_1 \ \cdots \ \tilde{\mathbf{p}}_4\,]$ and $\tilde{\mathbf{Q}} = [\,\tilde{\mathbf{q}}_1 \ \cdots \ \tilde{\mathbf{q}}_4\,]$ defined as in Theorem 1 from [23]. In the case of linear MMSE-based equalizers, assuming an SNR of 10 dB, one has the following matrices:

$$\begin{aligned} \mathbf{K} &= \mathbf{H}_0^H(\mathbf{H}_0\mathbf{H}_0^H + 10^{-1}\mathbf{I}_3)^{-1} \\ &\approx \begin{bmatrix} (0.2285-\jmath 0.1811) & (0.0920+\jmath 0.0752) & (-0.0631+\jmath 0.0362) \\ (0.0998+\jmath 0.2335) & (0.0682-\jmath 0.1677) & (0.0920+\jmath 0.0752) \\ (-0.3299-\jmath 0.1315) & (0.0998+\jmath 0.2335) & (0.2285-\jmath 0.1811) \end{bmatrix}, \end{aligned} \tag{D.36}$$

$$\begin{aligned} \nabla_{\mathbf{Z}_1,\mathbf{Z}_{-1}}(\mathbf{K}) &= \mathbf{P}\mathbf{Q}^T \\ &\approx \begin{bmatrix} (-0.4219-\jmath 0.2067) & (0.1630+\jmath 0.1973) & (0.4570-\jmath 0.3621) \\ (0.1604-\jmath 0.0134) & 0 & (0.0367+\jmath 0.2696) \\ 0 & (-0.1604+\jmath 0.0134) & (-0.2379-\jmath 0.0563) \end{bmatrix}, \end{aligned} \tag{D.37}$$

in which

$$\mathbf{P} \approx \begin{bmatrix} 0.0107 & 0.0009 & (-0.2285 + \jmath 0.1811) & (1.0163 - \jmath 0.0993) \\ (-0.0030 + \jmath 0.0045) & (-0.0112 - \jmath 0.0056) & (-0.0998 - \jmath 0.2335) & (-0.1643 + \jmath 0.0123) \\ (-0.0048 - \jmath 0.0076) & (0.0528 + \jmath 0.0154) & (0.3299 + \jmath 0.1315) & (-0.0427 + \jmath 0.4172) \end{bmatrix}, \tag{D.38}$$

$$\mathbf{Q} \approx \begin{bmatrix} (-1.1875 - \jmath 0.4174) & (-0.0477 - \jmath 0.0762) & (-0.0522 + \jmath 0.4020) & (-0.3299 - \jmath 0.1315) \\ (0.3116 + \jmath 0.5233) & (-0.0296 + \jmath 0.0448) & (-0.1702 + \jmath 0.0213) & (0.0998 + \jmath 0.2335) \\ (0.4478 - \jmath 0.3621) & 0.1067 & (-0.9623 - \jmath 0.0993) & (0.2285 - \jmath 0.1811) \end{bmatrix}, \tag{D.39}$$

$$\tilde{\mathbf{P}} \approx \begin{bmatrix} (-0.0029 + \jmath 0.0031) & (-0.0425 - \jmath 0.0098) & (-0.0015 - \jmath 0.0791) & (-0.8094 - \jmath 0.3302) \\ -0.0250 & (0.0381 - \jmath 0.0505) & (0.6596 - \jmath 0.6042) & (-0.7691 + \jmath 0.2088) \\ (-0.0040 - \jmath 0.0031) & (0.0016 + \jmath 0.0603) & (0.0274 + \jmath 0.1401) & (-1.4704 + \jmath 0.4194) \end{bmatrix}, \tag{D.40}$$

$$\tilde{\mathbf{Q}} \approx \begin{bmatrix} (-1.2890 - \jmath 0.8668) & (-0.0885 - \jmath 0.1275) & (0.6548 + \jmath 0.0970) & (-0.5317 - \jmath 0.2007) \\ (-1.1057 + \jmath 0.6504) & (-0.1429 + \jmath 0.0064) & (1.3879 + \jmath 0.4822) & (-0.3551 + \jmath 0.1978) \\ (1.0513 + \jmath 1.3028) & (-0.0886 + \jmath 0.1211) & (0.8444 - \jmath 0.2814) & (0.2012 + \jmath 0.5461) \end{bmatrix}. \tag{D.41}$$

By observing the elements of the vectors $\tilde{\mathbf{p}}_r$ and $\tilde{\mathbf{q}}_r$, with $r \in \{1, 2, 3, 4\}$ (see the column vectors in Eqs. (D.40) and (D.41)), it is hard to see any relationship between pairs of such vectors (there are a total of eight distinct column vectors). Actually, these vectors come from the relations [23]

$$\tilde{\mathbf{P}} = -\sqrt{3}\mathbf{W}_3\mathbf{P}, \tag{D.42}$$

$$\tilde{\mathbf{Q}} = \sqrt{3}\mathbf{W}_3 \left(\text{diag}\{e^{\jmath\frac{\pi}{3}m}\}_{m=0}^{2}\right) \mathbf{Z}_{-1}\mathbf{Q}, \tag{D.43}$$

in which $\mathbf{P}$ and $\mathbf{Q}$ are defined in Eqs. (D.38) and (D.39), respectively. In other words, in order to compute the equalizer taps, one might first determine the matrices $\mathbf{P}$ and $\mathbf{Q}$. After that, the equalizer taps are calculated employing $\mathcal{O}(M \log_2 M)$ operations.

Now, with the exception of $\mathbf{q}_4 = -\mathbf{J}_3\mathbf{p}_3$ (see the column vectors in Eqs. (D.38) and (D.39)), with

$$\mathbf{J}_3 = \begin{bmatrix} 0 & 0 & 1 \\ 0 & 1 & 0 \\ 1 & 0 & 0 \end{bmatrix}, \tag{D.44}$$

it is still hard to see any relationship between pairs of column vectors in matrices $\mathbf{P}$ and $\mathbf{Q}$. In fact, such an observation is not new. In [24], p. 161, the authors state that the coefficient vectors which define the displacements related to generalized Bezoutians[2] are solutions of certain "fundamental equations." These coefficient

[2]The inverse of a Toeplitz matrix, $\mathbf{T}$, is also known as a Toeplitz-Bezoutian matrix, or simply,

vectors are related to each other in a quite complicated manner, with exception of centrosymmetric Bezoutian matrices [24]. A similar remark is pointed out in Theorem 3.1 of [49], in which eight linear systems have to be solved in order to define the generator pair $(\mathbf{P}, \mathbf{Q})$.

Nevertheless, in the case of ZF receiver, in which the receiver matrix is essentially the inverse of the Toeplitz effective channel matrix, the relationship between pairs of column vectors within the resulting matrices $\mathbf{P}$ and $\mathbf{Q}$ is rather simple [24]. This fact simplifies the determination of the equalizer taps associated with ZF minimum-redundancy systems. Indeed, in the case of ZF equalizers, one has the following matrices for the chosen channel model:

$$\mathbf{H}_0^{-1} \approx \begin{bmatrix} (0.2345 - \jmath 0.1862) & (0.0897 + \jmath 0.0759) & (-0.0634 + \jmath 0.0386) \\ (0.1034 + \jmath 0.2414) & (0.0690 - \jmath 0.1724) & (0.0897 + \jmath 0.0759) \\ (-0.3448 - \jmath 0.1379) & (0.1034 + \jmath 0.2414) & (0.2345 - \jmath 0.1862) \end{bmatrix}, \tag{D.45}$$

$$\begin{aligned} \nabla_{\mathbf{Z}_1, \mathbf{Z}_{-1}}(\mathbf{H}_0^{-1}) &= \mathbf{P}\mathbf{Q}^T \\ &\approx \begin{bmatrix} (-0.4345 - \jmath 0.2138) & (0.1669 + \jmath 0.2028) & (0.4690 - \jmath 0.3724) \\ (0.1655 - \jmath 0.0138) & 0 & (0.0400 + \jmath 0.2800) \\ 0 & (-0.1655 + \jmath 0.0138) & (-0.2552 - \jmath 0.0621) \end{bmatrix}, \end{aligned} \tag{D.46}$$

in which

$$\mathbf{P} \approx \begin{bmatrix} (-0.2345 + \jmath 0.1862) & (1.0248 - \jmath 0.1021) \\ (-0.1034 - \jmath 0.2414) & (-0.1655 + \jmath 0.0138) \\ (0.3448 + \jmath 0.1379) & (-0.0483 + \jmath 0.4207) \end{bmatrix}, \tag{D.47}$$

$$\mathbf{Q} \approx \begin{bmatrix} (-0.0483 + \jmath 0.4207) & (-0.3448 - \jmath 0.1379) \\ (-0.1655 + \jmath 0.0138) & (0.1034 + \jmath 0.2414) \\ (-0.9752 - \jmath 0.1021) & (0.2345 - \jmath 0.1862) \end{bmatrix}, \tag{D.48}$$

$$\tilde{\mathbf{P}} \approx \begin{bmatrix} (-0.0069 - \jmath 0.0828) & (-0.8110 - \jmath 0.3324) \\ (0.6837 - \jmath 0.6261) & (-0.7793 + \jmath 0.2178) \\ (0.0267 + \jmath 0.1503) & (-1.4841 + \jmath 0.4208) \end{bmatrix}, \tag{D.49}$$

$$\tilde{\mathbf{Q}} \approx \begin{bmatrix} (0.6575 + \jmath 0.1204) & (-0.5482 - \jmath 0.2125) \\ (1.4101 + \jmath 0.4907) & (-0.3690 + \jmath 0.2056) \\ (0.8579 - \jmath 0.3048) & (0.2138 + \jmath 0.5655) \end{bmatrix}. \tag{D.50}$$

Note that in the ZF case, there are four distinct vectors which define the equalizer matrices $\mathbf{D}_{\tilde{\mathbf{p}}_r}$ and $\mathbf{D}_{\tilde{\mathbf{q}}_r}$, with $r \in \{1, 2\}$, (two column vectors in Eq. (D.49) and two column vectors in Eq. (D.50)), being very hard to see any relationship which is able to link such vectors. However, by using Eqs. (D.42) and (D.43), the distinct vectors that compose the matrices $\tilde{\mathbf{P}}$ and $\tilde{\mathbf{Q}}$ can be calculated from Eqs. (D.47) and (D.48), which could be summarized using two distinct vectors only, since $\mathbf{q}_1 = \mathbf{J}\mathbf{p}_2 - [0\ 0\ 2]^T$ and $\mathbf{q}_2 = -\mathbf{J}\mathbf{p}_1$. It is worth mentioning that the computation of matrices $\mathbf{D}_{\tilde{\mathbf{p}}_r}$ and

a T-Bezoutian matrix. It is possible to show that $\text{rank}\{\nabla_{\mathbf{Z}_\xi, \mathbf{Z}_\eta}(\mathbf{T}^{-1})\} \leq 2$. In general, a matrix $\mathbf{B}$ which respects $\text{rank}\{\nabla_{\mathbf{Z}_\xi, \mathbf{Z}_\eta}(\mathbf{B})\} \leq R$ is a (generalized) Bezoutian matrix. See, for example, [23, 24]. The MMSE-based receiver matrix pertains to this class of matrices.

$\mathbf{D}_{\tilde{\mathbf{q}}_r}$ is performed in the equalizer design stage (see Chapter J). If the channel does not vary, then matrices $\mathbf{D}_{\tilde{\mathbf{p}}_r}$ and $\mathbf{D}_{\tilde{\mathbf{q}}_r}$ are constant matrices as well.

D.3 Suboptimal MMSE Equalizers with Minimum Redundancy

An interesting fact concerning the MMSE and the ZF solutions in the case of standard OFDM and SC-FD systems is that both induce the same equalizer structure at the receiver end. For example, in an SC-FD system, the process of "inserting and discarding" redundancy induces an effective circulant channel matrix. For such a matrix, the related MMSE- and ZF-receiver matrices are both circulant as well. Note that this resemblance does not happen in the case of minimum-redundancy systems, since the effective channel matrix $\mathbf{H}_0$ is Toeplitz. Indeed, for the single-carrier solution, the related ZF-receiver matrix is a *T-Bezoutian matrix*, whereas the related MMSE-receiver matrix is a (*generalized*) *Bezoutian matrix*.

These facts, along with the practical necessity of designing simpler equalizers, led us to investigate the "best" T-Bezoutian matrix that still takes into account the presence of noise. Thus, instead of using a generalized Bezoutian matrix $\mathbf{K}$ as in the optimal MMSE solution [23], we shall describe how to design another matrix $\bar{\mathbf{K}}$, which is the "closest" T-Bezoutian matrix to $\mathbf{K}$. An additional constraint is that the method to achieve this new suboptimal solution must be computationally cheap.

The low-complexity requirement motivated us to work with the compressed form of $\mathbf{K}$ and $\bar{\mathbf{K}}$. This means that we will operate on at most $4M$ coefficients per matrix, instead of M^2. Hence, we now derive a pair $(\bar{\mathbf{P}}, \bar{\mathbf{Q}}) \in \mathbb{C}^{M\times R} \times \mathbb{C}^{M\times R}$, with $R \in \{\, 2,\, 3 \,\}$, from a known pair $(\mathbf{P}, \mathbf{Q}) \in \mathbb{C}^{M\times 4} \times \mathbb{C}^{M\times 4}$, where $\nabla_{\mathbf{Z_1},\mathbf{Z_{-1}}}(\bar{\mathbf{K}}) = \bar{\mathbf{P}}\bar{\mathbf{Q}}^T$ and $\nabla_{\mathbf{Z_1},\mathbf{Z_{-1}}}(\mathbf{K}) = \mathbf{P}\mathbf{Q}^T$. In order to do this, we will employ the useful result stated in Lemma 7 (see Chapter C), which shows how one can choose the closest (in the Euclidean-norm sense) matrix to a predefined matrix, using the knowledge about the SVD associated with such a predefined matrix.

Thus, by applying Lemma 7, we can use a similar reasoning as in [25, 45] in order to derive a new generator pair $(\bar{\mathbf{P}}, \bar{\mathbf{Q}}) \in \mathbb{C}^{M\times R} \times \mathbb{C}^{M\times R}$ related to a matrix $\bar{\mathbf{K}}$ based on the SVD of $\mathbf{P}\mathbf{Q}^T$. Therefore,

$$\bar{\mathbf{P}} = \text{first } R \text{ columns of } \left\{\mathbf{U}\bar{\mathbf{\Sigma}}\right\} \text{ and } \bar{\mathbf{Q}} = \text{first } R \text{ columns of } \{\mathbf{V}\}\,, \tag{D.51}$$

where $\mathbf{P}\mathbf{Q}^T = \mathbf{U}\mathbf{\Sigma}\mathbf{V}^T$ and $R \in \{\, 2,\, 3 \,\}$ (for T-Bezoutian matrices, $R = 2$). This is a suboptimal MMSE solution in the sense that the resulting displacement matrix is the closest one to the displacement matrix of the optimal MMSE solution, where the closeness is measured by the induced Euclidean norm of matrices.

However, this solution is based on SVD of $M \times M$ matrices, which, in general, requires $\mathcal{O}(M^3)$ computations [44]. We now describe a way to simplify these SVD computations by taking into account the structure of the matrices. The resulting computational complexity for this specific SVD process is only $\mathcal{O}(M)$ operations.

The aforementioned SVD computations may be efficiently performed by first computing QR decompositions of the matrices $\mathbf{P}$ and $\mathbf{Q}$ [45]. The QR algorithm decomposes a given matrix $\mathbf{X}$ into a unitary matrix $\boldsymbol{Q}$ and an upper triangular matrix $\boldsymbol{R}$ [44]. There are several versions for the QR algorithm [44]. Among them, the Householder-based QR factorization is one of the most popular. Thus, by applying a complex version of Algorithm 5.2.1 described in [44] (see also Sections 5.1.2, 5.1.3, and 5.1.4 of this reference), it is possible to calculate four matrices $\boldsymbol{Q}_{\mathbf{P}}$, $\boldsymbol{R}_{\mathbf{P}}$, $\boldsymbol{Q}_{\mathbf{Q}}$, and $\boldsymbol{R}_{\mathbf{Q}}$, such that $\boldsymbol{Q}_{\mathbf{P}}\boldsymbol{R}_{\mathbf{P}} = \mathbf{P}$ and $\boldsymbol{Q}_{\mathbf{Q}}\boldsymbol{R}_{\mathbf{Q}} = \mathbf{Q}$. All these computations require only $\mathcal{O}(M)$ operations since they are based on computationally efficient Householder reflections [44].

In addition, as $\mathbf{P}$ and $\mathbf{Q}$ are $M \times 4$ matrices, then $\mathbf{P}\mathbf{Q}^T = \boldsymbol{Q}_{\mathbf{P}}(\boldsymbol{R}_{\mathbf{P}}\boldsymbol{R}_{\mathbf{Q}}^T)\boldsymbol{Q}_{\mathbf{Q}}^T$ is such that

$$\boldsymbol{R}_{\mathbf{P}}\boldsymbol{R}_{\mathbf{Q}}^T = \begin{bmatrix} \bar{\boldsymbol{R}}_4 & \mathbf{0}_{4\times(M-4)} \\ \mathbf{0}_{(M-4)\times 4} & \mathbf{0}_{(M-4)\times(M-4)} \end{bmatrix}. \tag{D.52}$$

The resulting matrix $\bar{\boldsymbol{R}}_4$ is 4×4. Thus, a general SVD algorithm may be applied now to this reduced-dimension matrix. This can be done using $\mathcal{O}(4^3)$ numerical operations [44]. Hence, assuming that $\bar{\boldsymbol{R}}_4 = \mathbf{U}_4\boldsymbol{\Sigma}_4\mathbf{V}_4^T$, with $\mathbf{U}_4$ and $\mathbf{V}_4$ being unitary matrices, we have

$$\mathbf{P}\mathbf{Q}^T = \underbrace{\boldsymbol{Q}_{\mathbf{P}} \begin{bmatrix} \mathbf{U}_4 & \\ & \mathbf{I}_{M-4} \end{bmatrix}}_{=\mathbf{U}} \underbrace{\begin{bmatrix} \boldsymbol{\Sigma}_4 & \\ & \mathbf{0}_{M-4} \end{bmatrix}}_{=\boldsymbol{\Sigma}} \underbrace{\left(\boldsymbol{Q}_{\mathbf{Q}} \begin{bmatrix} \mathbf{V}_4 & \\ & \mathbf{I}_{M-4} \end{bmatrix} \right)^T}_{=\mathbf{V}^T}. \tag{D.53}$$

Therefore, we can apply Eq. (D.51) to derive the proposed solutions. The number of operations to obtain the generator pair $(\bar{\mathbf{P}}, \bar{\mathbf{Q}})$ from the generator pair $(\mathbf{P}, \mathbf{Q})$ is around $(72 + R)M$. In our case, $R = 2$, which means that the actual number of operations is around $74M$.

We have assumed that $(\mathbf{P}, \mathbf{Q})$ is known. In fact, these matrices completely define the MMSE equalizer, since they are the only ones that contain information about the channel. Nevertheless, these matrices must be previously computed in the so-called *receiver-design stage* [23]. This task can be performed using up to $\mathcal{O}(M \log_2^2 M)$ operations [23]. We have shown that the design of $(\bar{\mathbf{P}}, \bar{\mathbf{Q}})$ does not increase substantially the complexity of the receiver-design stage, since $M \log_2^2 M > M$, for all $M > 2$. Besides, there are many applications in which the equalizer-design problem

is not frequently solved. In wireline communications systems, the channel model is not updated so often. This means that the main problem is the *equalization*. Taking these facts into account, this chapter proposes suboptimal MMSE solutions that considerably reduce the computational effort during the MMSE-based equalization process.

It is worth mentioning that the proposed suboptimal solution is not the optimal T-Bezoutian-MMSE solution. Indeed, we had attempted to design a T-Bezoutian matrix $\mathbf{K}'$, such that $\|\mathbf{s} - \hat{\mathbf{s}}\|_2$ is minimized, where $\hat{\mathbf{s}} = \mathbf{K}'(\mathbf{H}_0\mathbf{F}_0\mathbf{s} + \mathbf{v}')$. However, after lengthy calculations, we verified that the solution to such a problem requires the use of optimization techniques that employ more than $\mathcal{O}(M)$ operations. Even though our proposals are not the optimal T-Bezoutian-MMSE solution, the simulations indicate that suboptimal solutions perform rather close to the optimal MMSE solutions (generalized Bezoutians) in a number of situations.

D.4 Simulation Results

This section aims at evaluating the performance of the DFT-based transceivers with minimum redundancy in some particular scenarios. The figures of merit adopted here are the uncoded BER and the throughput. The uncoded BER is defined as the bit-error rate without considering the protection of channel coding. The throughput is defined as

$$\text{Throughput} = br_c\frac{M}{M+K}(1 - \text{BLER})f_s \quad \text{bps}, \tag{D.54}$$

in which b denotes the number of bits required to represent one constellation symbol, r_c denotes the code rate considering the protection of channel coding, K denotes the amount of redundancy, f_s denotes the sampling frequency, where symbol and channel models use the same sampling frequency, and stands for block-error rate, assuming that a data block is discarded when at least one of its original bits is incorrectly decoded at the receiver end. In addition, the definition of the signal-to-noise ratio (SNR) used throughout the simulations is the ratio between the mean energy of the transmitted symbols at the input of the multipath channel and the power-spectral density of the additive noise at the receiver front-end. Besides, we also consider that both synchronization and channel estimation are perfectly performed at the receiver end.

Optimal MMSE Equalizers With Minimum Redundancy

In this example, we transmit 200 blocks, each one containing $M = 32$ BPSK [34, 35, 69] data symbols (without taking redundancy into account), and compute the un-

coded BER and throughput by using a Monte-Carlo averaging process with $10,000$ simulations. Consider these symbols are sampled at a frequency $f_s = 1.0$ GHz and that they are transmitted through a channel with a model operating at the same frequency as the symbols and with long impulse response of order $L = 30$. All the channel taps have the same variance, and the channel model is always normalized, that is, $\mathsf{E}[\|\mathbf{h}\|_2^2] = 1$. Both the imaginary and real parts of the channel are independently drawn from a white and Gaussian sequence (random Rayleigh channel) [70]. For each simulation a new channel is generated. Due to the randomness in the choice of these realizations, it is very likely that the amount of congruous zeros related to the channel is smaller than the amount of redundancy, which guarantees the existence of ZF solutions [33, 57, 71, 72].

Furthermore, since the proposed transceivers use zeros as redundant elements, the adopted OFDM and SC-FD systems in the simulations are the ZP-OFDM-OLA and ZP-SC-FD-OLA [37], where ZP and OLA stand for zero-padding and overlap-and-add, respectively (see Subsections B.3.2 and B.3.4). Like the traditional cyclic-prefix-based systems, these ZP-based transceivers also induce a circulant channel matrix. We have chosen these transceivers as benchmarks since they are superfast transceivers that transmit L redundant zeros for each M data symbols. **In summary, from now on we shall consider that OFDM means ZP-OFDM-OLA and SC-FD means ZP-SC-FD-OLA in all results throughout the entire text**.

Figure D.3 and Figure D.4 show the uncoded BER curves[3] for the OFDM, the SC-FD, the multicarrier minimum-redundancy block transceiver (MC-MRBT), and the single-carrier minimum-redundancy block transceiver (SC-MRBT), using both ZF and MMSE designs. By observing these figures it is possible to verify that the MMSE-MC-MRBT outperforms its counterpart, the MMSE-OFDM. As expected [73], the MMSE-OFDM has the same performance as the ZF-OFDM. On the other hand, the MMSE-SC-FD outperforms the MMSE-SC-MRBT for the whole SNR range. As expected, for the ZF solutions, the BER performances of the transceivers are only comparable with the MMSE when the SNR is large.

[3]The uncoded BER is the bit-error rate computed before the channel-decoding process at the receiver end.

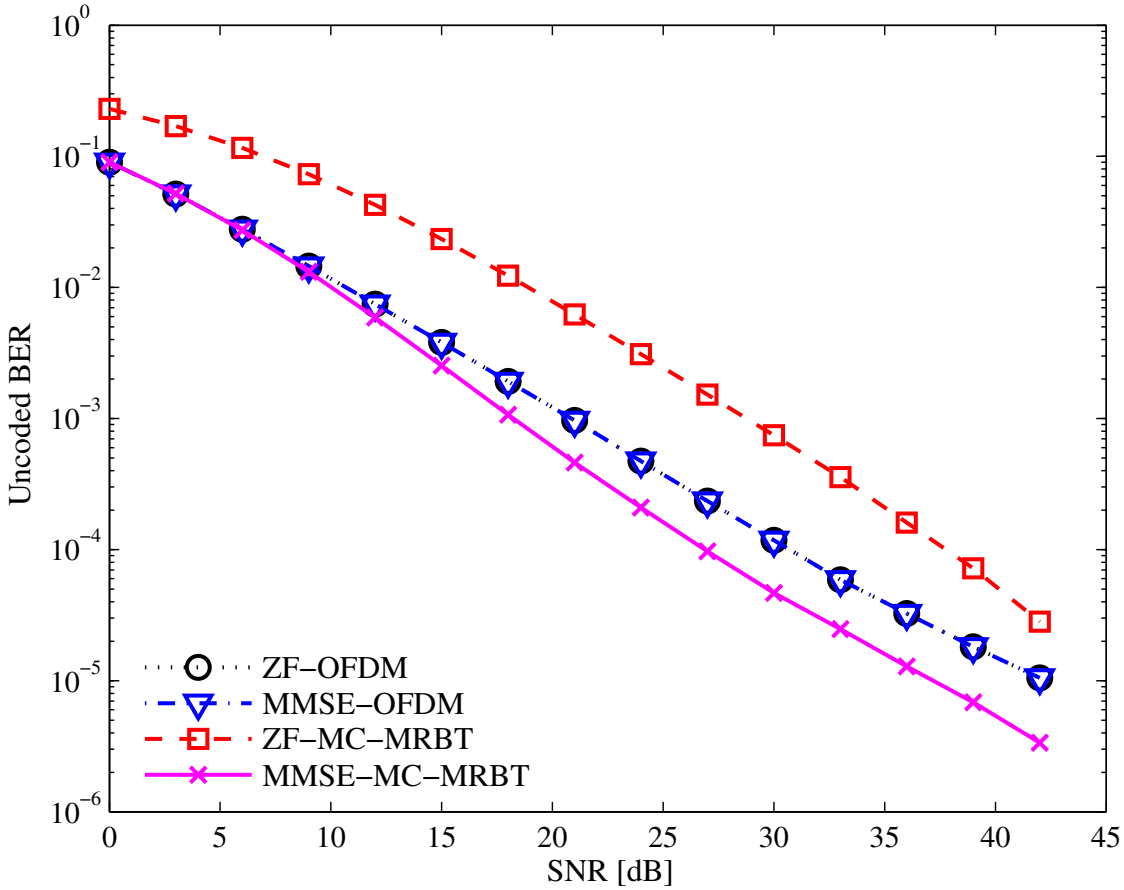

Figure D.3: Uncoded BER as a function of SNR [dB] for random Rayleigh channels, considering DFT-based multicarrier transmissions.

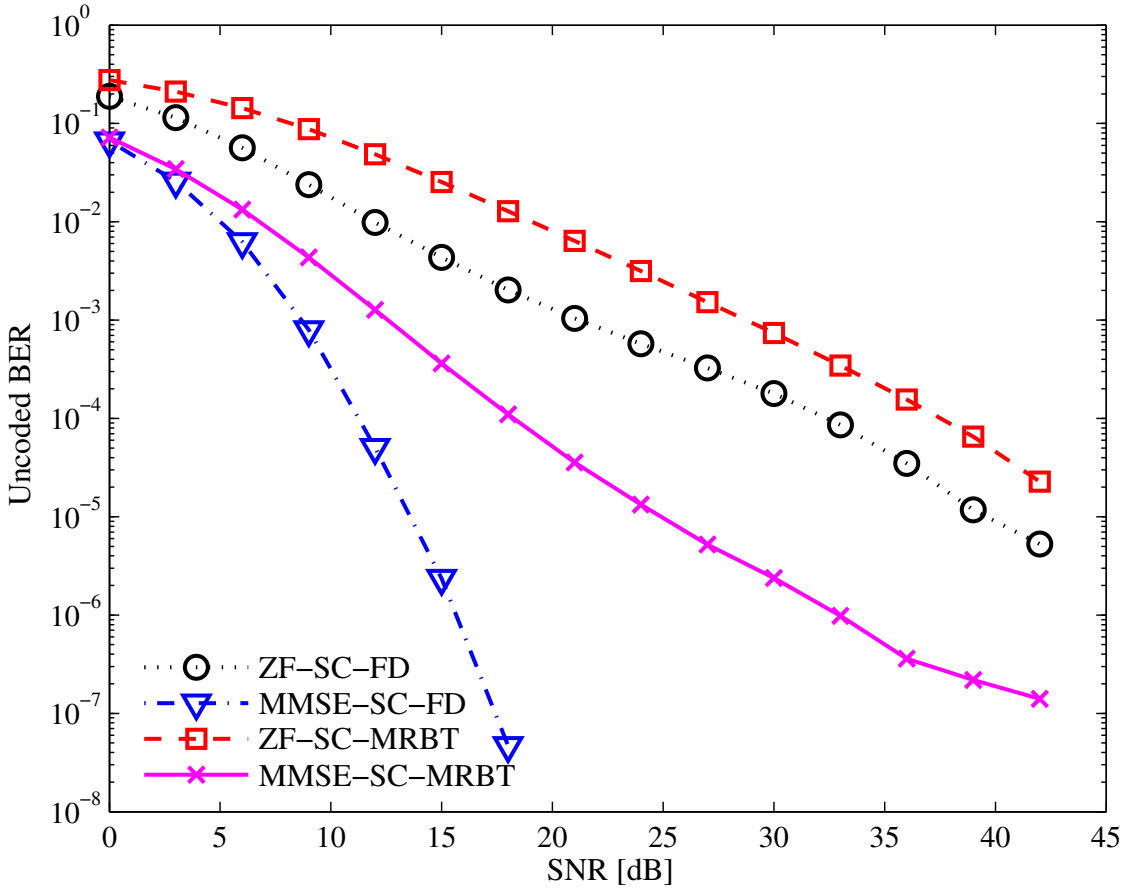

Figure D.4: Uncoded BER as a function of SNR [dB] for random Rayleigh channels, considering DFT-based single-carrier transmissions.

As observed in Figure D.5 and Figure D.6, the throughput performances of the proposed transceivers are much better than the traditional ones, except for SNRs lower than 12 dB in the ZF solutions. In this example, we use a convolutional code with constraint length 7, $r_c = 1/2$, and generators $\mathbf{g_0} = [\mathbf{133}]$ (octal) and $\mathbf{g_1} = [\mathbf{165}]$ (octal). This configuration is adapted from the 3G-LTE specifications [74]. In addition, for the BLER computation, we consider that a block (16 bits) is lost if, at least, one of its received bits is incorrect. We have employed a MATLAB implementation of a hard-decision Viterbi decoder. We do not make any restriction on the channel model in terms of condition number of the effective channel matrix. Note that such favorable result stems from the choices for M and L (delay constrained applications in very dispersive environments). These types of applications are suitable for the proposed transceivers. In the cases where $M \gg L$, the traditional OFDM and SC-FD solutions are more adequate.

In fact, for $M \gg L$, it was observed that the noise enhancement is even higher in the proposed transceivers. For example, consider the results depicted in Figure D.7 and Figure D.8, where $M = 64$, $L = 6$, and the throughput is computed as previously. The ZF-MC-MRBT and ZF-SC-MRBT have poor throughput performance due to the noise enhancement. However, the MMSE-MC-MRBT and MMSE-SC-MRBT may be used when the designer is willing to pay the price of a higher computational complexity.

Suboptimal MMSE Equalizers With Minimum Redundancy

In order to evaluate the performance of the proposed suboptimal solutions, four channel models were considered:

- *Channel A* [32], whose transfer function is

$$H_{\mathrm{A}}(z) = 0.1659 + 0.3045z^{-1} - 0.1159z^{-2} - 0.0733z^{-3} - 0.0015z^{-4}. \quad \text{(D.55)}$$

- *Channel B* [12], whose transfer function is

$$\begin{aligned} H_{\mathrm{B}}(z) = &- (0.3699 + \jmath 0.5782) - (0.4053 + \jmath 0.5750)z^{-1} - (0.0834 - \jmath 0.0406)z^{-2} \\ &+ (0.1587 - \jmath 0.0156)z^{-3} + 0z^{-4}. \end{aligned} \quad \text{(D.56)}$$

- *Channel C* [75], whose transfer function is

$$H_{\mathrm{C}}(z) = 1 + 0.5z^{-1} - 0.7z^{-2} + 0.9z^{-3} + z^{-4}. \quad \text{(D.57)}$$

- *Channel D* [31], whose zeros are $1, 0.9\jmath, -0.9\jmath$, and $1.3\exp(\jmath\frac{5\pi}{8})$.

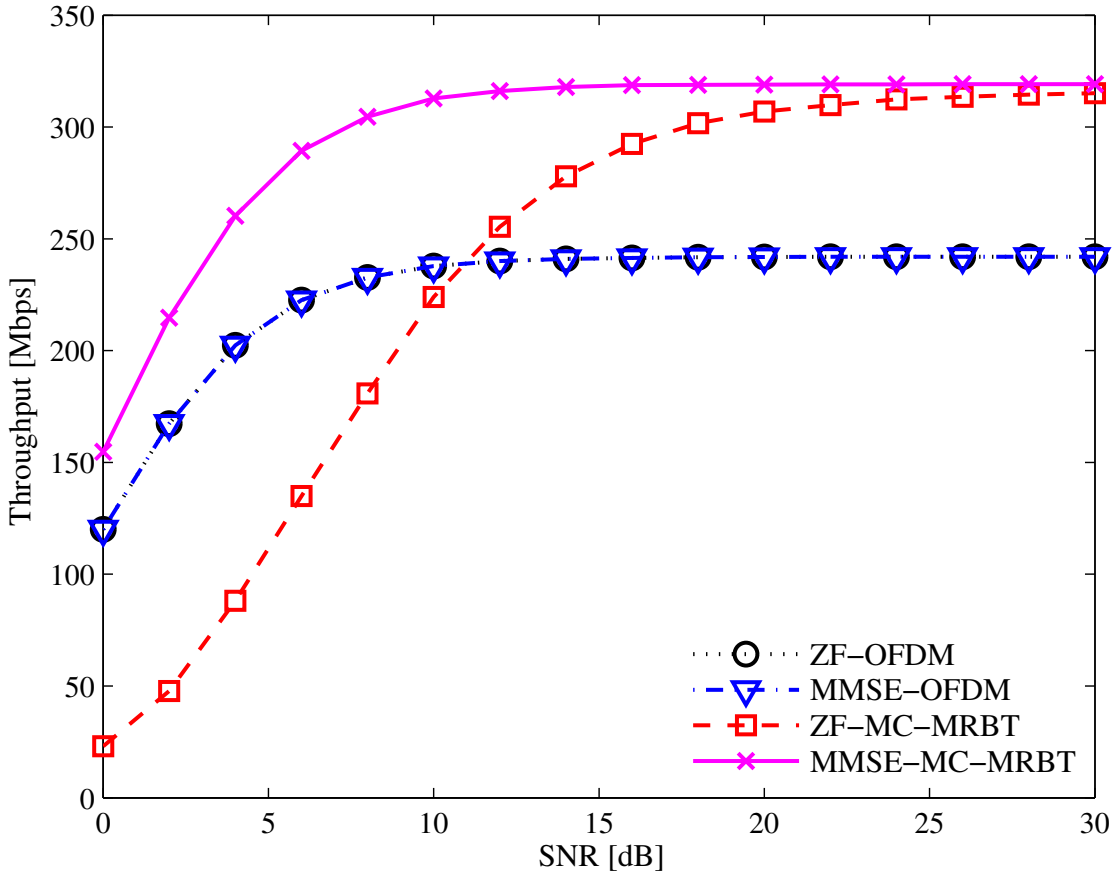

Figure D.5: Throughput [Mbps] as a function of SNR [dB] for random Rayleigh channels, considering DFT-based multicarrier transmissions ($M = 32$ and $L = 30$).

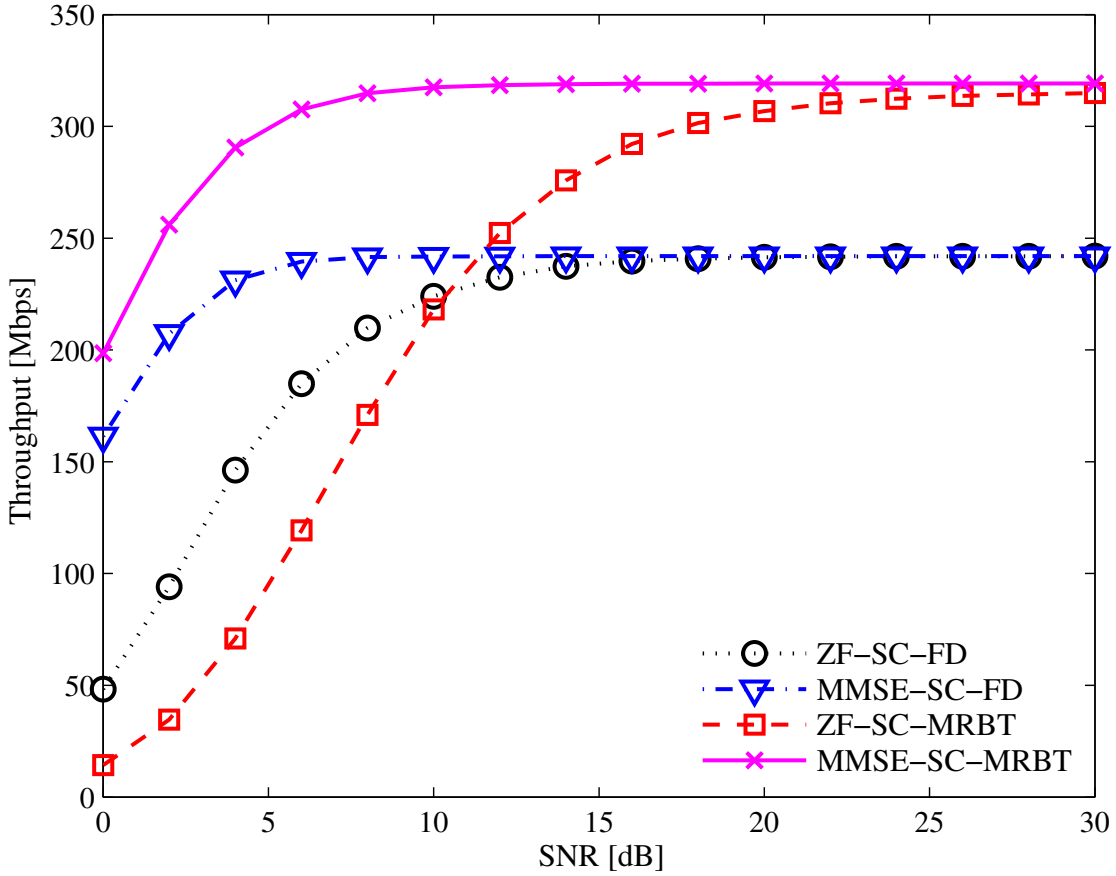

Figure D.6: Throughput [Mbps] as a function of SNR [dB] for random Rayleigh channels, considering DFT-based single-carrier transmissions ($M = 32$ and $L = 30$).

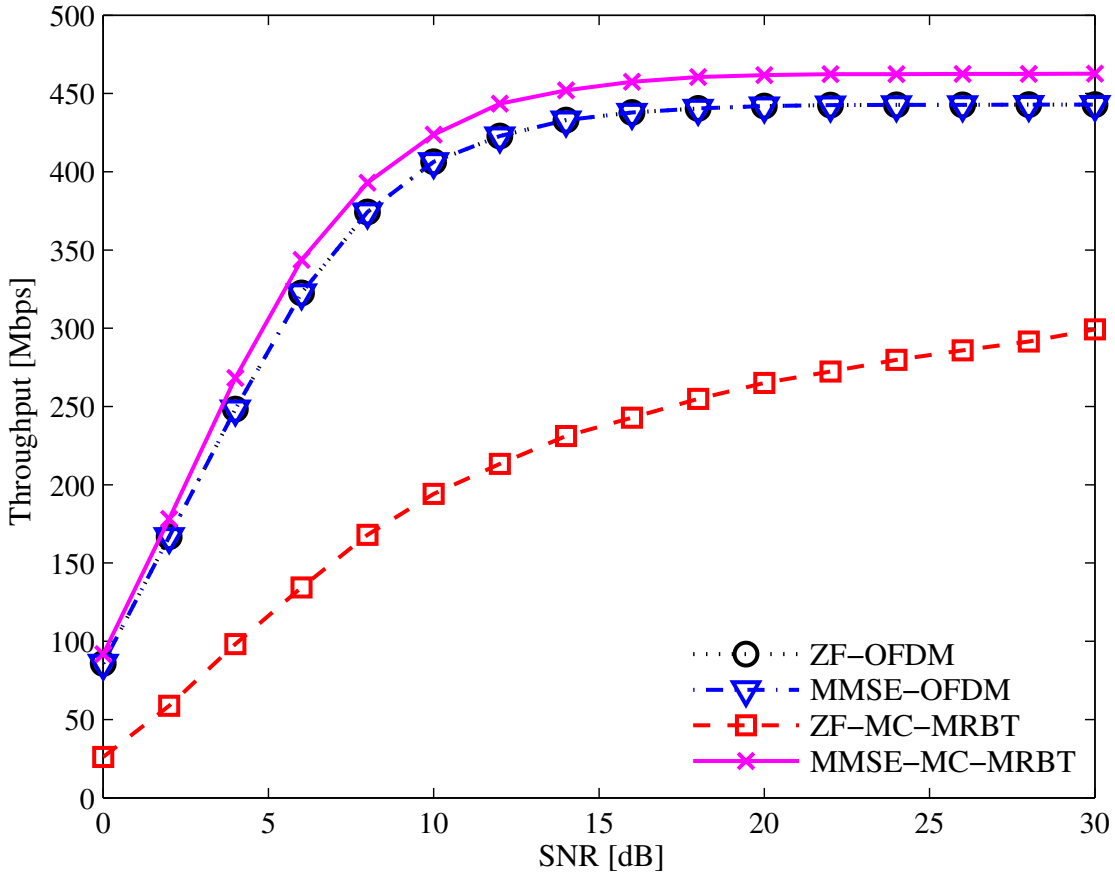

Figure D.7: Throughput [Mbps] as a function of SNR [dB] for random Rayleigh channels, considering DFT-based multicarrier transmissions ($M = 64$ and $L = 6$).

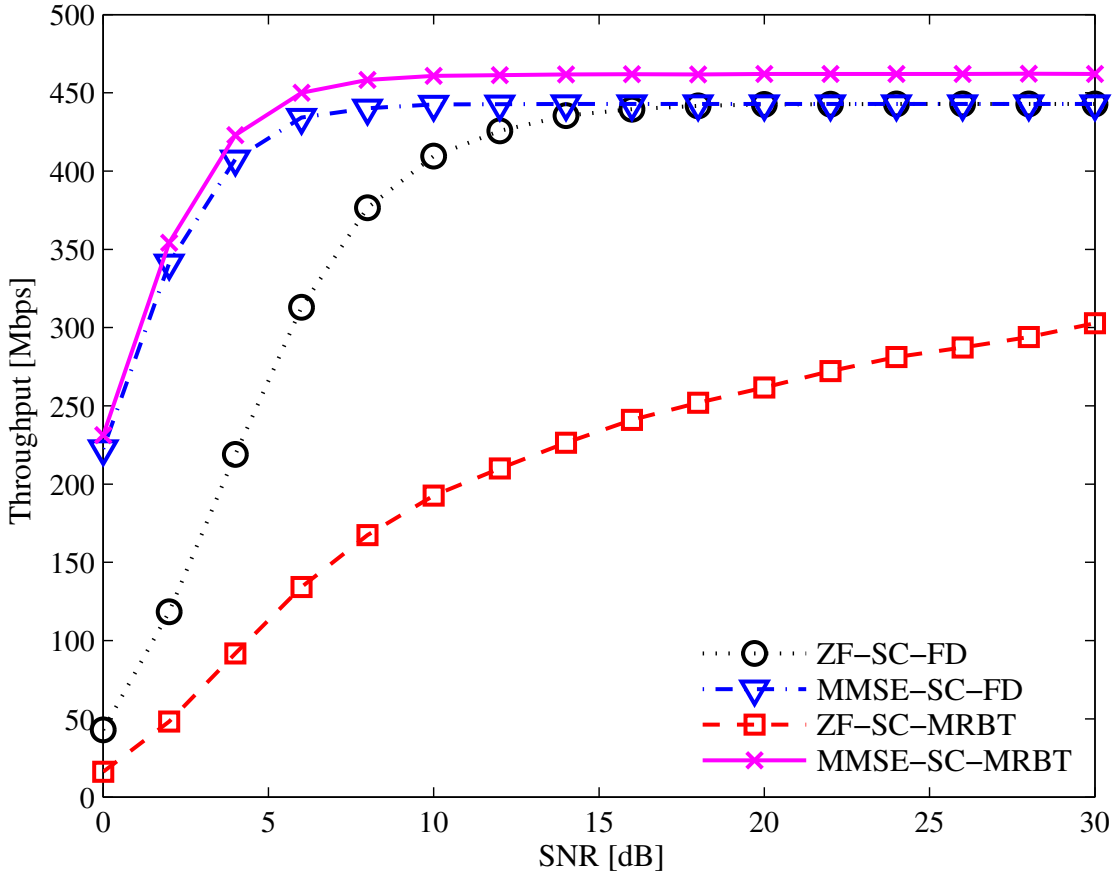

Figure D.8: Throughput [Mbps] as a function of SNR [dB] for random Rayleigh channels, considering DFT-based single-carrier transmissions ($M = 64$ and $L = 6$).

We transmitted $100,000$ blocks containing 16 data bits (8 data bits for Channel A) that generates 32 bits (16 bits for Channel A) after passing through a convolutional encoder with constraint length 7, $r_c = 1/2$, and generators $\mathbf{g_0} = [\mathbf{133}]$ (octal) and $\mathbf{g_1} = [\mathbf{165}]$ (octal) [74]. These bits are then mapped into $M = 16$ QPSK symbols using a Gray-mapping scheme (8 symbols for Channel A). After the redundancy insertion, the resulting block is transmitted through Channels A, B, C, and D, whose orders are[4] $L = 4$. At the receiver end, a data block is discarded when at least one of the original 16 bits (8 bits for Channel A) is incorrectly decoded.

Figures D.9, D.10, D.11, D.12, D.13, D.14, D.15, D.16 depict the obtained results. For each setup, we compare four transceivers: the MMSE-OFDM or MMSE-SC-FD systems, the multicarrier or single-carrier minimum redundant block transceivers (MC-MRBT or SC-MRBT) proposed in Section D.2, and the suboptimal MMSE proposals, which discard the two smallest single-values of $\mathbf{PQ}^T$, yielding a T-Bezoutian matrix.

From Figure D.9 one can observe that the suboptimal MMSE solution for this transmission is as good as the optimal one, being both of them much better than the MMSE-OFDM system. One can verify in Figure D.10 that our proposal is again very efficient with respect to the throughput, especially for large SNRs. It is possible to verify that the T-Bezoutian-ZF solution (see Eq. (D.7) and Chapter 4 in [23]) should not be used in the setup of Figure D.11, but the proposed T-Bezoutian-MMSE solution is a good choice. A similar observation applies to Figure D.12, except for the fact that none of the minimum-redundancy transceivers are better than the MMSE-SC-FD system. Figures D.13, D.14, D.15, D.16 also illustrate the fact that the proposed T-Bezoutian-MMSE solutions enhance the T-Bezoutian-ZF proposed originally in [23].

Table D.1 contains the relative importance (in percentage) of the singular-values related to the compressed form of the optimal MMSE solution $\mathbf{PQ}^T$ for Channels A, B, C, and D. The last row of each table shows how much we are discarding of the total sum of singular-values to get the suboptimal solution. Let us consider Channel A, for instance, for an SNR of 20 dB, we discard 9.1% of the total sum of the singular-values, i.e., $9.1\% \approx (\sigma_2^2 + \sigma_3^2)/(\sigma_0^2 + \sigma_1^2 + \sigma_2^2 + \sigma_3^2)$. Note that the first two singular-values are extremely important for the representation of $\mathbf{PQ}^T$ for all SNRs, confirming the fact that a T-Bezoutian is a good choice for a suboptimal MMSE solution.

[4]These setups exemplify delay constrained applications in very dispersive environments since $L = M/2$ or $L = M/4$.

Table D.1: Relative importance (percentage) of the singular-values of $\mathbf{PQ}^T$.

Channel A

SNR [dB]	0	10	20	30	40
σ_0^2	61.8	57.8	72.6	55.9	51.4
σ_1^2	34.4	35.0	18.3	44.0	48.6
σ_2^2	2.8	5.7	7.9	0.1	0.0
σ_3^2	1.0	1.5	1.2	0.0	0.0
$\sigma_2^2 + \sigma_3^2$	3.8	7.2	9.1	0.1	0.0

Channel B

SNR [dB]	0	10	20	30	40
σ_0^2	56.6	58.1	57.0	56.3	56.4
σ_1^2	38.8	32.9	34.8	36.4	36.5
σ_2^2	4.5	8.7	7.8	6.9	6.7
σ_3^2	0.1	0.3	0.4	0.4	0.4
$\sigma_2^2 + \sigma_3^2$	4.6	9.0	8.2	7.3	7.1

Channel C

SNR [dB]	0	10	20	30	40
σ_0^2	57.0	47.6	56.4	59.0	59.1
σ_1^2	28.5	24.2	34.1	40.2	40.8
σ_2^2	8.7	18.6	6.2	0.5	0.1
σ_3^2	5.8	9.6	3.3	0.3	0.0
$\sigma_2^2 + \sigma_3^2$	14.5	28.2	9.5	0.8	0.1

Channel D

SNR [dB]	0	10	20	30	40
σ_0^2	61.0	54.3	56.9	59.9	60.4
σ_1^2	24.8	20.9	31.3	38.3	39.4
σ_2^2	10.7	16.8	7.2	1.1	0.1
σ_3^2	3.5	8.0	4.6	0.8	0.1
$\sigma_2^2 + \sigma_3^2$	14.2	24.8	11.8	1.9	0.2

D.5 Concluding Remarks

In this chapter we described the basic zero-padded zero-jammed model to be used throughout this text. By using the displacement-rank concepts we were able to propose a simpler structure for the DFT-based optimal MMSE equalizer with minimum redundancy. In addition, new suboptimal MMSE equalizers requiring only half the amount of redundancy used in standard OFDM and SC-FD systems were proposed. Compared to previous proposals, the obtained multicarrier and single-carrier transceivers have the same structure of the ZF solutions with minimum redundancy, which perform around half the computations of the related optimal MMSE solutions. We presented some simulation results that confirm the throughput improvements of

the proposed solutions over the traditional OFDM and SC-FD systems for delay constrained applications in very dispersive environments. A key feature of the proposals refers to the computational complexity for the equalization, requiring $\mathcal{O}(M \log_2 M)$ operations, which is the same asymptotic complexity of OFDM and SC-FD systems.

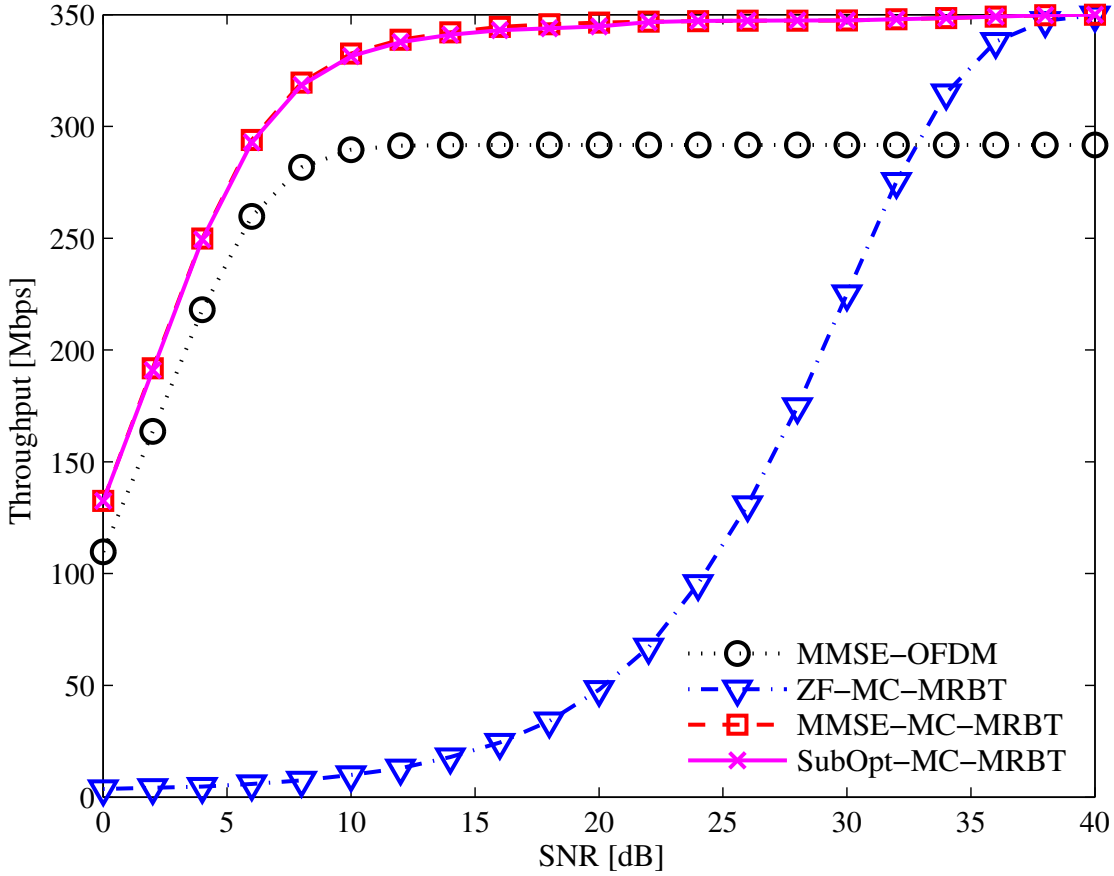

Figure D.9: Throughput [Mbps] as a function of SNR [dB] for Channel A, considering DFT-based multicarrier transmissions.

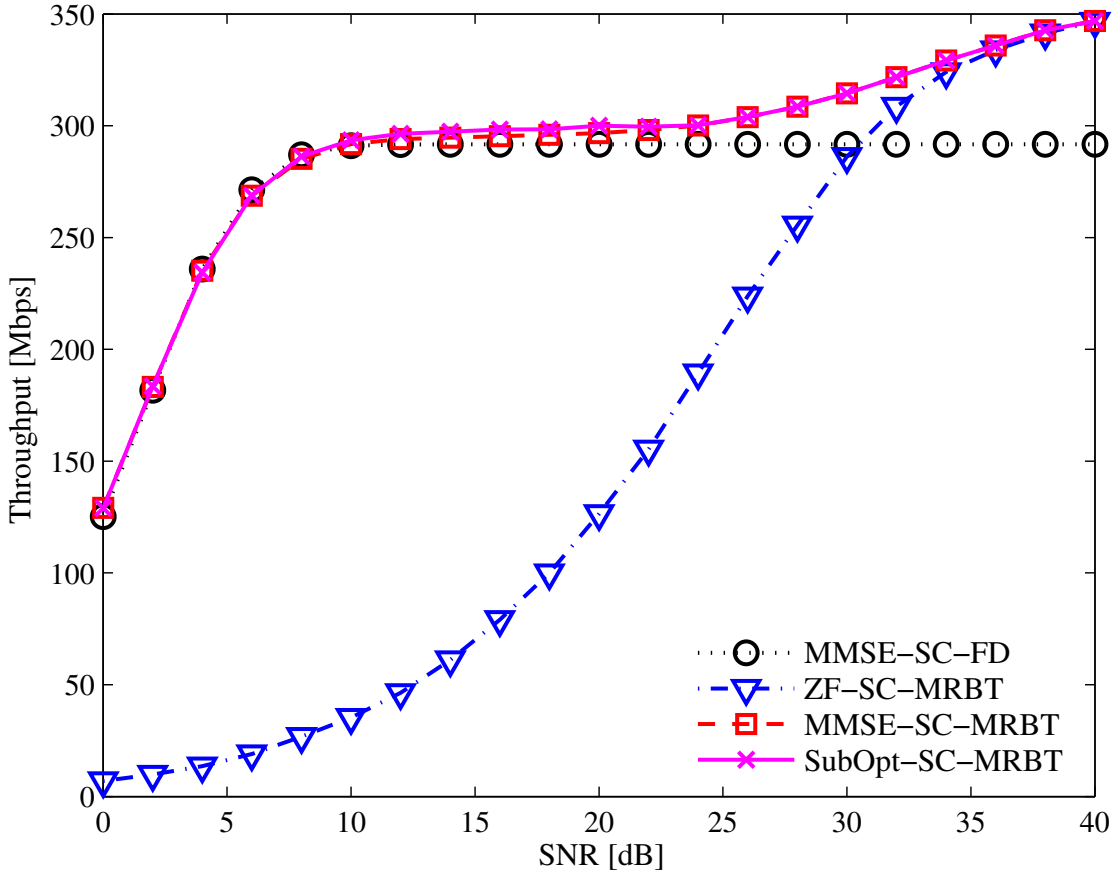

Figure D.10: Throughput [Mbps] as a function of SNR [dB] for Channel A, considering DFT-based single-carrier transmissions.

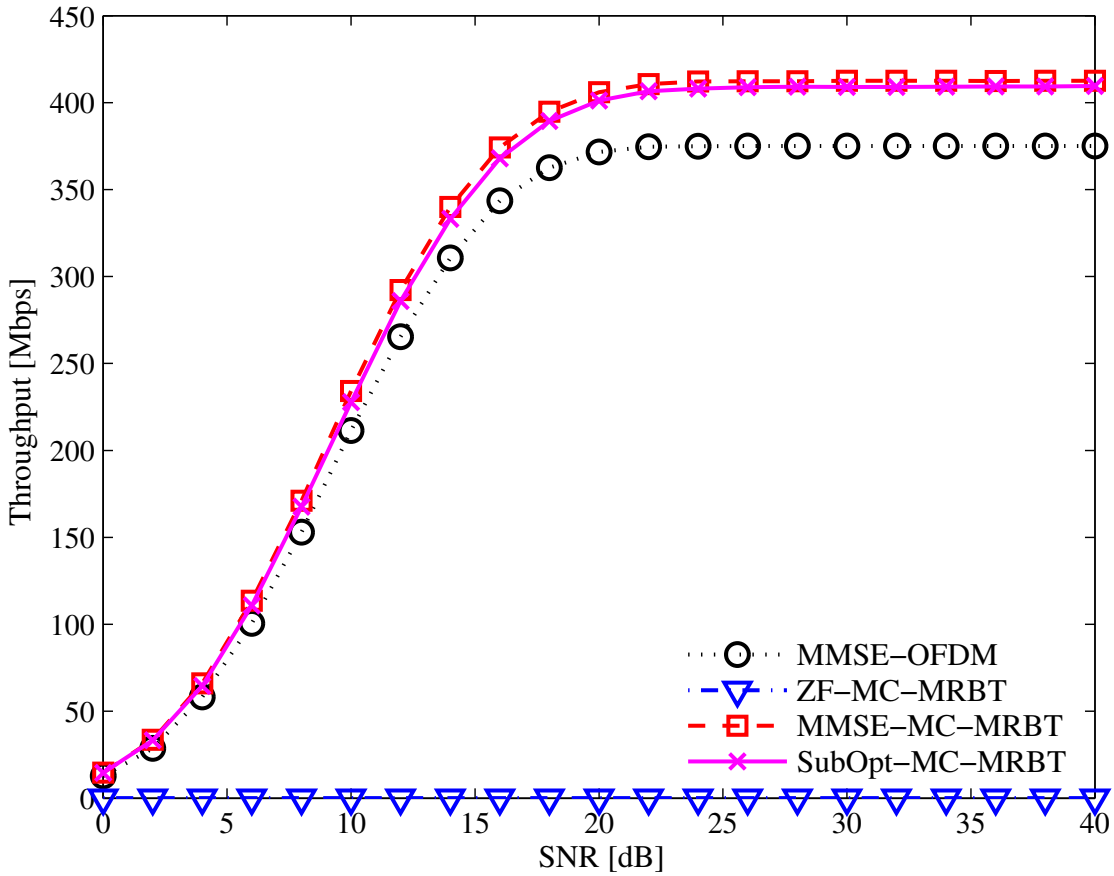

Figure D.11: Throughput [Mbps] as a function of SNR [dB] for Channel B, considering DFT-based multicarrier transmissions.

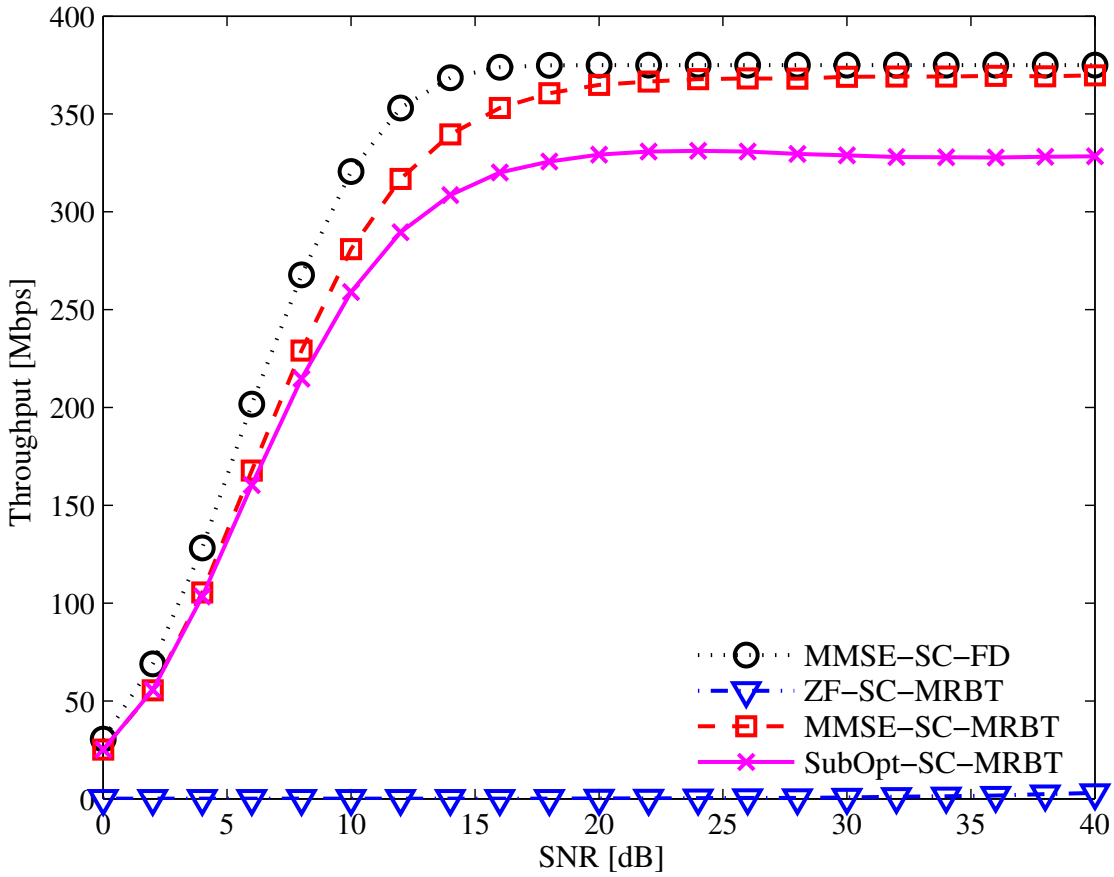

Figure D.12: Throughput [Mbps] as a function of SNR [dB] for Channel B, considering DFT-based single-carrier transmissions.

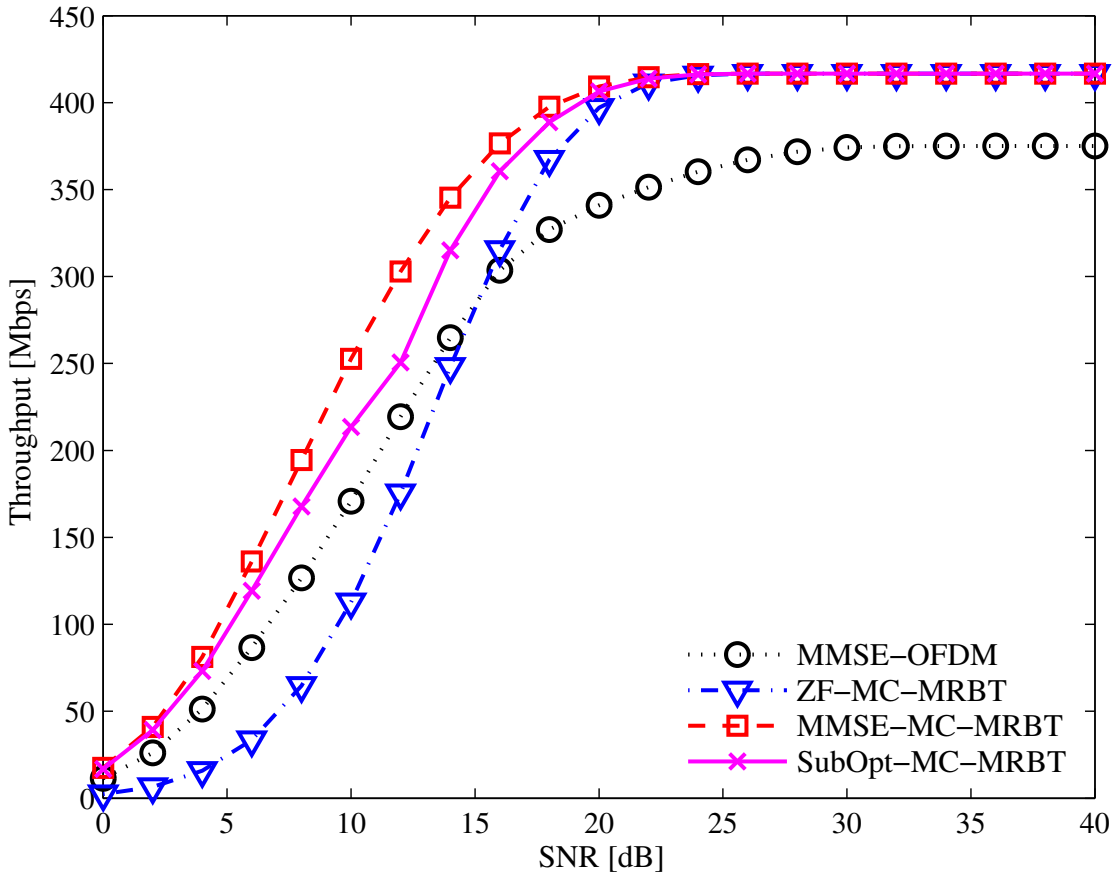

Figure D.13: Throughput [Mbps] as a function of SNR [dB] for Channel C, considering DFT-based multicarrier transmissions.

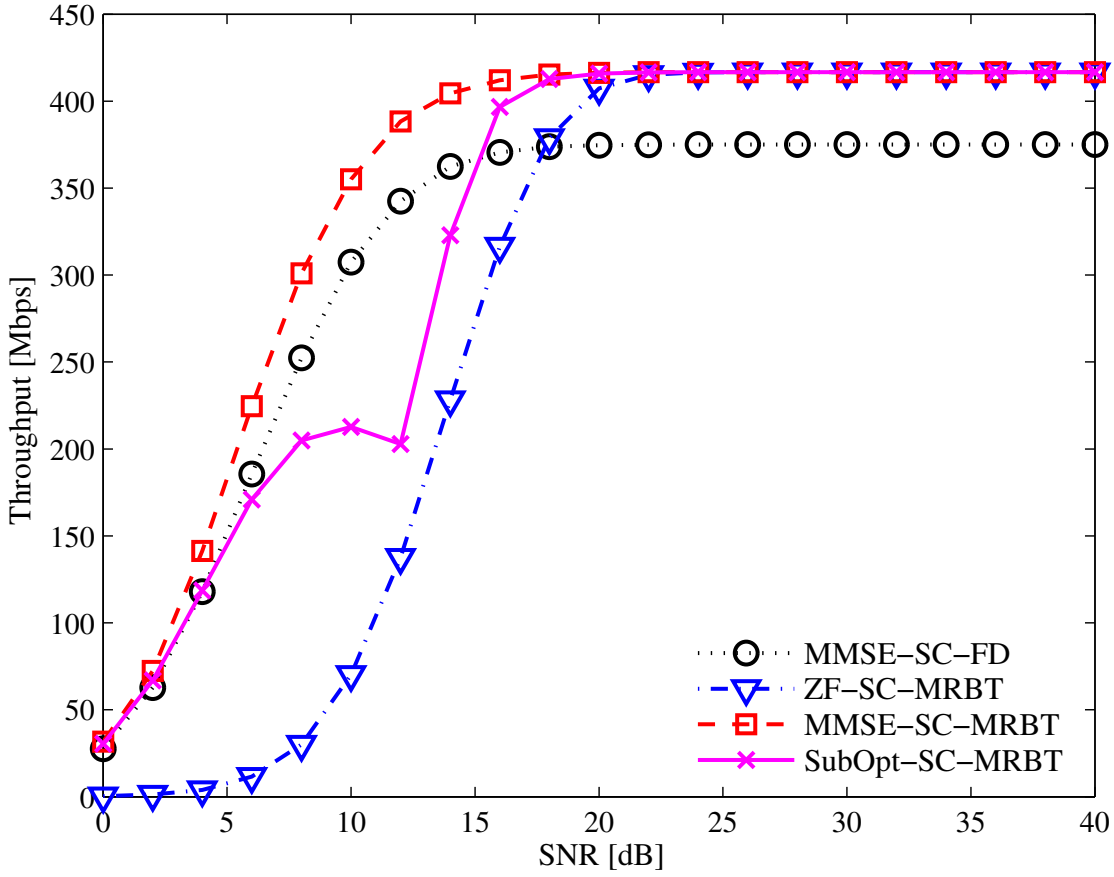

Figure D.14: Throughput [Mbps] as a function of SNR [dB] for Channel C, considering DFT-based single-carrier transmissions.

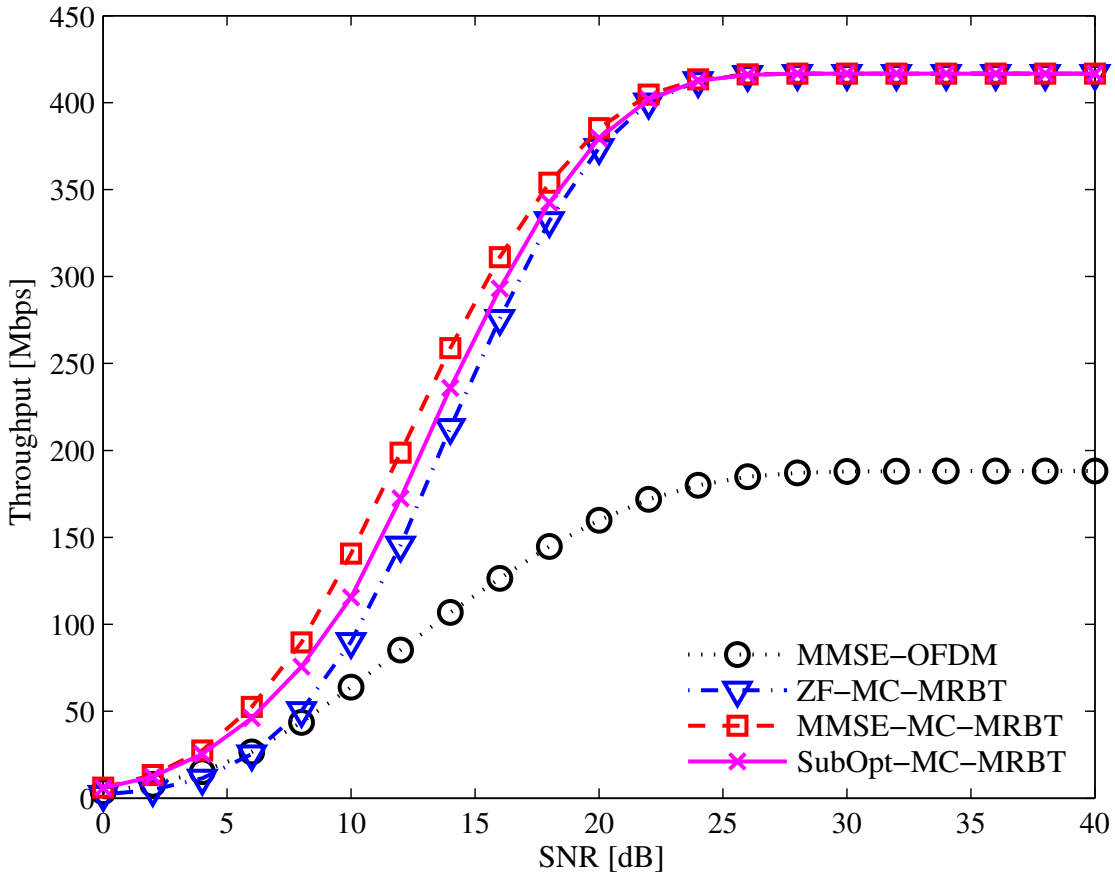

Figure D.15: Throughput [Mbps] as a function of SNR [dB] for Channel D, considering DFT-based multicarrier transmissions.

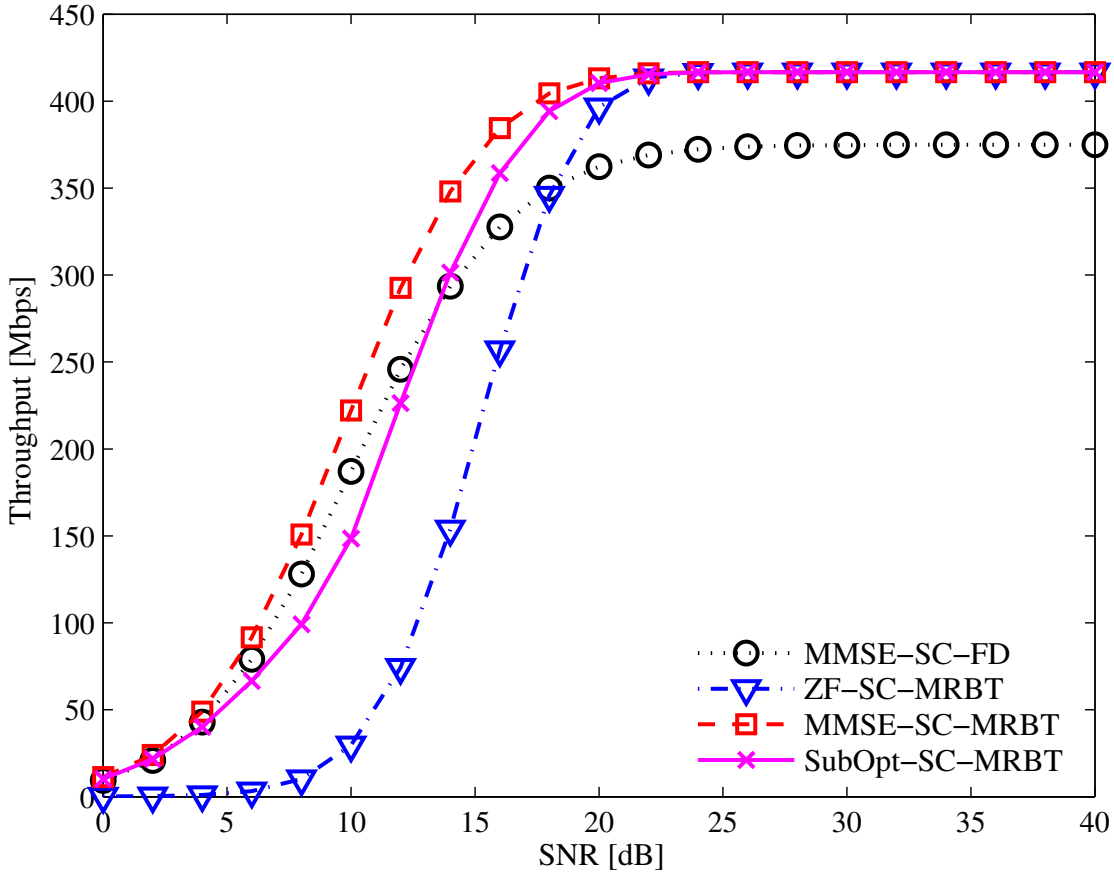

Figure D.16: Throughput [Mbps] as a function of SNR [dB] for Channel D, considering DFT-based single-carrier transmissions.

Apêndice E

DHT-Based Transceivers with Minimum Redundancy

The performance of real transform-based transceivers using L redundant elements has been studied in some works [46, 47]. Some key advantages of employing these transceivers rely on the following three facts [46, 47]: (*i*) real transforms, such as, discrete sine and discrete cosine transforms (DST and DCT, respectively) have larger sidelobe attenuation than DFT. This implies less intercarrier interference (ICI) leakage to adjacent subcarriers for MC-based transceivers; (*ii*) MC systems may benefit greatly from using real transforms along with real baseband modulations, such as PAM, since the transmission of inphase/quadrature (I/Q) data is not required, avoiding I/Q–imbalance problems; and (*iii*) DST, DCT, and DHT have superfast[1] implementations, keeping a competitive asymptotic computational complexity for the number of numerical operations, $\mathcal{O}(M \log_2 M)$, for M data symbols.

When dealing with minimum-redundancy systems, the first proposal of real transform-based transceivers in [23] has shown the possibility of implementing communications systems using only DHT and diagonal matrices. However, the proposed transceivers require a symmetric channel impulse response. This condition may be met with the introduction of a prefilter at the receiver front-end in order to turn the effective channel impulse response symmetric. This approach was also adopted in [46].

The aim of this chapter is to propose a technique that eliminates the aforementioned symmetry requirement on the FIR channel model. For this purpose, some new fixed and memoryless block-based systems are proposed. These new transceivers do not constrain the channel impulse response to have any kind of symmetry. They may be multicarrier or single-carrier, with either ZF or MMSE receivers. The transceivers only use DHT, diagonal, and antidiagonal matrices in their structures. For this rea-

[1] That is, transceivers that require $\mathcal{O}(M \log^d M)$ operations, for $d \leq 3$ [25].

son, the proposed designs are computationally as simple as OFDM and SC-FD systems, while being much more efficient with respect to the bandwidth usage.

The displacement rank theory [25] is applied in order to derive such new transceivers, using new representations of structured matrices. These new representations are heavily based on the decompositions proposed in [48]. The differences between this chapter and [48] rely on the fact that the restriction of only working with real matrices, as well as the necessity of extending the involved matrices with zeros are no longer present in this chapter. These features eventually allow us to work with channel models comprised of complex-valued taps and to design multicarrier transceivers, which are not possible by using the same formulation proposed in [48].

This chapter is organized as follows. Section E.1 contains the definitions of all types of DHTs and DFTs that will be used throughout this chapter. Section E.2 describes the two main results of this chapter related to the development of new ZF and MMSE superfast transceivers based on DHTs, diagonal, and antidiagonal matrices. Simulation results are described in Section E.3, whereas the concluding remarks of the chapter are in Section E.4.

E.1 Definitions of DHT and DFT Matrices

Before introducing the superfast transceivers based on discrete Hartley transforms, it is necessary to define other three transforms, which are slight modifications of the traditional DHT and, for this reason, are also called DHTs. These DHTs are directly associated with modifications of the traditional DFT, as follows.

Let us define the following angles

$$\theta_{\mathrm{I}}(i,j) = \frac{2ij\pi}{M} \tag{E.1}$$

$$\theta_{\mathrm{II}}(i,j) = \frac{i(2j+1)\pi}{M} \tag{E.2}$$

$$\theta_{\mathrm{III}}(i,j) = \frac{(2i+1)j\pi}{M} \tag{E.3}$$

$$\theta_{\mathrm{IV}}(i,j) = \frac{(2i+1)(2j+1)\pi}{2M} \tag{E.4}$$

for all $(i,j) \in \{\,0,1,\cdots,M-1\,\}^2$. Thus, the orthogonal DHT-X matrix is defined as [48, 49]:

$$[\boldsymbol{\mathcal{H}}_X]_{ij} = \frac{\sin[\theta_X(i,j)] + \cos[\theta_X(i,j)]}{\sqrt{M}}, \tag{E.5}$$

whereas the unitary DFT-X matrix is defined as [48, 49]:

$$[\mathbf{W}_X]_{ij} = \frac{\cos[\theta_X(i,j)] - \jmath\sin[\theta_X(i,j)]}{\sqrt{M}}, \tag{E.6}$$

with $\jmath^2 = -1$ and $X \in \{\mathrm{I}, \mathrm{II}, \mathrm{III}, \mathrm{IV}\}$.

With such definitions we can describe the proposed DHT-based systems employing minimum redundancy.

E.2 DHT-Based Superfast Transceivers with Minimum Redundancy

This section contains the main contributions of this chapter: new structures for DHT-based transceivers with minimum redundancy. Consider the MMSE receiver described by the matrix $\mathbf{G}_{0,\min}^{\mathrm{MMSE}}$ in Eq. (D.6). As pointed out before, in general the transmitter matrix $\mathbf{F}_0$ is first chosen in such a way that $\mathbf{F}_0\mathbf{F}_0^H = \mathbf{I}_M$ (unitary precoder). In this case, $\mathbf{G}_{0,\min}^{\mathrm{MMSE}} = \mathbf{F}_0^H\mathbf{K}_{\mathrm{MMSE}}$, in which

$$\mathbf{K}_{\mathrm{MMSE}} = \mathbf{H}_0^H\left(\mathbf{H}_0\mathbf{H}_0^H + \frac{\sigma_v^2}{\sigma_s^2}\mathbf{I}\right)^{-1}. \tag{E.7}$$

The matrix $\mathbf{K}_{\mathrm{MMSE}}$ can be efficiently compressed as proved in Theorem 6. Indeed, $\nabla_{\mathbf{Z}_1,\mathbf{Z}_{-1}}(\mathbf{K}_{\mathrm{MMSE}}) = \mathbf{P}\mathbf{Q}^T$, where

$$\mathbf{P} = \left[\frac{\sigma_v^2}{\sigma_s^2}\left(\mathbf{H}_0^H\mathbf{H}_0 + \frac{\sigma_v^2}{\sigma_s^2}\mathbf{I}\right)^{-1}\hat{\mathbf{P}}' \qquad -\mathbf{K}_{\mathrm{MMSE}}\hat{\mathbf{P}}\right]_{M\times 4}, \tag{E.8}$$

$$\mathbf{Q} = \left[\left(\mathbf{H}_0\mathbf{H}_0^H + \frac{\sigma_v^2}{\sigma_s^2}\mathbf{I}\right)^{-T}\hat{\mathbf{Q}}' \qquad \mathbf{K}_{\mathrm{MMSE}}^T\hat{\mathbf{Q}}\right]_{M\times 4}, \tag{E.9}$$

with $(\hat{\mathbf{P}}, \hat{\mathbf{Q}}) \in \mathbb{C}^{M\times 2} \times \mathbb{C}^{M\times 2}$ and $(\hat{\mathbf{P}}', \hat{\mathbf{Q}}') \in \mathbb{C}^{M\times 2} \times \mathbb{C}^{M\times 2}$ being the displacement generator pairs of $\nabla_{\mathbf{Z}_{-1},\mathbf{Z}_1}(\mathbf{H}_0)$ and $\nabla_{\mathbf{Z}_1,\mathbf{Z}_{-1}}(\mathbf{H}_0^H)$, respectively, i.e., $\nabla_{\mathbf{Z}_{-1},\mathbf{Z}_1}(\mathbf{H}_0) = \hat{\mathbf{P}}\hat{\mathbf{Q}}^T$ and $\nabla_{\mathbf{Z}_1,\mathbf{Z}_{-1}}(\mathbf{H}_0^H) = \hat{\mathbf{P}}'{\hat{\mathbf{Q}}'}^T$.

Now, let us define $\mathbf{J}' = [\,\mathbf{e}_1 \;\; \mathbf{e}_M \;\; \cdots \;\; \mathbf{e}_3 \;\; \mathbf{e}_2\,]$ and $\mathbf{J}'' = [\,-\mathbf{e}_1 \;\; \mathbf{e}_M \;\; \cdots \;\; \mathbf{e}_3 \;\; \mathbf{e}_2\,]$. By performing operations on the compressed representation of $\mathbf{K}_{\mathrm{MMSE}}$ it is possible to show the following result:

Theorem 7. *Given a unitary or an orthogonal transmitter matrix $\mathbf{F}_0$, the related MMSE-receiver matrix is*

$$\mathbf{G}_{0,\min}^{\mathrm{MMSE}} = \frac{M}{2}\mathbf{F}_0^H\boldsymbol{\mathcal{H}}_{\mathrm{III}}\left(\sum_{r=1}^{4}\boldsymbol{\mathcal{X}}_{\bar{\mathbf{p}}_r}\boldsymbol{\mathcal{H}}_{\mathrm{II}}\boldsymbol{\mathcal{H}}_{\mathrm{IV}}\boldsymbol{\mathcal{X}}_{\bar{\mathbf{q}}_r}\right)\boldsymbol{\mathcal{H}}_{\mathrm{IV}}, \tag{E.10}$$

where $\boldsymbol{\mathcal{X}}_{\bar{\mathbf{p}}_r} = (\alpha\mathbf{D}_{\bar{\mathbf{p}}_r} - \beta\mathbf{J}''\mathbf{D}_{\bar{\mathbf{p}}_r})$, $\boldsymbol{\mathcal{X}}_{\bar{\mathbf{q}}_r} = (\alpha\mathbf{D}_{\bar{\mathbf{q}}_r} - \beta\mathbf{D}_{\bar{\mathbf{q}}_r}\mathbf{J})$, $\alpha = (1+\jmath)/2$, $\beta = (1-\jmath)/2$, $\mathbf{D}_{\bar{\mathbf{p}}_r} = \mathrm{diag}\{\bar{\mathbf{p}}_r\}$, $\mathbf{D}_{\bar{\mathbf{q}}_r} = \mathrm{diag}\{\bar{\mathbf{q}}_r\}$, $\bar{\mathbf{P}} = [\,\bar{\mathbf{p}}_1 \;\cdots\; \bar{\mathbf{p}}_4\,] = \boldsymbol{\mathcal{H}}_{\mathrm{I}}(\jmath\mathbf{P}_+ + \mathbf{P}_-)$, *and* $\bar{\mathbf{Q}} = [\,\bar{\mathbf{q}}_1 \;\cdots\; \bar{\mathbf{q}}_4\,] = \boldsymbol{\mathcal{H}}_{\mathrm{III}}(-\jmath\mathbf{Q}_+ + \mathbf{Q}_-)$. *The matrices* $\mathbf{P}_\pm$ *and* $\mathbf{Q}_\pm$ *are defined as* $\mathbf{P}_\pm = (\mathbf{P} \pm \mathbf{J}'\mathbf{P})/2$, $\mathbf{Q}_\pm = (\mathbf{Z}_{-1}\mathbf{Q} \pm \mathbf{J}''\mathbf{Z}_{-1}\mathbf{Q})/2$, *with* $(\mathbf{P}, \mathbf{Q})$ *given as in (E.8) and (E.9).*

Proof. Before demonstrating Theorem 7, it will be helpful to state some supporting results, as follows:

Lemma 8 ([23])**.** *The four DFT matrices defined in Section E.1 obey the following identities:*

$$\mathbf{Z}_1 = \mathbf{W}_{\mathrm{I}}^H\mathbf{D}_{\mathbf{1}}\mathbf{W}_{\mathrm{I}} = \mathbf{W}_{\mathrm{II}}^H\mathbf{D}_{\mathbf{1}}\mathbf{W}_{\mathrm{II}}, \tag{E.11}$$

$$\mathbf{Z}_{-1} = \mathbf{W}_{\mathrm{III}}^H\mathbf{D}_{-\mathbf{1}}\mathbf{W}_{\mathrm{III}} = \mathbf{W}_{\mathrm{IV}}^H\mathbf{D}_{-\mathbf{1}}\mathbf{W}_{\mathrm{IV}}, \tag{E.12}$$

where $\mathbf{D}_{\mathbf{1}} = \mathrm{diag}\,\{W_M^m\}_{m=0}^{M-1}$ *contains all the* Mth *unit roots, and* $\mathbf{D}_{-\mathbf{1}} = \mathrm{diag}\left\{W_M^m \exp\left(-\jmath\frac{\pi}{M}\right)\right\}_{m=0}^{M-1}$ *contains all the* Mth *roots of* -1*, with* $W_M = \exp(-\jmath\frac{2\pi}{M})$.

Proof. First, consider that $j \in \{\,0,\,1,\,\cdots,M-2\,\}$. Thus,

$$\begin{aligned}
[\mathbf{D}_{\mathbf{1}}\mathbf{W}_{\mathrm{I}}]_{ij} &= \frac{1}{\sqrt{M}}W_M^i W_M^{ij} \\
&= \frac{1}{\sqrt{M}}W_M^{i(j+1)} \\
&= [\mathbf{W}_{\mathrm{I}}]_{i(j+1)} \\
&= [\mathbf{W}_{\mathrm{I}}\mathbf{Z}_1]_{ij}\,.
\end{aligned} \tag{E.13}$$

Second, consider that $j = M-1$. In this case, it follows that

$$\begin{aligned}
[\mathbf{D}_{\mathbf{1}}\mathbf{W}_{\mathrm{I}}]_{i(M-1)} &= \frac{1}{\sqrt{M}}W_M^i W_M^{i(M-1)} \\
&= \frac{1}{\sqrt{M}}W_M^{iM} \\
&= \frac{1}{\sqrt{M}} \\
&= [\mathbf{W}_{\mathrm{I}}]_{i0} \\
&= [\mathbf{W}_{\mathrm{I}}\mathbf{Z}_1]_{i(M-1)}\,.
\end{aligned} \tag{E.14}$$

The other three identities can be analogously proved. □

A vector $\boldsymbol{\nu} \in \mathbb{C}^{M\times 1}$ is *even* if $\mathbf{J}'\boldsymbol{\nu} = \boldsymbol{\nu}$, it is *odd* if $\mathbf{J}'\boldsymbol{\nu} = -\boldsymbol{\nu}$, it is *quasi-even* if $\mathbf{J}''\boldsymbol{\nu} = \boldsymbol{\nu}$, and it is *quasi-odd* if $\mathbf{J}''\boldsymbol{\nu} = -\boldsymbol{\nu}$. The definitions of quasi-even and quasi-odd were necessary in order to fix a related lemma stated in [49]. The authors of the referred paper did not distinguish between quasi-even/odd and even/odd vectors.

Lemma 9 ([23, 49]). *Given an even vector $\boldsymbol{\nu}_e \in \mathbb{C}^{M\times 1}$, an odd vector $\boldsymbol{\nu}_o \in \mathbb{C}^{M\times 1}$, a quasi-even vector $\boldsymbol{\nu}_{qe} \in \mathbb{C}^{M\times 1}$, and a quasi-odd vector $\boldsymbol{\nu}_{qo} \in \mathbb{C}^{M\times 1}$, it follows that:*

$$\mathbf{W}_{\mathrm{I}}\boldsymbol{\nu}_e = \boldsymbol{\mathcal{H}}_{\mathrm{I}}\boldsymbol{\nu}_e \tag{E.15}$$

$$\mathbf{W}_{\mathrm{I}}\boldsymbol{\nu}_o = -\jmath\boldsymbol{\mathcal{H}}_{\mathrm{I}}\boldsymbol{\nu}_o \tag{E.16}$$

$$\mathbf{W}_{\mathrm{III}}\boldsymbol{\nu}_{qe} = -\jmath\boldsymbol{\mathcal{H}}_{\mathrm{III}}\boldsymbol{\nu}_{qe} \tag{E.17}$$

$$\mathbf{W}_{\mathrm{III}}\boldsymbol{\nu}_{qo} = \boldsymbol{\mathcal{H}}_{\mathrm{III}}\boldsymbol{\nu}_{qo}. \tag{E.18}$$

Proof. See [49]. □

Lemma 10 ([23]). *Given $(\mathbf{P}, \mathbf{Q}) \in \mathbb{C}^{M\times R} \times \mathbb{C}^{M\times R}$, with $R \in \mathbb{N}$, then*

$$\jmath\mathbf{W}_{\mathrm{I}}\mathbf{P} = \boldsymbol{\mathcal{H}}_{\mathrm{I}}(\jmath\mathbf{P}_+ + \mathbf{P}_-) = \bar{\mathbf{P}} \tag{E.19}$$

$$\mathbf{W}_{\mathrm{III}}\mathbf{Z}_{-1}\mathbf{Q} = \boldsymbol{\mathcal{H}}_{\mathrm{III}}(-\jmath\mathbf{Q}_+ + \mathbf{Q}_-) = \bar{\mathbf{Q}}, \tag{E.20}$$

where $\mathbf{P}_\pm = (\mathbf{P} \pm \mathbf{J}'\mathbf{P})/2$ and $\mathbf{Q}_\pm = (\mathbf{Z}_{-1}\mathbf{Q} \pm \mathbf{J}''\mathbf{Z}_{-1}\mathbf{Q})/2$.

Proof. Since $\mathbf{P}_\pm = (\mathbf{P} \pm \mathbf{J}'\mathbf{P})/2$ and $\mathbf{Q}_\pm = (\mathbf{Z}_{-1}\mathbf{Q} \pm \mathbf{J}''\mathbf{Z}_{-1}\mathbf{Q})/2$, then each column vector of $\mathbf{P}_+$ is an even vector, whereas each column vector of $\mathbf{Q}_+$ is a quasi-even vector. In addition, the columns of $\mathbf{P}_-$ and $\mathbf{Q}_-$ are odd and quasi-odd vectors, respectively. By applying Lemma 9, one has

$$\begin{aligned}\jmath\mathbf{W}_{\mathrm{I}}\mathbf{P} &= \jmath\boldsymbol{\mathcal{H}}_{\mathrm{I}}\mathbf{P}_+ + \boldsymbol{\mathcal{H}}_{\mathrm{I}}\mathbf{P}_- \\ &= \boldsymbol{\mathcal{H}}_{\mathrm{I}}(\jmath\mathbf{P}_+ + \mathbf{P}_-) \\ &= \bar{\mathbf{P}}\end{aligned} \tag{E.21}$$

and

$$\begin{aligned}\mathbf{W}_{\mathrm{III}}\mathbf{Z}_{-1}\mathbf{Q} &= -\jmath\boldsymbol{\mathcal{H}}_{\mathrm{III}}\mathbf{Q}_+ + \boldsymbol{\mathcal{H}}_{\mathrm{III}}\mathbf{Q}_- \\ &= \boldsymbol{\mathcal{H}}_{\mathrm{III}}(-\jmath\mathbf{Q}_+ + \mathbf{Q}_-) \\ &= \bar{\mathbf{Q}}.\end{aligned} \tag{E.22}$$

□

Lemma 11 ([48, 49]). *The Hartley transforms $\boldsymbol{\mathcal{H}}_{\mathrm{II}}$ and $\boldsymbol{\mathcal{H}}_{\mathrm{IV}}$ obey the following relationship:*

$$[\boldsymbol{\mathcal{H}}_{\mathrm{II}}\boldsymbol{\mathcal{H}}_{\mathrm{IV}}]_{ij} = \frac{1}{M}\frac{1}{\sin\left(\frac{(2i+2j+1)\pi}{2M}\right)}. \tag{E.23}$$

Proof. See [48, 49]. □

In addition to these results, one can use Eq. (E.6) in order to verify that [48, 49]:

$$\mathbf{W}_{\text{II}} = \text{diag}\left\{\exp\left(-\jmath\frac{\pi}{M}m\right)\right\}_{m=0}^{M-1}\mathbf{W}_{\text{I}}, \tag{E.24}$$

$$\mathbf{W}_{\text{IV}} = \text{diag}\left\{\exp\left(-\jmath\frac{\pi}{2M}(2m+1)\right)\right\}_{m=0}^{M-1}\mathbf{W}_{\text{III}}. \tag{E.25}$$

It is now possible to prove Theorem 7. As shown in Lemma 8, $\mathbf{Z}_1 = \mathbf{W}_{\text{II}}^H\mathbf{D_1}\mathbf{W}_{\text{II}}$ and $\mathbf{Z}_{-1} = \mathbf{W}_{\text{IV}}^H\mathbf{D_{-1}}\mathbf{W}_{\text{IV}}$. By using these facts while applying the Stein displacement $\Delta_{\mathbf{D_1},\mathbf{D_{-1}}}$ to the matrix $\tilde{\mathbf{K}} = \mathbf{W}_{\text{II}}\mathbf{K}_{\text{MMSE}}\mathbf{W}_{\text{IV}}$, it follows that:

$$\begin{aligned}\Delta_{\mathbf{D_1},\mathbf{D_{-1}}}(\tilde{\mathbf{K}}) &= \tilde{\mathbf{K}} - \mathbf{D_1}\tilde{\mathbf{K}}\mathbf{D_{-1}} \\ &= \tilde{\mathbf{K}} - (\mathbf{W}_{\text{II}}\mathbf{Z}_1\mathbf{W}_{\text{II}}^H)\tilde{\mathbf{K}}(\mathbf{W}_{\text{IV}}^*\mathbf{Z}_{-1}^T\mathbf{W}_{\text{IV}}) \\ &= \mathbf{W}_{\text{II}}(\mathbf{K}_{\text{MMSE}} - \mathbf{Z}_1\mathbf{K}_{\text{MMSE}}\mathbf{Z}_{-1}^T)\mathbf{W}_{\text{IV}}.\end{aligned} \tag{E.26}$$

But, we know that

$$\mathbf{K}_{\text{MMSE}} - \mathbf{Z}_1\mathbf{K}_{\text{MMSE}}\mathbf{Z}_{-1}^T = \Delta_{\mathbf{Z}_1,\mathbf{Z}_{-1}^T}(\mathbf{K}_{\text{MMSE}}). \tag{E.27}$$

Thus, by using the result $\Delta_{\mathbf{X},\mathbf{Y}^{-1}}(\mathbf{U}) = -\nabla_{\mathbf{X},\mathbf{Y}}(\mathbf{U})\mathbf{Y}^{-1}$ (see Eq. (D.13)) and the fact that $\mathbf{Z}_{-1}^T = \mathbf{Z}_{-1}^{-1}$, one gets

$$\Delta_{\mathbf{D_1},\mathbf{D_{-1}}}(\tilde{\mathbf{K}}) = -\mathbf{W}_{\text{II}}\nabla_{\mathbf{Z}_1,\mathbf{Z}_{-1}}(\mathbf{K}_{\text{MMSE}})\,\mathbf{Z}_{-1}^T\mathbf{W}_{\text{IV}}. \tag{E.28}$$

As $\nabla_{\mathbf{Z}_1,\mathbf{Z}_{-1}}(\mathbf{K}_{\text{MMSE}}) = \mathbf{P}\mathbf{Q}^T$, one has

$$\Delta_{\mathbf{D_1},\mathbf{D_{-1}}}(\tilde{\mathbf{K}}) = (-\mathbf{W}_{\text{II}}\mathbf{P})(\mathbf{W}_{\text{IV}}\mathbf{Z}_{-1}\mathbf{Q})^T. \tag{E.29}$$

Similarly as done in [23], it is straightforward to verify that:

$$\begin{aligned}[\tilde{\mathbf{K}}]_{ij} &= \frac{[(-\mathbf{W}_{\text{II}}\mathbf{P})(\mathbf{W}_{\text{IV}}\mathbf{Z}_{-1}\mathbf{Q})^T]_{ij}}{\left(1 - e^{-\jmath\frac{(2i+2j+1)\pi}{M}}\right)} \\ &= \frac{e^{\jmath\frac{i\pi}{M}}[(-\mathbf{W}_{\text{II}}\mathbf{P})(\mathbf{W}_{\text{IV}}\mathbf{Z}_{-1}\mathbf{Q})^T]_{ij}e^{\jmath\frac{(2j+1)\pi}{2M}}}{e^{\jmath\frac{(2i+2j+1)\pi}{2M}} - e^{-\jmath\frac{(2i+2j+1)\pi}{2M}}} \\ &= \frac{[(\jmath\mathbf{W}_{\text{I}}\mathbf{P})(\mathbf{W}_{\text{III}}\mathbf{Z}_{-1}\mathbf{Q})^T]_{ij}}{2\text{sin}\left(\frac{(2i+2j+1)\pi}{2M}\right)},\end{aligned} \tag{E.30}$$

where we employed the identities in Eq. (E.24) and in Eq. (E.25).

As shown in Lemma 10, $\jmath\mathbf{W}_{\text{I}}\mathbf{P} = \boldsymbol{\mathcal{H}}_{\text{I}}(\jmath\mathbf{P}_+ + \mathbf{P}_-) = \bar{\mathbf{P}}$ and $\mathbf{W}_{\text{III}}\mathbf{Z}_{-1}\mathbf{Q} = \boldsymbol{\mathcal{H}}_{\text{III}}(-\jmath\mathbf{Q}_+ + \mathbf{Q}_-) = \bar{\mathbf{Q}}$, where $\mathbf{P}_\pm = (\mathbf{P} \pm \mathbf{J}'\mathbf{P})/2$ and $\mathbf{Q}_\pm = (\mathbf{Z}_{-1}\mathbf{Q} \pm \mathbf{J}''\mathbf{Z}_{-1}\mathbf{Q})/2$.

Then, it follows that:

$$[\tilde{\mathbf{K}}]_{ij} = \frac{[\bar{\mathbf{P}}\bar{\mathbf{Q}}^T]_{ij}}{2\sin\left(\frac{(2i+2j+1)\pi}{2M}\right)}. \tag{E.31}$$

This equation along with Lemma 11 yield:

$$\mathbf{W}_{\text{II}}\mathbf{K}_{\text{MMSE}}\mathbf{W}_{\text{IV}} = \frac{M}{2}\left(\sum_{r=1}^{4}\mathbf{D}_{\bar{\mathbf{p}}_r}\boldsymbol{\mathcal{H}}_{\text{II}}\boldsymbol{\mathcal{H}}_{\text{IV}}\mathbf{D}_{\bar{\mathbf{q}}_r}\right), \tag{E.32}$$

where $\bar{\mathbf{P}} = [\,\bar{\mathbf{p}}_1 \;\cdots\; \bar{\mathbf{p}}_4\,]$, $\bar{\mathbf{Q}} = [\,\bar{\mathbf{q}}_1 \;\cdots\; \bar{\mathbf{q}}_4\,]$, $\mathbf{D}_{\bar{\mathbf{p}}_r} = \text{diag}\{\bar{\mathbf{p}}_r\}$, and $\mathbf{D}_{\bar{\mathbf{q}}_r} = \text{diag}\{\bar{\mathbf{q}}_r\}$.

Since it is easy to verify that:[2]

$$\boldsymbol{\mathcal{H}}_{\text{III}}\mathbf{W}_{\text{II}} = \frac{(1-\jmath)\mathbf{I}+(1+\jmath)\mathbf{J}}{2} = \left[\frac{(1+\jmath)\mathbf{I}+(1-\jmath)\mathbf{J}}{2}\right]^{-1}, \tag{E.33}$$

$$\mathbf{W}_{\text{IV}}\boldsymbol{\mathcal{H}}_{\text{IV}} = \frac{(1-\jmath)\mathbf{I}-(1+\jmath)\mathbf{J}}{2} = \left[\frac{(1+\jmath)\mathbf{I}-(1-\jmath)\mathbf{J}}{2}\right]^{-1}, \tag{E.34}$$

and by taking into account the fact that $\mathbf{J}\boldsymbol{\mathcal{H}}_{\text{III}} = -\boldsymbol{\mathcal{H}}_{\text{III}}\mathbf{J}''$ and that $\boldsymbol{\mathcal{H}}_{\text{IV}}\mathbf{J} = \mathbf{J}\boldsymbol{\mathcal{H}}_{\text{IV}}$ [48, 49], then

$$\mathbf{K}_{\text{MMSE}} = \frac{M}{2}\boldsymbol{\mathcal{H}}_{\text{III}}\left(\sum_{r=1}^{4}\boldsymbol{\mathcal{X}}_{\bar{\mathbf{p}}_r}\boldsymbol{\mathcal{H}}_{\text{II}}\boldsymbol{\mathcal{H}}_{\text{IV}}\boldsymbol{\mathcal{X}}_{\bar{\mathbf{q}}_r}\right)\boldsymbol{\mathcal{H}}_{\text{IV}}, \tag{E.35}$$

where $\boldsymbol{\mathcal{X}}_{\bar{\mathbf{p}}_r} = (\alpha\mathbf{D}_{\bar{\mathbf{p}}_r} - \beta\mathbf{J}''\mathbf{D}_{\bar{\mathbf{p}}_r})$, $\boldsymbol{\mathcal{X}}_{\bar{\mathbf{q}}_r} = (\alpha\mathbf{D}_{\bar{\mathbf{q}}_r} - \beta\mathbf{D}_{\bar{\mathbf{q}}_r}\mathbf{J})$, $\alpha = (1+\jmath)/2$, and $\beta = (1-\jmath)/2$. Hence, the result of Theorem 7 follows. □

Theorem 7 is the first contribution of this chapter related to the design of practical block-based transceivers with minimum redundancy using DHTs. It is based on a similar mathematical result of [48]. Unlike the polynomial approach adopted in [48], a matrix approach was used based on the Sylvester and Stein displacement operators. This approach allowed us to derive transformations without requiring extension with zeros of the involved matrices as in [48], leading to efficient designs of multicarrier transceivers, which is not possible by using the same formulation presented in [48]. Another key feature that distinguishes Theorem 7 from the results in [48] is that the adopted approach allows us to work with complex-valued matrices. This is important for baseband channel models that have complex-valued taps. Moreover, Theorem 7 does not assume a centro-symmetry structure of the involved matrix as in [23].

Note that, when $\sigma_v^2/\sigma_s^2 \to 0$ and $\mathbf{H}_0\mathbf{F}_0$ is invertible, then $\mathbf{G}_{0,\min}^{\text{MMSE}} \to \mathbf{G}_{0,\min}^{\text{ZF}}$ (see Eq. (D.5) and Eq. (D.6)). Thus, $\nabla_{\mathbf{z}_1,\mathbf{z}_{-1}}(\mathbf{K}_{\text{MMSE}}) = \mathbf{P}\mathbf{Q}^T \to (-\mathbf{H}_0^{-1}\hat{\mathbf{P}})(\mathbf{H}_0^{-T}\hat{\mathbf{Q}})^T$

[2] A similar relationship between the standard DHT and DFT matrices was verified in [47].

(see Eq. (E.8) and Eq. (E.9)). These facts, along with Theorem 7, justify the following new contribution:

Theorem 8. *Given a unitary or an orthogonal transmitter matrix* $\mathbf{F}_0$*, the related ZF-receiver matrix is*

$$\mathbf{G}_{0,\min}^{\mathrm{ZF}} = \frac{M}{2}\mathbf{F}_0^H \boldsymbol{\mathcal{H}}_{\mathrm{III}} \left(\sum_{r=1}^{2} \boldsymbol{\mathcal{X}}_{\bar{\mathbf{p}}_r} \boldsymbol{\mathcal{H}}_{\mathrm{II}} \boldsymbol{\mathcal{H}}_{\mathrm{IV}} \boldsymbol{\mathcal{X}}_{\bar{\mathbf{q}}_r} \right) \boldsymbol{\mathcal{H}}_{\mathrm{IV}}, \tag{E.36}$$

where all matrices are analogously defined as in Theorem 7, except for the generator pair $(\mathbf{P}, \mathbf{Q}) = (-\mathbf{H}_0^{-1}\hat{\mathbf{P}},\ \mathbf{H}_0^{-T}\hat{\mathbf{Q}})$*, with* $\nabla_{\mathbf{Z}_{-1},\mathbf{Z}_1}(\mathbf{H}_0) = \hat{\mathbf{P}}\hat{\mathbf{Q}}^T$*.*

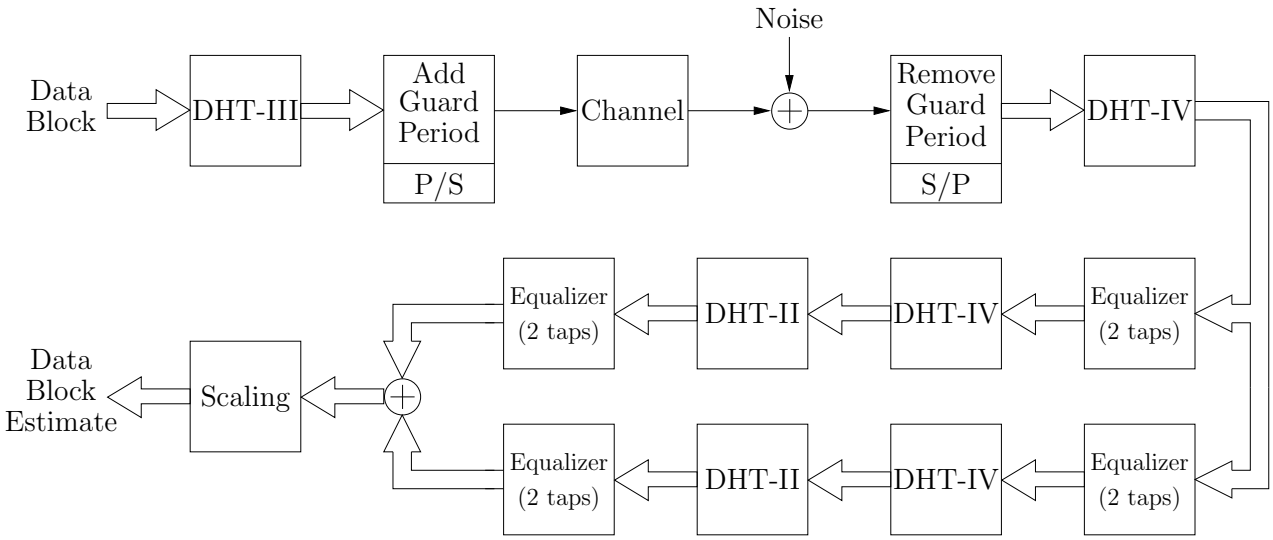

Figure E.1: DHT-based zero-forcing multicarrier minimum-redundancy block transceiver: ZF-MC-MRBT.

Based on Theorems 7 and 8, the single-carrier solution can be designed by setting $\mathbf{F}_0 = \mathbf{I}$, whereas the multicarrier solution can be designed by setting $\mathbf{F}_0 = \boldsymbol{\mathcal{H}}_{\mathrm{III}}$ for both MMSE and ZF designs.

Figure E.1 depicts the resulting multicarrier transceiver structure for the zero-forcing receiver. In this transceiver, the guard period consists of $L/2$ zeros. After removing the guard period, the DHT-IV is applied to the received vector. The first equalization step is performed on the data vector, that is, the resulting data vector is simultaneously processed by two different branches of the transceiver. The equalizers at this stage are the matrices $\boldsymbol{\mathcal{X}}_{\bar{\mathbf{q}}_1}$ and $\boldsymbol{\mathcal{X}}_{\bar{\mathbf{q}}_2}$. These matrices contain at most two nonzero elements in each row (2-tap equalizers). Figure E.2 depicts the structure of these equalizer matrices, where all matrix entries are zero, except the ones placed at the gray entries. A final equalization step is performed in each branch, after the application of the DHT-IV and DHT-II. Once again, the equalizers at this stage ($\boldsymbol{\mathcal{X}}_{\bar{\mathbf{p}}_1}$ and $\boldsymbol{\mathcal{X}}_{\bar{\mathbf{p}}_2}$) have a special structure depicted in Figure E.2.

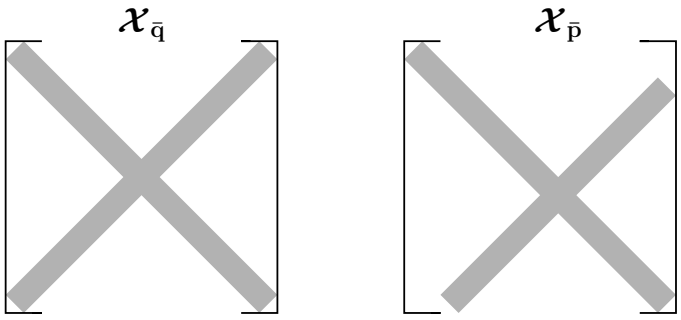

Figure E.2: Equalizer-matrix structures.

Note that the overall equalization process has an asymptotic complexity of $\mathcal{O}(M \log_2 M)$, as the standard OFDM transceiver. Obviously, the proposals require more numerical operations than OFDM transceivers in the practical non-asymptotic case. In fact, both the proposed solution and OFDM entail numerical complexities in the order of $M \log_2 M$, however, the former requires about 3 times the amount of computation of OFDM. Nevertheless, as illustrated in Figure E.1, it is possible to take advantage of the inherent parallel structure in order to reduce the processing time.

E.3 Simulation Results

The aim of this section is to compare the throughput performance of the proposed DHT-based transceivers against the traditional OFDM and SC-FD systems through simulations. In order to do so, we transmit 500 blocks with $M = 32$ QPSK data symbols, without taking into account the redundant zeros required. The transmitting process is repeated 10,000 times and a new channel is generated for each transmission. All channels have order $L = 20$, representing delay constrained applications in very dispersive environments. The real and imaginary parts of the channel coefficients are independently drawn from a white and Gaussian stochastic process, resulting in a Rayleigh channel with constant-power profile [16]. The sampling frequency is $f_s = 500$ MHz. Moreover, the adopted figure of merit is the throughput achieved by each technique, whose definition was given in Section D.4.

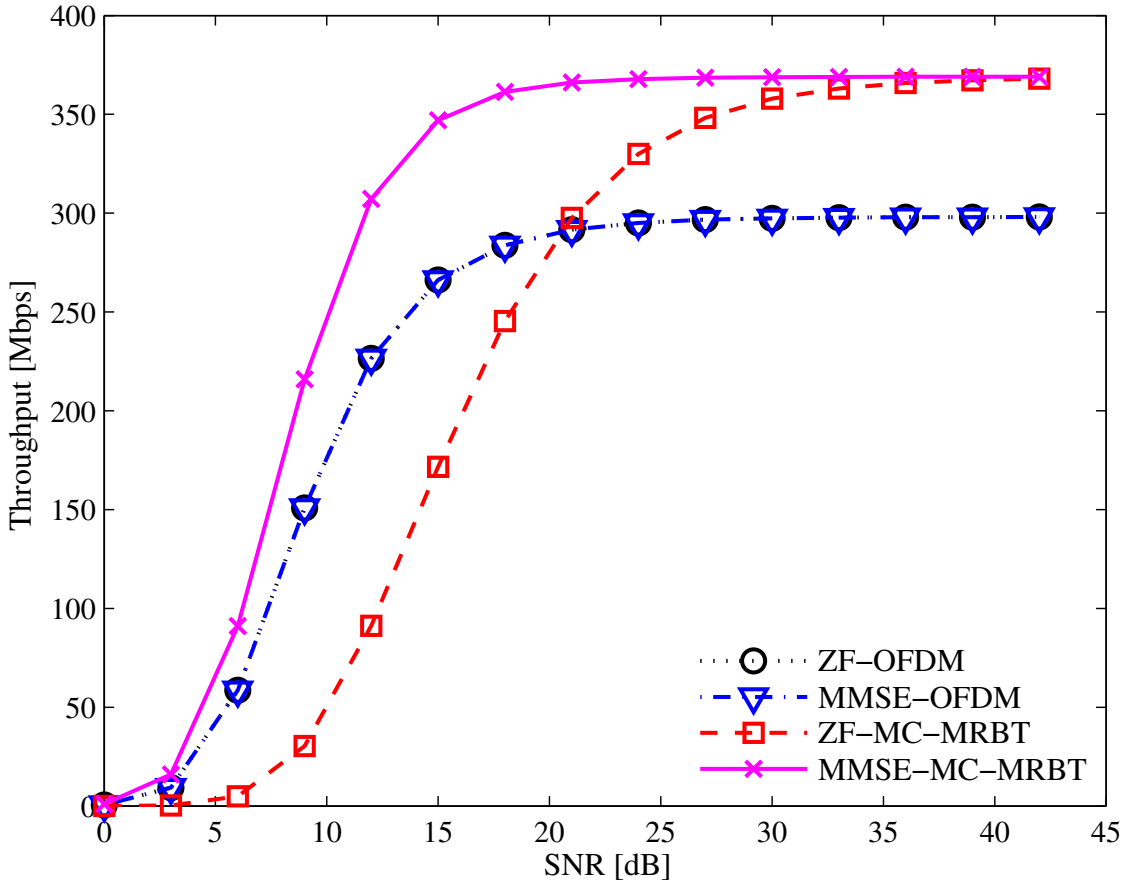

Figure E.3: Throughput [Mbps] as a function of SNR [dB] for random Rayleigh channels, considering DHT-based multicarrier transmissions ($M = 32$ and $L = 20$).

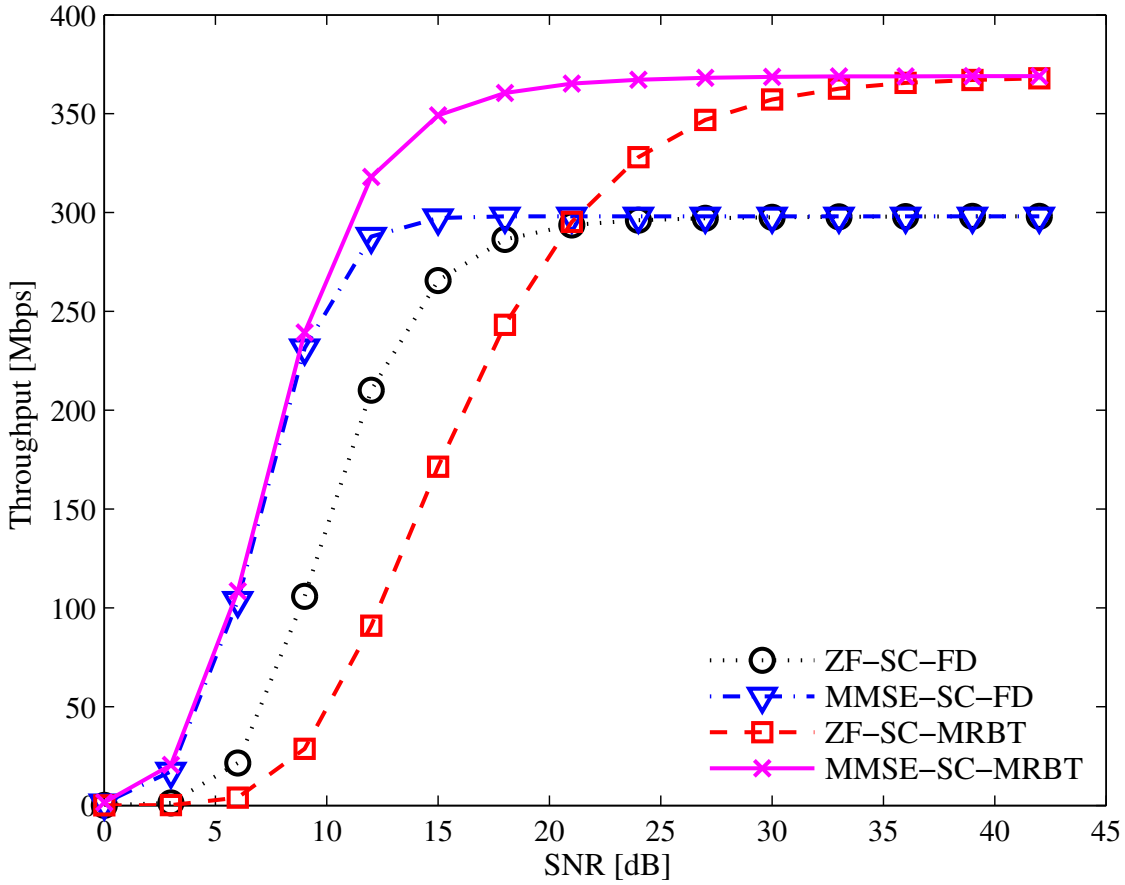

Figure E.4: Throughput [Mbps] as a function of SNR [dB] for random Rayleigh channels, considering DHT-based single-carrier transmissions ($M = 32$ and $L = 20$).

As observed in Figures E.3 and E.4, the throughput performances of the proposed multicarrier and single-carrier minimum-redundancy block transceivers (MC-MRBT and SC-MRBT, respectively) are better than the traditional systems, except for SNRs lower than 21 dB in the ZF solutions. The proposed ZF solutions are effective only for high SNRs, since most of the Toeplitz matrices, such as $\mathbf{H}_0$, induce larger noise enhancements than circulant matrices, for the same channel model.[3] This implies that, even though the proposed ZF solutions use only half the amount of redundancy of standard ZF-OFDM and ZF-SC-FD systems, more data blocks are discarded due to bit errors after channel decoding. Nonetheless, the advantages of using the proposed MMSE transceivers is remarkable in both multicarrier and single-carrier transmissions.

The proposals presented in this chapter are suitable for delay constrained transmissions in very dispersive environments, i.e., setups where the assumption $L \ll M$ is not reasonable. The above example can be cast as delay constrained application in dispersive environment, since $L \approx 0.6M$. For those transmissions where $L \ll M$, one may prefer to use the traditional OFDM or SC-FD systems for two main reasons: (i) it may not be worth increasing the non-asymptotic computational complexity of the transceiver in order to decrease the redundancy that is already small; and (ii) the noise enhancement associated with the proposed transceivers is larger when $L \ll M$. In order to give an example, consider a transmission with all parameter values equal to the previous example, except for the fact that now $M = 32$ and $L = 6$.

Figures E.5 and E.6 depict the results for both multicarrier and single-carrier transmissions, respectively. Once again, the proposed MMSE transceivers are more efficient than the standard MMSE systems. However, it is clearer now that the proposed ZF solutions is more sensitive to the presence of noise than the standard ZF-OFDM and ZF-SC-FD systems, whenever $L \ll M$.

As a final example, we transmit 100,000 data blocks, each one of them with $M = 16$ QPSK symbols, through a channel whose transfer function is [75]:

$$H(z) = 1 + 0.5z^{-1} - 0.7z^{-2} + 0.9z^{-3} + z^{-4}. \tag{E.37}$$

In this case, $L = 4$ and all the other parameter values are the same as in the previous examples.[4]

[3] We have observed this fact empirically.

[4] We do not consider random channels here since they are considered in the previous examples. In this case, our aim is to verify the performance in a slow-variant channel (modeled as a fixed channel), a typical setup of practical wireline applications.

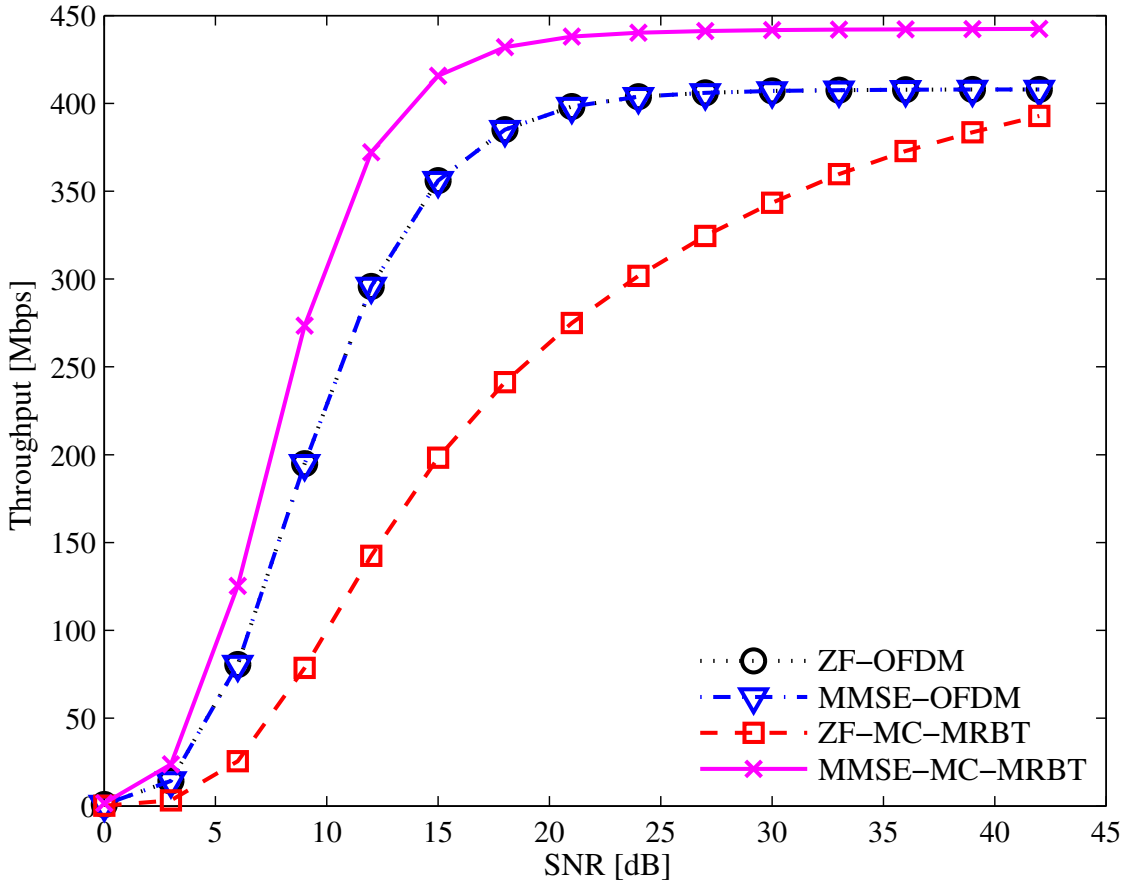

Figure E.5: Throughput [Mbps] as a function of SNR [dB] for random Rayleigh channels, considering DHT-based multicarrier transmissions ($M = 32$ and $L = 6$).

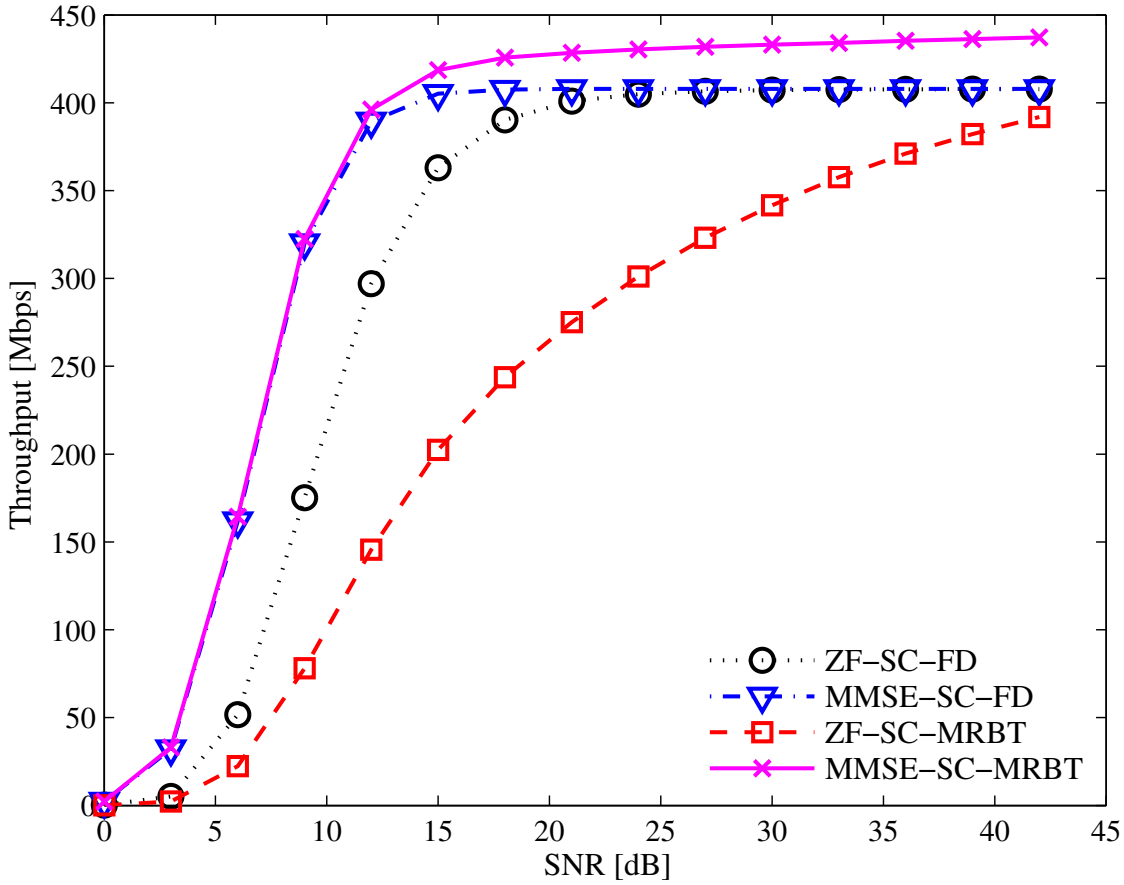

Figure E.6: Throughput [Mbps] as a function of SNR [dB] for random Rayleigh channels, considering DHT-based single-carrier transmissions ($M = 32$ and $L = 6$).

Figures E.7 and E.8 contain the obtained results. One may observe a similar behavior of the proposed transceivers for this particular channel. The proposed MMSE solutions with minimum redundancy are always better than their traditional counterparts, whereas the proposed ZF-MC-MRBT transceiver achieves higher throughputs than the traditional ZF-OFDM system for SNRs greater than 15 dB (see Figure E.7). On the other hand, the proposed ZF-SC-MRBT transceiver always outperforms the ZF-SC-FD system in this example, as depicted in Figure E.8. In order to illustrate the BER performance of the proposed transceivers, we also include here Figures E.9 and E.10.

E.4 Concluding Remarks

In this chapter we proposed transceivers using real discrete Hartley transforms with minimum redundancy for block data transmission. The ZF and MMSE solutions employ only DHT, diagonal, and antidiagonal matrices, making the new transceivers computationally efficient. Our approach relied on the properties of structured matrices using the concepts of Sylvester and Stein displacements. These concepts aimed at exploiting the structural properties of typical channel matrix representations. New DHT-based representations of Toeplitz inverses and pseudo-inverses were derived. Such new representations were the key tools to reach the proposed solutions for the multicarrier and single-carrier systems. A key feature of the proposed schemes is that no constraint is imposed on the channel model. Simulation results demonstrate that the solutions allow higher throughput in a number of situations, revealing the potential usefulness of the DHT-based transceivers.

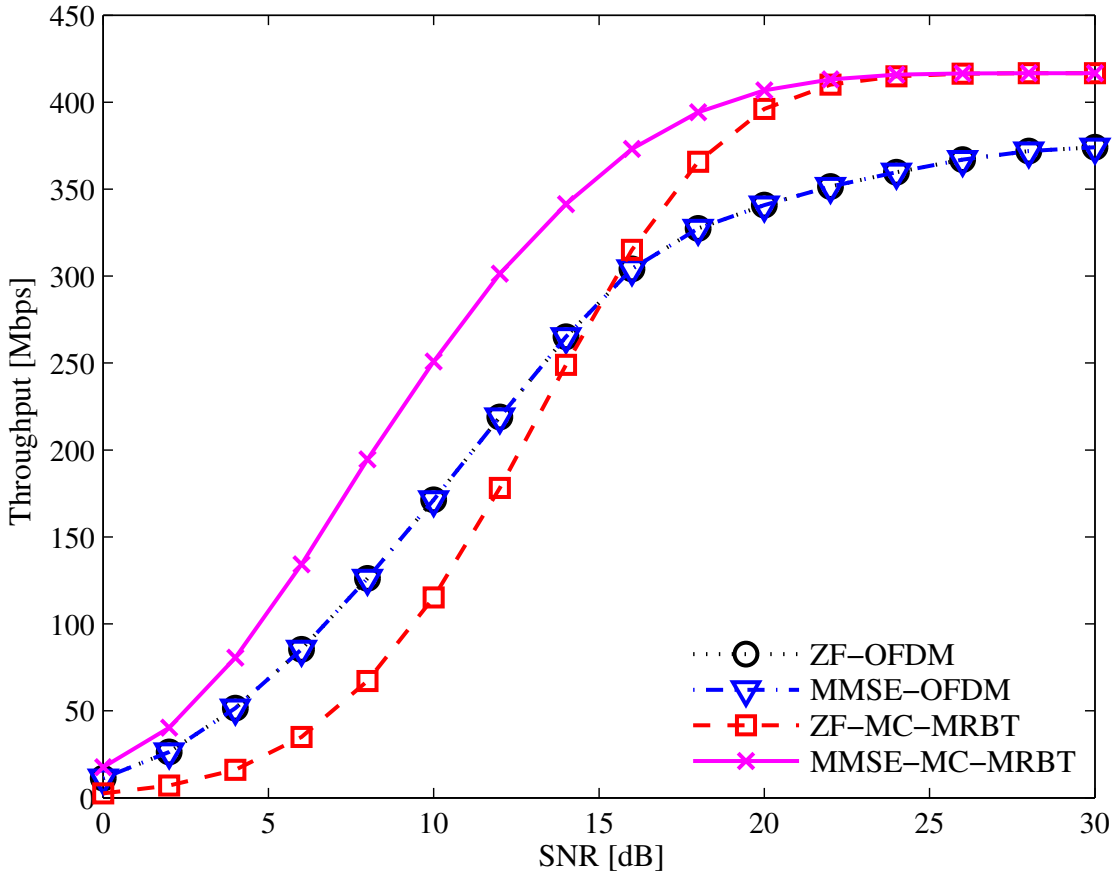

Figure E.7: Throughput [Mbps] as a function of SNR [dB] for the channel in Eq. (E.37), considering DHT-based multicarrier transmissions ($M = 16$ and $L = 4$).

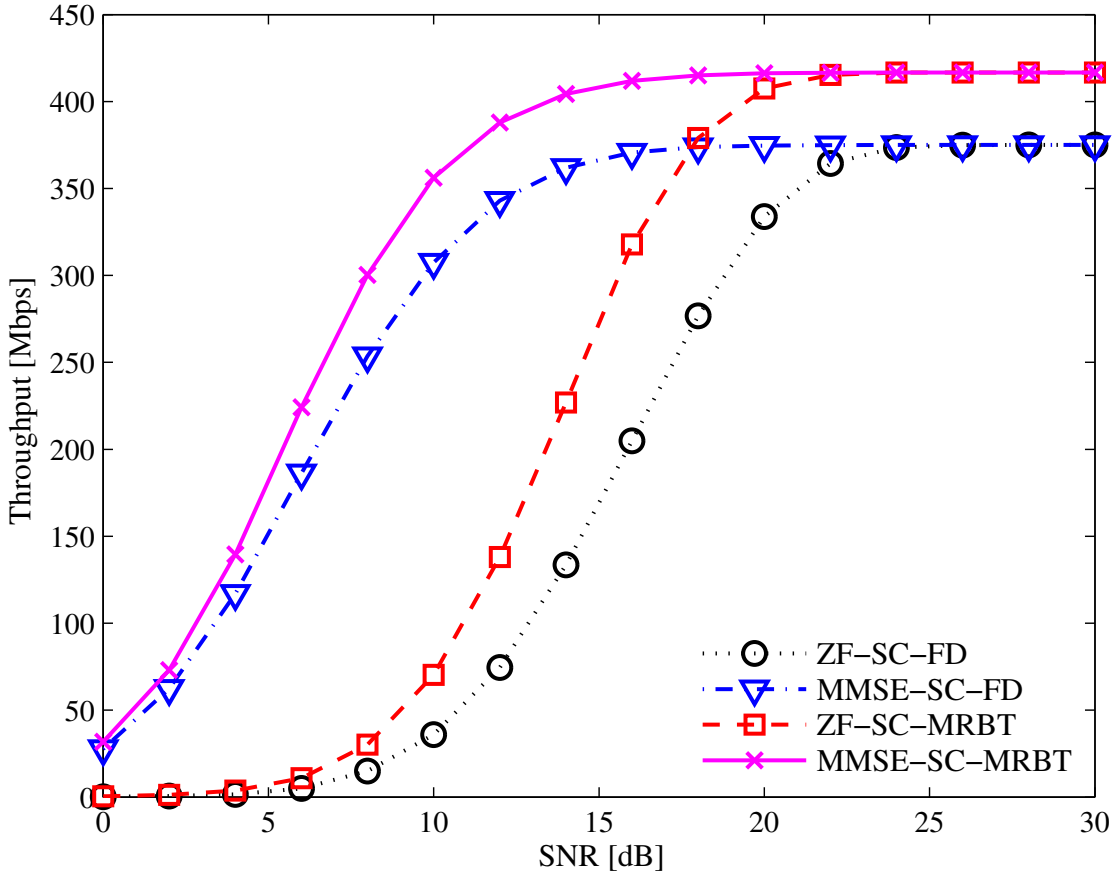

Figure E.8: Throughput [Mbps] as a function of SNR [dB] for the channel in Eq. (E.37), considering DHT-based single-carrier transmissions ($M = 16$ and $L = 4$).

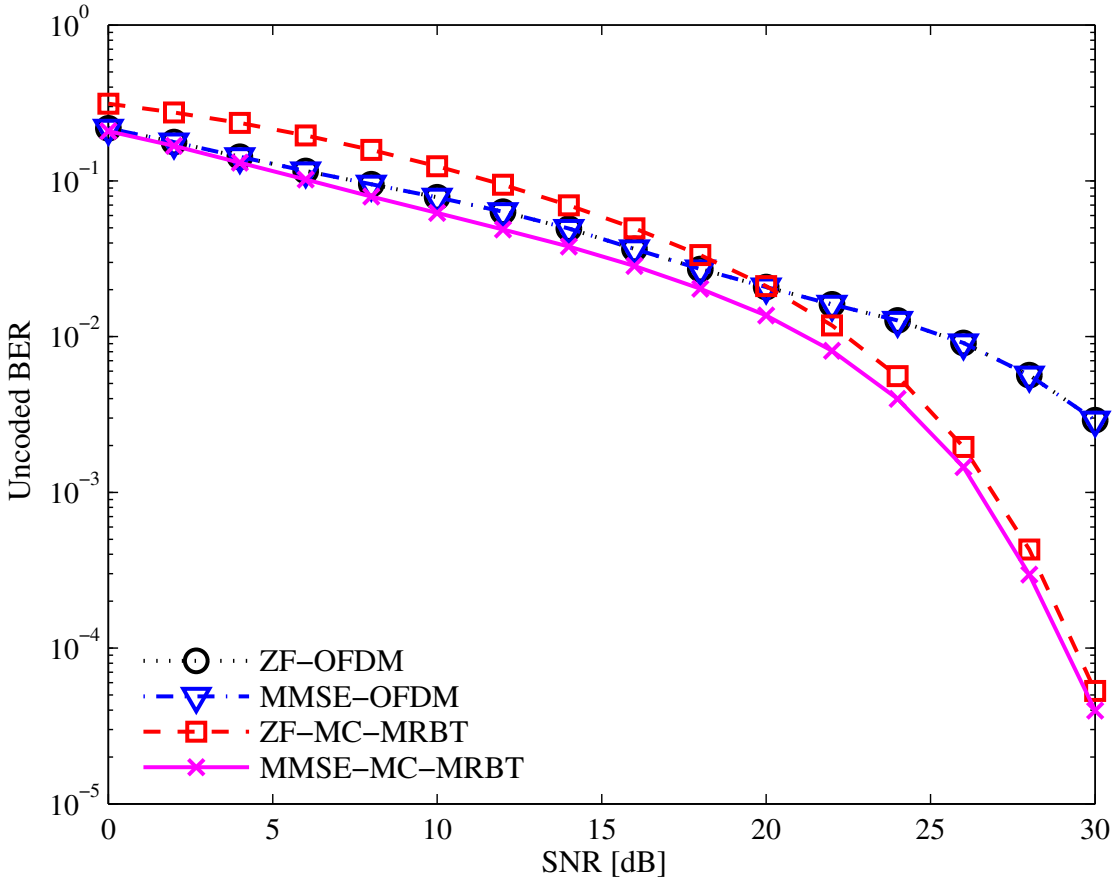

Figure E.9: Uncoded BER as a function of SNR [dB] for the channel in Eq. (E.37), considering DHT-based multicarrier transmissions ($M = 16$ and $L = 4$).

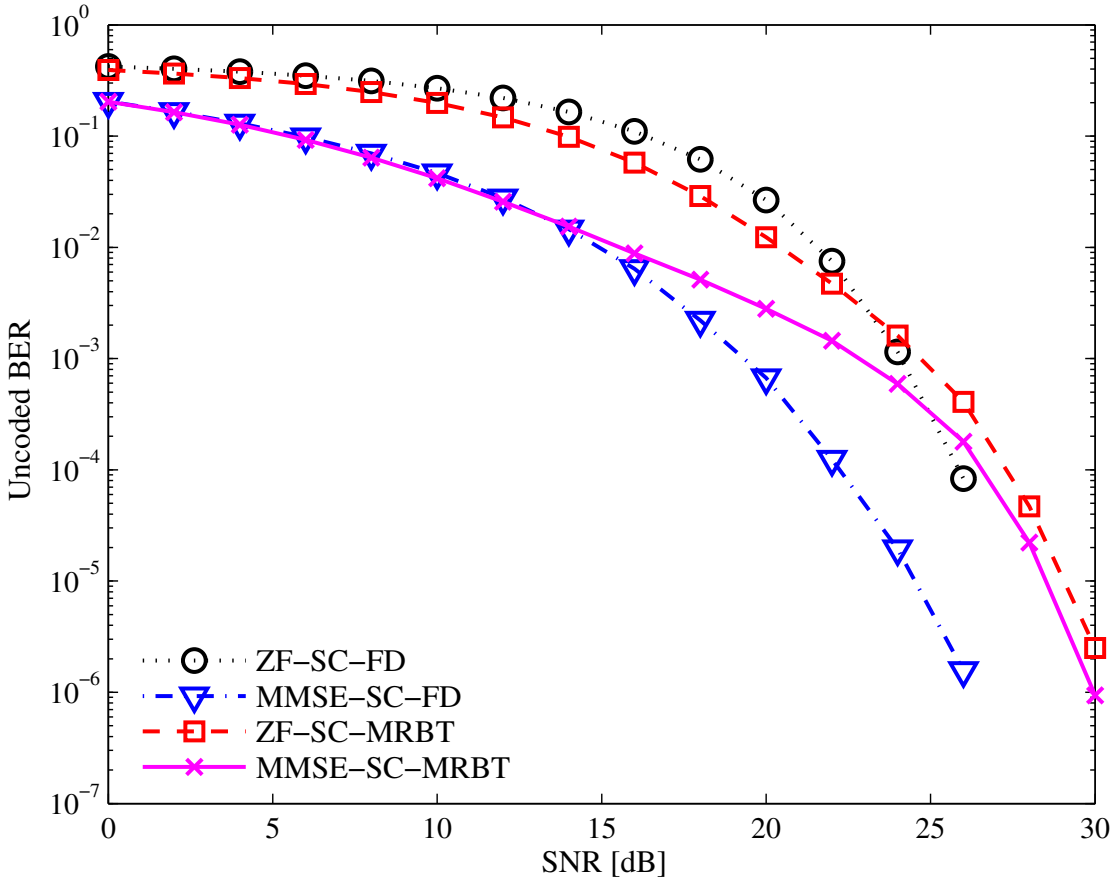

Figure E.10: Uncoded BER as a function of SNR [dB] for the channel in Eq. (E.37), considering DHT-based single-carrier transmissions ($M = 16$ and $L = 4$).

Part II

Reduced-Redundancy Systems

Apêndice F

DFT-Based Transceivers with Reduced Redundancy

This chapter presents new linear time-invariant (LTI) block-based transceivers which employ a reduced amount of redundancy to eliminate the interblock interference. The proposals encompass both multicarrier and single-carrier systems with either zero-forcing or minimum mean-square error (MSE) equalizers. The amount of redundancy ranges from the minimum, $\lceil L/2 \rceil$, to the most commonly used value, L, assuming a channel-impulse response of order L. The resulting transceivers allow for superfast equalization of the received data blocks, since they only use fast Fourier transforms and single-tap equalizers in their structures. The chapter also includes an MSE analysis of the proposed transceivers with respect to the amount of redundancy. Indeed, we demonstrate that larger amounts of transmitted redundant elements lead to lower MSE of symbols at the receiver end. Several computer simulations indicate that, by choosing an appropriate amount of redundancy, our proposals can achieve higher throughputs than the standard superfast multicarrier and single-carrier systems, while keeping the same asymptotic computational complexity for the equalization process.

In this chapter, we shall consider the zero-padding zero-jamming (ZP-ZJ) model [16, 41] that allows one to transmit with smaller amount of redundancy, while avoiding IBI. In fact, the minimum-redundancy ZP-ZJ transceivers proposed in [23] may be regarded as the state of the art in this particular topic, which naturally lead us to the question: why investigating reduced-redundancy transceivers when minimum-redundancy transceivers are already available? The answer to this question and the strategy to devise such new superfast transceivers will be key contributions of this chapter.

This chapter is organized as follows. Section F.1 discusses why reduced redundancy may be better than minimum redundancy. In order to introduce the new decompositions of rectangular structured matrices, Section F.2 briefly presents the

main ideas of the displacement theory applied to rectangular matrices. By applying the displacement-rank theory, we describe the two main results of this chapter related to the development of new ZF and MMSE superfast transceivers in Section F.3. The simulation results are described in Section F.4, whereas the concluding remarks of the chapter are in Section F.5.

F.1 Is Reduced Redundancy Better than Minimum Redundancy?

The performance of reduced-redundancy transceivers has been assessed by simulations in some works [16, 57]. By comparing the BER among systems with different amounts of redundancy, the authors in [16, 57] verify that transmitting using larger amounts of redundancy leads to lower the BER of such systems. In addition, the author in [43] also shows that, even when one transmits in a single-carrier system with full-redundancy ($K = L$), if not all the redundant elements are used at the receiver end during the equalization process, then the mean-square error of the symbols is also a monotone decreasing function of the number of redundant symbols used for the equalization. In fact, such behavior is present in a broader class of ZP optimal transceivers, as proved in Chapter C.

If on one hand we want to reduce the transmitted redundancy in order to save bandwidth, on the other hand we need to use as much redundancy as possible in order to have a good BER or MSE performance. The throughput is a good figure of merit to study the tradeoff between bandwidth usage and error performance. In general, however, throughput is also a function of the bit-error protection that is implemented at higher layers of a given communication protocol, entailing a sort of cross-layer design. The focus of our work is on the physical-layer design, rather than on the cross-layer design. Consequently, we shall analytically evaluate the performance of the ZP-ZJ systems based on the MSE of symbols only, since this figure of merit does not depend upon neither the particular constellation used (as in the BER case), nor the channel-coding scheme used (as in the throughput case).

With this in mind, consider a ZP-ZJ system that employs $K \in \mathcal{K}_L \triangleq \{\lceil L/2 \rceil, \lceil L/2 \rceil + 1, \cdots, L\}$ redundant symbols in order to transmit M data symbols through an Lth-order FIR channel. Given the received vector after the jamming processing

$$\mathbf{y}(K, M) \triangleq \mathbf{H}_0(K, M)\mathbf{F}_0(M)\mathbf{s}(M) + \mathbf{v}_0(K, M) \in \mathbb{C}^{(M+2K-L)\times 1}, \tag{F.1}$$

we define the error vector $\mathbf{e}(K,M)$ after the receiver processing as

$$\begin{aligned}\mathbf{e}(K,M) &\triangleq \hat{\mathbf{s}}(M)-\mathbf{s}(M)\\ &\triangleq \mathbf{G}_0(K,M)\mathbf{y}(K,M)-\mathbf{s}(M)\\ &= [\mathbf{G}_0(K,M)\mathbf{H}_0(K,M)\mathbf{F}_0(M)-\mathbf{I}_M]\mathbf{s}(M)+\mathbf{G}_0(K,M)\mathbf{v}_0(K,M),\end{aligned} \quad \text{(F.2)}$$

where in all variables the dependency on L is omitted, since the channel order will remain constant throughout this chapter. In addition, the average MSE (AMSE) of symbols is defined as

$$\begin{aligned}\mathrm{AMSE}(K,M) &\triangleq \frac{1}{M}\mathsf{E}\{\mathbf{e}^H(K,M)\mathbf{e}(K,M)\}\\ &= \frac{1}{M}\mathrm{tr}\{\mathsf{E}[\mathbf{e}(K,M)\mathbf{e}^H(K,M)]\}\\ &= \frac{1}{M}\sigma_s^2\mathrm{tr}\left\{[\mathbf{G}_0(K,M)\mathbf{H}_0(K,M)\mathbf{F}_0(M)-\mathbf{I}_M]\right.\\ &\times \left.[\mathbf{G}_0(K,M)\mathbf{H}_0(K,M)\mathbf{F}_0(M)-\mathbf{I}_M]^H\right\}\\ &+ \frac{1}{M}\sigma_v^2\mathrm{tr}\left\{\mathbf{G}_0(K,M)\mathbf{G}_0^H(K,M)\right\}\\ &= \frac{\sigma_s^2\|\mathbf{G}_0(K,M)\mathbf{H}_0(K,M)\mathbf{F}_0(M)-\mathbf{I}_M\|_{\mathrm{F}}^2}{M}+\frac{\sigma_v^2\|\mathbf{G}_0(K,M)\|_{\mathrm{F}}^2}{M}\\ &= \frac{\sigma_s^2}{M}\left(\|\mathbf{G}_0(K,M)\mathbf{H}_0(K,M)\mathbf{F}_0(M)-\mathbf{I}_M\|_{\mathrm{F}}^2+\rho\|\mathbf{G}_0(K,M)\|_{\mathrm{F}}^2\right),\end{aligned} \quad \text{(F.3)}$$

where $\rho \triangleq \sigma_v^2/\sigma_s^2 > 0$ is the reciprocal of the SNR and $\|\cdot\|_{\mathrm{F}}$ is the Frobenius norm. Considering such definitions, we are now able to state the first contribution of this chapter in Theorem 9.

Theorem 9. *The MMSE receiver defined in Eq. (D.4) yields the following average MSE of symbols:*

$$\begin{aligned}\mathrm{AMSE}^{\mathrm{MMSE}}(K,M) &= \frac{\sigma_v^2}{M}\mathrm{tr}\left\{\left[\mathbf{H}_0^H(K,M)\mathbf{H}_0(K,M)+\rho\mathbf{I}_M\right]^{-1}\right\}\\ &= \frac{\sigma_v^2}{M}\sum_{m\in\mathcal{M}}\frac{1}{\sigma_m^2(K,M)+\rho},\end{aligned} \quad \text{(F.4)}$$

where $\mathcal{M} \triangleq \{0,1,\cdots,M-1\}$ *and each* $\sigma_m^2(K,M) \in \mathbb{R}_+$ *is an eigenvalue of* $\mathbf{H}_0^H(K,M)\mathbf{H}_0(K,M)$.

Proof. For the sake of simplicity, we shall omit from all variables the dependency on K and M. Assume that the singular-value decomposition of the effective channel matrix is $\mathbf{H}_0 = \mathbf{U}\boldsymbol{\Sigma}\mathbf{V}^H$, where both the $(M+2K-L)\times(M+2K-L)$ matrix $\mathbf{U}$ and the $M\times M$ matrix $\mathbf{V}$ are unitary. In addition, the $(M+2K-L)\times M$

matrix $\mathbf{\Sigma}$ has zero entries except for the main-diagonal entries $[\mathbf{\Sigma}]_{m,m} = \sigma_m > 0$, with $m \in \mathcal{M}$. From Eq. (D.4) one has

$$\mathbf{G}_0 = \mathbf{F}_0^H \mathbf{V} \left(\mathbf{\Sigma}^T \mathbf{\Sigma} + \rho \mathbf{I}_M \right)^{-1} \mathbf{\Sigma}^T \mathbf{U}^H, \tag{F.5}$$

which implies that

$$\mathbf{G}_0 \mathbf{H}_0 \mathbf{F}_0 = \mathbf{F}_0^H \mathbf{V} \left(\mathbf{\Sigma}^T \mathbf{\Sigma} + \rho \mathbf{I}_M \right)^{-1} \mathbf{\Sigma}^T \mathbf{\Sigma} \mathbf{V}^H \mathbf{F}_0, \tag{F.6}$$

yielding

$$\begin{aligned} \mathbf{G}_0 \mathbf{H}_0 \mathbf{F}_0 - \mathbf{I}_M &= \mathbf{F}_0^H \mathbf{V} \left[\left(\mathbf{\Sigma}^T \mathbf{\Sigma} + \rho \mathbf{I}_M \right)^{-1} \mathbf{\Sigma}^T \mathbf{\Sigma} - \mathbf{I}_M \right] \mathbf{V}^H \mathbf{F}_0 \\ &= \mathbf{F}_0^H \mathbf{V} \left[-\rho \left(\mathbf{\Sigma}^T \mathbf{\Sigma} + \rho \mathbf{I}_M \right)^{-1} \right] \mathbf{V}^H \mathbf{F}_0, \end{aligned} \tag{F.7}$$

Hence, by substituting both Eqs. (F.5) and (F.7) into Eq. (F.3), and by taking into account that the Frobenius norm of a given matrix is the sum of its square singular values, we have

$$\begin{aligned} \mathrm{AMSE}^{\mathrm{MMSE}} &= \frac{\sigma_s^2}{M} \left[\sum_{m \in \mathcal{M}} \frac{\rho^2}{(\sigma_m^2 + \rho)^2} + \rho \sum_{m \in \mathcal{M}} \frac{\sigma_m^2}{(\sigma_m^2 + \rho)^2} \right] \\ &= \frac{\rho \sigma_s^2}{M} \sum_{m \in \mathcal{M}} \frac{\sigma_m^2 + \rho}{(\sigma_m^2 + \rho)^2} \\ &= \frac{\sigma_v^2}{M} \sum_{m \in \mathcal{M}} \frac{1}{(\sigma_m^2 + \rho)} \\ &= \frac{\sigma_v^2}{M} \mathrm{tr} \left\{ \left(\mathbf{H}_0^H \mathbf{H}_0 + \rho \mathbf{I}_M \right)^{-1} \right\}, \end{aligned} \tag{F.8}$$

as desired. □

The reader should notice the close relationship between the average MSE of symbols and the singular values of the effective-channel matrix. Indeed, the smaller the singular values of the effective-channel matrix are, the larger the average MSE of symbols is. In addition, a direct consequence of such a result is the description of the average MSE of symbols associated with the ZF-based ZP-ZJ transceivers, as described in Corollary 4.

Corollary 4. *The ZF receiver defined in Eq. (D.3) yields the following average MSE of symbols:*

$$\begin{aligned} \mathrm{AMSE}^{\mathrm{ZF}}(K, M) &= \frac{\sigma_v^2}{M} \mathrm{tr} \left\{ \left[\mathbf{H}_0^H(K, M) \mathbf{H}_0(K, M) \right]^{-1} \right\} \\ &= \frac{\sigma_v^2}{M} \sum_{m \in \mathcal{M}} \frac{1}{\sigma_m^2(K, M)}. \end{aligned} \tag{F.9}$$

Proof. As the mapping of a nonsingular matrix into its inverse is a continuous mapping, then $\mathbf{G}_0^{\mathrm{MMSE}} \to \mathbf{G}_0^{\mathrm{ZF}}$, when $\rho \to 0$. Thus, by considering that σ_v^2 is constant while $\rho \to 0$, then the result follows from Theorem 9 straightforwardly. □

Now that we have an explicit expression for the average MSE of symbols, we can compare the performance of systems that use different amounts of redundancy in a given environment. For that, we shall first state a very useful result in Lemma 12, as follows.

Lemma 12. *Given two fixed integer numbers L and M, let us assume that each matrix $\mathbf{H}_0(K, M) \in \mathbb{C}^{(M+2K-L)\times M}$ is constructed from the same Lth-order channel-impulse response, with $K \in \mathcal{K}_L$. Then*

$$\sigma_m(K+1, M) \geq \sigma_m(K, M),\ \forall (m, K) \in \mathcal{M} \times (\mathcal{K}_L \setminus \{L\}), \tag{F.10}$$

where each $\sigma_m(K, M) \in \mathbb{R}_+$ is a singular value of $\mathbf{H}_0(K, M)$, for each pair $(m, K) \in \mathcal{M} \times \mathcal{K}_L$.

Proof. For the sake of simplicity, we shall omit from all variables the dependency on M. Let us focus on the structure of $\mathbf{H}_0(K+1)$. By assuming that $K \in (\mathcal{K}_L \setminus \{L\})$, the relationship between $\mathbf{H}_0(K+1)$ and $\mathbf{H}_0(K)$ is given by

$$\mathbf{H}_0(K+1) = \begin{bmatrix} \mathbf{h}_{\mathrm{f}}^H(K+1) \\ \mathbf{H}_0(K) \\ \mathbf{h}_{\mathrm{l}}^H(K+1) \end{bmatrix} \in \mathbb{C}^{(M+2K+2-L)\times M}, \tag{F.11}$$

where

$$\mathbf{h}_{\mathrm{f}}^H(K+1) \triangleq [\, h(L-K-1)\ \ h(L-K-2)\ \ \cdots\ \ h(0)\ \ 0\ \ \cdots\ \ 0\,], \tag{F.12}$$

$$\mathbf{h}_{\mathrm{l}}^H(K+1) \triangleq [\, 0\ \ \cdots\ \ 0\ \ h(L)\ \ \cdots\ \ h(K+2)\ \ h(K+1)\,], \tag{F.13}$$

in which the subscript f stands for first row, whereas the subscript l stands for last row, both of them associated with the matrix $\mathbf{H}_0(K+1)$. We know that the 2-norm of a matrix $\mathbf{X} \in \mathbb{C}^{M_1\times M_2}$ is defined as $\|\mathbf{X}\|_2 \triangleq \max\|\mathbf{X}\mathbf{y}\|_2$, for $\mathbf{y}$ in the set $\mathbb{C}^{M_2\times 1}$ and such that $\|\mathbf{y}\|_2 = 1$. In addition, we also know that $\|\mathbf{X}\|_2 = \sigma_{\max}(\mathbf{X})$. We

therefore have

$$\begin{aligned}
\|\mathbf{H}_0(K+1)\|_2 &= \sigma_0(K+1) \\
&= \left\| \begin{bmatrix} \mathbf{h}_{\mathrm{f}}^H(K+1) \\ \mathbf{H}_0(K) \\ \mathbf{h}_{\mathrm{l}}^H(K+1) \end{bmatrix} \right\|_2 \\
&= \max_{\|\mathbf{x}\|_2=1} \left\| \begin{bmatrix} \mathbf{h}_{\mathrm{f}}^H(K+1) \\ \mathbf{H}_0(K) \\ \mathbf{h}_{\mathrm{l}}^H(K+1) \end{bmatrix} \mathbf{x} \right\|_2 \\
&= \max_{\|\mathbf{x}\|_2=1} \left\| \begin{bmatrix} \mathbf{h}_{\mathrm{f}}^H(K+1)\mathbf{x} \\ \mathbf{H}_0(K)\mathbf{x} \\ \mathbf{h}_{\mathrm{l}}^H(K+1)\mathbf{x} \end{bmatrix} \right\|_2 \\
&= \max_{\|\mathbf{x}\|_2=1} \sqrt{\|\mathbf{H}_0(K)\mathbf{x}\|_2^2 + |\mathbf{h}_{\mathrm{f}}^H(K+1)\mathbf{x}|^2 + |\mathbf{h}_{\mathrm{l}}^H(K+1)\mathbf{x}|^2} \\
&\geq \max_{\|\mathbf{x}\|_2=1} \|\mathbf{H}_0(K)\mathbf{x}\|_2 \\
&= \|\mathbf{H}_0(K)\|_2 \\
&= \sigma_0(K). \qquad \text{(F.14)}
\end{aligned}$$

Now, by taking into account the SVD decomposition of the matrix $\mathbf{H}_0(K+1)$, one has

$$\mathbf{H}_0(K+1) = \sum_{m \in \mathcal{M}} \sigma_m(K+1)\mathbf{u}_m(K+1)\mathbf{v}_m^H(K+1). \qquad \text{(F.15)}$$

In addition, one can also define a reduced-rank approximation for $\mathbf{H}_0(K+1)$ as follows:

$$\mathbf{H}_{(M-R-1)}(K+1) \triangleq \sum_{r=0}^{R} \sigma_r(K+1)\mathbf{u}_r(K+1)\mathbf{v}_r^H(K+1), \ \forall R \in \mathcal{M}, \qquad \text{(F.16)}$$

where $\mathbf{H}_{(M-R-1)}(K+1)$ is a rank-$(R+1)$ matrix.

Moreover, let us assume that $R \in (\mathcal{M} \setminus \{M-1\})$ and that each eigenvector $\mathbf{u}_r(K+1)$ can be written as

$$\mathbf{u}_r(K+1) = [[\mathbf{u}_r(K+1)]_{\mathrm{f}} \ \ \bar{\mathbf{u}}_r^T(K+1) \ \ [\mathbf{u}_r(K+1)]_{\mathrm{l}}]^T, \qquad \text{(F.17)}$$

where $[\mathbf{u}_r(K+1)]_{\mathrm{f}}$ is the first element of $\mathbf{u}_r(K+1)$, $[\mathbf{u}_r(K+1)]_{\mathrm{l}}$ is the last element of $\mathbf{u}_r(K+1)$, and $\bar{\mathbf{u}}_r(K+1) \in \mathbb{C}^{(M+2K-L)\times 1}$ contains the remaining elements of

$\mathbf{u}_r(K+1)$. Thus, by using Lemma 7 (see Chapter C), one has

$$
\begin{aligned}
\sigma_{(R+1)}(K+1) &= \|\mathbf{H}_0(K+1) - \mathbf{H}_{(M-R-1)}(K+1)\|_2 \\
&= \left\| \begin{bmatrix} \underbrace{\mathbf{h}_{\mathrm{f}}^H(K+1) - \sum_{r=0}^{R} \sigma_r(K+1)[\mathbf{u}_r(K+1)]_{\mathrm{f}} \mathbf{v}_r^H(K+1)}_{\boldsymbol{\delta}_{\mathrm{f}}^H} \\ \underbrace{\mathbf{H}_0(K) - \sum_{r=0}^{R} \sigma_r(K+1)\bar{\mathbf{u}}_r(K+1)\mathbf{v}_r^H(K+1)}_{\boldsymbol{\Delta}_{\mathbf{H}_0}} \\ \underbrace{\mathbf{h}_{\mathrm{l}}^H(K+1) - \sum_{r=0}^{R} \sigma_r(K+1)[\mathbf{u}_r(K+1)]_{\mathrm{l}} \mathbf{v}_r^H(K+1)}_{\boldsymbol{\delta}_{\mathrm{l}}^H} \end{bmatrix} \right\|_2 \\
&= \left\| \begin{bmatrix} \boldsymbol{\delta}_{\mathrm{f}}^H \\ \boldsymbol{\Delta}_{\mathbf{H}_0} \\ \boldsymbol{\delta}_{\mathrm{l}}^H \end{bmatrix} \right\|_2 \\
&= \max_{\|\mathbf{x}\|_2=1} \left\| \begin{bmatrix} \boldsymbol{\delta}_{\mathrm{f}}^H \\ \boldsymbol{\Delta}_{\mathbf{H}_0} \\ \boldsymbol{\delta}_{\mathrm{l}}^H \end{bmatrix} \mathbf{x} \right\|_2 \\
&= \max_{\|\mathbf{x}\|_2=1} \left\| \begin{bmatrix} \boldsymbol{\delta}_{\mathrm{f}}^H \mathbf{x} \\ \boldsymbol{\Delta}_{\mathbf{H}_0} \mathbf{x} \\ \boldsymbol{\delta}_{\mathrm{l}}^H \mathbf{x} \end{bmatrix} \right\|_2 \\
&= \max_{\|\mathbf{x}\|_2=1} \sqrt{\|\boldsymbol{\Delta}_{\mathbf{H}_0}\mathbf{x}\|_2^2 + |\boldsymbol{\delta}_{\mathrm{f}}^H \mathbf{x}|^2 + |\boldsymbol{\delta}_{\mathrm{l}}^H \mathbf{x}|^2} \\
&\geq \max_{\|\mathbf{x}\|_2=1} \|\boldsymbol{\Delta}_{\mathbf{H}_0}\mathbf{x}\|_2 \\
&= \|\boldsymbol{\Delta}_{\mathbf{H}_0}\|_2 \\
&= \left\| \mathbf{H}_0(K) - \sum_{r=0}^{R} \sigma_r(K+1)\bar{\mathbf{u}}_r(K+1)\mathbf{v}_r^H(K+1) \right\|_2 \\
&\geq \left\| \mathbf{H}_0(K) - \mathbf{H}_{(M-R-1)}(K) \right\|_2 \\
&= \sigma_{(R+1)}(K), \qquad \text{(F.18)}
\end{aligned}
$$

as desired. □

Note that Lemma 12 guarantees that the singular values associated with the effective channel matrix is a monotone increasing function of the number of transmitted redundant elements, which can vary from the minimum value, $\lceil L/2 \rceil$, to the limit value, L. With the help of Lemma 12, we can now state another key contribution of this chapter.

Theorem 10. *The average MSE of symbols related to both the MMSE and ZF*

receivers are monotone decreasing functions of $K \in (\mathcal{K}_L \setminus \{L\})$*, i.e.*

$$\text{AMSE}^{\text{MMSE}}(K+1, M) \leq \text{AMSE}^{\text{MMSE}}(K, M),\ \forall K \in (\mathcal{K}_L \setminus \{L\}) \tag{F.19}$$

$$\text{AMSE}^{\text{ZF}}(K+1, M) \leq \text{AMSE}^{\text{ZF}}(K, M),\ \forall K \in (\mathcal{K}_L \setminus \{L\}). \tag{F.20}$$

Proof. This result is a direct consequence of Theorem 9, Corollary 4, and Lemma 12. □

Theorem 10 states that if one aims to reduce the bandwidth usage on redundant data by decreasing the amount of transmitted redundant elements, then the resulting AMSE performance will degrade (or will be at most the same). On the other hand, we have proved in Chapter C that if one tries to enhance the spectral efficiency of a full-redundancy ZP transceiver by increasing the block size M, one ends up loosing performance as well. Indeed, the AMSE of a full-redundancy ZP system follows a similar pattern presented in Theorem 10, as described in the following proposition.

Proposition 4. *The average MSE of symbols related to both the MMSE and ZF full-redundancy block transceivers are monotone increasing functions of* M*, i.e.*

$$\text{AMSE}^{\text{MMSE}}(L, M) \leq \text{AMSE}^{\text{MMSE}}(L, M+1),\ \forall M \in (\mathbb{N} \setminus \mathcal{L}) \tag{F.21}$$

$$\text{AMSE}^{\text{ZF}}(L, M) \leq \text{AMSE}^{\text{ZF}}(L, M+1),\ \forall M \in (\mathbb{N} \setminus \mathcal{L}). \tag{F.22}$$

Proof. See [40, 42] and Chapter C. □

Theorem 10 and Proposition 4 show that, whenever one tries to increase the bandwidth efficiency of a block-based transmission, whether reducing the number of transmitted redundancy or increasing the amount of transmitted data symbols in a traditional full-redundancy system, one will end up losing performance with respect to the MSE of symbols. Based on these facts, it is key to look for the adequate system that allows one to achieve the target bandwidth efficiency and MSE (or BER) performance. As the analytical results indicate, the adopted transceiver, either reduced-redundancy or full-redundancy with larger block sizes, depends on the particular type of application. Hence, different channel models may call for distinct transceiver choices.

Now, let us assume that the ZP-ZJ system with full-redundancy using a large amount of data symbols is the best option[1] for achieving a target throughput performance. In this case, superfast implementations of this system are readily available and there is no additional challenge to the designer. On the other hand, if the best choice is the ZP-ZJ system with reduced-redundancy, how should we implement such

[1] Considering only the transceivers treated in this chapter.

systems? Do they have superfast implementations as well? This chapter proposes some answers to these questions, as described in the next section.

F.2 New Decompositions of Rectangular Structured Matrices

Many engineering models induce structural patterns in their matrix-based mathematical descriptions. Such structural patterns may bring about efficient means for exploiting features of the related problems. Besides, computations involving structured matrices can be further simplified by taking into account these structural patterns. As we have pointed out in Section D.1, the effective channel matrix associated with ZP-ZJ systems is a rectangular Toeplitz matrix. It is therefore natural to expect that linear equalizers, such as linear MMSE or ZF equalizers, can take advantage from the structure of this channel matrix. In this context, three questions arise: (i) How to recognize a structured matrix by using analytical tools? (ii) How to represent the linear optimal solutions (either MMSE or ZF) by employing such analytical tools? and (iii) How to effectively take advantage of such representations?

This section describes the answers to those questions in the context of rectangular structured matrices. Subsection F.2.1 describes the extension of the displacement-rank approach when one is dealing with rectangular structured matrices instead of square matrices. Subsection F.2.2 shows how to represent ZF- and MMSE-based receiver matrices by using the displacement approach. Subsection F.2.3 contains the results demonstrating how to decompose a wide class of structured matrices, the so-called Bezoutian matrices, using only DFT and diagonal matrices. Such results are relevant since the Bezoutian matrices encompass both the ZF- and MMSE-based receiver matrices.

F.2.1 Displacement-Rank Approach

Similarly as performed in Subsection D.1.3, let us assume that $\mathbf{X} \in \mathbb{C}^{M_1 \times M_1}$ and $\mathbf{Y} \in \mathbb{C}^{M_2 \times M_2}$ are two given *operator matrices*, where M_1 and M_2 are positive integers. Thus, the linear transformations [25]

$$\begin{aligned} \nabla_{\mathbf{X},\mathbf{Y}} : \mathbb{C}^{M_1 \times M_2} &\to \mathbb{C}^{M_1 \times M_2} \\ \mathbf{U} &\mapsto \nabla_{\mathbf{X},\mathbf{Y}}(\mathbf{U}) \triangleq \mathbf{X}\mathbf{U} - \mathbf{U}\mathbf{Y}, \end{aligned} \tag{F.23}$$

$$\begin{aligned} \Delta_{\mathbf{X},\mathbf{Y}} : \mathbb{C}^{M_1 \times M_2} &\to \mathbb{C}^{M_1 \times M_2} \\ \mathbf{U} &\mapsto \Delta_{\mathbf{X},\mathbf{Y}}(\mathbf{U}) \triangleq \mathbf{U} - \mathbf{X}\mathbf{U}\mathbf{Y} \end{aligned} \tag{F.24}$$

are the extensions of Sylvester and Stein displacement operators to the rectangular-matrix case.

As we have already highlighted in Chapter D, the displacement approach is comprised of compression, operation, and decompression stages [25]. In order to illustrate the compression capability of the displacement operators dealing with rectangular matrices, let us consider the application of the Sylvester displacement operator $\nabla_{\mathbf{Z}_{1/\eta},\mathbf{Z}_\xi}$, in which $\mathbf{Z}_{1/\eta} \in \mathbb{C}^{M_1\times M_1}$ and $\mathbf{Z}_\xi \in \mathbb{C}^{M_2\times M_2}$, on an $M_1 \times M_2$ complex-valued Toeplitz matrix $\mathbf{T}$, with $[\mathbf{T}]_{m_1,m_2} \triangleq t_{(m_1-m_2)}$, as follows:

$$\nabla_{\mathbf{Z}_{1/\eta},\mathbf{Z}_\xi}(\mathbf{T}) = \mathbf{Z}_{1/\eta}\mathbf{T} - \mathbf{T}\mathbf{Z}_\xi \tag{F.25}$$

$$= \begin{bmatrix} (1/\eta)t_{M_1-1} & (1/\eta)t_{M_1-2} & \cdots & (1/\eta)t_{M_1-M_2} \\ t_0 & t_{-1} & \cdots & t_{1-M_2} \\ \vdots & \vdots & \ddots & \vdots \\ t_{M_1-2} & t_{M_1-1} & \cdots & t_{M_1-M_2-1} \end{bmatrix}$$

$$- \begin{bmatrix} t_{-1} & \cdots & t_{1-M_2} & \xi t_0 \\ \vdots & \ddots & \vdots & \xi t_1 \\ t_{M_1-3} & \cdots & t_{M_1-M_2-1} & \vdots \\ t_{M_1-2} & \cdots & t_{M_1-M_2} & \xi t_{M_1-1} \end{bmatrix} \tag{F.26}$$

$$= \underbrace{\begin{bmatrix} 1 \\ 0 \\ \vdots \\ 0 \end{bmatrix}}_{\triangleq\hat{\mathbf{p}}_1} \underbrace{\begin{bmatrix} (1/\eta)t_{M_1-1} - t_{-1} & \cdots & (1/\eta)t_{M_1-M_2+1} - t_{1-M_2} & (1/\eta)t_{M_1-M_2} \end{bmatrix}}_{\triangleq\hat{\mathbf{q}}_1^T}$$

$$+ \underbrace{\begin{bmatrix} -\xi t_0 \\ t_{1-M_2} - \xi t_1 \\ \vdots \\ t_{M_1-M_2-1} - \xi t_{M_1-1} \end{bmatrix}}_{\triangleq\hat{\mathbf{p}}_2} \underbrace{\begin{bmatrix} 0 & 0 & \cdots & 1 \end{bmatrix}}_{\triangleq\hat{\mathbf{q}}_2^T} \tag{F.27}$$

$$= \hat{\mathbf{p}}_1\hat{\mathbf{q}}_1^T + \hat{\mathbf{p}}_2\hat{\mathbf{q}}_2^T = [\,\hat{\mathbf{p}}_1\ \hat{\mathbf{p}}_2\,] \begin{bmatrix} \hat{\mathbf{q}}_1^T \\ \hat{\mathbf{q}}_2^T \end{bmatrix} \triangleq \hat{\mathbf{P}}\hat{\mathbf{Q}}^T. \tag{F.28}$$

Note that the resulting displacement matrix $\nabla_{\mathbf{Z}_{1/\eta},\mathbf{Z}_\xi}(\mathbf{T})$ can be represented by the *displacement generator pair* of matrices $(\hat{\mathbf{P}}, \hat{\mathbf{Q}}) \in \mathbb{C}^{M_1\times 2} \times \mathbb{C}^{M_2\times 2}$. Thus, if one assumes that M_1 and M_2 are integer numbers much larger than 2, then the former example shows that rectangular Toeplitz matrices can always be compressed, since the matrix $\nabla_{\mathbf{Z}_{1/\eta},\mathbf{Z}_\xi}(\mathbf{T})$ has rank at most 2.

F.2.2 Displacement of ZF- and MMSE-Receiver Matrices

This subsection exemplifies the operation stage associated with the displacement-rank approach applied to rectangular matrices. In order to do that, let us define the transmitter-independent receiver matrix $\mathbf{K} \triangleq \mathbf{F}_0\mathbf{G}_0 \in \mathbb{C}^{M\times(M+2K-L)}$. From Eqs. (D.3) and (D.4), one can easily verify that $\mathbf{K}_{\text{ZF}} = \mathbf{H}_0^{\dagger}$, whereas $\mathbf{K}_{\text{MMSE}} = (\mathbf{H}_0^H\mathbf{H}_0 + \rho\mathbf{I}_M)^{-1}\mathbf{H}_0^H$. Observe that, for both the ZF and the MMSE solutions, the related transmitter-independent receiver matrix $\mathbf{K}$ is obtained from operations upon the effective channel matrix $\mathbf{H}_0$. Theorem 11 contains a result for the MMSE case that shows how to operate on the displacement-generator pairs of $\mathbf{H}_0$ and $\mathbf{H}_0^H$ in order to derive the displacement-generator pair of $\mathbf{K}_{\text{MMSE}}$.

Theorem 11. *Given the operator matrices* $\mathbf{Z}_\xi \in \mathbb{C}^{M\times M}$ *and* $\mathbf{Z}_{1/\eta} \in \mathbb{C}^{(M+2K-L)\times(M+2K-L)}$*, the MMSE-based transmitter-independent receiver matrix* $\mathbf{K}_{\text{MMSE}}$ *yields the displacement matrix* $\nabla_{\mathbf{Z}_\xi,\mathbf{Z}_{1/\eta}}(\mathbf{K}_{\text{MMSE}}) = \mathbf{P}\mathbf{Q}^T$*, in which*

$$\mathbf{P} = \left[\rho\left(\mathbf{H}_0^H\mathbf{H}_0 + \rho\mathbf{I}_M\right)^{-1}\hat{\mathbf{P}}' \quad -\mathbf{K}_{\text{MMSE}}\hat{\mathbf{P}}\right]_{M\times 4}, \tag{F.29}$$

$$\mathbf{Q} = \left[\left(\mathbf{H}_0\mathbf{H}_0^H + \rho\mathbf{I}_{(M+2K-L)}\right)^{-T}\hat{\mathbf{Q}}' \quad \mathbf{K}_{\text{MMSE}}^T\hat{\mathbf{Q}}\right]_{(M+2K-L)\times 4}, \tag{F.30}$$

with $(\hat{\mathbf{P}},\hat{\mathbf{Q}}) \in \mathbb{C}^{(M+2K-L)\times 2}\times\mathbb{C}^{M\times 2}$ *and* $(\hat{\mathbf{P}}',\hat{\mathbf{Q}}') \in \mathbb{C}^{M\times 2}\times\mathbb{C}^{(M+2K-L)\times 2}$ *being the displacement-generator pairs of* $\nabla_{\mathbf{Z}_{1/\eta},\mathbf{Z}_\xi}(\mathbf{H}_0)$ *and* $\nabla_{\mathbf{Z}_\xi,\mathbf{Z}_{1/\eta}}(\mathbf{H}_0^H)$*, respectively. These generator pairs are easily determined by using Eqs.* (F.25)*,* (F.26)*,* (F.27)*,* (F.28)*.*

Proof. In this proof we shall refer to several known results from the literature [25], which are the extensions of the results expressed in Eqs. (D.12), (D.13), (D.14), and (D.15) to deal with rectangular matrices.

Thus, let us compute the Sylvester displacement $\nabla_{\mathbf{Z}_\xi,\mathbf{Z}_\xi}(\mathbf{H}_0^H\mathbf{H}_0)$, as follows:

$$\nabla_{\mathbf{Z}_\xi,\mathbf{Z}_\xi}(\mathbf{H}_0^H\mathbf{H}_0) = \underbrace{\left[\hat{\mathbf{P}}' \quad \mathbf{H}_0^H\hat{\mathbf{P}}\right]}_{\triangleq\bar{\mathbf{P}}}\underbrace{\begin{bmatrix}\hat{\mathbf{Q}}'^T\mathbf{H}_0 \\ \hat{\mathbf{Q}}^T\end{bmatrix}}_{\triangleq\bar{\mathbf{Q}}^T} = \bar{\mathbf{P}}\bar{\mathbf{Q}}^T, \tag{F.31}$$

in which we have employed Eq. (D.14) adapted to rectangular matrices.

As the Sylvester displacement $\nabla_{\mathbf{Z}_\xi,\mathbf{Z}_\xi}(\mathbf{I}_M)$ is an $M\times M$ all-zero matrix, then the related displacement of the term $\mathbf{H}_0^H\mathbf{H}_0 + (\sigma_v^2/\sigma_s^2)\mathbf{I}_M$ present in Eq. (D.4) is $\bar{\mathbf{P}}\bar{\mathbf{Q}}^T$ as well. In other words, if one defines

$$\mathbf{A} \triangleq \mathbf{H}_0^H\mathbf{H}_0 + (\sigma_v^2/\sigma_s^2)\mathbf{I}_M, \tag{F.32}$$

then $\nabla_{\mathbf{Z}_\xi,\mathbf{Z}_\xi}(\mathbf{A}) = \bar{\mathbf{P}}\bar{\mathbf{Q}}^T$. Now, by applying Eq. (D.12) one gets:

$$\nabla_{\mathbf{Z}_\xi,\mathbf{Z}_\xi}\left(\mathbf{A}^{-1}\right) = -\mathbf{A}^{-1}\nabla_{\mathbf{Z}_\xi,\mathbf{Z}_\xi}\left(\mathbf{A}\right)\mathbf{A}^{-1} = \underbrace{\left[-\mathbf{A}^{-1}\bar{\mathbf{P}}\right]}_{\triangleq\check{\mathbf{P}}}\underbrace{\left[\mathbf{A}^{-T}\bar{\mathbf{Q}}\right]^T}_{\triangleq\check{\mathbf{Q}}^T} = \check{\mathbf{P}}\check{\mathbf{Q}}^T. \tag{F.33}$$

Now, by applying Eq. (D.14) adapted to rectangular matrices, one has

$$\nabla_{\mathbf{Z}_\xi,\mathbf{Z}_{1/\eta}}\left(\mathbf{A}^{-1}\mathbf{H}_0^H\right) = \underbrace{\begin{bmatrix}\check{\mathbf{P}} & \mathbf{A}^{-1}\hat{\mathbf{P}}'\end{bmatrix}}_{\triangleq\mathbf{P}}\underbrace{\begin{bmatrix}\check{\mathbf{Q}}^T\mathbf{H}_0^H \\ \hat{\mathbf{Q}}'^T\end{bmatrix}}_{\triangleq\mathbf{Q}^T} = \mathbf{P}\mathbf{Q}^T. \tag{F.34}$$

Hence, the displacement generator of the MMSE solution is given by the pair

$$\mathbf{P} = \begin{bmatrix}-\mathbf{A}^{-1}\hat{\mathbf{P}}' & -\mathbf{K}_{\text{MMSE}}\hat{\mathbf{P}} & \mathbf{A}^{-1}\hat{\mathbf{P}}'\end{bmatrix}_{M\times 6}, \tag{F.35}$$

$$\mathbf{Q} = \begin{bmatrix}\mathbf{K}_{\text{MMSE}}^T\mathbf{H}_0^T\hat{\mathbf{Q}}' & \mathbf{K}_{\text{MMSE}}^T\hat{\mathbf{Q}} & \hat{\mathbf{Q}}'\end{bmatrix}_{(M+2K-L)\times 6}. \tag{F.36}$$

Now, let us compute the product $\mathbf{P}\mathbf{Q}^T$ as follows:

$$\begin{aligned}\mathbf{P}\mathbf{Q}^T =& -\left(\mathbf{H}_0^H\mathbf{H}_0 + \frac{\sigma_v^2}{\sigma_s^2}\mathbf{I}_M\right)^{-1}\hat{\mathbf{P}}'\hat{\mathbf{Q}}'^T\mathbf{H}_0\left(\mathbf{H}_0^H\mathbf{H}_0 + \frac{\sigma_v^2}{\sigma_s^2}\mathbf{I}_M\right)^{-1}\mathbf{H}_0^H \\ &- \left(\mathbf{H}_0^H\mathbf{H}_0 + \frac{\sigma_v^2}{\sigma_s^2}\mathbf{I}_M\right)^{-1}\mathbf{H}_0^H\hat{\mathbf{P}}\hat{\mathbf{Q}}^T\left(\mathbf{H}_0^H\mathbf{H}_0 + \frac{\sigma_v^2}{\sigma_s^2}\mathbf{I}_M\right)^{-1}\mathbf{H}_0^H \\ &+ \left(\mathbf{H}_0^H\mathbf{H}_0 + \frac{\sigma_v^2}{\sigma_s^2}\mathbf{I}_M\right)^{-1}\hat{\mathbf{P}}'\hat{\mathbf{Q}}'^T \\ =& \left(\mathbf{H}_0^H\mathbf{H}_0 + \frac{\sigma_v^2}{\sigma_s^2}\mathbf{I}_M\right)^{-1}\hat{\mathbf{P}}'\hat{\mathbf{Q}}'^T\left[\mathbf{I}_{(M+2K-L)} - \mathbf{H}_0\left(\mathbf{H}_0^H\mathbf{H}_0 + \frac{\sigma_v^2}{\sigma_s^2}\mathbf{I}_M\right)^{-1}\mathbf{H}_0^H\right] \\ &- \left(\mathbf{H}_0^H\mathbf{H}_0 + \frac{\sigma_v^2}{\sigma_s^2}\mathbf{I}_M\right)^{-1}\mathbf{H}_0^H\hat{\mathbf{P}}\hat{\mathbf{Q}}^T\left(\mathbf{H}_0^H\mathbf{H}_0 + \frac{\sigma_v^2}{\sigma_s^2}\mathbf{I}_M\right)^{-1}\mathbf{H}_0^H.\end{aligned} \tag{F.37}$$

Thus, by applying the matrix inversion lemma, it is possible to show that

$$\begin{aligned}\mathbf{P}\mathbf{Q}^T =& \frac{\sigma_v^2}{\sigma_s^2}\left(\mathbf{H}_0^H\mathbf{H}_0 + \frac{\sigma_v^2}{\sigma_s^2}\mathbf{I}_M\right)^{-1}\hat{\mathbf{P}}'\hat{\mathbf{Q}}'^T\left(\mathbf{H}_0\mathbf{H}_0^H + \frac{\sigma_v^2}{\sigma_s^2}\mathbf{I}_{(M+2K-L)}\right)^{-1} \\ &- \left(\mathbf{H}_0^H\mathbf{H}_0 + \frac{\sigma_v^2}{\sigma_s^2}\mathbf{I}_M\right)^{-1}\mathbf{H}_0^H\hat{\mathbf{P}}\hat{\mathbf{Q}}^T\left(\mathbf{H}_0^H\mathbf{H}_0 + \frac{\sigma_v^2}{\sigma_s^2}\mathbf{I}_M\right)^{-1}\mathbf{H}_0^H.\end{aligned} \tag{F.38}$$

One can therefore redefine the matrix-generator pair $(\mathbf{P}, \mathbf{Q})$ in a more compact manner, in such a way that each generator matrix has four columns, instead of six,

as follows:

$$\mathbf{P} \triangleq \left[\frac{\sigma_v^2}{\sigma_s^2}\left(\mathbf{H}_0^H\mathbf{H}_0 + \frac{\sigma_v^2}{\sigma_s^2}\mathbf{I}_M\right)^{-1}\hat{\mathbf{P}}' \quad -\mathbf{K}_{\text{MMSE}}\hat{\mathbf{P}}\right]_{M\times 4}, \tag{F.39}$$

$$\mathbf{Q} \triangleq \left[\left(\mathbf{H}_0\mathbf{H}_0^H + \frac{\sigma_v^2}{\sigma_s^2}\mathbf{I}_{(M+2K-L)}\right)^{-T}\hat{\mathbf{Q}}' \quad \mathbf{K}_{\text{MMSE}}^T\hat{\mathbf{Q}}\right]_{(M+2K-L)\times 4}, \tag{F.40}$$

as desired. □

Theorem 11 describes the compressed form for the MMSE-based transmitter-independent receiver matrix. This compressed representation will be very useful in the design of superfast transceivers with reduced-redundancy. The ZF-based transceivers are obtained when one considers that $\rho \to 0$. In this particular case, the following Corollary 5 holds.

Corollary 5. *Given the operator matrices* $\mathbf{Z}_\xi \in \mathbb{C}^{M\times M}$ *and* $\mathbf{Z}_{1/\eta} \in \mathbb{C}^{(M+2K-L)\times(M+2K-L)}$*, the ZF-based transmitter-independent receiver matrix* $\mathbf{K}_{\text{ZF}}$ *yields the displacement matrix* $\nabla_{\mathbf{Z}_\xi,\mathbf{Z}_{1/\eta}}(\mathbf{K}_{\text{ZF}}) = \mathbf{P}\mathbf{Q}^T$*, in which*

$$\mathbf{P} = \left[\left(\mathbf{H}_0^H\mathbf{H}_0\right)^{-1}\hat{\mathbf{P}}' \quad -\mathbf{K}_{\text{ZF}}\hat{\mathbf{P}}\right]_{M\times 4}, \tag{F.41}$$

$$\mathbf{Q} = \left[\left[\mathbf{I}_{(M+2K-L)} - \mathbf{H}_0\mathbf{K}_{\text{ZF}}\right]^T\hat{\mathbf{Q}}' \quad \mathbf{K}_{\text{ZF}}^T\hat{\mathbf{Q}}\right]_{(M+2K-L)\times 4}, \tag{F.42}$$

with $(\hat{\mathbf{P}},\hat{\mathbf{Q}}) \in \mathbb{C}^{(M+2K-L)\times 2}\times\mathbb{C}^{M\times 2}$ *and* $(\hat{\mathbf{P}}',\hat{\mathbf{Q}}') \in \mathbb{C}^{M\times 2}\times\mathbb{C}^{(M+2K-L)\times 2}$ *being the displacement-generator pairs of* $\nabla_{\mathbf{Z}_{1/\eta},\mathbf{Z}_\xi}(\mathbf{H}_0)$ *and* $\nabla_{\mathbf{Z}_\xi,\mathbf{Z}_{1/\eta}}(\mathbf{H}_0^H)$*, respectively.*

Proof. First of all, as the mapping of a nonsingular matrix into its inverse is a continuous mapping, then $\mathbf{K}_{\text{MMSE}} \to \mathbf{K}_{\text{ZF}}$, when $\frac{\sigma_v^2}{\sigma_s^2} \to 0$. In addition, all the operations employed to compute the displacement-generator pair of $\mathbf{K}_{\text{MMSE}}$ are also continuous. Hence, in order to determine the displacement-generator pair of $\mathbf{K}_{\text{ZF}}$, we can evaluate the generator pair of $\mathbf{K}_{\text{MMSE}}$ when $\frac{\sigma_v^2}{\sigma_s^2} \to 0$. Thus, by making $\frac{\sigma_v^2}{\sigma_s^2} \to 0$ in Eq. (F.37), we get:

$$\begin{aligned}\mathbf{P}\mathbf{Q}^T &= \left(\mathbf{H}_0^H\mathbf{H}_0\right)^{-1}\hat{\mathbf{P}}'\hat{\mathbf{Q}}'^T\left[\mathbf{I}_{(M+2K-L)} - \mathbf{H}_0\left(\mathbf{H}_0^H\mathbf{H}_0\right)^{-1}\mathbf{H}_0^H\right]\\ &\quad - \left(\mathbf{H}_0^H\mathbf{H}_0\right)^{-1}\mathbf{H}_0^H\hat{\mathbf{P}}\hat{\mathbf{Q}}^T\left(\mathbf{H}_0^H\mathbf{H}_0\right)^{-1}\mathbf{H}_0^H\\ &= \left(\mathbf{H}_0^H\mathbf{H}_0\right)^{-1}\hat{\mathbf{P}}'\hat{\mathbf{Q}}'^T\left[\mathbf{I}_{(M+2K-L)} - \mathbf{H}_0\mathbf{K}_{\text{ZF}}\right] - \mathbf{K}_{\text{ZF}}\hat{\mathbf{P}}\hat{\mathbf{Q}}^T\mathbf{K}_{\text{ZF}},\end{aligned} \tag{F.43}$$

as desired. □

Theorem 11 and Corollary 5 show that, for both ZF and MMSE receivers, one always has $\nabla_{\mathbf{Z}_\xi,\mathbf{Z}_{1/\eta}}(\mathbf{K}) = \mathbf{P}\mathbf{Q}^T$, where $(\mathbf{P},\mathbf{Q}) \in \mathbb{C}^{M\times 4}\times\mathbb{C}^{(M+2K-L)\times 4}$. Thus, the transmitter-independent receiver matrix $\mathbf{K}$ can be regarded as a particular kind of

rectangular Bezoutian matrix, since a rectangular Bezoutian matrix is any matrix $\mathbf{B}$ such that $\nabla_{\mathbf{Z}_{\lambda_1},\mathbf{Z}_{\lambda_2}}(\mathbf{B}) = \mathbf{P}_{\mathbf{B}}\mathbf{Q}_{\mathbf{B}}{}^T$, where $(\mathbf{P}_{\mathbf{B}}, \mathbf{Q}_{\mathbf{B}}) \in \mathbb{C}^{M_1\times R} \times \mathbb{C}^{M_2\times R}$, with $M_1 \gg R$ and $M_2 \gg R$ [25].

F.2.3 DFT-Based Representations of Rectangular Bezoutians

Let $\boldsymbol{\nu} \triangleq [\nu_0\ \nu_1\ \cdots\ \nu_{M-1}]^T$ be a given complex-valued vector. An $M \times M$ matrix $\mathbf{V}_{\boldsymbol{\nu}}$ is a Vandermonde matrix when $[\mathbf{V}_{\boldsymbol{\nu}}]_{m_1,m_2} \triangleq (\nu_{m_1})^{m_2}$, for all ordered pair (m_1, m_2) within the set $\mathcal{M}^2$.

Now, we have all the required tools for stating the main mathematical results of this chapter aiming at decomposing rectangular Bezoutian matrices employing only DFT, diagonal, and Vandermonde matrices.

Theorem 12. *Given two nonzero complex numbers η and ξ, and given two natural numbers M_1 and M_2, let us assume that $\mathbf{B}$ is an $M_2 \times M_1$ complex-valued Bezoutian matrix such that $\nabla_{\mathbf{Z}_\xi,\mathbf{Z}_{1/\eta}}(\mathbf{B}) = \mathbf{P}\mathbf{Q}^T$, where the operator matrices have compatible dimensions. The generator pair $(\mathbf{P}, \mathbf{Q})$ is within the set $\mathbb{C}^{M_2\times R} \times \mathbb{C}^{M_1\times R}$, in which the natural number R is the rank of the related Sylvester displacement matrix. Thus, if $M_1 \geq M_2$, then*

$$\mathbf{B} = \sqrt{M_1 M_2}\mathbf{V}_{\boldsymbol{\xi}}^{-1}\left[\sum_{r=1}^{R}\mathrm{diag}\{\bar{\mathbf{p}}_r\}\mathbf{W}_{M_2}\left[\,\mathrm{diag}\{(\xi_0\eta_0)^{m_2}\}_{m_2=0}^{M_2-1}\quad \mathbf{0}_{M_2\times(M_1-M_2)}\,\right]\times\right.$$
$$\left.\times\ \mathbf{W}_{M_1}\mathrm{diag}\{\bar{\mathbf{q}}_r\}\right]\mathbf{V}_{\boldsymbol{\eta}}^{-T}, \tag{F.44}$$

where the $M_1 \times 1$ vector $\boldsymbol{\eta}$ contains the M_1th roots of η, i.e., for each index $m_1 \in \mathcal{M}_1 \triangleq \{0, 1, \cdots, M_1 - 1\}$, one has $[\boldsymbol{\eta}]_{m_1} = \eta_{m_1} \triangleq \eta_0 W_{M_1}^{m_1}$, with $W_{M_1} \triangleq \mathrm{e}^{-\jmath\frac{2\pi}{M_1}}$ and $\eta_0 \triangleq |\eta|^{1/M_1}\mathrm{e}^{\jmath\frac{\angle\eta}{M_1}}$, whereas the $M_2 \times 1$ vector $\boldsymbol{\xi}$ contains the M_2th roots of ξ, i.e., for each index $m_2 \in \mathcal{M}_2 \triangleq \{0, 1, \cdots, M_2 - 1\}$, one has $[\boldsymbol{\xi}]_{m_2} = \xi_{m_2} \triangleq \xi_0 W_{M_2}^{m_2}$, with $\xi_0 \triangleq |\xi|^{1/M_2}\mathrm{e}^{\jmath\frac{\angle\xi}{M_2}}$. Moreover, one also has

$$\bar{\mathbf{P}} \triangleq [\,\bar{\mathbf{p}}_1\ \cdots\ \bar{\mathbf{p}}_R\,] = -\mathbf{V}_{\boldsymbol{\xi}}\mathbf{P} \tag{F.45}$$

$$\bar{\mathbf{Q}} \triangleq [\,\bar{\mathbf{q}}_1\ \cdots\ \bar{\mathbf{q}}_R\,] = \left(\mathrm{diag}\left\{\frac{1}{1-\xi\eta_{m_1}^{M_2}}\right\}_{m_1=0}^{M_1-1}\right)\mathbf{V}_{\boldsymbol{\eta}}\mathbf{Z}_{\eta}\mathbf{Q}, \tag{F.46}$$

in which we have assumed that $\xi\eta_{m_1}^{M_2} \neq 1$, for all $m_1 \in \mathcal{M}_1$.

Proof. In order to prove that the decomposition proposed in Theorem 12 is valid, let us first verify the structure of the $M_2 \times M_1$ matrix $\tilde{\mathbf{B}} \triangleq \mathbf{V}_{\boldsymbol{\xi}}\mathbf{B}\mathbf{V}_{\boldsymbol{\eta}}^T$. We shall follow the same steps employed in Section 3.3 of [23]. Thus, let us consider the Stein displacement $\Delta_{\mathbf{D}_{\boldsymbol{\xi}},\mathbf{D}_{\boldsymbol{\eta}}}$ applied to $\tilde{\mathbf{B}}$. Note that $\mathbf{D}_{\boldsymbol{\xi}}$ is an $M_2 \times M_2$ diagonal matrix,

whereas $\mathbf{D}_{\boldsymbol{\eta}}$ is an $M_1 \times M_1$ diagonal matrix. From Lemma 1 of [23], we know that $\mathbf{D}_{\boldsymbol{\xi}} = \mathbf{V}_{\boldsymbol{\xi}}\mathbf{Z}_{\xi}\mathbf{V}_{\boldsymbol{\xi}}^{-1}$ and $\mathbf{D}_{\boldsymbol{\eta}} = \mathbf{V}_{\boldsymbol{\eta}}^{-T}\mathbf{Z}_{\eta}^{T}\mathbf{V}_{\boldsymbol{\eta}}^{T}$. Hence, by using these results, one has

$$\begin{aligned}
\Delta_{\mathbf{D}_{\boldsymbol{\xi}},\mathbf{D}_{\boldsymbol{\eta}}}(\tilde{\mathbf{B}}) &= \Delta_{(\mathbf{V}_{\boldsymbol{\xi}}\mathbf{Z}_{\xi}\mathbf{V}_{\boldsymbol{\xi}}^{-1}),(\mathbf{V}_{\boldsymbol{\eta}}^{-T}\mathbf{Z}_{\eta}^{T}\mathbf{V}_{\boldsymbol{\eta}}^{T})}(\tilde{\mathbf{B}}) \\
&= \mathbf{V}_{\boldsymbol{\xi}}\mathbf{B}\mathbf{V}_{\boldsymbol{\eta}}^{T} - (\mathbf{V}_{\boldsymbol{\xi}}\mathbf{Z}_{\xi}\mathbf{V}_{\boldsymbol{\xi}}^{-1})(\mathbf{V}_{\boldsymbol{\xi}}\mathbf{B}\mathbf{V}_{\boldsymbol{\eta}}^{T})(\mathbf{V}_{\boldsymbol{\eta}}^{-T}\mathbf{Z}_{\eta}^{T}\mathbf{V}_{\boldsymbol{\eta}}^{T}) \\
&= \mathbf{V}_{\boldsymbol{\xi}}\left(\mathbf{B} - \mathbf{Z}_{\xi}\mathbf{B}\mathbf{Z}_{\eta}^{T}\right)\mathbf{V}_{\boldsymbol{\eta}}^{T} \\
&= \mathbf{V}_{\boldsymbol{\xi}}\Delta_{\mathbf{Z}_{\xi},\mathbf{Z}_{\eta}^{T}}(\mathbf{B})\mathbf{V}_{\boldsymbol{\eta}}^{T} \\
&= -\mathbf{V}_{\boldsymbol{\xi}}\nabla_{\mathbf{Z}_{\xi},\mathbf{Z}_{1/\eta}}(\mathbf{B})\mathbf{Z}_{\eta}^{T}\mathbf{V}_{\boldsymbol{\eta}}^{T} \\
&= \underbrace{(-\mathbf{V}_{\boldsymbol{\xi}}\mathbf{P})}_{\triangleq\tilde{\mathbf{P}}\in\mathbb{C}^{M_2\times R}}\underbrace{(\mathbf{V}_{\boldsymbol{\eta}}\mathbf{Z}_{\eta}\mathbf{Q})^{T}}_{\triangleq\tilde{\mathbf{Q}}^{T}\in\mathbb{C}^{R\times M_1}} \\
&= \tilde{\mathbf{P}}\tilde{\mathbf{Q}}^{T},
\end{aligned} \tag{F.47}$$

where in the last line we have used the fact that $\Delta_{\mathbf{Z}_{\xi},\mathbf{Z}_{\eta}^{T}}(\mathbf{B}) = -\nabla_{\mathbf{Z}_{\xi},\mathbf{Z}_{1/\eta}}(\mathbf{B})\mathbf{Z}_{\eta}^{T}$ (see Eq. (D.13)). On the other hand, by the definition of the Stein displacement operator, one has

$$[\Delta_{\mathbf{D}_{\boldsymbol{\xi}},\mathbf{D}_{\boldsymbol{\eta}}}(\tilde{\mathbf{B}})]_{m_2,m_1} = (1-\xi_{m_2}\eta_{m_1})[\tilde{\mathbf{B}}]_{m_2,m_1}, \tag{F.48}$$

for each pair (m_2, m_1) within the set $\mathcal{M}_2 \times \mathcal{M}_1$. Thus, by using Eq. (F.47), we get

$$[\tilde{\mathbf{B}}]_{m_2,m_1} = \frac{[\tilde{\mathbf{P}}\tilde{\mathbf{Q}}^{T}]_{m_2,m_1}}{1-\xi_{m_2}\eta_{m_1}} = \sum_{r=1}^{R}\frac{[\tilde{\mathbf{p}}_r\tilde{\mathbf{q}}_r^{T}]_{m_2,m_1}}{1-\xi_{m_2}\eta_{m_1}},\ \forall(m_2,m_1)\in\mathcal{M}_2\times\mathcal{M}_1. \tag{F.49}$$

Note that the term $1/(1-\xi_{m_2}\eta_{m_1})$ appears in all of the components of the above summation. It is therefore convenient to verify whether this term can be efficiently decomposed. We know that $\xi_{m_2} = \xi_0 W_{M_2}^{m_2}$ is an M_2th root of ξ, for all $m_2 \in \mathcal{M}_2$, whereas $\eta_{m_1} = \eta_0 W_{M_1}^{m_1}$ is an M_1th root of η, for all $m_1 \in \mathcal{M}_1$. From Remark 2 in Chapter 3 of [23], we also know that

$$\mathbf{V}_{\boldsymbol{\xi}} = \sqrt{M_2}\mathbf{W}_{M_2}\mathrm{diag}\{\xi_0^{m_2}\}_{m_2=0}^{M_2-1}, \tag{F.50}$$

$$\mathbf{V}_{\boldsymbol{\eta}} = \sqrt{M_1}\mathbf{W}_{M_1}\mathrm{diag}\{\eta_0^{m_1}\}_{m_1=0}^{M_1-1}. \tag{F.51}$$

Now, let us compute the (m_2, m_1)th coefficient of the matrix

$\mathbf{V}_{\boldsymbol{\xi}} \left[\mathbf{I}_{M_2} \;\; \mathbf{0}_{M_2 \times (M_1 - M_2)} \right] \mathbf{V}_{\boldsymbol{\eta}}^T$:

$$\begin{aligned}
\left[\mathbf{V}_{\boldsymbol{\xi}} \left[\mathbf{I}_{M_2} \;\; \mathbf{0}_{M_2 \times (M_1 - M_2)} \right] \mathbf{V}_{\boldsymbol{\eta}}^T \right]_{m_2, m_1} &= \sqrt{M_1 M_2} \left[\mathbf{W}_{M_2} \left[\operatorname{diag}\{(\xi_0 \eta_0)^{m_2}\}_{m_2=0}^{M_2-1} \;\; \mathbf{0}_{M_2 \times (M_1 - M_2)} \right] \times \right. \\
&\quad \left. \times \; \mathbf{W}_{M_1}^T \right]_{m_2, m_1} \\
&= \sum_{m=0}^{M_2-1} \xi_0^m \eta_0^m W_{M_2}^{m_2 m} W_{M_1}^{m_1 m} \\
&= \frac{1 - (\xi_0 \eta_0 W_{M_2}^{m_2} W_{M_1}^{m_1})^{M_2}}{1 - (\xi_0 W_{M_2}^{m_2})(\eta_0 W_{M_1}^{m_1})} \\
&= \frac{1 - \xi \eta_{m_1}^{M_2}}{1 - \xi_{m_2} \eta_{m_1}}. \qquad \text{(F.52)}
\end{aligned}$$

Hence, if we assume that $1 - \xi \eta_{m_1}^{M_2} \neq 0$, the above expressions imply

$$\frac{1}{1 - \xi_{m_2} \eta_{m_1}} = \frac{\sqrt{M_1 M_2}}{1 - \xi \eta_{m_1}^{M_2}} \left[\mathbf{W}_{M_2} \left[\operatorname{diag}\{(\xi_0 \eta_0)^{m_2}\}_{m_2=0}^{M_2-1} \;\; \mathbf{0}_{M_2 \times (M_1 - M_2)} \right] \mathbf{W}_{M_1}^T \right]_{m_2, m_1}. \qquad \text{(F.53)}$$

By using Eq. (F.53), we can rewrite Eq. (F.49) as follows

$$\begin{aligned}
\tilde{\mathbf{B}} &= \mathbf{V}_{\boldsymbol{\xi}} \mathbf{B} \mathbf{V}_{\boldsymbol{\eta}}^T \\
&= \left(\sum_{r=1}^{R} \mathbf{D}_{\tilde{\mathbf{p}}_r} \mathbf{W}_{M_2} \left[\operatorname{diag}\{(\xi_0 \eta_0)^{m_2}\}_{m_2=0}^{M_2-1} \quad \mathbf{0}_{M_2 \times (M_1 - M_2)} \right] \mathbf{W}_{M_1} \times \right. \\
&\quad \left. \times \operatorname{diag} \left\{ \frac{\sqrt{M_1 M_2}}{1 - \xi \eta_{m_1}^{M_2}} \right\}_{m_1=0}^{M_1-1} \right) \mathbf{D}_{\tilde{\mathbf{q}}_r} \\
&= \sqrt{M_1 M_2} \sum_{r=1}^{R} \mathbf{D}_{\bar{\mathbf{p}}_r} \mathbf{W}_{M_2} \left[\operatorname{diag}\{(\xi_0 \eta_0)^{m_2}\}_{m_2=0}^{M_2-1} \quad \mathbf{0}_{M_2 \times (M_1 - M_2)} \right] \mathbf{W}_{M_1} \mathbf{D}_{\bar{\mathbf{q}}_r}, \qquad \text{(F.54)}
\end{aligned}$$

in which, by using Eq. (F.47), we have

$$\bar{\mathbf{P}} = [\, \bar{\mathbf{p}}_1 \;\; \cdots \;\; \bar{\mathbf{p}}_R \,] = \tilde{\mathbf{P}} = -\mathbf{V}_{\boldsymbol{\xi}} \mathbf{P} \qquad \text{(F.55)}$$

$$\begin{aligned}
\bar{\mathbf{Q}} = [\, \bar{\mathbf{q}}_1 \;\; \cdots \;\; \bar{\mathbf{q}}_R \,] &= \left(\operatorname{diag} \left\{ \frac{1}{1 - \xi \eta_{m_1}^{M_2}} \right\}_{m_1=0}^{M_1-1} \right) \tilde{\mathbf{Q}} \\
&= \left(\operatorname{diag} \left\{ \frac{1}{1 - \xi \eta_{m_1}^{M_2}} \right\}_{m_1=0}^{M_1-1} \right) \mathbf{V}_{\boldsymbol{\eta}} \mathbf{Z}_{\eta} \mathbf{Q}. \qquad \text{(F.56)}
\end{aligned}$$

□

F.3 DFT-Based Superfast Transceivers with Reduced Redundancy

This section presents the proposals of new transceivers with reduced redundancy that employ FFT-based algorithms. We shall tailor the previously proposed efficient decompositions of Bezoutian matrices (see Section F.2) to the particular cases of MMSE and ZF receiver matrices. As a result, a novel family of superfast multicarrier and single-carrier linear transceivers are proposed with their respective structures.

As we have already pointed out in Subsection F.2.2, the transmitter-independent receiver matrix $\mathbf{K}$ is a Bezoutian matrix for both MMSE- and ZF-based solutions. Thus, if one carefully chooses both parameters ξ and η, then one can apply Theorem 12 in order to design the referred matrices. Indeed, let us assume that $\xi = 1$ and $\eta = \mathrm{e}^{-\jmath\frac{\pi}{M}}$. Thus, by considering the compressed form of the Bezoutian matrix $\mathbf{K}$ described in Theorem 11 for the MMSE solution or in Corollary 5 for the ZF solution, one can use Theorem 12 to demonstrate the following general result.

Theorem 13. *The transmitter-independent receiver matrix* $\mathbf{K}$ *can be represented as follows:*

$$\mathbf{K} = \mathbf{W}_M^H \left[\sum_{r=1}^{4} \mathbf{D}_{\bar{\mathbf{p}}_r} \mathbf{W}_M \begin{bmatrix} \mathbf{D}_M & \mathbf{0}_{M\times(2K-L)} \end{bmatrix} \mathbf{W}_{(M+2K-L)} \mathbf{D}_{\bar{\mathbf{q}}_r} \right] \mathbf{W}_{(M+2K-L)}^H \mathbf{D}_{(M+2K-L)}^H, \tag{F.57}$$

in which $\mathbf{D}_N \triangleq \mathrm{diag}\{\mathrm{e}^{\frac{-\jmath\pi n}{MN}}\}_{n=0}^{N-1}$ *is an* $N \times N$ *diagonal matrix, for any given natural number* N*. The pair of matrices* $(\bar{\mathbf{P}}, \bar{\mathbf{Q}}) \in \mathbb{C}^{M\times 4} \times \mathbb{C}^{(M+2K-L)\times 4}$ *can be determined using Theorem 12 along with either Theorem 11 (for the MMSE-based system) or Corollary 5 (for the ZF-based system), considering that* $\xi = 1$ *and* $\eta = \mathrm{e}^{-\jmath\frac{\pi}{M}}$*.*

Proof. From either Theorem 11 or Corollary 5, note that $\mathbf{K}$ is an $M \times (M+2K-L)$ Bezoutian matrix, where $2K \geq L$. Thus, Theorem 13 is a straightforward consequence of Theorem 12. Indeed, if one chooses $\xi = 1$ and $\eta = \mathrm{e}^{-\jmath\frac{\pi}{M}}$, then

$$\xi_0 = |\xi|^{1/M} \mathrm{e}^{\jmath\frac{\angle\xi}{M}} = 1 \times \mathrm{e}^0 = 1 \tag{F.58}$$

and

$$\eta_0 = |\eta|^{1/(M+2K-L)} \mathrm{e}^{\jmath\frac{\angle\eta}{(M+2K-L)}} = 1 \times \mathrm{e}^{\frac{-\jmath\pi}{M(M+2K-L)}} = \mathrm{e}^{\frac{-\jmath\pi}{M(M+2K-L)}}. \tag{F.59}$$

These facts imply that

$$\mathbf{V}_{\boldsymbol{\xi}} = \sqrt{M}\mathbf{W}_M, \tag{F.60}$$

whereas

$$\mathbf{V}_{\boldsymbol{\eta}} = \sqrt{M+2K-L} \times \mathbf{W}_{(M+2K-L)} \text{diag}\{\mathrm{e}^{\frac{-\jmath\pi m}{M(M+2K-L)}}\}_{m=0}^{(M+2K-L-1)}. \tag{F.61}$$

We can therefore apply the decomposition presented in Theorem 12 to obtain the desired result.

Note that the choices of ξ and η were quite arbitrary. We have chosen $\xi = 1$, since we would like to cancel out the last IDFT matrix employed at the receiver end in the case of multicarrier systems. Indeed, in the multicarrier systems, the receiver matrix is $\mathbf{G}_0 = \mathbf{W}_M\mathbf{K}$. If $\xi \neq 1$, one would not be able to cancel out the DFT matrix with the last IDFT matrix presented in the decomposition of $\mathbf{K}$. After fixing $\xi = 1$, we have chosen η in such a way that $1 - \xi\eta_m^M = 1 - \eta_m^M \neq 0$, for all m within the set $\{0, 1, \cdots, M+2K-L-1\}$. There are infinite possible choices for η and we have arbitrarily chosen $\eta = \mathrm{e}^{-\jmath\frac{\pi}{M}}$ (when M is very large, then this choice yields $\eta \approx 1$). Note that, for this choice of η,

$$\begin{aligned}
\eta_m^M &= (\eta_0 W_{(M+2K-L)}^m)^M \\
&= \mathrm{e}^{\frac{-\jmath\pi}{(M+2K-L)}} \mathrm{e}^{\frac{-\jmath 2\pi m M}{(M+2K-L)}} \\
&= \mathrm{e}^{\frac{-\jmath\pi(2mM+1)}{(M+2K-L)}} \\
&\neq 1,
\end{aligned} \tag{F.62}$$

for all m within the set $\{0, 1, \cdots, M+2K-L-1\}$, since $\frac{2mM+1}{M+2K-L}$ is not an even number. □

A multicarrier system can be designed by setting $\mathbf{F}_0 = \mathbf{W}_M^H$ and $\mathbf{G}_0 = \mathbf{F}_0^{-1}\mathbf{K} = \mathbf{W}_M\mathbf{K}$, yielding

$$\mathbf{G}_0 = \left[\sum_{r=1}^{4} \mathbf{D}_{\bar{\mathbf{p}}_r} \mathbf{W}_M \begin{bmatrix} \mathbf{D}_M & \mathbf{0}_{M\times(2K-L)} \end{bmatrix} \mathbf{W}_{(M+2K-L)} \mathbf{D}_{\bar{\mathbf{q}}_r}\right] \mathbf{W}_{(M+2K-L)}^H \mathbf{D}_{(M+2K-L)}^H, \tag{F.63}$$

where the definitions of the vectors $\bar{\mathbf{p}}_r$ and $\bar{\mathbf{q}}_r$ depend on whether the ZF or the MMSE is chosen (see Theorem 11 or Corollary 5). In any case, the resulting multicarrier structure is depicted in Figure F.1.

By comparing Figure F.1 with the scheme depicted in Figure D.2 of Chapter D, one can observe that the reduced-redundancy transceivers always use four equalizer branches (instead of two branches in the minimum-redundancy ZF system first proposed in [23]), no matter whether the ZF or MMSE solution is chosen. Another important difference between those schemes is the fact that reduced-redundancy systems require two distinct DFT sizes, instead of only one size as in Figure D.2

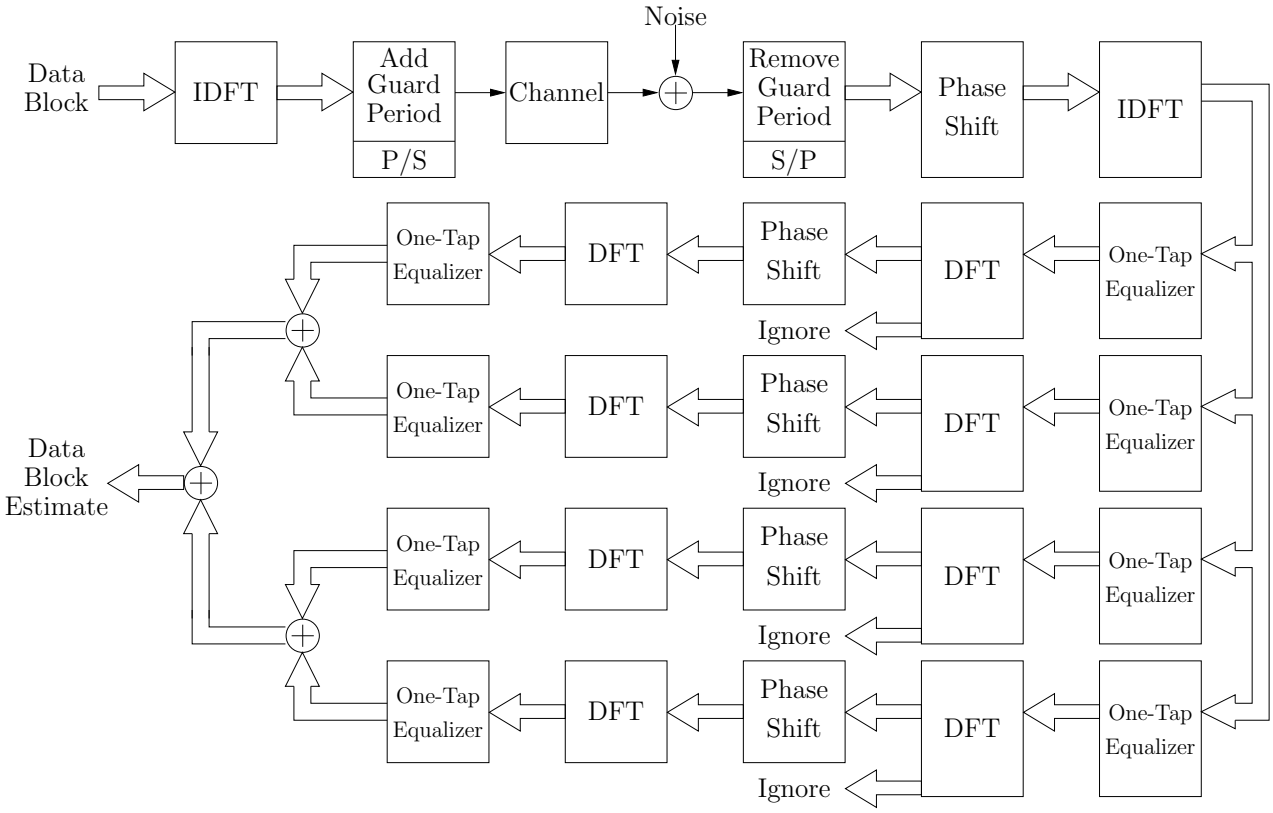

Figure F.1: DFT-based multicarrier reduced-redundancy block transceiver (MC-RRBT).

of Chapter D. Nevertheless, it is possible to verify that the structure depicted in Figure F.1 coincides with the scheme in Figure D.2 of Chapter D when minimum-redundancy is employed.

A single-carrier system can be designed by setting $\mathbf{F}_0 = \mathbf{I}_M$ and $\mathbf{G}_0 = \mathbf{F}_0^{-1}\mathbf{K} = \mathbf{K}$, yielding

$$\mathbf{G}_0 = \mathbf{W}_M^H \left[\sum_{r=1}^{4} \mathbf{D}_{\bar{\mathbf{p}}_r} \mathbf{W}_M \begin{bmatrix} \mathbf{D}_M & \mathbf{0}_{M\times(2K-L)} \end{bmatrix} \mathbf{W}_{(M+2K-L)} \mathbf{D}_{\bar{\mathbf{q}}_r} \right] \mathbf{W}_{(M+2K-L)}^H \mathbf{D}_{(M+2K-L)}^H, \tag{F.64}$$

in which, once again, the definitions of the vectors $\bar{\mathbf{p}}_r$ and $\bar{\mathbf{q}}_r$ depend on whether the ZF or the MMSE is chosen.

The superfast multicarrier and single-carrier proposals of this chapter yield an additional degree of freedom in the ZP-ZJ-based transmissions, for the amount of redundancy can vary from the minimum value, $\lceil L/2 \rceil$, to the limit value, L. Nonetheless, one must deal with two distinct DFT sizes, M and $M+2K-L$. When M is a power of 2, then $M+2K-L$ is not necessarily a power of two. Thus, a radix-2 FFT algorithm could only be applied to implement those DFTs with size M. As for the DFTs with size $M+2K-L$, one could implement the operations using a radix-2

FFT of size $2M$ (which is assumed to be larger than $M + 2K - L$), along with zero-padding of the related signals. Another possibility is to choose the amount of redundant elements in such a way that $M+2K-L$ can be decomposed as a product of small prime numbers, leading to fast implementations as well. We shall address this topic in future works.

F.3.1 Complexity Comparisons

Let us assume that an FFT algorithm requires $\frac{M}{2}\log_2 M - \frac{3M}{2} + 2$ complex multiplications [26] for size-M data blocks. In addition, we shall assume that $L = \frac{M}{4}$, as performed in [37]. Thus, it is possible to derive the results of Table F.1, which contains the number of complex-valued multiplications required by the proposed multicarrier reduced-redundancy system, as well as both the overlap-and-add (OLA) and fast proposals of zero-padded OFDM systems described in [37].

In the MC-RRBT, it is possible to implement part of the receiver side using parallel processing (see Figure F.1). In this case, if we consider that the required time to perform a generic complex-valued multiplication is T seconds, then the MC-RRBT requires $T(3M\log_2 M + 2(2K - L) + 8)$ seconds, whereas the ZP-OFDM-OLA requires $T(M\log_2 M - 2M + 4)$ seconds and ZP-OFDM-FAST requires $T\left(\frac{5M}{4}\log_2 M - 5M + 20\right)$ seconds.

We have assumed that the pair of matrices $(\mathbf{P}, \mathbf{Q})$ is known. In fact, these matrices completely define the reduced-redundancy equalizers, since they are the only ones that contain information about the channel. These matrices, however, must be previously computed in the so-called *receiver-design stage*, which can be performed using up to $\mathcal{O}(M\log_2^2 M)$ operations. Besides, there are many applications in which the receiver-design problem is not frequently solved. In wireline communications systems, the channel model is not updated so often. In this case, the main problem is the *equalization* itself.

F.4 Simulation Results

This section aims at evaluating the performance of the transceivers with reduced redundancy in some particular scenarios. The figures of merit adopted here are the uncoded BER and the throughput.

In [23], we have shown that minimum-redundancy systems may significantly improve the throughput performance of multicarrier and single-carrier transmissions. Nevertheless, we have pointed out in [23] that the minimum-redundancy transceivers may incur in high noise enhancements induced by the "inversion" of the Toeplitz effective channel matrix in the equalization process. In our first example here, we

Table F.1: Number of complex-valued multiplications.

System	Arithmetic Complexity
ZP-OFDM-OLA	$M \log_2 M - 2M + 4$
ZP-OFDM-FAST	$\frac{5M}{4} \log_2 M - 5M + 20$
MC-RRBT	$\frac{15M}{2} \log_2 M - \frac{9M}{2} + 20 + 5(2K - L)$

chose a fourth-order channel model (see [41], pp. 306–307)

$$H_{\mathrm{A}}(z) \triangleq 0.1659 + 0.3045z^{-1} - 0.1159z^{-2} - 0.0733z^{-3} - 0.0015z^{-4} \qquad \text{(F.65)}$$

for which the performance of the minimum-redundancy systems proposed in [23] is poor. For this channel (Channel A), we transmit 50,000 data blocks carrying $M = 16$ symbols of a 64-QAM constellation ($b = 6$ bits per symbol). In fact, each data block stems from 48 data bits that, after channel coding, yield 96 bits to be baseband modulated. The channel coding has constraint length 7, code rate $r_c = 1/2$, and octal generators $\mathbf{g_0} \triangleq [\mathbf{133}]$ and $\mathbf{g_1} \triangleq [\mathbf{165}]$ [74]. We assume that the sample frequency is $f_s = 100$ MHz.

Figures F.2, F.3, F.4, F.5 depict the obtained uncoded-BER results. For multicarrier transmissions, we compare four different transceivers, as shown in Figure F.2 and Figure F.3: the ZP-OFDM-OLA and the three possible multicarrier reduced-redundancy block transceivers (MC-RRBT). There are three possible MC-RRBT systems since the amount of redundant elements respects the inequality $\frac{L}{2} \leq K \leq L$ (i.e., $K \in \{2, 3, 4\}$). In addition, for single-carrier transmissions, we also compare four different transceivers, as shown in Figure F.4 and Figure F.5: the traditional SC-FD and the three possible single-carrier reduced-redundancy block transceivers (SC-RRBT). From Figure F.2, one can observe that the minimum-redundancy multicarrier system (MC-RRBT for $K = 2$) that employs a ZF equalizer is not able to produce a reliable estimate for the transmitted bits. However, if just one additional redundant element is included in the transmission, the resulting MC-RRBT system ($K = 3$) is enough to outperform the ZF-OFDM. Moreover, adding another redundant element in the transmission (MC-RRBT for $K = 4$) does not contribute to substantially improving the uncoded-BER performance in this case. Similar conclusions can be drawn from the analyses of Figure F.3, Figure F.4, and Figure F.5.

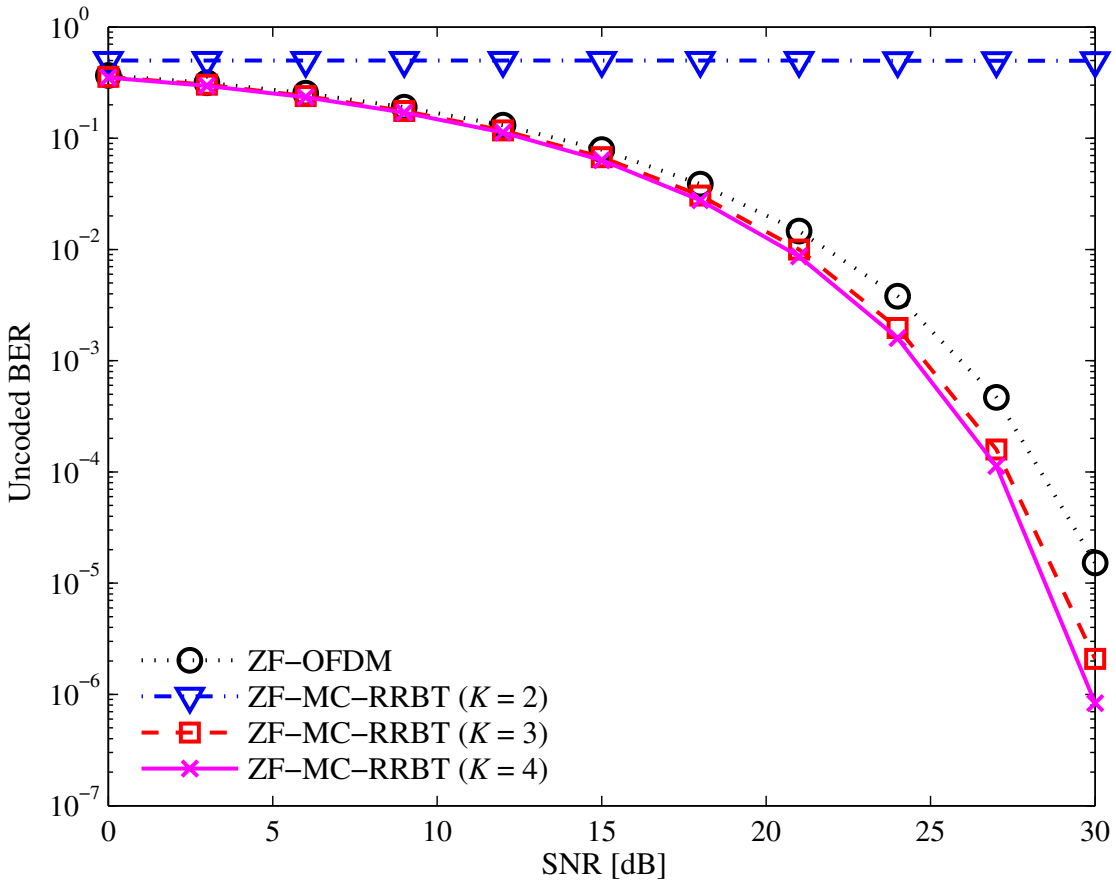

Figure F.2: Uncoded BER as a function of SNR [dB] for Channel A, considering ZF-based multicarrier transmissions employing DFT.

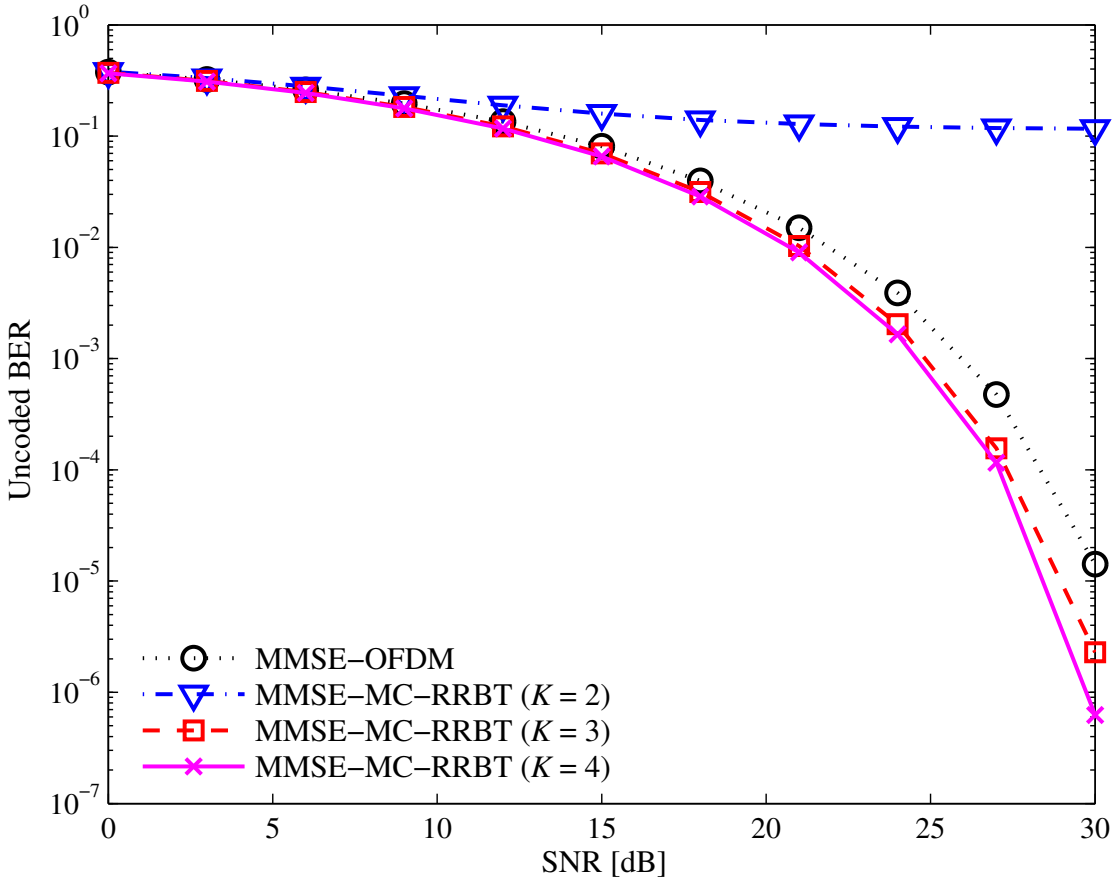

Figure F.3: Uncoded BER as a function of SNR [dB] for Channel A, considering MMSE-based multicarrier transmissions employing DFT.

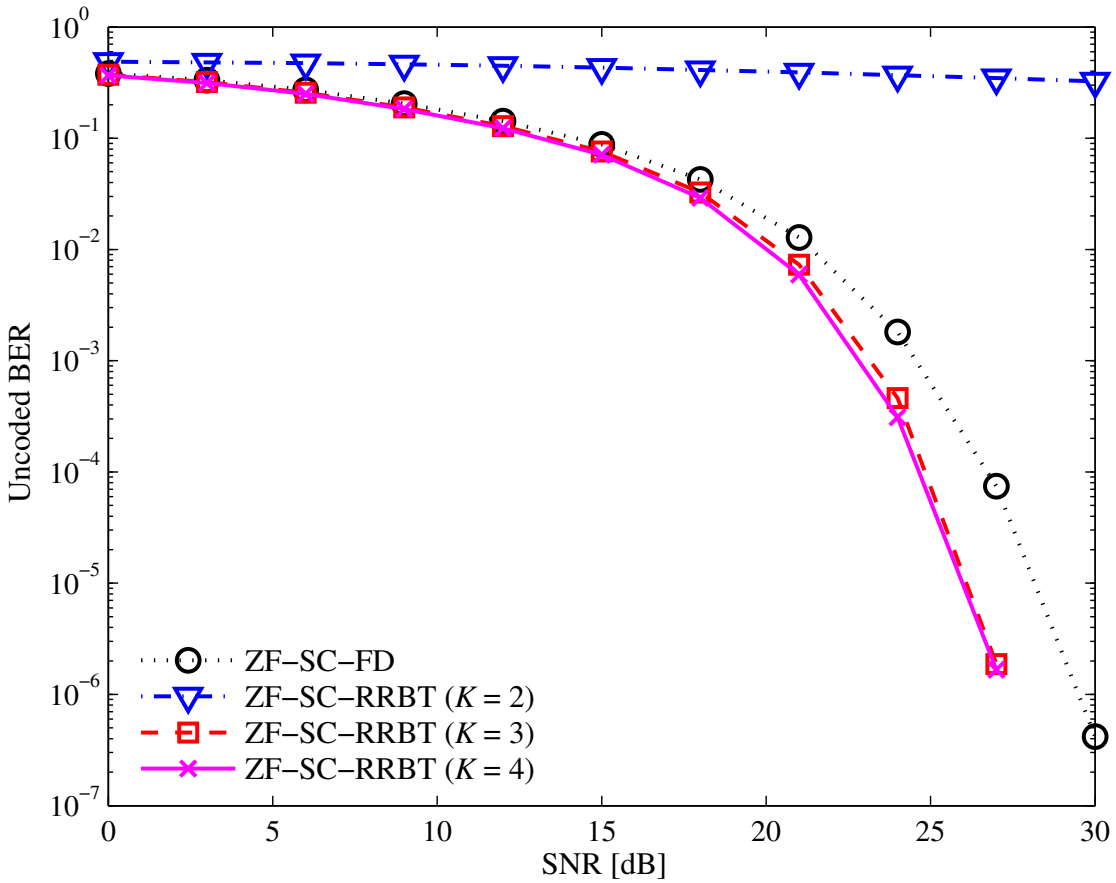

Figure F.4: Uncoded BER as a function of SNR [dB] for Channel A, considering ZF-based single-carrier transmissions employing DFT.

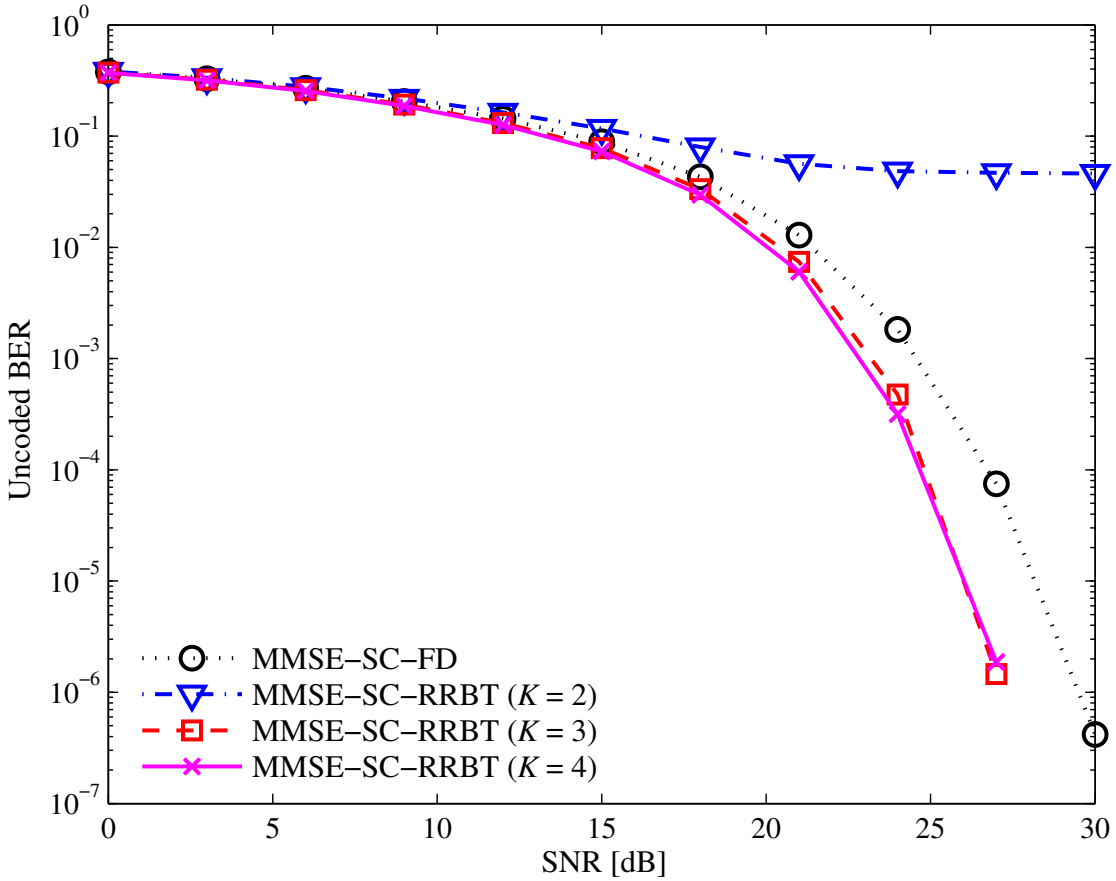

Figure F.5: Uncoded BER as a function of SNR [dB] for Channel A, considering MMSE-based single-carrier transmissions employing DFT.

Figures F.6, F.7, F.8, F.9 depict the obtained throughput results. Figure F.6 shows considerable throughput gains of using, for instance, an MC-RRBT system with $K = 3$, as compared to the traditional OFDM system. One should bear in mind that such throughput gains are attained without increasing substantially the computational complexity related to OFDM-based systems. Moreover, the MC-RRBT system with $K = 3$ also outperforms the MC-RRBT system with $K = 4$ in terms of throughput, especially for large SNR values. This occurs since both reduced-redundancy systems have similar uncoded-BER performances, but the MC-RRBT system with $K = 3$ saves bandwidth as compared to MC-RRBT system with $K = 4$. Similar conclusions can be drawn from the analyses of Figure F.7, Figure F.8, and Figure F.9.

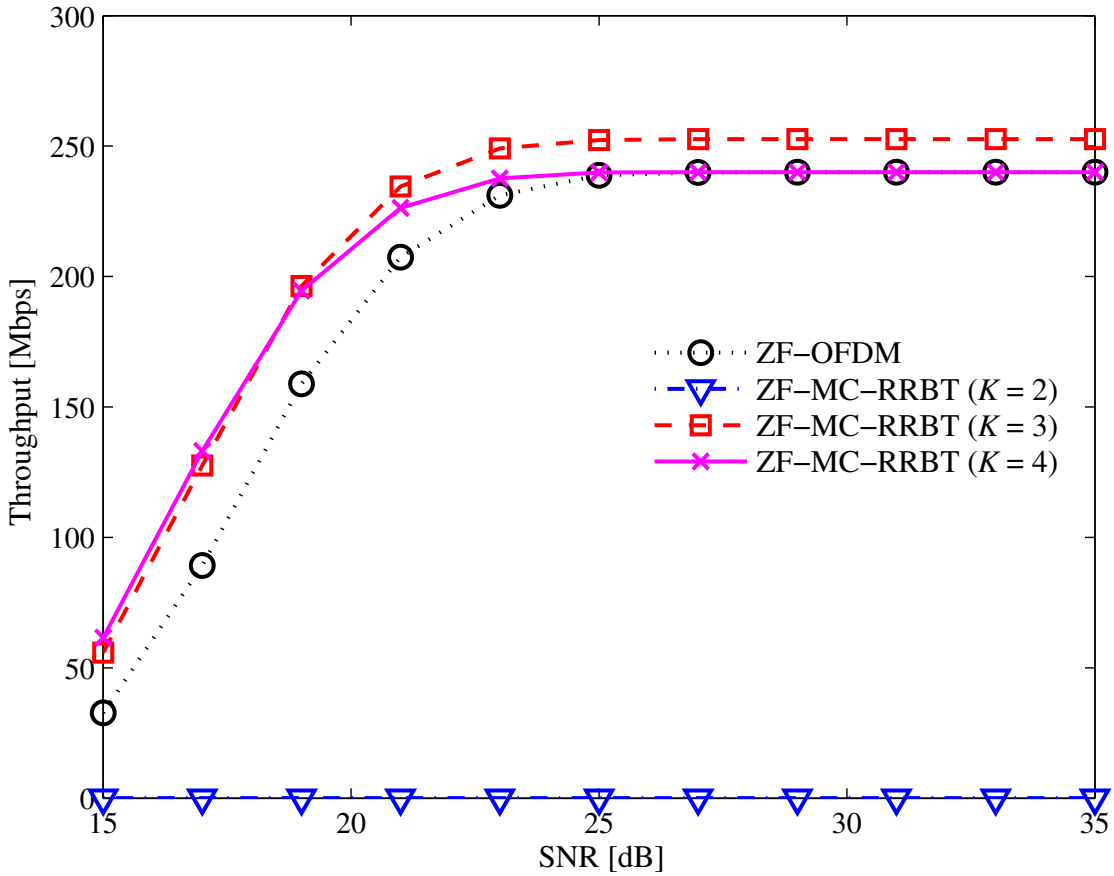

Figure F.6: Throughput [Mbps] as a function of SNR [dB] for Channel A, considering ZF-based multicarrier transmissions employing DFT.

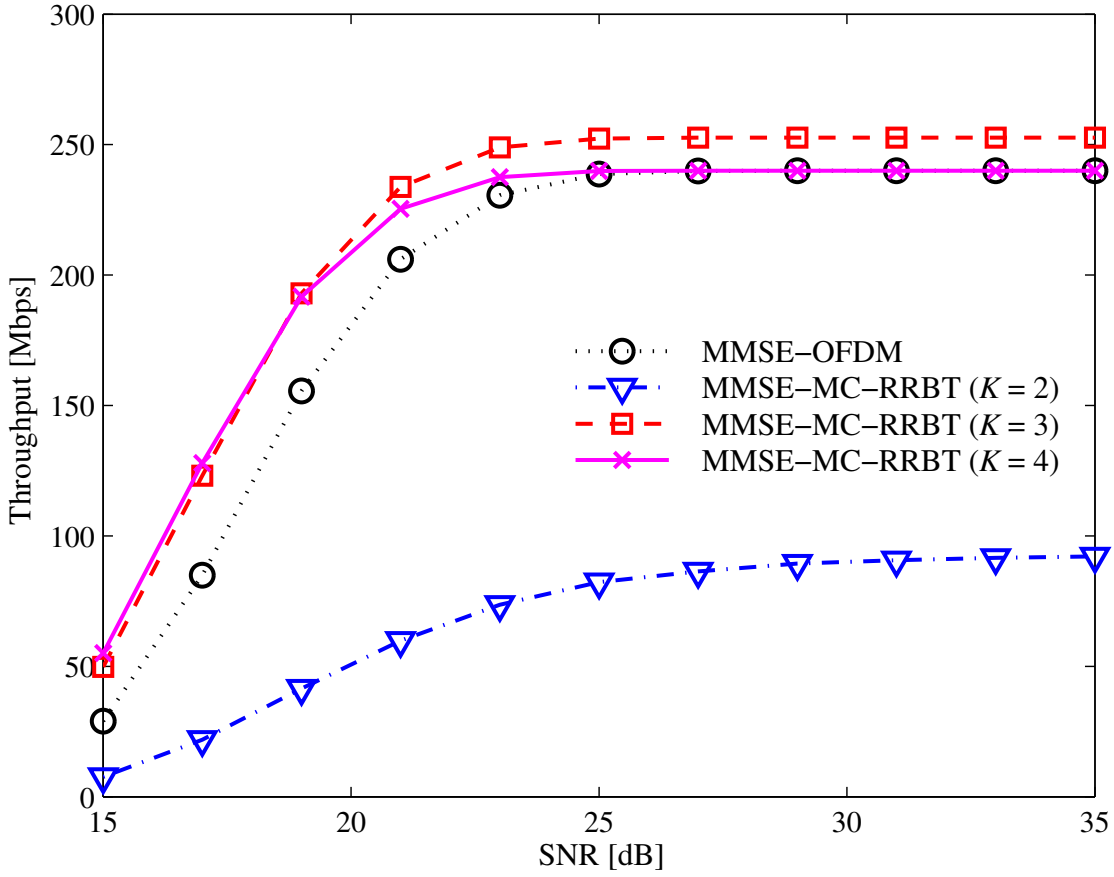

Figure F.7: Throughput [Mbps] as a function of SNR [dB] for Channel A, considering MMSE-based multicarrier transmissions employing DFT.

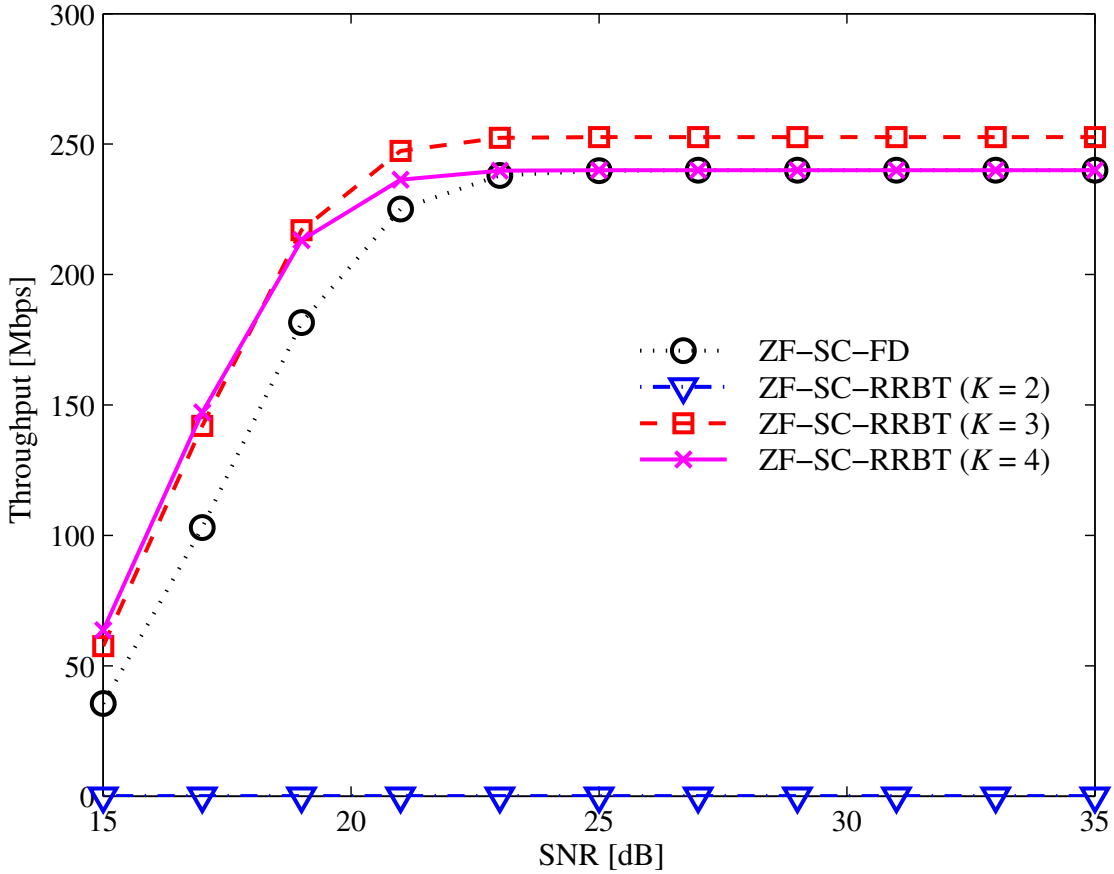

Figure F.8: Throughput [Mbps] as a function of SNR [dB] for Channel A, considering ZF-based single-carrier transmissions employing DFT.

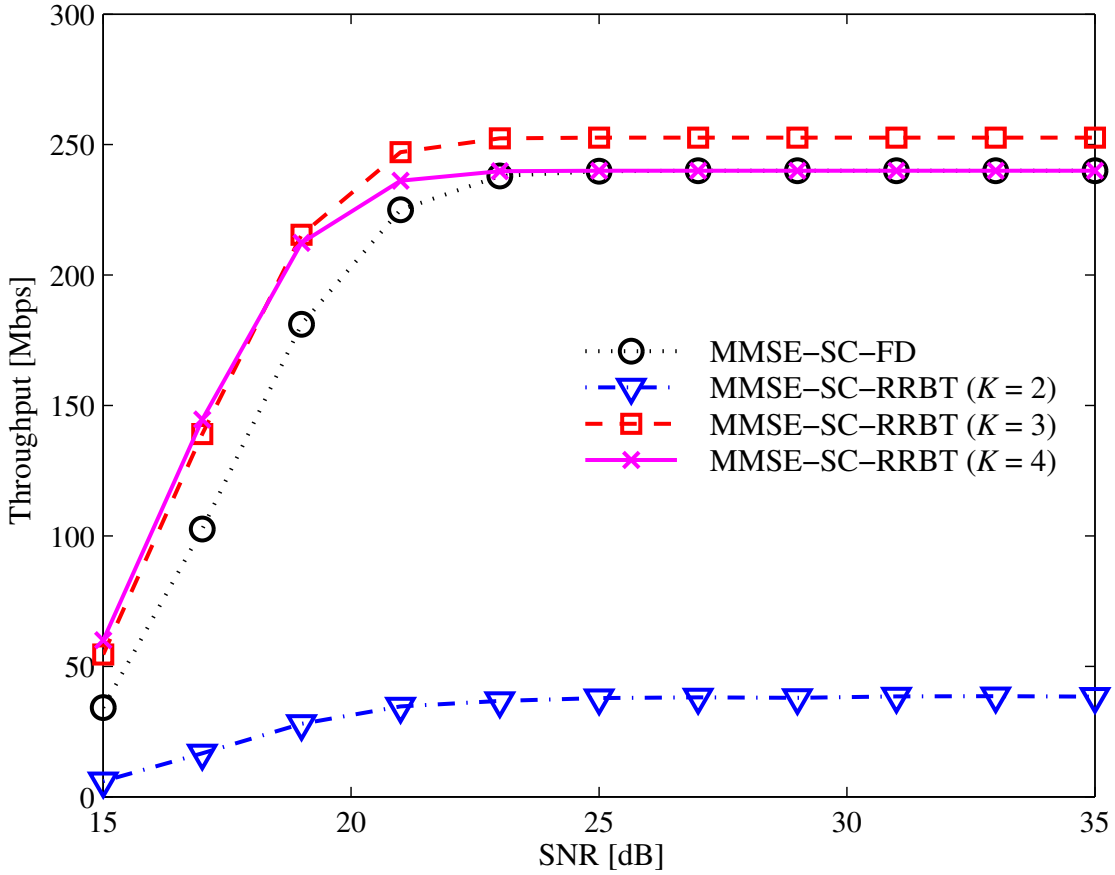

Figure F.9: Throughput [Mbps] as a function of SNR [dB] for Channel A, considering MMSE-based single-carrier transmissions employing DFT.

In our second experiment, we shall consider an FIR-channel model (Channel B) whose zeros are $0.8, -0.8, 0.5\jmath, -0.5\jmath$, and $-0.8\jmath$. The values of all simulation parameters are equal to the previous experiment, except for the fact that now $M = 32$, $b = 4$ (16-QAM constellation), and $L = 5$, which implies that $K \in \{3, 4, 5\}$. In addition, we only present the MMSE-based results for both multicarrier and single-carrier transmissions.

Figures F.10, F.11 contain the uncoded-BER and Figures F.12, F.13 contain the throughput results. For the multicarrier systems one can observe in Figure F.10 that neither MC-RRBT with $K = 3$ nor with MC-RRBT with $K = 4$ yield reliable data estimates. As can be verified in Figure F.12, it is much better to use the traditional OFDM system for this channel model when the SNR values are large, since the performances of both the ZP-OFDM-OLA and the proposed MC-RRBT with $K = 5$ are equivalent, but the ZP-OFDM-OLA performs less computations. An analogous observation also applies to the single-carrier case as seen in Figure F.11 and Figure F.13. The aim of this example is to show that the number of redundant elements required to yield a reliable transmission is strongly dependent on the type of channel. In this example, an additional redundant element (MC-RRBT with $K = 4$) is not enough to have good uncoded-BER and throughput performances, as in the experiment previously presented.

Note that, when the ZP-ZJ transceiver employs full redundancy ($K = 5$) in the transmission, the receiver defined in Eq. (D.4) is the well-known minimum norm ZF receiver [37]. Such type of transceiver enjoys several performance improvements as compared to ZP-OFDM-OLA and ZP-SC-FD-OLA, even though all of these transceivers transmit with the same amount of redundancy (see [37] for an in-depth description).

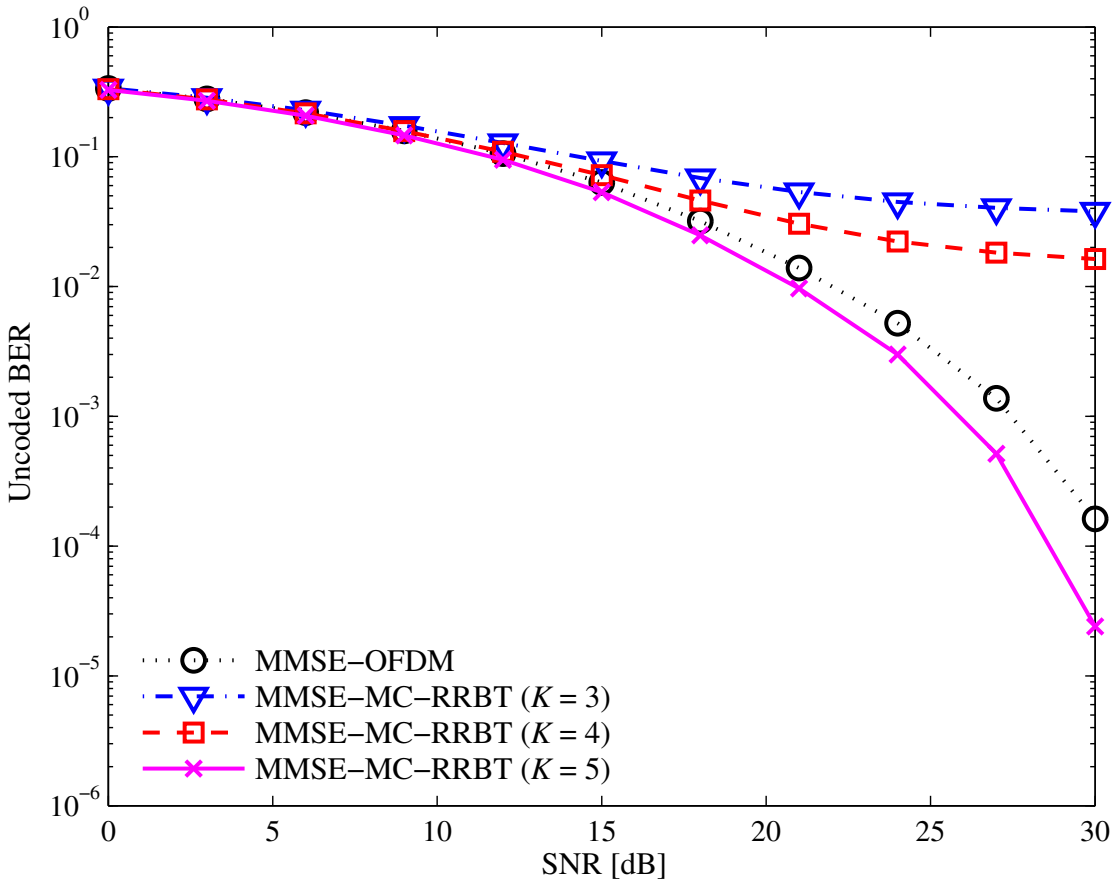

Figure F.10: Uncoded BER as a function of SNR [dB] for Channel B, considering MMSE-based multicarrier transmissions employing DFT.

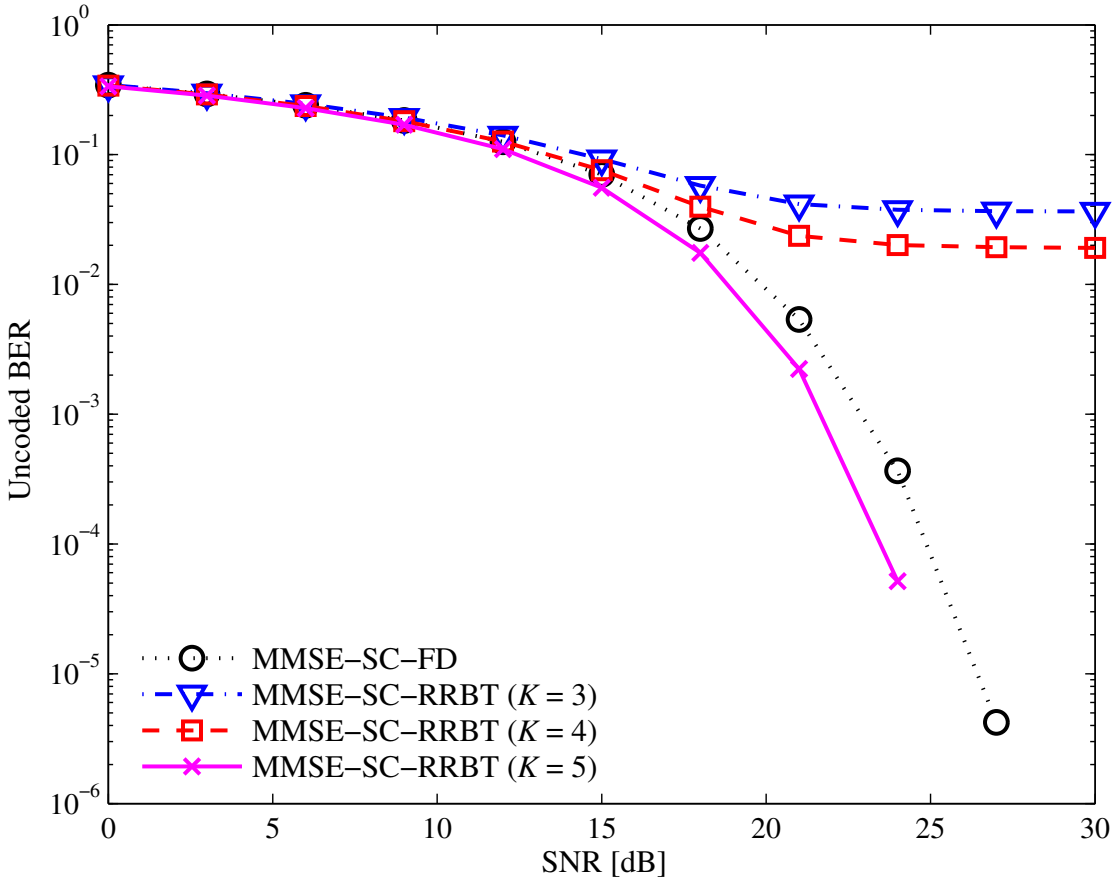

Figure F.11: Uncoded BER as a function of SNR [dB] for Channel B, considering MMSE-based single-carrier transmissions employing DFT.

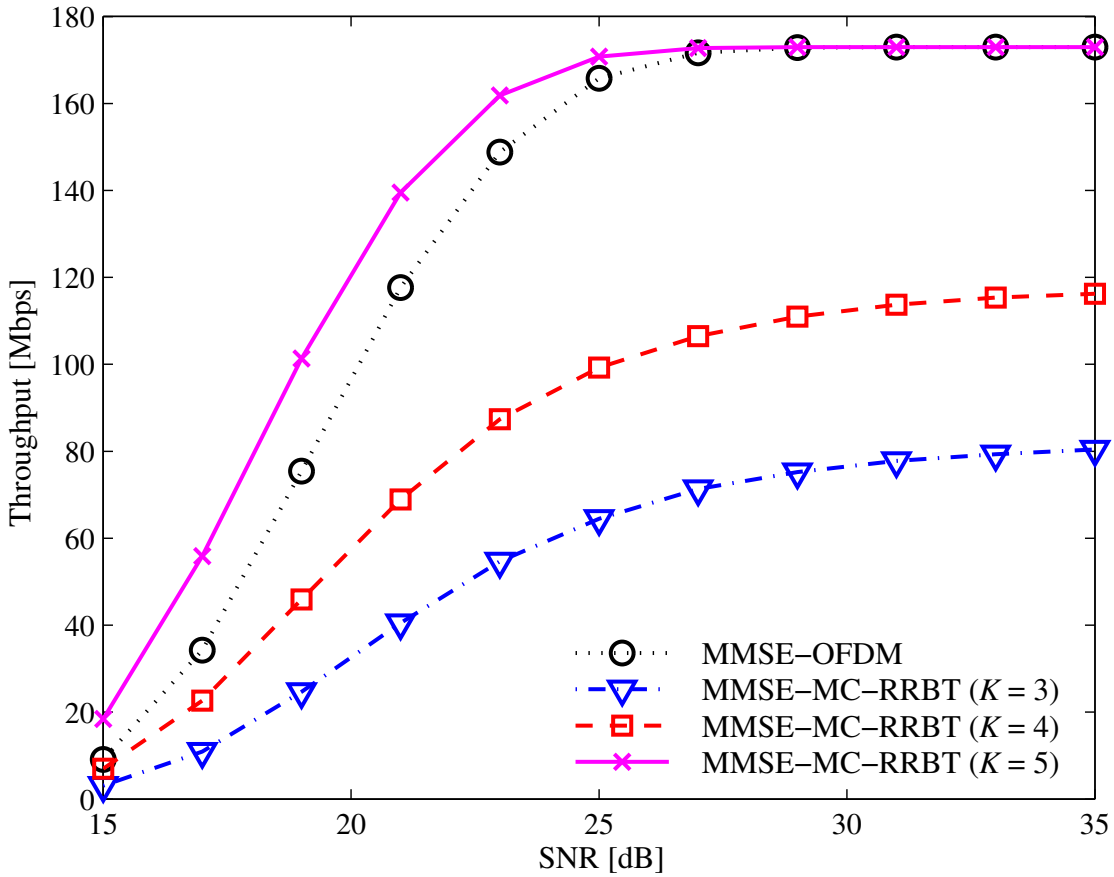

Figure F.12: Throughput [Mbps] as a function of SNR [dB] for Channel B, considering MMSE-based multicarrier transmissions employing DFT.

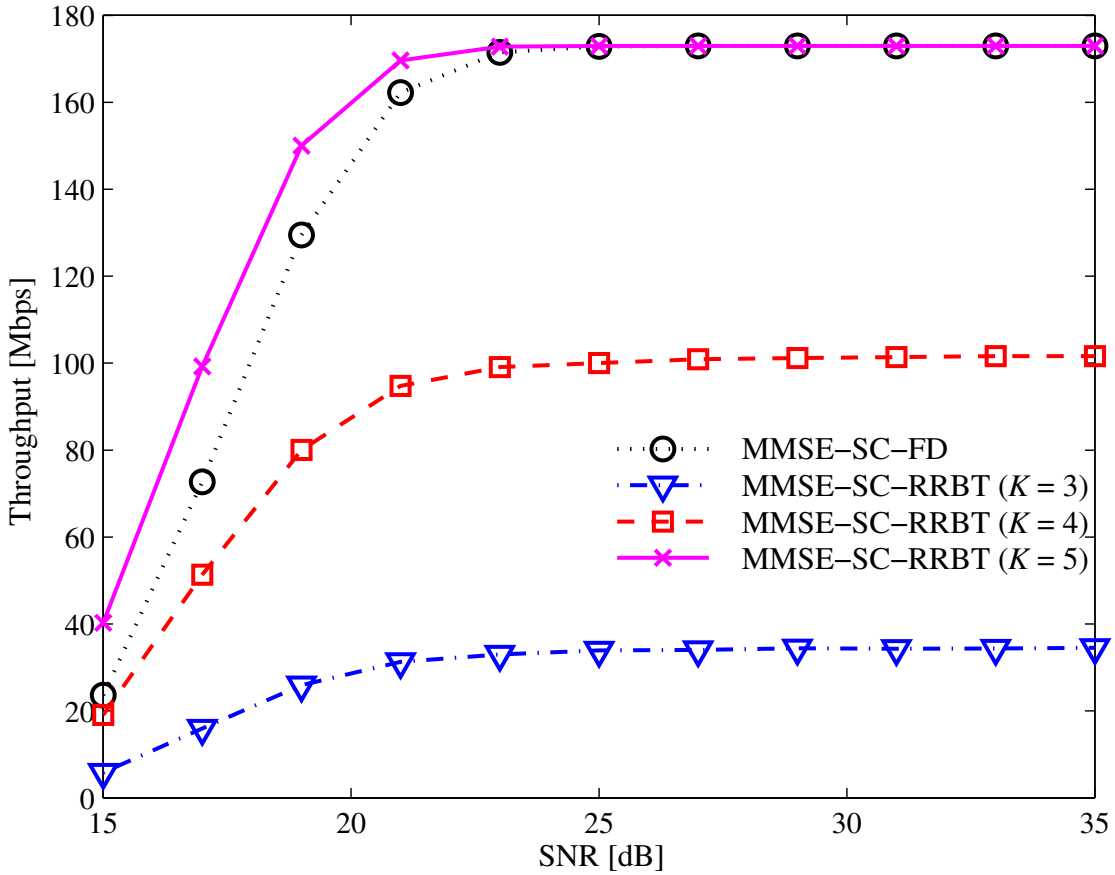

Figure F.13: Throughput [Mbps] as a function of SNR [dB] for Channel B, considering MMSE-based single-carrier transmissions employing DFT.

In our third example, we shall consider an FIR-channel model (Channel C) whose zeros are $0.999, -0.999, 0.7\jmath, -0.7\jmath$, and $-0.4\jmath$. This channel has zeros very close to the unit circle. Apart from the channel model, all simulation parameters are the same of the previous experiment. We therefore expect that the performances of the traditional OFDM and SC-FD systems should be rather poor. Figures F.14, F.15 depict the uncoded-BER and Figures F.16, F.17 depict the throughput results. One can observe that both the MC-RRBT and the SC-RRBT systems always outperform the traditional OFDM and SC-FD systems. Another important fact is that even though the uncoded-BER performance always improves as one increases the number of transmitted redundant elements, the throughput performance does not follow the same pattern. For example, for low SNR values, it is better to use a reduced-redundancy system that transmits with a larger amount of redundant elements, whereas for large SNR values, it is better to use a reduced-redundancy system that transmits with a smaller amount of redundant elements. Once again, it is important to highlight that the proposals of this chapter aim at showing how to transmit with a smaller amount of redundant elements while using superfast transforms and single-tap equalizers.

F.5 Concluding Remarks

In this chapter, we have proposed new linear time-invariant block-based transceivers with redundancies ranging from the minimum to the usual amount, which is in turn related to the channel-impulse response order. The proposals included practical solutions for multicarrier and single-carrier transceivers using varying redundancy. The transceivers ZF and MMSE solutions require only DFTs, inverse DFTs, and diagonal matrices, turning the new transceivers computationally efficient. The solutions were obtained by employing the framework of structured matrices using the concepts of Sylvester and Stein displacements. By using adequate displacement concepts applied to rectangular structured matrices we were able to derive the proposed solutions for the multicarrier and single-carrier block-based transceivers requiring redundancy ranging from the minimum to the channel order. Theoretical results have been derived proving for the first time that increase in the redundancy associated with zero-padding zero-jamming systems brings about performance benefits while decreasing bandwidth efficiency. In particular, for all proposed transceivers, by increasing the amount of redundancy we can witness a reduction in the average MSE as well as in the bit-error rate.

Simulations have confirmed these theoretical results, and have shown that the relative performance of the reduced-redundancy transceivers is highly dependent on the channel model characteristics. We believe that the results of this chapter answer,

for the first time, several open questions related to the insertion of redundancy in block-based transceivers.

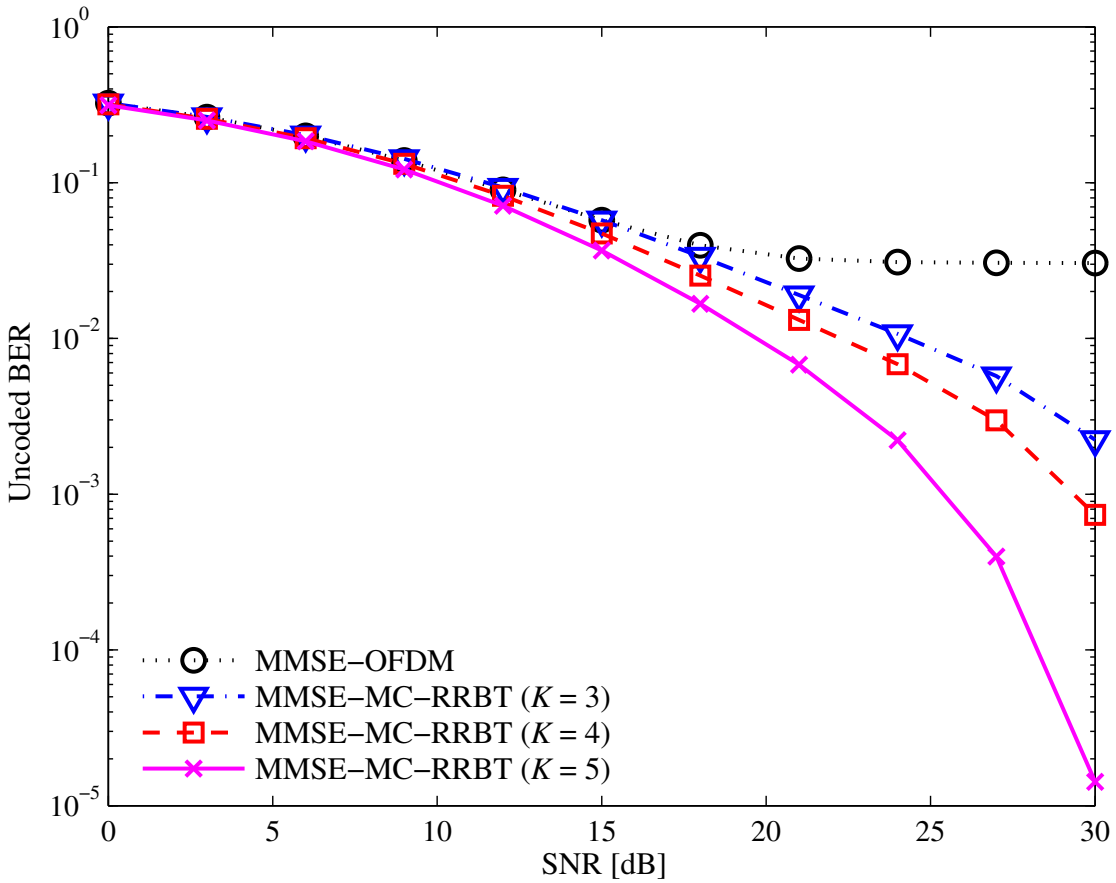

Figure F.14: Uncoded BER as a function of SNR [dB] for Channel C, considering MMSE-based multicarrier transmissions employing DFT.

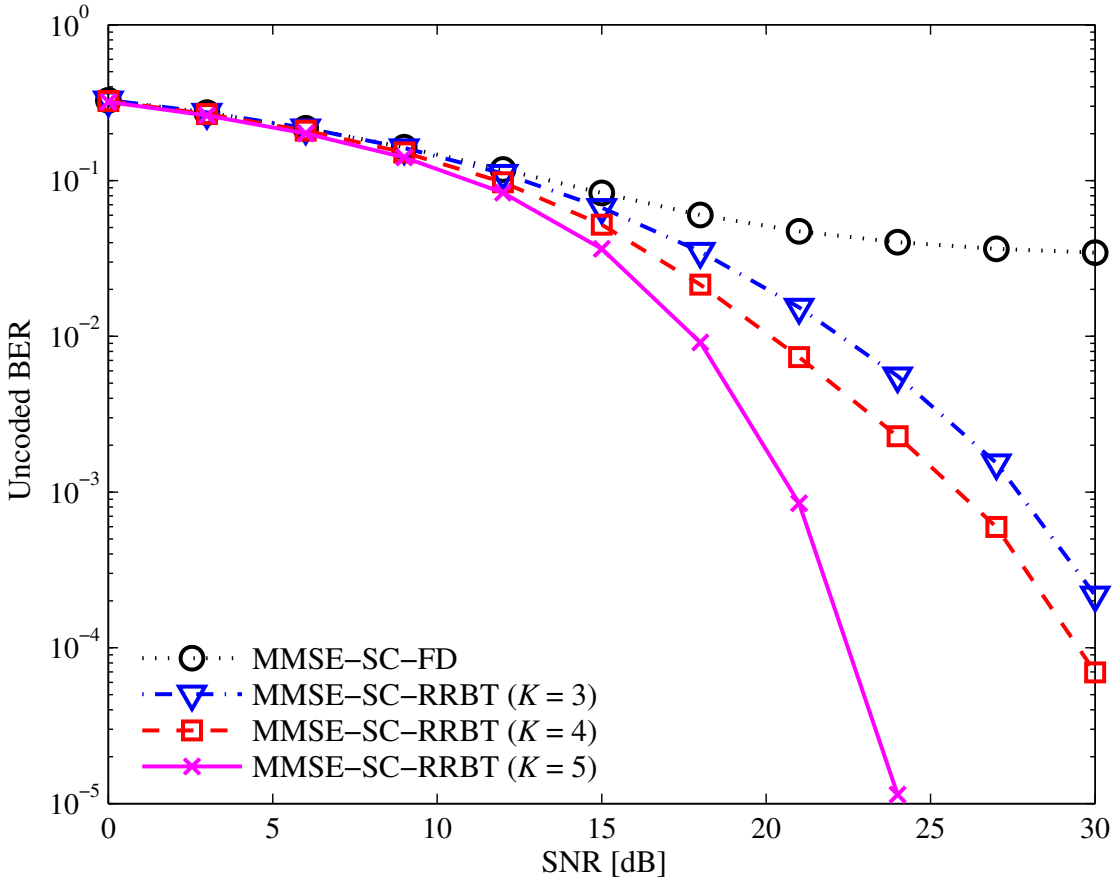

Figure F.15: Uncoded BER as a function of SNR [dB] for Channel C, considering MMSE-based single-carrier transmissions employing DFT.

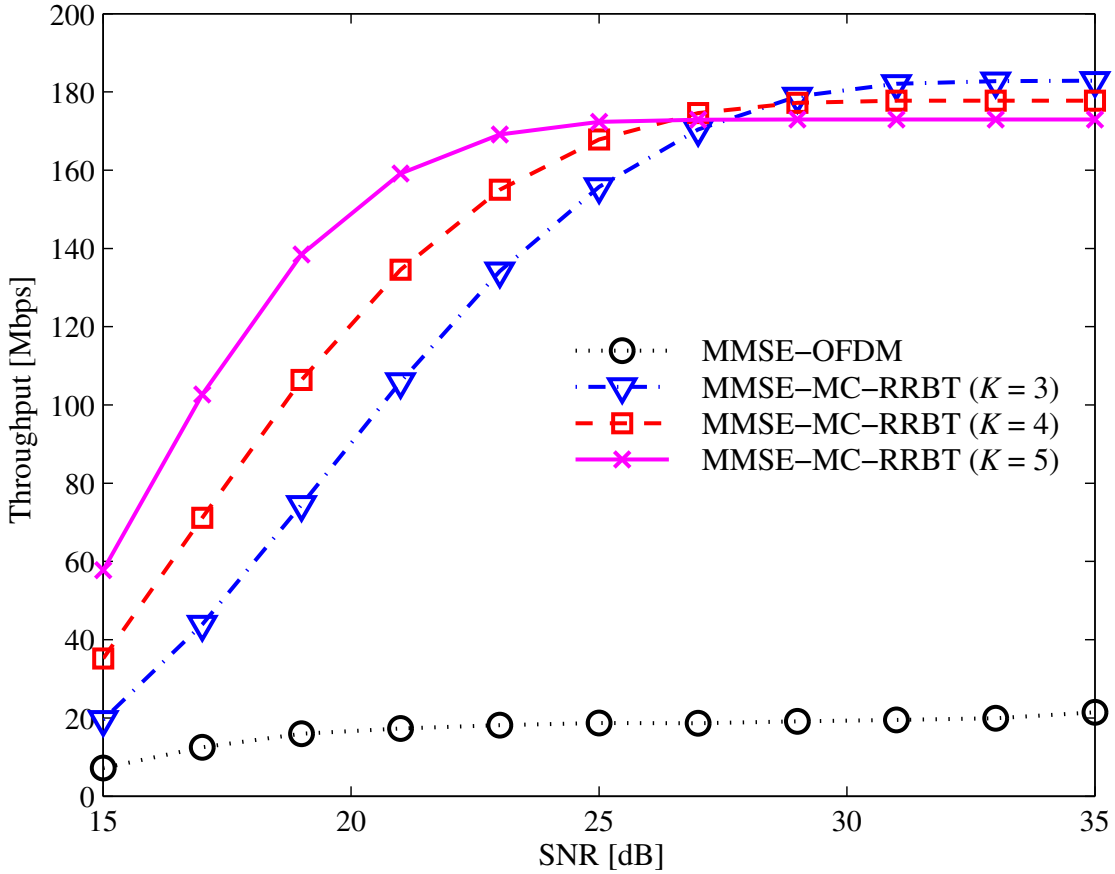

Figure F.16: Throughput [Mbps] as a function of SNR [dB] for Channel C, considering MMSE-based multicarrier transmissions employing DFT.

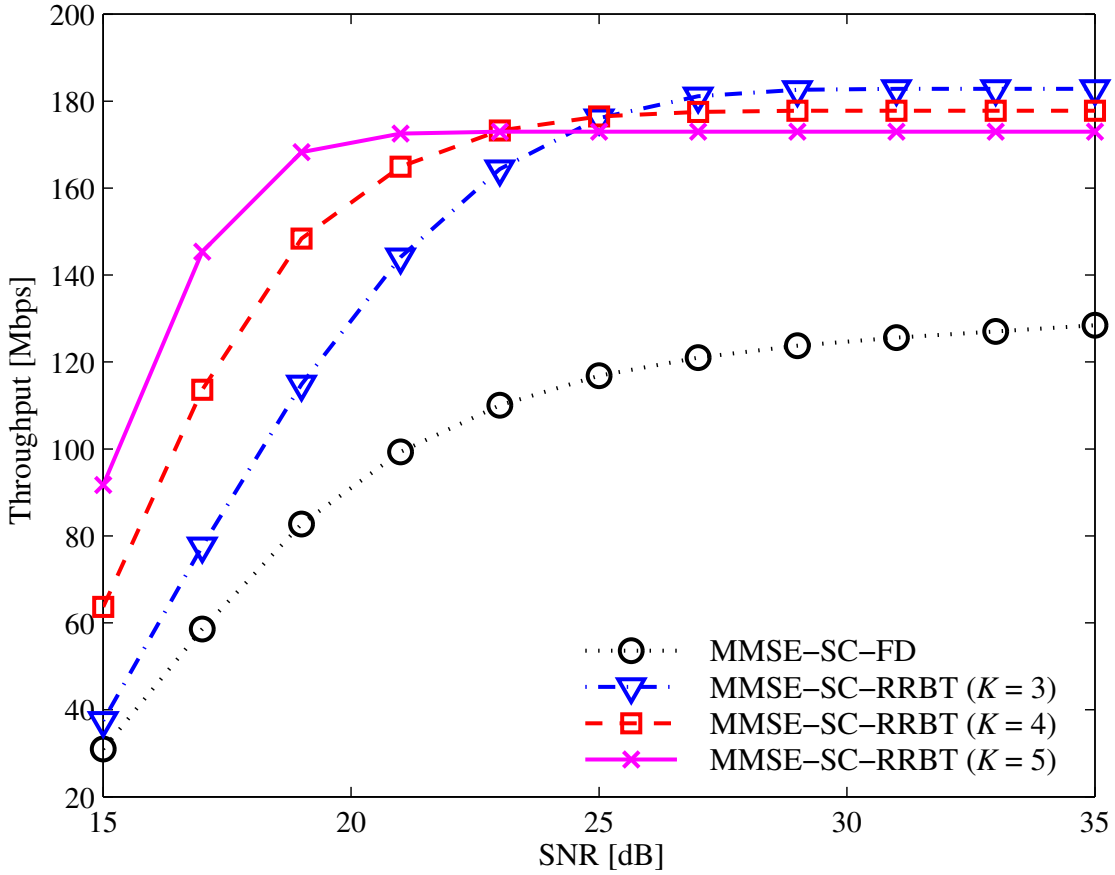

Figure F.17: Throughput [Mbps] as a function of SNR [dB] for Channel C, considering MMSE-based single-carrier transmissions employing DFT.

Apêndice G

DHT-Based Transceivers with Reduced Redundancy

As mentioned in Chapter E, there are some applications where employing real-transform-based multicarrier and single-carrier systems bring about many advantages over complex-transform-based transceivers. Chapter F introduced the reduced-redundancy transceivers based on discrete Fourier transform, which is a complex-value transform. The results of Chapter F can be used along with the results of Chapter E in order to derive reduced-redundancy transceivers based on discrete Hartley transform, which is a real-value transform.

In this chapter, we propose some possible structures for DHT-based transceivers with reduced redundancy. Starting from the derivations of both minimum-redundancy transceivers based on DHT and reduced-redundancy transceivers based on DFT, we can conceive the proposed structures for DHT-based transceivers with reduced redundancy by just adapting the results from Chapters E and F. As a result, this chapter is shorter than the previous two.

The proposed DHT-based superfast multicarrier and single-carrier transceivers with reduced redundancy is derived in Section G.1. The simulation results are in Section G.2, and the concluding remarks are in Section G.3.

G.1 DHT-Based Superfast Transceivers with Reduced Redundancy

We already know that the optimal linear solutions associated with block transceivers are particular types of Bezoutian matrices (see Subsection F.2.2). It is possible to derive DHT-based solutions by starting from a known efficient decomposition of a given Bezoutian matrix. Theorem 12 from Chapter F states that a given Bezoutian

matrix $\mathbf{B}$ of dimension $M_2 \times M_1$, with $M_1 \geq M_2$, admits the following decomposition

$$\mathbf{B} = \sqrt{M_1 M_2}\mathbf{V}_{\boldsymbol{\xi}}^{-1}\left[\sum_{r=1}^{R}\text{diag}\{\bar{\mathbf{p}}_r\}\mathbf{W}_{M_2}\left[\text{diag}\{(\xi_0\eta_0)^{m_2}\}_{m_2=0}^{M_2-1} \quad \mathbf{0}_{M_2\times(M_1-M_2)}\right]\times\right.$$
$$\left.\times\,\mathbf{W}_{M_1}\text{diag}\{\bar{\mathbf{q}}_r\}\right]\mathbf{V}_{\boldsymbol{\eta}}^{-T}, \tag{G.1}$$

in which, from Eqs. (F.50) and (F.51), we have

$$\mathbf{V}_{\boldsymbol{\xi}} = \sqrt{M_2}\mathbf{W}_{M_2}\text{diag}\{\xi_0^{m_2}\}_{m_2=0}^{M_2-1} \Leftrightarrow \mathbf{V}_{\boldsymbol{\xi}}^{-1} = \frac{1}{\sqrt{M_2}}\text{diag}\{\xi_0^{-m_2}\}_{m_2=0}^{M_2-1}\mathbf{W}_{M_2}^H, \tag{G.2}$$

$$\mathbf{V}_{\boldsymbol{\eta}} = \sqrt{M_1}\mathbf{W}_{M_1}\text{diag}\{\eta_0^{m_1}\}_{m_1=0}^{M_1-1} \Leftrightarrow \mathbf{V}_{\boldsymbol{\eta}}^{-T} = \frac{1}{\sqrt{M_1}}\mathbf{W}_{M_1}^H\text{diag}\{\eta_0^{-m_1}\}_{m_1=0}^{M_1-1}, \tag{G.3}$$

assuming that $\eta \neq 0 \neq \xi$, $\eta_0 = |\eta|^{1/M_1}\text{e}^{\jmath\frac{\angle\eta}{M_1}}$, and $\xi_0 \triangleq |\xi|^{1/M_2}\text{e}^{\jmath\frac{\angle\xi}{M_2}}$.

Now, let us recall the definitions of the normalized DFT matrices $\mathbf{W}_{M,X}$ given in Eq. (E.6), in which the sub-index $X \in \{\text{I}, \text{II}, \text{III}, \text{IV}\}$ indicates the type of the modified DFT matrix, whereas M denotes the dimension of the matrix ($M \times M$ DFT matrix).[1] Using these definitions, the following identities (see Eq. (E.24)) follow:

$$\begin{aligned}
\mathbf{W}_{M,\text{II}} = \mathbf{W}_{M,\text{III}}^T &= \text{diag}\left\{\exp\left(-\jmath\frac{\pi}{M}m\right)\right\}_{m=0}^{M-1}\mathbf{W}_{M,\text{I}} \\
&\Updownarrow \\
\mathbf{W}_{M,\text{III}} &= \mathbf{W}_{M,\text{I}}\text{diag}\left\{\exp\left(-\jmath\frac{\pi}{M}m\right)\right\}_{m=0}^{M-1} \\
&\Updownarrow \\
\mathbf{W}_{M,\text{III}}^H &= \text{diag}\left\{\exp\left(\jmath\frac{\pi}{M}m\right)\right\}_{m=0}^{M-1}\mathbf{W}_{M,\text{I}}^H,
\end{aligned} \tag{G.4}$$

where $\mathbf{W}_{M,\text{I}} = \mathbf{W}_M = \mathbf{W}_M^T$.

Now, we can set some values for ξ and η, for instance, by considering that $\xi = -1 = \exp(-\jmath\pi)$ and $\eta = 1$, we have $\xi_0 = \exp\left(-\jmath\frac{\pi}{M_2}\right)$ and $\eta_0 = 1$, yielding

$$\mathbf{V}_{-\mathbf{1}}^{-1} = \frac{1}{\sqrt{M_2}}\mathbf{W}_{M_2,\text{III}}^H, \tag{G.5}$$

$$\mathbf{V}_{\mathbf{1}}^{-T} = \frac{1}{\sqrt{M_1}}\mathbf{W}_{M_1,\text{I}}^H. \tag{G.6}$$

[1] In Chapter E, we omitted the sub-index M, since we were dealing only with $M \times M$ matrices in that chapter. In this chapter, since we also deal with rectangular matrices, the sub-index is required.

We therefore can rewrite Eq. (G.1) as

$$\mathbf{B} = \mathbf{W}_{M_2,\mathrm{III}}^H \left[\sum_{r=1}^{R} \mathrm{diag}\{\bar{\mathbf{p}}_r\} \mathbf{W}_{M_2,\mathrm{III}} \left[\mathbf{I}_{M_2} \quad \mathbf{0}_{M_2 \times (M_1 - M_2)} \right] \mathbf{W}_{M_1,\mathrm{I}} \mathrm{diag}\{\bar{\mathbf{q}}_r\} \right] \mathbf{W}_{M_1,\mathrm{I}}^H. \tag{G.7}$$

In order to describe the previous relation as a function of the Hartley transform, let us take into account the following facts (see also Eqs. (E.33) and (E.34)):

$$\begin{aligned}
\mathbf{W}_{M_2,\mathrm{III}} \boldsymbol{\mathcal{H}}_{M_2,\mathrm{II}} &= \frac{(1-\jmath)\mathbf{I}_{M_2} + (1+\jmath)\mathbf{J}_{M_2}}{2} \\
&\Updownarrow \\
\mathbf{W}_{M_2,\mathrm{III}} &= \left[\frac{(1-\jmath)\mathbf{I}_{M_2} + (1+\jmath)\mathbf{J}_{M_2}}{2} \right] \boldsymbol{\mathcal{H}}_{M_2,\mathrm{III}} \\
&\Updownarrow \\
\mathbf{W}_{M_2,\mathrm{III}}^H &= \boldsymbol{\mathcal{H}}_{M_2,\mathrm{II}} \left[\frac{(1+\jmath)\mathbf{I}_{M_2} + (1-\jmath)\mathbf{J}_{M_2}}{2} \right], \qquad \text{(G.8)} \\
\mathbf{W}_{M_1,\mathrm{I}} \boldsymbol{\mathcal{H}}_{M_1,\mathrm{I}} &= \frac{(1-\jmath)\mathbf{I}_{M_1} + (1+\jmath)\mathbf{J'}_{M_1}}{2} \\
&\Updownarrow \\
\mathbf{W}_{M_1,\mathrm{I}} &= \left[\frac{(1-\jmath)\mathbf{I}_{M_1} + (1+\jmath)\mathbf{J'}_{M_1}}{2} \right] \boldsymbol{\mathcal{H}}_{M_1,\mathrm{I}} \\
&= \boldsymbol{\mathcal{H}}_{M_1,\mathrm{I}} \left[\frac{(1-\jmath)\mathbf{I}_{M_1} + (1+\jmath)\mathbf{J'}_{M_1}}{2} \right] \\
&\Updownarrow \\
\mathbf{W}_{M_1,\mathrm{I}}^H &= \boldsymbol{\mathcal{H}}_{M_1,\mathrm{I}} \left[\frac{(1+\jmath)\mathbf{I}_{M_1} + (1-\jmath)\mathbf{J'}_{M_1}}{2} \right] \\
&= \left[\frac{(1+\jmath)\mathbf{I}_{M_1} + (1-\jmath)\mathbf{J'}_{M_1}}{2} \right] \boldsymbol{\mathcal{H}}_{M_1,\mathrm{I}}, \qquad \text{(G.9)}
\end{aligned}$$

in which we have used the identity $\boldsymbol{\mathcal{H}}_{\mathrm{I}} \mathbf{J'} = \mathbf{J'} \boldsymbol{\mathcal{H}}_{\mathrm{I}}$ [48]. Hence, we can rewrite Eq. (G.7) as

$$\mathbf{B} = \boldsymbol{\mathcal{H}}_{M_2,\mathrm{II}} \left[\sum_{r=1}^{R} \boldsymbol{\mathcal{X}}_{\bar{\mathbf{p}}_r} \boldsymbol{\mathcal{H}}_{M_2,\mathrm{III}} \left[\mathbf{I}_{M_2} \quad \mathbf{0}_{M_2 \times (M_1 - M_2)} \right] \boldsymbol{\mathcal{H}}_{M_1,\mathrm{I}} \boldsymbol{\mathcal{X}}_{\bar{\mathbf{q}}_r} \right] \boldsymbol{\mathcal{H}}_{M_1,\mathrm{I}}, \tag{G.10}$$

where, for each $r \in \{1, 2, \cdots, R\}$, we have

$$\boldsymbol{\mathcal{X}}_{\bar{\mathbf{p}}_r} = \left[\frac{(1+\jmath)\mathbf{I}_{M_2} + (1-\jmath)\mathbf{J}_{M_2}}{2} \right] \mathrm{diag}\{\bar{\mathbf{p}}_r\} \left[\frac{(1-\jmath)\mathbf{I}_{M_2} + (1+\jmath)\mathbf{J}_{M_2}}{2} \right], \tag{G.11}$$

$$\boldsymbol{\mathcal{X}}_{\bar{\mathbf{q}}_r} = \left[\frac{(1-\jmath)\mathbf{I}_{M_1} + (1+\jmath)\mathbf{J'}_{M_1}}{2} \right] \mathrm{diag}\{\bar{\mathbf{q}}_r\} \left[\frac{(1+\jmath)\mathbf{I}_{M_1} + (1-\jmath)\mathbf{J'}_{M_1}}{2} \right]. \tag{G.12}$$

Now, let us consider the transmitter-independent receiver matrix $\mathbf{K} = \mathbf{F}_0\mathbf{G}_0 \in \mathbb{C}^{M\times(M+2K-L)}$ as the Bezoutian matrix (see Subsection F.2.2 for more detailed information). We already know that $\mathbf{K}_{\text{ZF}} = \mathbf{H}_0^{\dagger}$ and $\mathbf{K}_{\text{MMSE}} = (\mathbf{H}_0^H\mathbf{H}_0 + \rho\mathbf{I}_M)^{-1}\mathbf{H}_0^H$. We can therefore sum up all previous developments in Theorem 14 as follows.

Theorem 14. *The transmitter-independent receiver matrix* $\mathbf{K}$ *can be written as*

$$\mathbf{K} = \boldsymbol{\mathcal{H}}_{M,\text{II}}\left[\sum_{r=1}^{R}\boldsymbol{\mathcal{X}}_{\bar{\mathbf{p}}_r}\boldsymbol{\mathcal{H}}_{M,\text{III}}\begin{bmatrix}\mathbf{I}_M & \mathbf{0}_{M\times(2K-L)}\end{bmatrix}\boldsymbol{\mathcal{H}}_{(M+2K-L),\text{I}}\boldsymbol{\mathcal{X}}_{\bar{\mathbf{q}}_r}\right]\boldsymbol{\mathcal{H}}_{(M+2K-L),\text{I}}, \tag{G.13}$$

where $\boldsymbol{\mathcal{X}}_{\bar{\mathbf{p}}_r}$ *and* $\boldsymbol{\mathcal{X}}_{\bar{\mathbf{q}}_r}$ *are defined in Eqs.* (G.11) *and* (G.12)*. In addition, we consider that* $\bar{\mathbf{P}} = [\,\bar{\mathbf{p}}_1\ \cdots\ \bar{\mathbf{p}}_4\,]$ *and* $\bar{\mathbf{Q}} = [\,\bar{\mathbf{q}}_1\ \cdots\ \bar{\mathbf{q}}_4\,]$ *are defined as in Eqs.* (F.55) *and* (F.56)*.*

Note that, in Eqs. (F.55) and (F.56), we must consider that $R = 4$, $\xi = -1$, and $\eta_m^M = \mathrm{e}^{\frac{-\jmath 2mM\pi}{(M+2K-L)}}$, for all m within the set $\{0, 1, \cdots, M+2K-L-1\}$, following our aforementioned hypotheses of $\xi = -1$ and $\eta = 1$. In fact, in this case, Eq. (F.56) only makes sense when $\mathrm{e}^{\frac{-\jmath 2mM\pi}{(M+2K-L)}} \neq -1$. In other words, $\frac{2mM}{M+2K-L}$ cannot be an odd number, for all possible m. We know that $M \leq M+2K-L \leq M+L \leq 2M$, since $L/2 \leq K \leq L$ and $L \leq M$. Now, if one assumes that $M = 2^k$, for some natural number k, and if $L < M = 2^k$, then one has that $\frac{2mM}{M+2K-L}$ is an integer number only when $K = L/2$, and, for this case, $\frac{2mM}{M+2K-L} = 2m$, which is an even number. Thus, we shall assume from now on that M is a power of 2 and that L is strictly smaller than M, since these conditions are sufficient to guarantee that Eq. (F.56) is well defined.[2]

Furthermore, the definition of the pair of matrices $(\mathbf{P}, \mathbf{Q}) \in \mathbb{C}^{M\times 4}\times\mathbb{C}^{(M+2K-L)\times 4}$ that appears in the definition of $(\bar{\mathbf{P}}, \bar{\mathbf{Q}})$ in Eqs. (F.55) and (F.56) depends on whether the ZF (see Eqs. (F.41) and (F.42) from Corollary 5) or MMSE (see Eqs. (F.29) and (F.42) from Theorem 11) solution is chosen.

Now that we have an efficient decomposition for the transmitter-independent receiver matrix $\mathbf{K}$, we can easily devise multicarrier and single-carrier systems. Indeed, a multicarrier system can be designed by setting $\mathbf{F}_0 = \boldsymbol{\mathcal{H}}_{M,\text{II}}$ and $\mathbf{G}_0 = \mathbf{F}_0^{-1}\mathbf{K} = \boldsymbol{\mathcal{H}}_{M,\text{III}}\mathbf{K}$, yielding

$$\mathbf{G}_0 = \left[\sum_{r=1}^{4}\boldsymbol{\mathcal{X}}_{\bar{\mathbf{p}}_r}\boldsymbol{\mathcal{H}}_{M,\text{III}}\begin{bmatrix}\mathbf{I}_M & \mathbf{0}_{M\times(2K-L)}\end{bmatrix}\boldsymbol{\mathcal{H}}_{(M+2K-L),\text{I}}\boldsymbol{\mathcal{X}}_{\bar{\mathbf{q}}_r}\right]\boldsymbol{\mathcal{H}}_{(M+2K-L),\text{I}}. \tag{G.14}$$

As for the single-carrier system, one can set $\mathbf{F}_0 = \mathbf{I}_M$ and $\mathbf{G}_0 = \mathbf{F}_0^{-1}\mathbf{K} = \mathbf{K}$,

[2]Actually, one could also take into account the case in which $L = M$ as long as full-redundancy is not employed ($K < L$), as can be noted from the discussions above.

yielding

$$\mathbf{G}_0 = \boldsymbol{\mathcal{H}}_{M,\mathrm{II}} \left[\sum_{r=1}^{4} \boldsymbol{\mathcal{X}}_{\bar{\mathbf{p}}_r} \boldsymbol{\mathcal{H}}_{M,\mathrm{III}} \left[\mathbf{I}_M \quad \mathbf{0}_{M\times(2K-L)} \right] \boldsymbol{\mathcal{H}}_{(M+2K-L),\mathrm{I}} \boldsymbol{\mathcal{X}}_{\bar{\mathbf{q}}_r} \right] \boldsymbol{\mathcal{H}}_{(M+2K-L),\mathrm{I}}. \tag{G.15}$$

In any case, the definitions of the vectors $\bar{\mathbf{p}}_r$ and $\bar{\mathbf{q}}_r$ depend on whether the ZF or the MMSE solution is chosen. As an illustrative example, Figure G.1 depicts the resulting multicarrier structure. The reader should notice the similarities between Figure G.1 and Figure F.1 (note, however, that the DHT-based transceivers require two-tap equalizers in their structures).

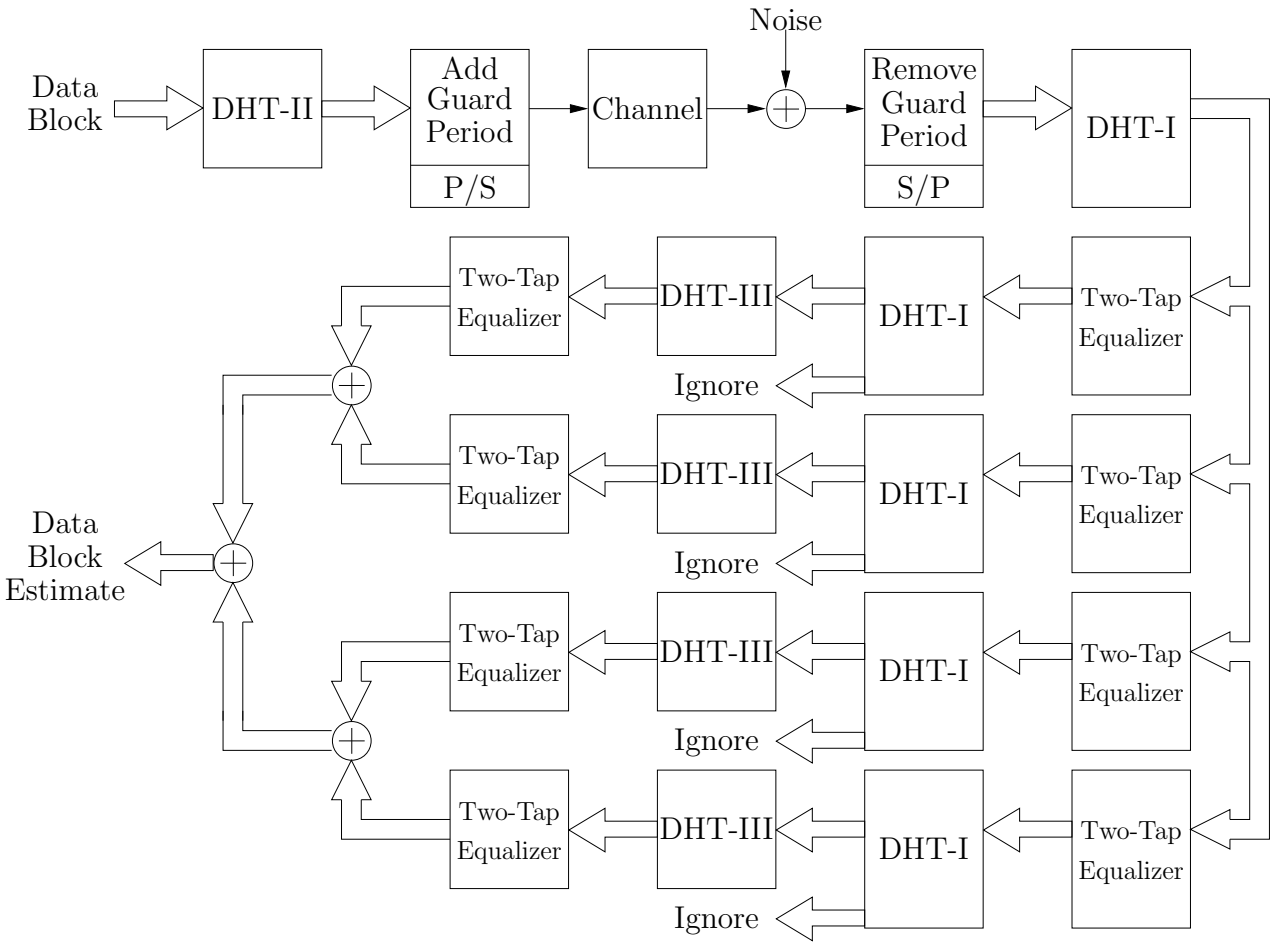

Figure G.1: DHT-based multicarrier reduced-redundancy block transceiver.

It is worth mentioning that, when both $K = L/2$ and the zero-forcing solution is adopted, then the number of equalizer branches at the receiver end in Figure G.1 reduces to only two, instead of four (see Eqs. (F.41) and (F.42) from Corollary 5). Nevertheless, even in this minimum-redundancy case, we end up with a structure which does not coincide with the proposal depicted in Figure E.1. This occurs since we have deduced the DHT-based reduced-redundancy systems in a different manner

from that in Chapter E.

G.2 Simulation Results

The aim of this section is to assess the performance of the proposed DHT-based transceivers with reduced redundancy, considering the same scenarios described in Section F.4. As in Chapter F, the figures of merit adopted here are the uncoded BER and the throughput. For the sake of clarity, we shall describe once again the channel models:

- Channel A, whose transfer function is $0.1659 + 0.3045z^{-1} - 0.1159z^{-2} - 0.0733z^{-3} - 0.0015z^{-4}$. We transmitted 50,000 data blocks carrying $M = 16$ symbols of a 64-QAM constellation ($b = 6$ bits per symbol);

- Channel B, whose zeros are $0.8, -0.8, 0.5\jmath, -0.5\jmath$, and $-0.8\jmath$. We transmitted 50,000 data blocks carrying $M = 32$ symbols of a 16-QAM constellation ($b = 4$ bits per symbol);

- Channel C, whose zeros are $0.999, -0.999, 0.7\jmath, -0.7\jmath$, and $-0.4\jmath$. We transmitted 50,000 data blocks carrying $M = 32$ symbols of a 16-QAM constellation ($b = 4$ bits per symbol).

The channel coding employed in all throughput-based simulations has constraint length 7, code rate $r_c = 1/2$, and octal generators $\mathbf{g_0} \triangleq [\mathbf{133}]$ and $\mathbf{g_1} \triangleq [\mathbf{165}]$ [74]. We assume that the sample frequency is $f_s = 100$ MHz.

Figures G.2, G.3, G.4, G.5 depict the obtained uncoded-BER results for DHT-based transmissions through Channel A. For multicarrier transmissions, four different transceivers are compared, as shown in Figure G.2 and Figure G.3: the traditional OFDM and the three possible DHT-based multicarrier reduced-redundancy block transceivers (MC-RRBT). There are three possible DHT-based MC-RRBT systems since the amount of redundant elements respects the inequality $\frac{L}{2} \leq K \leq L$ (i.e., $K \in \{2, 3, 4\}$). In addition, for single-carrier transmissions, we also compare four different transceivers, as shown in Figure G.4 and Figure G.5: the traditional SC-FD and the three possible DHT-based single-carrier reduced-redundancy block transceivers (SC-RRBT). The reader should notice in Figure G.2 that the DHT-based minimum-redundancy multicarrier system (MC-RRBT for $K = 2$) that employs a ZF equalizer is not able to produce a reliable estimate for the transmitted bits (the same conclusion was drawn for DFT-based systems in Section F.4). However, when additional redundant elements are included in the transmission, the resulting DHT-based MC-RRBT systems ($K = 3$ and $K = 4$) outperform the ZF-OFDM.

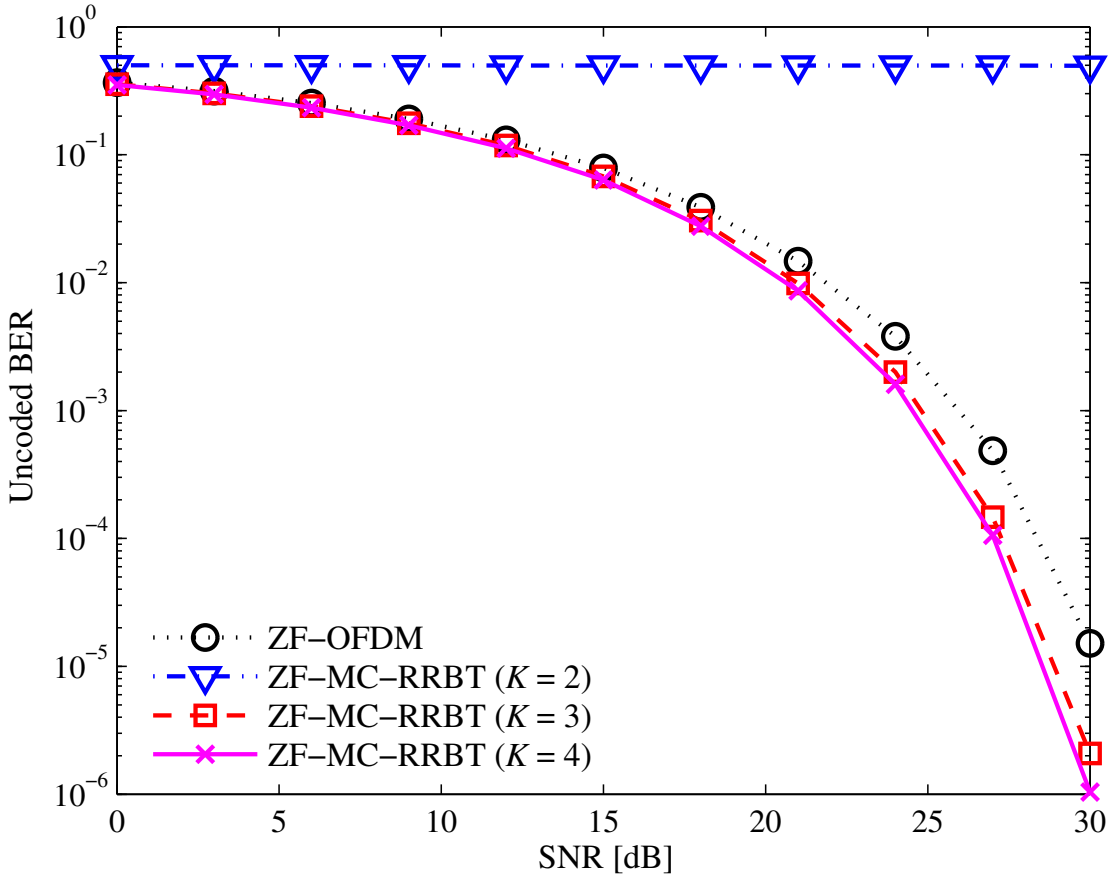

Figure G.2: Uncoded BER as a function of SNR [dB] for Channel A, considering ZF-based multicarrier transmissions employing DHTs.

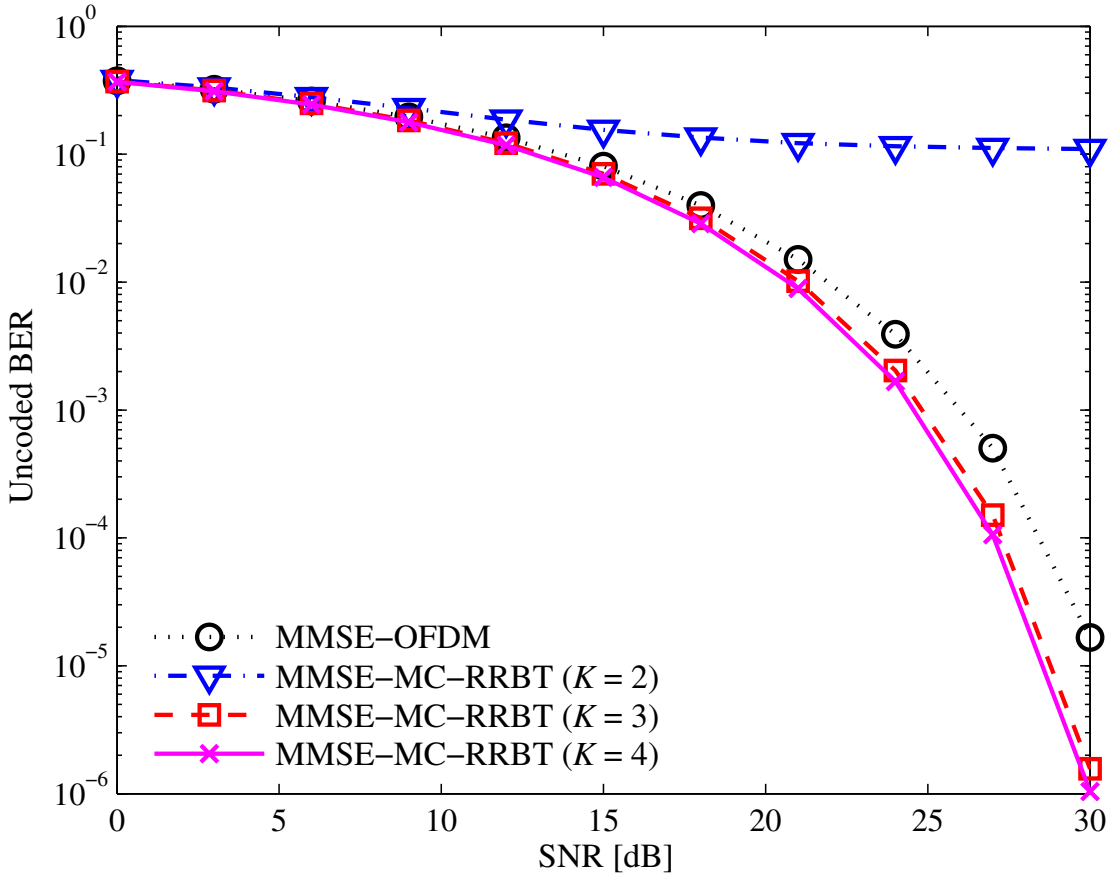

Figure G.3: Uncoded BER as a function of SNR [dB] for Channel A, considering MMSE-based multicarrier transmissions employing DHTs.

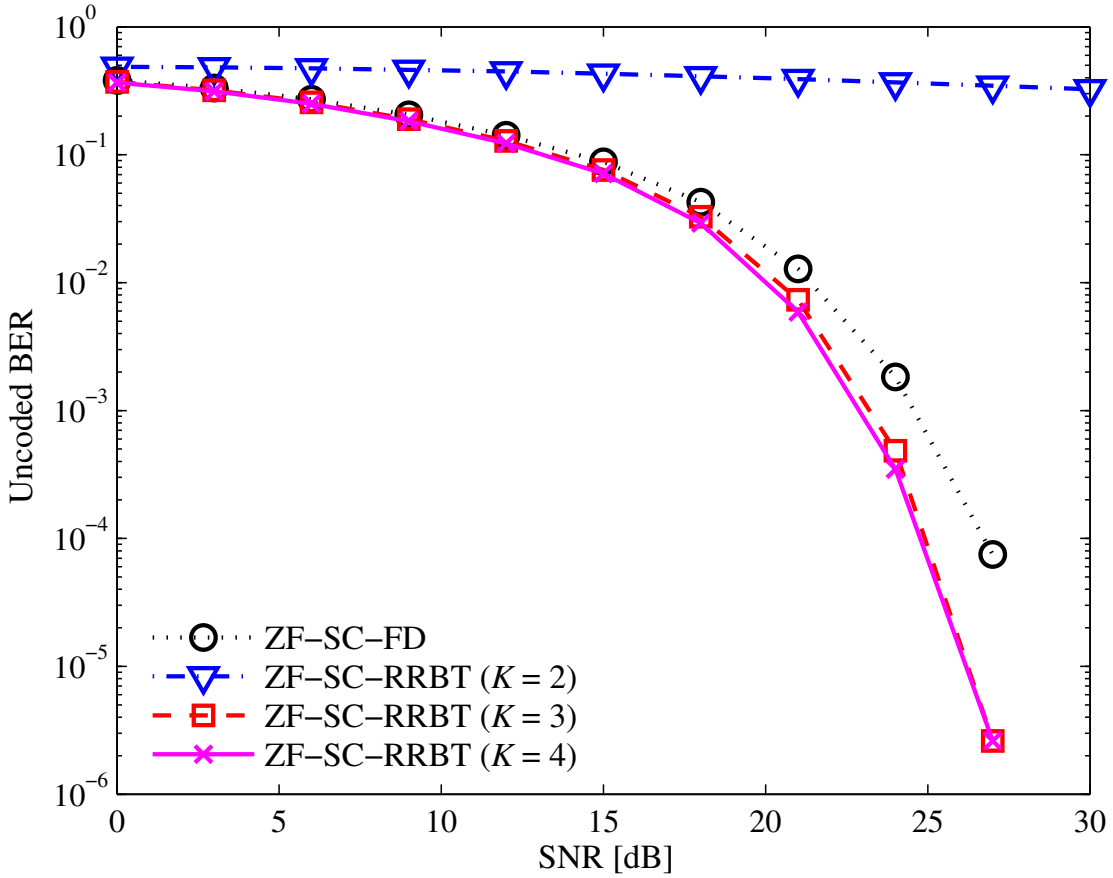

Figure G.4: Uncoded BER as a function of SNR [dB] for Channel A, considering ZF-based single-carrier transmissions employing DHTs.

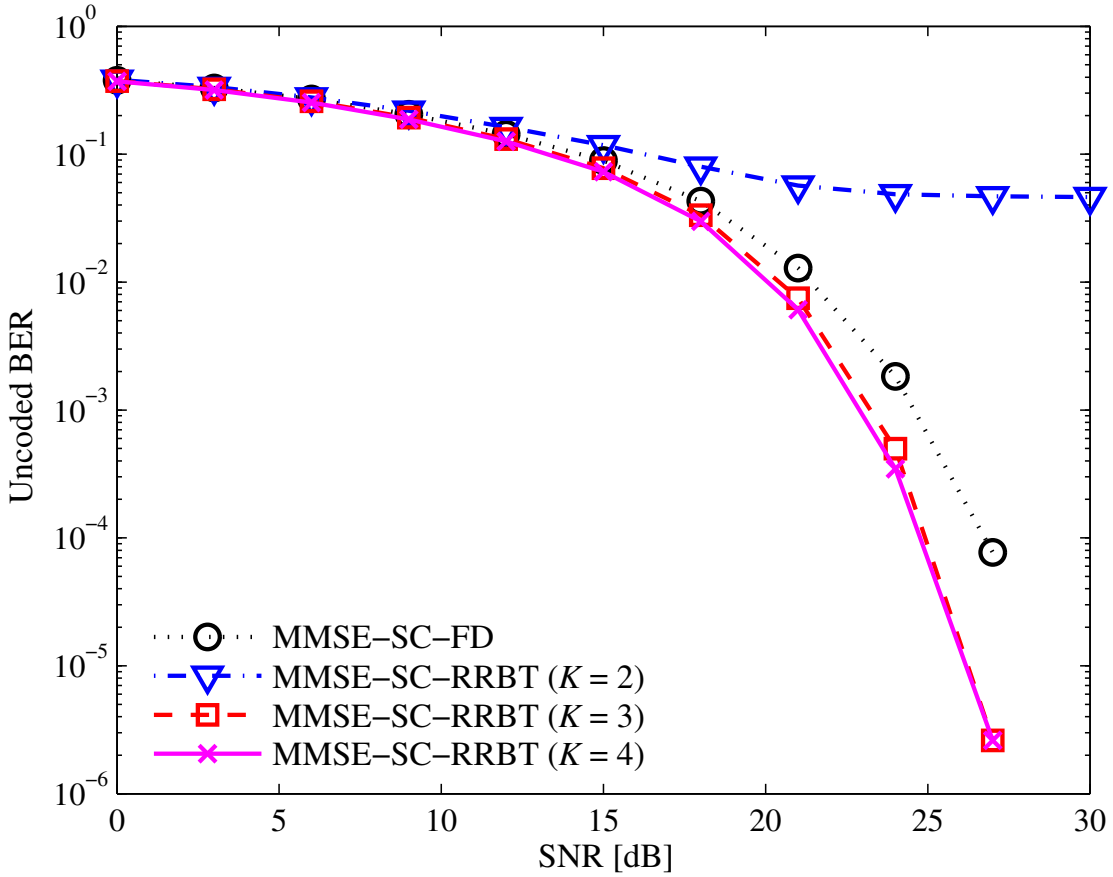

Figure G.5: Uncoded BER as a function of SNR [dB] for Channel A, considering MMSE-based single-carrier transmissions employing DHTs.

Figures G.6, G.7, G.8, G.9 depict the obtained throughput results. Figure G.6 shows that using a DHT-based MC-RRBT system with $K = 3$ is the best option from a throughput point of view, as compared to the other three options, including OFDM. Similar conclusions can be drawn from the analyses of Figure G.7, Figure G.8, and Figure G.9.

Figures G.10, G.11 contain the uncoded-BER and Figures G.12, G.13 contain the throughput results when Channel B is considered (only MMSE-based solutions). For the multicarrier systems one can observe in Figure G.10 that neither DHT-based MC-RRBT with $K = 3$ nor with DHT-based MC-RRBT with $K = 4$ yield reliable data estimates. This behavior was also observed in the results described in Section F.4 of this thesis. As can be verified in Figure G.12, it is much better to use the traditional OFDM system for this channel model when the SNR values are large ($\geq$ 27 dB). Nevertheless, for low SNR values, both the reduced-redundancy system with $K = 4$ and the full-redundancy system with $K = 5$ outperform the throughput results related to OFDM.

Figures G.14, G.15 depict the uncoded-BER and Figures G.16, G.17 depict the throughput results when Channel C is considered (only MMSE-based solutions). One can observe that both the DHT-based MC-RRBT and the DHT-based SC-RRBT systems always outperform the traditional OFDM and SC-FD systems. Another important fact is that even though the uncoded-BER performance always improves as one increases the number of transmitted redundant elements, the throughput performance does not follow the same pattern. For example, for low SNR values, it is better to use a DHT-based reduced-redundancy system that transmits with a larger amount of redundant elements, whereas for large SNR values, it is better to use a reduced-redundancy system that transmits with a smaller amount of redundant elements. Once again, such a behavior was also observed in Chapter F.

G.3 Concluding Remarks

In this chapter we proposed transceivers with reduced redundancy for block data transmission. More specifically, we extended the results from Chapter F by using Hartley transforms, instead of Fourier transforms. The ZF and MMSE solutions employ only DHTs, diagonal, and antidiagonal matrices. This feature makes the new transceivers computationally efficient. Our approach exploited the structural properties of typical channel matrix representations described in Chapter E and Chapter F. The obtained results corroborate the good throughput properties inherent to the new proposals.

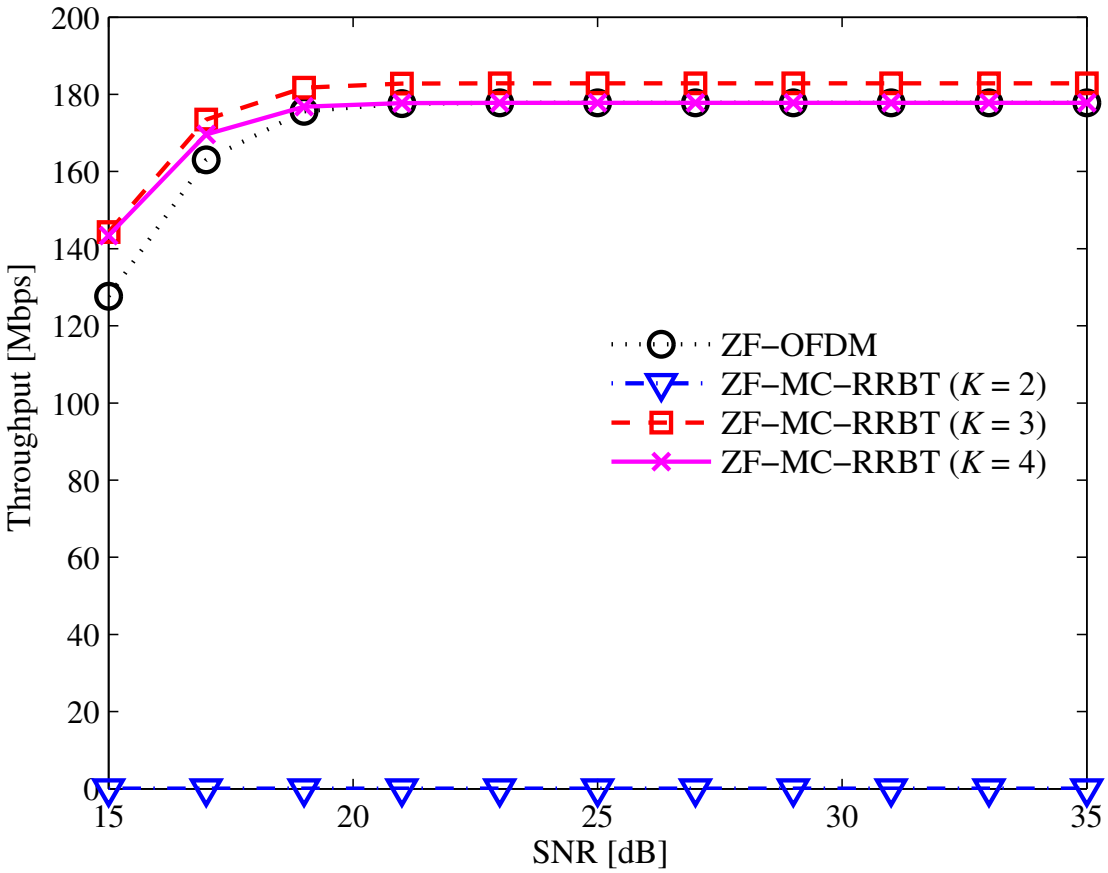

Figure G.6: Throughput [Mbps] as a function of SNR [dB] for Channel A, considering ZF-based multicarrier transmissions employing DHTs.

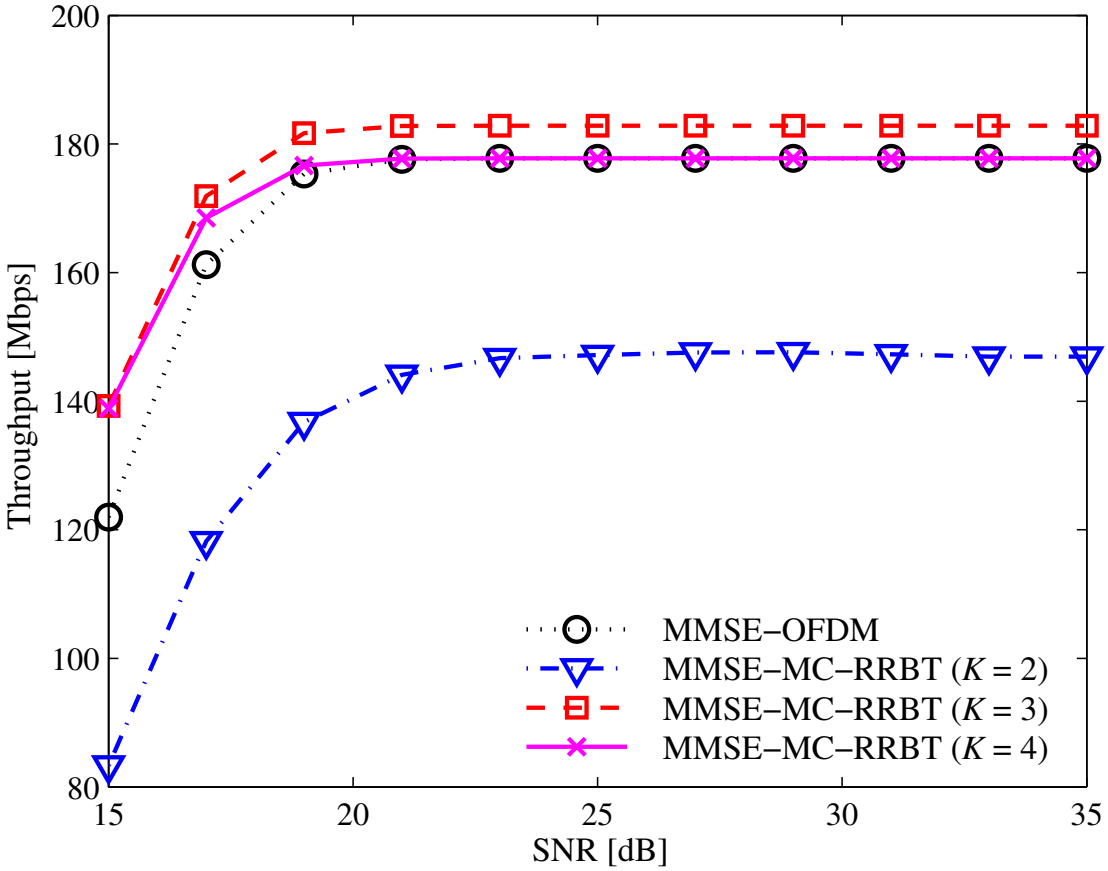

Figure G.7: Throughput [Mbps] as a function of SNR [dB] for Channel A, considering MMSE-based multicarrier transmissions employing DHTs.

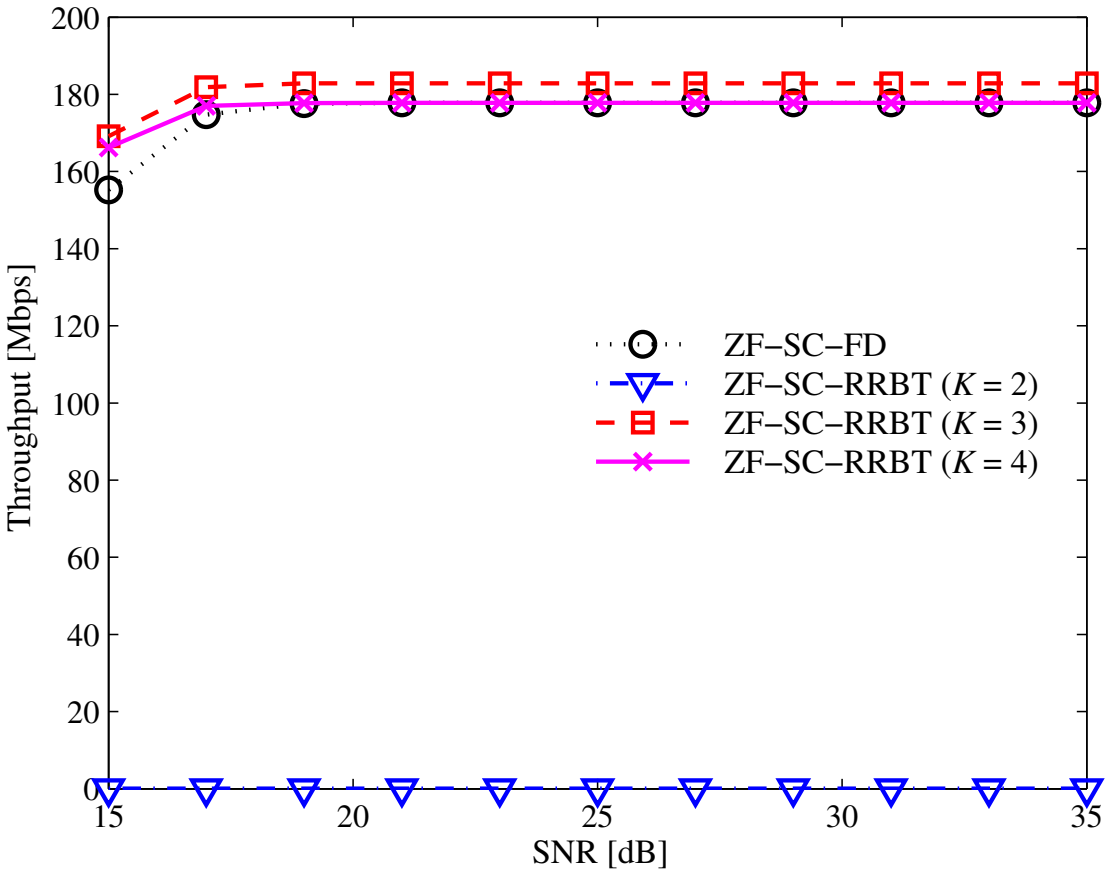

Figure G.8: Throughput [Mbps] as a function of SNR [dB] for Channel A, considering ZF-based single-carrier transmissions employing DHTs.

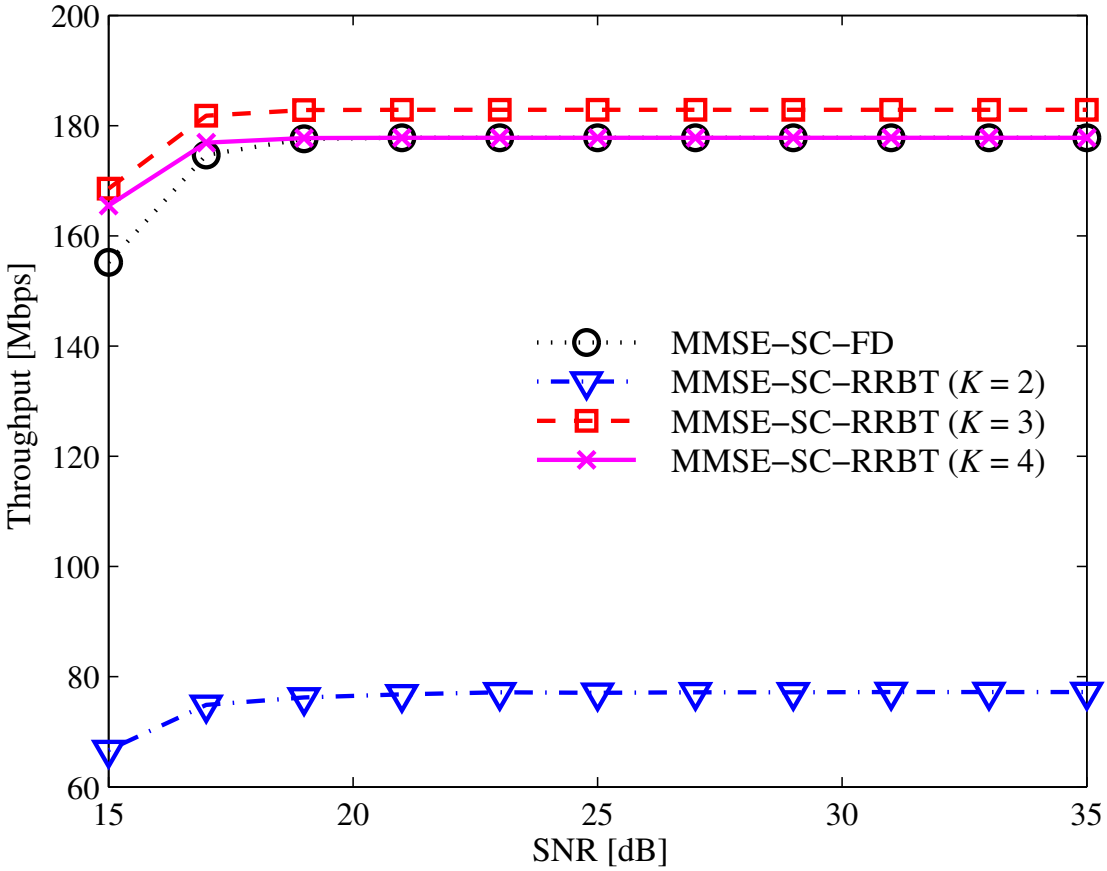

Figure G.9: Throughput [Mbps] as a function of SNR [dB] for Channel A, considering MMSE-based single-carrier transmissions employing DHTs.

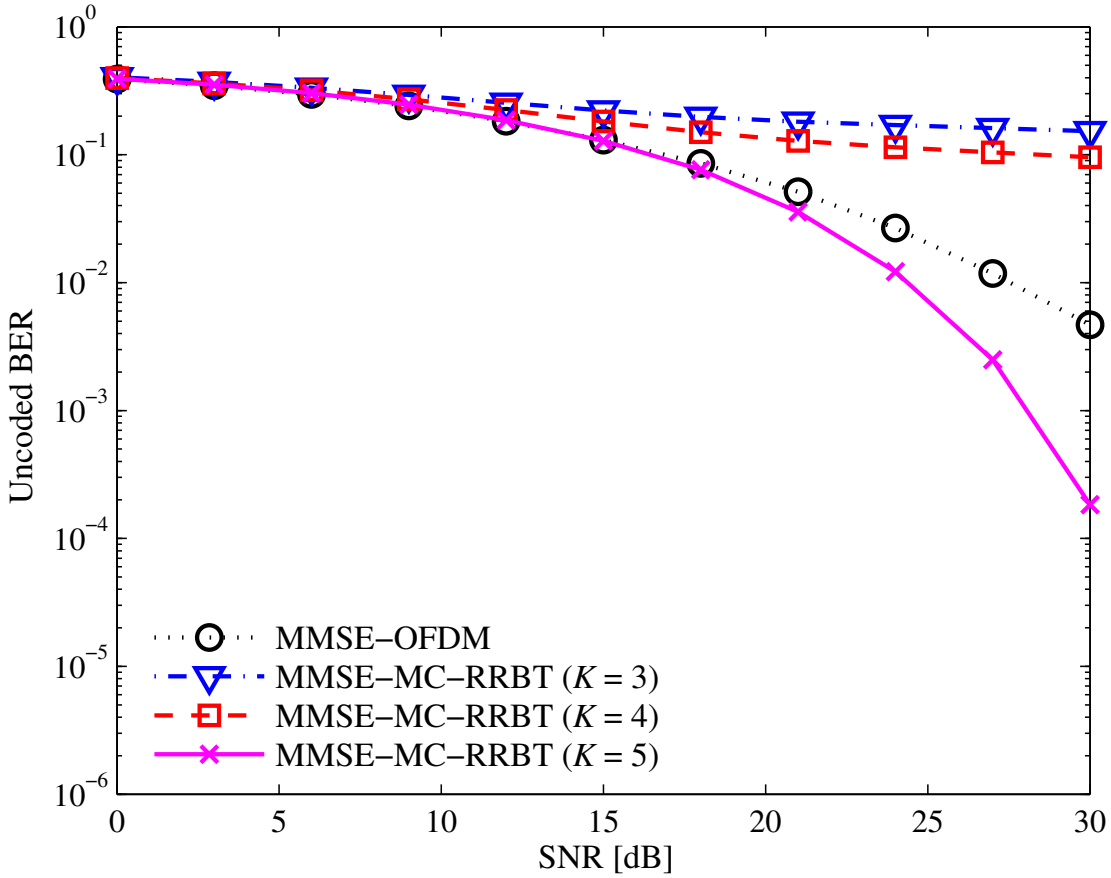

Figure G.10: Uncoded BER as a function of SNR [dB] for Channel B, considering MMSE-based multicarrier transmissions employing DHTs.

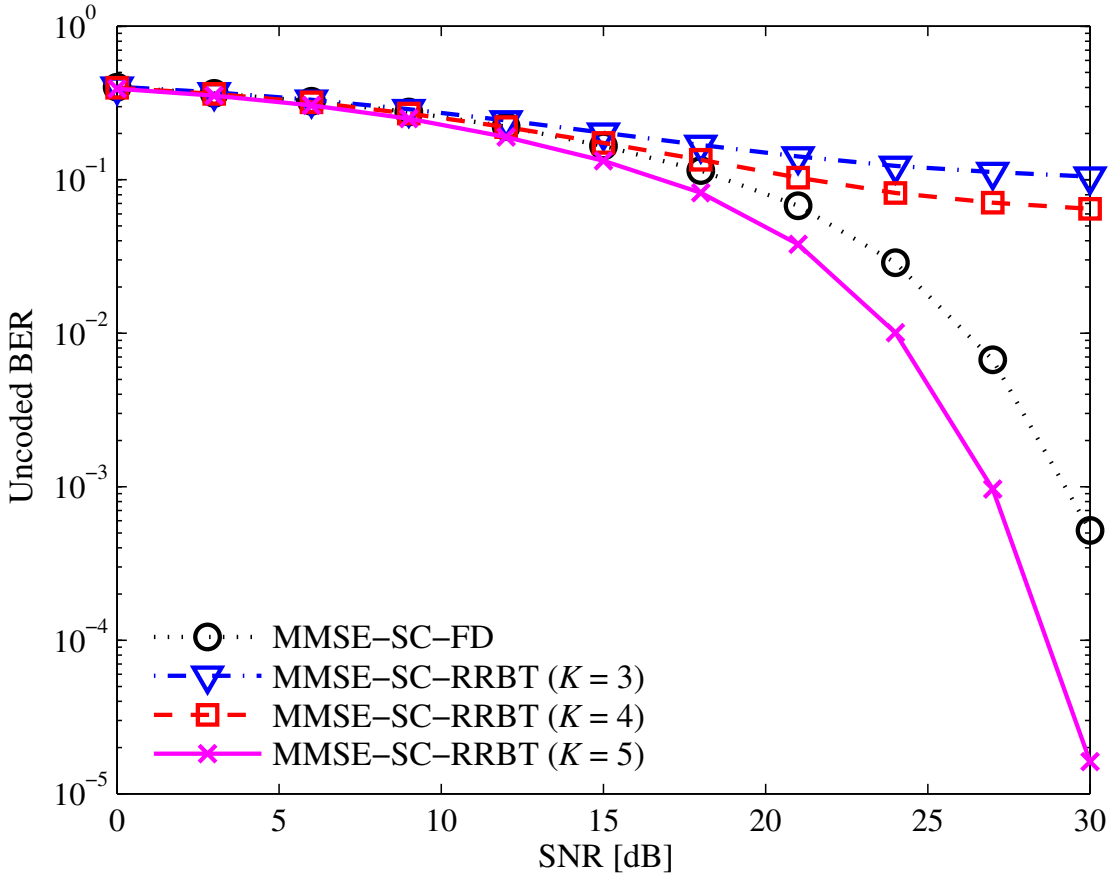

Figure G.11: Uncoded BER as a function of SNR [dB] for Channel B, considering MMSE-based single-carrier transmissions employing DHTs.

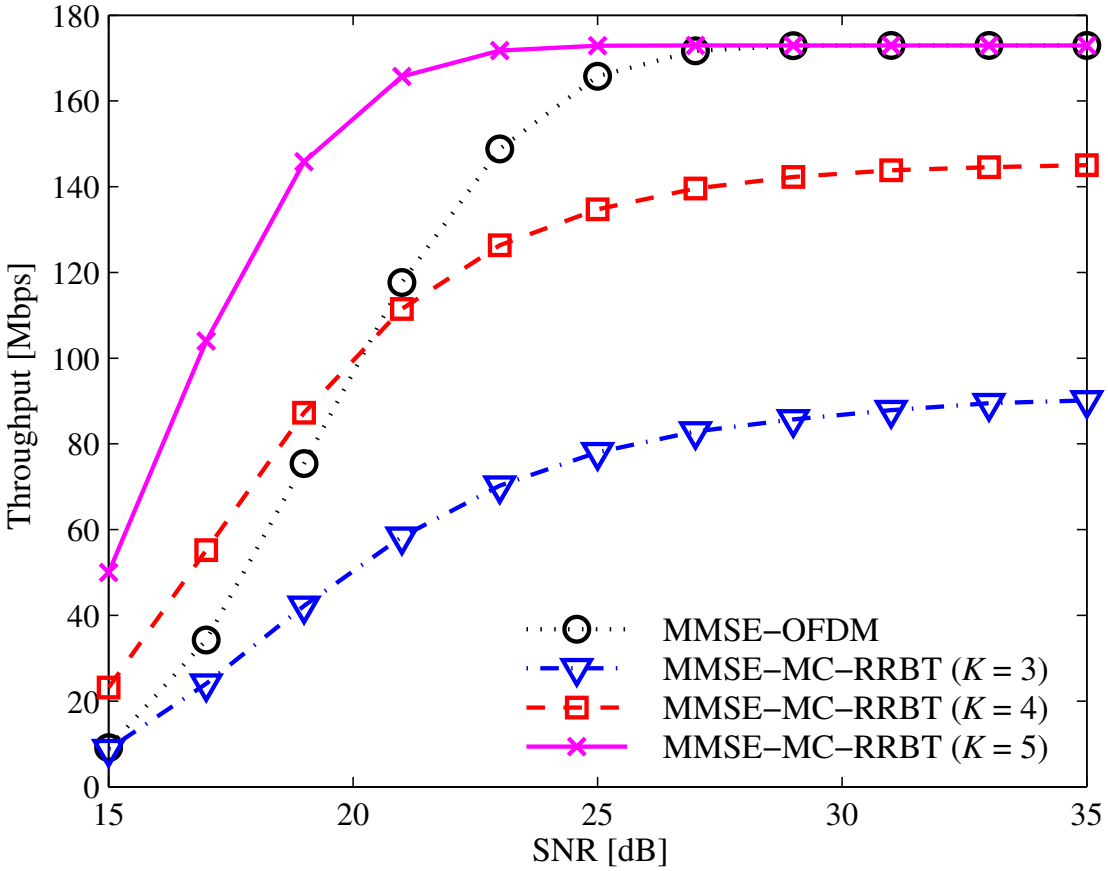

Figure G.12: Throughput [Mbps] as a function of SNR [dB] for Channel B, considering MMSE-based multicarrier transmissions employing DHTs.

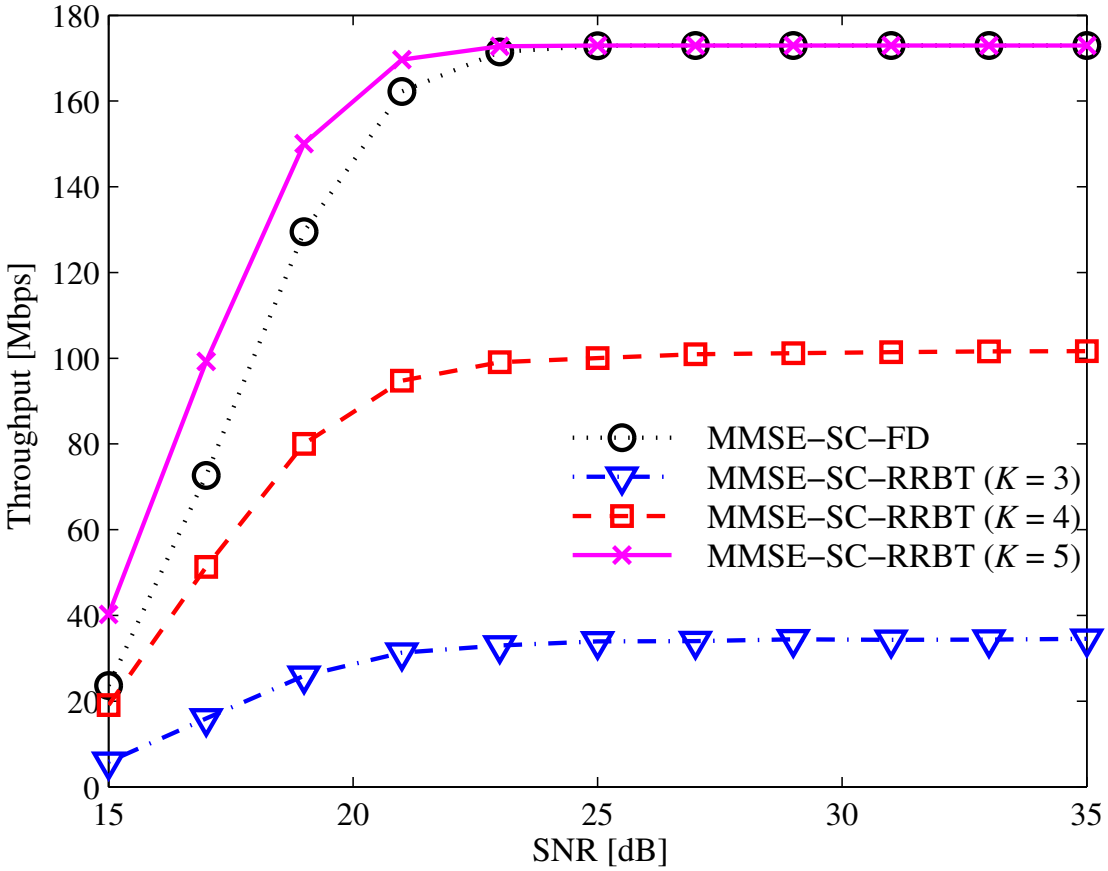

Figure G.13: Throughput [Mbps] as a function of SNR [dB] for Channel B, considering MMSE-based single-carrier transmissions employing DHTs.

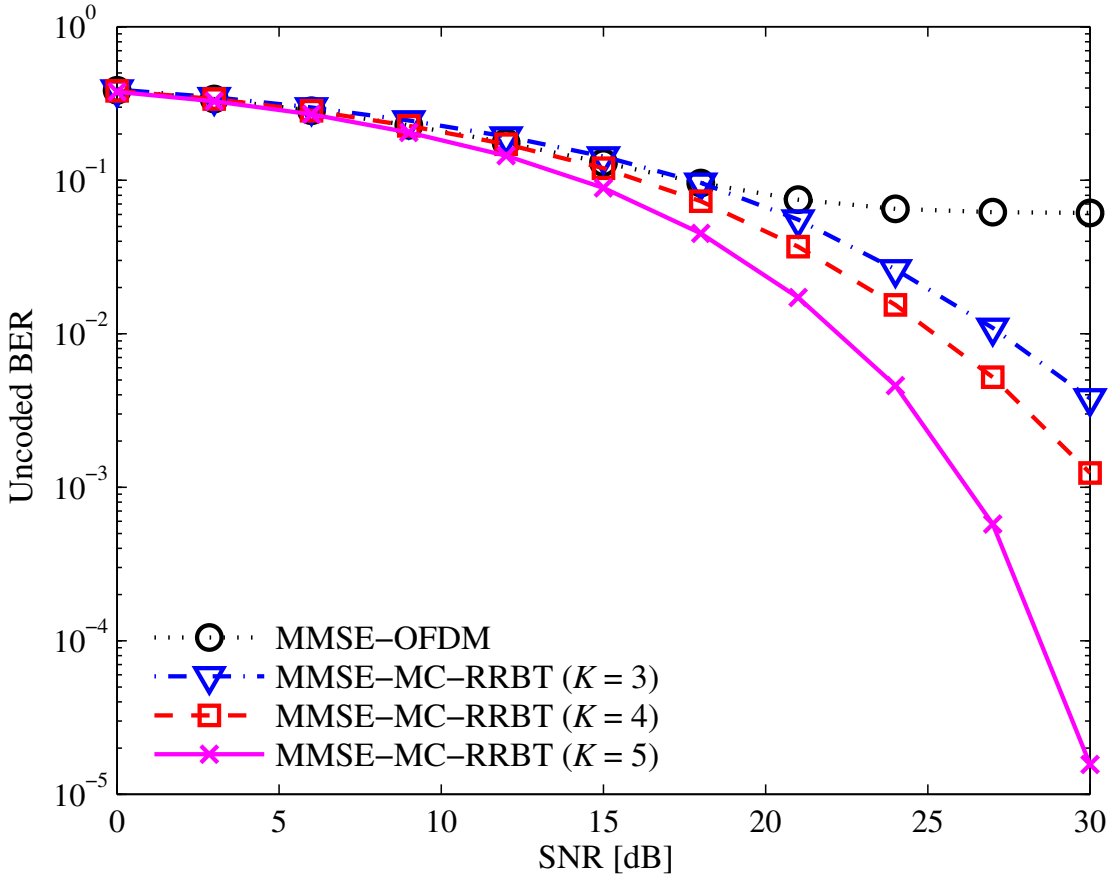

Figure G.14: Uncoded BER as a function of SNR [dB] for Channel C, considering MMSE-based multicarrier transmissions employing DHTs.

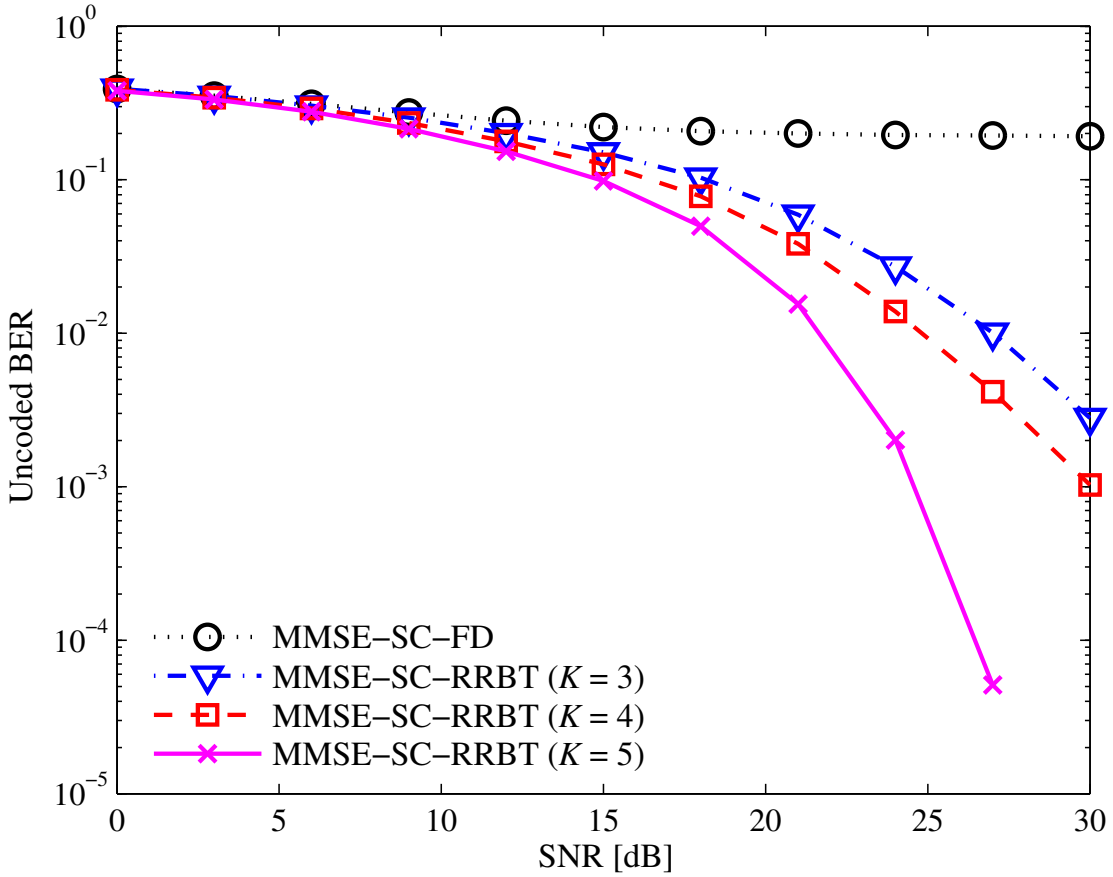

Figure G.15: Uncoded BER as a function of SNR [dB] for Channel C, considering MMSE-based single-carrier transmissions employing DHTs.

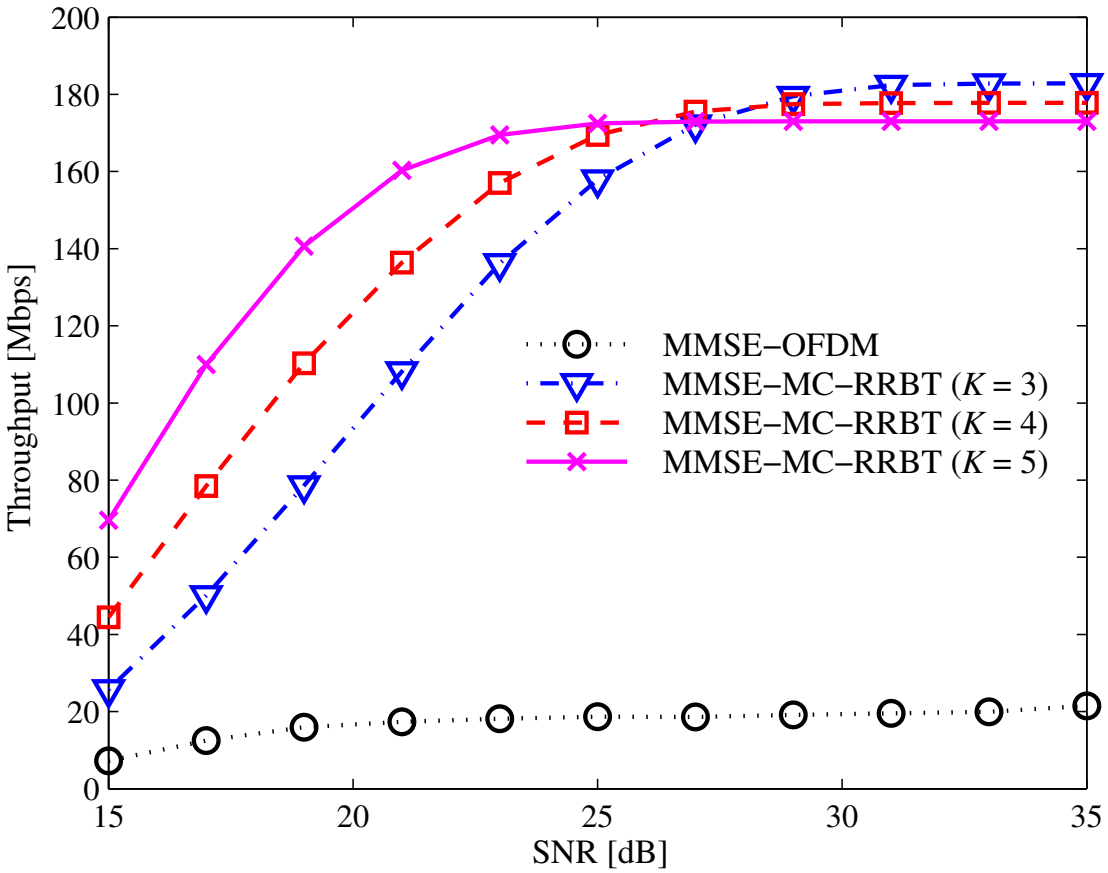

Figure G.16: Throughput [Mbps] as a function of SNR [dB] for Channel C, considering MMSE-based multicarrier transmissions employing DHTs.

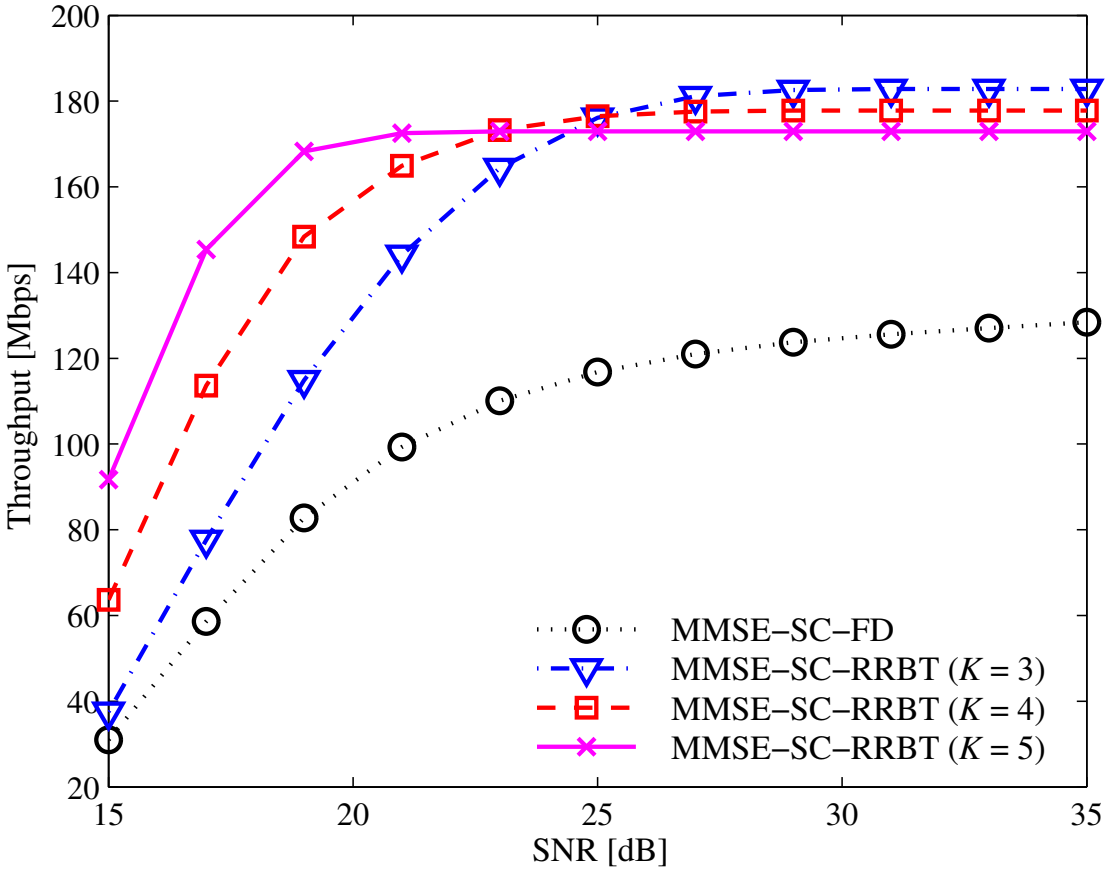

Figure G.17: Throughput [Mbps] as a function of SNR [dB] for Channel C, considering MMSE-based single-carrier transmissions employing DHTs.

Part III

Additional Contributions

Apêndice H

Power Allocation in Transceivers with Minimum Redundancy

It has been observed that, after the equalization process, minimum-redundancy transceivers may suffer from noise gains more than traditional OFDM and SC-FD systems do (see Chapter 4 in [23]). This occurs because of the additional difficulty in equalizing the Toeplitz effective channel matrix induced by the minimum-redundancy transceivers, as compared to the circulant channel matrix associated with OFDM and SC-FD systems [23].[1] This fact motivated us to perform research on methods to minimize these noise gains.

In this chapter, we consider a scheme where minimum-redundancy block transceivers have CSI available at the transmitter end. We use this information to distribute the available transmitter power among the symbols. The power allocation is performed in order to minimize the noise gains at the receiver end.

The proposed power-allocation method is implemented by multiplying each symbol to be transmitted by a positive real number. These real numbers are the solutions of a constrained optimization problem: to minimize the power of the noise vector after the receiver processing, without changing the average transmission power of the transmitted data block.

The proposed power-allocation method is derived in Section H.1. Numerical examples are presented in Section H.2. The chapter ends with some concluding remarks in Section H.3.

H.1 Optimal Power Allocation

The multicarrier transceivers with minimum redundancy proposed in [23] were not designed to take into account channel-state information at the transmitter end.

[1] It is common that Toeplitz matrices are more ill-conditioned than circulant matrices, considering the same channel model.

Hence, they do not apply any kind of bit and/or power loading to the subchannels. Rather, they transmit equal-power signals on every subchannel. In fact, the problem of power loading aiming at maximizing the channel capacity has not been addressed in the context of practical minimum-redundancy transceivers. This problem appears to be more complex than in the traditional DMT schemes (employing full-redundancy), since the effective channel matrix is not diagonalized in minimum-redundancy transceivers.

This section describes mathematically the proposal of this work. The idea is simple: to include at the transmitter and receiver ends two real-valued diagonal matrices $\mathbf{T}^{-1}$ and $\mathbf{T}$, respectively (see Figure H.1 and consider now that $\mathbf{T} \neq \mathbf{I}$). The matrix $\mathbf{T}$ is designed *in order to minimize the mean-square value of the noise after the processing at the receiver end, while keeping the same overall transmitter power*.[2] Note that this is not a unitary-precoder problem [40], since $\mathbf{T}$ is not a unitary or an orthogonal matrix. An analogous problem was proposed and solved in [39] for cyclic-prefix-based OFDM systems. This work, however, considers only a diagonal matrix $\mathbf{T}$ in order to avoid increasing the computational complexity of the transceiver significantly.

Given a noise vector $\mathbf{v}_0$ drawn from a zero-mean white process containing M independent and identically distributed (i.i.d.) elements, the resulting processed noise at the receiver end is $\mathbf{T}\mathbf{G}_0\mathbf{v}_0$. Thus, the average noise power (ANP) after the receiver processing is given by:

$$\begin{aligned} \text{ANP} &\triangleq \frac{1}{M}\mathsf{E}\left\{\text{tr}\left[\mathbf{T}\mathbf{G}_0\mathbf{v}_0\mathbf{v}_0^H\mathbf{G}_0^H\mathbf{T}^H\right]\right\} \\ &= \frac{\sigma_v^2}{M}\text{tr}\{\mathbf{T}^H\mathbf{T}\mathbf{G}_0\mathbf{G}_0^H\}, \end{aligned} \tag{H.1}$$

where $\mathsf{E}\{\mathbf{v}_0\mathbf{v}_0^H\} = \sigma_v^2\mathbf{I}$, with $\sigma_v^2 \in \mathbb{R}_+$. Hence, by defining the mth diagonal element of $\mathbf{T}$ as t_m, and the mth row-vector of $\mathbf{G}_0$ as $\mathbf{g}_m$, we have the following optimization problem:

$$\min \sum_{m=0}^{M-1} t_m^2 \|\mathbf{g}_m\|_2^2 \,, \quad \text{subject to} \quad \sum_{m=0}^{M-1} t_m^{-2} = M. \tag{H.2}$$

The constraint in Eq. (H.2) models the fact that, for a zero-mean white input $\mathbf{s}$ such that $\mathsf{E}\{\mathbf{s}\mathbf{s}^H\} = \sigma_s^2\mathbf{I}$, with $\sigma_s^2 \in \mathbb{R}_+$, the average transmission power (ATxP) is

[2] A more appropriate figure of merit would be throughput. Nevertheless, throughput is a rather complicated function of $\mathbf{T}$ and we were not able to deal with such a figure of merit.

kept constant, that is

$$\begin{aligned}\text{ATxP} &\triangleq \frac{1}{M}\mathsf{E}\left\{\text{tr}\left[\mathbf{F}_0\mathbf{T}^{-1}\mathbf{s}\mathbf{s}^H\mathbf{T}^{-H}\mathbf{F}_0^H\right]\right\}\\ &= \frac{\sigma_s^2}{M}\text{tr}\{\mathbf{T}^{-1}\mathbf{T}^{-H}\mathbf{F}_0^H\mathbf{F}_0\}\\ &= \frac{\sigma_s^2}{M}\text{tr}\{\mathbf{T}^{-2}\} = \frac{\sigma_s^2}{M}\sum_{m=0}^{M-1} t_m^{-2}\\ &= \sigma_s^2 = \frac{1}{M}\mathsf{E}\left\{\text{tr}\left[\mathbf{s}\mathbf{s}^H\right]\right\},\end{aligned} \tag{H.3}$$

since $\mathbf{F}_0^H\mathbf{F}_0 = \mathbf{I}$ and $\text{tr}\{\mathbf{T}^{-2}\}$ is constrained to be M. By applying the Lagrange-multiplier method, we have the following cost-function (see also [39]):

$$J(t_0,\cdots,t_{M-1}) \triangleq \sum_{m=0}^{M-1} t_m^2\|\mathbf{g}_m\|_2^2 + \lambda\left(\sum_{m=0}^{M-1} t_m^{-2} - M\right), \tag{H.4}$$

which can be optimized by finding its associated extreme points, as follows:

$$\frac{\partial J(t_0,\cdots,t_{M-1})}{\partial t_{m'}} = 2t_{m'}\|\mathbf{g}_{m'}\|_2^2 - 2\lambda t_{m'}^{-3}\,. \tag{H.5}$$

Thus, for $m \in \{0,1,\cdots,M-1\}$, we have

$$\frac{\partial J(t_0,\cdots,t_m^*,\cdots,t_{M-1})}{\partial t_m} = 0 \Leftrightarrow t_m^* = \sqrt[4]{\frac{\lambda}{\|\mathbf{g}_m\|_2^2}}\,, \tag{H.6}$$

in which we only considered the positive real root. Now, we can substitute the values t_m^* into the constraint described in Eq. (H.2) in order to determine λ. Hence, we have

$$\sum_{m=0}^{M-1}\frac{\|\mathbf{g}_m\|_2}{\sqrt{\lambda}} = M \Leftrightarrow \sqrt{\lambda} = \frac{\sum_{m=0}^{M-1}\|\mathbf{g}_m\|_2}{M}. \tag{H.7}$$

Now, by using Eq. (H.7) in Eq. (H.6), we obtain the optimal solution

$$t_m^* = \sqrt{\frac{\sum_{m'=0}^{M-1}\|\mathbf{g}_{m'}\|_2}{M\|\mathbf{g}_m\|_2}}, \quad \forall m \in \{0,1,\cdots,M-1\}. \tag{H.8}$$

Note that this solution is associated with the minimization of the cost-function $J:\mathbb{R}^M \longrightarrow \mathbb{R}$, defined in Eq. (H.4). In fact, from (H.5), we have

$$\frac{\partial^2 J(t_0,\cdots,t_{M-1})}{\partial t_{m''}\partial t_{m'}} = 6\lambda t_{m'}^{-4}\delta[m'-m'']\,, \tag{H.9}$$

where $\delta[x] = 1$ when $x = 0$, and $\delta[x] = 0$ otherwise. Thus, the Hessian matrix associated with the cost-function J is a diagonal matrix. From (H.7), we know that $\lambda > 0$. Each diagonal element of the Hessian matrix is, therefore, positive, yielding a positive-definite Hessian matrix.

Figure H.2 depicts the detailed structure of the zero-forcing multicarrier transceiver with minimum redundancy. This transceiver employs the optimal power-allocation scheme that we have just derived. The first step of the transmitter processing is to multiply each symbol in a data block by a real number (optimal weight $1/t_m^*$, for the mth symbol in the data block). After that, the entire block is transformed through the application of the IDFT and the $L/2$ guard-zeros are introduced. At the receiver end, a prefilter may be included in order to shorten the channel. After removing the guard period, M parallel phase shifts are performed, where the mth phase shifter, or rotator, is defined as $e^{-\jmath\frac{\pi}{M}m}$. The first equalization step is performed after the application of the IDFT on the data vector. Then, the resulting data vector is simultaneously processed by two different branches of the transceiver. The 1-tap equalizers in this stage are the elements of the vectors $\tilde{\mathbf{q}}_1$ and $\tilde{\mathbf{q}}_2$. After the application of the DFT, phase shifts are performed again, but now the mth rotator is defined as $e^{\jmath\frac{\pi}{M}m}$. Another equalization step is performed in each branch, after the application of the DFT on the phase-shifted data vectors. The 1-tap equalizers in this stage are the elements of the vectors $\tilde{\mathbf{p}}_1$ and $\tilde{\mathbf{p}}_2$. The last step of the receiver processing is to equalize the power throughout the whole data block. This is implemented by multiplying the mth symbol estimate by t_m^*. The related MMSE transceiver has a similar structure, except for the four parallel branches at the receiver end.

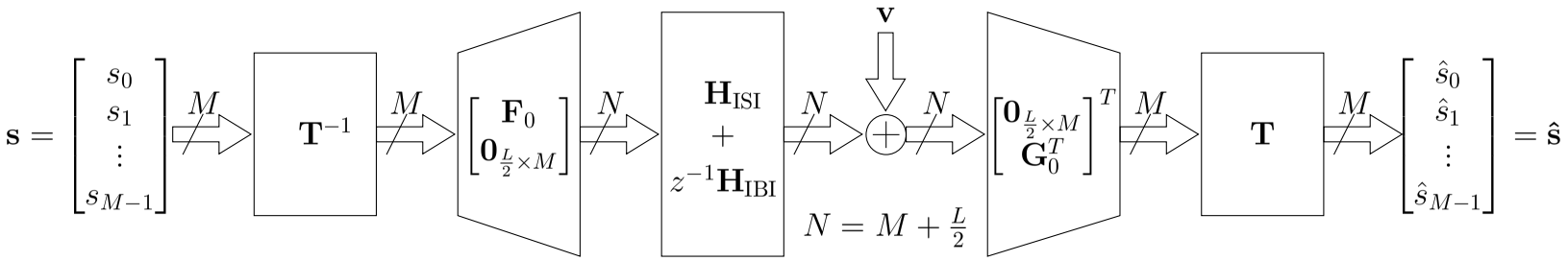

Figure H.1: Mathematical transceiver model with a diagonal precoder (power allocation).

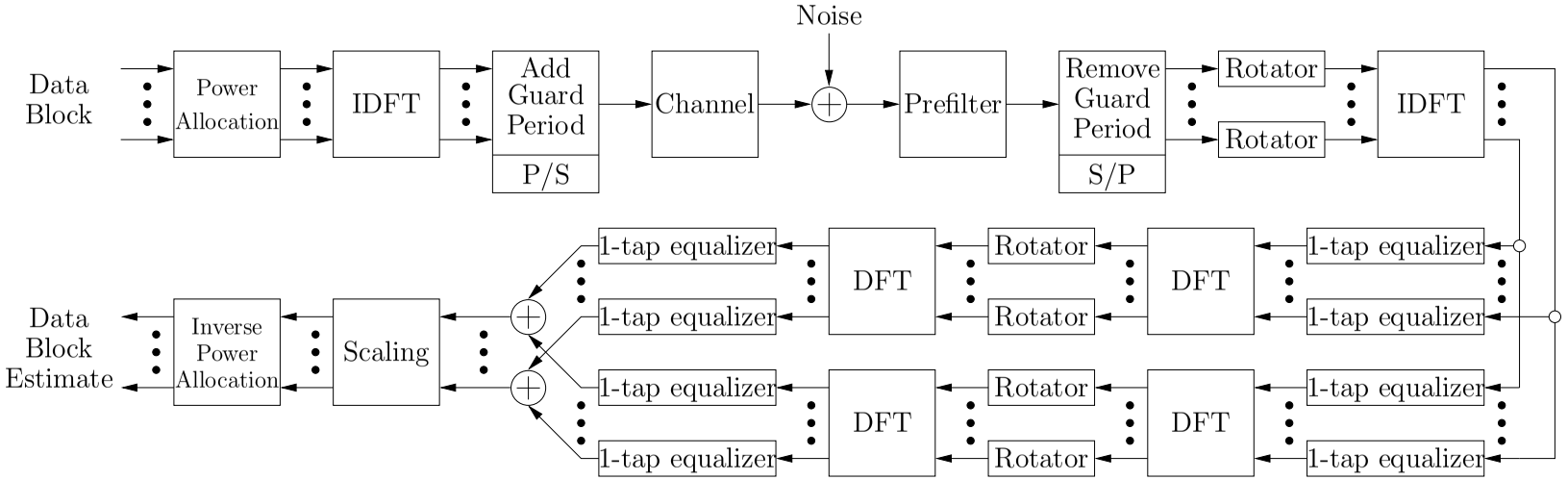

Figure H.2: DFT-based zero-forcing multicarrier minimum-redundancy block transceiver (ZF-MC-MRBT) with power allocation.

H.2 Simulation Results

We transmit 10,000 data blocks carrying $M = 16$ symbols of a 16-QAM constellation. In fact, each data block stems from 32 data bits that, after channel coding (with constraint length 7, code rate $r_c = 1/2$, and octal generators $\mathbf{g_0} = [\mathbf{133}]$ and $\mathbf{g_1} = [\mathbf{165}]$) [74], yield 64 bits to be baseband modulated. We assume that both symbol and channel models use the sample frequency $f_s = 100$ MHz. In addition, we only consider multicarrier systems, since we verified that the proposals are not effective for single-carrier systems.

In our first experiment, we assess the uncoded-BER and throughput performances of the multicarrier minimum-redundancy block transceivers (MC-MRBT) in two configurations: without precoding and with per-symbol precoding (each $1/t_m^*$ in Eq. (H.8) multiplies an element of the vector $\mathbf{s}$), *which is always indicated by the letter P*. In addition, we also depict the results for the OFDM-based systems as a reference. The channel model used here (Channel A [76]) has zeros 1.2, -1.2, $0.7\jmath$, and $-0.7\jmath$, implying that $L = 4$. From Figure H.3 and Figure H.4, one can verify that, in the SNR range above 15 dB, the gain from using the power-allocation method proposed in this work is noticeable. The throughput results are depicted in Figure H.5 and Figure H.6.

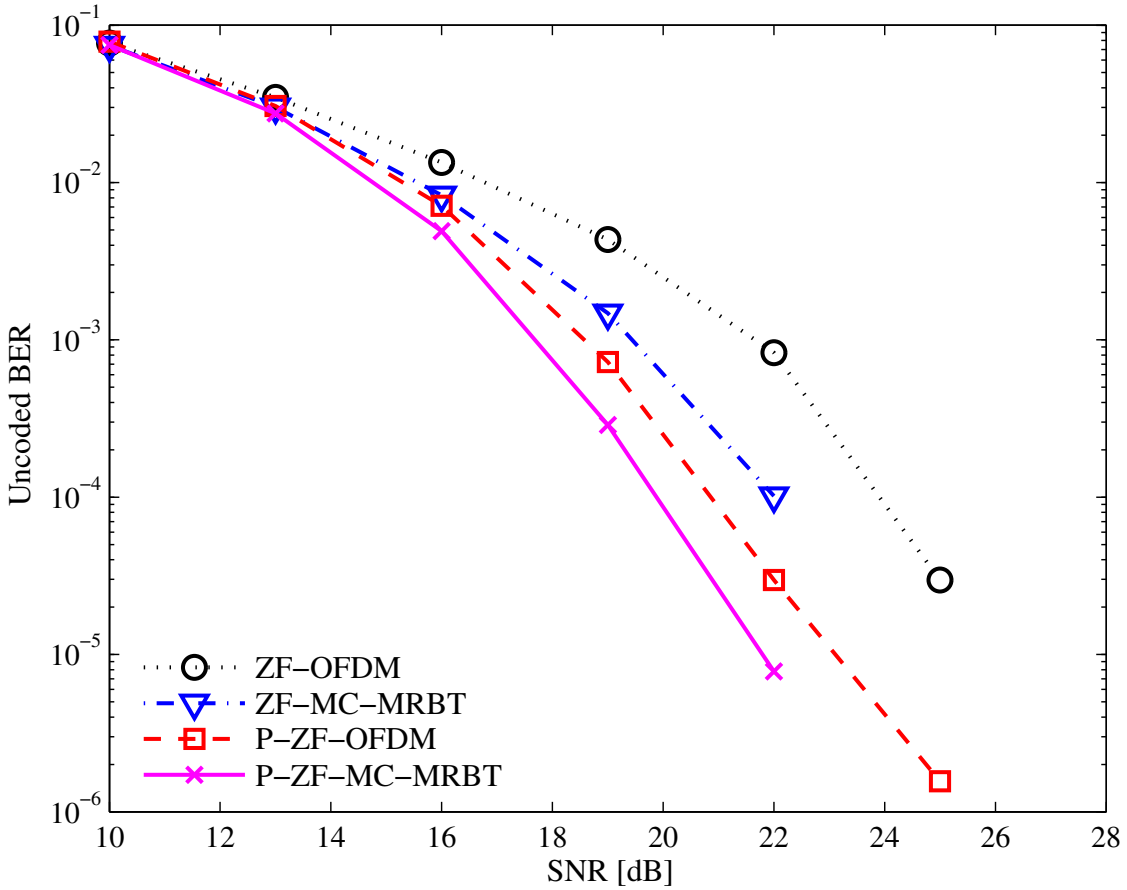

Figure H.3: Uncoded BER as a function of SNR [dB] for Channel A, considering ZF-based multicarrier transmissions.

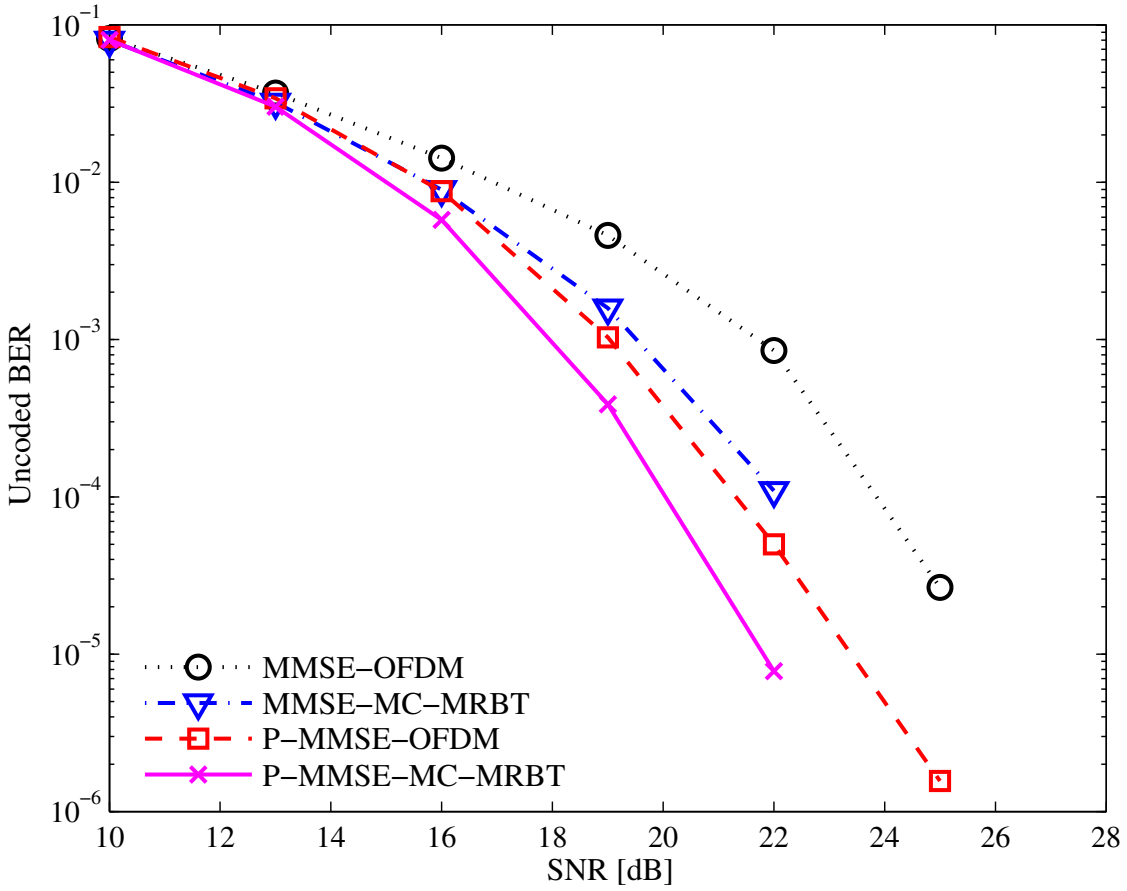

Figure H.4: Uncoded BER as a function of SNR [dB] for Channel A, considering MMSE-based multicarrier transmissions.

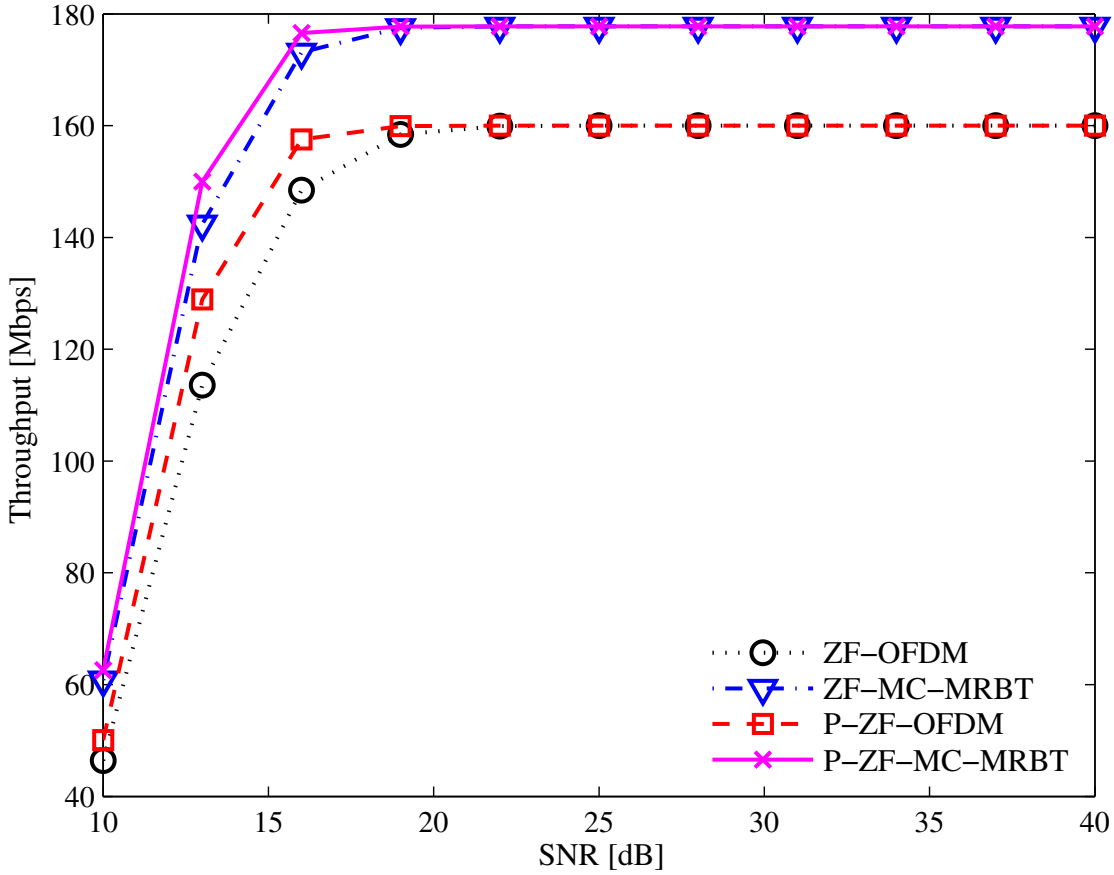

Figure H.5: Throughput [Mbps] as a function of SNR [dB] for Channel A, considering ZF-based multicarrier transmissions.

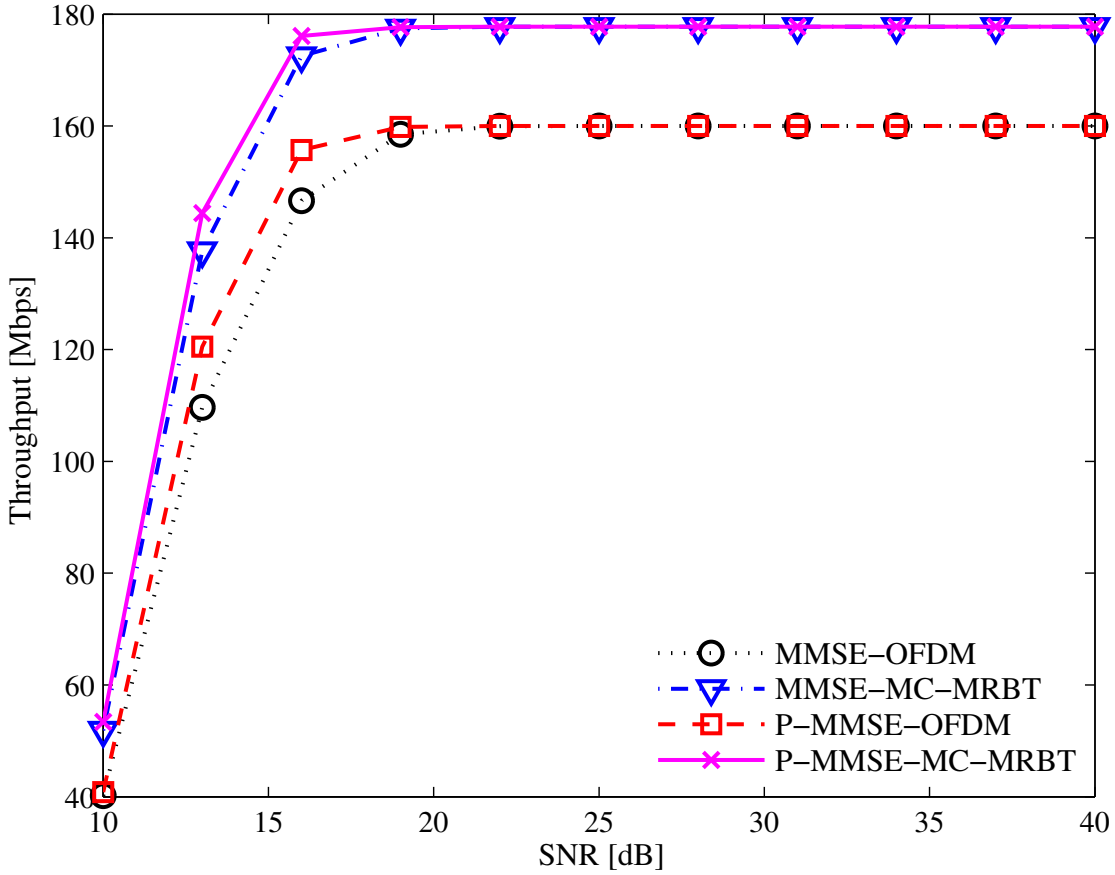

Figure H.6: Throughput [Mbps] as a function of SNR [dB] for Channel A, considering MMSE-based multicarrier transmissions.

In our second experiment, we assess the performance of the same transceivers previously discussed. The channel model (Channel B [75]) is

$$H(z) = 1 + 0.5z^{-1} - 0.7z^{-2} + 0.9z^{-3} + z^{-4}. \tag{H.10}$$

From Figures H.7, H.8, H.9, H.10, one can verify the throughput gains due to the proposed power allocation.

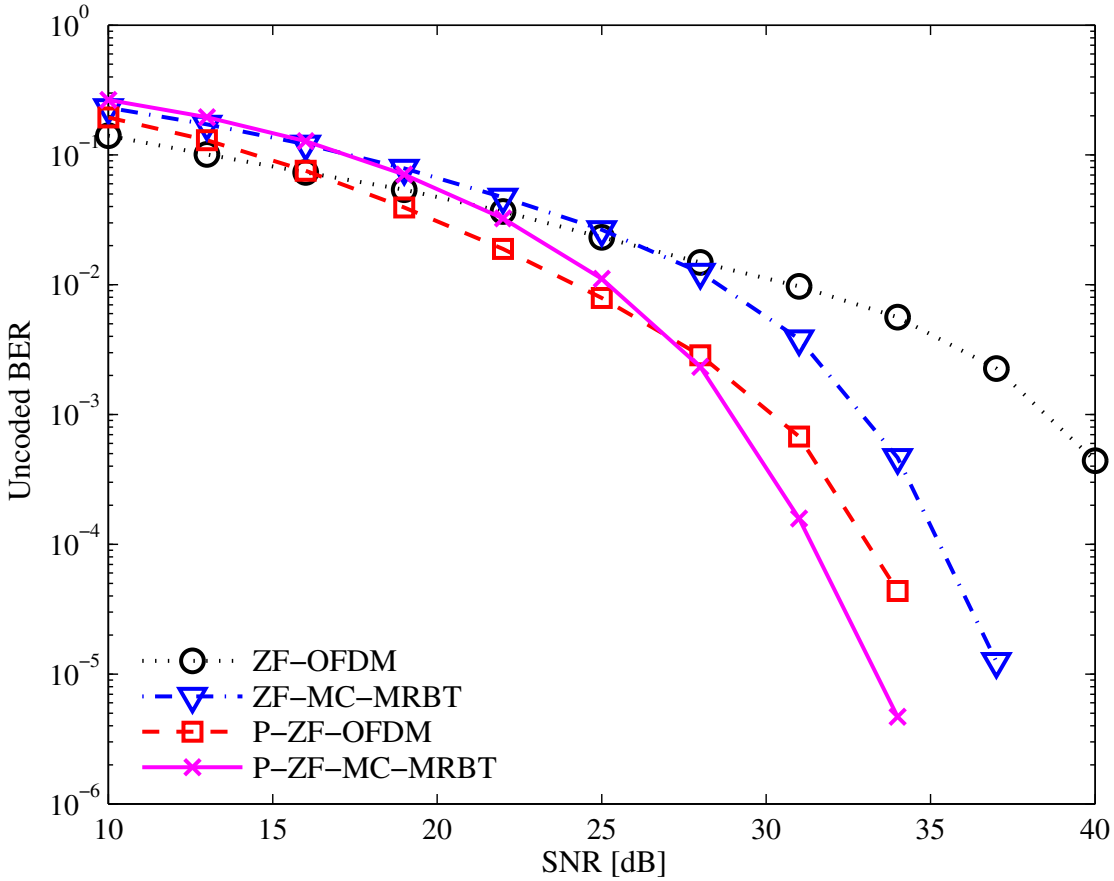

Figure H.7: Uncoded BER as a function of SNR [dB] for Channel B, considering ZF-based multicarrier transmissions.

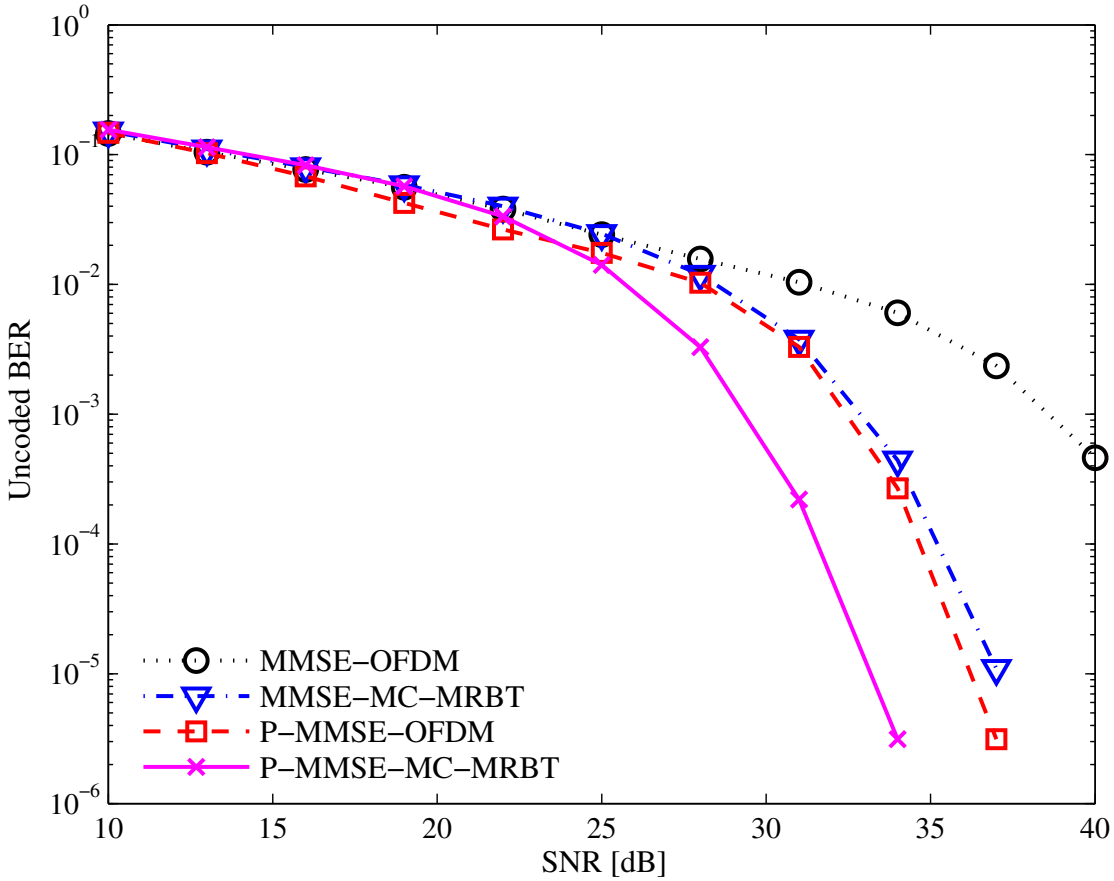

Figure H.8: Uncoded BER as a function of SNR [dB] for Channel B, considering MMSE-based multicarrier transmissions.

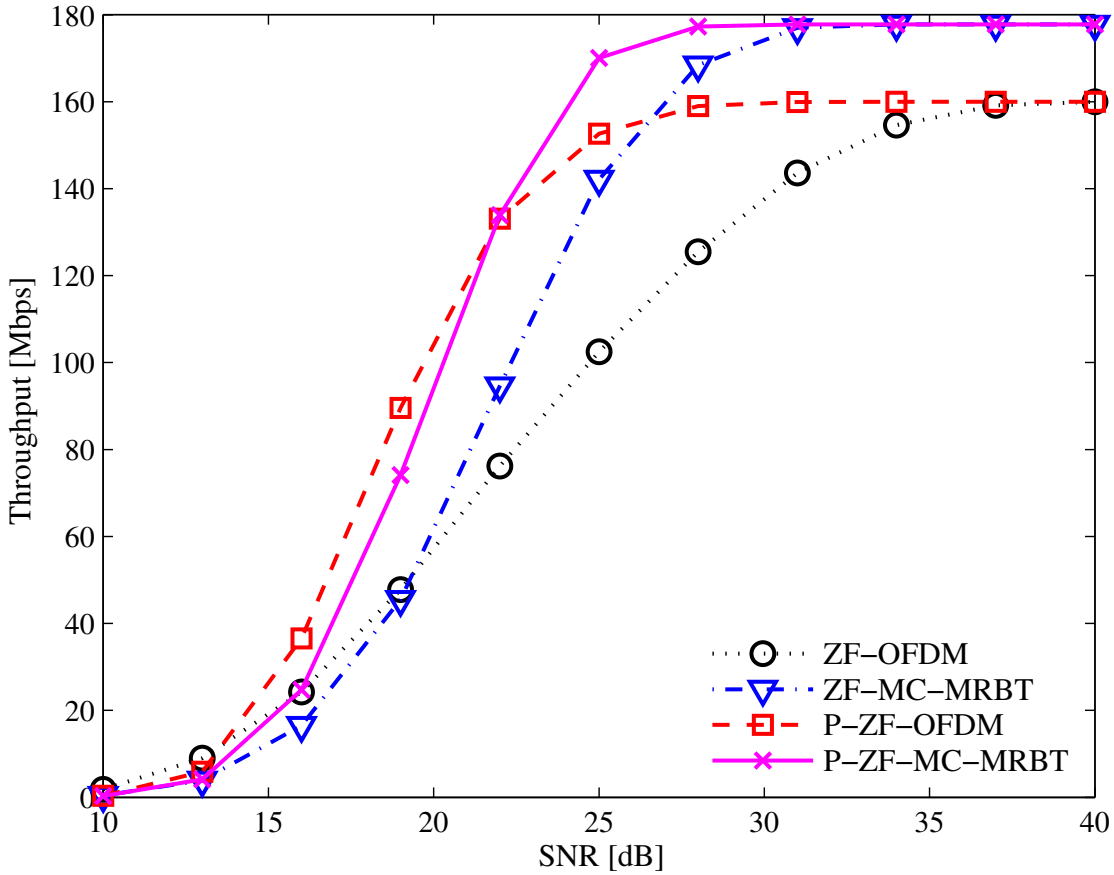

Figure H.9: Throughput [Mbps] as a function of SNR [dB] for Channel B, considering ZF-based multicarrier transmissions.

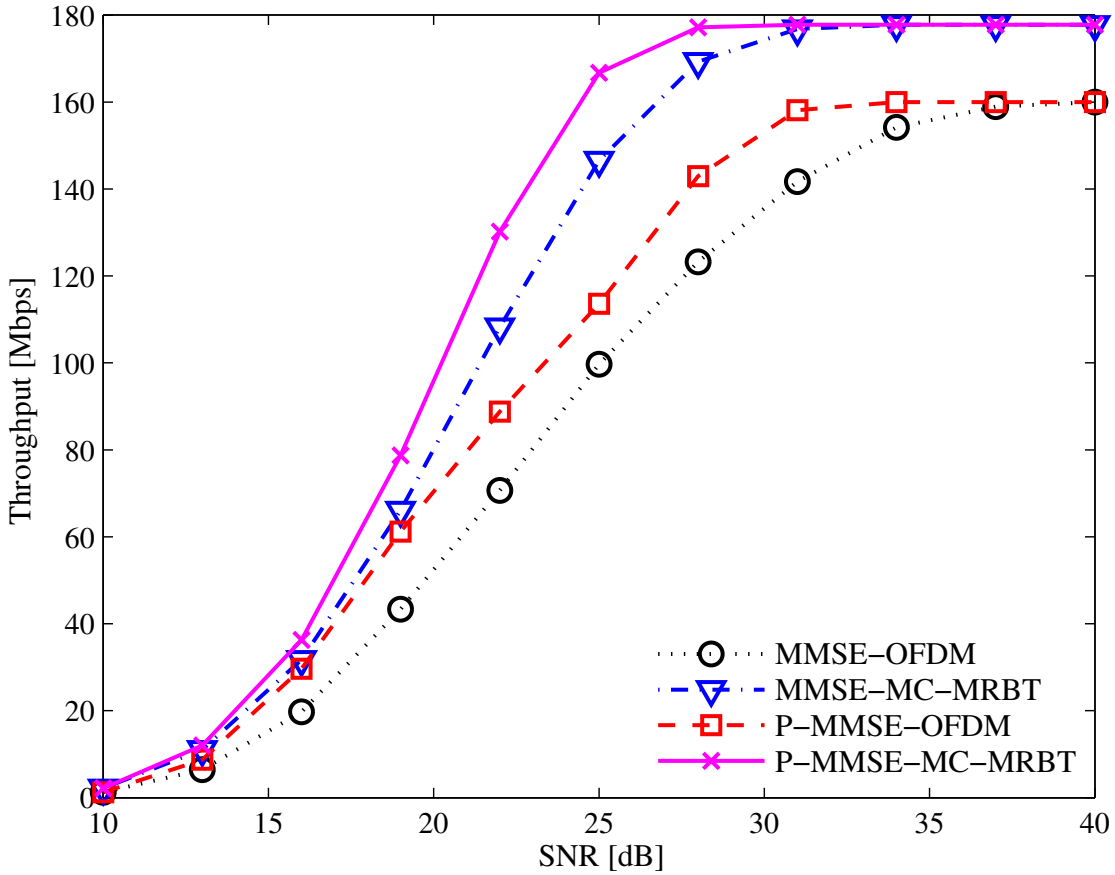

Figure H.10: Throughput [Mbps] as a function of SNR [dB] for Channel B, considering MMSE-based multicarrier transmissions.

The third experiment is equal to the previous one, except for the channel model (Channel C [31]), whose zeros are 1, $0.9\jmath$, $-0.9\jmath$, and $1.3e^{\jmath 5\pi/8}$. Once again, the new proposals outperform the existing systems, as depicted in Figures H.11, H.12, H.13, H.14. Moreover, the performances of the minimum-redundancy systems are much better than the performances of both the traditional OFDM system and the precoded OFDM system. This occurs since OFDM-based systems have poor performances when the channel model has zeros on the unit circle [31, 40].

H.3 Concluding Remarks

We presented in this chapter a power-allocation method specially designed to minimize the noise gains inherent to block-based transceivers with minimum redundancy. The resulting transceivers still require $\mathcal{O}(M \log_2 M)$ complex-valued numerical operations to equalize a received vector. In addition, the throughput performance is enhanced as the simulation results illustrate.

The problem of power allocation aiming at maximizing the channel capacity remains open and should be addressed in a future work.

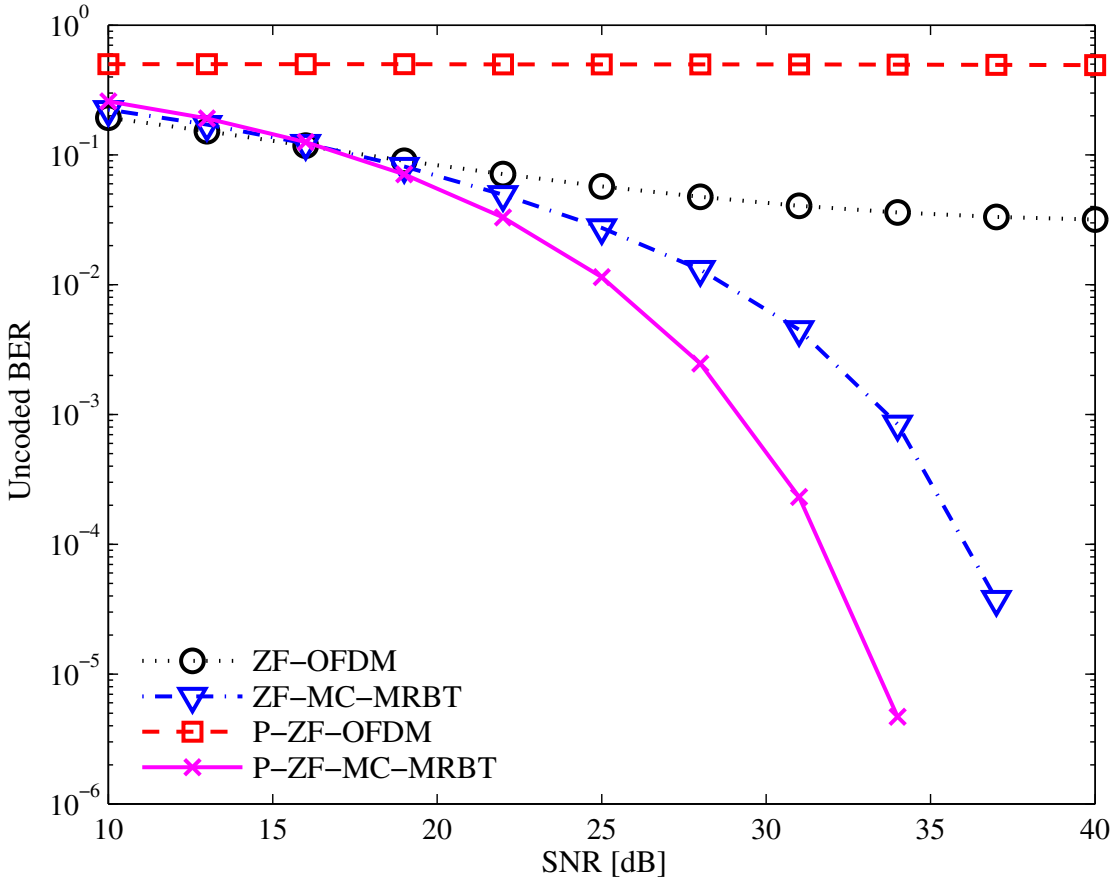

Figure H.11: Uncoded BER as a function of SNR [dB] for Channel C, considering ZF-based multicarrier transmissions.

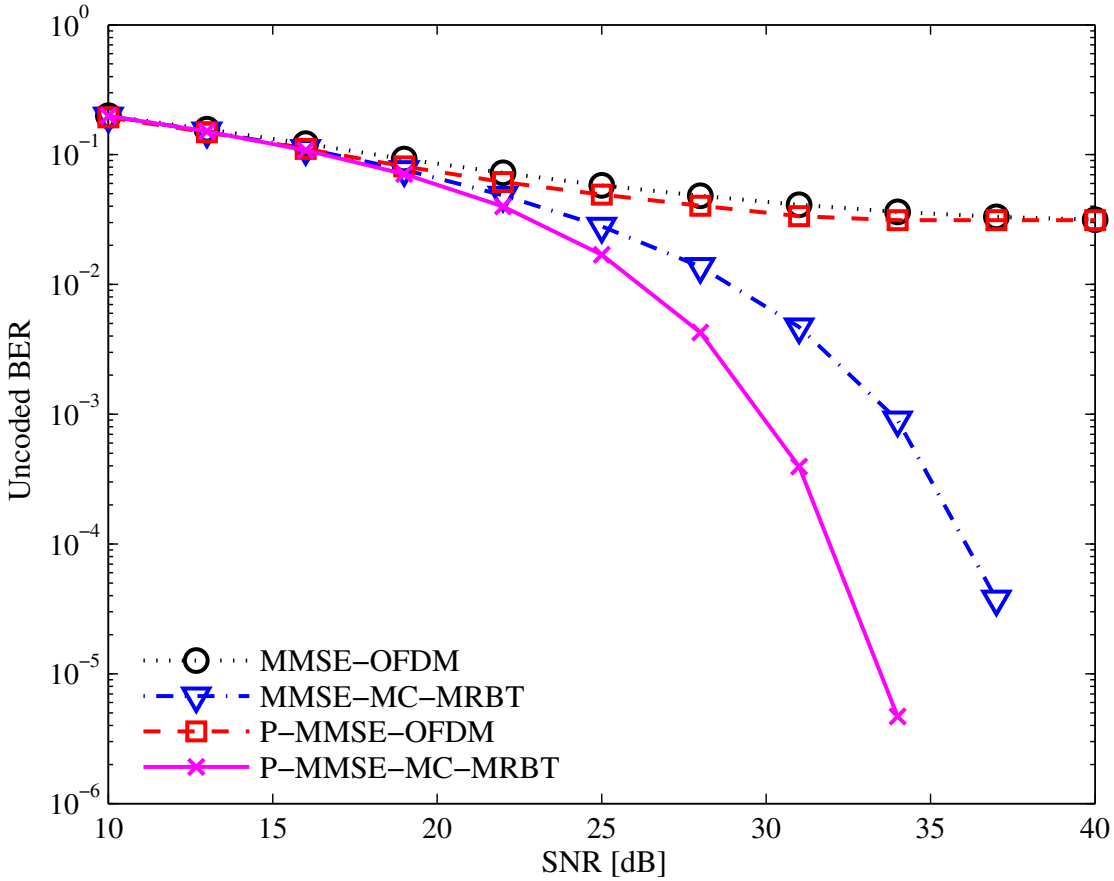

Figure H.12: Uncoded BER as a function of SNR [dB] for Channel C, considering MMSE-based multicarrier transmissions.

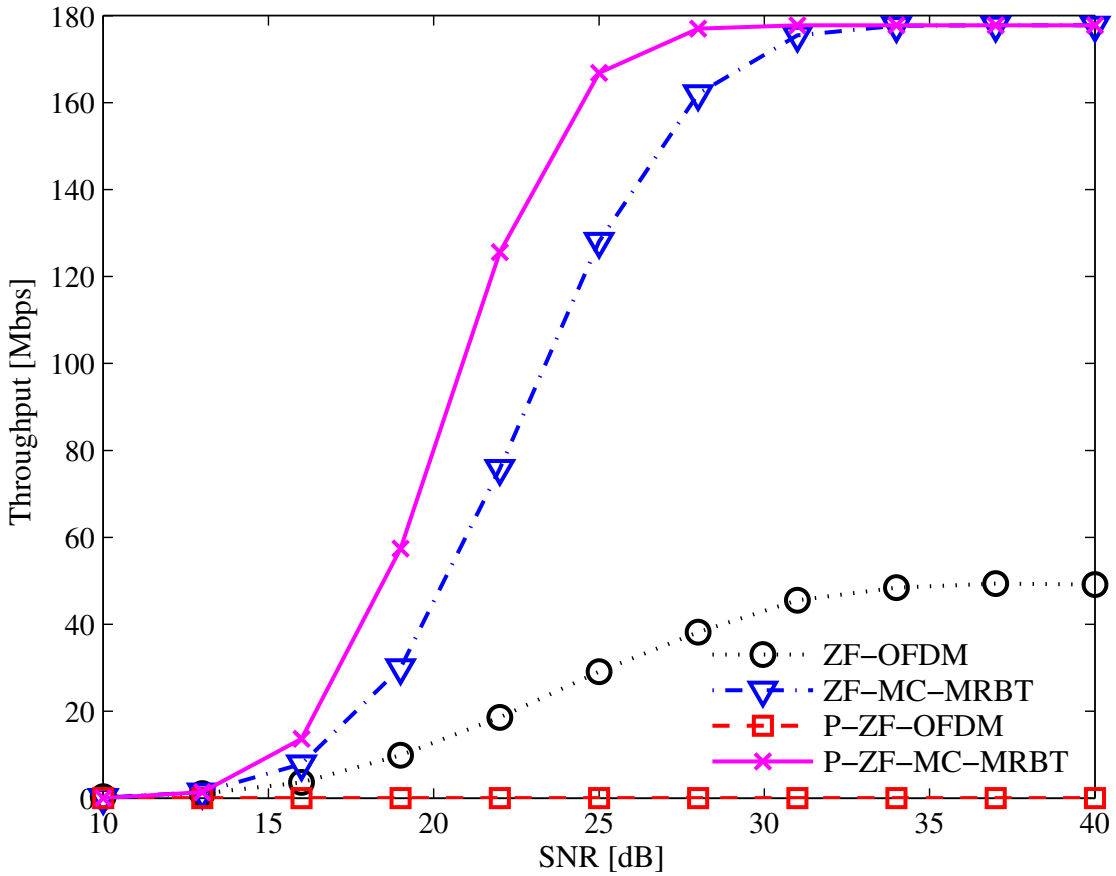

Figure H.13: Throughput [Mbps] as a function of SNR [dB] for Channel C, considering ZF-based multicarrier transmissions.

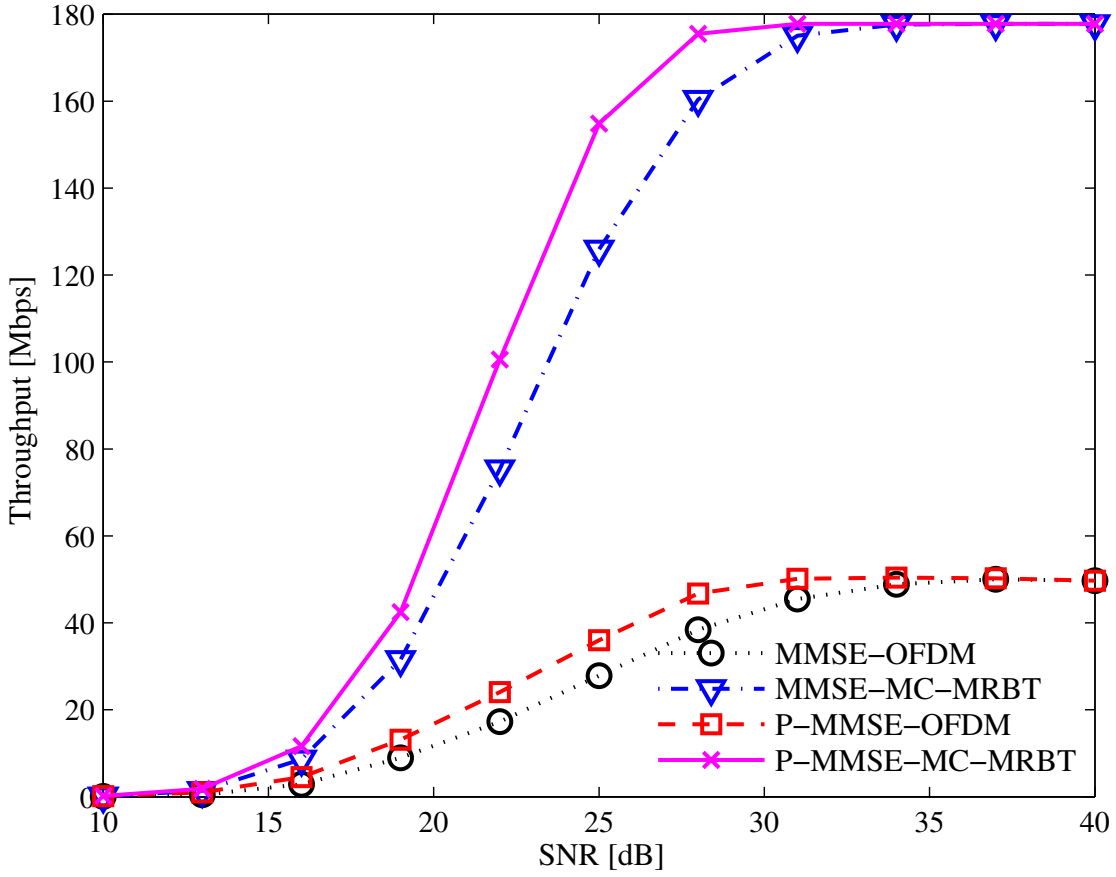

Figure H.14: Throughput [Mbps] as a function of SNR [dB] for Channel C, considering MMSE-based multicarrier transmissions.

Apêndice I

Block-Based DFEs with Reduced Redundancy

Equalization plays an important role in any modern digital transmission scheme. Linear equalizers are still the preferred choice in practical systems due to their computational simplicity. However, the constant performance improvements of digital processors have enabled the use of nonlinear equalizers as well. The nonlinearities induce certain degrees of freedom which are not exploited in linear equalization. Among the nonlinear receivers, decision-feedback equalizers (DFE) [40, 50–52] are the most popular since they feature good tradeoff between performance improvements and computational complexity.

In modern communications, it is common practice to segment the overall data string into smaller blocks that are transmitted separately in the so-called block-based transmission. Such separation in blocks is rather useful in block-based DFEs, since any symbol error within a given data block is not propagated across different blocks. Nonetheless, the undesired superposition of signals inherent to broadband communications generates interblock interference (IBI) between adjacent transmitted data blocks. IBI can be eliminated by transmitting redundant signals, such as zero-padded or cyclic-prefixed signals [7, 40]. However, one should optimize the use of the spectral resources in broadband transmissions. A possible way to address this problem is to reduce the amount of redundancy required by block transmissions to avoid interblock interference. An efficient solution is to employ zero-padding zero-jamming (ZP-ZJ) transceivers, which allow the transmission with reduced redundancy. Nevertheless, just few works have employed ZP-ZJ transceivers and all of them consider only linear equalizers.

This chapter shows that ZP-ZJ techniques can also be successfully applied in the context of DFE systems. The chapter describes how to apply known minimum mean-square error (MMSE) solutions with zero-forcing (ZF) constraints to block-based DFEs within the context of reduced-redundancy systems. The chapter also

includes some mathematical results which describe the monotone behavior of several figures of merit related to ZP-ZJ DFE systems (such as MSE of symbols, mutual information, error probability of symbols, etc.) The proposed analyses indicate that the reduction in the amount of redundancy leads to loss in performance of these figures of merit, not including the throughput. In fact, throughput may increase by reducing the amount of redundant signals, as will be clearer in the simulation results.

This chapter is organized as follows: Section I.1 contains the description of the proposed block-based DFE with reduced redundancy. In Section I.2 we state some mathematical results which describe formally the monotone behavior of several figures of merit associated with the proposed DFEs. The simulation results are in Section I.3, whereas the concluding remarks are in Section I.4.

I.1 DFE with Reduced Redundancy

As we have been doing throughout this thesis, let us assume that we want to transmit a vector $\mathbf{s} \in \mathcal{C}^{M\times 1} \subset \mathbb{C}^{M\times 1}$, with $M \in \mathbb{N}$ symbols drawn from a given constellation $\mathcal{C}$, through an FIR channel whose transfer function is

$$H(z) \triangleq h(0) + h(1)z^{-1} + \cdots + h(L)z^{-L}, \tag{I.1}$$

with $h(l) \in \mathbb{C}$, for each $l \in \{0, 1, \cdots, L\} \subset \mathbb{N}$. We already know that the matrix representation of such block-transmission scheme is given as

$$\mathbf{H}(z) \triangleq \mathbf{H}_{\text{ISI}} + z^{-1}\mathbf{H}_{\text{IBI}} \in \mathbb{C}^{N\times N}[z^{-1}], \tag{I.2}$$

in which $\mathbb{N} \ni N \geq \max\{M, L\}$ is the number of transmitted elements in a block, while $\mathbf{H}_{\text{ISI}}$ and $\mathbf{H}_{\text{IBI}}$ are Toeplitz matrices.

The first row of $\mathbf{H}_{\text{ISI}}$ is $[h(0) \quad \mathbf{0}^T_{(N-1)\times 1}]$, whereas the first column is $[h(0) \quad h(1) \quad \cdots \quad h(L) \quad \mathbf{0}^T_{(N-L-1)\times 1}]^T$. In matrix $\mathbf{H}_{\text{IBI}}$, the first row is $[\mathbf{0}^T_{(N-L)\times 1} \; h(L) \; h(L-1) \; \cdots \; h(1)]$, whilst the first column is $\mathbf{0}_{N\times 1}$.

In order to eliminate the IBI effect modeled by matrix $\mathbf{H}_{\text{IBI}}$, one can append $K \triangleq N - M$ zeros to the transformed vector $\mathbf{Fs}$ at the transmitter end, in which $\mathbf{F} \in \mathbb{C}^{M\times M}$ is a precoder matrix. The received vector of size N will still suffer from IBI effects in its first $L - K$ elements. The receiver thus ignores these first $L - K$ signals, working only with the remaining $N - (L - K) = (M + K) - (L - K) = M + 2K - L$ elements. These elements are first transformed into M signals by the feedforward matrix $\mathbf{G} \in \mathbb{C}^{M\times(M+2K-L)}$, as depicted in Figure I.1.[1]

[1]For a more detailed alternative explanation, the reader should refer to Section D.1.

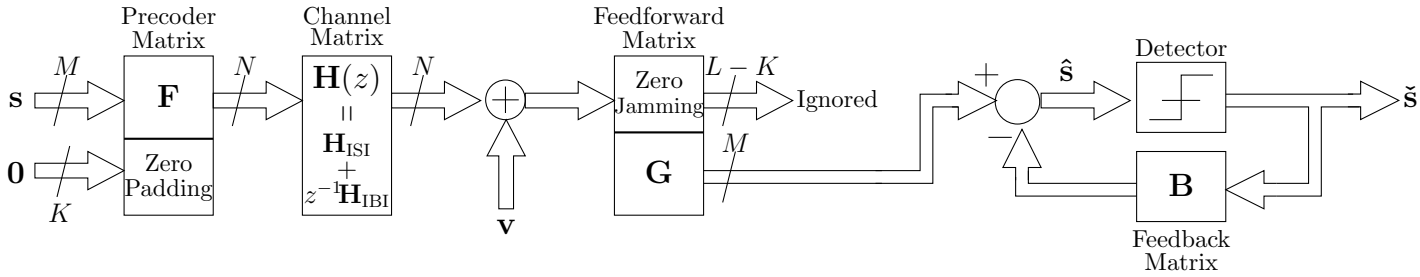

Figure I.1: General structure of the proposed ZP-ZJ block-based DFE.

As illustrated in Figure I.1, after the multiplication by the feedforward matrix, the received vector passes through a usual decision-feedback processing [40, 50–52]. In this figure, $\check{\mathbf{s}} \in \mathcal{C}^{M\times 1}$ denotes the vector containing the detected symbols and $\mathbf{B} \in \mathbb{C}^{M\times M}$ is the feedback matrix. As pointed out in Subsection C.1.2, this matrix is chosen strictly upper triangular, so that the symbol estimation within a data block is sequentially performed, guaranteeing the causality of the process [40].

The ZP-ZJ structure of the DFE proposed in Figure I.1 can be simplified if one incorporates the ZP-ZJ processing into the channel model, yielding an effective channel matrix $\mathbf{H}$,[2] which is Toeplitz and has dimension $(M + 2K - L) \times M$. In this case, the first row of $\mathbf{H}$ is $[h(L-K)\ h(L-K-1)\ \cdots\ h(0)\ \mathbf{0}^T_{(M+K-L-1)\times 1}]$, whereas the first column is $[h(L-K)\ h(L-K+1)\ \cdots\ h(L)\ \mathbf{0}^T_{(M+K-L-1)\times 1}]^T$. The equivalent structure is depicted in Figure I.2.

Under the common simplifying assumption of perfect decisions [40], one has $\check{\mathbf{s}} = \mathbf{s}$, yielding $\hat{\mathbf{s}} = (\mathbf{GHF} - \mathbf{B})\mathbf{s} + \mathbf{G}\bar{\mathbf{v}}$ (see Figure I.2). Hence, the overall MSE of symbols, $\mathcal{E}$, is given as (see Subsection C.1.2)

$$\mathcal{E} \triangleq \mathsf{E}\{\|\hat{\boldsymbol{s}} - \boldsymbol{s}\|_2^2\} = \sigma_s^2 \|\mathbf{GHF} - \mathbf{B} - \mathbf{I}_M\|_{\mathrm{F}}^2 + \sigma_v^2 \|\mathbf{G}\|_{\mathrm{F}}^2, \tag{I.3}$$

where we have assumed that the transmitted vector $\mathbf{s}$ and the channel-noise vector $\bar{\mathbf{v}}$ are respectively drawn from zero-mean jointly wide-sense stationary (WSS) random processes $\boldsymbol{s}$ and $\bar{\boldsymbol{v}}$. In addition, we have assumed that $\boldsymbol{s}$ and $\bar{\boldsymbol{v}}$ are uncorrelated, i.e., $\mathsf{E}\{\boldsymbol{s}\bar{\boldsymbol{v}}^H\} = \mathsf{E}\{\boldsymbol{s}\}\mathsf{E}\{\bar{\boldsymbol{v}}\}^H = \mathbf{0}_{M\times N}$, and that $\sigma_v^2, \sigma_s^2 \in \mathbb{R}_+$.

Now, the design of matrices $\mathbf{F}$, $\mathbf{G}$, and $\mathbf{B}$ can be formulated as an MSE-based

[2]Sometimes, we shall denote $\mathbf{H}$ as $\mathbf{H}(K)$ in order to emphasize that the related effective channel matrix is built considering the transmission of K redundant zeros.

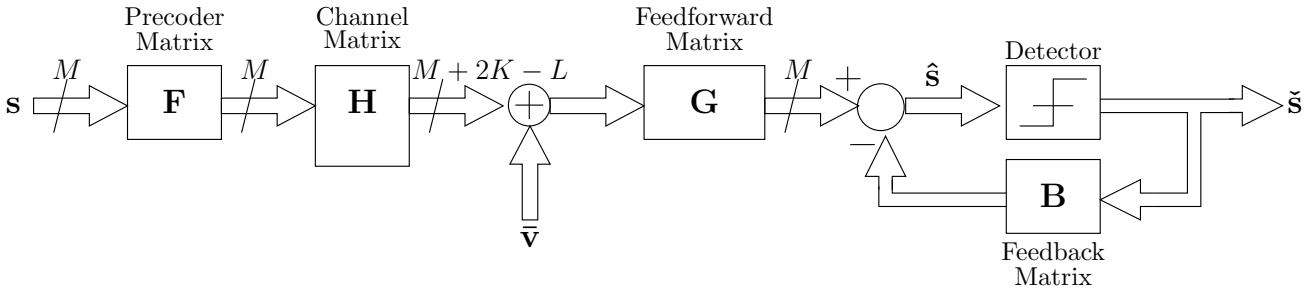

Figure I.2: Equivalent structure of the proposed ZP-ZJ block-based DFE.

optimization problem, as follows [40]:

$$\min_{\mathbf{F},\mathbf{G},\mathbf{B}} \left\{\sigma_s^2 \|\mathbf{GHF} - \mathbf{B} - \mathbf{I}_M\|_{\mathrm{F}}^2 + \sigma_v^2 \|\mathbf{G}\|_{\mathrm{F}}^2\right\}, \tag{I.4}$$

subject to:

$$(\mathbf{GHF} - \mathbf{B} - \mathbf{I}_M) = 0, \tag{I.5}$$

$$\|\mathbf{F}\|_{\mathrm{F}}^2 = M, \tag{I.6}$$

$$[\mathbf{B}]_{mn} = 0, \ \forall m \geq n, \tag{I.7}$$

where, in order to simplify the forthcoming mathematical descriptions, we focus only on MMSE solutions that meet the ZF constraint.

The equivalent structure of the proposed ZP-ZJ block-based DFE illustrated in Figure I.2 matches the general block-based DFE model described, for instance, in [40]. Therefore, the solutions to the above optimization problem are already known and can be described as [40] (p. 816):

$$\mathbf{F} = \mathbf{V}_{\mathbf{H}}\mathbf{S}, \tag{I.8}$$

$$\mathbf{G} = \mathbf{R}\mathbf{S}^H\mathbf{\Sigma}_{\mathbf{H}}^{-1}[\mathbf{I}_M \ \ \mathbf{0}_{M\times(2K-L)}]\mathbf{U}_{\mathbf{H}}^H, \tag{I.9}$$

$$\mathbf{B} = \mathbf{R} - \mathbf{I}_M, \tag{I.10}$$

in which the above matrices come from the SVD decomposition of $\mathbf{H}$ and the QRS decomposition [40] of $\mathbf{\Sigma}_{\mathbf{H}}$, as follows:

$$\mathbf{H} = \underbrace{\mathbf{U}_{\mathbf{H}}}_{(M+2K-L)\times(M+2K-L)} \underbrace{\begin{bmatrix} \mathbf{\Sigma}_{\mathbf{H}} \\ \mathbf{0}_{(2K-L)\times M} \end{bmatrix}}_{(M+2K-L)\times M} \underbrace{\mathbf{V}_{\mathbf{H}}^H}_{M\times M}, \tag{I.11}$$

$$\mathbf{\Sigma}_{\mathbf{H}} = \sqrt[M]{\prod_{m=0}^{M-1} \sigma_m}\mathbf{Q}\mathbf{R}\mathbf{S}^H, \tag{I.12}$$

where $\mathbf{\Sigma}_{\mathbf{H}} = \mathbf{\Sigma}_{\mathbf{H}}^H > O$ is an $M \times M$ diagonal matrix containing the M nonzero singular values of $\mathbf{H}$. The mth diagonal element of $\mathbf{\Sigma}_{\mathbf{H}}$ is denoted as σ_m. In addition,

$\mathbf{Q}$ and $\mathbf{S}$ are $M \times M$ unitary matrices, whereas $\mathbf{R}$ is an $M \times M$ upper triangular matrix containing only 1s in its main diagonal. See [40, 77] and references therein for further detailed information on QRS decompositions.

It is worth mentioning that other optimal solutions[3] can be derived for ZP-ZJ DFE systems whose equivalent building-block description is given in Figure I.2.

I.2 Performance Analysis

As in the case of full-redundancy ZP-based transceivers described in Chapter C, several physical-layer figures of merit related to the proposed ZP-ZJ DFE have close connections with the singular values of the effective Toeplitz channel matrix $\mathbf{H}$. The following lemma characterizes the monotone behavior of all of these singular values with respect to the number of transmitted redundant elements, K.

Lemma 13. *Given two fixed natural numbers L and M, let us assume that each effective channel matrix $\mathbf{H}(K) \in \mathbb{C}^{(M+2K-L)\times M}$ is constructed from the same Lth-order channel-impulse response, with $K \in \{\lceil L/2 \rceil, \lceil L/2 \rceil + 1, \cdots, L\}$. Then*

$$\sigma_m(K+1) \geq \sigma_m(K), \tag{I.13}$$

where each $\sigma_m(K) \in \mathbb{R}_+$ is a singular value of $\mathbf{H}(K)$.

Proof. See Lemma 12 in Chapter F. □

By using Lemma 13, we can derive a very general result (Theorem 15) that encompasses as particular cases the majority of the popular figures of merit of practical interest (e.g., MSE of symbols, mutual information, error probability of symbols).

Theorem 15. *Let us assume that, for each $m \in \{0, 1, \cdots, M-1\}$, there exists a function $f_m : \mathbb{R}_+ \to \mathbb{R}$ such that a performance measure $\mathcal{J} : \{\lceil L/2 \rceil, \lceil L/2 \rceil + 1, \cdots, L\} \to \mathbb{R}$ associated with the proposed ZP-ZJ DFE transceiver can be defined as*

$$\mathcal{J}(K) \triangleq \frac{1}{M} \sum_{m=0}^{M-1} f_m(\sigma_m(K)) \quad or \; \mathcal{J}(K) \triangleq \sqrt[M]{\prod_{m=0}^{M-1} f_m(\sigma_m(K))}. \tag{I.14}$$

If f_m is monotone increasing for all m, then $\mathcal{J}(K+1) \geq \mathcal{J}(K)$, for all K. Likewise, if f_m is monotone decreasing for all m, then $\mathcal{J}(K+1) \leq \mathcal{J}(K)$, for all K.

Proof. This is a straightforward application of Lemma 13. □

[3] For instance, MMSE-based solutions with channel-independent unitary precoder or Pure MMSE-based solutions [40].

Since the resulting MSE of symbols, $\mathcal{E}(K)$, the overall mutual information between transmitted and estimated symbols, $\mathcal{I}(K)$, and the average error probability of symbols, $\mathcal{P}(K)$, are respectively given by (see [40] and Chapter C):

$$\mathcal{E}(K) = M\sigma_v^2 \sqrt[M]{\prod_{m=0}^{M-1} \frac{1}{\sigma_m^2(K)}}, \tag{I.15}$$

$$\mathcal{I}(K) = M \ln\left(1 + \frac{\sigma_s^2}{\sigma_v^2} \sqrt[M]{\prod_{m=0}^{M-1} \sigma_m^2(K)}\right), \tag{I.16}$$

$$\mathcal{P}(K) = c\mathcal{Q}\left(A\sqrt{\frac{1}{\mathcal{E}(K)/M}}\right), \tag{I.17}$$

in which c and A are positive real constants that depend on the particular constellation $\mathcal{C}$, whereas $\mathcal{Q}(\cdot)$ is a decreasing function of its argument, being defined as

$$\mathcal{Q}(x) \triangleq \frac{1}{\sqrt{2\pi}} \int_x^\infty \mathrm{e}^{-x^2/2} \mathrm{d}x, \tag{I.18}$$

then, the following corollary holds.

Corollary 6. *Given the definitions in Lemma 13, we have*

$$\mathcal{E}(K+1) \leq \mathcal{E}(K), \;\; \mathcal{I}(K+1) \geq \mathcal{I}(K), \;\; \mathcal{P}(K+1) \leq \mathcal{P}(K), \tag{I.19}$$

with $K \in \{\lceil L/2 \rceil, \lceil L/2 \rceil + 1, \cdots, L-1\}$.

Proof. The inequalities come from the application of Theorem 15, along with the fact that $\mathcal{E}(K)$ is monotone decreasing, $\mathcal{I}(K)$ is monotone increasing, and $\mathcal{P}(K)$ is monotone decreasing with respect to each singular value $\sigma_m(K)$. □

Corollary 6 may lead us to a wrong conclusion that it is not worth reducing the amount of transmitted redundant elements. Nevertheless, if on one hand we need to use as much redundancy as possible in order to achieve lower probability of error or MSE of symbols (as described in Corollary 6), on the other hand we must reduce the transmitted redundancy to save bandwidth, which is paramount in high data-rate systems. In order to take both effects into account, one should consider throughput as figure of merit.

Section I.3 shows some setups where the proposed reduced-redundancy DFE outperforms the traditional full-redundancy zero-padding DFE with respect to the throughput performance.

I.3 Simulation Results

The aim of this section is to assess the throughput performance of the proposed DFE with reduced redundancy through a numerical example. We consider the transmission of $10,000$ data blocks containing $M = 16$ 16-QAM symbols through a 5th-order channel whose zeros are placed at 0.999, -0.999, $0.7\jmath$, $-0.7\jmath$, and $-0.4\jmath$. In this case, $K \in \{3, 4, 5\}$.

In order to generate each data block, we produce 32 random bits that, after passing through a convolutional channel-coding process with code rate $r_c = 1/2$, are transformed into 64 bits, which are mapped into 16 16-QAM symbols. The channel coding has constraint length 7 and octal generators $\mathbf{g_0} \triangleq [\mathbf{133}]$ and $\mathbf{g_1} \triangleq [\mathbf{165}]$. We assume that the sampling frequency is $f_s = 400$ MHz. In order to compute the BLER, we assume that a data block is discarded when at least one of the original bits is incorrectly decoded at the receiver end.

Figure I.3 depicts the obtained results. There are four curves in this figure which describe the performance of the following systems: (i) minimum-redundancy DFE ($K = 3$), (ii) reduced-redundancy DFE ($K = 4$), (iii) full-redundancy DFE ($K = 5$), and (iv) full-redundancy DFE ($K = 5$) with no error propagation, in which the exact symbols are fed back. This last system will be used as a benchmark for our comparisons.

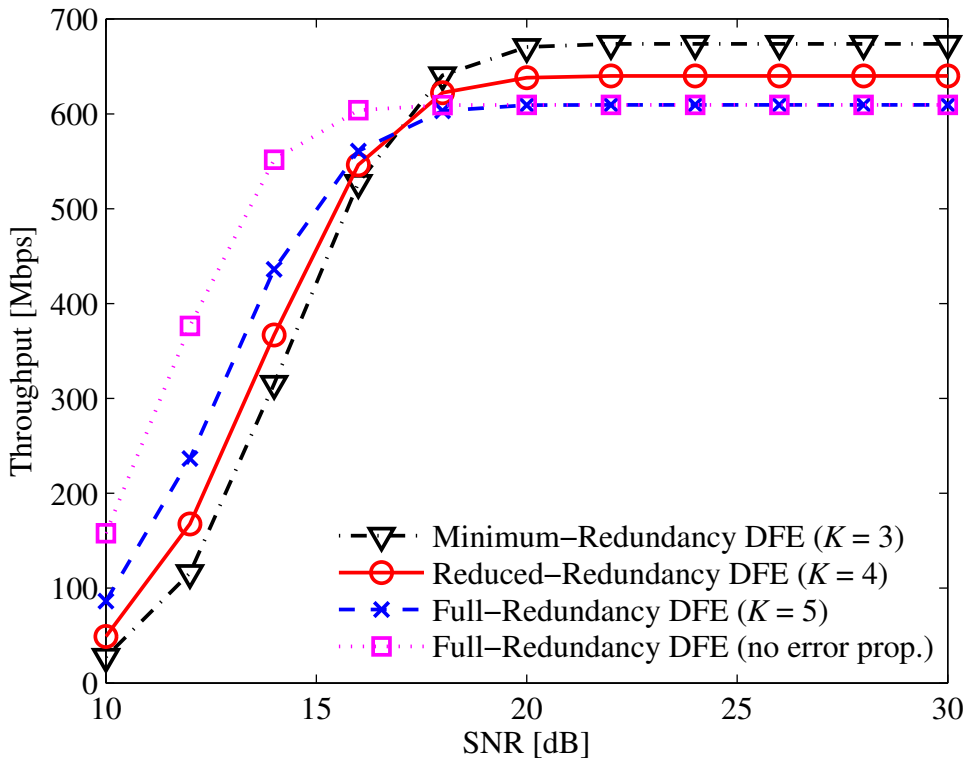

Figure I.3: Throughput [Mbps] $\times$ SNR [dB].

By observing Figure I.3, one can verify that, in this setup, the error propagation is critical since the already known full-redundancy DFE (or, simply, ZP DFE) without error propagation achieves much higher throughputs than the other transceivers for SNRs smaller than 16 dB. In this low SNR range, the proposed DFEs do not perform as well as the traditional full-redundancy DFE ($K = 5$). On the other hand, for SNRs larger than 16 dB, the proposed reduced-redundancy DFE ($K = 4$) can outperform the benchmark transceiver in up to 31 Mbps, whereas the proposed minimum-redundancy DFE ($K = 3$) can outperform the benchmark transceiver in up to 64 Mbps.

Other simulation results have shown that is possible to have better throughput performance with reduced-redundancy DFEs, rather than minimum-redundancy DFEs, for some particular channels.

I.4 Concluding Remarks

In this chapter we proposed the ZP-ZJ block-based transceivers with decision-feedback equalization. These transceivers allowed the tradeoff between transmission-error performance and data throughput, enabling the optimization of the spectral resources in broadband transmissions. This was possible by choosing the amount of redundancy ranging from the minimum to the channel order, which is usually employed. Some tools to analyze the transceivers were proposed based on the resulting MSE of symbols, mutual information between transmitted and estimated symbols, and average error probability of symbols.

The main conclusion from this chapter is that, for ZP-ZJ-based DFE transceivers, it is possible to increase the data throughput for a certain level of SNR at the receiver, without affecting the system performance, as confirmed by the simulation results. These are preliminary results from investigations that are in progress. An interesting future research direction is the development of efficient algorithms to implement the proposed optimal nonlinear solutions.

Apêndice J

Design of Transceivers with Minimum Redundancy

In Part I of this thesis, we have proposed multicarrier and single-carrier block-based transceivers with minimum redundancy which have proved to be an alternative to classical OFDM and SC-FD systems. As previously highlighted, these minimum-redundancy transceivers may have superior throughput performance than OFDM and SC-FD systems, requiring the same asymptotic complexity, viz. $\mathcal{O}(M \log_2 M)$, for M data symbols. However, the proposals of such transceivers rely on the CSI assumption. In addition, they also assume that the equalizer was previously designed, focusing on the equalization problem only.

The aim of this chapter is to present some theoretical results related to the design of the equalizers that employ minimum redundancy, without assuming CSI. More precisely, in this chapter we show how to estimate the channel when minimum-redundancy transceivers are employed and how to use this estimate in order to solve the linear systems of equations that define the equalizers. The key result of this chapter is to show that it is possible to design those equalizers based on pilot information and using fast-converging iterative algorithms that require $\mathcal{O}(M \log_2 M)$ operations per iteration. It must be pointed out that the proposals of this chapter are preliminary theoretical results of an ongoing research, which is not the mainstream of this thesis.

We organized this chapter in the following manner: the problem of estimating the channel-impulse response related to minimum-redundancy transceivers is addressed in Section J.1. The proposed equalizer designs are described in Sections J.2 and J.3. A numerical example is presented in Section J.4. The concluding remarks are in Section J.5. The chapter ends with some specific guidelines for further research in the design of minimum-redundancy transceivers.

J.1 Pilot-Aided Channel Estimation in The Time Domain

Traditional OFDM systems use the fact that, after the transmitter-receiver processing, the channel model is diagonalized and estimation of the channel-frequency response is much easier. Based on this fact, practical systems estimate only some bins in the frequency domain and, after that, perform an interpolation in order to estimate the whole channel-frequency response [20].

As highlighted in [20], an efficient technique is to estimate the channel-impulse response using least-squares (LS) estimation. Considering that $L+1 < M$, we have that the number of coefficients to be estimated in the time domain, $L+1$, is smaller than the number M in the frequency domain. In addition, we shall use the same reasoning developed in [20] in order to employ superfast algorithms for the implementation of the channel estimator.

Let us start with the single-carrier system with minimum redundancy. From Eq. (D.1), we have that, after discarding $L/2$ redundant elements,[1] the received vector $\mathbf{y} \in \mathbb{C}^{M\times 1}$ is given by:

$$\mathbf{y} = \mathbf{H}_0\mathbf{s} + \mathbf{v}', \tag{J.1}$$

where $\mathbf{v}' \in \mathbb{C}^{M\times 1}$ contains the last M elements of $\mathbf{v}$. Thus, assuming that the set $\mathcal{M} = \{\, 0, 1, \cdots, M-1 \,\}$ is partitioned in three disjoint sets

$$\mathcal{M}_0 = \{\, 0, 1, \cdots, L/2 \,\}, \tag{J.2}$$

$$\mathcal{M}_1 = \{\, L/2+1, L/2+2, \cdots, M-2-L/2 \,\}, \tag{J.3}$$

$$\mathcal{M}_2 = \{\, M-1-L/2, M-L/2, \cdots, M-1 \,\}, \tag{J.4}$$

then, the mth element of $\mathbf{y}$ can be expressed as:

$$y(m) = \begin{cases} \sum\limits_{l=0}^{\frac{L}{2}+m} h\left(\frac{L}{2}+m-l\right) s(l) + v'(m), & \forall m \in \mathcal{M}_0 \\ \sum\limits_{l=0}^{L} h\left(L-l\right) s\left(l+m-\frac{L}{2}\right) + v'(m), & \forall m \in \mathcal{M}_1 \\ \sum\limits_{l=0}^{(\frac{L}{2}+M-1-m)} h\left(L-l\right) s\left(l+m-\frac{L}{2}\right) + v'(m), & \forall m \in \mathcal{M}_2 \end{cases}. \tag{J.5}$$

After a change of variables and considering that the vector $\mathbf{r} = \mathbf{s}$ (single-carrier transmission) or $\mathbf{r} = \mathbf{W}_M^H\mathbf{s}$ (multicarrier transmission) contains only pilot signals,

[1] It is assumed that L is even.

the former equation can be rewritten as:

$$y(m) = \begin{cases} \sum\limits_{l'=0}^{\frac{L}{2}+m} r\left(\frac{L}{2}+m-l'\right)h(l') + v'(m), & \forall m \in \mathcal{M}_0 \\ \sum\limits_{l'=0}^{L} r\left(\frac{L}{2}+m-l'\right)h(l') + v'(m), & \forall m \in \mathcal{M}_1 \\ \sum\limits_{l'=(\frac{L}{2}-M+1+m)}^{L} r\left(\frac{L}{2}+m-l'\right)h(l') + v'(m), & \forall m \in \mathcal{M}_2 \end{cases}, \tag{J.6}$$

which yields the following identity:

$$\mathbf{y} = \mathbf{R}\mathbf{h} + \mathbf{v}', \tag{J.7}$$

where $\mathbf{R} \in \mathbb{C}^{M\times(L+1)}$ is a Toeplitz matrix containing the pilot signals. The first row of $\mathbf{R}$ is $[\, r(L/2) \quad r(L/2-1) \quad \cdots \quad r(0) \quad \mathbf{0}_{1\times L/2}\,]$ and the first column is $[\, r(L/2) \quad \cdots \quad r(M-1) \quad \mathbf{0}_{1\times L/2}\,]^T$. Moreover, the vector $\mathbf{h} \in \mathbb{C}^{(L+1)\times 1}$ contains the channel-impulse-response coefficients. The LS solution for the problem described in Eq. (J.7) is given by [20]:

$$\hat{\mathbf{h}} = \left(\mathbf{R}^H\mathbf{R} + \rho\mathbf{I}_{(L+1)}\right)^{-1}\mathbf{R}^H\mathbf{y}, \tag{J.8}$$

in which the regularization parameter $\rho \in \mathbb{R}_+$ may be chosen in a similar way as performed in MMSE-based solutions, i.e., it is possible to use the *a priori* knowledge about the signal-to-noise ratio (SNR) at the receiver front-end in order to set $\rho = 1/\text{SNR}$.

Note that, unlike in [20], the product $\mathbf{R}^H\mathbf{R}$ is not a Toeplitz matrix. This implies that we cannot use the Gohberg-Semencul formula [20, 25] to implement the product of the rectangular matrix $\left(\mathbf{R}^H\mathbf{R} + \rho\mathbf{I}_{L+1}\right)^{-1}\mathbf{R}^H$ by the received vector in a superfast way. This occurs since the traditional Gohberg-Semencul formula describes a superfast decomposition of inverses of Toeplitz matrices only. However, we still can adapt[2] the results of Theorem 13 from Chapter F in order to produce a superfast decomposition for the resulting rectangular matrix $\left(\mathbf{R}^H\mathbf{R} + \rho\mathbf{I}_{L+1}\right)^{-1}\mathbf{R}^H$. Hence, even though the pilot matrix does not induce a Toeplitz correlation-pilot matrix as in [20], we have verified that it is still possible to recover an estimate for all channel taps in the time-domain using up to $\mathcal{O}(M\log_2 M)$ operations, assuming that $M > L+1$ is a power of 2.

This discussion did not take into account the fact that, in order to apply Theorem 13 from Chapter F , we need to solve some structured linear systems of equations. A reasonable assumption is to consider that such linear systems of equations were previously solved [20] since they are related to pilot symbols only, which do not

[2]The adaptation consists in substituting $\mathbf{H}_0$ by $\mathbf{R}$ (see Chapter F).

have to be time-variant. In this case, $8(L+1)$ coefficients might be stored, since the minimum amount of pilots which guarantees that the matrix $\mathbf{R}^H\mathbf{R}$ is nonsingular is $L+1$ and, in addition to this, we need eight vectors ($\bar{\mathbf{p}}_1, \bar{\mathbf{p}}_2, \bar{\mathbf{p}}_3, \bar{\mathbf{p}}_4, \bar{\mathbf{q}}_1, \bar{\mathbf{q}}_2, \bar{\mathbf{q}}_3$, and $\bar{\mathbf{q}}_4$ defined in Theorem 13 from Chapter F) that are the solutions to the linear systems of equations. However, these linear systems can also be solved using the techniques described in Sections J.2 and J.3. As previously mentioned, these techniques also employ superfast algorithms.

J.2 Equalizer Designs Using Newton's Iteration

The equalizer-design problem consists in solving some linear systems of equations. We could solve such linear systems by employing Gaussian elimination [44]. However, the resulting computational complexity is higher than other methods that take into account the structure of the related matrices. In fact, the solutions of the linear systems can be achieved by using, for instance, Newton's iteration [25, 53].

The idea behind Newton's iteration is to generalize the traditional Newton's method to find zeros of a given function to the case in which the domain and the range of the function are comprised of matrices [25]. Thus, let us define the function

$$\begin{aligned} f_{\mathbf{X}} \,:\, \mathbb{C}^{M\times M} &\rightarrow \mathbb{C}^{M\times M} \\ \mathbf{U} &\mapsto \mathbf{U} - \mathbf{X}^{-1}, \end{aligned} \tag{J.9}$$

where $\mathbf{X} \in \mathbb{C}^{M\times M}$ is a nonsingular matrix, whose inverse we want to compute. It is possible to show that Newton's iteration improves an initial approximation $\mathbf{U}_0 \in \mathbb{C}^{M\times M}$ to the inverse of $\mathbf{X}$ by using the following iteration step [25, 53]:

$$\mathbf{U}_{i+1} = \mathbf{U}_i(2\mathbf{I} - \mathbf{X}\mathbf{U}_i), \tag{J.10}$$

for $i \in \mathbb{N}$. A sufficient constraint to guarantee convergence of the algorithm is that the initial approximation $\mathbf{U}_0$ must respect the following inequality [25, 53]:

$$\|\mathbf{I} - \mathbf{X}\mathbf{U}_0\|_2 < 1, \tag{J.11}$$

where $\|\cdot\|_2$ stands for the induced Euclidean norm of matrices [25, 53]. As all the involved matrices can be compressed using the displacement approach, it is possible to implement each recursion step using only $\mathcal{O}(M \log_2 M)$ operations [25, 53]. In addition, this algorithm features quadratic convergence rate, which is a very high speed of convergence when dealing with these types of problems [25, 53].

We now propose the following application of Newton's iteration method: consider that we have a previous estimate for the inverse of the effective channel matrix

$\mathbf{H}_0(k-1)$ at the time instant indexed by $k-1 \in \mathbb{N}$. Consider that, after applying the channel estimation method proposed in Section J.1, we also know the actual effective channel matrix $\mathbf{H}_0(k)$ at the current time instant k. The problem is to find $\mathbf{H}_0^{-1}(k)$, given that we know $\mathbf{H}_0(k-1)$, $\mathbf{H}_0^{-1}(k-1)$, and $\mathbf{H}_0(k)$. If the channel varies slowly with time, $\mathbf{H}_0^{-1}(k-1)$ is a good estimate for the inverse of $\mathbf{H}_0(k)$, in the sense that $\|\mathbf{I}-\mathbf{H}_0(k)\mathbf{H}_0^{-1}(k-1)\|_2 < 1$. Thus, by setting $\mathbf{U}_0 = \mathbf{H}_0^{-1}(k-1)$, we have that the application of Newton's iteration according to Eq. (J.10) has guaranteed (quadratic) convergence. The reader should refer to [25, 53] in order to verify the details related to the implementation of this recursion using only $\mathcal{O}(M \log_2 M)$ operations.

A fundamental assumption of the aforementioned method is that the channel varies slowly with time. However, this is a strong assumption in several applications, such as wireless systems. A possible solution to this case is to employ the homotopic Newton's iteration [25]. Once again, we assume that we know the matrices $\mathbf{H}_0(k-1)$, $\mathbf{H}_0^{-1}(k-1)$, and $\mathbf{H}_0(k)$, but now we define the homotopic transformation [25]:

$$\mathbf{H}_0^{(i)}(k) = \mathbf{H}_0(k-1) + [\mathbf{H}_0(k) - \mathbf{H}_0(k-1)]\tau_i, \tag{J.12}$$

for $i \in \mathcal{I} = \{0, 1, \cdots, I-1\} \subset \mathbb{N}$ and $\tau_i \in (\,0,\,1\,] \subset \mathbb{R}$. In addition, it is assumed that $0 < \tau_0 < \tau_1 \cdots < \tau_{(I-1)} = 1$. In particular, we can choose $\tau_i = (i+1)/I$. In such a case, the number I should be chosen as the smallest natural number that yields:

$$\left\| \mathbf{I} - \mathbf{H}_0^{(i)}(k) \left[\mathbf{H}_0^{(i-1)}(k) \right]^{-1} \right\|_2 < 1, \quad \forall i \in \mathcal{I} \setminus \{0\}. \tag{J.13}$$

Consequently, if I is properly chosen, we can apply Newton's iteration method for each $i \in \mathcal{I}\setminus\{0\}$, where we assume that we know $\mathbf{H}_0^{(i-1)}(k)$, $[\mathbf{H}_0^{(i-1)}(k)]^{-1}$, and $\mathbf{H}_0^{(i)}(k)$ in order to compute $[\mathbf{H}_0^{(i)}(k)]^{-1}$. At the end, we have that $[\mathbf{H}_0^{(I-1)}(k)]^{-1} \approx \mathbf{H}_0^{-1}(k)$. Nonetheless, this approach is much more complex than a direct approach that does not rely on the application of homotopic transformations.

There are other alternatives to solve the linear systems of equations that define the ZF and MMSE equalizers. Among them, the preconditioned conjugate gradient (PCG) algorithms play an important role.

J.3 Alternative Heuristics for Equalizer Designs

As the reader may have observed, there is a large number of superfast methods to compute inverses of structured matrices [25] that could be used to design the equalizers related to the proposed transceivers. The aim of this section is to describe two of them, as well as their applications to the problems at hand: preconditioned

conjugate gradient algorithm [54] and Pan's divide-and-conquer algorithm [25].

J.3.1 Preconditioned Conjugate Gradient Algorithm

The idea of PCG methods is to solve the problem $\mathbf{H}_0\mathbf{p} = \hat{\mathbf{p}}$ by solving the equivalent problem $\boldsymbol{\mathcal{P}}^{-1}\mathbf{H}_0\mathbf{p} = \boldsymbol{\mathcal{P}}^{-1}\hat{\mathbf{p}}$, which is better conditioned than the original problem, using conjugate gradient algorithms [54]. The matrix $\boldsymbol{\mathcal{P}}$ is the so-called *preconditioner matrix* and should be much easier to invert than matrix $\mathbf{H}_0$ and, simultaneously, should be a good approximation for $\mathbf{H}_0^{-1}$, that is, $\boldsymbol{\mathcal{P}}^{-1}\mathbf{H}_0 \approx \mathbf{I}$ [54]. As all involved matrices are structured, this type of algorithm can also be implemented using only $\mathcal{O}(M \log_2 M)$ operations per iteration.

The PCG method (see [54] and references therein) features superlinear convergence rate (slower than Newton's iteration). Nonetheless, it can be very useful when associated with Newton's iteration method. In fact, when the channel varies rapidly with time, the PCG approach can be used to refine the crude initial approximation $\mathbf{U}_0 = \mathbf{H}_0^{-1}(k-1)$ for the inverse of $\mathbf{H}_0(k)$ and, after that, to apply Newton's iteration or the homotopic Newton's iteration method [25].

J.3.2 Pan's Divide-and-Conquer Algorithm

Given a nonsingular Toeplitz matrix $\mathbf{T} \in \mathbb{C}^{M\times M}$ and a pair of vectors $\mathbf{x}, \mathbf{y} \in \mathbb{C}^{M\times 1}$, the linear system of equations $\mathbf{Tx} = \mathbf{y}$ can be efficiently solved through Pan's divide-and-conquer algorithm [25, 55]. In fact, assuming both that $M = 2^I$, for some $I \in \mathbb{N}$, and that the leading principal submatrix $\mathbf{T}_{00} \in \mathbb{C}^{\frac{M}{2}\times\frac{M}{2}}$ is nonsingular, then the original Toeplitz matrix $\mathbf{T}$ may always be represented as a 2×2 block matrix, as follows [19, 25, 55]:

$$\mathbf{T} = \begin{bmatrix} \mathbf{T}_{00} & \mathbf{T}_{01} \\ \mathbf{T}_{10} & \mathbf{T}_{11} \end{bmatrix} = \begin{bmatrix} \mathbf{I} & \mathbf{0} \\ \mathbf{T}_{10}\mathbf{T}_{00}^{-1} & \mathbf{I} \end{bmatrix} \begin{bmatrix} \mathbf{T}_{00} & \mathbf{0} \\ \mathbf{0} & \mathbf{S} \end{bmatrix} \begin{bmatrix} \mathbf{I} & \mathbf{T}_{00}^{-1}\mathbf{T}_{01} \\ \mathbf{0} & \mathbf{I} \end{bmatrix}, \tag{J.14}$$

where $\mathbf{S} = \mathbf{T}_{11} - \mathbf{T}_{10}\mathbf{T}_{00}^{-1}\mathbf{T}_{01} \in \mathbb{C}^{\frac{M}{2}\times\frac{M}{2}}$ is the *Schur complement* of the block $\mathbf{T}_{00}$ in the matrix $\mathbf{T}$ [19]. By using this decomposition, it is possible to verify that [19, 25, 55]:

$$\mathbf{T}^{-1} = \begin{bmatrix} \bar{\mathbf{T}}_{00} & \bar{\mathbf{T}}_{01} \\ \bar{\mathbf{T}}_{10} & \bar{\mathbf{T}}_{11} \end{bmatrix} = \begin{bmatrix} \mathbf{I} & -\mathbf{T}_{00}^{-1}\mathbf{T}_{01} \\ \mathbf{0} & \mathbf{I} \end{bmatrix} \begin{bmatrix} \mathbf{T}_{00}^{-1} & \mathbf{0} \\ \mathbf{0} & \mathbf{S}^{-1} \end{bmatrix} \begin{bmatrix} \mathbf{I} & \mathbf{0} \\ -\mathbf{T}_{10}\mathbf{T}_{00}^{-1} & \mathbf{I} \end{bmatrix}. \tag{J.15}$$

The main idea of Pan's divide-and-conquer algorithm is to apply such decompositions recursively up to the point where the matrix inversions reduce to inversions of nonzero scalars. This first step is the so-called *descending process* [25]. After that, a bottom-up procedure starts. Thus, the previously computed 1×1 matrices

are used to calculate the related 2×2 matrices, which are also used to compute the associated 4×4 matrices, and so forth. This second step is the so-called *lifting process* [25]. Accordingly, the following recursive iteration is implemented:

$$\mathbf{T}^{(i)} = \begin{bmatrix} \mathbf{T}_{00}^{(i+1)} & \mathbf{T}_{01}^{(i+1)} \\ \mathbf{T}_{10}^{(i+1)} & \mathbf{T}_{11}^{(i+1)} \end{bmatrix} = \mathbf{T}_{00}^{(i)} \in \mathbb{C}^{\frac{M}{2^i} \times \frac{M}{2^i}}, \tag{J.16}$$

where in this recursive iteration, $i \in \{\, 0,\, 1,\, \cdots,\, I-1 \,\}$ indicates the recursion level. Moreover, $\mathbf{T}^{(0)} = \mathbf{T}$ is the original Toeplitz matrix, whereas $\mathbf{T}_{00}^{(I)}$ is a scalar number.

Furthermore, the recursive version of Eq. (J.15) is:

$$(\mathbf{T}^{(i)})^{-1} = \begin{bmatrix} \bar{\mathbf{T}}_{00}^{(i+1)} & \bar{\mathbf{T}}_{01}^{(i+1)} \\ \bar{\mathbf{T}}_{10}^{(i+1)} & \bar{\mathbf{T}}_{11}^{(i+1)} \end{bmatrix}, \tag{J.17}$$

in which

$$\bar{\mathbf{T}}_{00}^{(i+1)} = (\mathbf{T}_{00}^{(i+1)})^{-1} + (\mathbf{T}_{00}^{(i+1)})^{-1}\mathbf{T}_{01}^{(i+1)}(\mathbf{S}^{(i+1)})^{-1}\mathbf{T}_{10}^{(i+1)}(\mathbf{T}_{00}^{(i+1)})^{-1}, \tag{J.18}$$

$$\bar{\mathbf{T}}_{01}^{(i+1)} = -(\mathbf{T}_{00}^{(i+1)})^{-1}\mathbf{T}_{01}^{(i+1)}(\mathbf{S}^{(i+1)})^{-1}, \tag{J.19}$$

$$\bar{\mathbf{T}}_{10}^{(i+1)} = -(\mathbf{S}^{(i+1)})^{-1}\mathbf{T}_{10}^{(i+1)}(\mathbf{T}_{00}^{(i+1)})^{-1}, \tag{J.20}$$

$$\bar{\mathbf{T}}_{11}^{(i+1)} = (\mathbf{S}^{(i+1)})^{-1}. \tag{J.21}$$

Regarding the computational complexity, consider the matrices $(\mathbf{T}_{00}^{(i+1)})^{-1}$, $(\mathbf{S}^{(i+1)})^{-1}$, $\mathbf{T}_{01}^{(i+1)}$, $\mathbf{T}_{10}^{(i+1)}$, and $\mathbf{T}_{11}^{(i+1)}$ already known before computing $(\mathbf{T}^{(i)})^{-1}$, at the ith recursion level. In this case, the number of multiplications to calculate $(\mathbf{T}^{(i)})^{-1}$ reduces to five matrix multiplications. In addition, assuming that these five matrix multiplications have an overall asymptotic complexity of $\mathcal{M}\left(\frac{M}{2^{i+1}}\right)$, then the inversion of the original matrix $\mathbf{T}^{(0)} = \mathbf{T}$ requires [55]

$$\sum_{i=0}^{I-1} 2^{i+1}\mathcal{M}\left(\frac{M}{2^{i+1}}\right) \quad \text{operations}, \tag{J.22}$$

since the algorithm must be applied recursively to calculate the inverse of $\mathbf{T}^{(i)}$, as well as the inverse of its related Schur complement.

As in each recursion step there are several multiplications of structured matrices, these multiplications may be performed with less numerical operations by using the compressed form of the resulting block matrices. A key result that helps in such a task is (see Theorem 1.5.6 in [25]):

$$\nabla_{\mathbf{X}_{i,i},\mathbf{Y}_{j,j}}(\mathbf{U}_{i,j}) = \boldsymbol{\nabla}_{i,j} - \mathbf{R}_{i,j} \tag{J.23}$$

in which

$$\mathbf{X} = (\mathbf{X}_{i,j})_{i,j=0}^{1} = \begin{bmatrix} \mathbf{X}_{0,0} & \mathbf{X}_{0,1} \\ \mathbf{X}_{1,0} & \mathbf{X}_{1,1} \end{bmatrix}, \tag{J.24}$$

$$\mathbf{Y} = (\mathbf{Y}_{i,j})_{i,j=0}^{1} = \begin{bmatrix} \mathbf{Y}_{0,0} & \mathbf{Y}_{0,1} \\ \mathbf{Y}_{1,0} & \mathbf{Y}_{1,1} \end{bmatrix}, \tag{J.25}$$

$$\mathbf{U} = (\mathbf{U}_{i,j})_{i,j=0}^{1} = \begin{bmatrix} \mathbf{U}_{0,0} & \mathbf{U}_{0,1} \\ \mathbf{U}_{1,0} & \mathbf{U}_{1,1} \end{bmatrix}, \tag{J.26}$$

$$\nabla_{\mathbf{X},\mathbf{Y}}(\mathbf{U}) = (\boldsymbol{\nabla}_{i,j})_{i,j=0}^{1} = \begin{bmatrix} \boldsymbol{\nabla}_{0,0} & \boldsymbol{\nabla}_{0,1} \\ \boldsymbol{\nabla}_{1,0} & \boldsymbol{\nabla}_{1,1} \end{bmatrix}, \tag{J.27}$$

and $\mathbf{R}_{i,j} = \mathbf{U}_{i,(1-j)}\mathbf{Y}_{(1-j),j} - \mathbf{X}_{i,(1-i)}\mathbf{U}_{(1-i),j}$, for $i, j \in \{0, 1\}$. For the particular case where $\nabla_{\mathbf{Z}_{-1},\mathbf{Z}_1}(\mathbf{H}_0) = \hat{\mathbf{P}}\hat{\mathbf{Q}}^T$, the partitions of the operator matrix $\mathbf{Z}_\lambda = [(\mathbf{Z}_\lambda)_{i,j}]_{i,j=0}^{1}$, for any $\lambda \in \mathbb{C}$, are:

$$(\mathbf{Z}_\lambda)_{00} = \begin{bmatrix} 0 & & & 0 \\ 1 & \ddots & & \\ & \ddots & \ddots & \\ & & 1 & 0 \end{bmatrix}_{\frac{M}{2}\times\frac{M}{2}}, \quad (\mathbf{Z}_\lambda)_{01} = \begin{bmatrix} 0 & & & \lambda \\ 0 & \ddots & & \\ & \ddots & \ddots & \\ & & 0 & 0 \end{bmatrix}_{\frac{M}{2}\times\frac{M}{2}} \tag{J.28}$$

$$(\mathbf{Z}_\lambda)_{10} = \begin{bmatrix} 0 & & & 1 \\ 0 & \ddots & & \\ & \ddots & \ddots & \\ & & 0 & 0 \end{bmatrix}_{\frac{M}{2}\times\frac{M}{2}}, \quad (\mathbf{Z}_\lambda)_{11} = \begin{bmatrix} 0 & & & 0 \\ 1 & \ddots & & \\ & \ddots & \ddots & \\ & & 1 & 0 \end{bmatrix}_{\frac{M}{2}\times\frac{M}{2}}, \tag{J.29}$$

where the blank entries contain zeros.

These partitions of $\mathbf{Z}_\lambda$-type operator matrices imply that $\mathbf{R}_{i,j}$ can always be computed very fast, since $\mathbf{X}_{0,1}, \mathbf{X}_{1,0}, \mathbf{Y}_{0,1}$, and $\mathbf{Y}_{1,0}$ have at most one nonzero coefficient. Thus, by using Eq. (J.23), it is possible to induce a compressed form into the block matrices of the partition, at each recursion. Hence, with this result, along with the application of Eqs. (D.12), (D.14), and (D.15), the inverse of $\mathbf{T}$ can be computed in an efficient way. In fact, as multiplications of $M \times M$ matrices using their generator pairs (with operator matrices of $\mathbf{Z}_\lambda$-type) can be calculated with $\mathcal{M}(M) = \mathcal{O}(M \log_2 M)$ operations (see Theorems 3.4 and 2.3 in [53]), the asymptotic computational complexity is $\mathcal{M}\left(\frac{M}{2^{i+1}}\right) = \mathcal{O}\left(\frac{M}{2^{i+1}} \log_2(\frac{M}{2^{i+1}})\right)$ operations, at the ith recursion level. Substituting this complexity in Eq. (J.22), one can verify that the overall asymptotic computational complexity to invert $\mathbf{T}$ is $\mathcal{O}(M \log_2^2 M)$ [25, 55].

Table J.1 contains a pseudo-code description of Pan's divide-and-conquer algorithm. Some important points must be highlighted:

Table J.1: Pseudo-code of Pan's divide-and-conquer algorithm to invert structured matrices.

Pan's Divide-and-Conquer Algorithm (PDCA)

$[\ \nabla_{\mathbf{Z}_\xi,\mathbf{Z}_\eta}(\mathbf{T}^{-1}),\ \text{IsEnd}\ ] = \text{pdca}(\mathbf{T},\ \nabla_{\mathbf{Z}_\eta,\mathbf{Z}_\xi}(\mathbf{T}),\ \text{IsEnd});$

$M = \text{dimension}\{\mathbf{T}\};$
Define $\mathbf{T}_{00}$, $\mathbf{T}_{01}$, $\mathbf{T}_{10}$, and $\mathbf{T}_{11}$ as in Eq. (J.14);
Define $(\mathbf{Z}_\lambda)_{00}$, $(\mathbf{Z}_\lambda)_{01}$, $(\mathbf{Z}_\lambda)_{10}$, and $(\mathbf{Z}_\lambda)_{11}$ as in Eq. (J.28) and Eq. (J.29), $\forall\lambda$;
Define $\nabla_{(\mathbf{Z}_\eta)_{00},(\mathbf{Z}_\xi)_{00}}(\mathbf{T}_{00})$, $\nabla_{(\mathbf{Z}_\eta)_{00},(\mathbf{Z}_\xi)_{11}}(\mathbf{T}_{01})$,
$\nabla_{(\mathbf{Z}_\eta)_{11},(\mathbf{Z}_\xi)_{00}}(\mathbf{T}_{10})$, and $\nabla_{(\mathbf{Z}_\eta)_{11},(\mathbf{Z}_\xi)_{11}}(\mathbf{T}_{11})$ as in Eq. (J.23);
If $(M = 2)$, then do
{
$\mathbf{T}_{00}^{-1} = 1/\mathbf{T}_{00}$;
$\mathbf{S}^{-1} = 1/(\mathbf{T}_{11} - \mathbf{T}_{10}\mathbf{T}_{00}^{-1}\mathbf{T}_{01})$;
IsEnd = TRUE;
}
if (IsEnd = FALSE), then do
{
$[\ \nabla_{(\mathbf{Z}_\xi)_{00},(\mathbf{Z}_\eta)_{00}}(\mathbf{T}_{00}^{-1}),\ \text{IsEnd}\ ] = \text{pdca}(\mathbf{T}_{00},\ \nabla_{(\mathbf{Z}_\eta)_{00},(\mathbf{Z}_\xi)_{00}}(\mathbf{T}_{00}),\ \text{IsEnd});$
}
if $(M \neq 2)$ and (IsEnd = TRUE), then do
{
$\nabla_{(\mathbf{Z}_\eta)_{11},(\mathbf{Z}_\eta)_{00}}(\mathbf{T}_{10}\mathbf{T}_{00}^{-1}) = \nabla_{(\mathbf{Z}_\eta)_{11},(\mathbf{Z}_\xi)_{00}}(\mathbf{T}_{10})\mathbf{T}_{00}^{-1} + \mathbf{T}_{10}\nabla_{(\mathbf{Z}_\xi)_{00},(\mathbf{Z}_\eta)_{00}}(\mathbf{T}_{00}^{-1});$
$\nabla_{(\mathbf{Z}_\eta)_{11},(\mathbf{Z}_\xi)_{11}}(\mathbf{T}_{10}\mathbf{T}_{00}^{-1}\mathbf{T}_{01}) = \nabla_{(\mathbf{Z}_\eta)_{11},(\mathbf{Z}_\eta)_{00}}(\mathbf{T}_{10}\mathbf{T}_{00}^{-1})\mathbf{T}_{01} + (\mathbf{T}_{10}\mathbf{T}_{00}^{-1})\nabla_{(\mathbf{Z}_\eta)_{00},(\mathbf{Z}_\xi)_{11}}(\mathbf{T}_{01});$
$\nabla_{(\mathbf{Z}_\eta)_{11},(\mathbf{Z}_\xi)_{11}}(\mathbf{S}) = \nabla_{(\mathbf{Z}_\eta)_{11},(\mathbf{Z}_\xi)_{11}}(\mathbf{T}_{11}) - \nabla_{(\mathbf{Z}_\eta)_{11},(\mathbf{Z}_\xi)_{11}}(\mathbf{T}_{10}\mathbf{T}_{00}^{-1}\mathbf{T}_{01});$
$[\ \nabla_{(\mathbf{Z}_\xi)_{11},(\mathbf{Z}_\eta)_{11}}(\mathbf{S}^{-1}),\ \text{“don't care”}\ ] = \text{pdca}(\mathbf{S},\ \nabla_{(\mathbf{Z}_\eta)_{11},(\mathbf{Z}_\xi)_{11}}(\mathbf{S}),\ \text{FALSE});$
}
$\nabla_{(\mathbf{Z}_\xi)_{11},(\mathbf{Z}_\eta)_{11}}(\bar{\mathbf{T}}_{11}) = \nabla_{(\mathbf{Z}_\xi)_{11},(\mathbf{Z}_\eta)_{11}}(\mathbf{S}^{-1});$
$\nabla_{(\mathbf{Z}_\xi)_{11},(\mathbf{Z}_\eta)_{00}}(\bar{\mathbf{T}}_{10}) = -\nabla_{(\mathbf{Z}_\xi)_{11},(\mathbf{Z}_\eta)_{11}}(\mathbf{S}^{-1})(\mathbf{T}_{10}\mathbf{T}_{00}^{-1}) - \mathbf{S}^{-1}\nabla_{(\mathbf{Z}_\eta)_{11},(\mathbf{Z}_\eta)_{00}}(\mathbf{T}_{10}\mathbf{T}_{00}^{-1});$
$\nabla_{(\mathbf{Z}_\xi)_{00},(\mathbf{Z}_\xi)_{11}}(\mathbf{T}_{00}^{-1}\mathbf{T}_{01}) = \nabla_{(\mathbf{Z}_\xi)_{00},(\mathbf{Z}_\eta)_{00}}(\mathbf{T}_{00}^{-1})\mathbf{T}_{01} + \mathbf{T}_{00}^{-1}\nabla_{(\mathbf{Z}_\eta)_{00},(\mathbf{Z}_\xi)_{11}}(\mathbf{T}_{01});$
$\nabla_{(\mathbf{Z}_\xi)_{00},(\mathbf{Z}_\eta)_{11}}(\bar{\mathbf{T}}_{01}) = -\nabla_{(\mathbf{Z}_\xi)_{00},(\mathbf{Z}_\xi)_{11}}(\mathbf{T}_{00}^{-1}\mathbf{T}_{01})\mathbf{S}^{-1} - (\mathbf{T}_{00}^{-1}\mathbf{T}_{01})\nabla_{(\mathbf{Z}_\xi)_{11},(\mathbf{Z}_\eta)_{11}}(\mathbf{S}^{-1});$
$\nabla_{(\mathbf{Z}_\xi)_{00},(\mathbf{Z}_\eta)_{00}}(\bar{\mathbf{T}}_{01}\mathbf{T}_{10}\mathbf{T}_{00}^{-1}) = \nabla_{(\mathbf{Z}_\xi)_{00},(\mathbf{Z}_\eta)_{11}}(\bar{\mathbf{T}}_{01})(\mathbf{T}_{10}\mathbf{T}_{00}^{-1}) + \bar{\mathbf{T}}_{01}\nabla_{(\mathbf{Z}_\eta)_{11},(\mathbf{Z}_\eta)_{00}}(\mathbf{T}_{10}\mathbf{T}_{00}^{-1});$
$\nabla_{(\mathbf{Z}_\xi)_{00},(\mathbf{Z}_\eta)_{00}}(\bar{\mathbf{T}}_{00}) = \nabla_{(\mathbf{Z}_\xi)_{00},(\mathbf{Z}_\eta)_{00}}(\mathbf{T}_{00}^{-1}) - \nabla_{(\mathbf{Z}_\xi)_{00},(\mathbf{Z}_\eta)_{00}}(\bar{\mathbf{T}}_{01}\mathbf{T}_{10}\mathbf{T}_{00}^{-1});$
Define $\nabla_{\mathbf{Z}_\xi,\mathbf{Z}_\eta}(\mathbf{T}^{-1})$ using both Eq. (J.23) and Eq. (J.27);

- All multiplications of displacements by matrices can be performed in a superfast way by using decompositions similar to the one in Theorem 13 from Chapter F. This explains why the algorithm does not calculate the inverse of the input matrix, but only the displacement of the inverse of the input matrix. For example, the product $\mathbf{T}_{00}^{-1}\nabla_{(\mathbf{Z}_\eta)_{00},(\mathbf{Z}_\xi)_{11}}(\mathbf{T}_{01})$ is implemented without using the matrix $\mathbf{T}_{00}^{-1}$, since the displacement $\nabla_{(\mathbf{Z}_\xi)_{00},(\mathbf{Z}_\eta)_{00}}(\mathbf{T}_{00}^{-1})$ is the only information required to compute this product in a superfast manner;

- After successive applications of Eq. (D.14), the generator-pair matrices may have more columns than their rank, eventually increasing the computational complexity. Nonetheless, this difficulty can be overcome by applying Theorem 4.6.4 of [25], which states that a generator pair $(\mathbf{P}, \mathbf{Q}) \in \mathbb{C}^{M\times S} \times \mathbb{C}^{M\times S}$, where $\text{rank}\{\mathbf{P}\mathbf{Q}^T\} = R < S$, may be transformed into a generator pair $(\bar{\mathbf{P}}, \bar{\mathbf{Q}}) \in$

$\mathbb{C}^{M\times R} \times \mathbb{C}^{M\times R}$ with only $\mathcal{O}(S^2 M)$ operations, where $\bar{\mathbf{P}}\bar{\mathbf{Q}}^T = \mathbf{P}\mathbf{Q}^T$;

- In order to apply Pan's algorithm to the ZF-based receiver design, the input of the algorithm must be the matrix $\mathbf{H}_0$ and its associated displacement matrix, whereas the output is $\nabla_{\mathbf{Z}_1,\mathbf{Z}_{-1}}\left(\mathbf{H}_0^{-1}\right)$. With the knowledge of the displacement of the channel matrix inverse, one may compute all vectors related to the equalizer design using only $\mathcal{O}(M\log_2 M)$ numerical operations;

- In order to use this algorithm to the MMSE-based receiver design, one may adapt Pan's algorithm and set $[\mathbf{H}_0\mathbf{H}_0^H + (\sigma_v^2/\sigma_s^2)\mathbf{I}]$ as the input matrix. The MMSE solution is calculated by applying the result of Eq. (D.14), with $\mathbf{U} = \mathbf{H}_0^H$ and $\mathbf{V} = [\mathbf{H}_0\mathbf{H}_0^H + (\sigma_v^2/\sigma_s^2)\mathbf{I}]^{-1}$. Once again, after running Pan's divide-and-conquer algorithm, all vectors related to the equalizer design may be computed employing $\mathcal{O}(M\log_2 M)$ operations.

  One may argue that the computation of the input, $[\mathbf{H}_0\mathbf{H}_0^H + (\sigma_v^2/\sigma_s^2)\mathbf{I}]$, of the Pan's divide-and-conquer algorithm may be costly. However, both matrices $\mathbf{H}_0$ and $\mathbf{H}_0^H$ can be represented using their displacements $\nabla_{\mathbf{Z}_{-1},\mathbf{Z}_1}(\mathbf{H}_0) \in \mathbb{C}^{M\times 2}$ and $\nabla_{\mathbf{Z}_1,\mathbf{Z}_{-1}}(\mathbf{H}_0^H) \in \mathbb{C}^{M\times 2}$. In addition, Theorem 4.7.2 of [25], p. 142, states that the maximum number of operations required for multiplying such types of structured matrices is[3]

$$\mathcal{O}\left(2\times 2\left[\mathcal{O}(M\log_2 M) + \mathcal{O}(M\log_2 M)\right]\right) = \mathcal{O}(M\log_2 M); \tag{J.30}$$

- Note that there are several practical applications where the equalizer-design problem is seldom solved. For instance, in many wireline communications systems, the channel model does not need to be updated often. This eventually means that the dominant problem is the equalization. The minimum-redundancy proposals in Part I solve the equalization problem in a very efficient way, requiring only $\mathcal{O}(M\log_2 M)$ computations. The aim of this section was to elucidate an application of Pan's divide-and-conquer algorithm to the situations where the equalizer design is also a concern. The described solution for the equalizer-design problem employs $\mathcal{O}(M\log_2^2 M)$ operations.

J.4 Simulation Results

Some experiments were included to verify the performance of some superfast algorithms previously described when applied to the design of minimum-redundancy transceivers. There are many different configurations to be tested, however, we assess the performance only when a PCG method is first employed in order to refine

[3] See also Theorems 3.4 and 2.3 in [53].

a crude initial approximation for the inverse of $\mathbf{H}_0$ and then Newton's iteration method is employed.

The channel model is a 3G-LTE-based extended typical urban (ETU) channel, whose power-delay profile is described in [74]. The resulting impulse response has order $L = 22$. We consider that $M = 32$. We generate 6000 distinct channels and each new channel used the inverse of the previous effective channel matrix as an initial approximation to the current inverse of the channel matrix. The performance assessment is based on the normalized error associated with the estimation of matrix $\mathbf{P}$ in a ZF solution (see Eq. (D.7)), i.e., the performance of the algorithms was verified based on the quantity $(\|\mathbf{P} - \bar{\mathbf{P}}\|_{\mathrm{F}})/\|\mathbf{P}\|_{\mathrm{F}}$, where $\|\cdot\|_{\mathrm{F}}$ is the usual Frobenius norm of matrices [25] and $\bar{\mathbf{P}}$ is the related estimate.

Figure J.1 depicts the empirical cumulative distribution function (CDF) of the variable $10\log_{10}\left[(\|\mathbf{P} - \bar{\mathbf{P}}\|_{\mathrm{F}})/\|\mathbf{P}\|_{\mathrm{F}}\right]$. The number of iterations of the PCG algorithm to achieve this performance is around 14 ± 3. We verified that the PCG algorithm would take much more iterations to further decrease the resulting normalized error. This justifies the use of a more sophisticated method, such as Newton's iteration. From Figure J.1, one may conclude that with just two or three Newton's itera-

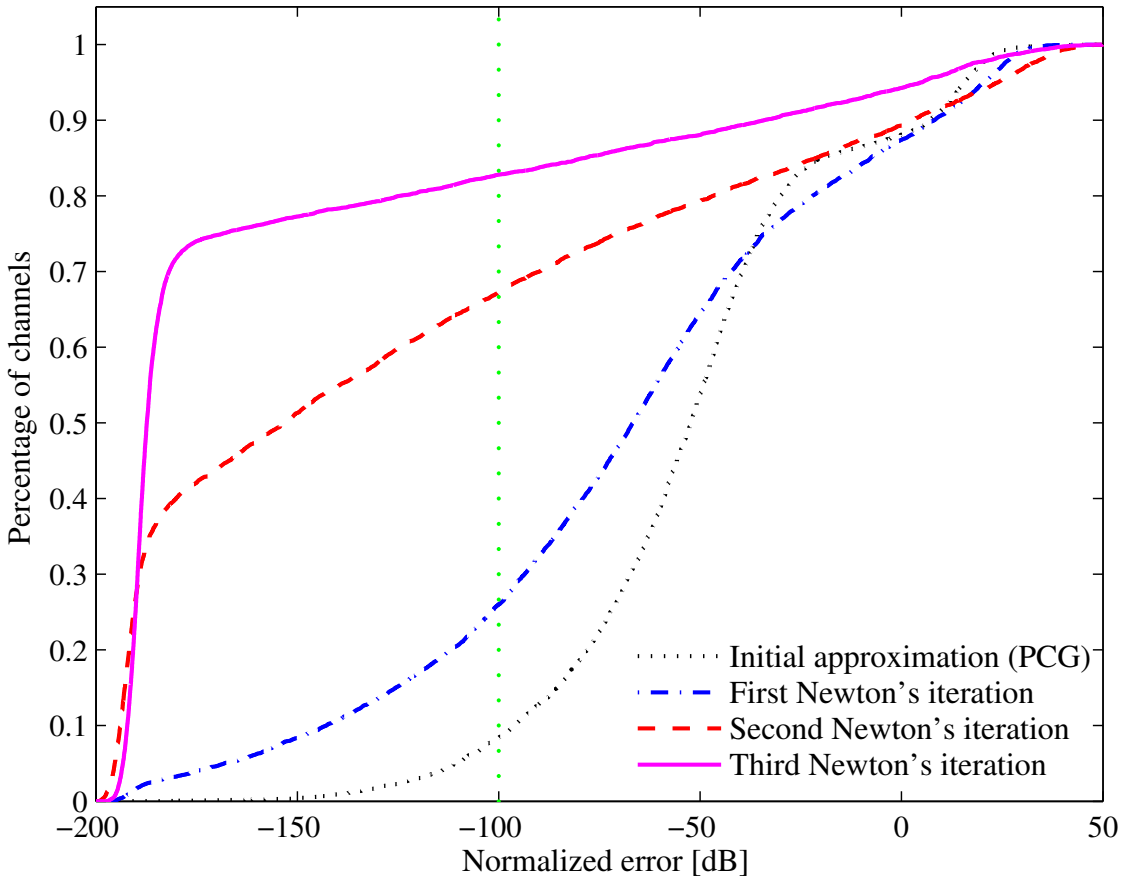

Figure J.1: Percentage of channels *versus* normalized error [dB]: CDF.

tions, the percentage of channels whose associated value $10\log_{10}\left[(\|\mathbf{P}-\bar{\mathbf{P}}\|_{\mathrm{F}})/\|\mathbf{P}\|_{\mathrm{F}}\right]$ is, e.g., lower than -100 dB is much higher than that when using the initial estimate obtained with the PCG method (blue line).

J.5 Concluding Remarks

In this chapter, we proposed new methods to design the channel-dependent parameter which define memoryless block-based equalizers with minimum redundancy. The new proposals are based on pilot transmission and require only $\mathcal{O}(M\log_2 M)$ to estimate the related time-domain model of the channel. In addition, the new proposals also employ iterative algorithms that require only $\mathcal{O}(M\log_2 M)$ operations per iteration. These are preliminary theoretical results from investigations that are in progress.

J.6 Guidelines for Further Research

All proposed methods to design block-based equalizers with minimum redundancy rely on the assumption that the channel is first estimated and, after this step, the equalizer is designed. In other words, the adopted approaches have three well-defined stages: channel estimation, equalizer design, and equalization. Nonetheless, channel estimation along with equalizer design could be addressed simultaneously. In fact, we could try to bypass the channel-estimation stage by directly designing the equalizer taps. This is a challenging open problem in the context of minimum- or reduced-redundancy transceivers. In this last section, we share some ideas about how one may attack this problem in future works.

Using Eq. (D.1) and the results from Section D.2, one has

$$\hat{\mathbf{s}} = \mathbf{G}_0 \underbrace{(\mathbf{H}_0\mathbf{F}_0\mathbf{s}+\mathbf{v}_0)}_{\triangleq\mathbf{y}_0} = \mathbf{G}_0\mathbf{y}_0, \tag{J.31}$$

in which the exact definition of the receiver matrix $\mathbf{G}_0$ depends on whether the ZF or MMSE solution is chosen. Let us focus on the MMSE solution, which takes the form

$$\mathbf{G}_0 = \frac{1}{2}\mathbf{F}_0^{-1}\mathbf{W}_M^H\left(\sum_{r=1}^{4}\mathbf{D}_{\bar{\mathbf{p}}_r}\mathbf{W}_M\mathbf{D}\mathbf{W}_M\mathbf{D}_{\bar{\mathbf{q}}_r}\right)\mathbf{W}_M^H\mathbf{D}^H. \tag{J.32}$$

One can rewrite Eq. (J.32) as follows:

$$\begin{aligned}\mathbf{G}_0 = \mathbf{A}\underbrace{\begin{bmatrix}\mathbf{D}_{\bar{\mathbf{p}}_1} & \mathbf{D}_{\bar{\mathbf{p}}_2} & \mathbf{D}_{\bar{\mathbf{p}}_3} & \mathbf{D}_{\bar{\mathbf{p}}_4}\end{bmatrix}}_{\triangleq\mathbf{X}_1}\times \\ \times\underbrace{\begin{bmatrix}\mathbf{W}_M\mathbf{D}\mathbf{W}_M & \mathbf{0} & \mathbf{0} & \mathbf{0}\\ \mathbf{0} & \mathbf{W}_M\mathbf{D}\mathbf{W}_M & \mathbf{0} & \mathbf{0}\\ \mathbf{0} & \mathbf{0} & \mathbf{W}_M\mathbf{D}\mathbf{W}_M & \mathbf{0}\\ \mathbf{0} & \mathbf{0} & \mathbf{0} & \mathbf{W}_M\mathbf{D}\mathbf{W}_M\end{bmatrix}}_{\triangleq\mathbf{C}}\underbrace{\begin{bmatrix}\mathbf{D}_{\bar{\mathbf{q}}_1}\\ \mathbf{D}_{\bar{\mathbf{q}}_2}\\ \mathbf{D}_{\bar{\mathbf{q}}_3}\\ \mathbf{D}_{\bar{\mathbf{q}}_4}\end{bmatrix}}_{\triangleq\mathbf{X}_2}\mathbf{B} \\ = \mathbf{A}\mathbf{X}_1\mathbf{C}\mathbf{X}_2\mathbf{B},\end{aligned}$$

where $\mathbf{A} \triangleq \frac{1}{2}\mathbf{F}_0^{-1}\mathbf{W}_M^H$ and $\mathbf{B} \triangleq \mathbf{W}_M^H\mathbf{D}^H$. Note that the matrices $\mathbf{X}_1$ and $\mathbf{X}_2$ contain the equalizer taps and can be considered the independent variables that must be updated in order to minimize the mean-square error $\mathsf{E}\left[\|\mathbf{s}-\hat{\mathbf{s}}\|_2^2\right]$, while all the remaining matrices are constant. In other words, we know the current matrices $\mathbf{X}_1$ and $\mathbf{X}_2$ and we want estimate new matrices $\mathbf{X}_1^{\text{new}}$ and $\mathbf{X}_2^{\text{new}}$, as we shall describe in the following developments.

Now, let $\mathbf{S} \triangleq \mathbf{A}^{-1}\mathbf{s} = 2\mathbf{W}_M\mathbf{F}_0\mathbf{s}$ be a known vector at the receiver end (a type of pilot signal). Note that we can define an estimate of $\mathbf{S}$ as:

$$\begin{aligned}\hat{\mathbf{S}} &\triangleq \mathbf{A}^{-1}\hat{\mathbf{s}} = \mathbf{A}^{-1}\mathbf{G}_0\mathbf{y}_0 = \mathbf{A}^{-1}(\mathbf{A}\mathbf{X}_1\mathbf{C}\mathbf{X}_2\mathbf{B})\mathbf{y}_0 \\ &= \mathbf{X}_1\underbrace{(\mathbf{C}\mathbf{X}_2\mathbf{B}\mathbf{y}_0)}_{\triangleq\mathbf{y}_1} = \mathbf{X}_1\mathbf{y}_1 = \mathbf{Y}_1\mathbf{x}_1,\end{aligned} \tag{J.33}$$

where $\mathbf{Y}_1$ is a *known* $M \times 4M$ matrix with the same structure of $\mathbf{X}_1$, whereas $\mathbf{x}_1$ is a vector containing $4M$ elements for which we want to determine a new estimate. We can estimate a new vector $\mathbf{x}_1^{\text{new}} \in \mathbb{C}^{4M\times 1}$ as follows:

$$\mathbf{x}_1^{\text{new}} = \mathbf{Y}_1^H(\mathbf{Y}_1\mathbf{Y}_1^H)^{-1}\mathbf{S}. \tag{J.34}$$

Note that $\mathbf{Y}_1\mathbf{Y}_1^H$ is an $M \times M$ diagonal matrix. Hence, if we already know $\mathbf{S}$ and $\mathbf{Y}_1$, then we can estimate a new vector $\mathbf{x}_1^{\text{new}}$ by employing $10M$ complex-valued multiplications. This means that we can update the final stage of equalizer taps (see vectors $\bar{\mathbf{p}}_1, \bar{\mathbf{p}}_2, \bar{\mathbf{p}}_3$, and $\bar{\mathbf{p}}_4$ in Figure D.2) using only $\mathcal{O}(M)$ operations, while we keep constant the first stage of equalizer taps (see vectors $\bar{\mathbf{q}}_1, \bar{\mathbf{q}}_2, \bar{\mathbf{q}}_3$, and $\bar{\mathbf{q}}_4$ in Figure D.2).

Now, define $\hat{\mathbf{t}} \triangleq \mathbf{X}_2(\mathbf{B}\mathbf{y}_0) = \mathbf{X}_2\mathbf{y}_2 = \mathbf{Y}_2\mathbf{x}_2$, where $\mathbf{y}_2 \triangleq \mathbf{B}\mathbf{y}_0$. Note that $\mathbf{Y}_2$ is a $4M \times 4M$ *known* diagonal matrix, whereas $\mathbf{x}_2$ is a vector containing $4M$ elements.

We can generate a reference $\mathbf{t} \in \mathbb{C}^{4M \times 1}$ for the vector $\hat{\mathbf{t}}$ as follows:

$$\mathbf{t} \triangleq \mathbf{C}^H (\mathbf{X}_1^{\text{new}})^H [\mathbf{X}_1^{\text{new}} \mathbf{C}\mathbf{C}^H (\mathbf{X}_1^{\text{new}})^H]^{-1} \mathbf{S} = \mathbf{C}^H (\mathbf{X}_1^{\text{new}})^H [\mathbf{X}_1^{\text{new}} (\mathbf{X}_1^{\text{new}})^H]^{-1} \mathbf{S}. \quad \text{(J.35)}$$

Thus, we can estimate a reference vector $\mathbf{t}$ by employing $14M$ complex-valued multiplications plus 8 DFTs.

The third step is to estimate a new vector $\mathbf{x}_2^{\text{new}}$ as follows:

$$\mathbf{x}_2^{\text{new}} = (\mathbf{Y}_2^H \mathbf{Y}_2)^{-1} \mathbf{Y}_2^H \mathbf{t} = \mathbf{Y}_2^{-1} \mathbf{t}. \quad \text{(J.36)}$$

Thus, if we already know $\mathbf{t}$, we can estimate a new vector $\mathbf{x}_2^{\text{new}}$ by employing $4M$ complex-valued multiplications. The total asymptotic complexity needed to determine $\mathbf{x}_2^{\text{new}}$ is therefore $\mathcal{O}(M \log_2 M)$.

The aforementioned process can be implemented iteratively, i.e., we can initiate once again the process by generating another estimate for $\mathbf{X}_1$ using the previous estimates for $\mathbf{X}_1$ and $\mathbf{X}_2$. After that, we can generate another estimate for $\mathbf{X}_2$, and so forth.

These theoretical guidelines give rise to several relevant practical questions:

- Is it possible to update only $\mathbf{X}_1$ without sacrificing the BER or throughput performances of the transceivers? In which situations this can be done?
- If the channel does not vary significantly from one block to another, then one could use a decision-direct scheme to generate $\mathbf{S}$ and, after that, using this vector to update the matrices $\mathbf{X}_1$ and $\mathbf{X}_2$. How fast the channel can vary without sacrificing significantly the BER or throughput performances of such transceivers?
- How many iterations are necessary to obtain good updates for $\mathbf{X}_1$ and $\mathbf{X}_2$ considering a given channel and SNR?

Apêndice K

Conclusion

In this work, we have proposed effective and practical solutions for multicarrier and single-carrier transceivers using minimum, or more generally, reduced redundancy. Their related ZF and MMSE solutions employ only DFTs, inverse DFTs, and diagonal matrices, or DHTs, diagonal, and antidiagonal matrices. This feature makes the new transceivers computationally efficient. The adopted framework relied on the properties of structured matrices using the concepts of Sylvester and Stein displacements. These concepts aimed at exploiting the structural properties of typical channel matrix representations, such as Toeplitz, Vandermonde, and Bezoutian matrices. By using adequate displacement properties we were able to derive DFT and DHT decompositions of generalized Bezoutians, which were the key tools to reach the proposed solutions for the multicarrier and single-carrier block-based transceivers requiring minimum/reduced redundancy.

Simulations had shown that the proposed transceivers can achieve substantially higher throughput (especially for long channels), as compared with the standard block-based systems, such as OFDM and SC-FD, while maintaining competitive asymptotic complexity for the equalization process, $\mathcal{O}(M \log_2 M)$.

K.1 Contributions

We now list in a more specific way the innovations presented in this work:

- A complete mathematical analysis of the MSE and the mutual information in block-based transceivers with full-redundancy that employ zero-padding was developed;

- A modification to the MMSE minimum-redundancy solution described in [23] was proposed. Indeed, the new proposed structure is simpler than the one proposed in [23], since it employs only four parallel branches at the receiver end instead of the previous five branches;

- Novel suboptimal MMSE equalizers with minimum redundancy that require the same amount of computations of ZF equalizers were proposed;
- New transceivers with practical ZF and MMSE receivers using DHT, diagonal, and antidiagonal matrices as building blocks were proposed. Such new transceivers do not impose a symmetry on the channel model as required in [23];
- New LTI transceivers with reduced redundancy based on DFTs were presented;
- New LTI transceivers with reduced redundancy based on DHTs were presented;
- An MSE analysis of the proposed reduced-redundancy transceivers with respect to the amount of redundancy was derived. Indeed, we demonstrated that larger amounts of transmitted redundant elements lead to lower MSE of symbols at the receiver end;
- An optimal power-allocation method that minimizes the noise gains when CSI is available at the transmitter end was conceived;
- Block-based DFE systems with reduced redundancy were proposed;
- Designs of minimum-redundancy equalizers based on pilot information and using fast-converging iterative algorithms [25, 53, 56] that require $\mathcal{O}(M \log_2 M)$ operations per iteration were proposed. Another proposed approach was: the application of Pan's divide-and-conquer algorithm [25, 55] to design the equalizers.

K.2 Future Works

We now list some possible future works:

- To develop time-varying transceivers following the same lines of the reduced-redundancy systems proposed in this thesis. Time-varying transceivers can use just one redundant element, regardless of the channel model, as described in [57];
- To develop MIMO versions of reduced-redundancy transceivers in order to deal with space-time diversity, beamforming, and spatial-multiplexing systems;
- To develop a multiple-access scheme based on the proposals of this thesis;
- To study I/Q imbalance problems in transceivers with reduced redundancy;

- To study the CFO effects and how to mitigate them in transceivers with reduced redundancy;
- To study the tradeoff between the insertion of redundant symbols (physical layer) and the insertion of redundant bits (channel coding implemented in the link layer, for example);
- To study the robustness of the proposed transceivers to errors in the channel-model estimation, which include errors in the values of the channel taps and/or errors in the delay spread of the channel.

Apêndice L

List of Publications and Invited Lectures

This chapter lists the published works which resulted from this thesis. The scientific contributions appeared in international conference proceedings, referred international journals, and parts of a book. In addition, we also list the invited lectures which resulted from this thesis and other related author's publications.

Journal Publications

1. Martins, W. A. and Diniz, P. S. R., "LTI transceivers with reduced redundancy," *IEEE Transactions on Signal Processing*, accepted in October 2011.

2. Martins, W. A. and Diniz, P. S. R., "Analysis of zero-padded optimal transceivers," *IEEE Transactions on Signal Processing*, vol. 59, no. 11, pp. 5443-5457, November 2011.

3. Martins, W. A. and Diniz, P. S. R., "Memoryless block transceivers with minimum redundancy based on Hartley transforms," *Signal Processing, EURASIP*, vol. 91, pp. 240-251, February 2011.

4. Martins, W. A. and Diniz, P. S. R., "Suboptimal linear MMSE equalizers with minimum redundancy," *IEEE Signal Processing Letters*, vol. 17, no. 4, pp. 387-390, April 2010.

5. Martins, W. A. and Diniz, P. S. R., "Block-based transceivers with minimum redundancy," *IEEE Transactions on Signal Processing*, vol. 58, no. 3, pp. 1321-1333, March 2010.

Conference Publications

1. Martins, W. A. and Diniz, P. S. R., "Combating noise gains in high-throughput block transceivers using CSI at the transmitter," in *Proc. 2010 IEEE International Symposium on Wireless Communications Systems*, York, UK, September 2010, pp. 275-279.

2. Martins, W. A. and Diniz, P. S. R., "Low-redundancy transceivers for wireless networks," (invited paper) in *Proc. 2010 IEEE International Conference on Systems, Signals and Image Processing*, Rio de Janeiro, Brazil, June 2010, pp. 20-23.

3. Martins, W. A. and Diniz, P. S. R., "Pilot-aided designs of memoryless block equalizers with minimum redundancy," in *Proc. 2010 IEEE International Symposium on Circuits and Systems*, Paris, France, May 2010, pp. 3112-3115.

Conference Submissions

1. Martins, W. A. and Diniz, P. S. R., "Block-based decision-feedback equalizers with reduced redundancy," submitted to IEEE ICASSP-2012.

Related Publications

1. Martins, W. A. and Diniz, P. S. R., "Minimum redundancy multicarrier and single-carrier systems based on Hartley transforms," *EURASIP News Letter*, vol. 20, no. 4, December 2009. This is the **same** conference paper described below, which was awarded *Best Student Paper Award* in EUSIPCO-2009.

2. Martins, W. A. and Diniz, P. S. R., "Minimum redundancy multicarrier and single-carrier systems based on Hartley transforms," in *Proc. 2009 European Signal Processing Conference*, Glasgow, Scotland, August 2009, pp. 661-665.

Related Books

1. Diniz, P. S. R., Martins, W. A., and Lima, M. V. S.; *Block transceivers: OFDM and Beyond*. Morgan & Claypool Publishers, 2012 (available soon).

Additional Publications

1. Martins, W. A., Diniz, P. S. R., and Huang, Y. F., "On the normalized minimum error-entropy adaptive algorithm: cost function and update recursion," in *Proc. 2010 IEEE Latin American Symposium on Circuits and Systems*, Foz do Iguaçu, Brazil, February 2010, pp. 160-163.

2. Martins, W. A., Lima, M. V. S., and Diniz, P. S. R., "Semi-blind data-selective equalizers for QAM," in *Proc. 2008 IEEE Workshop on Signal Processing Advances in Wireless Communications*, Recife, Brazil, July 2008, pp. 501-505.

3. Diniz, P. S. R., Lima, M. V. S., and Martins, W. A., "Semi-blind data-selective algorithms for channel equalization," in *Proc. 2008 IEEE International Symposium on Circuits and Systems*, Seattle, WA, May 2008, pp. 53-56.

4. Martins, W. A., Diniz, P. S. R., and Ferreira, T. N., "Mutual influence of techniques for CCI suppression in the GPRS," in *Proc. 2008 Brazilian Telecommunication Symposium*, Rio de Janeiro, Brazil, September 2008, pp. 1-6.

Additional Submissions

1. Lima, M. V. S., Gussen, C. M. G., Espíndola, B. N., Ferreira, T. N., Martins, W. A., and Diniz, P. S. R., "Open-source physical-layer simulator for LTE systems," submitted to IEEE ICASSP-2012.

Invited Lectures

1. Diniz, P. S. R., "*Efficient Block Transceivers*," **Plenary talk** at SBrT 2011, 28th Brazilian Telecommunications Symposium, Curitiba, Brazil, October 3rd, 2011.

2. Diniz, P. S. R., "*High-Throughput Block Transceivers*," University of Alcalá de Henares, Alcalá de Henares, Spain, May 31st, 2011.

3. Diniz, P. S. R., "*High-Throughput Block Transceivers*," **Plenary talk** at ISWCS 2010, 7th International Symposium on Wireless Communication Systems, York, UK, September 22nd, 2010.

4. Diniz, P. S. R., "*Low-Redundancy Transceivers for Wireless Networks*," **Plenary talk** at IWSSIP 2010, 17th International Conference on Systems, Signals and Image Processing, Rio de Janeiro, Brazil, June 17th, 2010.

5. Diniz, P. S. R., "*Low-Redundancy Transceivers for Wireless Networks*," Supelec, École Supérieure D'Électricité, Paris, France, June 3rd, 2010.

6. Diniz, P. S. R., "*Block-Based Transceivers for Wireless Networks*," **Plenary talk** at first IEEE Latin American Symposium on Circuits and Systems, Foz do Iguaçu, Brazil, February 25th, 2010.

7. Diniz, P. S. R., "*New Block-Based Transceivers with Minimum Redundancy*," University of Brasília, Brasília, Brazil, November 18th, 2009.

8. Diniz, P. S. R., "*New Block-Based Transceivers with Minimum Redundancy*," Munich University of Technology, Munich, Germany, June 4th, 2009.

Referências Bibliográficas

[1] SCAGLIONE, A., BARBAROSSA, S., GIANNAKIS, G. B. "Filterbank transceivers optimizing information rate in block transmissions over dispersive channels", *IEEE Transactions on Information Theory*, v. 45, n. 3, pp. 1019–1032, April 1999.

[2] LIN, Y. P., PHOONG, S. M. "Perfect discrete multitone modulation with optimal transceivers", *IEEE Transactions on Signal Processing*, v. 48, n. 6, pp. 1702–1711, June 2000.

[3] LIN, Y. P., PHOONG, S. M. "ISI-free FIR filterbank transceivers for frequency selective channels", *IEEE Transactions on Signal Processing*, v. 49, n. 11, pp. 2648–2658, November 2001.

[4] LIN, Y. P., PHOONG, S. M. "Optimal ISI-free DMT transceivers for distorted channels with colored noise", *IEEE Transactions on Signal Processing*, v. 49, n. 11, pp. 2702–2712, November 2001.

[5] ZHANG, W., MA, X., GESTNER, B., et al. "Designing low-complexity equalizers for wireless systems", *IEEE Communications Magazine*, v. 47, n. 1, pp. 56–62, January 2009.

[6] GUAN, R., STROMER, T. "Krylov subspace algorithms and circulant-embedding method for efficient wideband single-carrier equalization", *IEEE Transactions on Signal Processing*, v. 56, n. 6, pp. 2483–2495, June 2008.

[7] XIA, X. G. "New precoding for intersymbol interference cancellation using non-maximally decimated multirate filterbanks with ideal FIR equalizers", *IEEE Transactions on Signal Processing*, v. 45, n. 10, pp. 2431–2441, October 1997.

[8] AL-DHAHIR, N., DIGGAVI, S. N. "Guard sequence optimization for block transmission over linear frequency-selective channels", *IEEE Transactions on Communications*, v. 50, n. 6, pp. 938–946, June 2002.

[9] OHNO, S., GIANNAKIS, G. B. "Optimal training and redundant precoding for block transmissions with application to wireless OFDM", *IEEE Transactions on Communications*, v. 50, n. 12, pp. 2113–2123, December 2002.

[10] VOSOUGHI, A., SCAGLIONE, A. "Everything you always wanted to known about training: guidelines derived using the affine precoding framework and the CRB", *IEEE Transactions on Signal Processing*, v. 54, n. 3, pp. 940–954, March 2006.

[11] RIBEIRO, C. B. *Equalização de Canal em Sistemas de Comunicações Utilizando Transmissão em Blocos*. M.Sc. Thesis, Universidade Federal do Rio de Janeiro, Rio de Janeiro, Brazil, 2002.

[12] FURTADO JR., M. B., DINIZ, P. S. R., NETTO, S. L. "Redundant paraunitary FIR transceivers for single-carrier transmission over frequency selective channels with colored noise", *IEEE Transactions on Communications*, v. 55, n. 6, pp. 1125–1130, June 2007.

[13] FURTADO, M. B. *Otimização de Transceptores FIR Baseados em Bancos de Filtros Aplicados à Comunicação Digital Móvel e Fixa*. D.Sc. Thesis, Universidade Federal do Rio de Janeiro, Rio de Janeiro, Brazil, 2006.

[14] PANCALDI, F., VITETTA, G., KALBASI, R., et al. "Single-carrier frequency-domain equalization", *IEEE Signal Processing Magazine*, v. 25, n. 5, pp. 37–56, September 2008.

[15] WANG, Z., MA, X., GIANNAKIS, G. B. "OFDM or single-carrier block transmissions?" *IEEE Transactions on Communications*, v. 52, n. 3, pp. 380–394, March 2004.

[16] CHUNG, Y. H., PHOONG, S. M. "Low complexity zero-padding zero-jamming DMT systems". In: *Proc. 14th European Signal Processing Conference (EUSIPCO)*, pp. 1–5, Florence, Italy, September 2006.

[17] TRAUTMANN, S., FLIEGE, N. J. "Perfect equalization for DMT systems without guard interval", *IEEE Journal of Selected Areas in Communications*, v. 20, n. 5, pp. 987–996, June 2002.

[18] VEGA, L. R., GALARZA, C. G. "Capacity-approaching block-based transceivers with reduced redundancy", *Digital Signal Processing*, v. 19, n. 2, pp. 340–359, March 2009.

[19] KAILATH, T., SAYED, A. H. "Displacement structure: theory and applications", *SIAM Review*, v. 37, n. 3, pp. 297–386, September 1995.

[20] MERCHED, R. "Application of superfast algorithms to pilot-based channel estimation schemes". In: *Proc. IEEE 9th Workshop on Signal Processing Advances in Wireless Communications (SPAWC)*, pp. 141–145, Recife, Brazil, July 2008.

[21] CARBONELLI, C., VENDATAM, S., MITRA, U. "Sparse channel estimation with zero tap detection", *IEEE Transactions on Communications*, v. 6, n. 5, pp. 1743–1753, May 2007.

[22] GRAY, R. M. *Toeplitz and Circulant Matrices: A Review*. 1st ed. New York, Now Publishers Inc., 2006.

[23] MARTINS, W. A. *Transceptores em Bloco com Redundância Mínima*. M.Sc. Thesis, Universidade Federal do Rio de Janeiro, Rio de Janeiro, Brazil, 2009.

[24] HEINIG, G., ROST, K. "DFT representations of Toeplitz-plus-Hankel Bezoutians with application to fast matrix-vector multiplication", *Linear Algebra and its Applications*, v. 284, n. 1–3, pp. 157–175, November 1998.

[25] PAN, V. Y. *Structured Matrices and Polynomials: Unified Superfast Algorithms*. 1st ed. New York, Springer, 2001.

[26] DINIZ, P. S. R., DA SILVA, E. A. B., NETTO, S. L. *Digital Signal Processing: Systems Analysis and Design*. 2nd ed. Cambridge, Cambridge University Press, 2010.

[27] VAIDYANATHAN, P. P. *Multirate Systems and Filter Banks*. 1st ed. New Jersey, Englewood Cliffs, 1993.

[28] VAIDYANATHAN, P. P. "Filter banks in digital communications", *IEEE Circuits and Systems Magazine*, v. 1, n. 2, pp. 4–25, Second Quarter 2001.

[29] VAIDYANATHAN, P. P., VRCELJ, B. "Transmultiplexers as precoders in modern digital communication: a tutorial review". In: *Proc. IEEE 2004 International Symposium on Circuits and Systems (ISCAS)*, pp. 405–412, Vancouver, Canada, May 2004.

[30] AKANSU, A. N., DUHAMEL, P., L., et al. "Orthogonal transmultiplexers in communication: a review", *IEEE Transactions on Signal Processing*, v. 46, n. 4, pp. 979–995, April 1998.

[31] SCAGLIONE, A., GIANNAKIS, G. B., BARBAROSSA, S. "Redundant filterbank precoders and equalizers part I: unification and optimal designs",

IEEE Transactions on Signal Processing, v. 47, n. 7, pp. 1988–2006, July 1999.

[32] LIN, Y. P., PHOONG, S. M. "Minimum redundancy for ISI free FIR filterbank transceivers", *IEEE Transactions on Signal Processing*, v. 50, n. 4, pp. 842–853, April 2002.

[33] RIBEIRO, C. B. *Sistemas de Comunicações MIMO com Reconstrução Perfeita*. D.Sc. Thesis, Universidade Federal do Rio de Janeiro, Rio de Janeiro, Brazil, 2007.

[34] PROAKIS, J. G. *Digital Communications*. 4th ed. New York, McGraw-Hill, 2001.

[35] GALLAGER, R. G. *Principles of Digital Communication*. 1st ed. New York, Cambridge, 2008.

[36] DINIZ, P. S. R. *Adaptive Filtering: Algorithms and Practical Implementation*. 3rd ed. Boston, Springer, 2008.

[37] MUQUET, B., WANG, Z., GIANNAKIS, G. B., et al. "Cyclic prefixing or zero padding wireless multicarrier transmissions?" *IEEE Transactions on Communications*, v. 50, n. 12, pp. 2136–2148, December 2002.

[38] SAYED, A. H. *Fundamentals of Adaptive Filtering*. 1st ed. New York, Wiley, 2003.

[39] VRCELJ, B. *Multirate Signal Processing Concepts in Digital Communications*. Ph.D. Thesis, California Institute of Technology, California, USA, 2003.

[40] VAIDYANATHAN, P. P., PHOONG, S. M., LIN, Y. P. *Signal Processing and Optimization for Transceiver Systems*. 1st ed. New York, Cambridge Univ. Press, 2010.

[41] LIN, Y. P., PHOONG, S. M., VAIDYANATHAN, P. P. *Filter Bank Transceivers for OFDM and DMT Systems*. 1st ed. New York, Cambridge Univ. Press, 2011.

[42] OHNO, S. "Performance of single-carrier block transmissions over multipath fading channels with linear equalization", *IEEE Transactions on Signal Processing*, v. 54, n. 10, pp. 3678–3687, October 2006.

[43] VAIDYANATHAN, P. P. "On equalization of channels with ZP precoders". In: *Proc. IEEE 2007 International Symposium on Circuits and Systems (ISCAS)*, pp. 1329–1332, New Orleans, USA, May 2007.

[44] GOLUB, G. H., VAN LOAN, C. F. *Matrix Computations*. 3rd ed. Baltimore, Johns Hopkins Univ. Press, 1996.

[45] PAN, V. Y. "Concurrent iterative algorithm for Toeplitz-like linear systems", *IEEE Transactions on Parallel and Distributed Systems*, v. 4, n. 5, pp. 592–600, May 1993.

[46] AL-DHAHIR, N., MINN, H., SATISH, S. "Optimum DCT-based multicarrier transceivers for frequency-selective channels", *IEEE Transactions on Communications*, v. 54, n. 3, pp. 911–921, May 2006.

[47] MERCHED, R. "On OFDM and single-carrier frequency-domain systems based on trigonometric transforms", *IEEE Signal Processing Letters*, v. 13, n. 8, pp. 473–476, August 2006.

[48] HEINIG, G., ROST, K. "Hartley transform representations of symmetric Toeplitz matrix inverses with application to fast matrix-vector multiplication", *SIAM Journal on Matrix Analysis and Applications*, v. 22, n. 1, pp. 86–105, July 2000.

[49] HEINIG, G., ROST, K. "Hartley transform representations of inverses of real Toeplitz-plus-Hankel matrices", *Numerical Functional Analysis and Optimization*, v. 21, n. 1-2, pp. 175–189, February 2000.

[50] AUSTIN, M. E. *Decision feedback equalization for digital communication over dispersive channels*. Relatório Técnico 437, MIT Lincoln Lab., USA, Aug. 1967.

[51] SALZ, J. "Optimum mean square decision feedback equalization", *Bell System Technical Journal*, v. 52, pp. 1341–1373, Oct. 1973.

[52] XU, F., DAVIDSON, T. N., ZHANG, J.-K., et al. "Design of block transceivers with decision feedback detection", *IEEE Trans. Signal Process.*, v. 54, n. 3, pp. 965–978, Mar. 2006.

[53] PAN, V. Y., RAMI, Y., WANG, X. "Structured matrices and Newton's iteration: unified approach", *Linear Algebra and its Applications*, v. 343–344, pp. 233–265, March 2002.

[54] DOMÍNGUEZ-JIMÉNEZ, M. H., FERREIRA, P. J. S. G. "A new preconditioner for Toeplitz matrices", *IEEE Signal Processing Letters*, v. 16, n. 9, pp. 758–761, September 2009.

[55] PAN, V. Y. "A unified superfast divide-and-conquer algorithm for structured matrices over abstract fields". 1999. MSRI Preprint 1999-033, Mathematical Science Research Institute, Berkeley, CA.

[56] PAN, V. Y., WANG, X. "Inversion of displacement operators", *SIAM Journal on Matrix Analysis and Applications*, v. 24, n. 3, pp. 660–667, May 2003.

[57] RIBEIRO, C. B., DE CAMPOS, M. L. R., DINIZ, P. S. R. "Time-varying FIR transmultiplexers with minimum redundancy", *IEEE Transactions on Signal Processing*, v. 57, n. 3, pp. 1113–1127, March 2009.

[58] KAILATH, T., KUNG, S.-Y., MORF, M. "Displacement ranks of a matrix", *Bulletin of The American Mathematical Society*, v. 1, n. 5, pp. 769–773, September 1979.

[59] GIANNAKIS, G. B. "Filterbanks for blind channel identification and equalization", *IEEE Signal Processing Letters*, v. 4, n. 6, pp. 184–187, June 1997.

[60] AL-DHAHIR, N., CIOFFI, J. M. "Efficiently computed reduced–parameter input–aided MMSE equalizers for ML detection: a unified approach", *IEEE Transactions on Information Theory*, v. 42, n. 3, pp. 903–915, May 1996.

[61] BHATIA, R. *Positive Definite Matrices*. 1st ed. New Jersey, Princeton Univ. Press, 2007.

[62] JORSWIECK, E., BOCHE, H. *Majorization and Matrix-Monotone Functions in Wireless Communications*. 1st ed. New York, Now Publishers Inc., 2006.

[63] HANSEN, F., PEDERSEN, G. K. "Jensen's inequality for operators and Löwner's theorem", *Mathematische Annalen*, v. 258, n. 3, pp. 229–241, 1981/1982.

[64] MARSHALL, A. W., OLKIN, I. *Inequalities: Theory of Majorization and Its Application*. 1st ed. London, Academic Press, Inc., 1979.

[65] HJORUNGNES, A., GESBERT, D. "Introduction to complex-valued matrix differentiation", *IEEE Transactions on Signal Processing*, v. 55, pp. 2740–2746, 2007.

[66] REGALIA, P. A. *Adaptive IIR Filtering in Signal Processing and Control*. 1st ed. New York, Marcel Dekker, Inc., 1995.

[67] HALMOS, P. R. *Finite-Dimensional Vector Spaces*. 1st ed. Boston, Springer, 1974.

[68] STRANG, G. *Linear Algebra and Its Applications*. 3rd ed. San Diego, Harcourt Brace Jovanovich, 1988.

[69] HAYKIN, S. *Sistemas de Comunicação Analógicos e Digitais*. 4th ed. Porto Alegre, Bookman, 2004.

[70] POOR, H. V. *An Introduction to Signal Detection and Estimation*. 2nd ed. New York, Springer, 1994.

[71] RIBEIRO, C. B., DE CAMPOS, M. L. R., DINIZ, P. S. R. "FIR equalizers with minimum redundancy". In: *Proc. IEEE 2002 International Conference on Acoustics, Speech, and Signal Processing (ICASSP)*, pp. 2673–2676, Orlando, USA, May 2002.

[72] HJORUNGNES, A., DINIZ, P. S. R. "On the Relevancy of the Perfect Reconstruction Property When Minimizing the Mean Square Error in FIR MIMO Systems". In: *Proc. IEEE 2003 International Symposium on Circuits and Systems (ISCAS)*, pp. 49–52, Bangkok, Thailand, May 2003.

[73] LIN, Y. P., PHOONG, S. M. "BER minimized OFDM systems with channel independent precoders", *IEEE Transactions on Signal Processing*, v. 51, n. 9, pp. 2369–2380, September 2003.

[74] UNIVERSAL TERRESTRIAL RADIO ACCESS (E-UTRAN): MULTIPLEXING, E., CHANNEL CODING. *3rd Generation Partnership Project*. 3GPP TS 36212, v8.7.0, May 2009.

[75] HJORUNGNES, A., DINIZ, P. S. R., DE CAMPOS, M. L. R. "Jointly minimum BER transmitter and receiver FIR MIMO filters for binary signal vectors", *IEEE Transactions on Signal Processing*, v. 52, n. 4, pp. 1021–1036, April 2004.

[76] SCAGLIONE, A., GIANNAKIS, G. B., BARBAROSSA, S. "Redundant filterbank precoders and equalizers part II: blind channel equalization, synchronization, and direct equalization", *IEEE Transactions on Signal Processing*, v. 47, n. 7, pp. 2007–2022, July 1999.

[77] JIANG, Y., HAGER, W. W., LI, J. "The geometric mean decomposition", *Linear Alg. and Its Appl.*, pp. 373–384, 2005.